UNDERWATER ACOUSTIC COMMUNICATIONS

By

JONATHAN JAMES DAVIES

A thesis submitted to
The University of Birmingham
For the degree of
DOCTOR OF PHILOSOPHY

Cover + xiv + 268 pages

Department of Electrical and Electronic Engineering
The University of Birmingham

August 2002

Abstract and Statement of Originality

The underwater acoustic medium poses unique challenges to the design of robust, high throughput digital communications. The aim of this work is to identify modulation and receiver processing techniques to enable the reliable transfer of data at high rate, at range between two, potentially mobile parties using acoustics. More generally, this work seeks to investigate techniques to effectively communicate between two or more parties over a wide range of channel conditions where data rate is a key but not always the absolute performance requirement. Understanding the intrinsic ocean mechanisms that influence signal coherence, the relationship between signal coherence and optimum signal design, and the development of robust modulation and receiver processing techniques are the main areas of study within this work.

New and established signal design, modulation, synchronisation, equalisation and spatial processing techniques are investigated. Several new, innovative techniques are presented which seek to improve the robustness of 'classical' solutions to the underwater acoustic communications problem. The performance of these techniques to mitigate the severe temporal dispersion of the underwater channel and its unique temporal variability are assessed.

A candidate modulation, synchronisation and equalisation architecture is proposed based on a spatial-temporal adaptive signal processing (STAP) receiver. Comprehensive simulation results are presented to demonstrate the performance of the candidate receiver to time selective, frequency selective and spatially selective channel behaviour. Several innovative techniques are presented which maximise system performance over a wider range of operational and environmental conditions.

Field trials results are presented based on system evaluation over a wide range of geographically distinct environments demonstrating system performance over a diverse range of ocean bathymetry, topography and background noise conditions.

A real time implementation of the system is reported and field trials results presented demonstrating the capability of the system to support a wide range of data formats including video at useful frame rates.

Within this work, several novel techniques have been developed which have extended the state of the art in high data rate underwater communications:-

- Robust, high fidelity open loop synchronisation techniques capable of operating at marginal signal-to-noise ratios over a wide range of severely time spread environments. These high probability of synchronisation, low probability of false alarm techniques, provide the means for 'burst' open loop synchronisation in time, Doppler and space (bearing). The techniques have been demonstrated in communication and position fixing/navigation systems to provide repeatable range accuracy's to centimetric order.

- Novel closed loop synchronisation compensation for STAP receiver architectures. Specifically, this work has demonstrated the performance benefits of including both delay lock loop (DLL) and phase lock loop (PLL) support for acoustic adaptive receivers to offload tracking effort from the fractional feedforward equaliser section. It has been shown that the addition of a DLL/PLL outperforms the PLL only case for Doppler errors exceeding a few fractions of a knot.

- Recycling of training data has been demonstrated as a potentially useful means to improve equaliser convergence in difficult acoustic channels. With suitable processing power,

training data recycling introduces no additional transmission time overhead, which may be a limiting factor in battery powered applications.

- Forward and time reverse decoding of packet data has been demonstrated as an effective means to overcome some non-minimum phase channel conditions. It has also been shown that there may be further benefits in terms of improved bit error performance, by exploiting concurrent forward and backward symbol data under modest channel conditions.

- Several wideband techniques have been developed and demonstrated to be effective at resolving and coherently tracking difficult doubly spread acoustic channels. In particular, wideband spread spectrum techniques have been shown to be effective at resolving acoustic multipath, and with the aid of independent delay lock loops, track individual path arrivals. Techniques have been developed which can effect coherent or non-coherent recombination of these paths with a view to improving the robustness of an acoustic link operating at very low signal-to-noise levels.

- Demonstrated throughputs of up to 41kbps in a difficult, tropical environment, featuring significant biological noise levels for mobile platforms at range up to 1.5km.

- Demonstrated throughputs of between 300bps and 1600bps in a shallow, reverberant environment, at a range up to 21km at LF.

- Implemented and demonstrated all algorithms in real time systems.

Acknowledgements

The author wishes to acknowledge the following people and organisations for their support, funding and technical expertise:-

- QinetiQ Winfrith Deployables and acoustic communications team;
- MOD DSci (SEA) for funding the corporate research program into high data rate acoustic communications;
- MOD DEC(UWB) for continued funding in support of rapidly deployable sensors and sensor acoustic communications;
- QinetiQ for internal investment in support of several acoustic communication/acoustic positioning/acoustic velocity sensor systems;
- Mr Phil Atkins for his support and technical guidance as supervisor throughout this study;
- My family for their endless patience, support and the occasional cup of coffee...

The author would also like to acknowledge the efforst of the QinetiQ Winfrith Deployables and Acomms team for organising and executing trials, developing outboard array hardware and inboard MMI interfaces.

Mobile underwater vehicles present unique opportunities to explore the unique issues relevant to mobile underwater communications. The author would therefore like to acknowledge the underwater vehicle teams at Bincleaves, Weymouth and Newport Rhode Island for exploiting real time technology based on the work described herein.

The author would also like to acknowledge the efforts of the Winfrith Active sonar team in transmitting and recording waveforms using low frequency projectors for several long-range acoustic communications performance experiments.

The support and funding from military sponsors, DEC(UWB) and DSc(SEA) is also greatfully acknowledged both for research programmes into high data rate acoustic communications and ongoing research into acoustic modem technology for rapidly deployable sensors and systems.

List of contents

List of Tables

List of Figures

"The world should listen then- as I am listening now"

Percy Shelly, 'To a Skylark', 1819

1 PREAMBLE

1.1 Acoustic communications.

1.1.1 Sound and speech have played a key role in the evolution of mankind as a means to convey information and as a means of self-expression [1]. Speech, initially the most basic form of communication has now given way to the vast range of communications media and multimedia technologies characterising the digital information age [2].

1.1.2 Information carrier technology has evolved from the simple acoustic signals of early man to the complex wireless and optical infrastructures underpinning the very fabric of modern life. From personal mobile communications to the internet, from navigation to space exploration, modern digital communications technology has provided mankind the means to navigate and communicate reliably and effectively, at any time, at any place on the surface of the planet.

1.1.3 It is with some delicious irony then, that despite the sophistication of modern electromagnetic (EM) communications technologies, fundamental physics dictates that to communicate effectively in the underwater environment, one must come full circle and revisit that most basic of information carriers; sound.

1.1.4 It is probably not surprising that sound remains the most effective means to communicate underwater. Marine mammals have been using sound to communicate and hunt prey for millions of year's [3]. Dolphins are capable of detecting, classifying and localising prey using acoustic signals and biological signal processing many times more complex than

the most advanced man-made sonar systems of today. Whales, the largest of marine mammals can communicate over several thousands of miles under favourable conditions using low frequency whistles.

1.1.5 Whilst it is feasible to penetrate the ocean depths using low frequency EM transmission, as demonstrated by the extremely complex infrastructures in place for military submarine communications, there is no current solution to the problem of high data rate communications over reasonable range using EM technology.

1.1.6 Very low frequencies (VLF) EM technology can only penetrate to a few tens of metres. Extra low frequency (ELF) EM technology can potentially, penetrate several hundreds of metres, however in addition to the disadvantage of low data rate, these links are one way only, the infrastructures extremely expensive to install and maintain and the technology not without environmental concerns [4].

1.1.7 The main reason EM signals are so poorly suited to underwater communications stems from the large attenuation these signals experience as they propagate through water. The amount of energy lost (to heat) is dependent on many parameters, however the most significant is frequency. At low frequencies these losses, although high compared to acoustic signal losses, enable ELF and VLF transmissions to be received by submarines under the water surface. At higher medium frequencies (MF) through to very high frequencies (VHF) and beyond, the attenuation losses become extremely high making EM based telemetry impractical for all but the most limited of applications.

1.1.8 If one considers the propagation of acoustic waves within the ocean medium, the losses are orders of magnitude smaller. At frequencies below 1kHz absorption losses are so small that acoustic signals can, under favourable conditions, propagate hundreds or even thousands of miles depending upon the transmission power level [5]. Below 10kHz the

energy losses due to absorption are usually overtaken by other loss mechanisms such as those arising when the sound interacts with the ocean surface and sea floor.

1.1.9 The price paid for this greatly reduced absorption loss, is heavily weighted by the fundamentally different nature of acoustic propagation and the complexity of the ocean environment. These issues conspire to make acoustic communications quite unlike any terrestrial or extraterrestrial EM communication technology and many of the techniques established around these technologies, fail to work reliably in the harsh underwater environment.

1.1.10 The most obvious difference between electromagnetic and acoustic waves is the speed at which they propagate. In water, propagation speed is influenced by several factors including temperature, pressure and salinity. A typical benchmark figure representative of sea water is $1.5x10^3$ m/s. EM propagation speed is also subject to environmental factors, however a typical figure is $3x10^8$m/s (in a vacuum and considerably slower in the sea).

1.1.11 The ratio of these two propagation speeds is approximately 200,000; a fact which underlines the significantly different nature of the two wave types. If one for example, transmits a radio signal comprising a single bit of information 0.001s duration, this pulse of energy would occupy a physical length of 300km as it propagates out into space. The same signal transmitted acoustically underwater will occupy a physical length of only 1.5m. In air, where propagation speeds reduce even further, the pulse would occupy a physical space of only 30-40cm.

1.1.12 It is perhaps not difficult to see then, that the physically smaller acoustic pulse is much more likely to be distorted as it propagates within a complex medium such as the ocean. In such a constrained environment as the ocean, it is also perhaps not difficult to envisage this signal adopting many distinct paths to reach its destination. This received signal may

therefore comprise several versions of the transmitted signal, each arriving at a different time, with varying levels of distortion. The relative length of each of these paths or multipaths may well differ by several tens of metres; this for a signal itself occupying a space of only 1.5m! This multipath phenomenon, shown in Figure 1, is an extremely difficult problem in underwater acoustics since it effectively scrambles together the pieces of information one wishes to recover at the receiver.

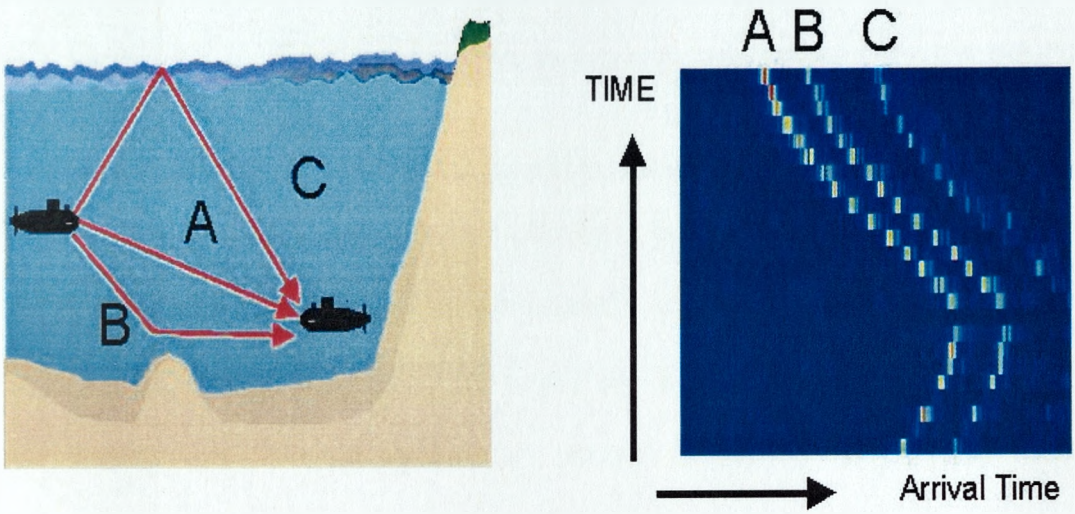

Propagation via different paths (MULTIPATH)

+ Path arrival time changes as platform moves (DOPPLER)

+ Path strength variability

+ Path arrival time variability

= DIFFICULT COMMUNICATIONS PROBLEM!

Figure 1; Acoustic multipath and Doppler phenomena

1.1.13 It is also perhaps not too difficult to envisage the effect on the transmitted signal if one party moves relative to the other. If one or other party moves at 5m/s, then from the start of the transmission to the end 0.001s later, this party has moved 5x0.001s = 5mm. This means that the space occupied by the pulse as it propagates through the water is effectively altered or, equivalently, the pulse duration has changed. If the transmitter moves toward the receiver the pulse duration reduces, i.e. the pulse seems to compress. If the transmitter moves away from the receiver the pulse duration increase, i.e. the pulse seems to expand.

1.1.14 This phenomenon, known as the Doppler effect [6] is another difficult problem to deal with in underwater acoustics since the receiver must know when the pulse arrives in order to extract the information from it. If one transmits several pulses, one after the other, then as the transmitter moves, each pulse will be slightly compressed or expanded such that its precise arrival time is difficult for the receiver to anticipate, particularly if the transmitter's motion is difficult to predict. Also as the pulse propagates, it will encounter changes in temperature, depth and possibly salinity. These changes will serve to add further uncertainty to the pulse arrival time since these factors influence the propagation speed of the pulse.

1.1.15 Changes in depth, temperature and water salinity, not only influence the speed of sound propagation, but also influence the direction of sound propagation [7]. Specifically, as sound propagates it is seen to 'bend' or refract as it encounters changes in propagation speed. The extent of path refraction is directly related to the speed change and the angle which the sound traverses the speed gradient. This relationship, known as Snells law, is a fundamental result of wave theory and applies not only to acoustic propagation but also to EM propagation. Refraction of EM transmissions in the upper ionosphere provides a means for signals to bounce or 'skip' very long distances via alternate reflections and

refraction's between the Earth and the ionosphere. In underwater acoustics the variation in sound propagation speed with depth or bathymetry, has a profound effect on the characteristics of the received signal. Unfavourable conditions may for example result in acoustic shadow zones i.e. regions where, as a result of the sound refraction phenomenon, little or no sound penetrates as shown Figure 2.

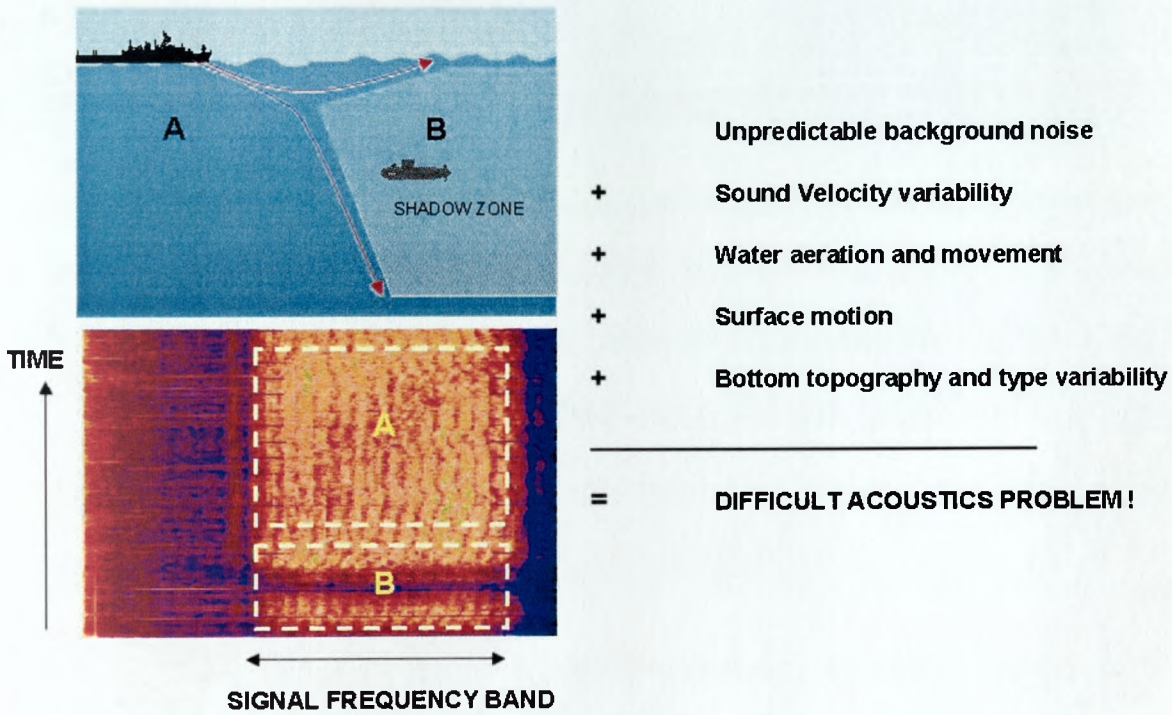

Figure 2; Technical difficulties involved in acoustic communications

1.1.16 Establishing a reliable communications link with a receiver within such a zone is extremely difficult. In many cases judicious positioning of the transmitter and/or receiver depth can make the difference between establishing a reliable link or no link at all. It is for this reason that understanding the physics of sound propagation and having some means of predicting how sound will propagate is an essential aspect of any sonar system, not least an acoustic communications system.

1.1.17 Multipath and Doppler are well known problems in the radio world and effective techniques have evolved to combat them. In the acoustic case, these problems are orders of magnitude more severe and it is perhaps not surprising that the evolution of acoustic communications technology has lagged somewhat behind RF technology.

1.1.18 Despite the difficulties many researchers have attempted to solve the problems using a wide variety of techniques. In the last ten years or so, there has been a paradigm shift in the performance of acoustic telemetry systems brought about by a combination of improved computing power, advances in signal processing algorithms and perhaps most importantly of all, a greater understanding of the acoustic environment. The ultimate aspiration for acoustic communications technology is to mirror the dramatic advances of terrestrial communications technology in the undersea environment. These advances have encompassed not only information bearer technology but also information access and routing technology with the advent of advanced networking infrastructures, most notably the Internet.

1.1.19 The fundamental physics of acoustic propagation conspires to make the application of established terrestrial networking technologies to the underwater networking problem, extremely difficult. This once again stems from the low propagation speed of acoustic waves. Since acoustic transmissions propagate 200,000 times slower than RF counterparts, this poses unique problems for high data rate multi-user applications. Traditional channel access protocols involving time and/or frequency division multiplexing, wherein parties are allocated unique 'round robin' time slots or frequency bands are unsuited to the extremely long propagation delays and multipath delays of the acoustic environment.

1.1.20 The solution to high data rate acoustic networking is therefore likely to be solved not by a single technique alone, but the application of several techniques specifically engineered to counteract the unique time, frequency and spatial characteristics of the underwater acoustic environment.

1.1.21 As a technology, acoustic communications is likely to play an increasingly important role within both commercial and military arenas as underwater sensor systems and vehicle technology evolves. Acoustic communications is a key enabling technology to underpin future advances in off platform systems and sensors. As oil exploration moves toward deeper water and more complex subsea well installations, the potential roles for acoustic communications are vast. Remote monitoring and operation of well head valves, riser anchorage point monitoring, seismic sensor data uplift, pipeline pigging, borehole tool sensor telemetry are just a few of the potential applications of 'in situ' acoustic communications. With the advent of new underwater vehicle technologies, acoustic communications provides a means to command and control the vehicle and a means of uplifting mission data remotely without distraction to the vehicle, enabling it to remain on station/mission.

1.1.22 A technology closely linked to underwater communications is underwater positioning and navigation. Indeed the technology underpinning underwater positioning represents a subset of acoustic communications technology; most notably synchronisation. Whilst there are many levels of synchronisation in a communications receiver, establishing the exact time of arrival of information is as important to a communications receiver as it is to an underwater navigation system.

1.1.23 The potential applications of underwater positioning technology are as diverse as underwater communications technology. The key features of an underwater positioning

system are range/position accuracy, update rate, robustness and the ability to support several users. UUV navigation, diver navigation, pipeline positioning, search and rescue beacon localisation are just a few examples of the potential applications of underwater navigation.

1.1.24 The ultimate aspiration in underwater acoustic communications research will be to mirror the paradigm shifts in terrestrial communications technology and networking capabilities in the undersea environment. Whilst signal processing algorithms and devices are key enablers to achieve this goal, the ultimate enabler is a comprehensive understanding of the underwater acoustic environment. Only if one can measure and understand the complex mechanisms of underwater acoustics can one really begin to exploit the environment effectively.

1.2 Historical Perspective

1.2.1 There have been many review papers on underwater acoustic communications spanning the last thirty years and numerous systems have been developed over this time [8-15]. It is perhaps testament to the complexity of the acoustic environment that despite significant research over this period, opinion remains divided regarding candidate technologies and methodologies to mitigate the severe dispersion of the acoustic environment.

1.2.2 Indeed an emergent trend is toward multimode modulation solutions [13,16] providing low rate robust communications under particularly difficult channel conditions and high rate communications where channel conditions are less harsh. Implicit in such an approach is the concept of environmental adaption whereby the modulation scheme and/or parameters are adapted to the environment, which is monitored either through explicit channel sounding or during the demodulation process itself.

1.2.3 As a consequence of the acoustic channel complexity, robust low rate modulation schemes have historically dominated much of the pioneering work in the field through the late seventies and early eighties [8-11]. The technical justification for this approach was based on the popular premise of the time that the acoustic channel was too complex for fully coherent modulation methods.

1.2.4 It was for this reason that incoherent multiple frequency shift keyed (MFSK) modulation was the dominant technology in underwater communications up until the latter part of the 1980's. The technique, however, is extremely bandwidth inefficient with bandwidth efficiencies rarely exceeding a few tenths of bps/Hz. This meant that given the low transducer bandwidths at low-to-medium frequencies, data rates were relatively modest; typically up to a 1000 bits per second (BPS) maximum.

1.2.5 Perhaps one of the major turning points in underwater communications has been the advent of spatial-temporal adaptive processing (STAP) [12-16] to realise fully coherent, high rate acoustic communications. Paradoxically these techniques have actually demonstrated the intrinsic delay stability of the underwater acoustic when using wideband modulation techniques. Up until the late 1980's the predominance of MFSK and the adoption of low data rates were a consequence of the perceived phase instability of the acoustic channel. This perception stemmed from the observed fading statistics of narrowband transmissions, which are inherently susceptible to violent frequency selective fading by virtue of the acoustic multipath problem. Wideband transmissions provide a form of frequency diversity, which makes transmissions more robust to the frequency selective fading problem.

1.2.6 It is not until relatively recently that the intrinsic delay stability of the acoustic channel has become more widely accepted and exploited through the emergence of wideband

modulation techniques which seek to exploit the inherent frequency diversity afforded by wideband transmission in frequency selective (multipath) environments. This has been demonstrated by the emergence of fully coherent wideband phase modulation schemes employing adaptive equalisation and beamforming to mitigate extreme channel conditions. Such techniques have led to a paradigm shift in the achievable data throughputs over a much wider range of environmental conditions.

1.2.7 The foundation for this shift has been the exploitation of adaptive temporal-spatial processing. Such structures are particularly powerful in underwater acoustic communications since the adaptive receiver can mitigate the channel spreading problem either temporally (equalisation), spatially coherently (null steering) or spatially incoherently (spatial diversity) depending on the channel coherence characteristics and the receiver architecture.

1.2.8 Whilst such techniques have become well established in the open literature, and impressive data throughputs achieved, the primary limiting factor to their widespread application is both system complexity and transmission robustness. The ability to achieve repeatable, low error rates over a wide range of environments is the ultimate goal in high rate underwater communications system design.

1.2.9 It is perhaps for this very reason that there exists, and will exist in the future, a need for robust low rate techniques which mitigate both severe channel conditions and extremely hostile noise environments.

1.2.10 A pervasive issue in undersea technology is the rapid advance of digital signal processing (DSP) technology. At the time of writing, current general purpose DSP devices provide throughputs approaching 500million floating point operations per second (Mflops) at power consumption's of typically 2-3W. Fixed point devices provide 300-400Million

instructions per second (Mips) at power consumption's of 0.2-0.3mA/Mip. The springboard effect of increased embedded signal processing performance will be to enable the application of more advanced algorithms and infrastructures for underwater acoustic communications.

1.3 Understanding the Ocean : Signal Coherence

1.3.1 A useful indication of the complexity of an environment as a communications channel is demonstrated by the temporal and spatial scales of the communicating waveform(s) and how these scales relate to the intrinsic temporal and spatial scales of variability's arising within the communications medium.

1.3.2 The above simple statement encapsulates much of the complexity of the underwater communications problem. In underwater acoustics the temporal and spatial scales of waveforms transmitted within the medium are poorly matched to the temporal and spatial scales of ocean variability by virtue of both the complexity of the ocean environment, the underlying propagation speed and physics, and the number and complexity of boundary interactions. The problem is compounded by the spatial and temporal variability of acoustic channel noise, volume scattering mechanisms and turbulence arising within the medium. In terms of digital communications system design the underwater acoustic channel poses unique challenges in modulation, equalisation and synchronisation design.

1.3.3 Since the ocean is bounded, non-stationary and non-homogenous it is intrinsically dispersive in time and Doppler. This is compounded by the spatial and temporal variability of acoustic background noise and localised noise mechanisms (ships, biological etc.).

1.3.4 Temporal dispersion manifests as multipath whereby acoustic energy is received via a number of discrete paths (macropaths) which can be acoustic or, at lower frequencies,

geo-acoustic. Each macropath may support a number of micropaths, representing a finer temporal resolution of arrival energy attributable to the temporal and spatial variability of thermal microstructure for example. Both multipath and micropath variability in amplitude and delay dictate the time and frequency coherence characteristics of the underwater acoustic channel and understanding the nature of this variability and its extent is central to realising robust signal design and receiver processing techniques.

1.3.5 Doppler dispersion arises since the ocean medium is not homogenous and is not static. Temporal variability of the sound velocity microstructure arising due to temperature variation, layer mixing, salinity variations etc. can introduce short time scale path length fluctuations. Scattering from moving wave facets introduces amplitude and phase modulation. Internal waves introduce a Doppler velocity vector resulting in long time scale phase variations. Tidal activity will introduce phase variations on a similar time scale.

1.3.6 For dynamic transmitter-receiver configurations, the different time evolved geometry for each path arrival results in differential Doppler between paths. This is particularly problematic at short range-depth ratios. Additionally, mobile platforms introduce several additional concerns including acoustic screening and scattering from wake aeration which serves to introduce rapid signal attenuation whilst wake turbulence serves to degrade the time coherence of the received signal.

1.3.7 It is important to emphasise the difficulty in isolating intrinsic channel coherence measurements from influences extrinsic to the channel itself. The channel scattering function which describes the redistribution of signal energy in time and frequency will be translated in time by the mean path propagation time and will be translated in Doppler by the mean relative platform velocity. Translations in space and angle can similarly be

ascribed. Inherent platform dynamics will serve to introduce slow time/phase variations about the mean delay and system parameters such as clock oscillator error, jitter, beam pointing error etc. introduce additional terms which serve to degrade the coherence properties of the received signal. A number of these extrinsic terms occur with comparable timescales to channel effects such that isolating the intrinsic channel scattering characteristics is often not straightforward. For example many measurements of the channel phase response presented in the literature exhibit pronounced phase variation commensurate with platform heave motion as will be shown in section 2.

1.3.8 For the mobile source the channel time-frequency-spatial dispersion becomes a much more adverse problem since relative motion between source and surface/bottom topography will introduce amplitude and phase modulation effects in addition to those introduced by moving scatterers within the medium. It is well known from active measurements for example, that the Doppler dispersion of a channel scales with environmental and system parameters i.e. windspeed, source velocity, beamwidth (and beamsteer), surface grazing angle etc.

1.3.9 So, when the 'mean' platform Doppler is removed, the channel will become more time selective due to fluctuations about the mean Doppler introduced by platform velocity variations, sound velocity variations and the variation in the scattering characteristics of the boundaries as functions of time, space and platform attitude. The nature of the underwater channel as a time-Doppler-angle convolver is illustrated in Figure 3.

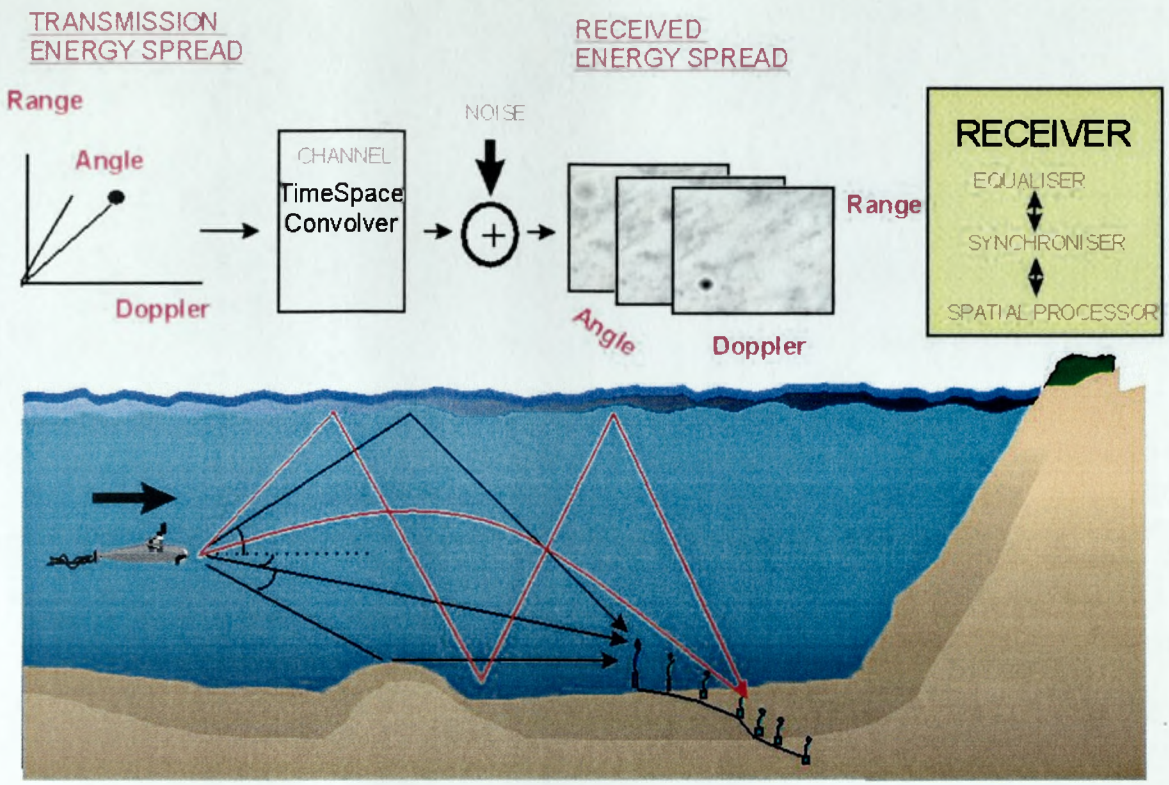

Figure 3: The acoustic channel as a time-Doppler-space convolution process.

1.3.10 Transmissions initiated from an underwater moving vehicle arrive at several spatially separated receivers via separate distinct paths. The time difference between path arrivals results in time spreading. As the geometry evolves, so the time difference of arrival between paths changes. In strongly refracting environments, paths may become unstable during the transition to higher-order path families. The path structure 'seen' by the receiver elements may be similar or disparate depending on how far apart the elements are placed and the particular geometry. The structure, temporal variability and spatial characteristics of the received path structures dictate the frequency, time and spatial coherence of the incident field. The basis of any communication is to develop techniques that are best suited to the coherence characteristics of the incident field. The task of the receiver is then to recover the original transmitted signal by three interrelated processes, synchronisation, equalisation and spatial processing. The precise implementation and

interdependence between these processing tasks ultimately depends on the choice of modulation scheme, the channel characteristics and sensor geometry.

1.3.11 In the broadest sense, the aim of this work is to identify modulation and receiver processing techniques to enable the reliable transfer of data at high rate, at range between two parties. More specifically, this work seeks to investigate techniques to effectively communicate between two or more parties over a wide range of channel conditions including low data rate techniques to augment high data rate capability. This multimode approach to the acoustic communications problem seeks to balance the conflicting needs for robustness and high data rate in difficult acoustic conditions. The starting point for such a task lies in establishing an understanding of the underwater environment and its influence on signal coherence. Only with this knowledge can one begin to consider signal designs and receiver processing methods to 'solve' the underwater acoustic communications problem.

1.4 Thesis Structure

1.4.1 This thesis is presented in 13 sections as depicted in Figure 4.

1.4.2 In section 1 a brief statement of the acoustic communications problem is presented and thesis structure defined.

1.4.3 In section 2 a discussion of a number of acoustic telemetry reviews is presented based on publications by a wide variety of authors over the last decade. The discussion serves as a roadmap of acoustic communications technology identifying technological trends and performance issues.

1.4.4 In section 3 a selection of papers are reviewed, that address the complex issue of acoustic channel coherence measurement. Measurements presented include tomographic

measurements, forward scattering, back scattering and surface scattering for a wide range of environments and operational parameters.

1.4.5 In sections 4 and 5 the intrinsic ocean mechanisms that influence signal coherence are reviewed and the problem of how one measures and quantifies the environment as a communications channel is addressed. This includes how one effectively models acoustic channel behaviour for the purposes of assessing acoustic communications signals and techniques.

1.4.6 Sections 6 and 7 constitute the start of a system wide perspective on the acoustic communications problem. In section 6, the problem of synchronising to an acoustic transmission is addressed including initial open loop acquisition and closed loop tracking algorithms. Techniques to characterise the channel are presented in section 7.

1.4.7 In section 8 the signal design problem for acoustic channels is addressed. The problem of how one effectively maps information to a physical waveform and the suitability of particular waveforms to particular channel characteristics is discussed.

1.4.8 In section 9, adaptive approaches to the acoustic receiver design problem are reviewed. The relative merits of several classes of adaptive algorithms are reviewed. The results of simulation studies are presented which seek to investigate the performance of a spatial-temporal adaptive processing receiver over a wide range of simulated ocean conditions.

1.4.9 In section 10 field trials results collated over a wide range of environments and systematic configurations are presented. This includes demonstrated data rates of up to 41kbps in difficult, tropical environments.

1.4.10 In section 11 the problem of real time implementation is addressed. The development of a multimode acoustic modem featuring a low rate bi-directional spread spectrum link, a high data rate uplink, and selective addressing and ranging capability, is discussed.

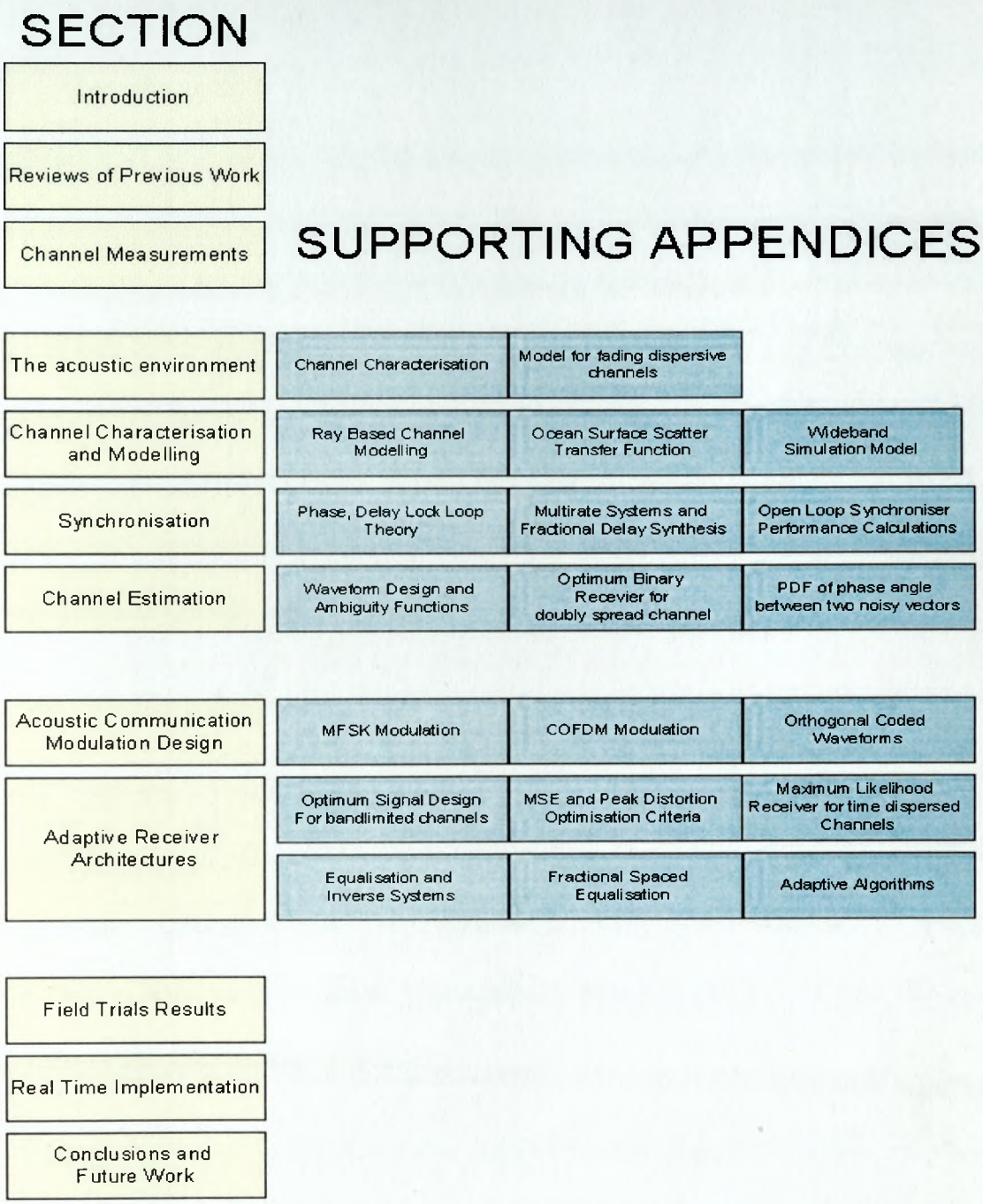

Figure 4; Thesis Structure

'Science is organised knowledge'

Herbert Spencer, Education (1861) ch.2

2 REVIEW OF PREVIOUS WORK

2.1 Preamble

2.1.1 In order to chart the evolution of communications technology over the past twenty years a small selection of review articles which span this timeframe are reviewed. These papers constitute a natural starting point for this literature review and serve to raise several key issues relating to the high data rate, acoustic communications problem. The key issues identified in this section are developed further in sections 4, 5 and 6 with a view to providing a more quantitative basis for understanding the physics of acoustic propagation and interaction, environmental measurement and characterisation, waveform design and acoustic communications system design.

2.2 Acoustic Telemetry Reviews

2.2.1 Berktay and Gazey [8] presented one of the earliest papers on underwater communications. Despite predating many of the more recent signal processing advances in underwater communications, the paper serves as a useful benchmark towards establishing many of the more fundamental issues relevant to the acoustic communications system design problem.

2.2.2 The authors consider the severity of carrier amplitude and phase fluctuations with range arising from multipath induced frequency selective fading and present theoretical results based on a 50kHz carrier which indicated a root mean square (rms) phase variability which increased linearly with the logarithm of range. The results indicated rms phase

fluctuations of between 0.1 to 1.0 radians over the operation ranges of interest (100m to 10km) and an amplitude variability of 0.1 to 0.7 over the same range.

2.2.3 Multipath propagation arising from boundary interactions is cited as the most complex aspect of the acoustic channel. The authors note that the time differential between paths had a greater impact on communications system performance than the micropath scattering associated with each path.

2.2.4 The use of diversity as a technique to combat the acoustic multipath problem was proposed for flat fading and frequency selective fading cases. Both frequency and spatial diversity techniques were suggested by the authors as means to combat the frequency selectivity problem, however the performance benefits of wideband signalling were developed for linear swept sine waveform designs only.

2.2.5 Under frequency selective conditions the use of pulse compression techniques to mitigate temporal spreading was advocated by the authors in order to overcome channel multipath. The performance benefits of energy raking techniques to combine multipath energies were reviewed, however the synchronisation implications of such a system whilst indicated, were not fully developed.

2.2.6 The paper concludes that the intrinsic fluctuations of the medium do not significantly degrade communications system performance. However, the existence of macropath and associated frequency selective fading do pose significant problems for reliable communications.

2.2.7 Despite being published some thirty years ago, this paper raises many technical issues featured in more contemporary papers. As will be discussed in subsequent sections, pulse compression and spread spectrum systems are emergent technologies in the acoustic

communications arena. Diversity methods in conjunction with adaptive signal processing now underpin recent advances in high rate, acoustic communication technology.

2.2.8 The issue of intrinsic channel phase stability degrading with range is open to some debate. As will be discussed later, there is evidence pointing to degraded phase stability and time spread at shorter range by virtue of greater boundary interaction and the more pronounced influence of platform dynamics on signal time coherence at shorter ranges.

2.2.9 In [9] and [10] Bagoroer and Quazi present overviews of the acoustic telemetry problem and review the data throughput requirements of a number of applications. Bagoerer proposes that there are typically three levels of data throughput required. At the lowest level, systems requiring command/control status telemetering will have modest data rate requirements, however this is offset by the need to make the link robust and error tolerant. Such systems would require data throughputs of 50-500bps. The next capability level would be for acoustic measurement systems such as seismic profiler's etc. which would require data throughputs of between 1-10kbps. The highest capability level would be the telemetering of video information at low frame rates, which require data throughputs of 10-100kbps.

2.2.10 An important aspect of system performance briefly reviewed by Bagoreor is the acoustic noise problem, particularly at low to medium frequencies in shallow water. Specific results cited indicate that in harsh shallow water environments such as offshore platforms noise levels can exceed ambient by up to 60-70dB.

2.2.11 Bagoroer observes that the extent of the channel time spread is actually longer at shorter ranges in very shallow channels at high frequency. This is attributed to the absorption losses within the medium and lossy bottom interactions. This view contrasts to that

forwarded by Gazey and highlights the importance of acoustic field coherence at short and long range in acoustic communications.

2.2.12 Bagorer advocates incoherent MFSK as a candidate technology to overcome the channel time spread problem and proposes the use of diversity to maximise system robustness. The extent of channel Doppler spreading is emphasised, as is the difficulty in isolating the intrinsic phase stability of the channel due to the inherent dynamics of the measurement platforms. This is a subtle point and one that is developed more fully in the context of ocean tomographic measurements and acoustic communications coherence measurements in later sections.

2.2.13 The peak power requirements of signal designs are briefly discussed. Although not stated, the ratio of peak-to-rms power of the transmitted waveform is an important factor for power amplifier dynamic range and linearity, particularly for non-linear modulation schemes such as MFSK and COFDM.

2.2.14 The performance benefits of forward error correction coding are reviewed in general terms, primarily from the single carrier perspective. The performance benefits of time-frequency interleaved coding to mitigate frequency and time selective channel behaviour in multicarrier systems are, however, not discussed.

2.2.15 In [11] Catapovic presents a comprehensive discussion on acoustic communications technology spanning the 1980's through to 1990's. He reviews many of the fundamental issues impacting on acoustic communications performance. Catapovic notes that the multipath problem itself is not the primary technical difficulty but rather it is the temporal variability of paths and path stability, which dictate channel complexity. This is a very understated fact in the open literature since whilst path structure defines the frequency

coherence of the channel, it is the temporal fluctuations and variability of paths which, coupled with the extent of the time spread, makes acoustic channels particularly difficult.

2.2.16 The authors discussion on ambient noise introduces the problems of bubble layer forward scattering and attenuation. He correctly highlights this as a significant problem when communicating from surface ships, particularly from stern aspect where water aeration can extend many metres below the surface. Such channels are extremely difficult since aeration has a rapid and dramatic influence on received signal coherence arising from the masking of favourable eigenrays.

2.2.17 Catapovic subdivides the acoustic telemetry problem into three operating range regimes. Long range systems operating in deep water over ranges exceeding 20km. Medium range systems operating between 2-20km and short range systems operating at less than 2km. The phase stability of the long range channel is noted as being good, and the use of waveform coding in the ocean tomographic community to characterise ocean behaviour cited as examples of the phase stability. This view aligns with that of Baggeor whereby intrinsic loss mechanisms, most notably bottom loss serve to improve signal coherence at longer ranges.

2.2.18 The medium range communications problem is subdivided into four categories. The synchronisation problem, the equalisation problem, the modulation design problem and the error correction coding problem. Catapovic reviews the theoretical performance of the classic delay lock loop. He does not however develop the full complexity of the synchronisation problem in terms of characterising the DLL phase discriminator for typical ocean environments where temporal and Doppler smear are both highly variable and highly coupled.

2.2.19 The problem of initial acquisition is reviewed. The use of the first arrival is proposed, as the author argues, this tends to be the strongest. This issue will be considered in more detail later since the choice of which path to synchronise to, is strongly influenced by the receiver synchronisation and equalisation strategy.

2.2.20 The possibility of synchronising on multiple paths with a view to improving system performance is proposed, however the author does not develop the techniques which would allow this to be done such as wideband correlation processing, spatial filtering etc.

2.2.21 The signal design discussion centres on the use of MFSK modulation schemes. Here the matching of the waveform set to the spreading characteristics of the channel is proposed and the design criteria for frequency guard bins and time guard bins reviewed. The use of a phase lock loop (PLL) for carrier phase tracking is introduced and the randomisation of carrier phase to reduce the transmission crest factor suggested. This technique seeks to reduce the peak to mean power of the transmission. This is necessary due to the peak power limitation of MFSK waveforms.

2.2.22 Despite the emphasis placed on the synchronisation problem, Catapovic does not develop the full impact of acoustic Doppler temporal scaling on the receiver synchronisation problem. Whilst not critical for non coherent MFSK signal designs, robust synchronisation is essential for fully coherent signal designs particularly so for coherent multi-carrier modulation strategies which will be discussed later.

2.2.23 For short-range systems Catapovic advocates the use of conventional RF technologies such as adaptive equalisers etc. He states that this channel is the most benign and subject to mild phase fluctuations. This view conflicts with that held by many researchers, and it will be shown later that the short-to-medium range shallow water channel can in fact be

one of the most challenging particularly where moving platforms are involved. Baggorer also advocates this view.

2.2.24 A relatively recent overview of acoustic telemetry is given by Stojanovic [12], which underlines the rapid advances in the use of phase coherent techniques with particular emphasis on bandwidth efficiency.

2.2.25 The author rightly distinguishes between macro and micropath and the strong spatial dependency of the received acoustic field and suggests that surface wave scattering is the dominant micropath mechanism for time variability in shallow water. The importance of internal waves on acoustic scattering is also mentioned for deep water, long range systems. The impact of bathymetry variations and topography variations in the case of moving platforms on time variability is only briefly considered.

2.2.26 Stojanovic correctly notes the importance of symbolling rate on system performance and presents simple first order calculations of surface wave scattering to identify Doppler spreading with a view to defining an appropriate system symbol rate. This is basically a statement of the requirement to sufficiently oversample the channel transfer function in order to track its variability. This is particularly relevant for receiver algorithms and acoustic conditions incurring significant tracking lag in closed loop such as adaptive equalisation and delay lock loop synchronisation.

2.2.27 In order to contain the time variable multipath problem the author defines the solution in terms of signal design and receiver design. The performance limitations of incoherent multicarrier systems are discussed in the context of channel time and frequency coherence. The inherent data throughput limitation of MFSK systems is emphasised. Alternative bandwidth efficient multicarrier techniques such as COFDM are not included in the discussion.

2.2.28 Stojanovic focuses on the use of spatial diversity combining and adaptive equalisation and synchronisation as a candidate technology to overcome the channel multipath problem. The author does not however discuss the spatial coherence of the shallow water acoustic field for moving platforms and for this reason the choice of term 'spatial diversity combining' is somewhat misleading, particularly as the spacing of the elements is not indicated. Later it will be shown that the role of the structure as a spatial diversity combiner or beamformer rests on the spatial coherence of the field relative to sensor separation, which is a function of the channel geometry and environment.

2.2.29 Experimental results in the form of receiver constellations are given for a static configuration. The signal design was a 15kHz carrier at 10-15ksym/s equating to 30-40kbps. The link range was 1852m in 25m water depth. Time spread was 10ms with 2-3 resolved multipath arrivals. Receiver configuration was 32 T/2 forward taps and 100 feedback taps. A single baseband phase lock loop is used for synchronisation. Due to the large range to depth ratio and the static configuration the channel was relatively benign.

2.2.30 The authors recommendations for future work focused primarily on algorithm complexity reduction. The adopted algorithm was recursive least squares where it is argued that the convergence properties are superior to the low complexity LMS. The authors do not consider the relative tracking performance of both algorithm types in non-stationary environments. Under these conditions the performance advantage of least squares algorithms is less well defined. Also the authors advocate the periodic rather than symbol by symbol update of the algorithm to relax computational complexity.

2.2.31 The performance benefits of self-optimisation such as adaption rate control and blind equalisation are reviewed and the mobile underwater communications problem discussed. The author rightly emphasises the difficulties inherent to mobile underwater

communications however fails to indicate how the Doppler problem impacts on the proposed receiver performance.

2.2.32 Recently a number of review articles have been published which present a snapshot of state of the art in underwater communications research technology based on US DoD sponsored programmes. In [14] Kilfoyle et al presents a perspective on the perceived evolution of acoustic telemetry technology. The author focuses on coherent signalling, networking and error correction coding. The discussion is relatively generic, however a number of noteworthy points are made. The author highlights the shift of opinion toward the intrinsic phase stability of the underwater channel. In the 1980's many researchers assumed the channel phase stability to be insufficient to support phase coherent methods. This was at the time when most systems were narrow band and it was only when researchers started to explore true wideband systems in earnest; either spread spectrum or single carrier that the intrinsic stability of the channel was demonstrated. The adoption of wideband techniques as a means to overcome the traditional limitations of the underwater environment has been advocated and pursued by this author over the last ten years [15,16]

2.3 Discussion

2.3.1 Despite the twenty-year span of the review articles, recurrent themes are evident. The fundamental physics of the acoustic channel is reviewed by all authors and underlines the complexity of the underwater communications problem. Invariably the extent and variability of the channel multipath problem is cited as the most complex aspect of acoustic telemetry and this is attributed to the non-stationary, non-homogenous nature of the ocean medium. It is perhaps appropriate to consider the acoustic communications problem in the context of the spatial and temporal scales of such variability's and to relate them to the temporal and spatial scales of the communication signal itself. This after all

determines how the medium interacts with the propagating signal and defines the coherence characteristics of the received signal.

2.3.2 The temporal and spatial scales of an acoustic communications signal are related through the medium propagation speed. An obvious, but often understated, feature of acoustic communications, is the fact that acoustic propagation speeds result in data symbol spatial scales orders of magnitude less than RF counterpart systems.

2.3.3 This is a fundamental reason why acoustic communication is so much more difficult than RF communications. In the acoustic case, the spatial scales of environmental variability due to surface wave effects, bottom topography, sound speed variations, turbulence etc. are comparable to the spatial scales of the data symbols themselves. Also, the time spread of acoustic channels extends to several tens or possibly hundreds of symbols. This obviously impacts on signal temporal, frequency and spatial coherence and underlines the radical differences between RF and acoustic communications channels.

2.3.4 Despite these significant differences few authors consider such fundamental aspects of the signal design problem. For example Baggoerer refers to the channel spreading characteristics but does not develop the signal design implications of the doubly spread channel. Stojanovic relates Doppler spreading to time coherence and highlights the performance advantages of rapid symbolling rates in such time selective channels. However she fails to emphasise that the acoustic channel is inherently doubly spread and as such increasing channel symbolling rate incurs additional equaliser complexity. In many cases the highly coupled nature of the equalisation, synchronisation and spatial processing solution is not discussed. Stojanovic touches on this point by emphasising the power of jointly adaptive equalisation and synchronisation, however the arguments relate

to phase variability rather than delay variability in the acoustic channel response and no consideration is given to the symbol timing recovery problem in mobile applications.

2.3.5 The emphasis Baggeor places on noise performance is well founded and an often understated aspect of acoustic telemetry performance. Whilst the off platform noise problem is severe, natural mechanisms can serve to significantly degrade signal-to-noise performance and system bit error performance in typical ocean environments. For example, observations by Nysten [17] on the spectral level of rain noise as a function of drop kinetic energy indicate significant (25dB+) increase in spectral level attributable to rain noise. The impact of biologics is also of particular importance in single carrier systems since such noise sources are spatially correlated, of high intensity and often transient in nature. Since single carrier systems exploit short duration, low energy, waveforms to combat channel time selectivity, these systems are particularly prone to 'bursty' errors under such conditions. Also, the small spatial scales of acoustic waveforms are subject to degradation when the water body itself is in motion. Water turbulence serves to rapidly degrade the time coherence of high frequency acoustic fields [18].

2.3.6 The review articles clearly define a demarcation in the technologies of underwater communications. Incoherent MFSK techniques, traditionally the most robust in severe channels are giving way to phase coherent techniques which afford almost an order of magnitude increase in data throughput. This shift in performance has largely been achieved by dispelling the myth that the acoustic channel phase stability is insufficiently stable to support phase coherent methods by exploiting channel bandwidth to resolve and track path arrivals. The robustness of such techniques for extreme channel conditions where communicating parties are moving, and where the channel is strongly non-minimum phase is not widely reported

2.3.7 In order to address the efficacy of such techniques in mitigating severe channel conditions, one must determine what constitutes a severe channel and how one measures or characterises it. Fortunately there are many acoustic measurements in the open literature covering a wide range of system and environmental parameters. Whilst these measurements are often disparate from the high data rate case, they are relevant, nonetheless, in defining acoustic channel behaviour, its temporal and spatial scales, and the influences on the signals which propagate within it.

2.3.8 In section 3, field and experimental results of several authors are discussed. These measurements encompass a wide range of operational, environmental and systematic parameters specific to the physical mechanism under investigation. This includes long range time of flight measurement, time/frequency/spatial coherence measurement, surface scattering measurement, bottom loss measurement and isolated refracted path measurement. Although disparate from the parameters one may use for a high data rate system, the results and observations serve to identify and quantify intrinsic ocean mechanisms, which directly relate to the high data rate, acoustic communications problem.

' Science is built up of facts, as a house is built of stones;

but an accumulation of facts is no more

a science than a heap of stones is a house'

Henri Poincare, Science and Hypotheses (1905), ch.9

3 ACOUSTIC CHANNEL MEASUREMENTS

3.1 Preamble

3.1.1 Whilst an extensive volume of acoustic channel measurements exist in the open literature, the measured temporal, frequency and spatial coherence measurements are often directed at isolating intrinsic ocean mechanisms occurring on scales (temporal, spatial and Doppler) incommensurate with the high data rate acoustic communications problem.

3.1.2 Low frequency tomographic measurements and analysis is normally directed at identifying internal wave, tidal and other macroscopic ocean behaviour which occurs on time scales (and spatial scales) many times longer than practical signalling rates for high throughput acoustic communications i.e. mesoscale effects.

3.1.3 The techniques attempt to extract information about the physical properties of the ocean based on the structure of the sound field propagation. To this end, acoustic travel time is often the parameter of interest. Since low frequencies and extensive averaging are used, time coherence measurements are directed at long time scale (hours/days) channel variation. The use of low frequencies to overcome channel absorption loses inevitably incurs a transmission bandwidth limitation which constrains the systems ability to resolve multipath components; in particular forward scattering artefacts are usually averaged out

in the receiver processing. The use of phase coded waveforms is well established in this field

3.1.4 In most tomographic measurements channel stationarity is assumed over substantial time intervals. This emphasises the point that channel stationarity is often interpreted in the context of the measurements being made and ultimately relates the ratio of the temporal and spatial scales of the transmitted waveforms to the temporal and spatial scales of the intrinsic ocean mechanisms under study.

3.1.5 Despite these limitations, the tomographic literature does offer valuable insight to acoustic channel behaviour and some of the more practical issues relating to signal design and signal processing to determine channel coherence. A brief review of selected tomographic literature is presented in section 3.2.

3.1.6 Surface scattering is often cited as one of the primary factors influencing signal time coherence. For this reason there are many papers in the open literature, which provide experimental results for both forward scattering and back scattering experimental configurations. From a communications perspective the measurements of interest relate primarily to the temporal, frequency and spatial coherence characteristics of the forward-scattered field. A brief review of surface scattering literature is presented in section 3.3.

3.2 Tomographic Literature Review

3.2.1 Aspects of tomographic signal processing are discussed by Spindel [19] who overviews the tomographic philosophy and qualifies time-of-flight techniques suited to the measurement of ocean sound velocity and current structure. An interesting point raised is the need for two way, simultaneous time-of-flight measurements to resolve ocean current behaviour. In such applications, system requirements demand long term timing

accuracy's of the order 10ms/year resolution, temporal resolution to 25ms, and temporal accuracy to 0.5ms.

3.2.2 In order to achieve the required signal-to-noise ratios the author advocates the use of pseudorandom noise (PRN) based signals by virtue of their correlation properties. The authors do however concede that the use of such waveforms is a compromise. For this application the authors use between 64 and 511 chips over an interval of 4-8s, a bandwidth of up to 100Hz and carrier frequencies up to 400Hz. Since the transmission frequencies are low and the bandwidths modest, the system is robust under modest time selective conditions even at 4-8s integration time.

3.2.3 Pulse integration techniques are used to further improve signal-to-noise ratio (SNR), which also provides a time diversity gain. At the receiver, interpolating the magnitude replica correlation output results in increased accuracy even for simple Gaussian interpolation. At such low SNR this technique is probably more robust than using complex phase information from the correlation process.

3.2.4 The author also considers the impact of timing oscillator accuracy and platform motion on overall timing accuracy. Rubidium based timing standards (and more recently GPS) are used to obtain time sync between stations. Platform movement is typically monitored using acoustic positioning sensors updated on an hourly basis. This is deemed sufficient for the measurements undertaken.

3.2.5 In practice platform dynamics have a significant role in the received sound field at high frequencies and data rates typical of the high data rate problem. In the tomographic case platform induced Doppler fluctuations would influence the receiver processing. For the proposed signal designs it can be shown using techniques presented in appendix N, that

decorrelation and range ambiguity would arise for platform motions up to 1m/s and accelerations up to $0.1ms^{-2}$.

3.2.6 Speisberger and Worcester [19] present acoustic fluctuation measurements based on three resolved multipath arrivals at a range of 900km and relate the observed results to theoretical predictions based on the Garret-Munk internal wave model. The channel sounding signal was a 220Hz, maximal length pseudorandom binary sequence (PRBS) transmission of duration 4s, and bandwidths of typically a few tens of Hz. Receiver processing was based on the coherent averaging of fourteen consecutive packets to improve SNR.

3.2.7 With this degree of averaging the intrinsic short duration time selectivity of the channel is lost. Indeed the author assumes the channel to be time invariant and linear over the transmission duration of 64s. Whilst biases due to platform drift and tx/rx oscillator drift were removed, it was noted that because of platform motion the time statistics of the received signal could not be determined.

3.2.8 This issue, also noted by Spindel, arises frequently in the literature, namely the importance of platform dynamics on the measurement process. From the Garret-Munk model, second order statistical characteristics, namely the time-lagged autocorrelation of the received signal were computed. In the model's fully saturated regime each deterministic multipath is considered scattered by internal waves into uncorrelated micropaths.

3.2.9 The frequency coherence and time coherence of this forward scattered energy are parameters of particular interest for long range acoustic communications. In this case the authors make a clear distinction between coherence measurements based on micropath

and multipath and attempt to reconcile the observed micropath coherence bandwidth with theoretical results derived from the Garret-Munk model.

3.2.10 Here the micropath bandwidth function Q, is formulated in terms of a characteristic scale η_0 measured in Hz. The characteristic scale is empirically related to a strength parameter Φ and a diffraction parameter, Λ which are dimensionless and derived from the Garret-Munk model. For the three ray arrivals considered, the normalised micropath bandwidth coherence measurement reduces to 0.5 for frequency separation of typically 50Hz.

3.2.11 The bandwidth used for the experimental results was approximately 30Hz, which is comparable with the measured micropath coherence bandwidth. Despite this the authors found that experimental autocorrelation measurements were significantly broader than theoretically predicted which was attributed to reverberation effects. Another possible cause would be the effect of platform motion over the long integration intervals used, which would serve to temporally smear the time lagged correlation result.

3.2.12 The paper raises a number of issues. Firstly the use of such low bandwidths begs the question at what point does one consider a path arrival as resolved and how, in a communications sense, does one relate channel coherence measurements to the signal design issue if the channel exhibits micropath and multipath spreading.

3.2.13 Secondly the authors have used a stochastic noise signal to measure the frequency selective behaviour of the channel and the impact of platform motion and intrinsic channel time selectivity on the measured results have not been fully developed. Specifically the authors do not consider the signal ambiguity and decorrelation losses.

3.2.14 Thirdly, the authors attempt to reconcile the observed results with an internal wave scattering model only. This means that intrinsic ocean effects such as turbulence, surface

wave scattering, thermal mixing and sound velocity fluctuations are largely averaged out in the receiver in addition to extrinsic effects such as platform dynamics and oscillator jitter. It is however such effects which are of paramount influence in the high data rate problem.

3.2.15 The feasibility of coherently combining multipath signals propagated over a long range deep water channel is considered in the paper by Williams and Battestin [21]. The authors propose the feasibility of deconvolving the influence of the acoustic channel on a low frequency transmission by measuring the channel impulse response. The technical approach relies, somewhat tenuously on the autocorrelation properties of the channel impulse response as it is assumed that this function approximates a delta function. In practice this is rarely the case. By estimating the channel impulse h(t) and cross correlating this estimate with the received signal r(t), the output $X(\tau)$, represents an energy raking process. The authors argue that if this function is subsequently correlated with the original signal the resulting function exhibits a single main peak attributable to the coherently summed rays and smaller peaks or sidelobes due to the 'suppressed arrivals'.

3.2.16 The approach is in fact very similar to the rake receiver concept used in spread spectrum systems. However in this case, the authors rely on an explicit impulse channel sounding waveform for the channel estimate and on the channel time coherence being sufficiently long (6s) to ensure the channel does not change appreciably between soundings.

3.2.17 The results presented are however somewhat ambiguous as the 'raked' normalised correlation output is actually less than the unraked normalised output which the authors attribute to the use of hardlimiting correlators introducing noise, thereby reducing the normalised correlation.

3.2.18 There are many other factors affecting the performance of such a raking technique. For example the authors implicitly assume the signal autocorrelation to be zero outside of the reciprocal bandwidth. This is comparable to the ideal rake assumption where signal self noise arising from sidelobes, are ignored. This assumption is however only valid for perfectly synchronised high BT signals or perfectly orthogonal signal designs, both of which are theoretical ideals which are difficult to achieve in practical acoustic channel conditions.

3.2.19 Further, the experiments were performed for a drifting platform at 1.2kts. The long integration time (4s) used for the hyperbolic chirp would be susceptible to Doppler and Doppler variability within this integration period.

3.2.20 In a more recent paper Spiesberger et al [22] pay closer attention to the channel time selectivity problem. In this paper pulsed and continuous transmissions at 133Hz were transmitted over a range of 4000m with bandwidth 13Hz with the aim of monitoring travel time fluctuations. In this experiment the signal energy integration time is 31s and time delay estimates are made from the average formed from each multipath arrival. This has the obvious advantage of reducing uncorrelated delay fluctuations between paths.

3.2.21 In the paper Spiesberger considers the integrated phase fluctuations due to sound speed variability arising from internal wavefields over the path length. The author suggests that this results in a random walk process on the received signal phase. By considering the phase changes from record to record Spiesberger derives expressions for the variance of this phase difference term and the associated phase noise error term. For M complex baseband samples of the transmitted signal, it is shown that the phase error variance is reduced by a factor M. This indicates the benefits of using increased integration times for phase averaging during the correlation process. In their analysis the authors derive

expressions for the power spectral density of the random walk phase, so called extended phase, and also for the phase differences, the rationale being that the techniques are more suited to identifying long and short timescale mechanisms respectively. In their measurements the authors identify a rms phase variance of 0.95 radians which equates to a spatial scale of 1.7m in a two minute interval.

3.2.22 The receiver processing methodology used is of interest in that the authors use both absolute and differential phase measurements derived from the complex baseband replica correlation to identify intrinsic ocean mechanisms. The use of differential phase is an established semi-coherent technique used in many communications systems to mitigate channel time selective behaviour. In the tomographic application of this paper, the technique fails to demonstrate the more dynamic features of multipath variability due to the extensive averaging of the complex baseband correlator outputs.

3.2.23 In the paper by Jobst and Dominijanni [23] the temporal, spatial and frequency stability of a long range acoustic channel is considered. Results are presented for a low frequency (206Hz) phase coded sounding signal of null-null bandwidth 25.75Hz. Receiver processing used extensive block sequence averaging to improve SNR based on an integration window of 5.3minutes. A feature of this paper is the care exercised to reduce the number of refracted arrivals and the choice of transmitter and receiver location to ensure low energy reflected arrivals. Despite the low operational bandwidth the authors highlight the ability of the system to achieve centimetric accuracy provided sufficient SNR is available. This is an important, often overlooked point. By exploiting the processing gain inherent to a coherent complex correlation receiver it is possible to achieve high phase accuracy's at low SNR subject to channel stationarity over the integration interval. The results presented demonstrate path length oscillations attributable to tidal activity. In their analysis of channel coherence bandwidth the authors concede that

the time spreading measurement is subject to the resolution capability of the transmitted waveform. No account is made of the influence of the doubly spread nature of the channel on the measurement technique.

3.2.24 The propagational stability of a doubly spread acoustic channel is considered by Veenkant [24]. The author considers the feasibility of instantaneous channel characterisation based on phase coded transmissions at 420Hz and null-null bandwidth 40Hz. The author notes that when the product of the channel frequency spread (B) and time spread (T) is less than unity the channel can be unambiguously characterised with an appropriate signal design. In order to characterise the acoustic channel, the authors propose the use of a CW pulse train. This is designed such that the pulse separation $T_p >$ channel time spread and the discrete components in the resulting signals line spectrum are separated in frequency by more than the channel frequency spread i.e. $L<1/T_p<B$.

3.2.25 It is to be noted that the experiment was performed for a static geometry, otherwise these frequency guardbands may have been compromised. In the experiment the pulse separation was set at 1.2s the pulse duration was 20ms resulting in a transmission null-null bandwidth of 100Hz. The use of a pseudorandom phase modulated waveform provided approximately 15dB process gain.

3.2.26 Since the transmission comprised a broadband line spectrum, the authors argue that it is possible to determine the spreading characteristics of the channel by isolating narrowband and broadband components of the received signal. In this case the authors isolate a narrowband component at the carrier frequency, a broadband component from the filtered line spectra, and a noise component. Since the former measurement estimates narrowband signal energy, and the latter measurement is an estimate of the broadband signal energy,

the authors argue that the time variability of each measurement indicates frequency selective and frequency non selective fading effects.

3.2.27 The results presented consider the time variability of each component for bottom reflection and surface reflection dominated channels. In each case the filtered narrowband carrier component is subject to differing degrees of fading. In the bottom reflected path which consists of many coalesced path arrivals the energy undergoes extensive fading up to 20-30dB, however in the surface reflected path, no fading occurs. In both cases the broadband signal energy undergoes modest variability indicating that the channel is subject to rapid frequency selective fading in the bottom-reflected case.

3.2.28 In contrast, the surface reflected path exhibits greater out-of-band energy due to frequency spreading (typically 3dB), and greater variability, both in terms of Doppler spreading and slow fading effects.

3.2.29 Veenkants approach to channel characterisation is somewhat refreshing as it actively addresses the doubly spread nature of the acoustic channel, the degree of coupling between the temporal and spectral spreading mechanisms, and highlights the importance of signal design to overcome these effects. Specifically the proposed signal exhibited time and frequency guards to isolate the dispersion mechanisms. The results obtained for a bottom-refracted path however clearly indicate that the transmission was subject to frequency selective fading despite the adoption of time guardbands.

3.2.30 Although not stated, this was likely due to the poor temporal resolution of the signal. At such low frequencies the bandwidths available to resolve the multipath structure are extremely modest, typically 10-50Hz. This means that path arrivals within 10-30m are not resolved. The problem is compounded by the fact that the carrier wavelength is typically

1-2 orders of magnitude less than the temporal resolution of the system. This means that correlation processing cannot isolate discrete micropath structure.

3.2.31 The difficulty in resolving forward scattering micropath is addressed in a paper by Ewart [25]. Once again the emphasis is on tomographic measurements however in this case the frequencies used are higher and the ranges shorter. The main feature of this paper is the care taken to isolate a single refracted path for analysis. The transmission comprised a pulsed continuous wave (CW) transmission of bandwidth 50Hz at centre frequencies 4.2kHz and 8.3kHz received by three receivers. Since the received pulse SNR was high, coherent averaging of received pulses was not performed. The analysis focuses on a single path arrival which the authors believe is uncontaminated by multipath despite the limited resolution of the transmission signal. The pulse repetition rate (PRF) used was one pulse every 30s which invariably undersamples any rapid phase fluctuations of interest for high data rate communications.

3.2.32 The power spectrum formed from the observed phases demonstrate most energy below 1Hz falling by approximately $1/\omega^3$ above 1Hz. The measured phase variance was typically 380μs for both 4kHz and 8kHz transmissions corresponding to a spatial scale of the order 50cm. In both cases the phase distribution is Gaussian. Since both transmitter and receiver were bottom mounted the observed phase variability is attributed to the integrated variation in sound velocity over the measurement path.

3.2.33 For a high data rate system the spatial scale of transmitted symbols will typically be 5-15cm which is significantly shorter than the spatial scale of the observed phase fluctuations.

3.2.34 An interesting link between the ocean tomography community and the underwater communications problem is presented in a paper by Birdsall [26]. Here the author exploits

the use of high energy phase coded waveforms to achieve both low data rate telemetry (measured in bits per second) and ocean tomographic measurement.

3.2.35 Based on purely physical reasoning Birdsall suggests that the intrinsic time scales of ocean variability are primarily due to ocean surface wave effects and to a lesser degree on receiver buoy movement. A salient point stressed by the author is the dominance of buoy motion and not intrinsic ocean mechanisms, in determining the time coherence of the channel. This is a recurrent theme in much of the literature presenting actual channel data. Another salient point stressed by the author is the time variability of forward scattered energy for discrete multipath arrivals.

3.2.36 The authors adopt the use of a multiphase pseudo-randomly coded waveform set for the telemetry link. An important point raised is the degradation in the waveform orthogonality characteristics when transmitted over real ocean channels. This is generically attributed to multipath, however it will be shown later that acoustic Doppler also significantly influences code orthogonality.

3.2.37 The proposed signal is designed to ensure that it is fully convolved with the channel response to enable tomographic measurements to be performed on all paths. Whilst the authors do not present any field experimental results, nor indeed any simulation results, the paper is noteworthy in that it links tomographic methods to the low rate underwater communications problem by addressing channel time and frequency coherence issues albeit on pseudo tomographic timescales.

3.2.38 The use of phase coded transmissions in the region 850-1325Hz for long range, timing and ranging measurements are considered by Coffey and Paquette [27]. The authors review conventional tracking algorithms based on time difference of arrival between hydrophone pairs and the computation of hyperbolic intersections; and spherical

intersection techniques based on known transmission/reception times. The authors argue that at very long range (up to 75 nautical miles) the dispersion introduced into the transmitted signal results in significant correlation degradation such that accurate range tracking of the signal becomes difficult. The proposed approach involved introducing environmental modelling data into the tracking process. In the technique the authors attempt to effectively pattern match the observed channel structure with that obtained from environmental model runs and using a maximum likelihood decision process to obtain the best range estimate. This technique is essentially a form of broadband matched field processing implemented against a known target.

3.2.39 The signal design comprised a 10s multicarrier transmission using 8 tones for Doppler estimation, 8 tones for channel ID and 24 tones based on 8-FSK for an 8 bit message. The ranging signal followed the multicarrier transmission after a 1s time guardband, and comprises three phase coded transmissions based on a 13bit Barker sequence of 160Hz bandwidth 0.325Hz, hopped between 920-1240Hz.

3.2.40 The environmental model used for channel characterisation was ray based, accepting bottom and surface conditions. The authors do not indicate if the model is range and time dependant. Initial synchronisation is achieved through energy detection techniques. The Doppler pilots are then used to determine Doppler compensation prior to correlation of the Barker code. The correlation results are then compared with the environmental predictions. In the majority of cases poor correlation between observed and simulated channel data was achieved. The authors consider the performance limitations of the environmental prediction model to be responsible for the discrepancy. In particular the authors highlight range dependence in the sound speed profile and suggest that extensive sound speed averaging prior to environmental modelling may have contributed to the poor performance.

3.2.41 Heard and Schumacher [28] present results from the analysis of phase coded M sequence waveforms transmitted over a range of over 170km from a moving source. An interesting aspect of this paper was the use of a closed loop Doppler tracking technique based on observing the received signal phase and re-sampling the received data accordingly. This process was performed at complex baseband and the authors do not indicate if any phase compensation was applied. This would be necessary since the re-sampling process addresses temporal-spectral scaling over the transmission band but not frequency translation. Unfortunately the authors do not indicate the bandwidth of the DLL tracking loop.

3.2.42 The preceding papers on tomographic measurements have underlined the relative stability of the long range, low-frequency channel, albeit at lower frequencies than those considered by the authors. This suggests that the discrepancies between measured and modelled channel were due primarily to the limitations of the model. This has in fact been a recurring issue in matched field processing techniques, which rely intimately on accurate environmental inputs. This is the focus of much current research in the field addressing such issues as global optimisation such as Gestoft and Gingras [29]) and sparse estimation techniques such as those discussed by Rouseff et al [30]. In the latter the underlying principle is that knowledge of the acoustic field at a specific location can be merged with existing environmental data with a view to extrapolating the acoustic field to other locations.

3.2.43 Long range channel characterisation results are presented in a more recent paper by Franlink et al [31] where the authors seek to determine the suitability of the channel for differentially coherent modulation schemes at ranges out to 120km. In this case the channel was well characterised from previous experiments and featured particularly low bottom losses at the frequencies of interest (800-1kHz). Channel time spreading was

measured using explosive charges however the resolution of arrivals was limited due to the bandlimiting at the receiver resulting in a resolution of 2ms. Such a channel sounding 'waveform' is well suited to characterise channel frequency coherence due to its impulsive, wideband characteristics. The time spreading measurements were conducted out to a range of 160km. The time spreading increased with range exhibiting typically 30ms+ at 160km. However of particular note were the very large time spreads arising at ranges of less 5km. At shorter ranges there are fewer bottom-surface interactions and so multipath energy is not dissipated. This often results in a much richer, much more variable multipath structure.

3.2.44 This fact is of particular importance to the high data rate communications problem since the operational frequencies and bandwidths incur large absorption and scattering losses, limiting the operational range to typically 2.5-7.5km depending on source level. At increased ranges, rays with high Rayleigh parameters are subject to much greater scattering losses at bottom and surface interfaces and also incur increased absorption losses through the medium with the result that their energies rapidly decay with range. This leads to the somewhat paradoxical situation that the channel often becomes less complex at increased ranges. At shorter range, the complex multipath structure is further complicated by the issue of differential Doppler, which will be discussed later.

3.2.45 The channel time coherence was measured based on CW soundings. Care was taken to decouple the projector from surface platform motion. The coherence measurements are particularly interesting in that they were obtained for a receiver moving at radial velocity of +10knots. The received pulse phase trajectory demonstrated sinusoidal variations on timescales of 14s with a corresponding spatial scale of 1.3m and peak Doppler 0.6knots. These variations are typical of platform motion.

3.2.46 Virovlyanskii et al [32] consider the Doppler spreading problem for a moving source for a narrowband transmission at 300Hz. The authors emphasise the phase stability of the underwater channel when surface scattering is not involved. In this case temporal fluctuations due to tides and internal wave behaviour dictate channel time coherence. A fundamental observation forwarded by the authors is the ability of an observer to infer information regarding the mode structure of the acoustic channel based on the different Doppler shifts attributable to each mode when one or both parties are moving. This differential Doppler problem is a significant limiting factor for high rate acoustic communications. The theoretical development focuses on the narrow band case under the assumption that the velocity - time integration product is much greater than a wavelength. Under these conditions mode interference (i.e. fast fading) is effectively averaged out and subsequent analysis assumes incoherent summation.

3.2.47 The authors note that velocity fluctuations result in spectral broadening. Expressions for this random perturbation spectrum are presented for the case of small and/or rapid velocity fluctuations resulting in a Lorentzian Spectral distribution and the case of large and/or slow velocity fluctuations result in a Gaussian spectral distribution.

3.2.48 Shallow water oceanographic variability and the influence of sea bottom interactions are considered in a review paper by Ali [33] that attempts to delineate the transition from shallow to deep water propagation. The author suggests the demarcation to be determined by the validity of ray versus normal mode treatment of the acoustic propagation problem. This definition is further refined in terms of the extent of interaction of the acoustic signal with the medium boundaries; an issue of notable importance from the preceding discussions.

3.2.49 Whilst focussing on very low frequency acoustic propagation and in particular geoacoustic coupling, the author attempts to categorise the temporal and spatial scales of ocean variability and their influence on acoustic propagation. Results presented for shallow water sound velocity emphasise the intrinsic microstructure and its temporal and spatial variability, which correspond to decisecond-centimetric scales.

3.3 Medium/high frequency Measurements and surface scattering

3.3.1 Inevitably as operational frequencies and information rates are increased, scattering from surface and bottom interfaces becomes increasingly important. This is a direct consequence of the reduced spatial scale of the symbolling waveforms and carrier wavelength.

3.3.2 The complexity of the sea surface as a signal scatterer has prompted much research, both acoustic and electromagnetic, geared to the understanding of the effect of surface wave scattering on both acoustic and electromagnetic signal coherence [34]

3.3.3 For radar applications, understanding surface wave and surface wave scattering is central to many military and commercial applications such as clutter suppression, wake detection, remote sensing etc. In underwater acoustic communications surface scattering is often considered the dominant mechanism affecting signal time coherence; certainly at higher sea states and at high-to-medium grazing angles. For this reason, many studies have been conducted to investigate the role of the sea surface on signal coherence for both forward and backscattered cases. These studies have included theoretical modelling of surface scattering, laboratory experiments and field measurements.

3.3.4 From the communications perspective one is particularly interested in the time, frequency and spatial coherence of the scattered signal as this ultimately impacts on receiver synchronisation, equalisation and spatial processing solutions. Unfortunately interpreting

the results presented in the open literature is ultimately complicated by the diversity of parameters, which influence the received acoustic field. Environmental parameters, signal designs, array configuration and experiment geometry are primary factors influencing the results presented.

3.3.5 Both system and environmental influences on signal coherence are considered in the paper by Robinson et al [35]. The main emphasis of this work is on characterising system and environmental influences on the received reverberation spectrum. The authors consider the reverberation spectrum due to the convolution of three main components. The spectrum describing source-receiver motion, the spectrum of the transmitted waveform and the spectrum of the random motion of the scatterers within the medium. Results presented for the surface reverberation spectrum of a 20kHz, 100ms pulse demonstrates significant variability, however the ensemble average tends toward a Gaussian distribution. The authors present a number of results, which serve to illustrate those mechanisms resulting in spectral smear and asymmetry in the smear. Surface reverberation spectra as a function of windspeed demonstrate increased spectrum bandwidth with increased windspeed with a total spectral smear up to 30Hz at 20knots based on a CW shaded pulse of duration 100ms. The influence of platform speed on spectral smear is demonstrated for a range of velocities up to 60knots for the broadside case. Here the Doppler shift component is zero however the received spectrum exhibits spectral smear which increases with velocity and tends to an asymmetrical distribution at higher platform velocities. This asymmetry also manifests as the system beamwidth is increased due to the beampattern becoming spread over more Doppler cells. Results presented as a function of vertical arrival angle indicates significant spectral smearing and asymmetry as the arrival angle approaches the horizontal since the scattering becomes less specular,

3.3.6 These results underline many of the important system wide and environmental issues relating to the ocean surface scatter channel model. Interpretation of the results is complicated by the choice of sounding waveform, which was both narrowband and of relatively long duration (100ms CW). The poor resolution and the low PRF of this waveform are inappropriate to fully characterise the time and Doppler spreading characteristics of the medium.

3.3.7 The impact of doubly spread shallow water acoustic channels on signal coherence and channel noise is considered in a review paper by Rice [36] that provides a comprehensive overview of the acoustic communications problem over such channels. The author focuses on the acoustic channel temporal and Doppler dispersion in the context of classic time varying channel characterisation. In the discussion the author considers a simple environmental model to demonstrate an overspread channel due to sea surface motion time and Doppler dispersion. Similar models are recurrent in the literature on acoustic communications.

3.3.8 The relevance of these arguments to the acoustic communications problem is however undermined by the nature of the acoustic Doppler problem, which manifests as both time varying phase variability and temporal scaling. Further, since the shallow water channel often exhibits discrete path structure it is often more appropriate to consider the channel dispersion characteristics in terms of forward-scattered components rather than as a lumped parameterisation. This is particularly so for wideband high rate communications where the system is capable of resolving such components and, in some cases, exploiting it.

3.3.9 Owen [37] considers the forward reflection and scattering characteristics of surface water motion for a scaled model telemetry channel under experimental conditions. Owen notes

that the influence of transducer depth introduces variability due to the effective change in grazing angle and also due to the change in surface isonified area. Since the fluctuation of the forward scattered signal is a function of the rms wave height, wave number and grazing angle Owen suggests that for small grazing angles the forward scattering strength increases with transducer depth. Expressions for the isonified surface footprint are defined for the pulse duration limited case, the beamwidth limited case and the wave facet case. Acoustic shadowing is accounted for using an empirically derived correction factor. In the experiment the frequencies employed were 3MHz with surface wave agitation to +/- 1.4mm and beamwidths 9deg x 2deg. Owen argues that the parameters were chosen to model a proposed acoustic data telemetry link operating at 50kHz for a geometrical scaling of 60:1.

3.3.10 The results presented highlight the role of wave facet scattering on received signal characteristics, and clearly indicates multiple forward-scattered returns attributable to leading wave edges traversing the experimental tank. For the chosen signal characteristics the pulse duration was sufficiently short (2.5us / 3.7mm) and the PRF sufficiently rapid (100Hz) to resolve individual returns. Owen concludes that large area surface isonification leads to time spreading and for more complex surface wave models, a two level surface roughness model encompassing swell and surface roughness is more appropriate for surface wave modelling. It is argued that adaptive equalisation schemes would be unable to track such fluctuations in long range channels, however the arguments to support this conclusion are not developed in the context of more general propagation considerations such as the rapid attenuation of large Rayleigh parameter rays with range.

3.3.11 Experimental measurements of surface wind generated wave scattering made under laboratory conditions are presented by Spindel and Schultheiss [38]. In the paper the authors consider the acoustic forward surface scattering as a linear random time varying

filter which they attempt to characterise using impulse response measurements. In their measurements the authors adopt a 1us-pulse length at a prf of 40Hz. This signal design was compatible with the temporal and spatial scales of the wind generated waves in the tank (rms height 1-2mm) however the PRF was short compared to the surface wave temporal correlation time measured to the first null (0.05s). Impulse response results presented for varying grazing angles are in agreement with simple theoretical predictions based on a two-ray path model both on axis and off axis rays.

3.3.12 However, time spreading estimates due to surface wave displacement only, fell somewhat short of the experimental observations. Due to the random behaviour of the observed instantaneous channel impulse measurements, the authors attempt to use ensemble averaging of the channel impulse response. Their rational is however somewhat unclear since the surface scatter is spatially and temporally varying. The results indicate a consistent secondary arrival. However, the associated time spread is inconsistent with Eckarts scattering theory. The result is most likely due to a standing wave component due to backward propagating waves reflected from the tank boundaries.

3.3.13 Despite this discrepancy the authors present both instantaneous and ensemble averaged channel transfer function estimates based on the Fourier transform of respective channel impulse response measurements. From these measurements the authors derive the channel spreading characteristics evaluated at frequencies between 50 and 500kHz. Spindel notes that the channel frequency spread increases as a function of carrier frequency and grazing angle with typical spreads between 10-20Hz. The suitability of the analysis technique for surface scatter exhibiting quasiperiodic structure in a spatial and temporal sense is unclear since the ensemble averaging process could remove the very structure one is interested in, particularly for high data rate acoustic communications. The time evolution of the channel impulse response presented by Owen clearly identifies the role of wave facet specular

reflections in the scattering process and the need to conduct averaging on a temporal and spatial scale compatible with that of the wave surface motion.

3.3.14 Olson and Nichols [39] consider the influence of surface wave forward scattering on pulsed stochastic signals at 300 and 750Hz transmitted at an incidence of 30degrees and received by two hydrophones at a range of 16km for a variety of waveheights ranging from 2-25ft. The pulse duration of 10s was chosen to be compatible with the wave period and the frequencies chosen to be compatible with the waveheights. Investigations were also conducted into the spatial coherence of the received signals based on the hydrophone receivers placed 500m apart. Average normalised cross correlation between hydrophones and single hydrophone replica correlation results are presented. Both data sets demonstrate an almost linear reduction in correlation coefficient with increasing waveheight. As expected, the single hydrophone replica correlation results are significantly higher than the hydrophone cross correlation results (cf. 0.8 - 0.6). Olson notes that the observed correlation results are significantly higher than previously published results and attributes this to the reduced integration time in the receiver.

3.3.15 Higher frequency, surface wave back scattering is considered by Boehme [40]. In the paper the author focuses on the frequency-spread characteristics of the backscattered field as a function of the acoustic incidence angle, wave vector and height, and second order descriptions of surface wave behaviour. In the experiments transmissions were made at 175kHz and 455kHz with corresponding beamwidths of 6x60deg and 12x12deg respectively. The authors do not indicate the scale of the isonified surface area, however the use of such relatively large beamwidths suggests that the footprint may have been quite large even at modest grazing angles. The authors make a number of observations regarding the datasets.

3.3.16 Firstly the observed frequency translation increases as the grazing angle reduces. Also the frequency translation scales with surface windspeed and is subject to saturation at high wind speeds. Frequency spreading was found to be independent of azimuth and to decrease with reduced grazing angle. The observed reverberation spectra were found to be notably asymmetric with greater energy evident in the Doppler sideband component for the downwind case. Since the beamwidths employed by Boheme were relatively large, the results are somewhat inconclusive from the viewpoint of understanding the intrinsic scattering mechanisms.

3.3.17 Malyshev and Gulin consider the statistical characteristics of surface wave scattering in a number of papers [41-45]. In the experimental results presented in [41], the authors consider the amplitude statistics of forward scattered pulsed 3ms CW at PRF 3-8Hz and frequencies between 3 and 36kHz at a range of 1.5km and water depth 80m. For the geometry, chosen surface and direct paths were clearly resolved. The authors note that the amplitude coefficient of variation was significantly higher for the surface path than for the direct path. Smaller variations in the direct path were attributed to surface platform motion and this was substantiated by the periodic nature of the signal autocorrelation. The authors also noted little variation in amplitude variation with range. Amplitude variations were found to increase with frequency, typically 0.02-0.07 at 4-7kHz and 0.05-0.1 at 11-15kHz. Results presented as a function of Rayleigh parameter demonstrated a linear dependence at low Rayleigh parameter and amplitude variation saturation at high Rayleigh. Boheme also noted this effect for the backscattered case.

3.3.18 The statistical analysis of the amplitude variability demonstrated slight deviation from the Rayleigh distribution, which was attributed to the high spatial correlation present in the surface waves resulting in increased dependence between scattered signal components and deviations from uniform phase distributions. The autocorrelation of the amplitude

variations demonstrated appreciable periodicity for the swell only data sets and the time scale is attributable to surface wave period. For increasing Rayleigh parameter, the autocorrelation time is seen to reduce for all the data sets presented which underlines the decorrelative effect of surface wave scattering at high grazing angles.

3.3.19 In [42] the authors turn their attention to the spatial correlation functions of the amplitude and phase fluctuations of surface scattered signals. The authors find periodic spatial trends in the amplitude correlation and rms phase coefficients for array orientation normal and perpendicular to sound propagation for low values of Rayleigh parameter. This spatial period is shown to relate to surface wave period and arises from wave facet scattering also observed by Owen. For the results presented this corresponds to spatial scale of 5-6m. At higher Rayleigh parameters spatial periodicity is lost and the spatial amplitude correlation coefficient decays rapidly over 3m with phase variability becoming too extreme to measure within 2π. For vertical orientation the authors note that the spatial coherence is much less than for the horizontal case typically 1m for small grazing angles.

3.3.20 Wilson et al [46] present results obtained for forward scattered direct and bottom paths for pulsed CW signals in the frequency range 20-180kHz over a range of 90m in water depth 30m. Direct and bottom paths were barely resolved for the 1ms pulse duration used. Despite this the authors present results for the amplitude variability of each path as a function of frequency. The results presented indicate that the direct and surface-bottom paths are subject to greater variability at higher frequencies with a marked peak occurring at 60kHz (sigma 0.8 versus 0.25). Since the phenomenon occurred on both direct and bottom paths the authors propose that the variation is due to microthermal variations in the water column causing path length fluctuations of typically 2-3cm (i.e. the wavelength at 60kHz). As the range is relatively short this is feasible, however since the direct and bottom paths coalesce in the receiver processing it is unclear how the authors clearly

discriminate direct and bottom paths. Also the authors attempt no measurement of the temporal coherence of the received signal and since the PRF was low (1s), the signal design is unsuited to characterising rapid time variation of the channel impulse response.

3.3.21 Zheng [47] presents statistical results for the envelope of a pulsed 20kHz CW signal transmitted over a 16m-depth channel at ranges 0.25-2NM. The analysis focuses on characterising the envelope probability density function (PDF) for direct and surface reflected paths. Results are also presented for channel temporal correlation. Zheng notes that the mainpath and multipath exhibit different amplitude statistics and that these statistics vary with range. At short range the surface multipath component exhibits Rayleigh statistics and the direct path exhibits Gaussian statistics. At increased range the direct path statistics tend toward Rayleigh. As the range increases for the surface reflected path the statistics also tend toward Rayleigh. At all ranges the multipath component is subject to greater amplitude variability compared to the direct component. The temporal coherence measurements indicate high coherence (0.9) for both direct and surface reflected paths. In all data sets the author notes a much higher coefficient of variation at shorter range.

3.4 Discussion

3.4.1 It is evident from the preceding discussion that it is not always possible to extrapolate the results from tomographic experimental coherence measurements to the high data rate acoustic communications problem by virtue of the modest bandwidths used and the extensive averaging. This underlines the importance of matching waveform spatial and temporal scales to the environmental mechanisms under study. In the tomographic case the relevant scales are one, possibly two orders of magnitude higher than for high data rate signalling waveforms. Despite this limitation, the tomographic discussion has

highlighted several issues of relevance to the high data rate acoustic communications problem:-

- Although modest bandwidths are employed in these systems, high temporal resolution can be achieved with sufficient signal-to-noise ratio based on interpolation and/or use of complex phase information in the baseband correlation information.

- A number of authors distinguish between signal coherence based on micropath or macropath. This is an important distinction which underlines the difficulty in characterising acoustic environments.

- Phase coded waveforms are well established in the tomographic field. The utility of this waveform for channel estimation and characterisation is intimately linked to its ambiguity function and the channel scattering function.

3.4.2 There are several issues arising from the experimental studies conducted on ocean surface scattering:

- High grazing angle surface scatter and backscatter returns, or equivalently returns with high Rayleigh parameters have poor time and frequency coherence. This observation would support the argument developed in section 2, namely short-range acoustic communications channels are often more difficult than longer range channels. This arises not only due to greater time spreads but also poorer time coherence.

- At high grazing angles there is evidence that coherence degradation saturates. This effect however has been investigated as a function of limited systematic parameters such as signal design, frequency, bandwidth, beamwidth etc.

- There is evidence pointing to the important role of wave facet scattering in determining in the forward scattered signal coherence characteristics. The observations by Owen

Malyshev and Gulin suggest a Bragg resonance effect as indicated by periodicity's in the time lagged autocorrelation of the received signal.

- The results on ocean surface scattering underline the importance of signal design when attempting to measure received signal coherence and the difficulty in isolating the physical mechanisms responsible for degrading signal coherence.

3.4.3 A key issue in performing any environmental measurement is to provide a quantitative measure of the coherence characteristics of the received signal field. This information is useful for determining appropriate modulation signal designs and diversity techniques to improve the reliability of a communications link. One may, for example attempt to transmit the same information in two or more frequency bands sufficiently separated to ensure that if one becomes corrupted then the other is not. Similarly, one may transmit the information at two distinct times to minimise the risk of both transmissions becoming corrupted. Finally one may use two or more receivers separated some distance apart such that signal corruption on one receiver does not affect the other. These techniques rely on knowledge of the coherence bandwidth, coherence time and spatial coherence of the received field.

3.4.4 In this section several studies have been reviewed concerning the coherence of the received signal field. Only passing account is made of the intrinsic ocean mechanisms contributing to signal coherence degradation. Understanding these mechanisms is a key element of the communications system design process. In section 4 several of these mechanisms are studied in greater detail and methods to measure the environment and model it are developed in section 5.

'Now the wild white horses play

Champ and chafe and toss in the spray",

Matthew Arnold, 'The Foresaken Merman,1849

"Roll on, thou deep and dark blue Ocean – roll!"

Childe Harolds Pilgrimage, Lord Byron, 1812

4 THE ACOUSTIC ENVIRONMENT

4.1 Preamble

4.1.1 In section 3, the experimental results of several researchers have been investigated with a view to more fully understanding the influence of the ocean environment on the signals that propagate within it. Specifically, it has been shown that the acoustic environment dramatically impacts upon the received signal coherence properties and these properties are strongly dependant on systematic parameters such as signal design (frequency, pulse width, bandwidth), beamwidth, sensor separation and number. It has also been shown that the received signal coherence properties are also strongly dependant on environmental parameters including bathymetry, bottom type, bottom topography, surface motion, relative motion, turbulence and water aeration.

4.1.2 Distinguishing between the systematic and environmental influence upon the measured signal coherence is a most important and difficult issue. In this section, physical mechanisms relating to the propagation of acoustic energy, acoustic interaction with boundaries and the influence of inhomogenities are developed.

4.2 Multipath

4.2.1 Multipath is an extremely difficult problem in underwater acoustics. Since the acoustic transmission occurs in a bounded medium, geometry plays an important role in determining the received path structure. The time difference of arrival between significant paths propagating within a bounded medium can extend to several tens of milliseconds or more depending upon environment and geometry. By comparison time spreads of EM transmissions rarely exceed a few microseconds.

4.2.2 Whilst geometry plays a key role in defining the structure of the received signal, the influence of the environment itself profoundly affects both the received path structure, its temporal and spatial variability.

4.2.3 Many authors define two regimes of multipath and multipath variability:-

- Macropath
- Micropath

4.2.4 Macropath relates to the broad structure attributable to the propagation geometry, micropath relates to the temporal smear attributable to interface scattering and scattering due to microstructure variations in the sound velocity profile in time and space. Figure 5 depicts a medium range, shallow water channel impulse response taken from Weymouth Bay in Summer 1998 illustrating three main ray arrivals corresponding to direct, bottom and surface returns. The surface path arrival is seen to comprise several coalesced paths. This micropath structure is due to scattering influence of the surface interaction and is much more dynamic than both direct and bottom paths. The extent of the macropath spread and the temporal variability of paths are the key factors which make high rate acoustic communications particularly challenging.

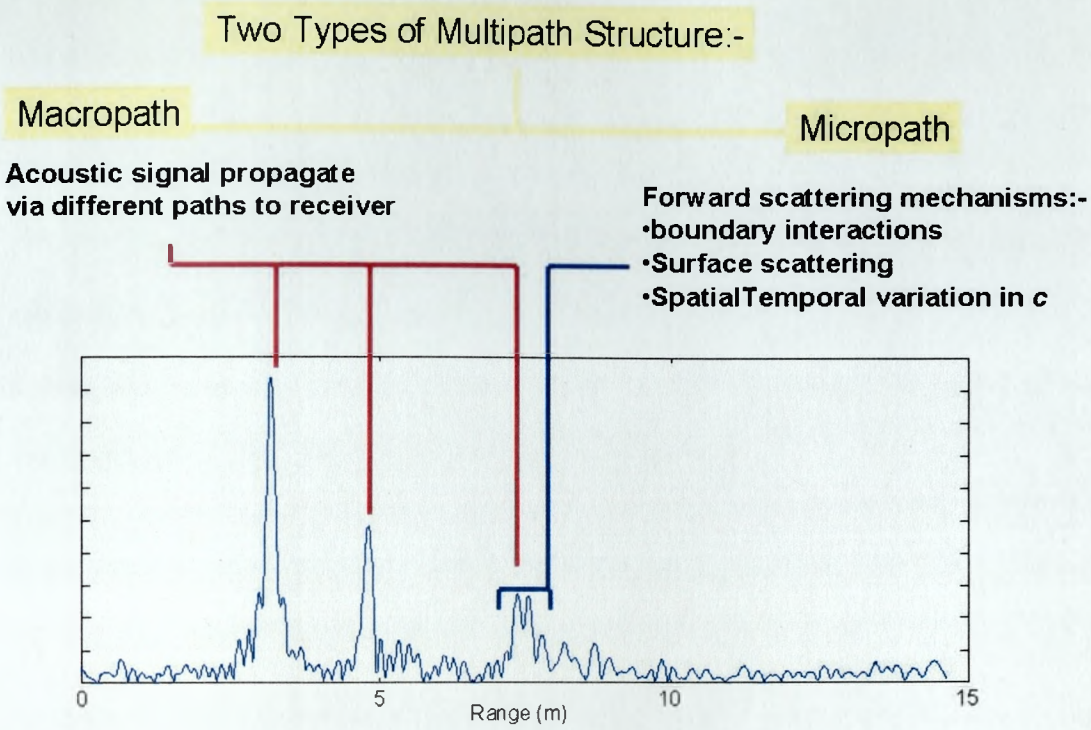

Figure 5: Macro and micro path structure

4.3 Doppler

4.3.1 The Doppler effect, often misrepresented as 'Doppler shift', relates to the apparent temporal compression or expansion of a signal transmitted from a source when relative movement exists between transmitter and receiver. In either case the velocity vector is referred relative to the signal propagation axis. Figure 6 illustrates the Doppler effect for a transmitter moving axially toward an observer.

4.3.2 The acoustic Doppler effect differs profoundly from the EM Doppler case by virtue of the much lower propagation speed, typically 1500m/s which is only three orders higher that typical platform speeds and some five orders of magnitude less than the EM case. This means that the physical distances moved by transmitting platforms, are a significant percentage of the spatial lengths of the transmitted pulse. For example acoustic signals transmitted from a platform moving radially toward an observer at $v = 15 m/s$ would be

compressed by a factor of 1%. So, for an acoustic communication transmission comprising 100 symbols, temporal compression due to Doppler would mean that the 100^{th} symbol would effectively slip by one complete symbol duration.

4.3.3 For an EM system temporal compression/expansion factors are of the order of a few millionths of 1%. This tiny factor, rarely impacts upon the baseband information of a RF carrier based communications system. It does however influence the passband signal by translating the carrier frequency term i.e. 'Doppler shift'.

4.3.4 In the acoustic case, platform motion, platform dynamics (heave/pitch etc), the motion of the medium itself (tides/currents), surface wave motion and even variations in the propagation speed introduce temporal/spatial scaling of the propagating wave. Further, this scaling may be appreciably different between paths both by virtue of the geometry and environment. This 'differential Doppler' raises several issues regarding high data rate receiver synchronisation and equalisation design, which will be discussed in later sections.

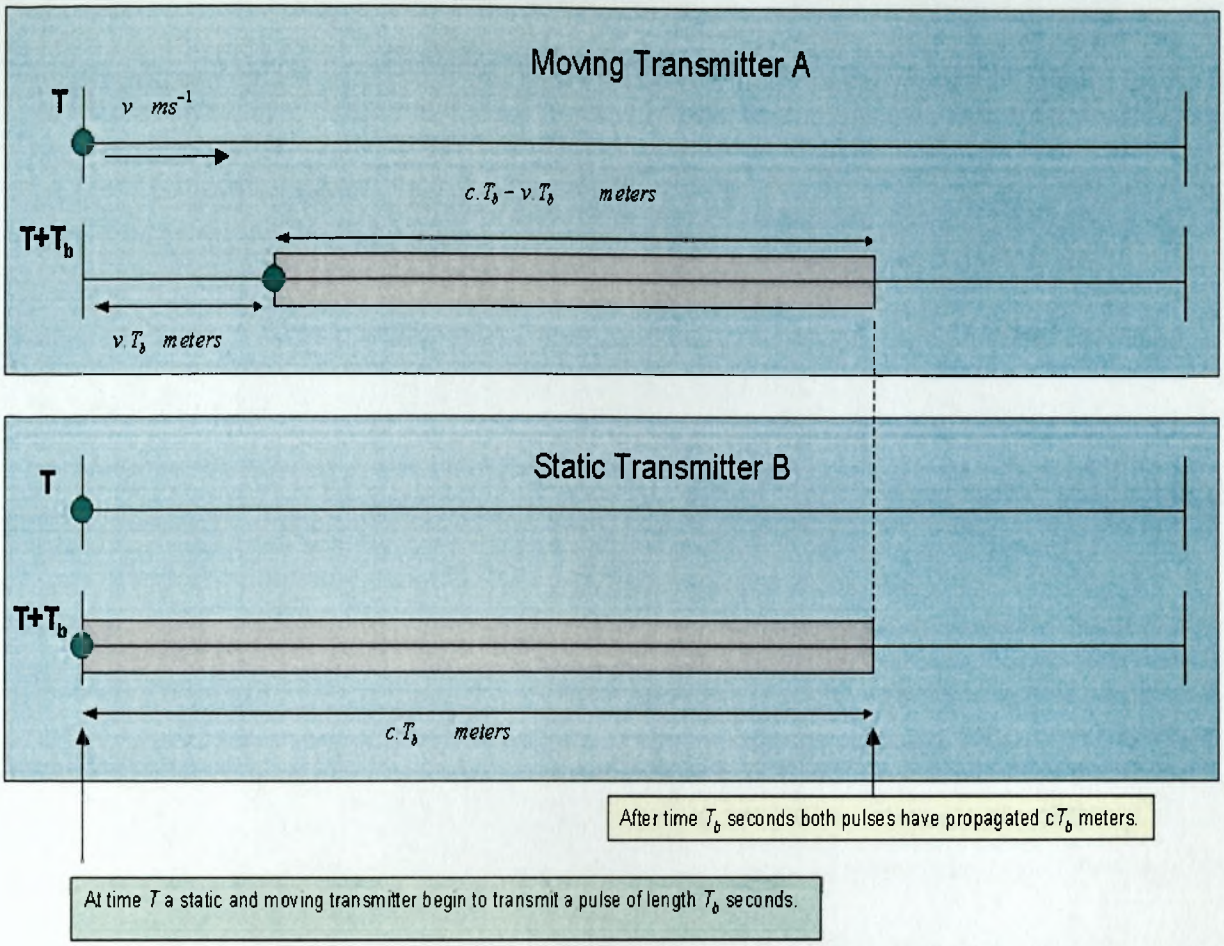

So the pulse transmitted from A is spatially compressed by

$$\alpha = \frac{cT_b - vT_b}{cT_b} = \frac{c \pm v\cos\theta}{c}$$

$v < 0$ *Expansion*

$v > 0$ *Compression*

Notes

- The velocity scalar v is the component of the platform vector $\boldsymbol{v}$ resolved along the acoustic propagation axis.
- Transmitted signal is time compressed or expanded.
- Case v>0 (transmitter approaching receiver) shown

Figure 6: Acoustic Doppler Effect

4.4 Bottom Loss

4.4.1 Bottom loss plays a significant role in high data rate, acoustic communication since it introduces energy dissipation by virtue of the reflection and transmission of the acoustic wave at the water-bottom interface. Energy transmitted into the bottom propagates by compressional and/or shear waves depending on the nature of the bottom type and the propagation attenuation is typically three to four orders of magnitude higher than that of water. The transmission of acoustic energy in the bottom media is determined by its geoacoustic properties. For low frequency signals the effective acoustic penetration depth can extend down to many tens of metres. For high frequencies typical of acoustic communications (say 5-30kHz) only the surface layer is of interest and only to a few metres.

4.4.2 In Table 1 the geoacoustic properties of continental shelf and slope environments as compiled in [48] are shown. Considering the table, it is evident that high frequencies are subject to very high losses when propagating in the various media. Assuming a frequency of 15kHz the compressional wave losses (which are smaller than the shear) range from 2dB/m in silt to around 10dB/m in sand, this compares with approximately 0.001dB/m in water. Evidently the role of the bottom in transmitting frequencies of interest in high rate acoustic communications is limited. More important are the energy losses when the bottom reflection is not perfect due to penetration into the bottom and scattering. The reflection and transmission coefficients, which relate the amplitudes of incident, reflected and transmitted acoustic amplitudes, are derived in [49]. These results may be used to calculate the reflections and transmission coefficients for an acoustic wave interacting with the bottom. In particular one is interested in the losses arising as a function of incident angle.

Type	Porosity $p(\%)$	Rel. Density ρ_b/ρ_w	Rel Speed c_p/c_w	Comp. Speed c_p(m/s)	Shear Speed c_s (m/s)	Comp Wave Attn α_p (dB/λ_p)	Shear Wave Attn α_s (dB/λ_s)
Clay	70	1.5	1.0	1500	<100	0.2	1.0
Silt	55	1.7	1.05	1575	$c_s^{(1)}$	1.0	1.5
Sand	45	1.9	1.1	1650	$c_s^{(2)}$	0.8	2.5
Gravel	35	2.0	1.2	1800	$c_s^{(3)}$	0.6	1.5
Moraine	25	2.1	1.3	1950	600	0.4	1.0
Chalk	-	2.2	1.6	2400	1000	0.2	0.5
Lime.	-	2.4	2.0	3000	1500	0.1	0.2
Basalt	-	2.7	3.5	5250	2500	0.1	0.2

$c_s^{(1)}=80z^{0.3}$, $c_s^{(3)}=110z^{0.3}$, $c_s^{(1)}=180z^{0.3}$, $c_w=1500$m/s , $\rho_w=1500$kg/m^3

Table 1: Geoacoustic properties of various bottom types

4.4.3 Considering a fluid-fluid interface which supports compressional waves only, a wave propagating at speed c_1 in a fluid medium of density ρ_1 and incident at an angle θ_1 to a fluid medium of density ρ_2 and propagation speed c_2 with a transmission angle θ_2. The transmission coefficient T and reflection coefficient R are given by:-

$$R = \frac{\frac{\rho_2 c_2}{\sin\theta_2} - \frac{\rho_1 c_1}{\sin\theta_1}}{\frac{\rho_2 c_2}{\sin\theta_2} + \frac{\rho_1 c_1}{\sin\theta_1}} \quad , \quad T = \frac{\frac{2\rho_2 c_2}{\sin\theta_2}}{\frac{\rho_2 c_2}{\sin\theta_2} + \frac{\rho_1 c_1}{\sin\theta_1}} \qquad \textit{Eqn 1}$$

4.4.4 From Snells law the critical grazing angle below which perfect reflection occurs is given by

$$\theta_c = a\cos(\frac{c_1}{c_2}) \qquad \textit{Eqn 2}$$

4.4.5 This evidently requires the sound speed in the second medium to be higher than the first. It is to be noted that in general the sound speed is normally complex enabling the modelling of lossy media and as such the reflection and transmission coefficients are complex resulting in phase shift with each bottom interaction.

Bottom Type	Critical Grazing Angle (deg)
Clay	0
Silt	17
Sand	25
Gravel	33
Basalt	73

Table 2: Critical grazing angles for a variety of bottom types

4.4.6 In Table 2 the critical angle for a number of bottom types is shown. The results demonstrate that for softer bottom types total reflection occurs only at very shallow grazing angles. The significance of this is that these bottom types introduce large losses to rays incident at steeper angles such that they are rapidly attenuated with range due to the number and extent of the losses at each bottom interaction.

4.4.7 Figure 7 shows the reflection coefficient versus grazing angle for a number of bottom types. The critical angles agree with those in the table. The figure shows that at low grazing angles, softer materials are subject to reduced reflectivity and as such introduce greater losses to rays at larger incident angles. So, for example an eigenray launched at an angle of 60 degrees would experience a loss of approximately 9dB per bottom bounce for clay, 5dB per bounce for gravel and zero loss for basalt.

4.4.8 In terms of channel behaviour this would reduce the time spread of the channel at increased ranges since rays at high grazing angles incur much greater losses by virtue of the larger number of bottom interactions with range. For harder bottom types this 'ray stripping' behaviour is less pronounced. Soft bottom environments exhibiting strongly downward refracting sound speed profiles are therefore the most difficult to achieve good range performance. Thus, in terms of channel complexity short range channels can be very difficult to deal with due to the more complex multipath structure, time spreading and, for moving platforms, Doppler spread. This results strongly support the observations of several researchers presented earlier, namely short range channels can have particularly poor coherence properties.

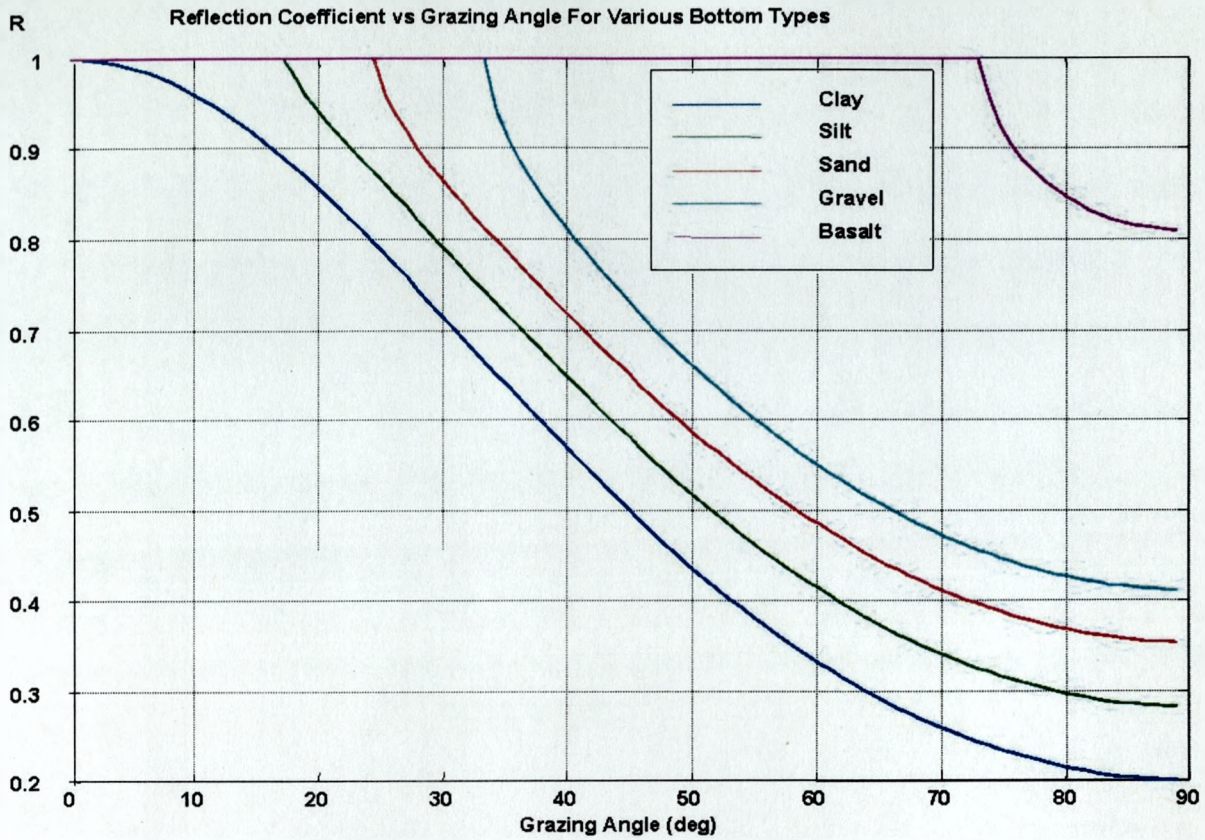

Notes

- Very soft clay bottoms are lossy at all incidence angles > 0
- Very hard Basalt bottoms are perfect reflectors up to 73 ° incidence
- Hard bottom = lots of strong paths at range
- Strongly downwardly refracting environments = higher grazing = lossier
- Soft bottom = paths attenuated at range

Figure 7: Reflection Coefficient vs Grazing Angle for various bottom types

4.5 Scattering

4.5.1 Scattering is a significant loss mechanism for high frequency acoustic signals and arises from bottom, volume and surface scattering effects. Scattering results in a reduction in the coherent component of a specularly reflected signal and so is an additional loss mechanism to bottom loss. If the bottom or surface interface can be modelled as randomly rough and the spatial scale of the roughness is small with respect to the acoustic wavelength, then a simple modification to the bottom reflection coefficient is often used to model scattering losses [7]

$$R'(\theta) = R(\theta)e^{-\frac{\Gamma^2}{2}} \qquad \textit{Eqn 3}$$

where

$\Gamma = 2k\sigma \sin\vartheta$

$k = 2\pi/\lambda$

λ is the wavelength of the incident acoustic signal.

σ is the rms surface roughness in metres.

θ is the grazing angle in degrees

4.5.2 For surface interaction R(θ)= -1 and for bottom interaction R(θ) will be determined by the bottom characteristics. Obviously the assumption of the roughness spatial scale being less than the acoustic wavelength is somewhat tenuous, particularly at the high frequencies and bandwidths employed in high rate acoustic communications. It is clear from earlier sections, that when the wavelengths and spatial scales of the symbolling waveforms are comparable to, or smaller than, the roughness spatial scale it is no longer appropriate to model surface scattering in terms of Rayleigh parameter. Indeed the results from several

authors presented earlier, indicate that whilst scattering parameters scale linearly with small Rayleigh parameter, at high Rayleigh parameters non-linear saturation effects arise.

4.5.3 In this case wave facet attitude and motion has a more pronounced influence on signal coherence. Models of surface wave scattering are well established in the open literature and a number of authors have derived expressions for the ocean scatter transfer function [50-55]. A more comprehensive discussion of this approach is presented appendix D.

4.5.4 The primary advantage of this modelling approach is that it seeks to determine second order characterisation functions for the ocean surface scattering function, which in turn can be used to determine channel coherence and ultimately appropriate modulation designs.

4.5.5 A less obvious mechanism for acoustic scattering arises from the influence of microstructure upon signal propagation. This fine structure which is both temporally and spatially variable, serves to disperse propagating signals in time due to both refraction effects and variations in propagating speed along the propagation path.

4.6 Bubble Scattering and water aeration

4.6.1 Water aeration, attributable to propeller cavitation for example, has a significant influence on the performance of acoustic communication systems since the bubble layers serve to scatter and mask the propagating sound field leading to a rapid deterioration in the received signal coherence.

4.6.2 Since gas bubbles are compliant elements tightly coupled with the water mass they are able to resonate such that their effective scattering cross section can be many hundreds of times their geometric size. The frequency of bubble resonance is a function of the bubble size and depth and is given by [56]

$$f_r = \frac{3.25x10^6}{a}\{1+0.1Z\}^{\frac{1}{2}} \qquad \textit{Eqn 4}$$

where

a is the bubble radius in microns

Z is the bubble depth.

4.6.3 The effective scattering cross section is dependent on the damping effect due to sound radiation, water viscosity and thermal conduction. The ratio of effective to geometric scattering cross section can be shown to be inversely proportional to the square of the damping term

$$\frac{\sigma_s}{\pi a^2} = \frac{4}{\delta^2} \qquad \textit{Eqn 5}$$

where

σ_s is the scattering cross section

δ is the bubble damping constant

4.6.4 For an acoustic communication system operating between 10-20kHz the damping constant at sea level is approximately 0.06. For a 0.3mm diameter bubble resonant around 15kHz, its effective scattering cross section is approximately 1000 times greater than its geometric cross section. In Figure 8 the resonant frequency of bubble diameters up to 2mm are shown for depths of 5,10,15 and 20m. The graph shows the rapid decrease in resonance frequency for bubbles up to 0.5mm. For operating band 10-20kHz, bubble diameters between 0.2mm and 0.4mm would cause the highest absorption losses.

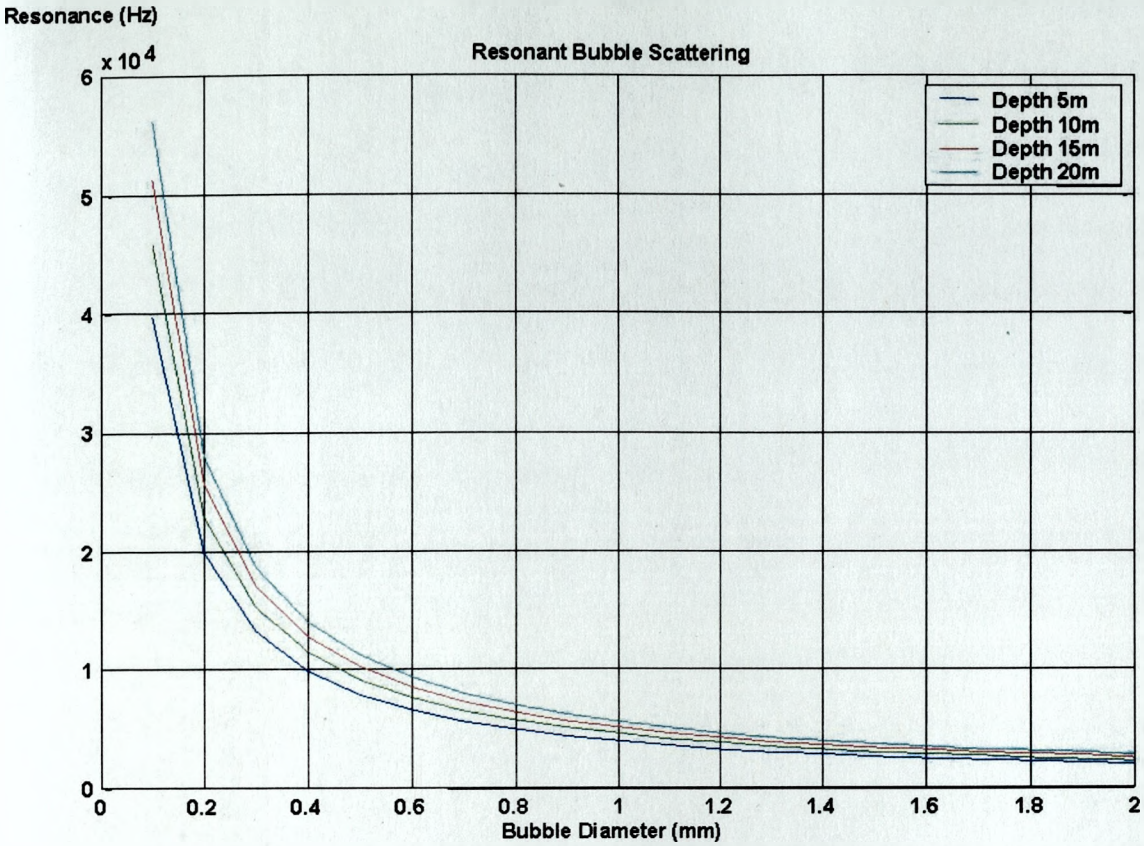

Notes

- Resonant bubbles effective cross sections increases 100-1000+ times
- Resonance frequency increases with depth
- Resonance frequency inversely proportional to bubble radius
- Bubbles resonant between 10-20kHz = 0.2-0.4mm radius

Figure 8: Bubble Resonance Frequency vs. Diameter

4.6.5 In highly aerated water significant attenuation, non-coherent scattering and dispersion occurs in the acoustic field and establishing reliable acoustic communications can be extremely difficult. This situation often occurs when attempting stern aspect acoustic communication from a surface vessel. In this scenario the significant eigenrays from transmitter to receiver would be those with large launch angles from the horizontal since direct and surface rays would be heavily attenuated. These significant rays would incur large bottom losses during bottom interaction by virtue of the large grazing angles and the numerous surface bottom interactions.

4.7 Acoustic Absorption

4.7.1 Acoustic absorption, i.e. the loss of acoustic energy to heat, is a significant loss mechanism that increases with frequency. Whilst absorption is primarily frequency dependent, temperature, pressure, salinity and acidity levels all influence loss. A most notable example is the influence of salinity. In the Baltic for example reduced salinity potentially enables the use of higher frequencies compared to open ocean. Differences between the acoustic absorption coefficient across a wideband transmission can lead to significant differences in the attenuation across the transmission bandwidth. A simplified expression for frequency (f in kHz) dependence of acoustic absorption is given by [7]

$$\alpha = 3.3x10^{-3} + \frac{0.11f^2}{1+f^2} + \frac{44f^2}{4100+f^2} + 3.0x10^{-4}f^2 \qquad (dB/km) \qquad \textit{Eqn 6}$$

4.7.2 This function is plotted in Figure 9. The graphs clearly demonstrate that a wideband transmission will undergo varying levels of attenuation due to differences in the absorption coefficient across the transmission bandwidth. For example, the acoustic absorption at 8 and 16 kHz is 0.81 and 2.77dB/km respectively. Table 3 depicts differential attenuation in dB at the band edges of this transmission at 1, 5 and 10km

range. The table indicates that differential absorption is likely to be evident at ranges in excess of 1km and problematic at ranges in excess of 5km. At 10km almost 20dB difference in absorption loss occurs between the band edges. At a receiver, equalising such a transmission would result in appreciable noise enhancement at the higher frequencies resulting in degraded performance. Wider operational bandwidths would lead to greater differences at comparable frequencies. The most obvious solution to this problem is to pre-emphasise the transmitted signal. Automating such a technique would require explicit channel sounding between communicating parties in order to determine an exact pre-emphasis transfer function. A simpler solution would be a short range/long range, pre-emphasis mode. This is discussed in subsequent sections.

Range	Diff. Attenuation (dB)
1km	1.96
5km	9.8
10km	19.6

Notes

- Acoustic absorption across the band becomes significant at ranges 5-10km
- Problem scales with bandwidth ... Pre-emphasis.

Table 3; Difference in attenuation at the band edges of a wideband transmission between 8-16kHz.

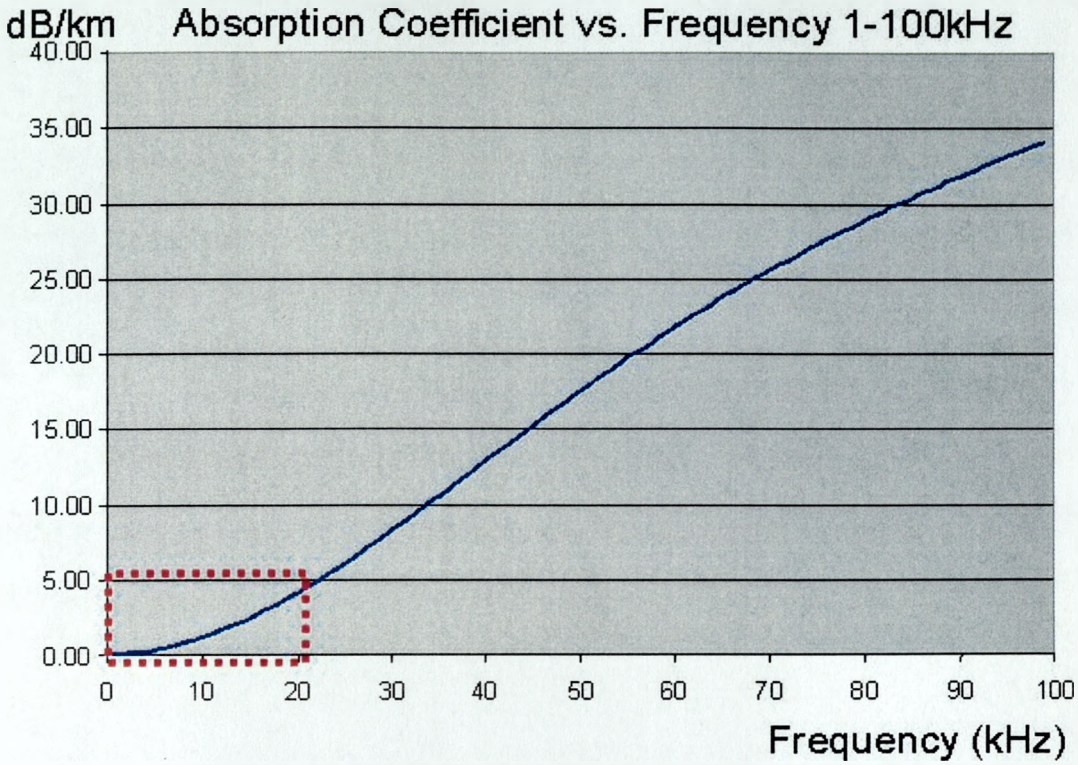

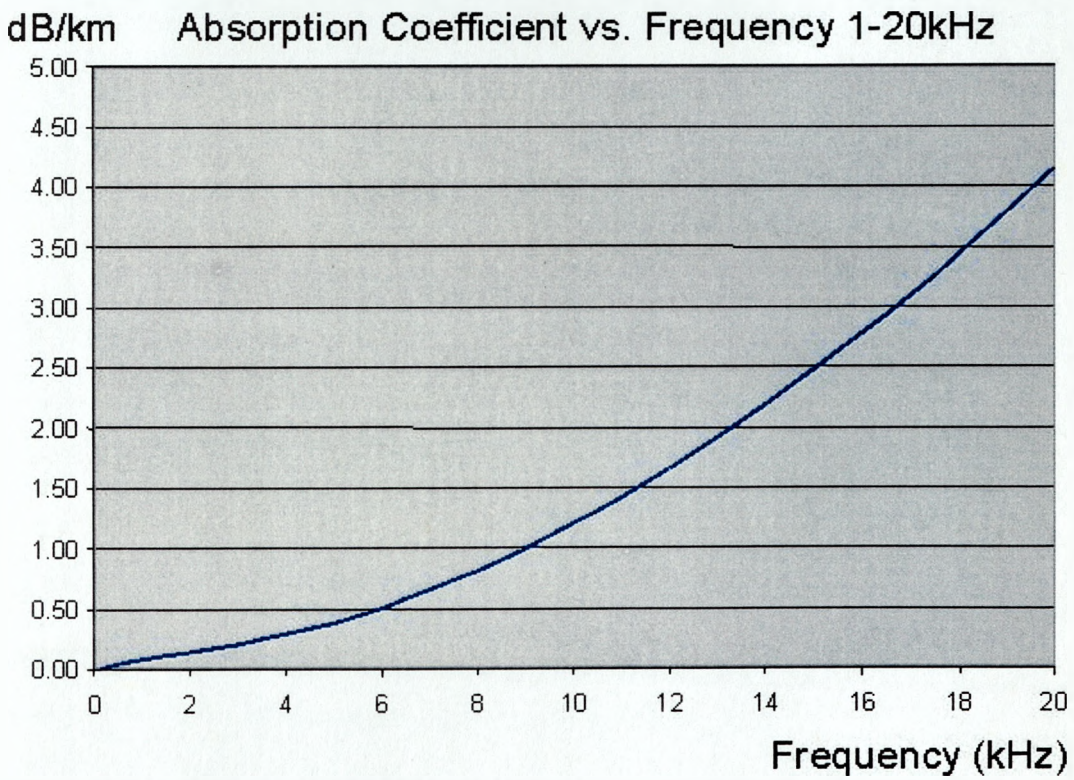

Figure 9; Absorption versus frequency (Top) 1-100kHz (Bottom) 1-20kHz

4.8 Discussion

4.8.1 In this section several aspects of acoustic signal propagation and interaction with the environment have been reviewed. The underlying aim has been to identify and discuss the key mechanisms responsible for signal coherence degradation. The aim has not been to develop rigorous arguments and theory relating to the underwater signal coherence problem, but to develop some of the more general issues raised by several authors in section 3 regarding the temporal and Doppler spread characteristics of underwater acoustic channels. In the next section the signal coherence issue is taken a step further by considering the problem of characterising and modelling an acoustic channel.

'Where observation is concerned, chance favours only the prepared mind',

Louis Pasteur, Address at the University of Lille December 1854

5 CHANNEL CHARACTERISATION AND MODELLING

5.1 Preamble

5.1.1 In section 3, the coherence characteristics of acoustic signals measured by several researchers was presented and discussed. It was highlighted that the temporal, frequency and spatial coherence characteristics of acoustic signals are profoundly influenced by both systematic and environmental factors.

5.1.2 In section 4, several key physical mechanisms responsible for degrading signal coherence were defined and discussed. These included multipath, Doppler, surface wave scattering, bottom loss and water aeration scattering.

5.1.3 Thus far, there has been no attempt to reconcile observed signal coherence characteristics with actual channel behaviour. Channel characterisation, has been extensively studied in the RF fraternity. Kailath, Bello and Root [57-63] for example, established the basis for the channel characterisation techniques used today. A more comprehensive review of channel characterisation theory and its role in understanding the acoustic channel is presented in appendix A. This also provides an historical perspective on the channel characterisation problem and develops the interrelationship between the time varying impulse response, transfer function, scattering function and bifrequency functions. Each of these functions provides information on the channel characteristics.

5.1.4 The gross characterisation of an environment based purely on the received signal statistics provides little understanding to the physical mechanisms responsible for coherence

degradation. In this section, a closer link between channel behaviour and signal coherence is developed. Techniques to measure and characterise the channel are discussed, including how these characteristics influence the coherence of the received signal field. This discussion is then further developed to address the problem of how one effectively models acoustic channel behaviour with a view to assessing candidate receiver algorithms.

5.1.5 In order to emphasise several of the key issues raised in the section, two data sets are initially presented. A low frequency data set is used to demonstrate the use of channel characterisation functions in defining channel behaviour. A high frequency data set is used to demonstrate the influence of channel geometry on channel complexity by comparing short and medium range channel sounding measurements. These results technically underpin the subsequent discussion on channel characterisation and modelling techniques developed later in the section.

5.2 Shallow Water Characterisation at 500Hz-1.5kHz

5.2.1 The following data set and discussion relates to data collected during shallow water trials off the Northwest coast of Italy during September 1995. The results presented are based on continuous PRN channel sounding of a 200m deep channel featuring a soft bottom and an isothermal layer at down to 30m. A towed transducer comprising two staggered, flooded rings provided a 3dB bandwidth between 500Hz and 1500Hz. The towing platform, RV Alliance described an offset circular manoeuvre at a range of 3.6km from a bottom moored vertical line receive array. Acoustic data from the array was received via a RF link inboard. Channel data from two hydrophones was recorded and analysed offline.

5.2.2 Figure 10 shows the channel characterisation functions and example impulse responses for this channel. The upper group of four graphs depict the channel characterisation functions as follows:-

- Top Left : Time varying channel impulse magnitude response

  - the channel impulse response demonstrates two stable, clearly resolved paths and at least five paths which are less stable and less clearly defined.

- Top Right: Time varying channel magnitude transfer function

  - the channel magnitude transfer function demonstrates deep fades due to the two significant paths. However the intermittent path arrivals lead to more complex structure over the observation interval.

- Bottom Left: Channel Spreading Function

  - the channel spreading function provides a measure of the delay/phase fluctuation of path arrivals. It is evident that there is notable variation in Doppler spread between arrivals. The two significant arrivals demonstrate modest Doppler spread of approximately 0.1Hz.

- Bottom Right: Channel Bifrequency Function

  - the channel bifrequency function demonstrates the temporal variability of the channel as a function of frequency. The inherent structure reflects the results from both the channel transfer function and spreading function. As the function is unnormalised in the frequency axis it is difficult to directly compare the Doppler spread as a function of frequency.

5.2.3 In Figure 11 the magnitude and phase trajectories of each of three rays A, B and C are labelled. These plots were generated by synchronising to each of the rays, and applying a delay lock loop in order to track delay fluctuations. The graphs demonstrate the magnitude and delay behaviour of each ray as follows

- Top: This image depicts the channel time varying magnitude response over a ten second window depicting two significant rays B,C and one of the less stable arrivals ,A.

- Middle Left: This graph shows the relative magnitudes of each of the path arrivals tracked over the ten second observation window. For this low frequency application the magnitudes are relatively stable and consistent over the observation period.

- Middle Right: This graph shows the ray phase trajectories over a 100s+ observation interval. The spatial scale based on 1kHz carrier is 1radian = 0.238m. For each ray it is evident that the trajectories are not equivalent indicating the change in channel geometry over the observation interval. An alternative view is that each ray is subject to different Doppler.

- Bottom Right: This graph considers a 20second observation interval from T+40 to T=60s in the coarse phase track graph. In this case the mean Doppler is removed from the data to allow comparison of the shorter timescale phase fluctuations on each ray. It is evident that each ray is subject to phase fluctuations. Ray B and C are subject to two scales of phase fluctuations. Both are subject to a long timescale phase variation on a spatial scale 1-2radians (25-50cm) and temporal scale 4-6s. Superimposed on the long timescale variations are much more rapid phase fluctuations on a spatial scale of 0.25radians (5cm). Ray C demonstrates the same long timescale variability however the short term phase fluctuations are much more dynamic. This is due primarily to the lower signal-to-noise on this path arrival which impacts on the DLL tracking performance

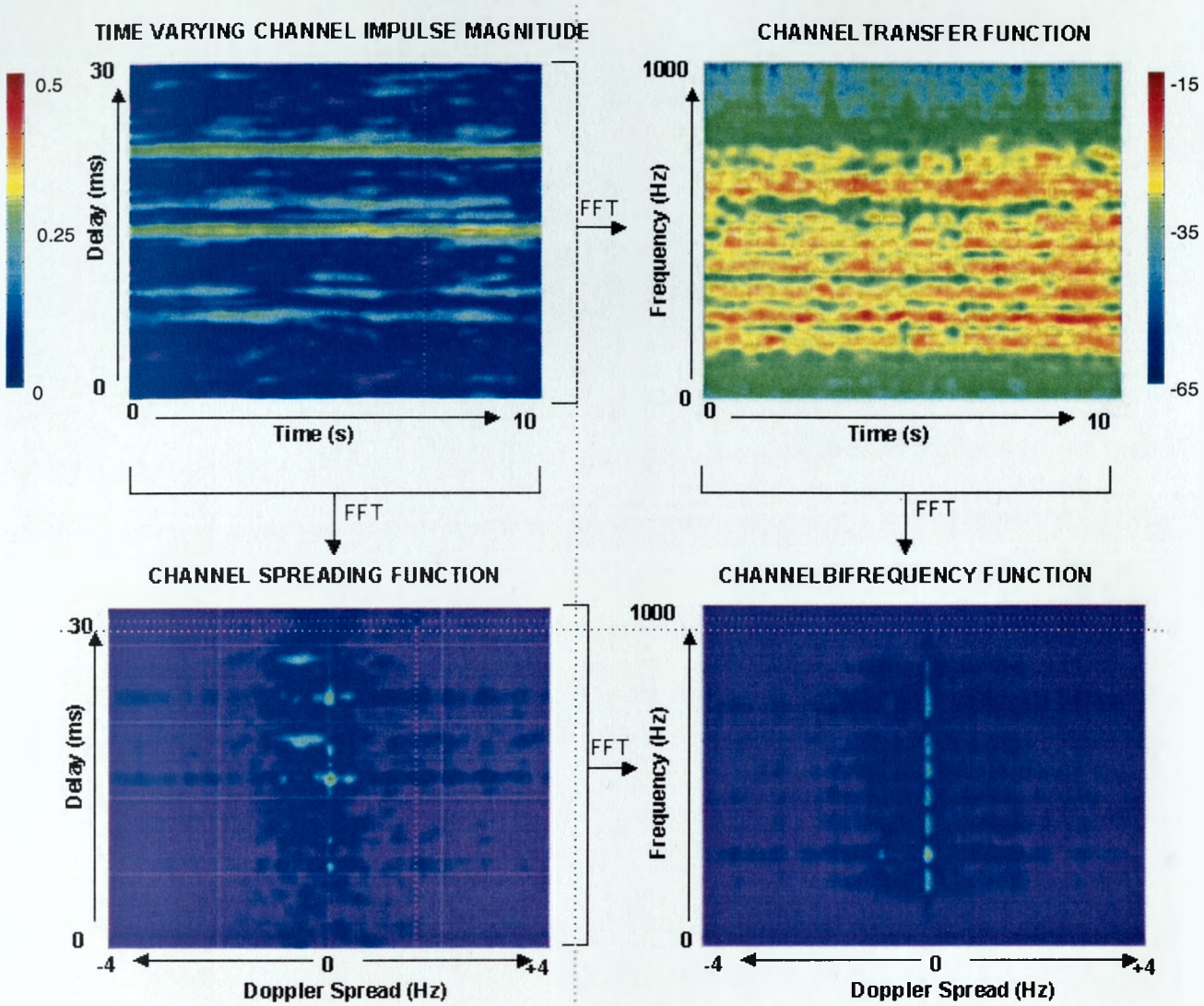

Notes

- Time varying channel impulse response (Top Left) shows two significant path
- Delay spread of channel of the order 10ms (Top Left)
- Channel transfer function exhibits deep, variable nulls (Top right)
- Spreading function indicates modest (1Hz) Doppler spread (Bottom Left)

Figure 10 Channel Characterisation Functions for PRN based channel Sounding at 500-1500Hz, 200m water depth, range 3.6km

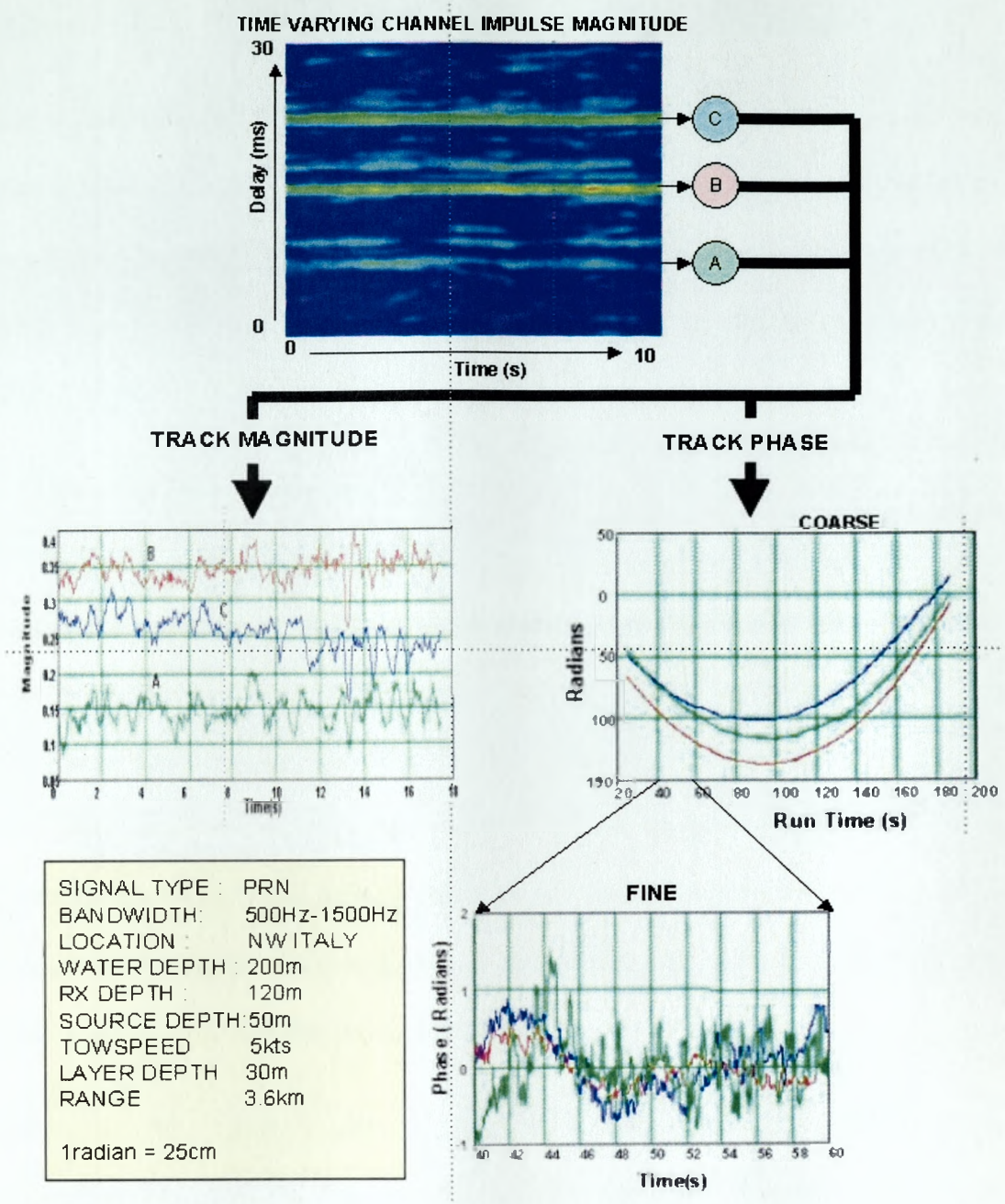

Notes

- Magnitudes relatively stable
- Coarse phase evolution demonstrates different range rates(differential Doppler)
- Phases extremely stable. Phase variance increases with reduced SNR.

Figure 11: Magnitude and Phase Tracking using 500-1500Hz PRN channel sounding.

5.3 Short Range vs Medium Range High frequency Channel Measurements

5.3.1 The importance of channel geometry, surface-bottom scattering loss and bottom loss was discussed in sections 3 and 4. Specifically it was noted that the temporal spread of the acoustic channel is often more severe at short range rather than longer range at high frequencies due to the importance of surface and bottom loss mechanisms and their dependence on grazing angle.

5.3.2 Figure 12 shows evolved channel soundings conducted at 400m and 1200m in a shallow water channel 30m deep, comprising a sandy-rocky bottom. The soundings were based on a 21ms chirp between 10-20kHz repeated at approximately 1s intervals. Transmitter and receiver were approximately mid-water. The 400m results (top) demonstrate a temporal spread equivalent to 3m and it is evident that the field temporal coherence is relatively poor due to the relative motion between transmitter and receiver of approximately 4knots (removed prior to processing). The 1200m results (bottom) show a temporal spread equivalent to 1m and that the field coherence is good. Specifically, the direct path is particularly well resolved and stable.

5.3.3 Also shown are the waterfall plots for the two transmissions. The results, which essentially show the time varying channel transfer function, demonstrate frequency selective fading typical of multipath channels. It is interesting to note that the fade depth in the shorter range channel is less than that for the longer range channel due to the more complex path structure. In the longer range channel the two first path arrivals result in the deep, time varying fades shown in the bottom right graph.

5.3.4 Figure 13 shows consecutive channel soundings at 400m demonstrating the complex path structure and more importantly the dynamic variability of the path structure over the 3 second observation interval. In particular it is evident that whilst paths delays are stable,

the path magnitudes are subject to significant variability. These results demonstrate that the channel sounding only provides a 'snapshot' of the highly dynamic, time varying channel estimate. It underlines the need to rapidly sample the channel to track its fluctuations and points to the need for 'closed loop' techniques to cope with channel variability during decoding. Figure 14 shows consecutive channel soundings at 1200m, which demonstrate the greater stability of this channel. This is a consequence of the increased range. Here platform heave dynamics have a less pronounced effect on the temporal coherence of the received field.

5.3.5 Figure 15 depicts the delay and magnitude of individually resolved paths based on channel sounding measurements taken in the 10 to 20kHz band. The results demonstrate a dynamic interchange in ray path magnitudes over the ten second observation interval. The path arrivals times are, in contrast, remarkably stable, with significant variability occurring on a time scale on the order of a few fractions of a second maximum.

5.3.6 Figure 16 shows the spatial relationship of correlation's obtained using an 8-16kHz LFM chirp received on an 8 element vertical line array receiver with λ spaced elements. The figure demonstrates a high degree of coherence for the direct path, however other paths exhibit greater spatial variability.

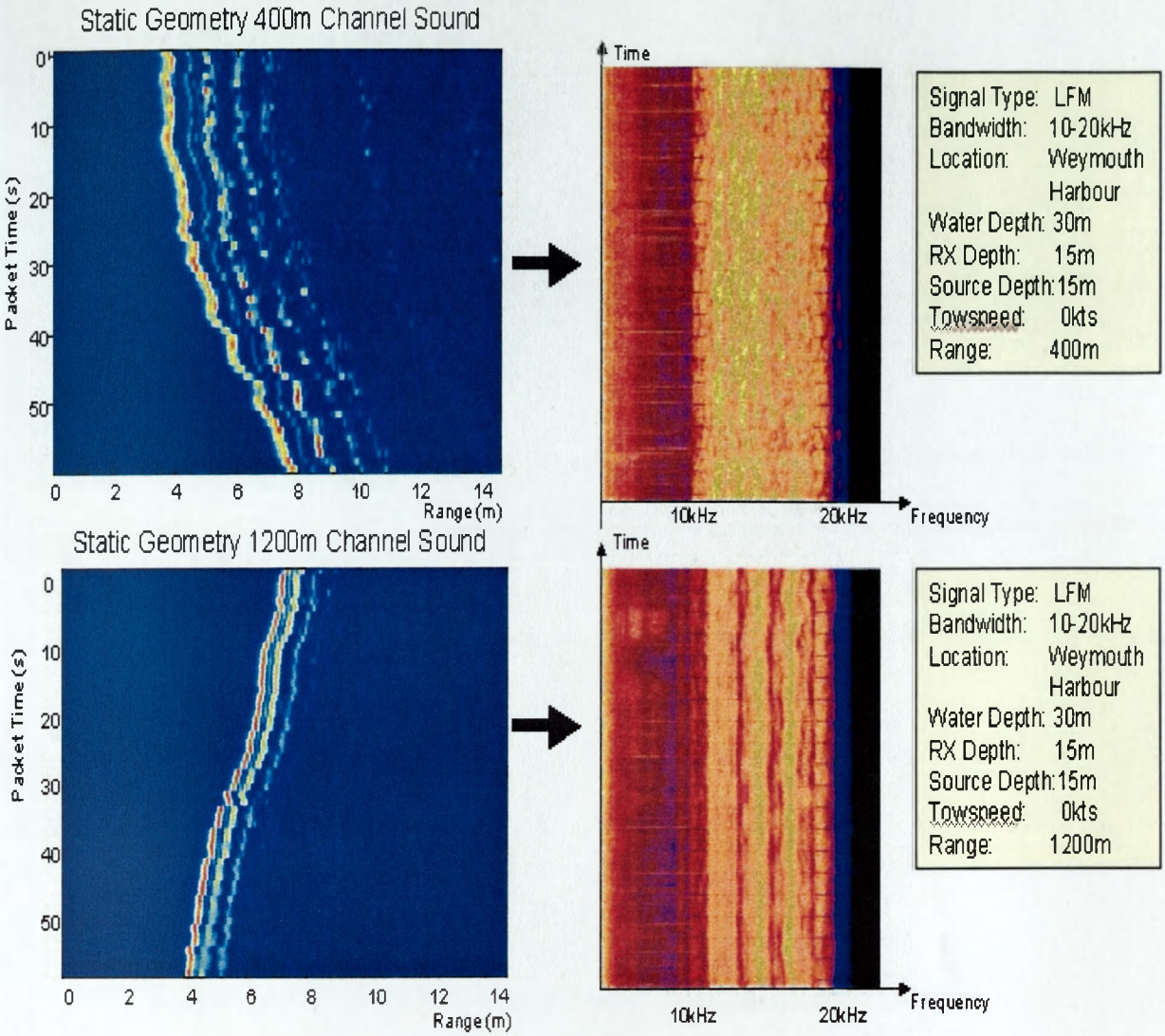

Notes

- Short Range Channel has longer time spread than medium range channel
- Short Range Channel paths rapidly time varying in magnitude
- Short Range Channel has more path arrivals
- Both channel demonstrate medium duration temporal variability
- Short range channel frequency nulls closer spaced and more dynamic
- Medium Range channel nulls clear defined. Path delay variability demonstrated

Figure 12: Short Range (400m) vs Medium Range (1200m) Ensemble Channel Measurements using chirp sounding between 10-20kHz

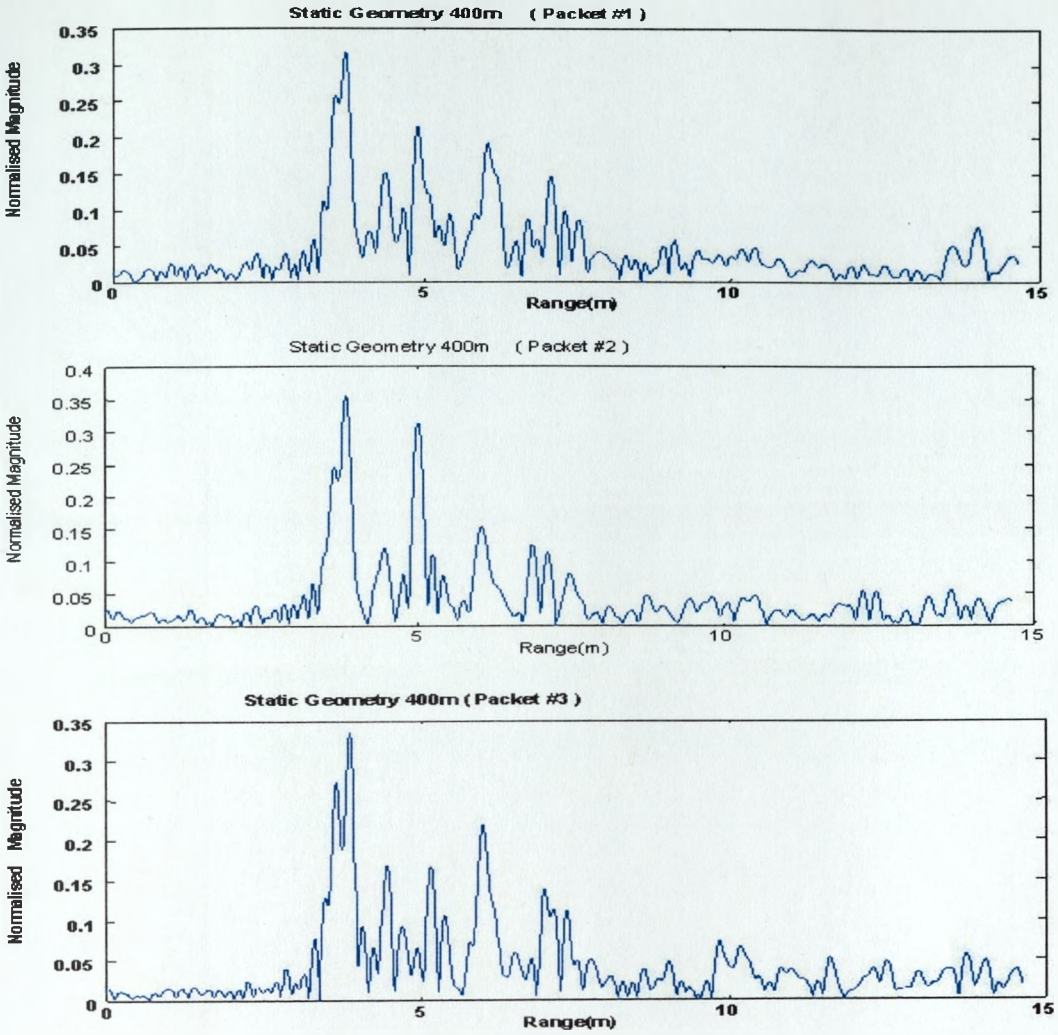

Notes

- Short range channel path structure exhibits in excess of 10 paths
- Transmission bandwidth resolves most (not all) resolving paths
- Short range path magnitudes highly dynamic. Range spread 5m.
- First arrival not necessarily the largest
- Short range path delay relatively stable.

Figure 13: Consecutive Chirp Channel Estimates at 400m

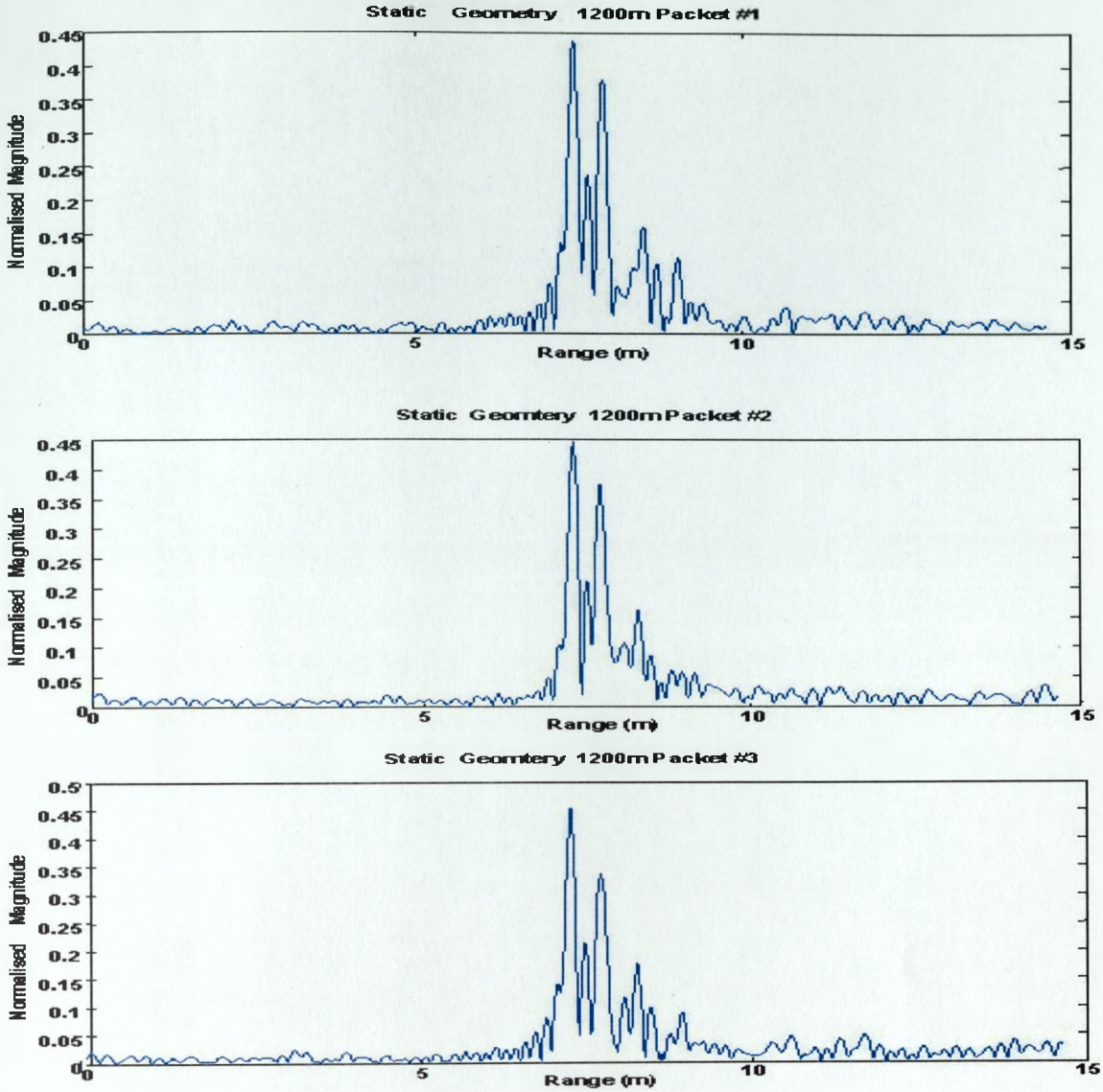

Notes

- Medium Range Channel path structure exhibits 5+ paths
- Transmission bandwidth resolves most (not all) paths
- Medium Range path magnitudes much more stable. First arrival largest
- Range spread 2-3m

Figure 14: Consecutive Chirp Channel Estimates at 1200m

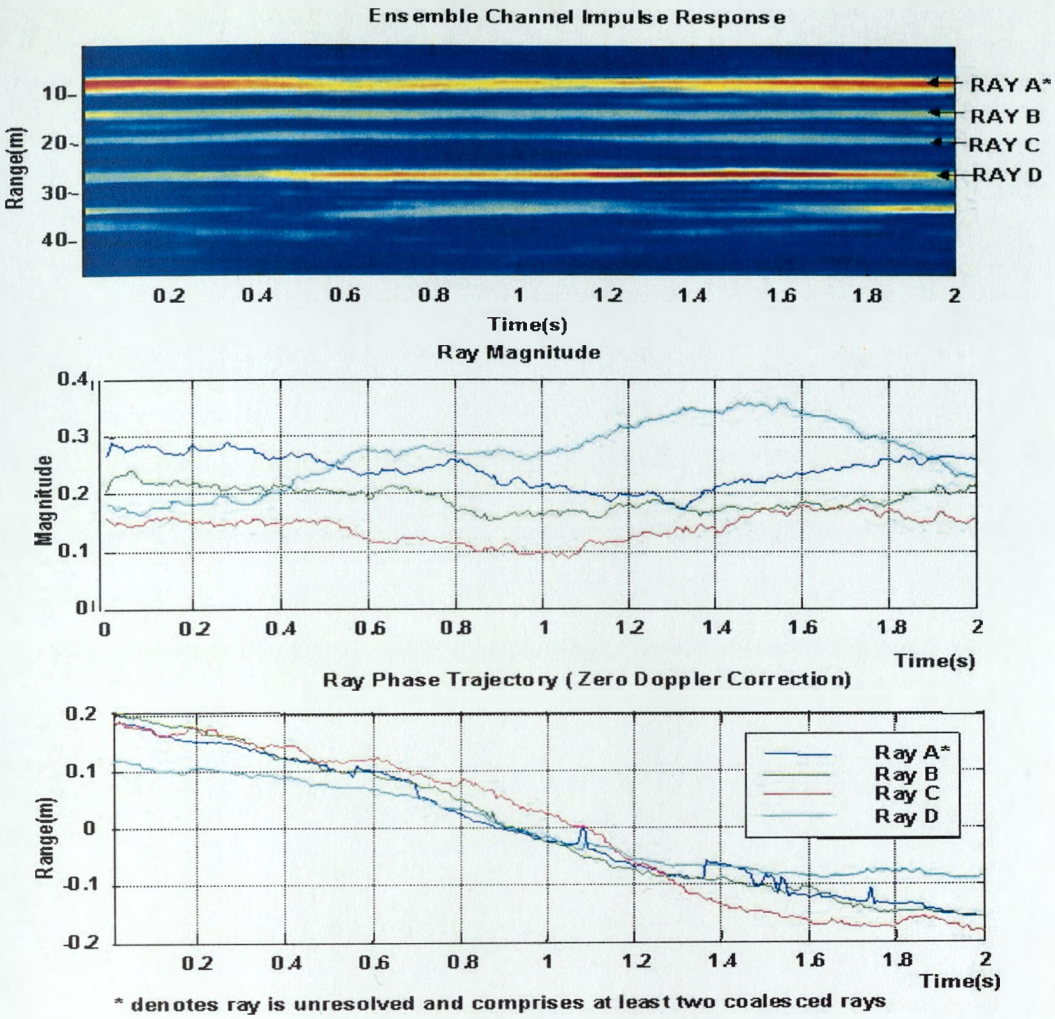

Notes

- Highly dynamic interchange in path magnitudes over 2s observation window
- First arrival largest at start and end of observation but not largest midway.
- Path phase/delay extremely stable, can be tracked to millimetric accuracy.
- Ray DLL tracking algorithm confused when rays are unresolved (Ray A)
- Rays demonstrate correlated delay variability over 10s observation interval

Figure 15 Magnitude and Phase Tracking using 10-20kHz PRN channel sounding.

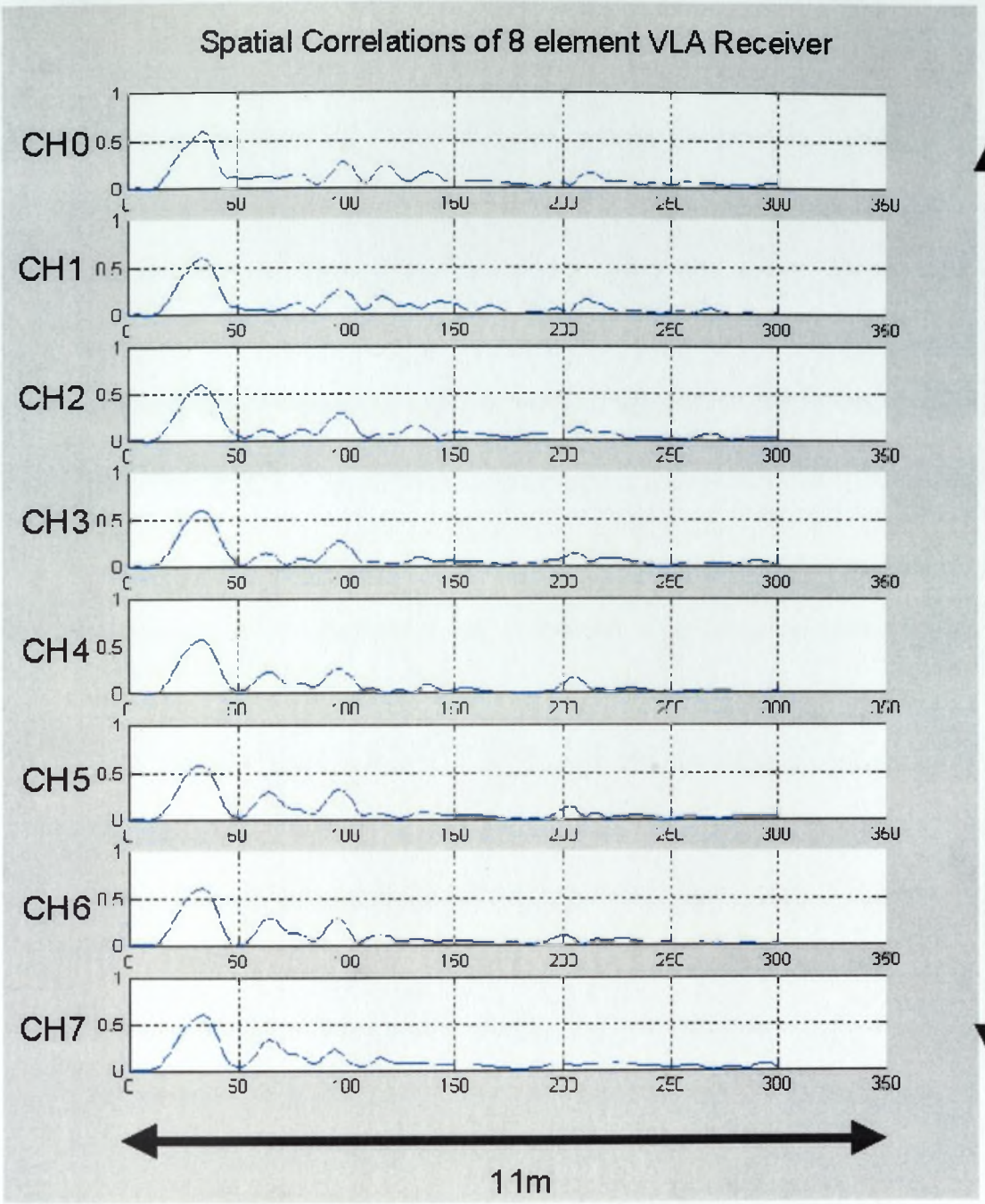

Figure 16 Spatial Correlations from 8 element vertical line array for shallow water channel in 8-16kHz band

5.4 Channel Characterisation and modelling

5.4.1 The preceding measurements have demonstrated the impact of the acoustic channel upon received signal coherence. The results have demonstrated the temporal smear attributable to both macropath and micropath and have shown how this impacts upon the frequency coherence of the received signal. It has also been shown that with sufficient bandwidth it is possible to resolve these paths and once resolved it is possible to track the dynamic magnitude and delay fluctuations which impact upon the temporal coherence of the received signal.

5.4.2 Channel characterisation provides a means to provide a quantitative basis for the assessment of the complexity of a channel as a communications medium. The time varying characteristics of many physical channels invariably raises a number of questions; 'how complex is the channel?', ' is channel A more complex than channel B ?','how can one optimise a signal design for a particular channel?'. Such considerations are particularly pressing in the underwater acoustic channel due to the degree and extent of the temporal and spatial variability, which is unlike any terrestrial channel. The measurement of channel characteristics, the interpretation of such characteristics and the development of a quantitative basis for signal design and modulation methodology are therefore important issues relevant to the underwater acoustic communications problem.

5.4.3 In the context of acoustic channel modelling, it is important that the model encompass those characteristics of the channel that influence acoustic communications system performance. Understanding what these characteristics are and how well suited particular models are to synthesising them is an important issue. For example, acoustic Doppler has been highlighted as a central issue in acoustic communications. However, many models attempt to model acoustic Doppler purely as a frequency translation effect rather than as a

temporal/spectral scaling effect. For example, established models for fading dispersive channels and their suitability to underwater acoustic channels is considered in appendix B.

5.4.4 Despite the vast literature available on acoustic modelling [64-72], there have been relatively few papers addressing acoustic modelling for communications system performance. Whilst there have been attempts to specifically model aspects of the acoustic environment such as the ocean surface in terms of channel scattering function [50-52], the vast majority of channel models for acoustic communications simulation are based on ray trace techniques [66-72] which offer computational simplicity and are inherently wideband. A more comprehensive review of these techniques is presented in appendix C.

5.4.5 Techniques to characterise an environment provide a means to better understand and ultimately model the environment. The acoustic channel modelling problem may be considered on two levels.

- Environment specific modelling
- Deterministic channel modelling

5.4.6 The former approach seeks to characterise the channel for a particular environment specified in terms of geometry, bathymetry, platform movement, topography etc. The latter approach seeks to specify the channel characteristics alone. This is a simpler approach to the modelling problem, however it does allow for greater control over channel behaviour during simulation studies. In ether case the channel model provides a quantitative basis for the assessment of acoustic receiver algorithms including synchronisation, equalisation, spatial processing, modulation techniques etc.

5.5 Simple Geometric Models

5.5.1 Geometric models, i.e. those which assume straight-line propagation are useful tools for quick look analysis of path structures at short range [66]. They are also useful in demonstrating the significant role of bottom and surface interactions on the received path structure and the effect of platform motion on individual ray Doppler [70]. In this section propagation through a bounded medium is investigated with a view to understanding the role of channel geometry, bottom type and sound velocity profile on received signal coherence. Simulations are presented to investigate the influence of channel geometry, bottom type and sound velocity profile on received signal coherence. The adopted approach is to begin with a simple geometric model to provide a quantitative basis for comparison with ray trace simulations using real sound velocity data. The parameters for the simulations were as follows

- Frequency 10000Hz
- Bottom types : sand and clay
- Spreading law 15logR
- Absorption 0.0015dB/m
- Number of Interactions 10
- Water Depth 50m and 200m
- TX depth 10m, RX Depth 25m and 100m

5.5.2 Figure 17 shows the simulated ray arrival structure at ranges from 0 to 5000m for water depths 200m (left) and 50m (right) for receiver at midwater. Immediately obvious from the figures is the large time spread between path arrivals at shorter ranges. At increased ranges the channel time spread reduces. Similarly, at shorter ranges the arrival angles of

paths will show greater spread than at longer ranges. The figure however does not convey the ray magnitudes associated with each path arrival. Since later rays are those which interact more times with the surface and bottom interfaces, they are subject to greater scattering and bottom losses. This is shown in Figure 18, which demonstrates the dramatic influence of these losses relative to spreading and absorption losses. The graphs are presented top to bottom spreading loss only, absorption loss, bottom-surface loss (sand). The results demonstrate that spreading loss is much more significant for this short-range case. However the ratio of direct path spreading loss to the spreading loss of the last arrival in the simulation is less than 10 to 1. If one considers the bottom-surface loss graph, the ratio between direct path loss and multipath loss increases significantly across all paths. The significance of this result is that the high incidence angle on paths at short range in deeper water, results in heavy losses which actually serve to reduce the complexity of the channel.

5.5.3 At longer ranges bottom losses are greatly reduced due to the reduced incidence angles such that for harder bottom types, rays which interact with the bottom only a few times are not attenuated. For soft bottom types all rays undergo attenuation. These results emphasise the importance of channel geometry and bottom type on acoustic communication performance. The range-depth ratio largely determines ray incidence angles on both surface and bottom. Although bottom loss has only been considered here, scattering losses are also strongly dependent on incidence and play a significant role in received field coherence.

5.5.4 A final point worth some consideration, is the role of the bottom when operational frequencies reduce. Specifically it was shown in section 4 that sound propagating in bottom media is subject to absorption losses that scale with frequency. At high frequencies these losses are sufficiently large as to allow bottom propagation to be ignored. At lower frequencies, geoacoustic propagation may occur and this will give rise to quite different path structures since propagation speeds in the denser media are higher than in water. Thus rays which undergo geoacoustic propagation may arrive before rays which propagate solely within the water column.

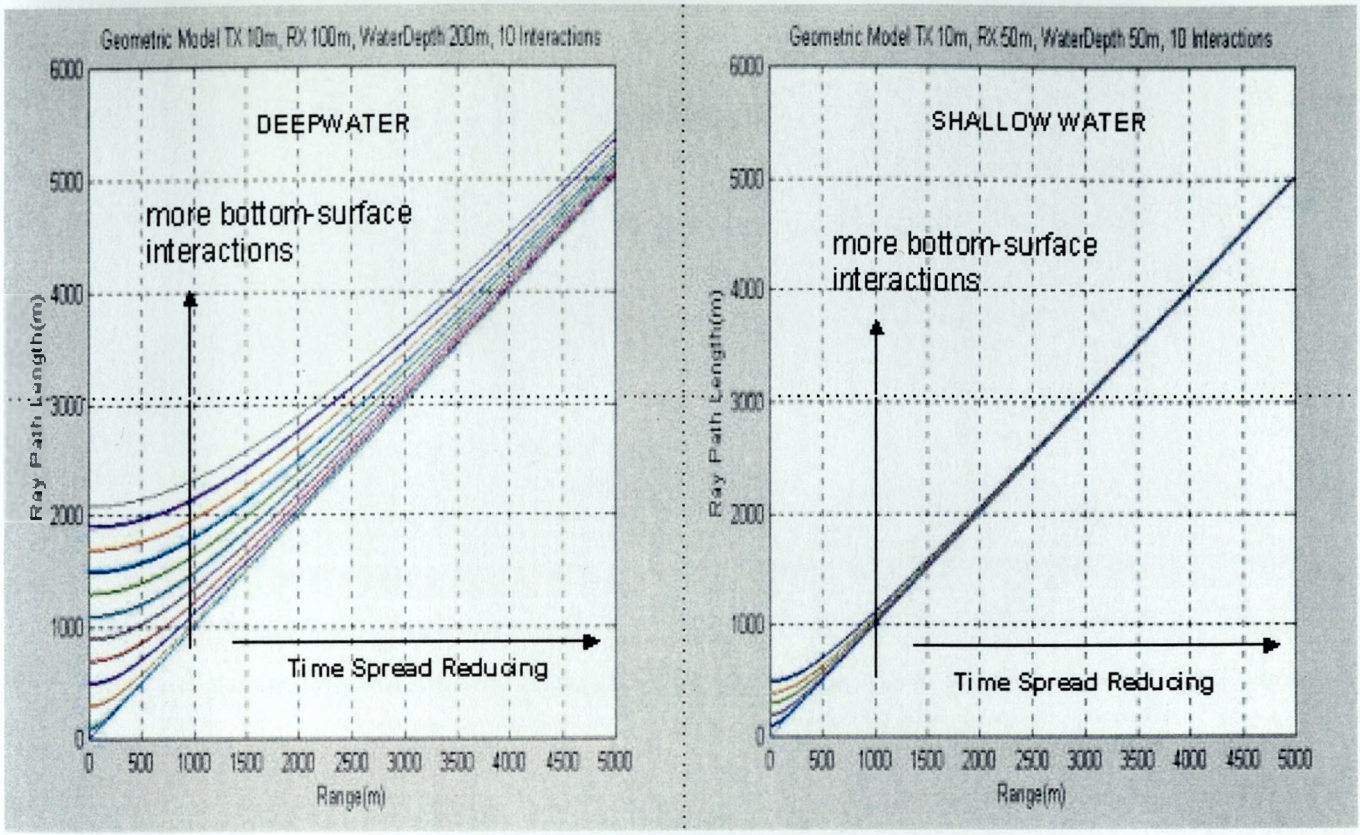

Notes

- Simple straight line propagation.
- Up to 10 bottom-surface interactions
- No account of bottom-surface interaction loss.
- Time spread greatest at short range
- Time spread greater for deep water channel
- Range evolution different between rays at short range = differential Doppler
- Large angular diversity @ short range. Small angular diversity @ long range.

Figure 17; Geometric Model Range vs Time Spread Deep (left) Shallow (Right)

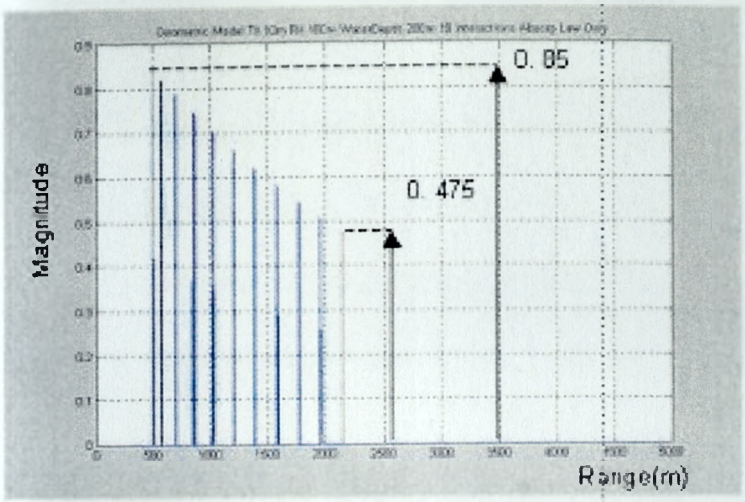

ABSORPTION LOSS

- Linear Scale
- Negligible multipath attn.

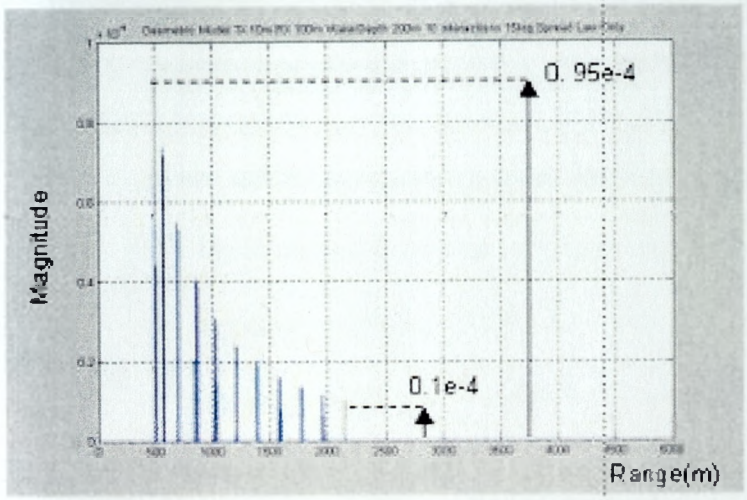

SPREAD LOSS

- Linear scale
- Modest multipath attn.

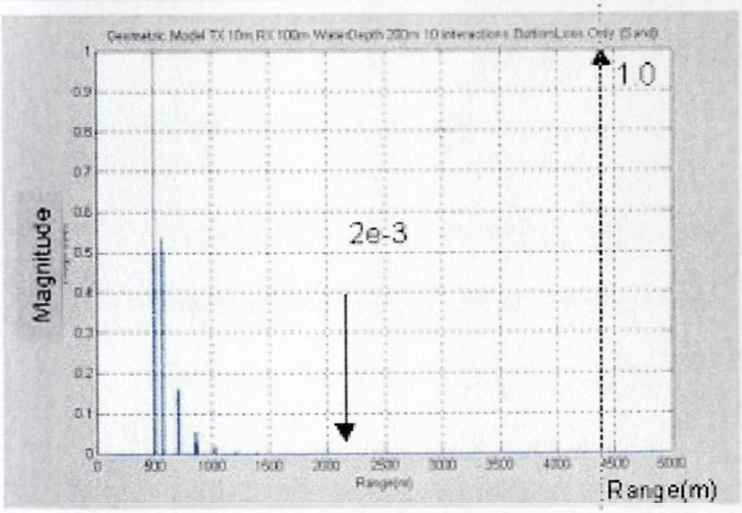

BOTTOM/SURFACE LOSS

- Linear scale
- Significant multipath attn.
- Ray 'stripping'

- TX Depth 10m
- RX Depth 100m
- Water Depth 200m
- Sandy Bottom
- TX-RX Separation 500m

Figure 18: Geometric Model Losses vs Range

5.6 A simple Ray Tracing Model

5.6.1 Whilst geometrical models are useful tools for quick look analysis, the utility of such models in 'real' ocean environments where significant ray refraction occurs is limited. In the context of acoustic communications system design, performance prediction and environmental modelling are important tools for optimising overall system performance. Indeed one could argue that such tools should form a highly integrated part of any acoustic communications system in order to determine optimum ranges and depths for specific environments [67].

5.6.2 There are many techniques to solve the full acoustic wave equation [7], however simple ray trace methods provide a means to provide an intuitive, quick look analysis of real propagation problems. Whilst ray tracing is a more complex simulation method compared to simple geometrical models it is more representative of 'real' acoustic propagation behaviour. In particular, it provides more meaningful information on transmission loss and signal coherence in strongly refracting environments where multiple bottom and/or surface interactions occur.

5.6.3 Formal mathematical derivation based on a ray series solution of the Helmholtz equation results in the series of equations known as the Eikonal equation and transport equations which may in turn be reduced to ordinary differential equations soluble using either Euler or Runge-Kutta numerical methods.

5.6.4 A less formal approach which is intuitively simple and easy to program is to exploit an important result of ray theory. Snells law states that for a ray transiting the interface between two layers with different propagation speeds $c_1, c_2, ..$ the incidence angles $\vartheta_1, \vartheta_2, ..$ are related to the sound velocities by

$$\frac{\cos\vartheta_1}{c_1} = \frac{\cos\vartheta_2}{c_2} \qquad \textit{Eqn 7}$$

5.6.5 This simple relationship forms the basis of most ray trace programs. Despite its simplicity, this ray propagation model provides a means to estimate the channel characteristics for a specified environment. In particular the model extends the geometric model functionality by accommodating ray refraction. This is a significant propagation issue since the degree to which a propagating signal interacts with both the surface and bottom will be profoundly influenced by the sound velocity profile of the medium.

5.6.6 A simple ray trace model based on the above model was developed which assumed a piecewise linear sound speed profile with intermediate results obtained by linear interpolation. As each ray propagates interactions with bottom and or surface incur scattering losses. These are computed based on empirical models such as those in appendix D. The main parameter for each interaction is the ray-grazing angle. As each ray is traced, propagation time is computed based on an average sound speed over the incremental distance. At each step a check is made as to whether the ray passes the receiver point using a simple depth bracketing and fine search algorithm. Each successful eigenray is stored along with its propagation distance, total surface losses, total bottom losses and arrival angle.

5.6.7 Whilst it is not intended to provide an exhaustive study of ocean propagation modelling here it is useful to consider a single scenario in order to underpin some of the issues raised in the opening literature survey regarding signal coherence such as geometry, range, beamwidths, thermal microstructure and spatial processing.

5.6.8 Figure 19 depicts a strongly refracting environment typical of the Baltic in the winter.

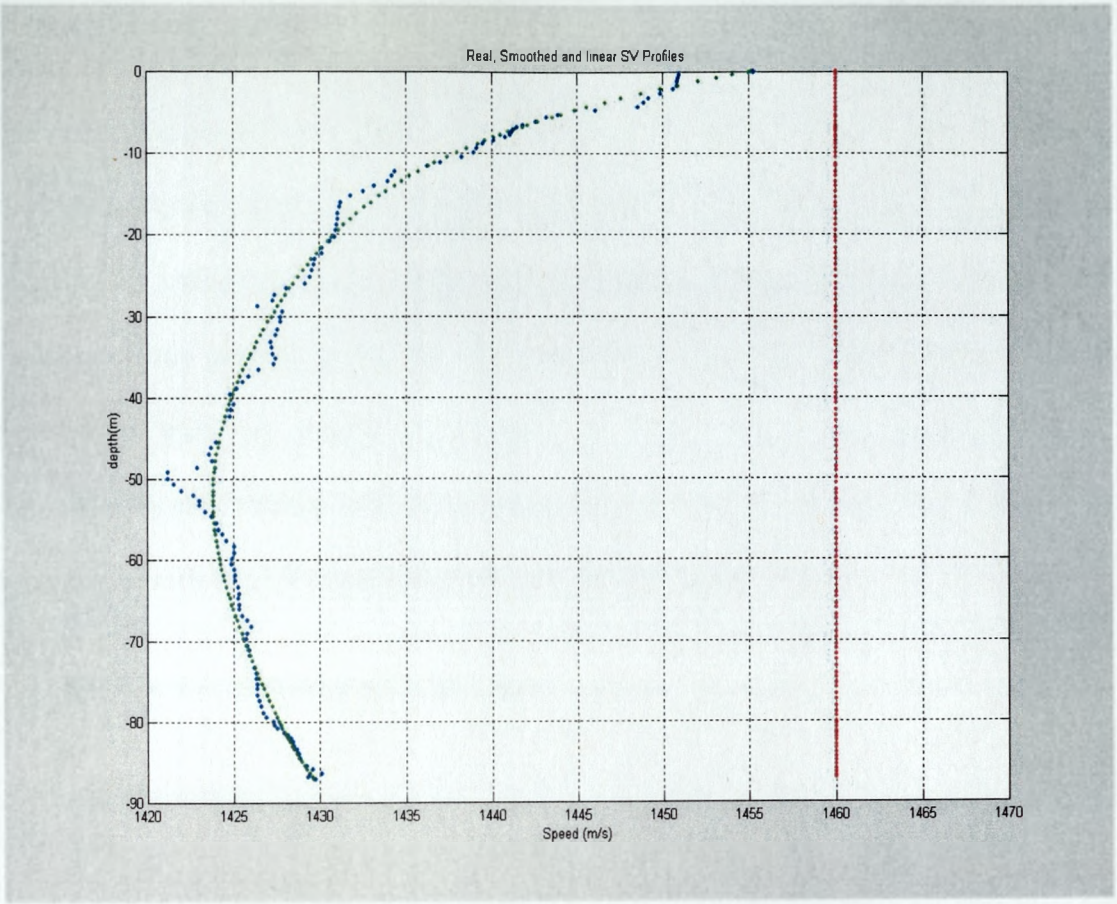

Figure 19: SV Profiles: Actual, Smoothed and Linear Profiles

5.6.9 The figure shows three profiles

- A linear constant profile at c=1460m/s;
- Actual SV profile demonstrating appreciable microstructure;
- Least Squares smoothed SV profile.

5.6.10 A number of simulations were performed to compute the channel characteristics as a function of range for each SV structure. For each case the simulation parameters were

- TX depth 5m
- RX depth 55m
- Water Depth 65m

- Ray Launch Angles –20 to +20 deg

5.6.11 The geometric model discussed earlier was used to provide a reference/sanity case. Figure 20 depicts the multipath arrival structure based on geometric and ray trace models for the linear sound speed profile c=1460m/s. The simulation is shown for ranges 250m to 900m. Three main ray groupings are shown. These groupings relate to the number of interface interactions each ray family undergoes. The first four arrivals correspond to direct, surface reflection, bottom and surface-bottom reflections. Subsequent groupings relate to ray arrivals with two or more surface/bottom interactions.

5.6.12 The simulation demonstrate several issues

- Good agreement between ray and geometric models for this simple case.
- Reduction in path delay spread with range
- Higher order ray families evident at increased range due to ray launch limit.

5.6.13 Figure 21 depicts the ray trace plots at four ranges denoted A,B,C,D. These ray traces serve as a reference to explain channel behaviour at several ranges of interest. Since the environment is strongly downwardly refracting down to 50m, then limiting cases are encountered whereby rays launched toward the surface will eventually coalesce with surface reflected rays. At this limiting point further opening of range results in the respective rays no longer being eigenrays and so are lost. In this case the next shortest path length eigenray is adopted as the reference for the remaining eigenrays. These results clearly demonstrate the significant role refraction plays in the received signal coherence. For example the simulation demonstrates that a receiver cannot rely on a direct path arrival for ranges exceeding 430m. It also shows that a receiver attempting to synchronise on a limiting ray is likely to experience difficulties if the ray is lost in dynamic scenarios.

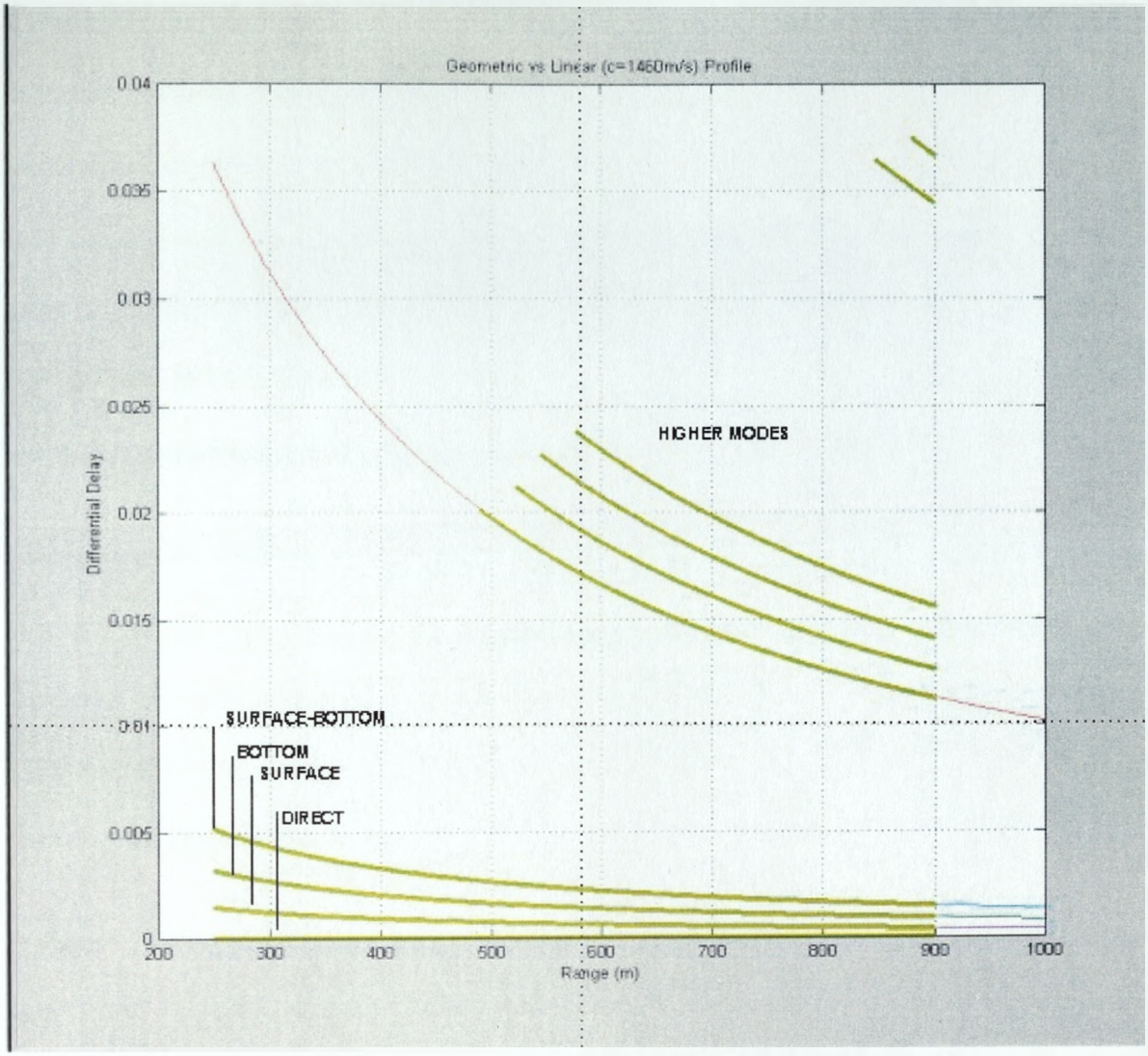

Notes

- Agreement between geometric and ray trace algorithms for linear profile case
- Delays referenced to first (direct) arrival
- Higher order ray families evident at increased range due to ray launch angle limit.
- Short ranges demonstrate longer time spreads

Figure 20: Raytrace Linear Profile Vs Geometric

5.6.14 Clearly this simulation represents a somewhat synthetic SV profile and this results in the somewhat dramatic discontinuities at 425 and 550m. In practice it is likely that the microstructure of the true SV profile would tend to 'blur' the transition to different ray families and would also introduce greater variability in the path arrival times. Figure 22 depicts the same ray trace simulation conducted with the smoothed (top) and unsmoothed SV profiles. Whilst the result is broadly similar to the linear SV case the influence of thermal macrostructure and microstructure is clearly evident

5.6.15 The path delay structure significantly differs from the linear/geometric case previously. Not only do the rays demonstrate markedly different trajectories as the simulation range increases but also at specific ranges rays are entirely lost due to the refraction process. This occurs at approximately 425m and 550m. The reason for this may be deduced from the ray trace plots in figure 21.

5.6.16 In figure 22 the transition between the surface and bottom reflected paths between 380m and 550m is less well pronounced. Indeed the results suggest that the surface reflected/refracted path persists over this range interval. This is most likely due to the fact that the unsmoothed SV trace exhibits a relatively constant speed in the first 2-3m whereas the smoothed profile results in a fixed rate of sound speed change over the same depth. Beyond 380m the rays show discontinuities which suggest a more gradual transition between ray families at 500m and onwards. Figure 23 depicts ray arrival angle versus range for linear, smoothed and unsmoothed SV profiles. The general trend toward broadside is evident in all cases. For refracted cases it is also evident that the arrival angles are generally greater by virtue of the downwardly refracting profile.

5.6.17 In the context of acoustic communications the preceding simulations have indicated several important factors relating to the performance of a high data rate link. Most

importantly the results have emphasised the important role of channel geometry, bathymetry, bottom and surface scattering losses on signal coherence. Results from both ray trace and geometric models have indicated the potential for short range channels to prove particularly difficult by virtue of the greater time spreads at short range and the reduced scattering losses on higher order ray families.

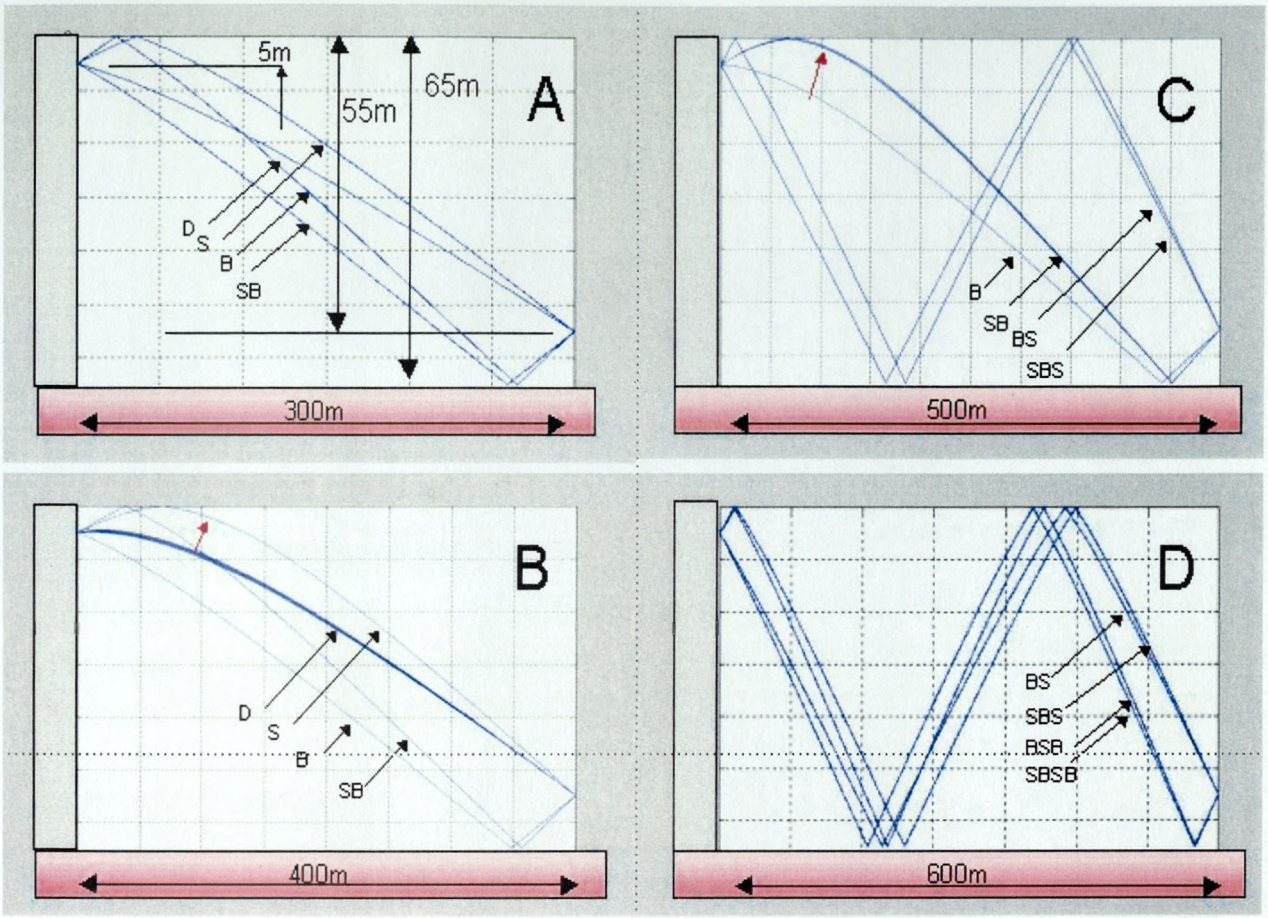

Notes

- D=direct, S=surface reflection, B=bottom reflection
- Path arrival structure notably different to geometric case
- From 250m to 450m D moves to coalesce with S.
- At 425m S limiting ray lost. B ray now first arrival.
- From 425m to 550m B moves to coalesce with SB.
- At 550m B limiting ray lost. BS ray now first arrival.
- Microstructure prevents limiting ray transition at 425m.
- Microstructure 'blurs' path transitions

Figure 21; Ray traces at positions A,B,C,D

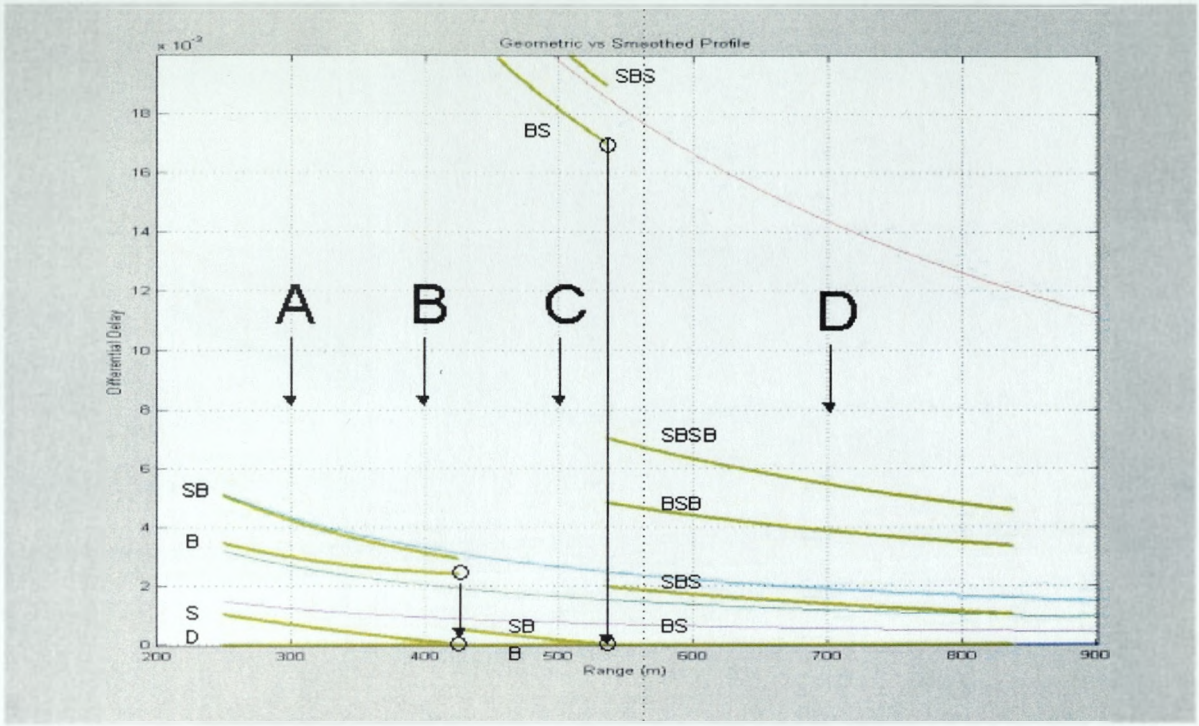

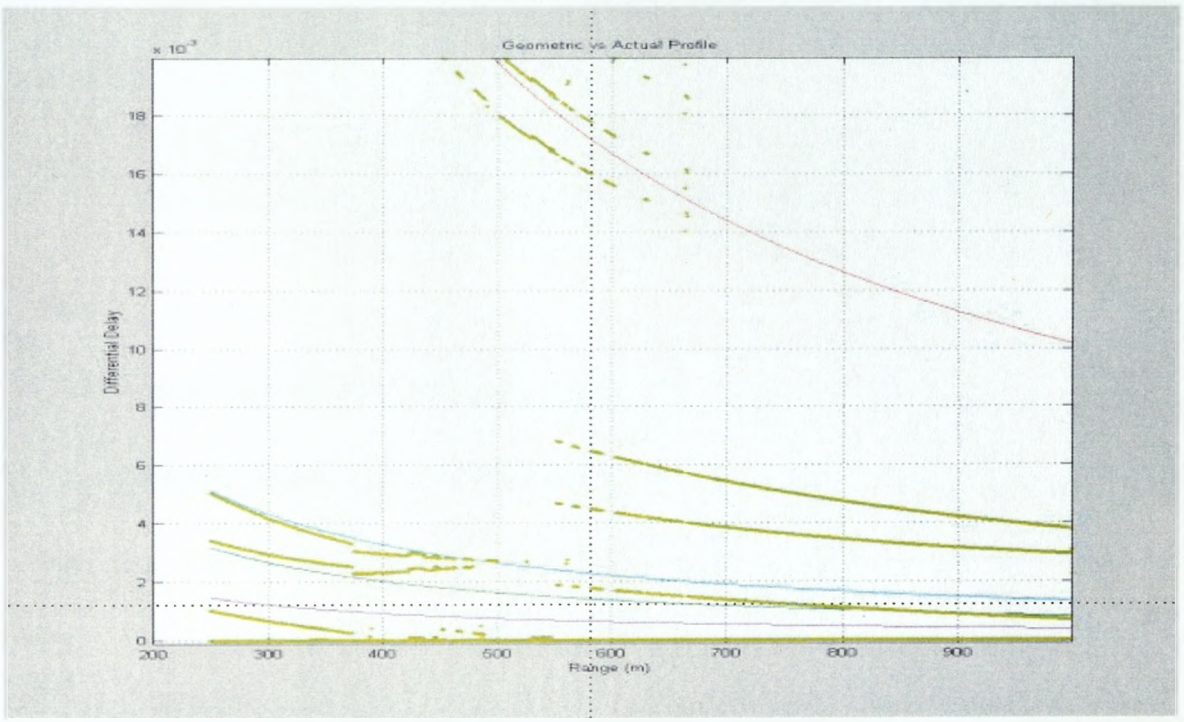

- Smoothed SV profile demonstrates distinct transition to higher modes with range
- Unsmoothed SV profile demonstrates 'blurred' transition to higher modes
- Thermal microstructure has dramatic influence on path structure and stability during transition

Figure 22:Raytrace Baltic Profile with (Top) Smoothed SV profile (Bottom) Unsmotthed Profile

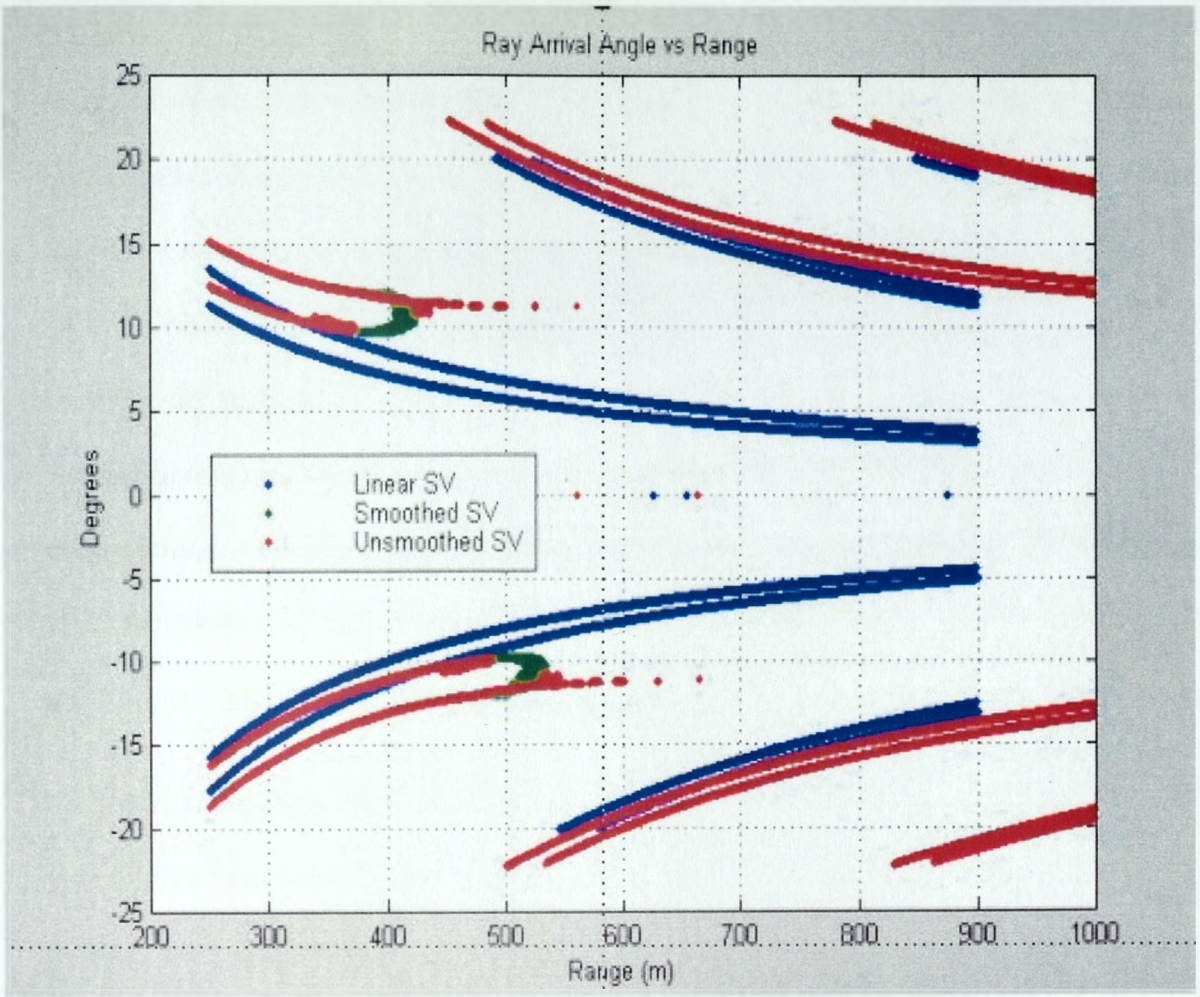

Notes

- Ray arrival angle reduces with range for all rays
- Arrival angle plateau's around 700-800m
- At 1km there is still appreciable angular diversity between rays.

Figure 23: Raytrace path arrival angle

5.6.18 Comparative simulations involving ray trace and geometric models have demonstrated significant path delay errors and path arrival angle errors if a geometric model is assumed. Comparative simulations using a ray trace model for smoothed and unsmoothed SV profiles have demonstrated the appreciable influence of thermal microstructure on path delay profiles particularly at shorter range. For the particular case of a strongly downwardly refracting environment, it has been shown that as range opens direct path propagation is quickly lost and more complex bottom interacting modes appear. As range opens further, rays must be launched at steeper angles. In the limiting case where these rays just reflect off the ocean surface, new ray modes occur. This can lead to quite dramatic changes in the path arrival structure.

5.6.19 The results presented here have provided a physical insight into the influence of channel geometry, sound velocity and bottom type on received signal coherence. The underlying aim has been to investigate and understand the physical mechanisms influencing sound propagation. Ultimately, the fidelity of any environmental modelling relies on how accurately, and to what resolution (both temporal and spatial), one is willing or able to characterise the environment.

5.6.20 A key issue in the development of a channel simulation model for communication system assessment is the need to control and isolate these physical mechanisms in order to determine the performance and sensitivities of candidate acoustic communications algorithms. Clearly this is difficult to achieve using the ray based modelling techniques investigated here and so an alternative approach is proposed in the next subsection.

5.7 A Broadband Channel Simulation Model

5.7.1 The preceding discussion has demonstrated the utility of ray trace modelling model to determine the time varying channel impulse response for underwater acoustic

communications system assessment. The diverse nature of propagation models, the varying degree of rigour employed when specifying the environment and the sensitivity of these models to environmental uncertainty underlines the difficulty in accurately relating real ocean behaviour to true channel behaviour. In the foregoing case the aim was to relate the observed time varying channel impulse response to the simulated eigenray structure of the channel. In so doing stochastic perturbations were not modelled, yet it is such time variability which is the most complex aspect of the acoustic channel. Whilst it is feasible to model such random factors as say, platform heave motion and/or temporal-spatial bathymetry variability, absolute fidelity would require an impractical degree of environmental detail.

5.7.2 An alternative approach to the channel modelling problem is to actively attempt to model environmental variability in a controlled manner, which is not specific to a particular environment. Such an approach allows tailored development of candidate modulation technologies, receiver processing methodologies etc and enables one to investigate signal modem designs against extremes of channel behaviour. At the most fundamental level any composite ray model defines a number of rays each with a characteristic arrival time and magnitude. However the time varying nature of the acoustic channel invariably requires that the model accommodate time varying path delay and its first derivative, Doppler. Also the use of spatially coherent processing is a powerful technique to mitigate multipath and so the modelling of ray arrival angle in a time dependent manner is also appropriate. Since the ratio of carrier to transmission bandwidth is low it is appropriate to implement the channel model as a passband model rather than a complex baseband model which is the conventional approach in all RF channel models thus:-

$$h(t,\tau,N_p) = \sum_{n=0}^{N_p-1} A_n(t)\delta(t-\tau_n(t))$$

where

N_p = *number of discrete paths or macropaths,* *Eqn 8*

$A_n(t)$ = *Complex Gaussian random process,*

$\tau'_n(t)$ = *Random process for n'th ray delay.*

5.7.3 Conventionally the random process $A_n(t)$ is considered as a circular complex valued Gaussian process and $\tau_n(t)$ is assumed time independent. This model is widely used for radio communication channel modelling, however it is unsuitable for acoustic channels due to the nature of the acoustic Doppler problem. In the RF model, time selective channel behaviour arises from variation of ray amplitude and phase in $A_n(t)$, which leads to frequency spreading. Since the spatial scales of the symbolling waveforms are great (of the order 10's km at kbps), relative to the carrier wavelength (typically 10's cm), then such a model is perfectly acceptable under most circumstances.

5.7.4 In the acoustic case however, where the propagation speed is orders of magnitude less than that of RF, it is inappropriate to model path time selective behaviour purely as a complex phasor since symbol spatial scales are comparable to the acoustic carrier wavelengths. At complex baseband this leads to not only tap rotation in $A_n(t)$, but also tap 'slippage' arising from time dependent fluctuations in the ray propagation time through environmental influences and the influence of platform relative motion. In order to model such acoustic channel behaviour it is therefore more appropriate to extend the RF model to incorporate temporal scaling.

5.7.5 The model can be further enhanced by considering the nature of the physical mechanisms influencing $A_n(t)$ and $\tau_n(t)$. Physical arguments would suggest that it is unlikely that the amplitude and delay/phase fluctuations of each ray are truly independent processes. Moreover it is more appropriate to consider the timescales of the physical mechanisms

influencing each. For example, previous results indicate that correlated delay/phase fluctuations occur on a medium-to-long time scale arising from platform motion and movement. Further it is reasonable to assume that the spatial-temporal variations in the medium propagation characteristics would lead to a medium to long time scale amplitude variations which would be correlated between rays.

5.7.6 It would therefore appear reasonable to consider both the random processes $A'_n(t)$ and $\tau'_n(t)$ in terms of correlated and uncorrelated components between rays. It is assumed that both processes are low pass and Gaussian in nature. Conventionally long time scale 'biases' to the channel scattering function are not considered such as propagation delay offset and oscillator errors.. Ultimately the demarcation depends on the nature of the communications modulation, synchronisation and equalisation and how these parameters relate to the channel scattering function.

5.7.7 Such a model is discussed more comprehensively in appendix E. This model is used in subsequent sections to simulate aspects of real ocean behaviour upon high rate receiver architectures.

5.8 Discussion

5.8.1 The preceding discussion and results have demonstrated that the acoustic channel exhibits both temporal dispersion and frequency dispersion and this dispersion is attributable to several physical mechanisms.

5.8.2 Methods to characterise communications channels have been discussed and developed for the acoustic channel case. It has been shown that multipath serves to degrade the frequency coherence of the incident acoustic field by virtue of the acoustic multipath problem. It has been shown that the temporal coherence of the incident acoustic field is

influenced by both platform motion, the propagation of the signal within the medium and its interaction with both surface and bottom interfaces.

5.8.3 Several approaches to the channel modelling problem have been considered with a view to realistically exercising candidate acoustic communications techniques and algorithms. Environmental simulations based on a simple geometrical and ray tracing algorithm have demonstrated the influence of ray refraction and bottom interaction upon signal coherence.

5.8.4 It has been shown that geometry, bathymetry and bottom characteristics can have a dramatic influence upon the received signal coherence characteristics. Platform motion in strongly refracting environments can introduce dramatic variations in the received path structure.

5.8.5 The distinction between narrow and wideband systems and the impact of signal coherence degradation upon each system has been developed. It has been shown that wideband systems enable path components to be resolved exploiting frequency diversity and path diversity. Narrowband systems have been shown to be much more susceptible to violent phase and magnitude fluctuation compared to wideband systems.

5.8.6 Field trials results have been presented to support the foregoing observations. By tracking paths individually, it has been shown that for wideband systems capable of resolving multipath components, path phase/delay is actually extremely stable, and it is path magnitude which exhibits greater variability.

5.8.7 Results for short and medium range shallow water channels have demonstrated a greater degree of channel complexity at shorter range. This supports the arguments presented previously which stress the key role of bottom interaction, geometry and platform motion in defining the complexity of the channel.

5.8.8 Thus far, evidence from several researchers, field results and simulation studies have provided a more in depth understanding of the underwater acoustic environment and its role in defining the coherence characteristics of signals propagating within it.

5.8.9 Subsequent sections now develop the techniques necessary to overcome the complexities of this difficult environment. This will include modulation techniques for mapping information to the physical waveforms that interact with the environment, techniques to minimise the influence of multipath and Doppler dispersion upon the receiver decoding process. This will include techniques such as beamforming, equalisation and waveform coding.

5.8.10 Before addressing these issues, the problem of how a receiver determines the presence or absence of a transmission is considered. In the next section, the extremely important and fundamental problem of synchronisation is considered. Synchronisation is as fundamental to acoustic communications as detection theory is to active sonar. In the context of underwater acoustic communications, synchronisation relates to the problem of a receiver establishing an appropriate time, Doppler and spatial reference prior to decoding.

5.8.11 Establishing these parameters in difficult, noisy, highly dispersed environments is not straightforward and it is for this reason that 'open loop' synchronisation is considered as the first of several 'blocks' constituting the acoustic communications system design.

'The times they are a-changin'

Bob Dylan, Song Title, 1964

6 SYNCHRONISATION

6.1 Synchronising in Time-Doppler Spread Channels

6.1.1 Synchronisation is perhaps the most understated and misunderstood aspect of acoustic telemetry. The open literature on synchronisation at carrier, symbol and word levels is sparse. In the majority of open literature on acoustic telemetry the issue of synchronisation is rarely developed beyond a brief discussion of the limitations of conventional phase lock loop techniques. Morgera [73] for example considers several techiques to establish optimum symbol timing in a simple pulse position modulation communication system. Ludecke [74] considers techniques to remove the temporal fluctuations arising from Doppler variability. Optimum synchronisation techniques are considered by Solimon [75] involving exhaustive searches of the time-frequency uncertainty based on a narrowband channel model. Sharif [76] considers a periodic sounding technique to estimate and compensate for Doppler variability. The unique nature of acoustic Doppler as a temporal scaling phenomenon introduces new challenges to wideband acoustic synchronisation. Established techniques for communications synchronisation and their limitations for acoustic systems are discussed in appendix G. In appendix L, the acoustic synchronisation problem is developed further with a view to defining signal processing techniques to compensate for Doppler variability.

6.1.2 In this section several techniques are investigated with a view to identifying robust and reliable synchronisation schemes for initial acquisition and closed loop tracking. Several

appendices provide a more complete discussion of the open loop (acquisition) and closed loop (tracking) problem.

6.1.3 In the acoustic channel, achieving robust synchronisation in all types of environments at low signal-to-noise is a particularly challenging problem. Since initial synchronisation or acquisition is so fundamental to the performance of any acoustic telemetry system it is deemed appropriate to address this issue before considering modulation, equalisation and spatial processing technologies.

6.1.4 The performance of any synchronisation scheme ultimately relies upon the scattering characteristics of the channel and upon the ambiguity characteristics of the signalling waveform. [75]. Optimum detection and synchronisation of these waveforms requires perfect knowledge of the channel scattering function; information which is rarely available to the receiver. Indeed the conventional formulation of the channel scattering function in terms of temporal and spectral energy smear must be interpreted with some caution for the underwater acoustic case due to the low ratio of transmission bandwidth to carrier frequency. The role of the channel scattering function and imprecise synchronisation upon digital receiver performance is discussed in greater detail in appendix M, where the problem of optimum receiver performance in fading dispersive channels is discussed.

6.2 Open Loop Synchronisation - Acquisition

6.2.1 Acquisition relates to the process by which a receiver detects the presence of a transmission and subsequently establishes three fundamental references prior to decoding:

- Time reference;
- Doppler reference;

- Bearing reference.

6.2.2 Prior to establishing these references, the receiver must be able to determine the presence or absence of a transmission. Whilst this may be straightforward in benign channels at high signal-to-noise, establishing the presence or otherwise of a transmission reliably, at low signal-to-noise in severely spread channels is a difficult problem reliant upon achieving a high probability of transmission detection and low probability of false alarm.

6.2.3 Once a transmission has been detected the receiver must subsequently establish an appropriate time reference. The accuracy to which this time reference has to be established is ultimately dependent upon several systematic factors. For practical systems employing packetised transmissions 'higher levels' of synchronisation may also be necessary to support techniques such as adaptive training, forward error correction coding, handshaking protocols etc. [76]

6.2.4 In addition to time synchronisation, the influence of platform motion and to a lesser extent, systematic issues such as clock misalignment, require the receiver to establish frequency or, more precisely, Doppler synchronisation. Conventionally in RF systems this form of synchronisation is assumed to be a carrier frequency offset. For the reasons developed in previous sections, this is inappropriate for acoustic systems and one must consider Doppler synchronisation as a temporal scaling correction analogous to a sample rate adjustment in a digital system.

6.2.5 Bearing synchronisation relates to the potential need to spatially synchronise prior to data decoding. This potentially affords numerous advantages. For example, in the vertical plane, beamforming may be used to combat multipath. In the horizontal plane beamforming may be used to improve signal-to-noise ratio. Since the transmitter bearing is unlikely to be known by a receiver, then the receiver cannot use the full (horizontal)

spatial processing gain of its receive array since it may not know where to point the receive beam. Obviously the receiver could form multiple, beams in parallel to capitalise on any DI advantage, however this would greatly increase the complexity of the synchroniser.

6.2.6 Time, Doppler and bearing accuracy ultimately rely upon the ability to accurately determine absolute time of arrival (time synchronisation) and time difference of arrival between signals arriving at two or more sensors (bearing accuracy) and/or two signals arriving at the same sensor (Doppler accuracy).

6.2.7 The local accuracy of the estimate of delay τ, and frequency ω (in a narrowband sense) is given in the classic text by H.Van Trees [78]. Specifically Van Trees shows that the local accuracy is bounded by

$$Var[\hat{\tau}-\tau] \geq \left[\frac{2\overline{E}_r}{N_0}.\frac{\overline{E}_r}{(\overline{E}_r+N_0)}\right]^{-1} \frac{1}{\overline{\omega^2}} \qquad \textit{Eqn 9}$$

$$Var[\hat{\omega}-\omega] \geq \left[\frac{2\overline{E}_r}{N_0}.\frac{\overline{E}_r}{(\overline{E}_r+N_0)}\right]^{-1} \frac{1}{\overline{t^2}} \qquad \textit{Eqn 10}$$

$$\overline{\omega^2} = \frac{1}{2\pi}\int_{-\infty}^{+\infty} \omega^2 \mid \tilde{F}(j\omega) \mid^2 d\omega \qquad \textit{Eqn 11}$$

$$\overline{t^2} = \int_{-\infty}^{+\infty} u^2 \mid \tilde{f}(u) \mid^2 du \qquad \textit{Eqn 12}$$

$\overline{\omega^2}$ and $\overline{t^2}$ are the un-normalised rms bandwidth and duration of a waveform $\tilde{f}(t)$, with spectrum $\tilde{F}(j\omega)$. ~ denotes complex variable, N_0 is the one sided noise spectral density and $\overline{E_r}$ is the mean received signal energy. $\hat{\omega}$ and $\hat{t}$ denote receiver estimates of the

waveform time and frequency. $Var[\hat{\tau}-\tau]$ denotes the lower limit of the variance of the time estimation error and $Var[\hat{\omega}-\omega]$ denotes the lower limit of the variance of the frequency estimation error.

6.2.8 The above result demonstrates that time accuracy is limited by the signal-to-noise ratio and the bandwidth of the transmitted waveform and the frequency estimate accuracy is limited by signal-to-noise ratio and time duration of the waveform.

6.2.9 Van Trees also demonstrates that the local accuracy of a particular waveform design can be expressed in terms of the waveform ambiguity function in the vicinity of the origin. This statement is borne out in appendices N and M wherein the waveform ambiguity function is defined and its role in digital receiver performance investigated. In a communications sense this would indicate the synchronisation performance once initial acquisition had been achieved (the global accuracy problem). This result indicates the pivotal role of transmission bandwidth in any synchronisation system.

6.2.10 It was shown in sections 3-5, that the impact of Doppler and the requirement for Doppler compensation arises due to several factors:-

- Doppler variability exists on two levels. Long time scale variations attributable to platform manoeuvres and short time scale variability attributable to platform dynamics and the influence of the ocean medium on signal propagation;
- Differential Doppler can exists between rays;
- Open loop compensation is required to remove Doppler bias for high velocity platforms.

6.2.11 The Doppler estimation problem is intimately linked to the receiver synchronisation problem. Synchronisation implies absolute time and frequency alignment of the received signal to an absolute time and frequency reference at the receiver. In the presence of

severe multipath and Doppler spread, obtaining an absolute time and frequency reference is often extremely difficult. This is especially so in noisy environments featuring excessive transient noise interference. In such environments matched filter based 'burst' synchronisers may be prone to unacceptable false alarm rates. Also the fact that each ray may be subject to different Doppler variably raises the issue of what the open loop Doppler estimate should be.

6.2.12 There are a number of methods by which one could address the Doppler estimation problem. An accurate, but computationally costly, technique is to use ambiguity analysis on a wideband channel sounding waveform. The technique relies on the ambiguity properties of the sounding waveform to provide accurate unambiguous range and Doppler estimation. This in turn relies on the ambiguity function exhibiting 'thumbtack' response; ideally with zero sidelobes in both time and Doppler axes.

6.2.13 Whilst signal designs exist with well behaved sidelobe levels in the time axis, maintaining good auto correlation performance in time and Doppler spread channels is not so straightforward. Appendix Q reviews a number of digital codes which exhibit such well behaved correlation performance.

6.2.14 Since the channel may exhibit multiple rays, which may have varying Doppler, the choice of which ray to use for this analysis is not often straightforward. In many channels (but not all) the first arrival is the highest energy and so is chosen for synchronisation. An alternative, lower complexity, technique, is to periodically sound the channel with a wideband signal and to use the resulting channel information to determine Doppler.

6.2.15 Wideband sounding provides information on the channel multipath structure. In evolving geometry's where relative Doppler exists, path delays are time varying and so by sampling the path delays at two instants it is possible to estimate Doppler in a mean sense

between the two sampling instants. The performance of the technique relies to a large degree on channel stationarity between soundings. Since the Doppler resolution of the technique is related to the time difference between channel sampling instants, this obviously conflicts with the need to sample sufficiently rapidly. Under acceleration conditions due to say, platform heave motion, this could lead to Doppler estimation error prior to closed loop tracking.

6.2.16 One feature of platform Doppler which can be exploited in severe multipath environments at medium to long range, is that the Doppler component will exhibit some degree of correlation between paths as demonstrated in section 5. At shorter range differential Doppler between rays becomes more significant. In such circumstances exploiting path diversity would require several separate Doppler-tracking loops for each path. As shown in section 5 the coherent tracking and exploitation of multipath is feasible provided the paths can be resolved.

6.2.17 At medium to longer ranges path differential Doppler is less of an issue as demonstrated by the simulations presented earlier. An open loop Doppler estimation technique developed for the high data rate application is to use the wideband channel correlation output structure from two successive wideband pulses to determine acoustic Doppler. Open loop Doppler correction requires specific signal processing to implement the time varying delay due to Doppler. The are several potential approaches to this problem [79-82] some of which are discussed in greater detail in appendix L.

6.3 Open Loop 2 Chirp Synchronisation

6.3.1 An important issue in the implementation of any correlation or matched filter based synchronisation scheme is the problem of false alarm rate. Indeed establishing a reliable

threshold for such schemes is greatly complicated by several aspects of the underwater channel:-

- 'bursty' noise levels

- wide range of temporal dispersion characteristics.

6.3.2 One approach to automating the detection threshold is based on normalising the matched filter output by the product of the received signal variance and replica variance. This enables a threshold to be set between 0 and 1 irrespective of the received signal-to-noise in an additive white Gaussian noise (AWGN) environment. Unfortunately such a thresholding scheme cannot be relied upon in multipath channels. This is because even though the received signal may be received at a high signal-to-noise ratio, the signal to multipath (noise) interference ratio may be low. Thus, in highly time spread channels at high signal-to-noise it is quite possible for the normalised correlation function to drop below a threshold derived from an AWGN channel model, despite the fact that the received signal-to-noise ratio may be high.

6.3.3 An alternative approach is not to normalise, and to base the threshold on received signal statistics. This assumes that the signal present, signal absent case can be isolated by the receiver. Such a technique is similar to the constant false alarm rate (CFAR) principles exploited in radar receivers.

6.3.4 The advantage of this approach is that, by establishing a threshold based on noise statistics, it is possible to detect the synchronisation signal even for severely time-dispersed environments. The disadvantage is that the system becomes more susceptible to non-coherent false alarms arising for example from impulsive clicks due to marine organisms. Such signals are inherently wideband and often high-energy, and as such are likely to feature a strong in-band component which may be admitted by the matched filter

synchroniser. This is a direct consequence of the fact one is trying to realise a synchronisation scheme capable of operating robustly in AWGN channels and also in difficult random scatter channels. In the latter, the received signal is more noiselike.

6.3.5 One solution to this dilemma is to exploit the time coherence of the acoustic channel. The technique is based on using two wideband channel sounding waveforms to explicitly sample the channel delay profile. Assuming the channel delay profile does not change significantly between the two soundings it is possible to use this information to improve the robustness of the initial synchronisation. The underlying assumption being that the false alarm rate of the system can be substantially reduced by exploiting the information from two rather than one channel sounding waveform. In addition the use of two channel sounding waveforms provides a means for the receiver to not only establish a time reference for data decoding but also a Doppler reference to resample the signal prior to decoding.

6.3.6 The synchronisation technique can be perceived as a form of post processor whereby several initial tentative detection's based on a threshold set by the received signal statistics are combined to improve robustness. Upon making a tentative detection decision the receiver processor cross checks the detection against the previous detection with a view to reducing system false alarm rate.

6.3.7 A common waveform used for channel sounding and synchronisation is the linear frequency modulated pulse (LFM) given by:-

$$s(t) = w(t)e^{j2\pi(f_o t+\frac{1}{2}mt^2)} \qquad \textit{Eqn 13}$$

where

$w(t)$ is an envelope window function defined over the interval -T/2 to +T/2.

$m = \frac{W}{T}$ is the sweep rate of the pulse
W is the signal bandwidth
T is the pulse duration

6.3.8 When subjected to Doppler the received signal is given by

$$s((1-\alpha)t) = w((1-\alpha)t)e^{j2\pi(f_o(1-\alpha)t+\frac{1}{2}m[(1-\alpha)t]^2)} \qquad \textit{Eqn 14}$$

which differs from the original signal by a frequency translation term $f_d = \sigma f_0$ and a slope mismatch term $\Delta m = (\sigma^2 - 2\sigma)m$ where $\sigma = 1-\alpha$ and α is the time compression factor discussed in section 4 and illustrated in figure 6 previously.

6.3.9 In the narrowband case the received signal is merely a frequency translated version of the transmitted signal. In the wideband case both frequency translation and slope mismatch serve to degrade correlator performance. In terms of synchronisation, frequency translation serves to introduce delay ambiguity. The range-Doppler ambiguity for a 10-20kHz LFM up chirp of duration 21ms sampled at 48kHz is shown in Figure 24. The figure shows unweighted and unilaterally weighted cases. Evident from the figure is the Doppler tolerance of this waveform (3dB output at +/-10knots). The slope of the ambiguity function indicates a range ambiguity of approximately 1.4samples per knot equating to approximately 5cm per knot. The delay ambiguity is influenced by both the LFM centre frequency and by the sweep rate. To contain the range ambiguity of the waveform it is desirable to :-

- reduce the carrier frequency f_o;
- increase the bandwidth W;
- reduce the pulse duration T.

6.3.10 In addition to the range ambiguity that is inherent to LFM designs the slope mismatch can lead to appreciable decorrelation in applications requiring high Doppler tolerance. The

application of a unilateral shading function can significantly improve the Doppler performance at the expense of waveform processing gain and range resolution. This arises since by applying the windowing function one is in essence de-emphasising the low and high frequency components of the chirp. Since the extreme frequency components suffer the most from slope misalignment, deemphasising by windowing reduces the overall loss arising from slope mismatch in the correlation output. In order to improve the performance of this waveform for open loop synchronisation consider two consecutive chirps given by:-

$$S_{12}((1-\sigma)t) = s((1-\sigma)t) + s((1-\sigma)(t-T)) \qquad \textit{Eqn 15}$$

6.3.11 Each waveform will undergo degradation as given by 14 and illustrated in Figure 24 resulting in range-Doppler ambiguity. However under the assumption that the channel is relatively stable over the 2T interval, which is reasonable where T is sufficiently short, then both waveforms undergo comparable Doppler degradation and comparable temporal smear due to multipath. Since only the relative time slip is of concern for Doppler estimation, provided the waveforms are themselves suitably robust to Doppler decorrelation, then it is possible to use the differential time difference between the first pulse arrival and second pulse arrival to estimate Doppler as shown in Figure 25.

6.3.12 Decorrelation losses due to slope mismatch may be avoided through the use of Doppler tolerant waveform designs such as Linear Period Modulation (LPM). This approach requires the use of an extended replica in order to realise the full potential processing gain of the signal. This is due to the fact that whilst the waveform design provides Doppler invariance it does not simulataneously provide time invariance. So, the time-frequency trajectory of a received signal subject to Doppler must be effectively time shifted to perfectly align with the extended replica time-frequency profile. In practice, the

performance benefits of LPM over LFM are strongly influenced by the role of windowing. Unilateral weighting serves to improve the Doppler performance of both waveform types and is a prerequistie to improve performance in extended multipath environments by containing correlation sidelobes. So whilst LPM has not been considered here it is a potentially useful alternative to LFM in very high Doppler applications.

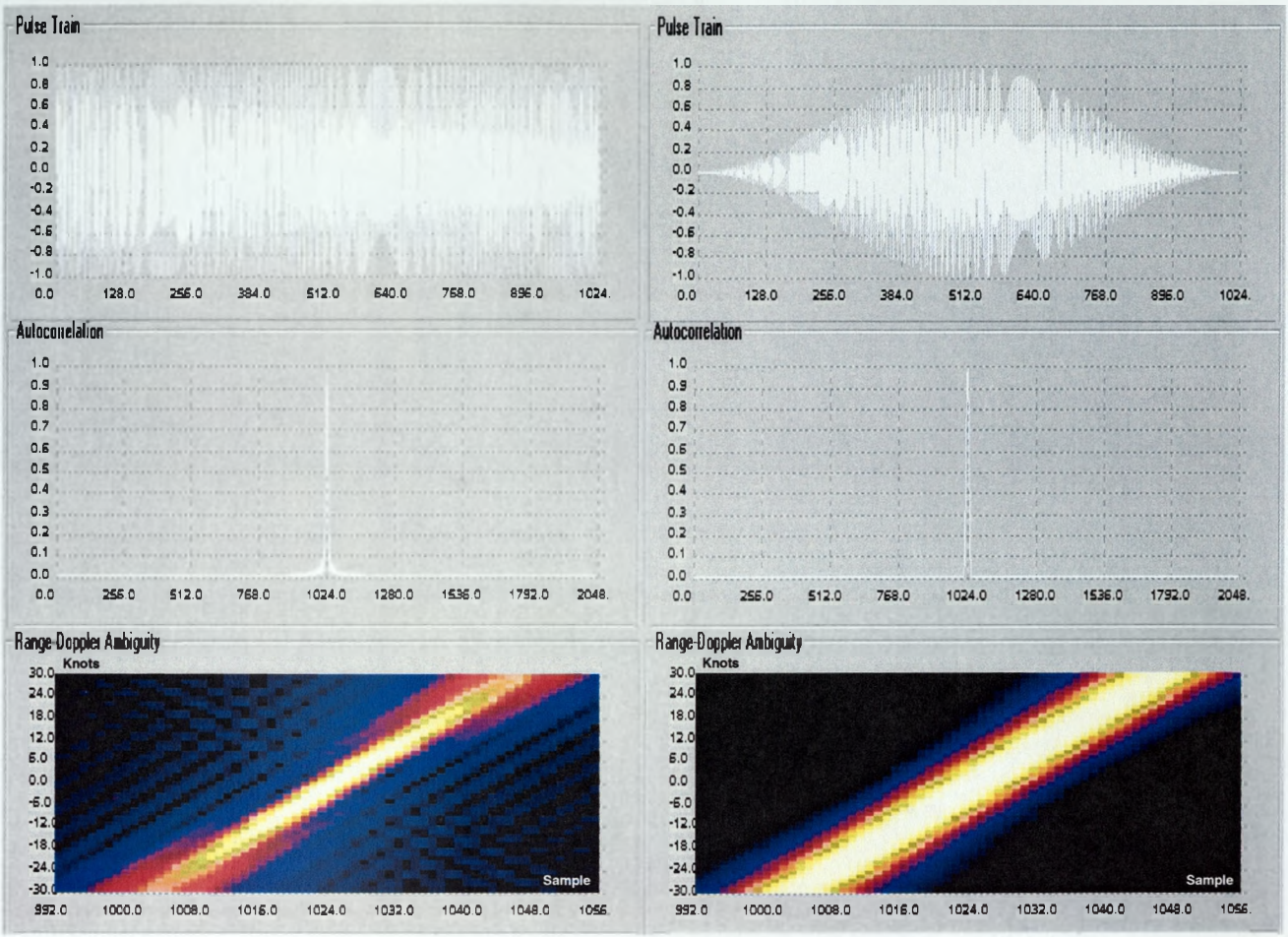

Notes

- (left) Unweighted (right) Unilateral Hanning weighting
- Range ambiguity approximately 1.4 samples per knot (approximately 5cm).
- Unilateral weighting (right) improves Doppler tolerance
- Unilateral weighting (right) reduces resolution
- Unilateral weighting (right) reduces sidelobe level
- LPM waveforms potentially afford greater tolerance for high Doppler platforms

Figure 24; LFM 'Chirp' 10-20kHz, 21ms, Range-Doppler Ambiguity for shaded and unshaded cases

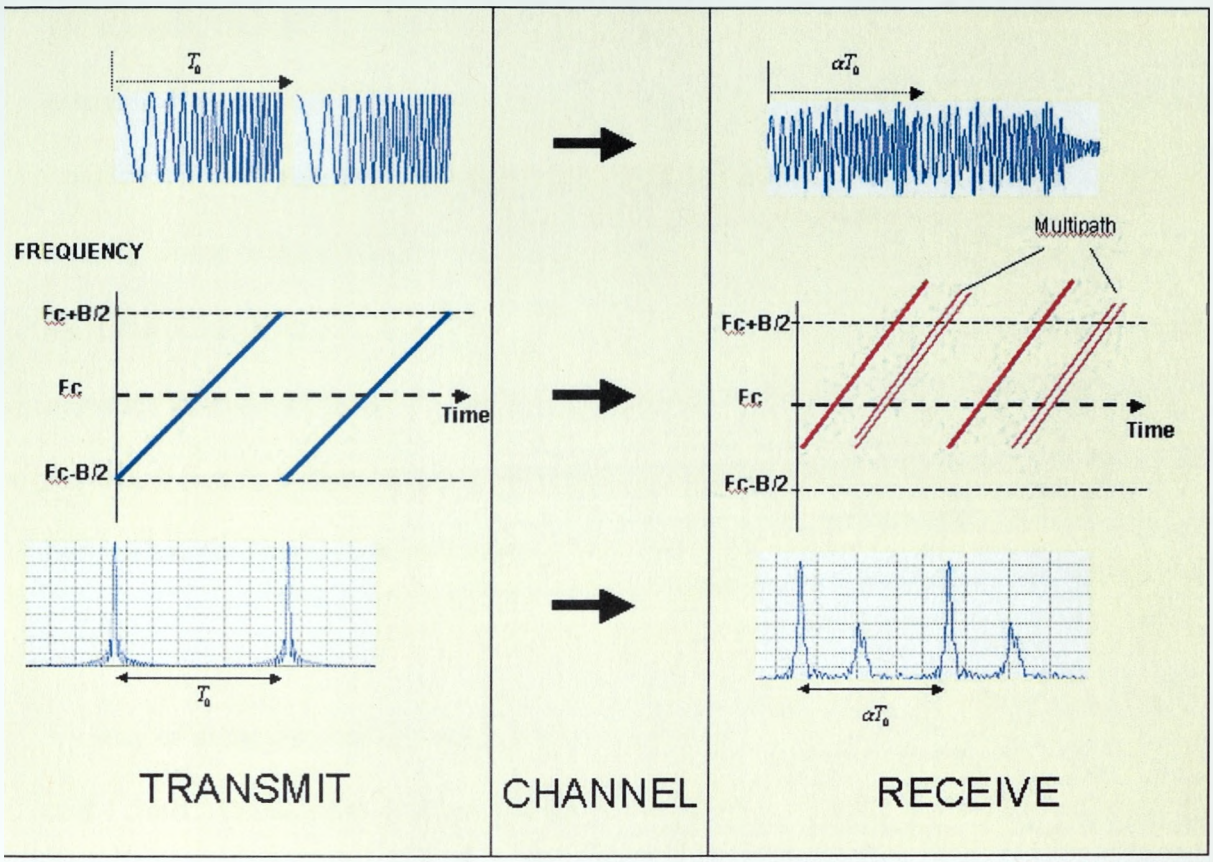

Notes

- T_0 assumed less than channel coherence time
- Received chirps centre frequency shifted by $\frac{1}{\alpha}.F_c$
- Chirp Time-Frequency slope now mismatched $F_c \pm \frac{B}{2} \rightarrow \frac{1}{\alpha}(F_c \pm \frac{B}{2})$
- Time between correlation peaks modified from T_0 to $\alpha.T_0$
- Use multiple paths to improve synchroniser robustness

Figure 25; Open Loop 2 Chirp Burst Synchroniser

6.3.13 The two wideband channel sounding waveforms are therefore used to explicitly sample the acoustic channel multipath structure. Provided sufficient bandwidth is available, path energies are resolved. In the presence of acoustic Doppler, temporal scaling occurs, which results in time translation of the second correlation multipath profile relative to the first by αT_0 where α is the Doppler temporal scaling factor ($0.99 < \alpha < 1.01$ for +/-30knots) and T_0 is the pulse duration. The output of cross correlating the two channel sounding profiles provides an estimate of the Doppler. This is shown in the bottom four graphs in Figure 26 for 0.0, 0.5, 1.0, 1.5m/s. Of note is the phase step between samples of approximately 2 radians which corresponds to the carrier phase for one sample delay (2π x 15kHz/ 48kHz = 1.96).

6.3.14 By way of example consider the correlation peak phase output for Doppler=0m/s, 0.5m/s and 1.5m/s. At 0m/s the peak output phase is 0 degrees as expected. At 0.5m/s the peak output phase as shown in the figure, retards by approximately 0.3-0.4 radians. The theoretical phase slip is given by $\alpha = \frac{c - v}{c}$ = (1500-0.5)/1500 = 0.99966667

Temporal Slip $\Delta\tau = (1-\alpha)T = (1-0.9996667) \cdot 512/48000 = 3.552$us

Phase Slip $= 2\pi\Delta\tau F_c = 2\pi.3.552e\text{-}6 \cdot 15000 = 0.35$rads

6.3.15 As the Doppler increases the correlation peak position changes such that at 1.5m/s the correlation peak is offset by one sample. In this case the theoretical phase slip is given by:

$\alpha = \frac{c - v}{c}$ =(1500-1.5)/1500 = 0.999

Temporal Slip $\Delta\tau = (1-\alpha)T = (1-0.999)$ x 512/48000 = 10.66667μs

Phase Slip $= 2.\pi .\Delta\tau.Fc = 2.\pi.10.6667e\text{-}6$ 15000 = 1rad

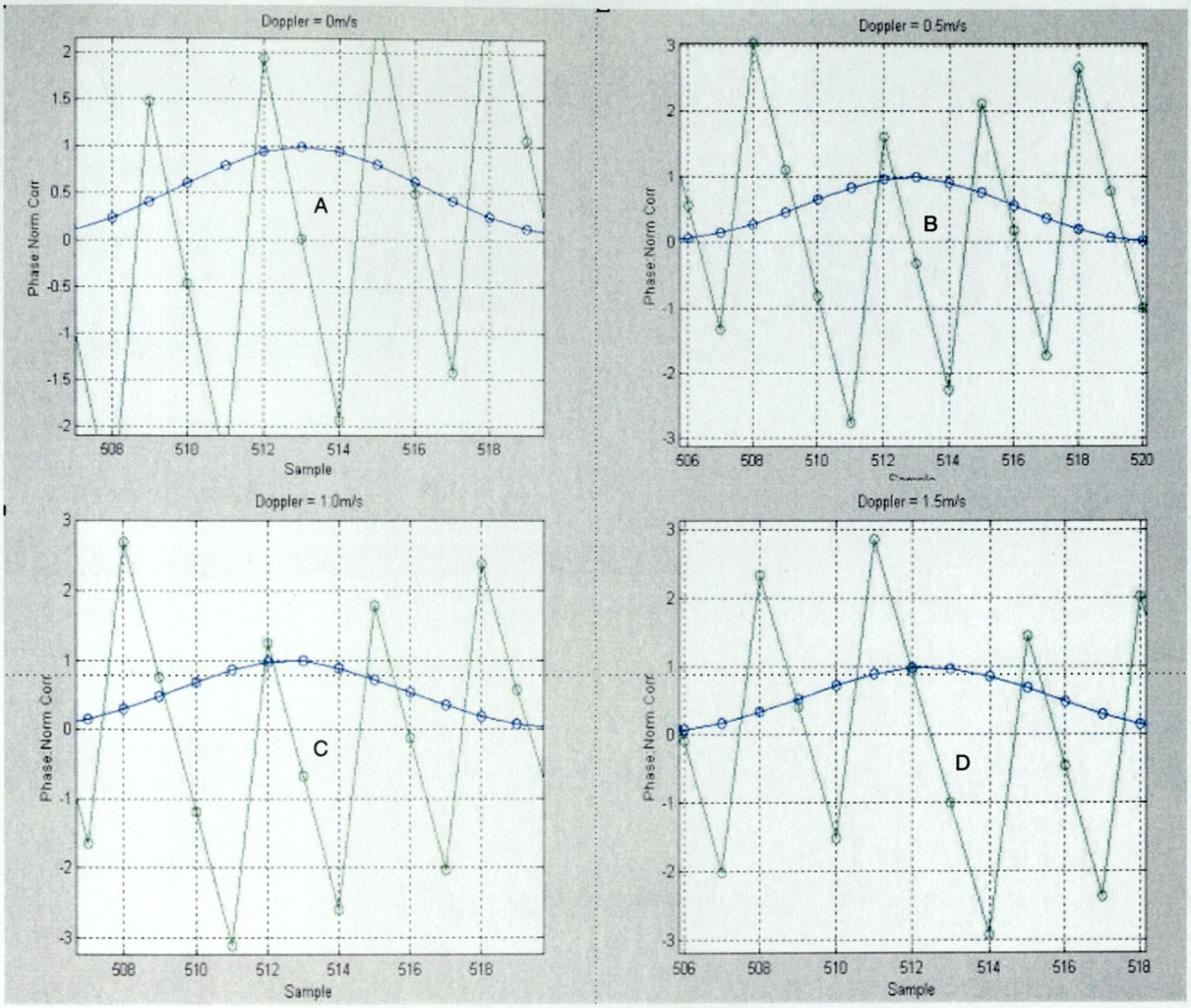

Notes

- Magnitude scale 0-1, Phase scale -2π to $+2\pi$ depicted on common axis
- (A) Zero Doppler case. Differential phase=0 radians, peak magnitude at sample 513.
- (B) Doppler = 0.5m/s. Differential phase = -0.35rads, peak magnitude at 513.
- (C) Doppler = 1m/s. Differential phase = -0.7rads, peak magnitude at 513.
- (D) Doppler = 1.5m/s. Differential phase = +1rads peak magnitude shifts to 512
- Phase and magnitude shift information may be used to improve fidelity of Doppler estimate. Refer 6.3.13 - 6.3.15 for theoretical calculation of phase and magnitude for above Doppler=0.5m/s and 1.5m/s.

Figure 26; Complex Correlator Output vs Doppler

6.3.16 The results demonstrate the ability to use the delay (in samples) and phase of the complex output from the two channel estimates to determine Doppler to a high degree of accuracy. This technique has been developed to measure the speed profiles of swimmers. A more comprehensive discussion of this complex problem is presented in appendix T.

6.3.17 In practice the fidelity of the estimate will be subject to the degree to which the system resolves path components, the extent of differential Doppler between paths and the number of paths. A simple model for determining the PDF of the phase angle between the two correlation outputs is considered in appendix I.

6.3.18 In a practical receiver implementation the correlation may be performed digitally in the frequency domain, thus:-

$$\phi_i(k) = \sum_{n=0}^{N-1} (\frac{1}{N}[R_i(n)X^*(n)]^* \exp(-j2\pi nk/N)$$

where

$$R_i(n) = \sum_{k=0}^{N-1} r_i(kT_s)\exp(-j2\pi nk/N) \qquad \textit{Eqn 16}$$

$$X(n) = \sum_{k=0}^{N-1} x(kT_s)\exp(-j2\pi nk/N)$$

where *r(t)*, and *x(t)* denote replica and received waveforms respectively, T_s is the system sampling rate and * denote complex conjugation. N represents the correlation size. Conventionally $R_I(n)$ *and* $X_I(n)$ would be obtained by the Fast Fourier Transform.

6.3.19 Since the received data is non-finite, then data sectioning is necessary to contain signal processing memory resources. For this reason the sampled received data r(k) and x(k) is zero padded to avoid end effects, specifically:

$$
\begin{aligned}
r_i(k) &= r(kT + iNT) \quad && k = 0,1,.....N-1 \\
&= 0 && k = N, N+1,....2N-1 \\
x(k) &= 0 && k = 0,1,....N-1 \\
&= x(kT) && k = N, N+1,.....2N-1
\end{aligned}
\qquad \textit{Eqn 17}
$$

6.3.20 In this case N denotes the number of samples representing receive sections and replica sections. Using the overlap add method of sectioning the output of each correlation block is added:-

$$\varphi_{i,k} = \phi_{i,k} + \phi_{i-1,k+N} \qquad k = 0,1,.....N-1 \qquad \textit{Eqn 18}$$

6.3.21 A number of practical issues arise using digital correlation based on sectioning techniques. Acoustic communications channels may often exhibit non-minimum phase characteristics such that the highest energy arrival may not be the first. In an unbuffered block processing correlation scheme, a decision is often made on a block by block basis as to whether to commit to synchronisation. This could lead to the situation whereby the system could synchronise to a low energy first arrival in the presence of much higher energy late arrivals if the subsequent data blocks were not monitored.

6.3.22 A second issue relating to digital implementation is the achievable resolution from the correlation process. Whilst the use of a short duration waveform benfits from Doppler tolerance and improved burst timing accuracy, in order to achieve sufficient Doppler resolution capability, the receiver correlator must be able to achieve sufficient temporal resolution over the two chirp period. This requires the chirps be long enough and sufficiently wideband. A final issue, which relates to the CFAR processing approach is the need to isolate signal statistics for the signal present and signal absent cases.

6.3.23 Assuming the signal is suitably processed to complex baseband at WT samples per inphase (I) and Quadriphase (Q) channel, or 2WT samples at passband, then the resolution of the correlation is often considered to be 1/W. However improved temporal

resolution can be achieved by exploiting interpolation techniques in conjunction with complex phase information from the complex matched filter output.

6.3.24 For correlations performed at passband, the phase information can easily be obtained by correlating I and Q versions of the received signal with the replica waveform. I and Q phase signals are readily obtained from the Fourier coefficients R_i obtained in equation 16 by multiplication by j. The resulting two channel correlation therefore retains all phase information.

6.3.25 By using two wideband-sounding waveforms, successive sectioned correlation results ϕ_i, ϕ_{i-1} can be compared to estimate channel Doppler. The correlation process serves to identify multipath power delay profile and so only rays exceeding a predetermined threshold are considered for Doppler estimation. One approach is to base this threshold on the variance of the magnitude of the correlation output given in 18 thus:-

$$E_T = \frac{1}{N}\sqrt{\sum_{k=0}^{k=N-1} |\phi_i|^2} \qquad \textit{Eqn 19}$$

$$\begin{array}{lcll} \psi_{i,k} & = & \phi_{i,k} & |\phi_{i,k}| > E_T \\ & = & 0 & \textit{otherwise} \end{array}$$

6.3.26 The thresholded complex, path energies stored in ψ_{i-1}, ψ_i are then correlated. The resulting complex correlation allows Doppler to be estimated based on the peak output, its position (in a digital implementation) and phase. A prerequisite for the technique to work is sufficient bandwidth to resolve multipath components. Under high noise conditions the processing gain afforded by the correlation process makes the technique very reliable under high noise conditions. The delay estimation error for broadband correlation increases nonlinearly with reduced SNR. This means that the variance of the Doppler

estimation error will also increase in high noise environments and in severely spread channels.

6.3.27 The path correlation result P_I is given by:

$$P_i(k) = \left| \sum_{n=0}^{N-1} \left(\frac{1}{N} [W_i(n) X(n)]^* \exp(-j2\pi nk / N) \right|^2 / Ep \right.$$

where

$$W_i(n) = \sum_{k=0}^{N-1} \psi_i(k) \exp(-j2\pi nk / N) \qquad \textit{Eqn 20}$$

$$X_i(n) = \sum_{k=0}^{N-1} \psi_{i-1}(k) \exp(-j2\pi nk / N)$$

6.3.28 Where *Ep* is a normalisation term computed from the variances of W_i, X_I. Max(P_I) forms the basis of the Doppler estimate and comprises three terms. A normalised magnitude from 0-1 (ζ), a sample offset (J) and a phase (θ). The normalised magnitude provides a confidence measure of the stationarity of the channel between each sounding. High confidence indicates that the output is due to the two sounding waveforms, low confidence indicates the output is noise only. Provided the confidence is high then the Doppler estimate may be computed from the sample delay and phase values.

6.3.29 In order to ensure robust synchronisation at marginal SNR and/or in adverse channel conditions, committing to synchronisation only occurs if ζ exceeds a threshold, the Doppler estimate is within operational parameters and both normalised peak correlations exceed a predetermined threshold. Figure 27 shows four consecutive block correlation outputs W,X,Y,Z computed using the overlap save correlation processing described. On the computation of each block, the receiver computes a threshold based on the noise variance in the earliest block Z. This threshold is used to normalise the peak correlation

values in blocks X and Y. If the peak value in block X and corresponding peak in Y exceed the detection threshold tentative synchronisation occurs.

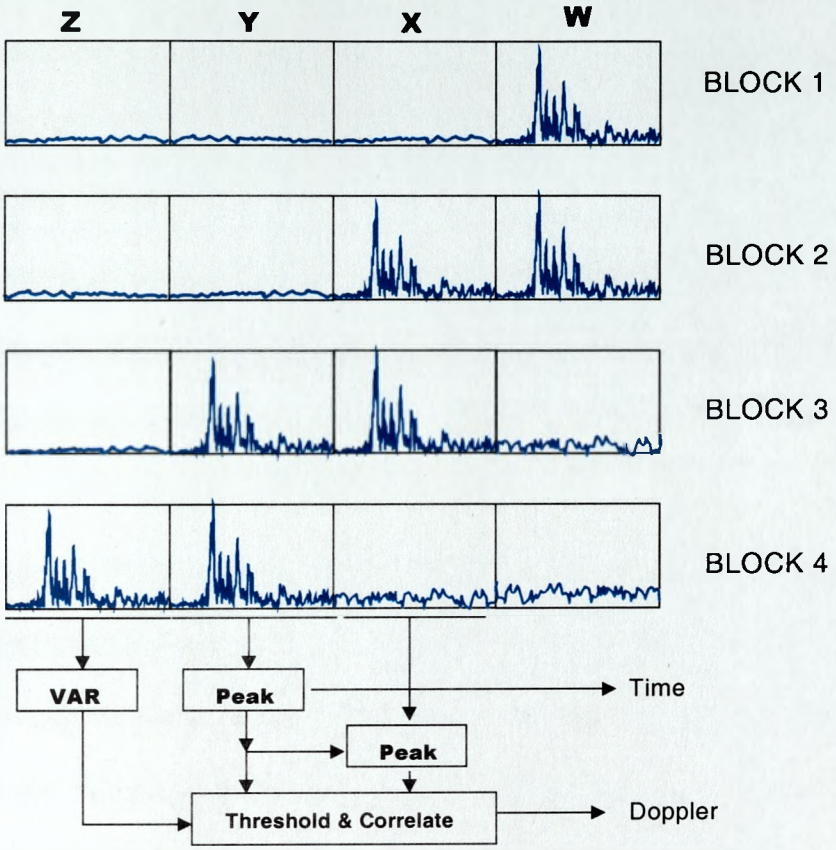

Notes

- Block overlap save FFT based correlation processing;
- Process and buffer four correlation blocks;
- Threshold computed based on noise statistics for block Z
- Peak to rms ratio computed for blocks X and Y.
- If both ratios exceed threshold, T_0 estimated and blocks X and Y thresholded then cross correlated. If Doppler estimate is within limits commit to decoding.

Figure 27; Two Chirp Block Sectioning Correlator Output

6.3.30 During block 3, the peak correlation output in block X and the corresponding peak in block Y exceeds the detection threshold. In this case the synchronisation algorithm brackets the complex correlation output around the peak positions in X and Y. Next the two time windowed correlation results are thresholded leaving only significant paths arrivals. Finally the complex result from the correlation of the two time windows is used to determine the open loop estimate based on the position and phase of the peak correlation output. Although the figure indicates a time spread less than the correlation waveform duration, under more severe time spread conditions the channel spread may exceed the correlation waveform duration. In this case delayed path components from the first sounding will coalesce with the components from the second sounding during correlation block X if the same sounding waveform is used for both soundings. Under these circumstances the resolved paths in the second sounding are contaminated with multipath components from the initial sounding. Ideally then, the sounding waveform duration should be comparable to the delay spread of the channel to minimise contamination. This is however offset by the fact that the two soundings occur at greater time separation and so, depending on the channel time coherence may be less correlated. Also, time spent sounding the channel is time not spend on data transmission and so should ideally be made as short as is practical. An alternative approach is to use consecutive sounding waveforms with low cross correlation properties (ideally orthogonal). Using up-chirp,down-chirp soundings for example, would reduce the multipath contamination problem, however it would be more difficult to automate the synchronisation algorithm for block correlation processing and for this reason is not considered further

6.3.31 In appendix J an example calculation is presented to determine the signal-to-noise performance of the synchroniser in a simple AWGN channel.

6.4 Closed Loop Tracking

6.4.1 Closed loop tracking relates to the process of maintaining receiver time-frequency synchronism during the decoding phase. A key issue with closed loop synchronisers for acoustic channel is the need to track not only phase but also delay perturbations. It is for this reason that phase and delay tracking loops, are an essential part of a phase coherent acoustic communications receiver. A more thorough discussion of PLL and DLL theory is presented in appendix I, and briefly summarised here.

6.4.2 The delay lock loop can be considered the broadband analogue of the phase lock loop and its importance in acoustic communications applications stems from the wideband nature of acoustic communications systems coupled with the acoustic Doppler problem. The analysis of the DLL closely follows that of the PLL with the primary difference being in the phase discriminator which usually involves two or more correlators for early and late versions of the signal replica. The performance analysis of the phase discriminator characteristic draws heavily on waveform design, specifically waveform ambiguity.

6.4.3 The delay discriminator is obtained from the difference in correlation outputs for early and late time lags. So, for example, if the received timing drifts one correlation output will exceed the other depending on the direction of the drift. It is important to stress that in practice the error signal characteristics will depend on the waveform ambiguity and channel scattering characteristics in addition to signal-to-noise ratio. Thus the performance of the delay lock loop in multipath channels which are not completely resolved will be degraded.

6.4.4 In RF systems, DLLs are often used in code tracking loops such as those used in direct sequence spread spectrum systems. Typically these correlators are realised by multiplying the received baseband code by early and late replicas of the code. The resulting signal is

then bandpass filtered and envelope detected. The combination of the multiplication and subsequent filtering realises the correlation operation. The noise and dynamic tracking performance of the DLL in an ideal channel is then heavily dependent on the filter bandwidth, the tracking loop filter and the relative time separation of each of the early-late arms.

6.4.5 It will be demonstrated that STAP processing with closed loop Doppler compensation can provide Doppler pull-in at low-to-medium platform speeds. This capability affords significant improvement in receiver complexity at low-to-medium velocities, as no explicit open loop correction is required. This is obtained at the expense of slightly increased algorithm convergence time that scales relative to the initial Doppler estimation error.

6.4.6 To augment closed loop Doppler tracking capability for high Doppler platforms (v>3-5kts say), and to provide initial pull-in, techniques for open loop Doppler compensation have been investigated. The requirement for open loop Doppler compensation is to provide a snapshot of the relative Doppler between transmitter and receiver and compensating for this Doppler prior to block demodulation.

6.5 Discussion

6.5.1 The techniques presented in this section provide the means for a receiver to initially synchronise to a transmission initiated by a second party whose range and relative velocity are unknown. Two approaches have been discussed. The first involving exhaustive search of range-Doppler uncertainty region are optimum, however they are computationally expensive. The second approach involves a novel, synchronisation technique involving the transmission of two wideband sounding waveforms. A cross correlating receiver then cross correlates the sampled channel path structure to estimate

Doppler under the assumption the sampling instants are sufficiently rapid such the path structure does not appreciably change. The technique affords several advantages over single matched filter based synchronisers

- Computationally inexpensive
- Low false alarm rate in noise limited environments
- Low false alarm rate in difficult, highly reverberant, random scatter channels

6.5.2 The adoption of a relatively simple channel sounding waveform, the LFM chirp, is driven by the need for modest Doppler tolerance and robust performance in multipath environments. In the next section, the signal design problem is revisited with a view to identifying signal designs for estimating the channel. The effectiveness of any channel sounding waveform is closely linked to its ambiguity function and the channel scattering function. Channel estimation has several potential roles in an acoustic communications receiver.

- It serves to provide a reference for the choice of modulation and modulation parameters.
- Optimum decoding of digital signals transmitted through a channel with memory requires a channel estimator
- In spread spectrum systems it provides a means to determine the choice of rakes

'If you cannot measure it, then it is not science',

Lord Kelvin, Popular lectures and Addresses Vol.1 (1889)

7 CHANNEL ESTIMATION

7.1 Optimum Signal Designs

7.1.1 The preceding discussions have centred upon understanding the acoustic communications channel, the concept of the channel scattering function and some important differences between typical RF channels and acoustic channels.

7.1.2 In RF communications waveform design, the performance of a particular waveform design is often assessed purely on the temporal dispersion of the channel. To this end waveforms exhibiting well-behaved autocorrelation functions are generally desirable for use in highly time spread channels. However it will be shown that the desirable correlation properties of such waveforms are severely disturbed by large time spreads arising in acoustic channels and the nature of acoustic Doppler. Indeed the latter can have a significantly more pronounced effect on waveform orthogonality degradation.

7.1.3 Viewed in terms of the channel scattering function, it is perhaps more appropriate to consider the signal design issue not just in terms of channel spread but in terms of channel time and Doppler spread. The challenge then becomes one of attempting to realise a waveform design, which can maintain good autocorrelation performance in the presence of both time, and Doppler spread.

7.1.4 The problem of designing acoustic signals for active sonars has been extensively studied over the last thirty years including the performance of linear frequency modulated (LFM) [83,85,86] and phase coded waveforms [84].

7.1.5 In the previous section techniques to provide open loop synchronisation both in time and Doppler were presented. These techniques provide the means for a receiver to establish the existence of a transmission and to synchronise in time and Doppler. The next block in the processing chain, which is now discussed, is the method by which the channel may be quantitatively measured.

7.2 Correlation Based Estimators

7.2.1 Fundamental matched filter theory states that the output signal-to-noise ratio of a matched filter detector is a function of the received signal energy and noise spectral density. For a fixed noise spectral density, signal energy can be increased either by increasing the signal power level or by increasing the signal duration.

7.2.2 The ultimate challenge in sonar signal design is to determine waveforms who's performance is ideally unaffected by the doubly spread nature of the acoustic channel. A detailed account of sonar signal design and the role of waveform ambiguity functions as a means for predicting the performance of signals in time and/or Doppler spread environments is presented in appendix N. The following discussion is based on the more detailed treatment presented in appendices N and Q.

7.2.3 Unfortunately the desirable correlation properties of coded waveforms are invariably degraded in real channel conditions. This is due to numerous factors

- Channel Time Spread;
- Channel Doppler Spread;
- Frequency Dependence (Scattering, absorption etc);
- Doppler.

7.2.4 The orthogonallity properties of digitally coded waveforms are largely based on the codes periodic correlation function of the code. This assumes that the correlation occurs in a cyclic manner. In practice realising this condition requires either that information is impressed upon the same code which repeats for each symbol or specific measures are taken to protect the code from orthogonality degradation in time spread (and ideally Doppler spread) channels.

7.2.5 Correlating on a subsequence of the code results in loss of orthogonality. This situation occurs in multipath channels when no provision is made to account for multipath. Since the time spread of RF channels forms a tiny fraction of the symbol duration, code orthogonality is often not significantly compromised. In acoustic channels multipath time spread can constitute a significant percentage of the symbol duration and so orthogonality degradation is a much more serious issue.

7.2.6 In this case, whilst the integration window may be perfectly aligned with a particular path arrival, post cursor (or pre cursor) multipath arrivals would not be so aligned, and the desirable correlation properties of the code are lost. So, whilst the synchronised path maintains its good autocorrelation properties, it would be subject to code sidelobe 'clutter' from multipath arrivals. One technique to overcome this problem is to modify the transmitted code to include a cyclic prefix and/or suffix. The duration of this prefix would be determined by the time spread characteristics of the channel. The purpose of the prefix and/or suffix is to preserve the orthogonality properties of the waveform in multipath channels.

7.2.7 This technique is employed in orthogonal Frequency Division Multiplex (OFDM) modulation schemes where the orthogonality of each sub-band carrier has to be preserved to minimise inter channel interference (ICI)[91]

7.2.8 A more comprehensive discussion of this modulation technique may be found in appendix O. In the OFDM technique the Fast Fourier Transform is used to generate orthogonal carriers for each symbolling period. In the presence of multipath (and Doppler dispersion), orthogonality of the carriers is not maintained. However, with the addition of a cyclic prefix of duration greater than, or equal to, the channel timespread, othogonality is maintained and interchannel interference reduced.

7.2.9 Evidently the addition of the prefix or time guard, reduces the system data rate and in practice the time guard duration is traded against other methods to contain ICI. These include powerful interleaved coding strategies and frequency domain equalisers which act on multiple sub-bands to reduce the ICI 'spillage' in a manner completely analogous to the time domain equaliser in combating intersymbol interference ISI. Provided the symbolling rate is sufficiently rapid, then it is possible for the frequency domain equaliser to contain ICI due to degraded orthogonality for multipath channels and for frequency spread channels. Whilst robustness to channel time spread usually drives the coded signal design problem from an RF perspective, in acoustics, channel time spread and channel Doppler spread can significantly degrade the correlation properties of phase coded signal designs. The temporal scaling influence of Doppler not only serves to rapidly decorrelate phase coded waveforms but also rapidly degrades their correlation properties. This is demonstrated in Figure 28 which shows simulated results obtained from transmitting a degree 8 maximal length (ML) code over a single path channel under zero noise conditions. In both cases the simulation involved bandlimiting prior to up conversion, transmission, channel simulation at passband, basebanding and correlation detection. Filtering stages in the processing chain served to contain the transmitted spectrum sidelobe levels and explains the small departures from the theoretical 1/N sideloble level in the zero Doppler case.

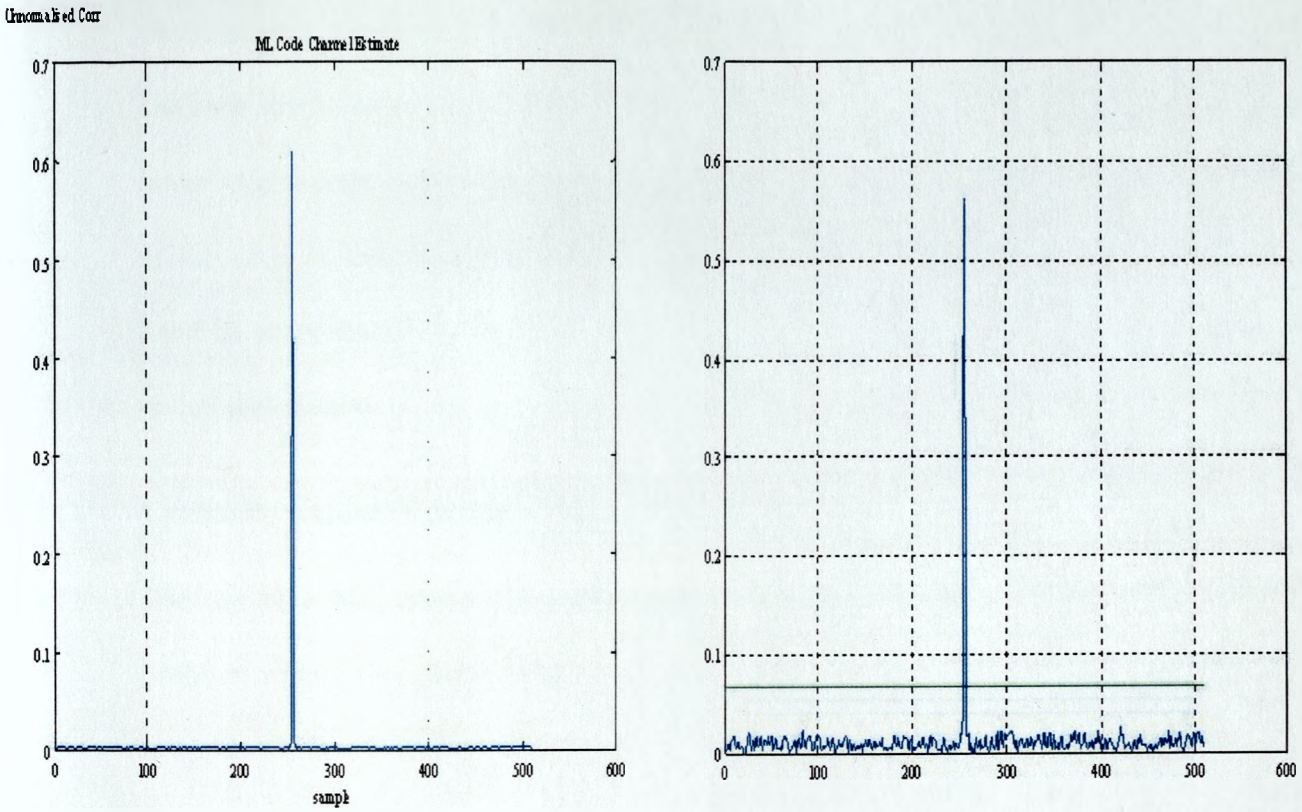

Note

- Maximal length sequence cyclic autocorrelation in ideal channel (left)
- Maximal length sequence cyclic autocorrelation in ideal channel for 1kt Doppler (right)
- Auto correlation peak value slightly reduced
- Significant sidelobe growth
- Typical detection threshold shown right.

Figure 28: ML Code Autocorrelation degradation for (left) zero Doppler and (right) 1 knot Doppler.

7.2.10 Under 1kt Doppler error, a small decrease in the main peak is evident due to decorrelation. More significantly however, the results demonstrate a clear increase in the sidelobe levels from approximately 0.002rms to 0.125rms. These sidelobes manifest as uncorrelated code noise which add on a power basis and serve to reduce the performance of the code in uncompensated, time selective channels. The simulation emphasises the need to compensate for Doppler in order to preserve the desirable properties of phase coded waveforms.

7.2.11 Cyclically Extend Maximal Code Simulation results

7.2.12 The use of a ML code with cyclic prefix is a useful method to combat the multipath problem when using phase coded waveforms. The technique is explained in greater detail in appendix Q in which orthogonal waveform designs are discussed and the role of cyclic extensions explained.

7.2.13 In applications where data is phase encoded onto the ML code, and the ML code is transmitted as a train, code orthogonality is observed, to a close approximation, where multiple carrier cycles occur within a chip. However in applications where data is encoded, in terms of separate codes for example, and the fractional bandwidth is small, then cyclic extension is necessary to preserve the code orthogonality properties. The utility of a cyclically prefixed ML code as a channel characterisation waveform is a potentially useful technique to provide a high-fidelity channel estimate. The technique is however heavily reliant upon removing the influence of Doppler temporal scaling on the received waveform prior to channel estimation. A number of simulations were performed to determine the performance of a ML code with cyclic prefix in a number of simple scenarios. The simulation involved the transmission of a cyclically prefixed channel sounding waveform formed from a 511chip ML code. The code was carrier modulated at 12kHz to give a null-null bandwidth of 12kHz and 3dB bandwidth of approximately

8kHz. A 64 tap FIR filter was used to band limit the signal prior to transmission. At the receiver the signal was quadrature downconverted, decimated to two samples per chip and I and Q channel correlations performed on the code replica. The resulting correlation is presented in unnormalised form.

7.2.14 The sounding waveform is preceded by two unshaded chirp waveforms used for the purposes of Doppler estimation and compensation of the ML_{chan} channel estimation code which is known (Figure 29). Subsequent ML codes convey data. As discussed in the previous section Doppler compensation is necessary to preserve the orthogonaility characteristics of the ML code.

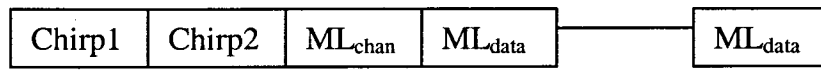

Note

- Two chirps used for burst time-Doppler synchronisation
- Cyclically extended Msequence(s) Doppler compensated prior to correlation

Figure 29: Cyclic Extension ML Code Channel Characterisation

7.2.15 Figure 30 depicts four graphs as follows from top to bottom

- Chirp1 Correlation result
- Chirp2 Correlation result
- ML Correlation result
- ML data symbols

7.2.16 The top figure shows the five simulated path arrivals resulting from the convolution of the channel impulse response with the transmitted chirp1. The figure shows the high sidelobe levels inherent in the chirp waveform design. This is also manifested in relative magnitudes of the path correlations since the second path magnitude is slightly smaller than the third by virtue of sidelobe contamination. In the second chirp result, the high correlation levels subsequent to path arrivals is due to the ML channel sounding codes in the same bandwidth as the chirps and as such manifest as uncorrelated noise. The ML channel sounding result clearly demonstrates reduced sidelobe levels both in the vicinity of the path arrivals and outside. Also of note is the fact the relative magnitude of each arrival is consistent with the simulated path weights, indicating the reduced influence of sidelobe contamination. The bottom figure shows subsequent ML correlation results from data decoding. In order to evaluate the technique in a more representative environment, an acoustic channel replaced the simulated channel. Here the signal was transmitted under a variety of multipath conditions and noise levels. Figure 31 shows the received results for a modestly complex channel. The graphs demonstrate a relatively simple multipath structure comprising a direct arrival and one or two weaker path arrivals. As in the simulated case the sidelobe levels on the ML channel estimate are noticeably less than for the chirp and the range resolution is also superior. Figure 32 shows a more complex multipath structure comprising direct and scattered arrivals. Here the sidelobe levels have increased, however the ML sounding waveform provides the best channel estimate in terms of resolution and noise.

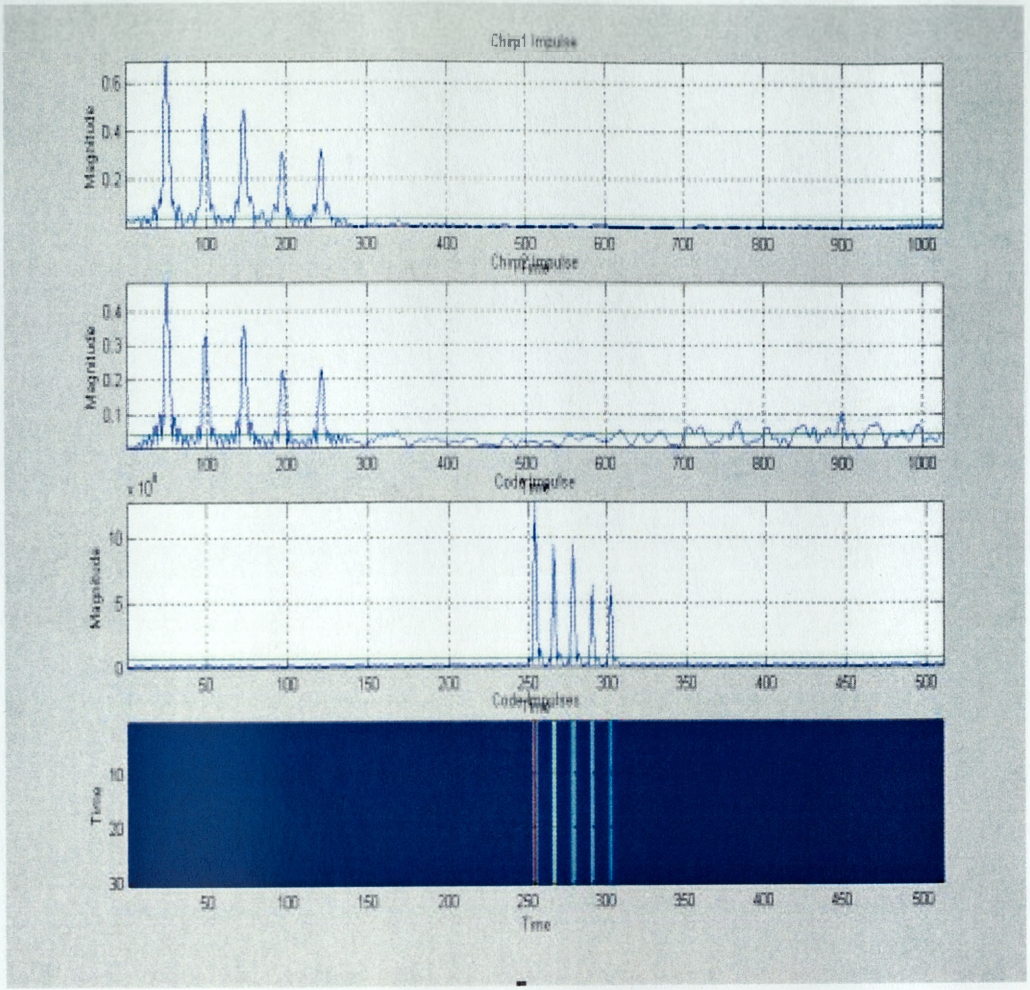

Note

- Simulated Channel
- High chirp sidelobe levels (unwindowed)
- Significant code noise breakthrough on second chirp correlator
- Negligible sidelobes for cyclically extended Msequence correlation

Figure 30: Simulation results $h(Z) = 1 + 0.75\,Z^{-50} + 0.75\,Z^{-100} + 0.5\,Z^{-150} + 0.5\,Z^{-200}$

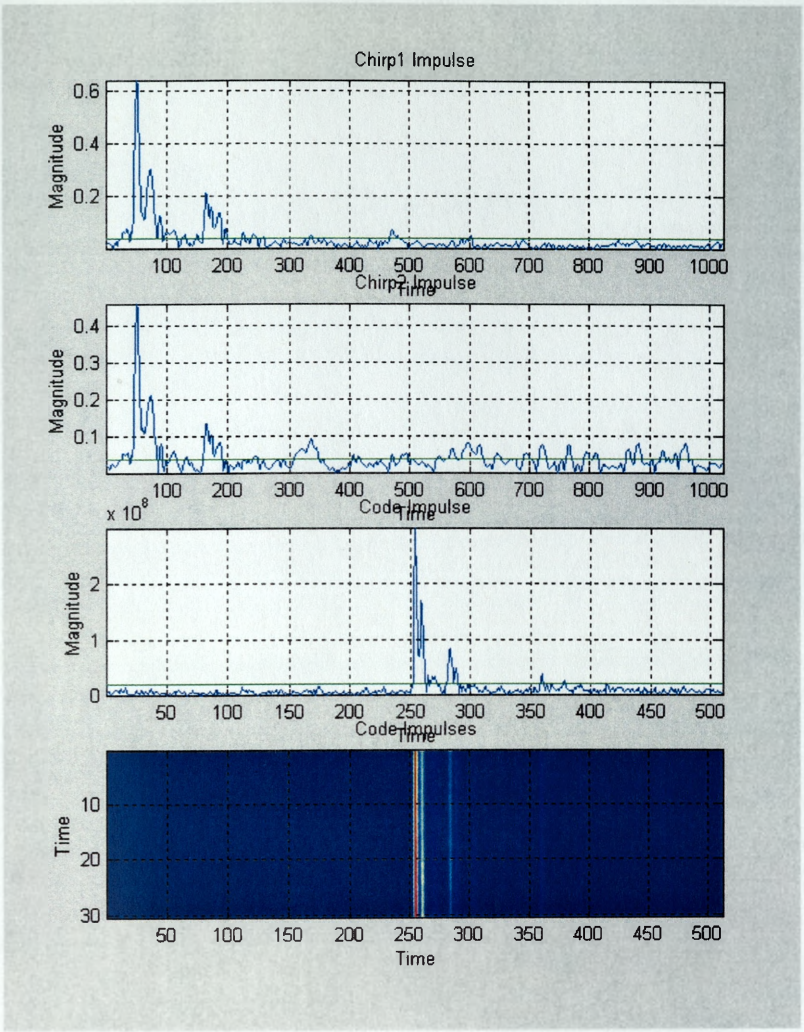

Note

- 'Simple' air acoustic channel
- Significant code breakthrough on second chirp correlator
- Negligible sidelobes for cyclically extended Msequence correlation

Figure 31: Air Acoustic Experiment Direct Separation 3m.

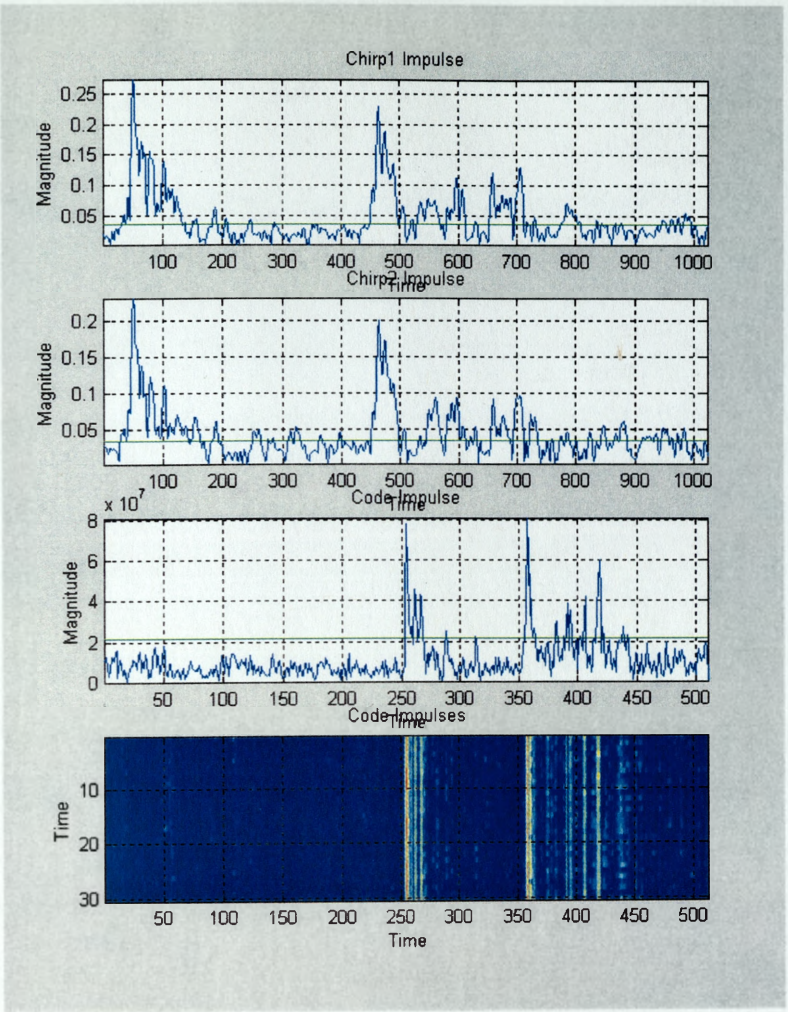

Note

- Complex air acoustic channel
- High chirp sidelobe levels (unwindowed)
- Improved path resolution on cyclically extended ML sequence
- Lower sidelobe contamination on cyclically extended ML sequence

Figure 32: Air acoustic experiment with more complex scattering

7.3 Correlation Detection in Time Selective Acoustic Channels

7.3.1 The preceding discussion has considered the effect of linear Doppler on waveform ambiguity. In practice Doppler will be time variable due to intrinsic ocean effects and platform dynamics. Intrinsic ocean variability arises by virtue of the spatial and temporal variation of the interfaces and medium. Time coherence is a parameter used to convey the time variability of a communications channel. It is often quoted as the reciprocal of the channel Doppler spread in a narrowband RF sense and its measurement is usually based on the complex channel scattering function. When the channel undergoes amplitude and phase variability on timescales comparable to the communication symbol duration, then the channel is termed time selective. If the timescales of variability are much longer than the communication symbol duration then the channel is termed time non-selective.

7.3.2 Conventionally the symbolling rate over communications channels must be sufficiently rapid to track the time varying channel impulse response of the channel. Ultimately the acoustic channel is much more complicated than the simple simulations presented here, however the results do indicate the vulnerability of phase coded waveform designs to channel time selective behaviour. This includes both delay and amplitude variability. Obviously if this variability is on a much longer timescale than the waveform itself, its impact on overall system performance is reduced. This underlines the importance of understanding and characterising acoustic channel behaviour.

7.3.3 In the RF channel case, equalisation and carrier phase synchronisation are effectively de-coupled by virtue of the relaxed Doppler problem. Since the symbols occupy a large spatial scale due to their high propagation speed, the channel impulse magnitude response changes slowly compared to the acoustic channel for moving platforms. However, since the carrier wavelength occupies a much smaller spatial scale the channel phase response

is much more dynamic. This is a much easier problem to deal with provided the symbolling rate is sufficiently rapid to implement phase lock loop techniques.

7.3.4 A fundamental requirement of any noise tolerant communications system is that the symbol duration be made as long as possible to maximise the signal energy since this maximises the receiver signal-to-noise performance after matched filter detection. In practice the dynamic nature of the ocean environment coupled with platform motion results in a complex time varying Doppler profile.

7.3.5 If the Doppler varies significantly within the symbol integration interval the detection performance will degrade. The level of degradation will be a function of the rate of Doppler change and the associated timescale. The need to maximise signal energy therefore conflicts with the need to sufficiently oversample the time varying channel impulse. Physical arguments, the results of channel measurements by several authors presented in section 3 and field measurements presented in section 4, suggest variations of Doppler of typically +/-0.5m/s occurring over a timescale of 1-2s. The actual variability would be determined by the dynamics of the communicating platforms, their size and prevalent sea state. The physical interpretation of this result is that if the symbol waveform duration used for communications is comparable to the timescales of Doppler variability arising for example, from platform dynamics, then significant degradation in system performance can arise.

7.3.6 Discussion

7.3.7 The doubly spread nature of the underwater acoustic channel makes the problem of channel estimation particularly difficult. Indeed where the product of the channel time and frequency spread is greater than unity one cannot unambiguously characterise the channel.

7.3.8 For RF systems the modest influence of Doppler on the (baseband) waveform design has meant that these designs are often driven by the desire to maintain good auto-correlation performance in time spread channels or cross correlation performance for families of waveform designs.

7.3.9 It has been shown that when subjected to acoustic Doppler the desirable correlation properties of these 'good' waveforms degrade. Thus if one is to actively attempt to exploit these properties in an acoustic environment one must implement complex synchronisation schemes to compensate for the Doppler problem. In the next section the signal design problem is revisited with a view to using waveforms or modifying waveform parameters to convey information i.e. modulation.

"Unstable as water, thou shalt not excel."

Genesis, ch.49, v.4

8 MODULATION DESIGN

8.1 Overview

8.1.1 The complexity of the underwater environment has stimulated much research into acoustic communication modem design and a broad range of technologies has been applied to the undersea communications problem. Despite the complexity of the acoustic underwater channel there have been many acoustic communications systems developed over the last 25 years. The technological approaches are diverse both in terms of modulation, equalisation, synchronisation and spatial processing methodologies which underlines the system wide nature of the acoustic communications problem.

8.1.2 Thus far, discussion has focussed on understanding the ocean environment, its impact upon signal coherence and potential means to measure and track the environment have been presented. The aim in this section is to consider the problem of how one impresses information upon physical waveforms, which propagate and interact with the environment.

8.1.3 The arguments closely parallel those presented for the problem of characterising the environment. The main difference stems from the additional constraints imposed by the need for high data rate. In this case more judicious use of available bandwidth is necessary to maximise data throughput.

8.1.4 It is however important to emphasise that the performance of any communications system cannot be assessed merely on modulation technique alone. Moreover overall system

performance is dependent on synchronisation, equalisation, spatial processing and coding elements which are likely to be specific to the choice of modulation.

8.1.5 Inevitably it is extremely difficult to assess modulation performance on a quantitative basis since there are many other factors which influence overall system performance. In [13] for example McDonald et al evaluate the performance of a diverse range of waveforms for the purpose of modem validation and comparison. A feature of this paper was the use of a composite waveform train designed to ascertain characteristics of the channel prior to modem evaluation. This included long CW to ascertain frequency spreading and multiple chirps to ascertain channel coherence on the decisecond timescales. Whilst the results presented were somewhat qualitative the paper demonstrates the efforts needed to provide a quantitative basis for the evaluation of modem performance and the necessary experimental configurations necessary to achieve this.

8.2 Single Carrier or Multiple Carrier?

8.2.1 The doubly spread nature of the acoustic channel [24,53,54] has a profound influence on the choice of signal design, and the time-frequency duality of the problem inherently means that the 'best' signal design is a trade off exercise. Some basic arguments can be developed based purely on the signalling rate.

8.2.2 If one chooses a single carrier modulation scheme (SCM) where the effective symbol rate is high, each transmitted symbol occupies the entire transmission bandwidth. If this bandwidth exceeds the channel coherence bandwidth, the channel is termed frequency selective and fading will occur selectively within the transmission bandwidth. Further, if the symbolling rate is higher than the channel time coherence the channel is time non-selective.

8.2.3 If one chooses a multicarrier modulation scheme (MCM) where the effective signalling rate is reduced, each transmitted symbol occupies a bandwidth less than the channel coherence bandwidth and so each undergoes 'flatter' (frequency non selective) fading. Since the symbolling rate is reduced, MCM systems are more prone to channel time selective effects however the channel equalisation problem is relaxed.

8.2.4 Since the underwater acoustic channel exhibits both time and frequency selectivity it is not immediately obvious whether SCM or MCM systems have the advantage, particularly since there are numerous receiver processing techniques to reduce the susceptibility of SCM to frequency selective behaviour and MCM to time selective behaviour.

8.2.5 However, it could be argued that MCM might have an advantage, since it affords a more scaleable option. One can increase or reduce the number of carriers and reduce/increase the symbolling rate to best match the carrier bandwidth to the channel coherence bandwidth and the symbolling time to channel coherence time.

8.2.6 In the context of underwater acoustic communications the choice of single carrier versus multicarrier represents a fundamental step in the system design process. The relative advantages of these two approaches to the system design problem are now developed.

8.3 MCM Acoustic Communications

8.3.1 Multicarrier schemes have historically been forwarded as a useful technique to relax the equalisation problem [88-92], however their application to UW communications problem has been mainly limited to non-coherent MFSK modulation schemes. The application of multicarrier coherent schemes to the underwater communications problem is relatively new [93,94,95]. A particularly elegant form of MCM is coded orthogonal frequency division multiplexing (COFDM) [91]. Here the modulation-demodulation process is realised using the FFT to generate carriers at the minimum frequency separation to ensure

orthogonality. A more comprehensive discussion of this technique is presented in appendix O and summarised here.

8.3.2 OFDM effectively reduces the symbol duration by a factor N where N is the number of carriers thereby reducing the signal bandwidth commensurate with the channel coherence bandwidth. Under such conditions the fading between carriers becomes independent and each channel can be considered as flat fading [89].

8.3.3 For such a channel the equalisation requirement reduces to a single (complex) tap per carrier in the frequency domain. The main constraint on symbol rate reduction is the channel time coherence. Extending the symbol duration can result in carrier orthogonality degradation which in turn results in energy 'smearing' between adjacent carriers. The performance of the multicarrier coherent approach therefore relies on achieving a symbol rate commensurate with the channel time coherence. The basic principle of multicarrier modulation is shown in Figure 33. For this frequency selective channel, deep fades are evident within the single carrier bandwidth, necessitating a receive equaliser. For the multicarrier system, each carrier has a greatly reduced bandwidth such that each sub-channel is effectively frequency non-selective. However one or two carrier are lost through the deep fade at 18kHz. To recover this data forward error correction coding is necessary. Figure 34 provides a concise summary of the relative merits and issues relevant to SCM and MCM modulation techniques.

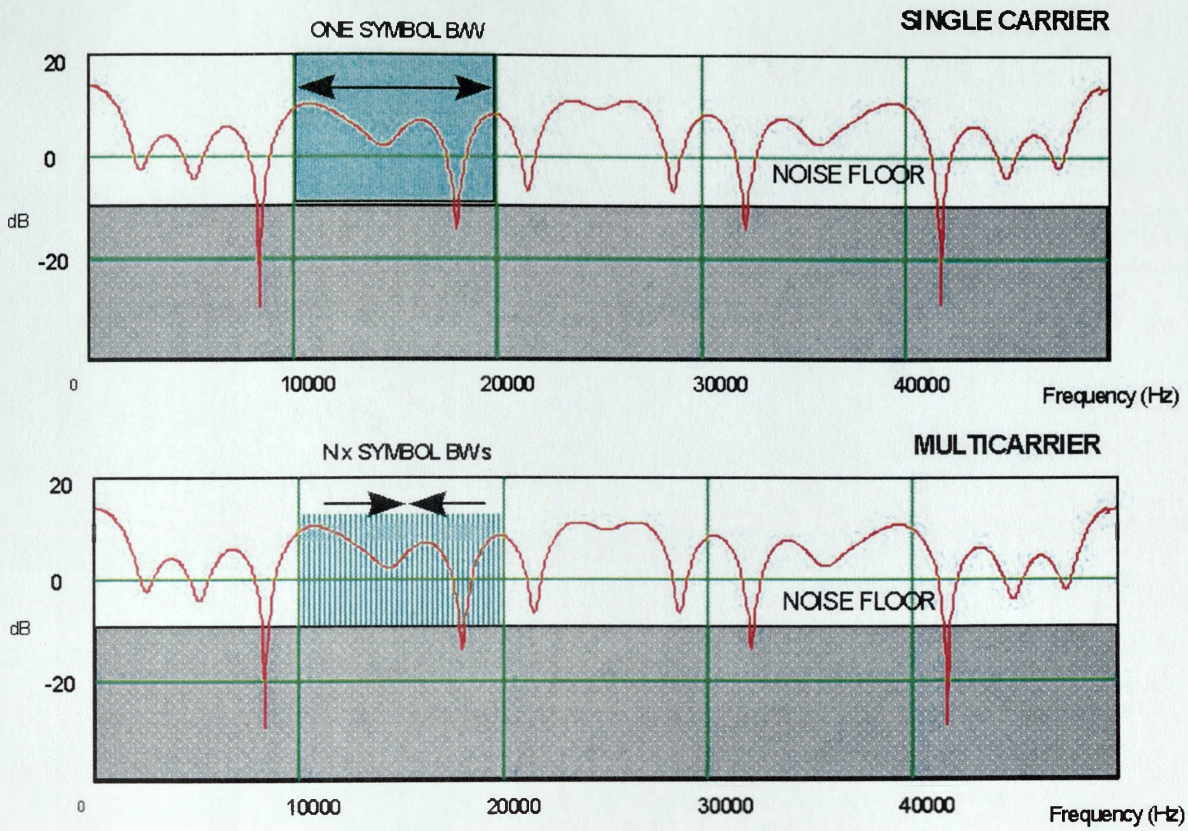

Note

- Frequency selective fading for wideband single carrier transmission
- Frequency non selective fading for wideband multicarrier transmission
- Deep fades occur within bandwidth
- Information lost in multicarrier system -> need coding !
- Noise enhancement in single carrier equaliser

Figure 33: Single carrier versus multicarrier modulation in frequency selective channels

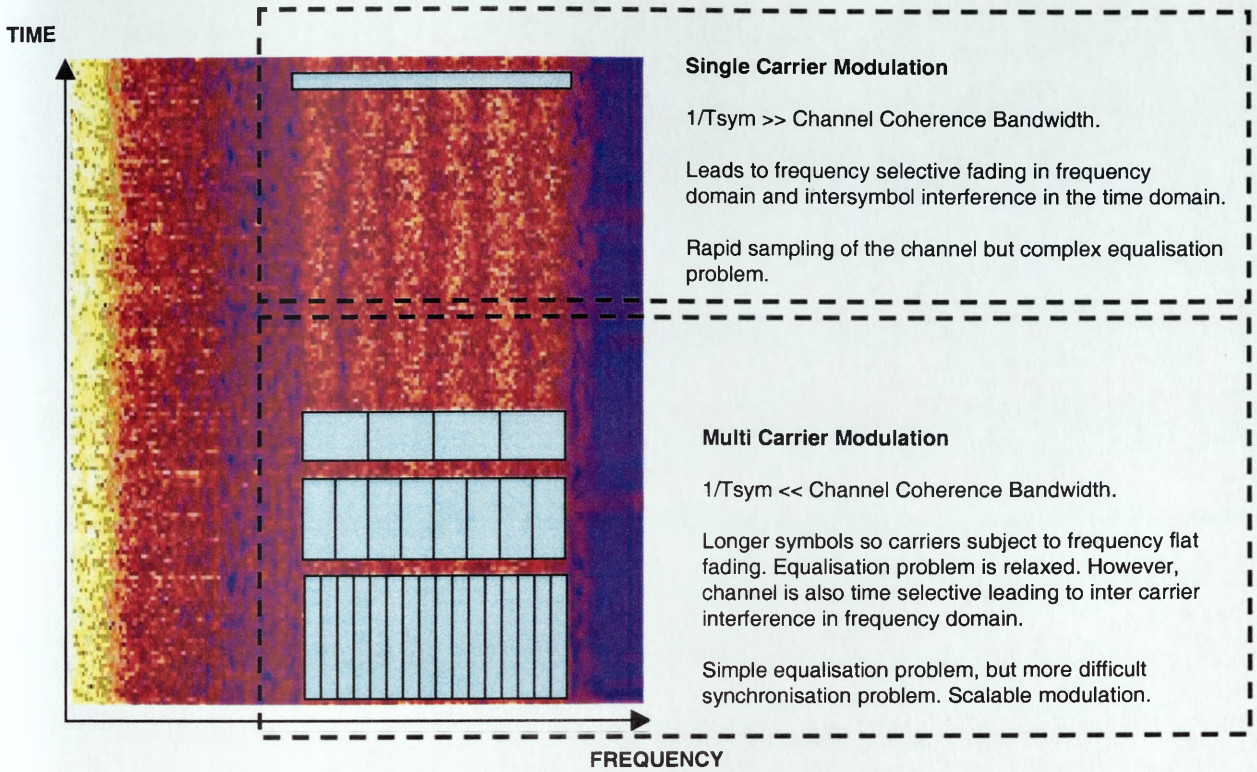

Note

- Single carrier modulation occupies entire bandwidth
- Single carrier modulation provides rapid sampling of channel bandwidth: better for time selective channels
- Complex equalisation required for single carrier modulation design
- Possibility of of tailored time-frequency signal design for time-frequency selective channels

Figure 34: Signal design issues: SCM versus MCM in time- frequency selective channels

8.3.4 For non-minimum phase channels exhibiting deep nulls, noise enhancement occurs around the null frequencies. If the nulls extend significantly below the noise floor, then some symbols cannot be recovered. For this reason OFDM systems must employ error correction coding to truly benefit from inherent frequency diversity. Since the number of carriers is large, then error correction coding can be applied in time and frequency domains. For each case the time-frequency interleave depth will be constrained to ensure that errors in time and frequency are uncorrelated.

8.3.5 Whilst MCM techniques are powerful against multipath, they are more susceptible to channel time selectivity. Since the effective symbolling rate is reduced, the effective channel sampling rate also reduces and symbol time coherence margin degrades. This means that the system is less able to track the amplitude and phase fluctuations for more dynamic channels and each carrier is subject to frequency domain dispersion.

8.3.6 The time selective channel serves to smear channel energy in frequency in a manner completely analogous to time domain spreading by frequency selective channels. The nature of the energy distribution will be a function of the carrier amplitude and phase modulation mechanism since both will serve to introduce spectral smear. In the MCM approach spectral smear between carriers manifests as additional noise terms or inter carrier interference (ICI) which is analogous to ISI in the time domain SCM system.

8.3.7 Much recent work has been directed at improving the performance of multicarrier techniques in the presence of single and doubly spread channels. Traditionally, in order to ensure carrier orthogonality between frame intervals, cyclic extensions to the data frame are used. These extensions effectively ensure that within the observation window the multipath components are circular convolved such that during demodulation, carrier orthoganality is maintained for multipath arrivals within the extension duration and the

equalisation requirement reduces to a single complex tap to equalise the ideal (flat) channel response.

8.3.8 For long multipath spreads where the use of a long cyclic extension is undesirable, frequency domain DFE equalisers have been proposed [91] which serve to re-establish carrier orthogonality by cancelling sidelobe energy 'spillage' contributions from adjacent carriers. Here the equaliser accepts symbols from a number of adjacent carrier channels and adapts the complex weightings to cancel energy leakage. Since the energy contribution falls as a sin(x)/x squared function, it can be argued that only contributions from neighbouring carriers are significant which relaxes the processing overhead. The feedback portion of the equaliser allows cancellation (in frequency) of multipath components spanning more than one symbol interval.

8.3.9 The timing and synchronisation requirements for the multicarrier approach are inherently more severe than the single carrier approach. Under high Doppler conditions the orthoganality condition is destroyed, however provided it is re-established using a sample rate adjustment prior to FFT demodulation, residual Doppler and timing errors could then be compensated by the frequency domain equaliser. Recall that initial timing and Doppler estimates are also necessary for the time domain DFE to ensure a useful data frame length.

8.3.10 Differential Doppler and Doppler acceleration are however much more difficult to control and will have a significant impact on the performance of a COFDM system. These effects degrade system performance on two levels. Carrier orthogonality is degraded within frame intervals and gives rise to dynamic variability in the channel null positions and overall phase response between frame intervals. Since phase transitions are most rapid near to interference nulls, single complex tap equalisers must track extremely rapid phase

fluctuations in these regions. In instances where many deep nulls exist and Differential Doppler occurs, the performance of COFDM will degrade substantially.

8.3.11 Frequency hop and frequency modulation techniques have also been developed as a means to overcome the difficult multipath conditions. In such systems the frequency selective fading problem is essentially addressed in the time domain [89] discriminating between multipath components by altering frequency sufficiently rapidly to ensure orthogonality.

8.4 SCM Acoustic Communications

8.4.1 For single carrier systems employing a bandwidth exceeding the coherence bandwidth of the channel, frequency selective fading occurs within the transmission bandwidth. This gives rise to intersymbol interference (ISI) in the time domain where time spreads due to multipath may span several tens or even hundreds of symbols. To counter the deleterious effects arising from ISI, an equaliser must be used [96]. The complexity of the equaliser will be dependent on the delay power profile and extent of the multipath spread i.e. the arrival time and energy of each multipath. Such an equaliser shown in Figure 35.

8.4.2 For a single path channel, which can be made minimum phase with an appropriate delay, equaliser implementation is straightforward. For a multiple path channel exhibiting non-minimum phase characteristics where a causal, stable channel inverse filter may not exist one must resort to non-linear equaliser architectures or more complex detection schemes such as maximum likelihood sequence estimation (MLSE). A more thorough discussion on channel invertability and non minimum phase systems is presented in appendix F. The adoption of single carrier modulation and complex equalisation structures has become firmly established in underwater acoustic telemetry [96]. However, this structure is, in itself not a solution to the problem as will be discussed in subsequent sections.

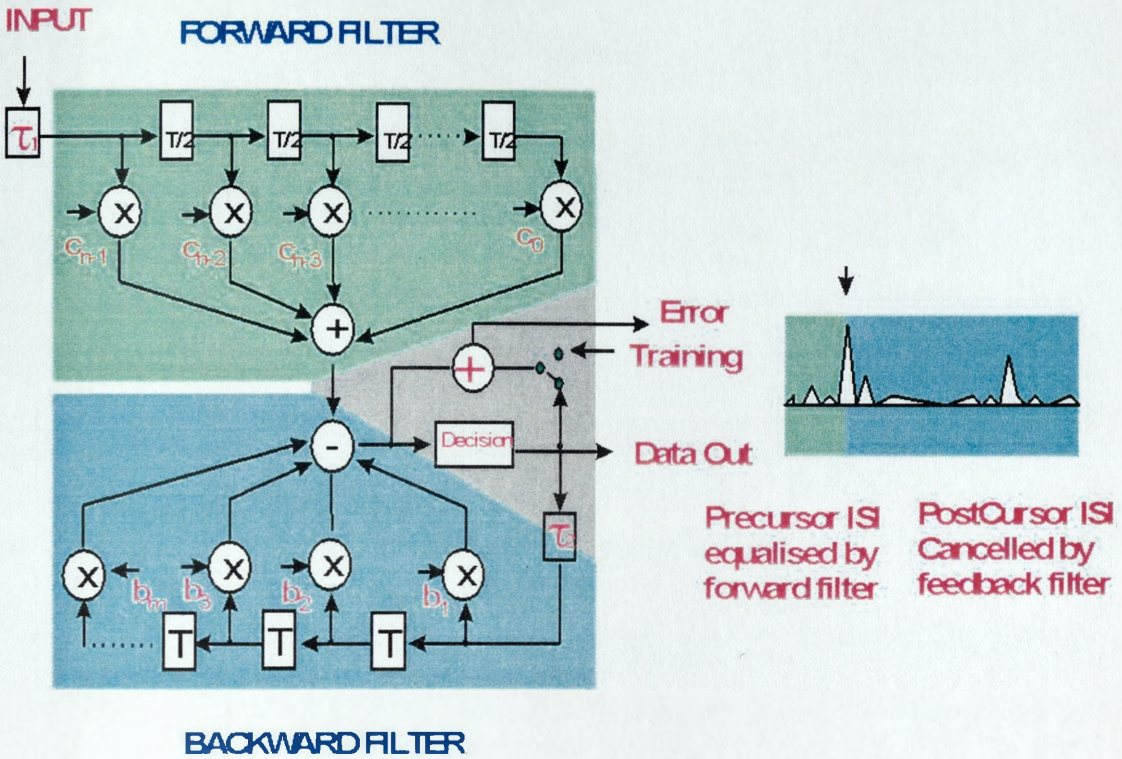

Figure 35: Decision feedback equaliser

8.4.3 Decision feedback equalisers (DFE) provide a low complexity non-linear solution to non minimum phase channels by avoiding noise enhancement near the unstable pole positions which arise in traditional linear equaliser designs [97]. The principle of operation is to cancel multipath components by feeding back the recovered data symbols (which are assumed error free), delaying and appropriately weighting them in a tapped delay line structure. Due to the time varying nature of many physical communications channels, adaptive equalisers have been the chosen solution for many RF terrestrial and underwater acoustic communications. Such adaptive structures are able to track the time varying character of the communications channel [98]. Figure 35 illustrates the typical form of a decision feedback equaliser comprising a fractionally spaced forward FIR section, a

symbol spaced feedback FIR section and a decision algorithm. The basic operation assumes error free decisions generated by the forward filter. These good symbols are then feed back through the feedback section to coherently cancel postcursor multipath.

8.4.4 Optimising coefficients for a particular channel can be based either on peak distortion or mean squared error criteria [97] as discussed in appendix H. In practice however the channel is not known and/or is time variant. For this reason coefficient update is normally done adaptively enabling the structure to adapt to and track the channel. To this end there are many adaptive algorithms and a comprehensive review is provided in appendix K.

8.4.5 The structure in the figure implicitly assumes that the channel structure is minimum phase, that is to say decisions are based on early arrivals to cancel later arrivals. For channels where significant paths arrive after smaller precursor, it is clear that the above structure is no longer suited to the equalisation task. This situation could occur for example, in low frequency propagation where geoacoustic propagating components arrive before the main waterborne arrivals. One solution to this problem is to time reverse the received data [99]. In this case received symbol data is buffered and time reversed prior to equalisation. In a conventional implementation of adaptive processing this would require training data at the start and at the end of each data packet in order to cope with both minimum and maximum phase channels.

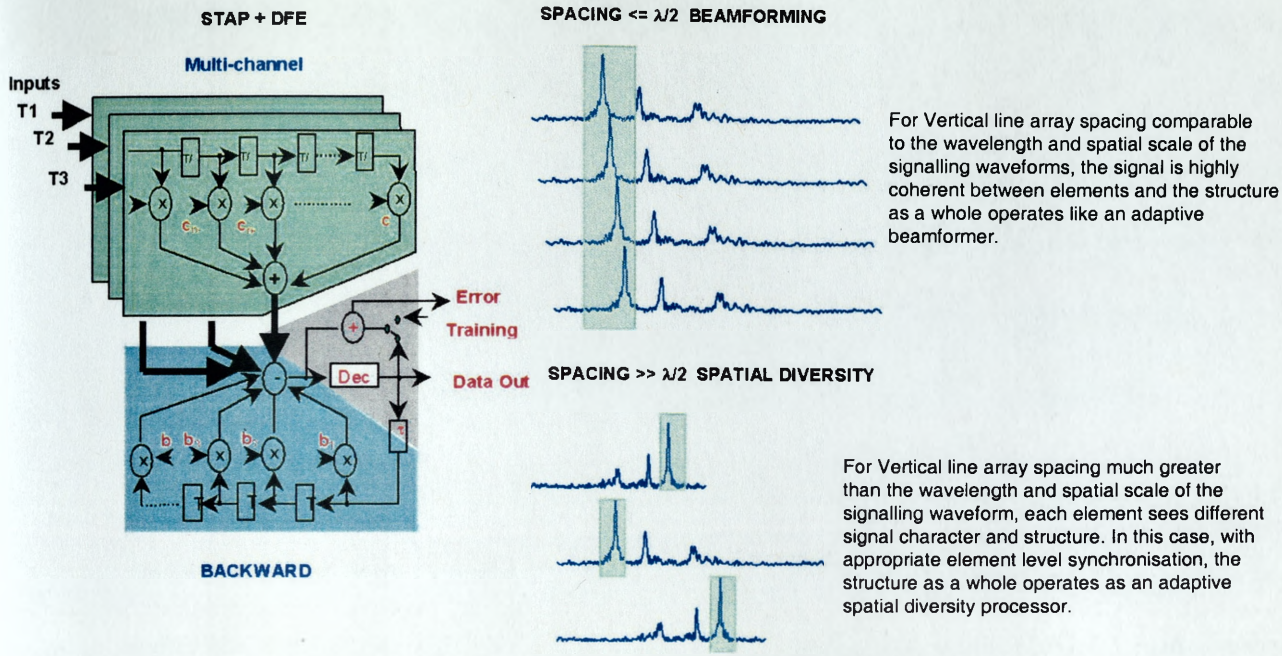

Figure 36; Spatial Temporal Adaptive Processor with Decision Feedback

8.4.6 Another solution to this problem is to implement the DFE structure in a multichannel form, as shown in Figure 36. This structure has been extensively studied in RF applications as a spatial diversity receiver [100] and more recently in underwater acoustic applications [96]. Here multiple feed forward sections from spatially separated receivers replace the single feed forward section. The output from each section is then summed and fed to the feedback section. In this case the structure is able to exploit spatial characteristics of the incident acoustic field in order to reduce the equalisation task. Spatial - temporal adaptive processing (STAP) is a particularly powerful processing technique to contain the multipath problem. Its ultimate performance is however closely related to the time, frequency, angular and spatial coherence characteristics of the incident field and the precise form of algorithm implementation (equaliser taps, adaptive algorithm, sensor separation etc).

8.4.7 For example, the spatial adaptive behaviour of the structure will depend upon the spatial coherence of the incident field. For small sensor separations the incident field between

sensors will be strongly correlated. For wide sensor separations the spatial coherence will degrade. In this case transmission bandwidth is exploited since the receiver can (with appropriate synchronisation) exploit energy from several independent paths. The precise definition of the receiver in either case (beamformer / spatial diversity processor / path diversity processor) is ultimately determined by the coherence characteristics of the incident field which itself will be a function of geometry and sensor separation.

8.4.8 This structure has recently become established in underwater communications, however its performance under channel Doppler and ray differential Doppler has not been widely reported. Indeed the issue of Doppler is largely dismissed as a secondary issue to the multipath problem and its impact on equaliser performance often misunderstood. There are however fundamental differences between RF terrestrial channels and underwater acoustic channels with regard to time selectivity, specifically Doppler. For a 200ksym/s RF terrestrial system such as GSM each symbol represents a propagation distance of 1.5km, for an acoustic system operating at 20ksym/s each symbol represents a propagation distance of only 7.5cm. This means that a platform moving at 1m/s will effectively traverse 13 symbols per second underwater compared to 0.0007 symbols per second above water. This demonstrates the marked difference in the Doppler problem between the two systems. Specifically symbol synchronisation is a greatly amplified problem for the underwater communications channel. Considering phase synchronisation, an acoustic system operating at 15kHz and an RF system operation at 3GHz each have a 10cm wavelength. A receiver moving at 1m/s experiences a phase rotation of 20π per second for either system. In the RF case phase synchronisation is achieved using a phase locked loop and the modest symbol timing requirements are performed separately [101]. In the acoustic case symbol timing slip occurs at a comparable rate to phase rotation such

that the carrier phase tracking and symbol timing recovery are much more tightly coupled and the problem as a whole is much more difficult.

8.4.9 Figure 37 demonstrates the influence of acoustic Doppler on phase coherent single carrier communications. The simulation involved a passband simulation of a 10ksps Nyquist shaped QPSK transmission at 30kHz centre frequency, over a single path ideal channel for a constant simulated Doppler 1m/s.

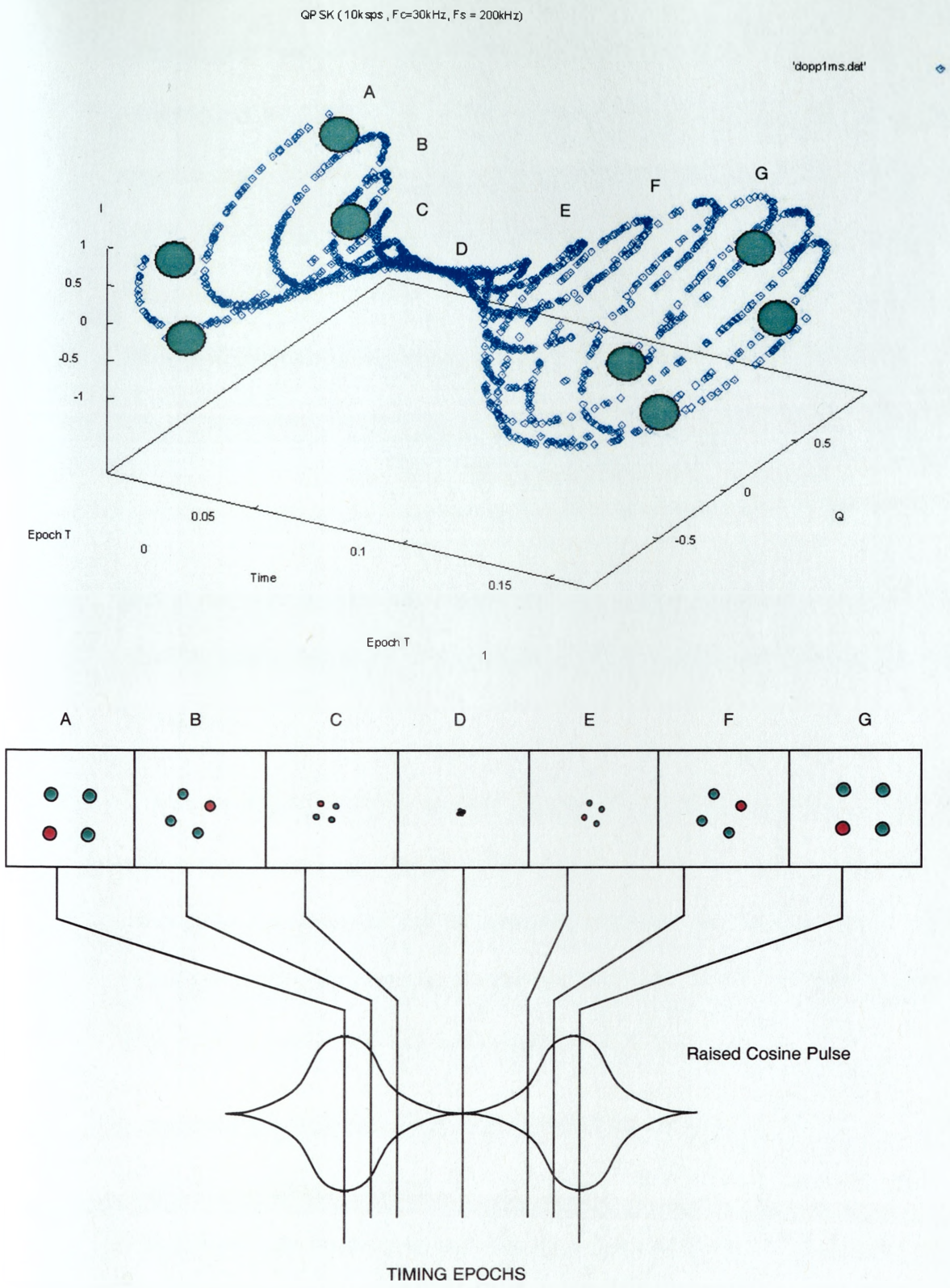

Figure 37: Doppler phase rotation and symbol timing slip at complex baseband

8.4.10 The figure shows baseband I and Q symbol data evolved over 0.15s comprising 1500symbols and demonstrates the phase rotation resulting from the 20Hz Doppler frequency translation of the carrier frequency. Over this time the constellation rotates approximately 1080degrees. Of more significance however is the slip in timing epoch which occurs over the 0.15s as demonstrated by the variation in the constellation size which describes the envelope of the Nyquist pulse design used in the simulation. Over the 1500 symbols the time slippage, in terms of symbols is a single symbol :-

$$\alpha = (1500+1)/1500 = 1.000666667$$
$$(1-\alpha)*1500 = 0.0006666*1500 = 1 \quad symbol$$

8.4.11 This is demonstrated by the fact that the I,Q envelope describes one complete pulse over the 1500 symbol duration. Thus, acoustic Doppler manifests as phase rotation and symbol timing slip.

8.4.12 In light of this argument it is clear that adaptive equalisers behave very differently for underwater channels compared to RF channels. In the RF case, carrier phase fluctuations are readily compensated for by complex equaliser tap rotation. Under high platform velocities where phase rotation is extremely dynamic, a single adaptive phase locked loop (PLL) can be used to off-load tracking effort from the equaliser.

8.4.13 In practice the adaptive PLL will off-load the Doppler shift arising from the mean Doppler component across all multipaths. Differential path Doppler shifts are compensated for by relative tap rotation in the main equaliser. However provided the differential Doppler is small (which will be the case at medium/long range), the tracking effort is unlikely to exceed the tracking capability of the equaliser.

8.4.14 In the acoustic case the equaliser not only has to track phase variations but also compensate for symbol timing slip. In practice, symbol timing compensation is achieved in the forward filters. By ensuring at least two samples per symbol at complex baseband, the structure can synthesise and compensate for slowly time varying delays:- so called fractional spacing. [102,103]. A more thorough discussion on the performance benefits of fractional spaced equalisation is presented in appendix P.

8.4.15 For acoustic channels, where significant platform Doppler and Doppler acceleration occurs as demonstrated in earlier sections, excessive tracking effort is required from the forward filters, not only for phase correction but also symbol timing jitter. Despite this limitation, the majority of researchers have adopted a single PLL to address the acoustic Doppler problem [104]. The problem of symbol timing recovery is largely left to the ability of the forward fractional filters to compensate for temporal variability in optimum sampling epoch. It will be shown later that PLL and DLL support have a key role in adaptive equaliser perfomance.

8.4.16 Whilst effective in RF communications the PLL does not fully address the acoustic Doppler problem. The PLL essentially implements a carrier phase adjustment to counteract the phase change arising from carrier frequency translation due to the Doppler effect. It does not, however account for the temporal scaling inherent in underwater communications which manifests as both carrier translation and bandwidth expansion/compression (i.e. symbol timing slip).

8.4.17 Since the transmission fractional bandwidth of high data rate signals is high, it is often more appropriate to treat the phase recovery and symbol timing problem together i.e. through the use of a front end multirate sampling adjustment to provide a passband Doppler correction prior to data demodulation. Even after compensating for the mean

platform Doppler component multipath time variations will still incur a significant tracking effort from the adaptive equaliser. This would be the case, for example, if accelerations occurred on a comparable timescale to data packet durations.

8.4.18 Consider a 10ksym/s system using a 32tap filter where each symbol has an effective spatial scale of 15cm. Channel characterisation results presented earlier indicated ray phase fluctuations of the order of 2 radians for a 1kHz carrier occurring on timescales less than 1second. This equates to a path length fluctuation of approximately 50cm i.e. more than 5 symbols at 10ksym/s. A considerable tracking effort is required when many multipaths arrive and where each undergoes delay and magnitude fluctuation.

8.4.19 This effort is offset by the rapid channel sampling effected by each transmitted symbol which occupies the entire transmission bandwidth. Increasing the symbolling rate provides a greater oversampling of the channel transfer function. For highly time spread channels a single equaliser span is likely to extend over many hundreds of symbols and so even with the fastest adaptive algorithms the channel must be greatly oversampled if acceptable channel tracking is to be achieved. The balance between fast channel sampling and equaliser tracking performance degradation is central to their performance.

8.4.20 It is therefore evident that the choice of single carrier systems using high symbolling rates with time domain adaptive equalisers is not a straightforward one. Indeed the need to perform initial Doppler estimation and compensation reduces the main advantage of SCM systems i.e. their tolerance to channel time selectivity. In addition, adaptive DFE's can experience problems equalising some extreme channel conditions. As demonstrated in earlier sections, minimum, maximum and non-minimum phase channel characteristics occur in underwater acoustics.

8.4.21 For maximum phase channels where precursor multipath dominates and there is insufficient angular separation for spatial filtering to improve performance, the DFE must be implemented with a time reversal structure to operate effectively [99]. For non-minimum phase channels which do not have a causal, stable inverse the convergence rate of the DFE becomes a significant issue

8.4.22 Even assuming the equaliser structure is suited to the prevalent channel conditions the equaliser must be trained prior to decision directed data detection in order to circumvent error propagation effects due to the equaliser closed loop structure.

8.4.23 It will be shown in subsequent sections that the multichannel decision feedback equaliser is not in itself a solution to the high data rate acoustic communications problem and its performance is heavily reliant on additional processing to alleviate the convergence and tracking burdens imposed by typical underwater acoustic channels.

8.5 Modulation Methods

8.5.1 The most fundamental aspect of any communications system is the modulation technique since this ultimately maps information to a physical waveform, which propagates and interacts with the environment. This interaction with the environment inevitably serves to distort the waveform and recovering the transmitted information from the distorted waveform is the ultimate goal of the receiver.

8.5.2 There are many ways in which to map information to a waveform. Conventionally these involve altering the characteristics of a carrier waveform in a predetermined manner known to the intended receiver. The class of linear modulation methods serve to alter either the magnitude or the phase of the carrier in a linear manner

- ASK – amplitude shift keying where the waveform magnitude conveys information

- BPSK – bi-phase shift keying where the waveform phase assumes one of two levels to convey information.

- MPSK – multiphase shift keying where the waveform phase assumes one of M levels to convey information

- DPSK –differential phase shift keying where the waveform phase difference from one symbol to the next assumes one of M levels.

- QAM – quadrature amplitude modulation where the waveform magnitude and phase assume one M levels in order to convey information

8.5.3 The class of non linear modulation methods serve to alter the phase of the carrier in a non linear manner

- MFSK – multiple frequency shift keying where the waveform instantaneous frequency assumes one of M possible values

- MSK – minimum frequency shift keying where the instantaneous frequency is stepped between symbols such that the phase assumes one of M discrete values.

- GMSK – Gaussian minimum frequency shift keying where the instantaneous frequency is smoothly altered between symbols such that the phase assumes one of M discrete values. The smooth adjustment serves to reduce sidelobe levels in the transmission waveform.

8.5.4 In more complex modulation schemes the above modulation methods act as an inner scheme to a more complex outer modulation scheme designed to improve the robustness of the system to channel impairments such as multipath. Two such methods are

- Direct sequence spread spectrum

- Coded Orthogonal Frequency Division Multiplexing.

8.5.5 A further class of modulation schemes are those based on pulse position techniques whereby information is encoded in to the pulse arrival time either absolutely or differentially. The robustness of this technique may be significantly improved through the use of coded waveforms to enable the system to resolve and exploit multipath.

8.6 PPM

8.6.1 One of the earliest techniques proposed for underwater communications is the use of pulse position modulation (PPM). Riter [105] presents a number of design considerations in applying PPM techniques to the underwater channel. Riter assumes the narrowband case and derives expressions for the error performance of generic PPM systems as a function of BT product and received signal-to-noise ratio. The influence of channel delay spread on PPM system performance is not analysed, however it is argued that by increasing the pulse duration beyond the delay spread and increasing the threshold level, channel time dispersion can be contained.

8.6.2 This effectively ensures the pulse transmission is subject to frequency flat fading. However moderate channel time selectivity would ensure that the signal remains in fade for a duration less than the symbol duration. Similarly Riter does not consider the influence of acoustic Doppler on system performance. Uncompensated relative Doppler would temporally scale the received signal and as such introduce unknown bias in the demodulated signal. This is a consequence of the need to obtain unambiguous estimates of delay relative to some known reference on a pulse by pulse basis.

8.6.3 In the presence of acoustic Doppler and possible acoustic Doppler variation over the pulse integration interval (channel time selectivity), achieving reliable delay estimates is not trivial as the delay reference itself is time varying in a random manner albeit on a slow

timescale. The application of the PPM technique to the underwater acoustic communications problem is therefore not without limitations. An alternative implementation of the PPM principle based on wideband correlation processing affords numerous advantages over narrowband processing. Specifically signal bandwidth allows resolution of multipath. It will be shown in subsequent discussion that differential delay modulation using phase coherent broadband correlation methods is a powerful technique to overcome severe channel conditions.

8.7 Spread Spectrum Systems

8.7.1 Spread spectrum is a generic modulation technique whereby the transmission bandwidth is deliberately increased beyond that of the fundamental data rate. In direct sequence systems bandwidth expansion is achieved through the use of specially designed codes and data recovery achieved through code correlation. This process imparts the modulation technique many desirable properties [106-109]

- the spreading process reduces the power spectral density of the transmission making the transmission difficult to detect and jam [108,109];
- provided the spreading process extends the transmission bandwidth beyond the channel coherence bandwidth, the correlation detection process enables multipaths to be resolved and combined. This micro-diversity [107] may be exploited by a receiver to improve system performance;
- the spreading-despreading process inherently affords the spread spectrum system noise immunity.

- by selecting code designs with low cross correlation properties it is possible for many transmissions to occupy the same time-frequency space enabling multiple users to share a common bandlimited channel [114].

8.7.2 Spread spectrum systems based on frequency hopped signal designs operate in a different manner to direct sequence systems. In fast hop systems the transmission frequency hops many times within a single symbol period. In slow hop systems the hop occurs on a symbol by symbol basis. Ayela and Reste [110,111] consider a form of frequency hopping based on the modulation of a linearly swept carrier, which seeks to mitigate multipath using a tracking filter synchronised to the sweep rate to reject multipath components. LeBlanc [112] considers the use of a broadband LFM based signalling scheme to mitigate the channel multipath problem. The authors note that the shallow water, short-range channel is particularly hostile and indicate that at increased range the channel problem relaxes. To combat discretely spread channels the authors propose a linear frequency sweep modulation technique, which enables path resolution and isolation using simple narrowband filters. The technique relies on a sufficiently fast sweep rate to ensure that multipath components delayed relative to a strong first arrival lie outside the bandwidth of a narrow band frequency-tracking filter, which is trained on the main sweep. Experimental results are presented demonstrating decoded message outputs, however no indication is given on channel complexity, signal-to-noise etc.

8.7.3 Other researchers have sought to exploit digital waveform orthogonality as a means to enable the bandlimited acoustic channel to be used by multiple users [114-116]. In all these papers the impact of the acoustic channel on waveform orthogonality is not addressed and yet this issue is key to the efficient use of the technique for multi-user communications.

8.8 COFDM

8.8.1 Coded orthogonal frequency division multiplex modulation is a technique, which seeks to exploit the benefits of wideband operation without the equalisation complexity normally associated with wideband single carrier systems. The potential benefits of multicarrier modulation techniques were presented earlier in the section. A more comprehensive discussion of COFDM is presented in appendix O.

8.8.2 In COFDM, data is modulated and coded across multiple orthogonal carriers separated such that each will undergo frequency flat fading for a given channel coherence bandwidth [90]. In multipath channels several carriers will go in deep fade and will be lost. However, these lost data symbols may be recovered by exploiting the time-frequency interleaved coding across all carriers.

8.8.3 In such a system equalisation is usually conducted in the frequency domain and comprises a single complex tap per carrier. Equalisation across carriers may be performed as it is across symbols in a time domain equaliser. In the frequency case the equaliser combats inter carrier interference in a manner completely analogous to the way a time domain equaliser combats inter symbol interference (ISI).

8.8.4 The main difficulty with COFDM techniques is maintaining carrier othogonality under time and Doppler spread channels and the more complex synchronisation requirements as a result of the reduced symbolling rate.

8.9 Coherent, Semi Coherent and Non Coherent

8.9.1 Coherent systems rely on the receiver being able to establish and maintain a frequency and phase synchronised local carrier. Information is thus encoded as an absolute or differential carrier phase change relative to this reference. In some non-linear modulation

techniques, data is conveyed in terms of carrier phase changes that are introduced by specific frequency shifts. Such continuous phase frequency shift keyed systems (CPFSK) are particularly bandwidth efficient for example minimum shift keying (MSK) uses two frequencies fc+1/4T and fc-1/4T, separated by 1/2T, to ensure phase continuity.

8.9.2 In earlier sections it was shown that both environmental and systematic factors influence the delay stability of multipaths propagating within the ocean medium and establishing an absolute time and Doppler synchronisation reference can be difficult, however the individual delay stability of paths is extremely good. In semi-coherent systems, information is encoded in terms of phase and/or magnitude differences between symbols. Thus, provided the phase error between received carrier and local carrier is fixed or varies slowly over a single symbol period, then reliable data recovery is possible. Phase error variation may arise from imprecise frequency synchronisation due to initial open loop residual error, tracking lag in the closed loop phase tracking system or delay fluctuations introduced by the acoustic propagation path or transmitter-receiver platforms. The performance of a differential phase system is therefore reliant on establishing, and maintaining carrier frequency synchronisation to an accuracy determined by the symbolling rate, symbol ordinate Euclidean separation and the overall motional dynamics of the transmitter and receiver.

8.9.3 Non coherent systems do not rely on the generation of a phase synchronised carrier since phase information is not used. A popular implementation of the non-coherent technique involves mapping information to two or more carrier frequencies to realise a M'ary system whereby one of M symbols are transmitted. This M'ary frequency modulation technique dominated underwater digital communication system design up until the late 1980's and early 1990's. [117-121]

8.9.4 Galvin et al [117] consider field results from a 50kHz DPSK acoustic link and attempt to reconcile observed performance with a theoretical model. The range:depth ratios tested practically ranged between 70 to 150:1. Both transmit and receive transducers were directional featuring narrow beamwidths in the vertical plane (3-4°) with bandwidth 10kHz. The reported results indicated good system performance for reasonably benign channel conditions (strong first arrival) however under more severe weather conditions the system failed to perform reliably. The channel soundings which were based on pulsed CW snapshots and indicated greater temporal spreading in the second case. The adopted channel sounding waveform was a ten cycle (0.2ms) CW pulse. Evident from the second sounding was significant envelope variability indicative of frequency selective fading, probably due to one or more forward scattering micropaths.

8.9.5 Catapovic et al [118] consider the use of incoherent MFSK techniques to combat the acoustic channel dispersion problem. The rationale for incoherent signalling is based on the assumption that the channel will not support coherent signalling. As will be seen later, this statement is valid only for narrowband systems, for broadband systems exceeding the channel coherence bandwidth the phase stability of the channel is in fact incredibly stable. The proposed system is based on 16 tones in the 45-55kHz band with a dedicated pilot tone at 60kHz for Doppler tracking using a dedicated PLL.

8.9.6 The ability of such an approach to compensate for Doppler where severe, discrete multipath occurs is extremely limited. For example if the pilot goes into deep fade then the phase and amplitude fluctuations become extremely severe resulting in loss of lock. The field performance of the technique is not reported.

8.9.7 The experimental performance of the MFSK system is presented. Channel characterisation results based on the fading statistics of each of the frequency bins are

discussed and demonstrate rapid magnitude fading. Phase results are not presented. Frequency coherence measurements at short and long range demonstrate a coherence bandwidth of the order 2kHz commensurate with a channel delay spread of 0.5-1ms, which can be considered a relatively benign channel. Despite this the system falls short of the theoretical predictions based on Mary orthogonal non-coherent signals in a Rayleigh Channel. Typically such theoretical bounds assume independent fading between carriers. For the proposed system carrier separation was much less than the channel coherence bandwidth and so the predictions were an upper bound on system performance. Typically performance was 3-5 dB worse than predicted.

8.9.8 The author attributes much of this loss to hardware transmission and reception imperfections. A more likely candidate are errors in the system synchronisation. Such errors can easily lead to performance degradations of 5dB or more.

8.9.9 Eck and Porta [121] consider a dual mode acoustic telemetry solution to provide a low rate robust command control link for command control and a high rate system for data transmission.. The technical approach essentially draws from many established methods to contain the multipath problem. Conventional spatial processing is used to provide narrow transmit beams and to maximise signal-to-noise performance.

8.9.10 The low rate transmission modulation scheme is based on simple incoherent FSK using a 2ms pulse duration with 8ms time guardband. Such a scheme would incur significant performance degradation for channel time spreads exceeding 10ms; which is not uncommon in shallow water environments. The high rate mode uses a frequency hopping technique based on six sub-bands. Pulse duration's are not indicated however the quoted data rate of 2.4kbaud implies a symbol duration of approximately 0.4ms with a total transmission bandwidth of approximately 10kHz. Typical shallow water time spreads

extending beyond 10ms would again likely result in significant performance degradation of this system. Experimental results are not given.

8.9.11 MFSK modulation is the basis for a system proposed by Catapovic [121] for the telemetering of deep-ocean mooring data. In this application the deep water vertical channel is relatively benign however a design criteria is for very low power deep water transmitter which introduces added criteria to the system design process. The system employs MFSK incoherent modulation in the 22-27kHz band where M can be varied between 4-16. Both upper and lower sidebands of the signal are transmitted. The authors argue that this increases system robustness based on frequency diversity. The signal design comprises a synchronisation pulse (design not stated) followed by 1 of M FSK realised through FFT processing (time and frequency guard bands are not reported). The frame duration is reported at 12.8ms resulting in a data throughput of 5000bps based on 64MFSK. The authors do not develop any of the more fundamental issues relating to the use of MFSK in frequency selective channels. For example the use of frequency guardbands to account for Doppler frequency scaling, the requirement for forward error correction coding to protect data in fast frequency fading channels are not developed.

8.9.12 A very similar system is reported by Frietag and Catapovic [119] where the application is specific to ROV communications. In this paper the synchronisation requirement is further developed. The authors consider the application of the delay lock loop and rightly note that DLL performance is tightly coupled with the multipath problem. DLL implementation is not discussed. Indeed its proposed use for a multicarrier narrowband system is somewhat confusing.

8.9.13 One assumes the authors are considering a narrow band delay lock loop approach based on periodic channel sampling enabling data resampling on a packet-by-packet basis. The

use of pilot tones is proposed for Doppler tracking. However, whilst the authors advocate the benefits of Doppler tracking, they do not expand on the tracking algorithm. The Doppler compensation is implemented as a sampling frequency change at the receiver front end. The adjustment is discrete although the resolution is not reported. A simple channel estimate equalisation scheme is reported based on echo cancellation. The underlying algorithm is not reported whilst fundamental issues such as noise enhancement and channel non minimum phase characteristics are not developed.

8.10 Discussion

8.10.1 The extent and nature of the time and Doppler spread inherent to acoustic channels radically impacts upon the choice of modulation scheme. The relative merits of single carrier modulation techniques, multicarrier modulation techniques and spread spectrum modulation techniques have been presented.

8.10.2 The results of preceding chapters have highlighted the unique nature of acoustic channel behaviour. In particular it has been shown that there is no definitive solution to the modulation problem.

8.10.3 Multicarrier systems have been shown to provide a means to relax the equalisation requirement. In particular the use of multicarrier techniques provide a means to reduce the sub-band carrier bandwidth to less than the channel coherence bandwidth such that individual carriers are subject to frequency flat fading and so equalisation reduces to a single complex tap per band.

8.10.4 The bandwidth efficiency of MCM systems may approach that of SCM systems if the carrier spacing is the minimum to ensure orthogonality between carriers. The penalty paid for relaxed equalisation is a more difficult synchronisation problem. Since the effective rate at which one samples the channel is reduced, closed loop adaptive equalisation and

synchronisation tracking schemes must adapt and track more dynamically. Since the acoustic channel is particularly time selective for mobile transmitter-receiver geometry's the choice of modulation design is ultimately driven by the time and frequency coherence characteristics of the channel.

8.10.5 Arguments advocating a multicarrier modulation solution are therefore tempered by the problem of acoustic channel temporal variability. In previous sections it was shown that the influence of geometry and environment results in time dependant variability between the relative time of arrivals of individual rays. In the frequency domain this temporal variability in the channel impulse response results in highly dynamic fluctuations in the phase response of the channel transfer function in the vicinity of the channel fading nulls.

8.10.6 Single carrier systems employing bandwidths exceeding the channel coherence bandwidth, are subject to frequency selective fading. It has been shown that such systems require complex equalisers in order to overcome the fading phenomenon. It has also been shown that for difficult multipath channels, spatial processing and non-linear equaliser structures provide a means to overcome non-minimum phase channels under certain conditions. In particular it has been shown that appropriate spatial filtering may provide a means to make a nonminimum phase channel minimum phase by reducing multipath contamination. The main benefit of a single carrier system stems from the rapid sampling of the channel which readily lends to the closed loop adaptive schemes for channel equalisation and synchronisation.

8.10.7 A key issue relevant to both SCM and/or MCM techniques is the need to track and compensate for unpredictable channel behaviour. This may be viewed as a closed loop equalisation/synchronisation problem that may be combated in either the time or frequency domain.

8.10.8 In the next section algorithms are presented which enable a receiver to cope with unpredictable channel behaviour based on optimum filtering theory. These adaptive algorithms are considered for receiver structures involving two or more spatially separated receivers. The performance limitations of the algorithms are assessed by simulation studies to investigate algorithm performance for a variety of ocean mechanisms discussed in earlier sections.

'...

Blow, bugle, blow, set the wild echoes flying,

Blow bugle; answer echoes, dying, dying, dying.'

Alfred Lord Tennyson, The princess (1847) p.4

9 ADAPTIVE SPATIAL-TEMPORAL RECEIVER ARCHITECTURES

9.1 Review

9.1.1 In the previous section technical arguments were presented contrasting the relative benefits of single carrier and multicarrier modulation techniques. It was concluded that the doubly spread nature of the acoustic channel posed unique challenges to both modulation techniques and these issue demanded varying levels of synchronisation and equalisation complexity depending upon the choice of modulation scheme.

9.1.2 A requirement common to both modulation techniques is the need to cope with the time varying nature of acoustic channel behaviour. For a receiver to reliably recover information in a time varying channel, it must be able to track and compensate for channel variability. This variability exists both in the extent of the multipath and its temporal variability. As discussed in earlier sections the operations of synchronisation and equalisation are particularly closely related for underwater acoustic channels.

9.1.3 In Section 6 techniques were presented to provide an open loop estimate of the time and Doppler characteristics of the channel. These techniques however, only provide a snap shot of the channel impulse response and closed loop tracking is necessary to reliably decode information over the transmission duration. Since multipath is itself a time domain phenomenon, it is perhaps natural to assume a time domain structure to compensate for its

effects. The most common structure is the linear transversal filter that effects a convolution process between the received signal and a filter transfer function derived from an optimisation process. Appendix H details the two most common filter optimisation criteria, the zero forcing equaliser and the minimum mean square error (MMSE) equaliser. For time varying channels it is useful to reformulate the optimisation problem to enable the filter to cope with time varying behaviour. Such selfadapting algorithms are now well established in various signal-processing fields. In this section the properties and behaviour of these adaptive algorithms are considered and their suitability to the underwater acoustic communications problem assessed.

9.2 Adaptive Algorithms : Two Ray Channel Simulation

9.2.1 The algorithms considered comprise a tiny subset of the many adaptive methods that can be applied to the adaptive equalisation problem. In order to contain the analysis the following algorithms are considered

- Least Mean Square (LMS)
- Normalised Least Mean Square (NLMS)
- Recursive Least Square (RLS)
- QR Recursive Least Square (QR-RLS)

9.2.2 Notable omissions from the above are the order recursive adaptive filter families based on lattice structures and non-linear adaptive methods for blind deconvolution. The respective performance of each of the algorithms is shown in Figure 38 which demonstrates the convergence for a simple two ray channel of the form

$$H(z^{-1}) = 1 + 0.75z^{-5} \qquad \textit{Eqn 21}$$

9.2.3 Despite its apparent simplicity, this channel model provides a useful measure of the respective adaptive algorithm convergence properties. In all cases the desired response was a bandlimited, complex Gaussian noise process and the filters implemented in complex form. Algorithm performance is shown for a number of adaption constants. Evident from the figure is the superior convergence properties of the least squares algorithms over the stochastic gradient. Of all the algorithms the QR-RLS demonstrates the most rapid convergence followed by the conventional RLS, the normalised LMS and finally standard LMS. It is evident that the reformulation of the least squares problem in terms of the root of the correlation matrix has a significant impact on the performance of the algorithm. This underlines the difficulty in assessing the relative merits of adaptive algorithms since, whilst the optimisation criteria are the same the reformulation can lead to significantly different behaviour. This is also demonstrated by the convergence of the LMS and NLMS. Here the convergence rate improves with increasing μ up to a point beyond which convergence degrades. In the case of the LMS algorithm the transition occurs between 0.2 and 0.3. In the NLMS case the transition occurs between 0.06 and 0.08. This is a consequence of the close relationship between adaption parameter and channel eigenvalue spread. The simplicity of the channel model obviously limits the conclusions one can draw from the algorithm convergence simulation. The main point to be is the disparity between algorithm behaviour even for a relatively simple channel using a single channel equaliser.

9.2.4 An important point to note is that the simulations were conducted for a noiseless input. Of course, practical application of the algorithms results in noise from finite precision arithmetic. Under more severe input signal to noise conditions (say less than 10dB) the convergence superiority of the RLS algorithms indicated in the simulation presented here, is not so well defined. For example in [157], equalisation simulations are presented which

demonstrate comparable convergence rates between LMS and RLS for a stationary environment with an eigenvalue spread of 11 at a signal to noise of 10dB. The simulations demonstrate a reduction in algorithm convergence relative to the noise free case. This result further underlines the fact that whilst RLS based algorithms have several advantages over LMS in high noise, stationary environments, these advantages are much less clearly defined in non stationary, noisey environments typified by the underwater acoustic channel.

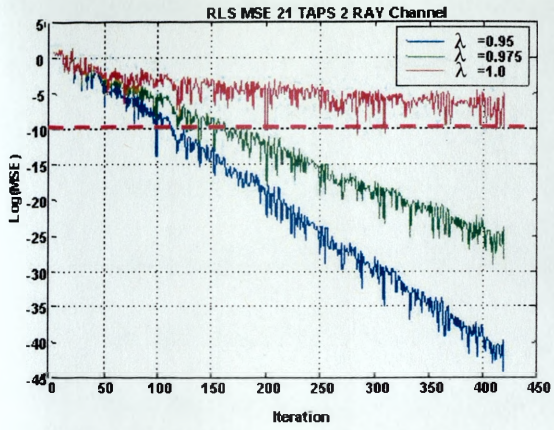

λ=0.95 RLS MSE Convergence to 0.1 in 110 iterations
λ=0.975 RLS MSE Convergence to 0.1 in 165 iterations
λ=1.0 RLS MSE Convergence to 0.1 in >400 iterations

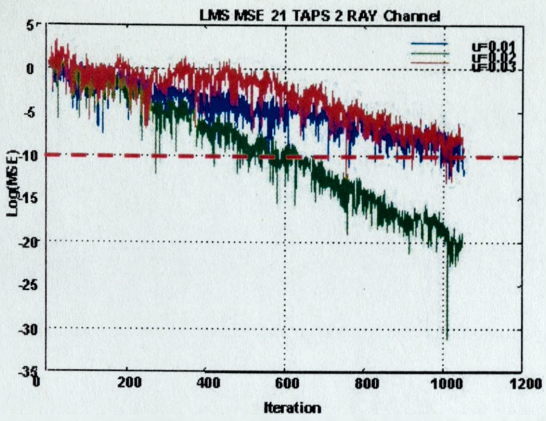

μ =0.03 LMS MSE Convergence to 0.1 in 600 iterations
μ =0.02 LMS MSE Convergence to 0.1 in 1000 iterations
μ =0.01 LMS MSE Convergence to 0.1 in >1000 iterations

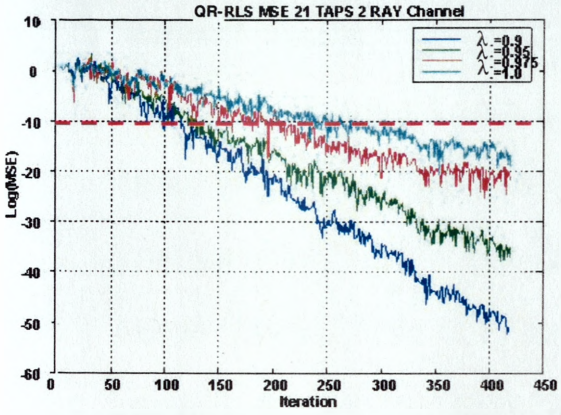

λ =0.9 QR-RLS MSE Convergence to 0.1 in 100 iterations
λ =0.95 QR-RLS MSE Convergence to 0.1 in 125 iterations
λ =0.975 QR-RLS MSE Convergence to 0.1 in 200 iterations
λ =1.0 QR-RLS MSE Convergence to 0.1 in 250 iterations

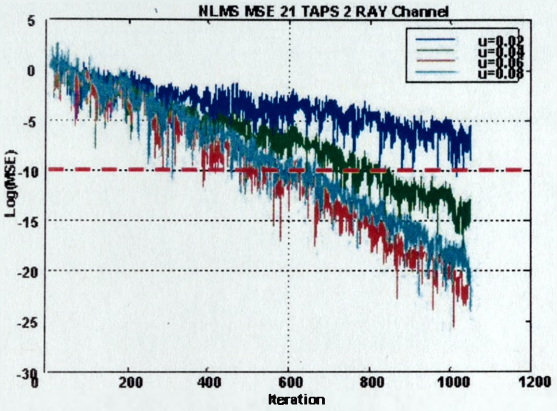

μ =0.08 NLMS MSE Convergence to 0.1 in 550 iterations
μ =0.06 NLMS MSE Convergence to 0.1 in 600 iterations
μ =0.04 NLMS MSE Convergence to 0.1 in 800 iterations
μ =0.02 NLMS MSE Convergence to 0.1 in >1000 iterations

Note

- Adaption constants μ and λ dictate intrinisic convergence properties of LMS and RLS algorithms
- RLS based algorithms have superior convergence properties than LMS for high signal to noise.
- IQRLS provides most rapid convergence followed by RLS, then NLMS and finally LMS
- (N)LMS convergence properties improve with increasing μ until value of μ exceeds eigenvalue spread.
- Performance benefits of RLS based algorithms not so well defined in non stationary, noisey environements.

Figure 38: Comparison of LMS, NLMS RLS and QRLS algorithms

9.3 Decision Feedback Equalisation (DFE)

9.3.1 A key limitation of the linear transversal equaliser structure in combating multipath channels is the noise enhancement effect arising from the deep fades from path arrivals of comparable intensity. This results in significant noise enhancement in the vicinity of nulls in the equaliser frequency response. Since the optimisation criteria for an MMSE equaliser is to minimise error power at the equaliser output regardless of origin (noise and/or ISI), the optimum operating condition in the presence of noise is unlikely to be the reciprocal channel impulse response (as in a zero forcing equaliser approach). For example many channels may not have a stable causal inverse filter and/or the noise background may be significantly coloured. In these instances the MMSE operating condition would result in an equalisation response quite distinct from the inverse channel transfer function. For many such cases, an optimised MMSE transversal delay line equaliser may prove insufficient and alternative structures are necessary. One approach is to use equaliser structures, which seek an optimum operating condition based not on a single filter but a combination of two or more filters. A classic example of this approach is the decision feedback equaliser shown previously in Figure 35, which exploits known past decisions to cancel or reduce multipath arrivals. A key issue with such a structure is that it reduces the noise enhancement problem since the equalisation task no longer rests with a single transversal filter.

9.3.2 The DFE is however, not without its own set of problems. Since the operating principle relies upon the integrity of the feedback decisions, the closed loop nature of the DFE can lead to a rapid breakdown in performance when erroneous decisions transit through the feedback stage [122]. These erroneous decisions constitute a form of feedback noise. The analysis of such noise on the performance of the decision feedback equaliser is complicated by its inherently non linear structure.

9.4 Multichannel DFE

9.4.1 Whilst the decision feedback equaliser can significantly improve system performance in difficult channels, it is not optimum and its performance will degrade with increasing channel complexity. For example it can be shown [97] that the signal-to-noise advantage of MLSE relative to DFE scales with channel complexity and for the results presented this is typically 5-7dB. The influence of feedback errors accounts for a performance loss of typically 2-3dB.

9.4.2 In practical terms the addition of the decision feedback section of the equaliser essentially enables the structure greater flexibility to achieve the desired optimisation criteria namely the minimisation of the error formed between the sum of the forward and backward sections and a desired response.

9.4.3 From the previous discussions relating to the nature of the acoustic environment it is perhaps not difficult to see the potential performance benefits of using data from several spatially separated receive elements and feed this data to separate forward equalisers, one for each channel. The technical arguments for such an approach is based on exploiting the different, information available to each sensor to improve the overall performance of the system, namely to minimise the MSE. Such a structure was shown previously in Figure 36.

9.4.4 Thus the behaviour of the adaptive structure is driven as much by the spatial characteristics of the incident sound field as it is by the temporal and frequency characteristics. Also, the greatly reduced propagation speed of acoustic waveforms relative to their RF counterparts results in centimetric symbol spatial scales rather than kilometric scales. This has a profound influence on the behaviour of an acoustic multichannel decision feedback equaliser. Specifically the process of spatial combining,

equalisation and synchronisation become much more tightly coupled and the minimum mean square operating condition may be achieved through the combined influences of spatial combining/forward equalisation and decision feedback cancellation. Such a structure which uses spatial-temporal adaptive processing (STAP) is particularly powerful in combating a wide range of acoustic behaviour.

9.4.5 It is well known that in shallow water environments, the vertical sound field is particularly complex [123] and recent efforts in high data rate acoustic communications have sought to identify means to exploit the vertical coherence properties of the sound field to overcome the mulitpath problem [124-143].

9.4.6 However it is important to stress that STAP and DFE techniques are not in themselves solutions to the high data rate underwater acoustic communications problem, but provide the basis for several techniques which together, constitute an effective high data rate receiver processing system. In this section the fundamental behaviour of this basic structure is investigated

9.5 Spatial Temporal Adaptive Processing

9.5.1 STAP Simulations

9.5.2 In order to explore the performance and behaviour of the multichannel decision feedback equaliser a number of simulations were conducted to investigate the behaviour of this structure under real acoustic conditions using a parametric channel model described in appendix B.

9.5.3 The following parameters were adopted for the simulation

- 4 channels
- Number of forward fractionally spaced taps 32

- Number of Backward, symbol spaced taps 64
- PLL GAIN 0.004
- DLL GAIN 500
- Forward adaption constant during training 0.001
- Backward adaption constant during training 0.001
- Forward adaption constant during decoding 0.001
- Backward adaption contant during decoding 0.001
- Sampling Rate 48000Hz
- Carrier frequency 12kHz
- Data rate 6ksym/s QPSK

9.6 Algorithm Convergence : Recycling Training Data

9.6.1 Stochastic gradient algorithms such as the (N)LMS [129,130,133,134,135,137] seek to attain the optimum Weiner solution through iterative jumps toward a global minimum. In channel equalisation, the algorithm is initially steered toward this global minimum using a known training sequence and, once trained, the algorithm then reverts to decision directed mode whereby tentative output decisions are quantised and the results used in the decision directed mode. A key issue in the use of stochastic gradient algorithms is the speed and reliability of convergence prior to entering the decision directed mode [143]. In appendix K convergence properties of various adaptive algorithms are compared and the issues affecting convergence discussed. An under exploited feature of stochastic gradient algorithms is the fact that the training process will result in a particular solution in the M dimensional solution space for a particular start point. If one alters the start point (i.e. initialise the filter taps with some other initial estimate) then the resulting endpoint will be

different even though the same training data is used during the convergence process. This fact can be exploited during the equaliser-training mode in order to improve the reliability and robustness of algorithm training in difficult channels. Specifically, after the first training pass the filter achieves an M dimensional solution nearer to the global minimum. By recycling the training data, the algorithm can be driven nearer to the global minimum by retraining using the same data with a different start solution. The practical significance of this result is that it may potentially improve real time system performance by recycling training data until an acceptable MSE is achieved prior to decoding. The benefit of this approach is that the training sequence length does not need to be increased in the transmission and so overall throughput rate is not affected. The technique does of course introduce additional processing overhead on the decoder.To verify the retraining principle, a number of simulations were performed whereby training data was recycled during the equaliser training phase. This was performed for a number of channel models for which convergence of the LMS is particularly poor, namely channels with path arrivals of comparable energy.

9.6.2 Figure 39 demonstrates the magnitude squared error training curves for the NLMS algorithm for channel models $H(z)=1$, $H(z)=1+ z^{-30}$,$H(z) =1+z^{-30} +z^{-60}$. For the single path model it is evident that after the first training iteration (512 symbols) the algorithm has converged to an MSE value of 0.1 and subsequent training iterations offer no improvement in decoding performance. For the two-path model the results indicate that an accepatable MSE is not achieved after the first iteration. However subsequent passes provide convergence toward a better solution, with acceptable MSE of 0.25 achieved after 3-4 passes. The solution moves nearer the optimum during the decision directed mode and achieves a MSE of 0.1 at the end of the decoding phase. The results for the three-path channel demonstrate a longer convergence period. After six passes the algorithm has

converged to a non optimal solution providing an MSE of better than 0.5. This is sufficient for the algorithm to operate in decision directed and the solution moves nearer to the optimal Weiner solution duringthis phase, achieving an MSE of 0.2 after 10000 iterations.

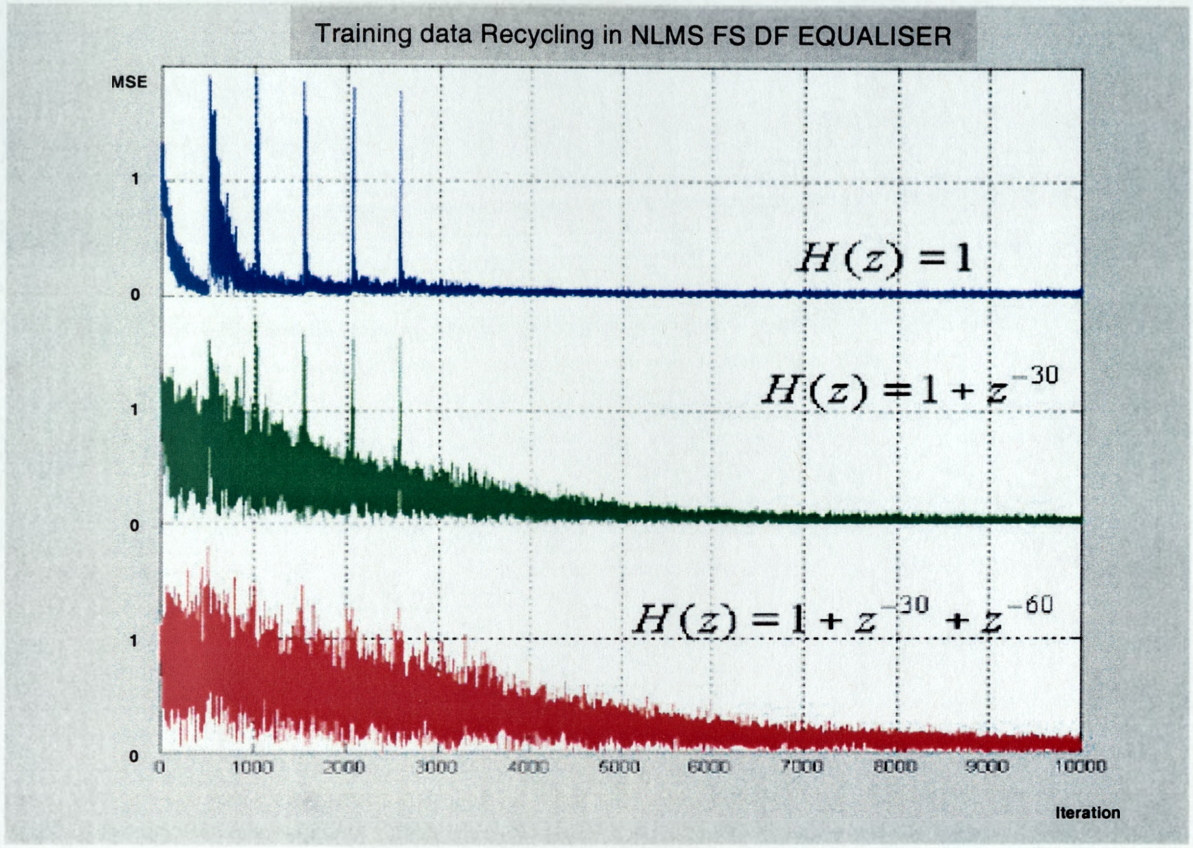

Note

- Recycling of training data for ideal channel offers no improvement in performance
- For medium to high complexity channel three to six recycles ensure sufficent convergence for decision directed decoding.
- Technique enables relatively short training sequences to be 're-used .
- Transient MSE increases at each iteration due to discontinuity in input data during recycling. In practice the training iteration period would be limited at at each recycling stage so as to avoid large discontinuities that may occur in non-stationary environments.

Figure 39; MSE training curves for recycled equaliser training

9.7 Performance Vs Channel Complexity

9.7.1 Figure 40 depicts the performance of a single channel fractional spaced equaliser as a function of channel complexity and illustrates the performance advantage of including a decision feedback section. The simulation parameters were as follows:-

- 30 forward taps
- 64 backward taps
- 512 training symbols
- NLMS adaption
- μ_f =0.001
- μ_b=0.0002
- 6ksym/s QPSK @ Fs=48kHz
- Channel Models (All rays arrival angle=0deg)
  - $H(z)=1+0.25z^{-30}$
  - $H(z)=1+0.5z^{-30}$ (FS equaliser only)
  - $H(z)=1+0.5z^{-30}$(FS equaliser + DF section)

9.7.2 The results demonstrate the significant degradation in equaliser performance as the channel complexity increases. In this case the noise enhancement due to equalising channels with deeper nulls serves to degrade bit error performance. The results show that the addition of a decision feedback section afford a 2-3dB improvement in performance at BER 10^{-3}. This is still 3dB down on the single channel case and demonstrates the impact of decision error propagation and tap jitter using decision feedback techniques.

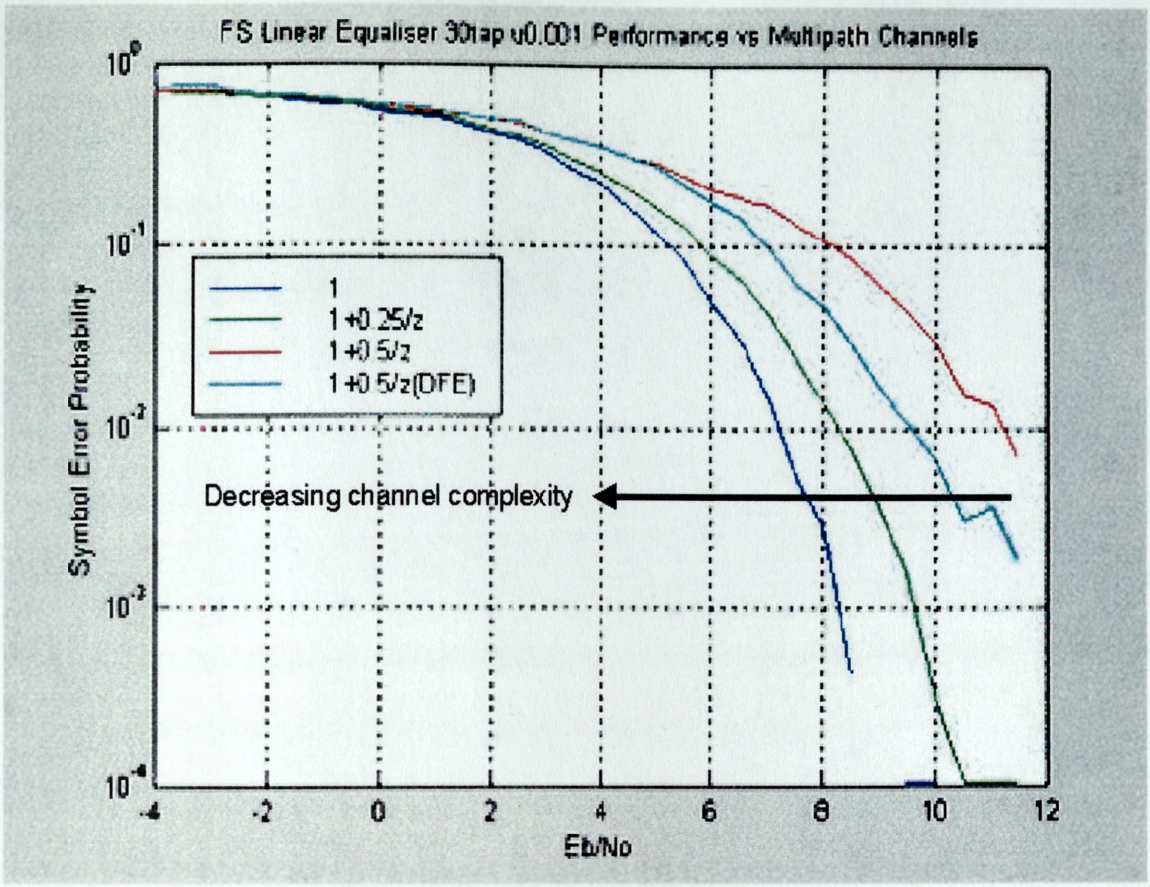

Note

- Single fractional spaced equaliser performance degrades with increasing channel complexity
- Addition of DFE provides 2-3dB improvement in system performance
- Greater performance gains using DFE in more complex channels

Figure 40; Error performance curves for single FS equaliser with and without DFE

9.8 Performance vs. Number of Channels in Isotropic noise

9.8.1 Figure 41 depicts the performance of a multichannel (N=1,2,4,8) FS equaliser with DF section using the same parameters with channel separation of 0.1m. In this simulation a fixed channel model was adopted $H(z)=1+0.5z^{-30}$ and system performance evaluated as a function of receiver elements. In each case both path arrivals were simulated for broadside arrival. The results indicate improvement in receiver performance with number of receiver channels as one would expect in an isotropic noise field. Whilst 4 channels afford approximately 3.5dB performance improvement at SER=1e-3 over the single channel case, less than 1dB improvement is achieved by increasing the number channels to 8. These results suggest that for channels exhibiting broadside path arrivals in isotropic noise the computational complexity of additional channels (more than 8) are likely to be outweigh any significant performance benefits. For environments featuring several path arrivals with appreciable angular diversity, the MMSE criteria is driven quite differently than for the AWGN case. Here the structure seeks to attain the MMSE criteria by spatially filtering arrivals and isotropic noise plays a lesser role (depending on SNR).

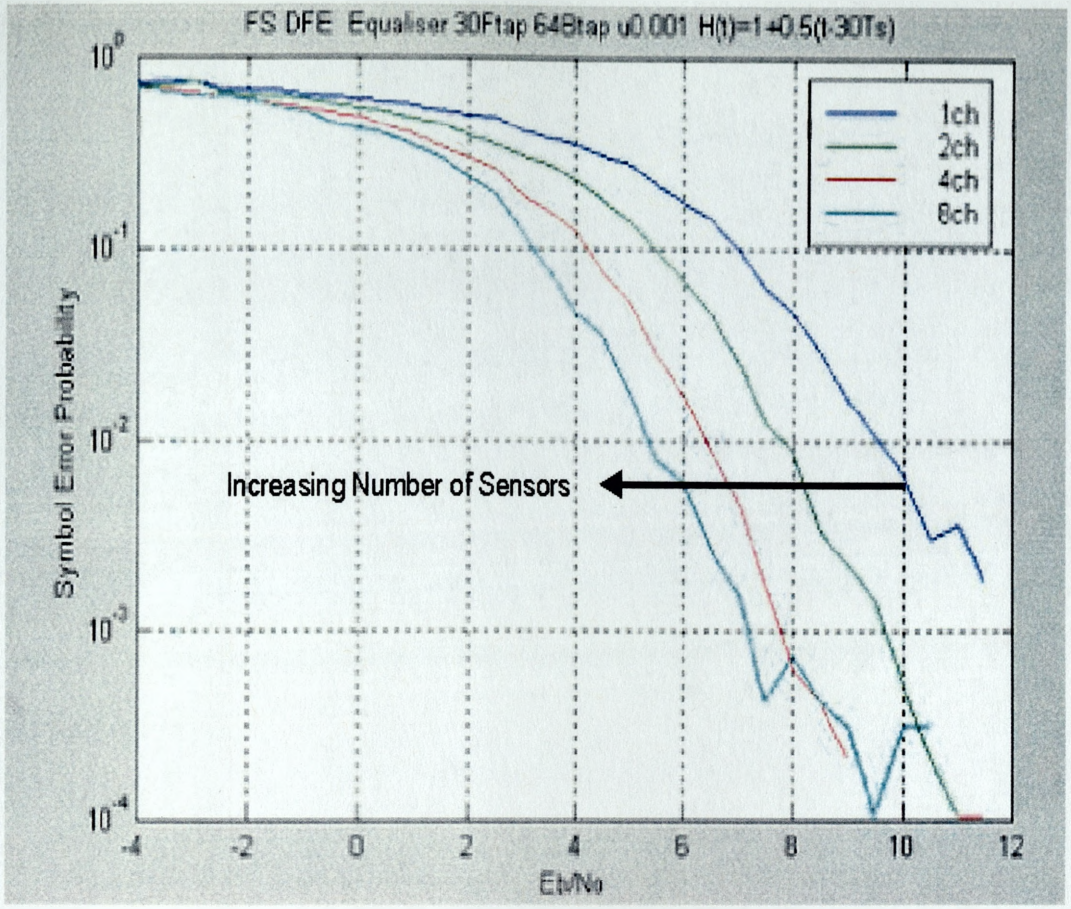

Note

- Two channels provide 2-3dB over single channel
- Eight channels provide 4-5dB improvement over single channel
- Only modest improvements attained for greater than 8 channels

Figure 41; Error performance curves vs. number of elements

9.9 Performance vs. Path Arrival Angle Separation

9.9.1 Figure 42 depicts system performance for the four channel case (N=4) for a two ray channel $H(z)=1+0.5z^{-30}$ where arrivals are subject to an increased angular spread (0,5,10,20degrees). The results demonstrates the ability of the multichannel receiver to exploit the spatial characteristics of incident field by providing improved performance with angular separation of incident rays. A more significant result that is not indicated in the figure is the much more robust convergence of the algorithms in difficult channels when there is appreciable angular spread between arrivals. The result clearly demonstrates the ability of the STAP structure achieve the MMSE criteria solely though spatial filtering.

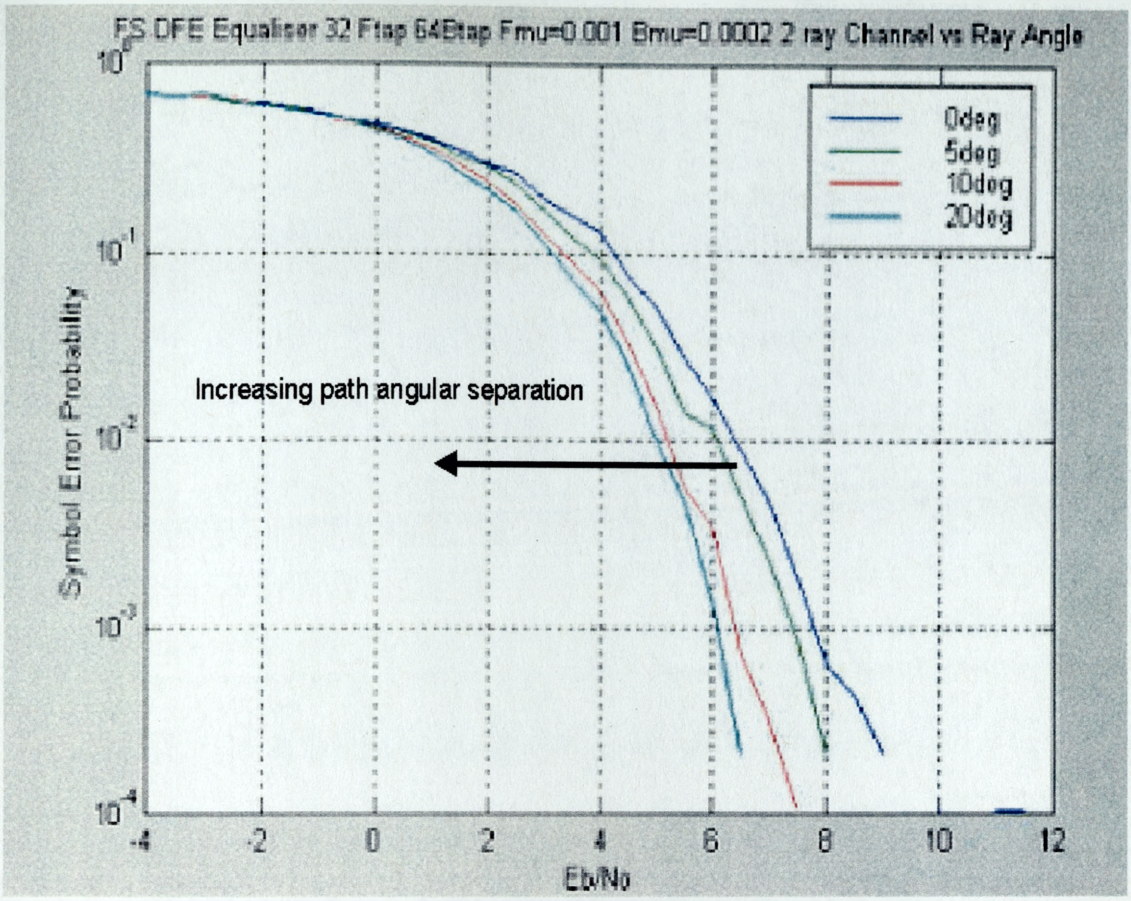

Note

- STAP receiver able to exploit spatial characteristics of incident sound field
- Up to 2-3dB improvement for 0.1m sensor separation
- Much more rapid convergence for angular separated paths

Figure 42; Error performance curves vs. path angular separation

9.10 Open Loop Performance vs Doppler

9.10.1 Since acoustic Doppler manifests as a temporal scaling of the received symbol train, then the forward adaptive equaliser must adapt to compensate. This means that the significant forward filter taps must not only rotate to compensate for the frequency translation of the carrier (i.e. Doppler 'shift'), but also temporally adjust to compensate for variations in the path arrival time. The effect is demonstrated in Figure 43 which shows receiver performance for an ideal channel submitted to a sinusoidal 0.5 m/s Doppler variation at 1Hz.

- **Top Left** : This image depicts the forward filter magnitude response at the end of decoding. The Y ordinate is space (channel), the X ordinate is time.

- **Top Middle**: This graph depicts the backward decision feedback filter magnitude response at the end of decoding. The X ordinate is time, the Y ordinate is magnitude.

- **Top Right**: This graph depicts the received data constellation for the complete packet. The X ordinate is the real component, the Y ordinate is the imaginary component.
- **Bottom Left**: This graph depicts the magnitude squared error over the complete packet duration including training phase. The X ordinate is iteration number, the Y ordinate is magnitude squared error.
- **Bottom Middle**: This graph depicts the time evolution of the mid channel forward filter magnitude response. The X ordinate is time (channel tap), the Y ordinate is iteration.
- **Bottom Right**: This graph depicts the phase error between decisions and quantised decisions over the packet duration. The X ordinate is iteration, the Y ordinate is degrees.

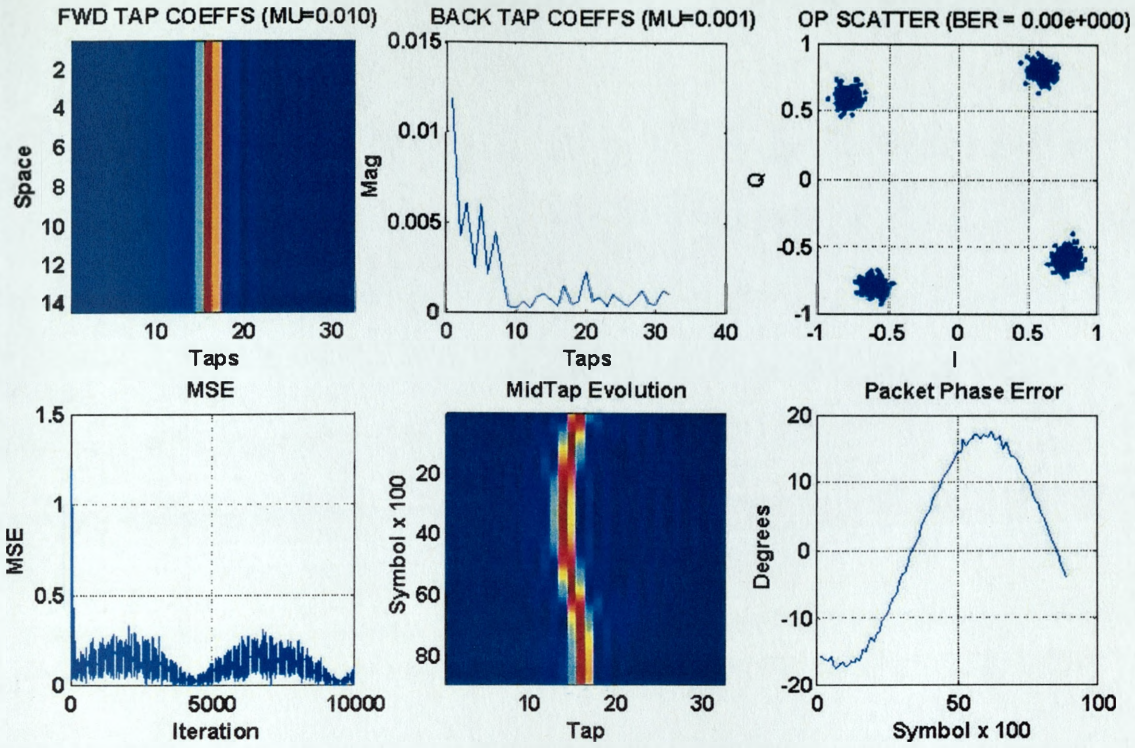

Single Ray Sinusoidal Doppler = 0.5 x cos(2 π t) m/s

-

Note

- Fractionally spaced forward filters able to compensate for temporal scaling due to Doppler (see midtap evolution)
- Doppler scaling results in residual phase tracking error which follows Doppler profile
- MSE error increases with high Doppler errors

Figure 43; STAP-DFE decoder performance for time varying Doppler error

9.10.2 The figure demonstrates several important issues regarding the behaviour of the structure under acoustic Doppler conditions. Perhaps most important is the ability of the structure to track and compensate for Doppler variability over the packet duration. Obviously the ability of the structure to track and compensate for Doppler variability is strongly influenced by the adaption constant. Inherent in any closed loop tracking process is a lag error which scales inversely with the system bandwidth. In the simulation the tracking error is clearly demonstrated by the residual phase tracking error. In addition to demonstrating the ability of the structure to track Doppler shift arising from translation of the system carrier frequency, the simulation also demonstrates the ability of the system to compensate for the temporal scaling. This is evidenced by the time evolution of the central forward filter taps shown bottom middle. Here the tap positions are seen to adjust in order to re-establish the optimum sampling epoch at the receiver output. The capability of the structure to track and compensate for this kind of distortion is strongly driven by the use of fractional spacing in the forward section. The response of the STAP-DFE structure to acoustic Doppler highlights the need to offload tracking effort from the forward filters. Specifically it can be seen that when the Doppler profile is maximum (0.5m/s) tracking effort is significantly increased as demonstrated by increase in MSE (bottom left). This points to two potential aids to tracking performance.

- Phase Lock Loop

- Delay Lock Loop

9.10.3 A phase lock loop is required to compensate for phase rotation arising from the Doppler shift frequency error. A delay lock loop is also needed to compensate for the temporal scaling influence of acoustic Doppler. In order to investigate the potential performance benefits of closed loop phase and delay support several simulations were conducted.

9.10.4 Figure 44 demonstrates receiver performance in the presence of residual Doppler error for two values of tracking parameter mu=0.001 and 0.0025 respectively. In each case receiver performance is shown for residual Doppler errors of 0,0.05,0.075,0.1and 0.15kts. It should be pointed out that this range of velocities represents just a few tens of centimetres per second underlining the inherent sensitivity of these structures to Doppler error.

9.10.5 For the lower tracking constant (mu=0.001) it is clearly demonstrated that small Doppler errors do have an impact on receiver performance. Most noticeable is the impact upon initial convergence. This is demonstrated by the high signal-to-noise ratios necessary to achieve convergence at the higher Doppler rates. At 0.15kts convergence is not achieved until the SNR is 3dB or higher, thereafter the performance is marginally degraded relative to lower Doppler errors by virtue of the increased tracking effort of the structure. The tracking effort is demonstrated by the 0.5-1dB spread across the Doppler error range when the structures have converged and are operating in the normal decision directed mode.

9.10.6 For the higher tracking constant (mu=0.0025) it is evident that the residual Doppler problem is noticeably reduced and convergence is achieved at lower SNR. Also there is a much smaller spread between curves when converged and operating in the normal decision directed mode. This indicates the reduced tracking lag and improved tracking performance at higher adaption constant.

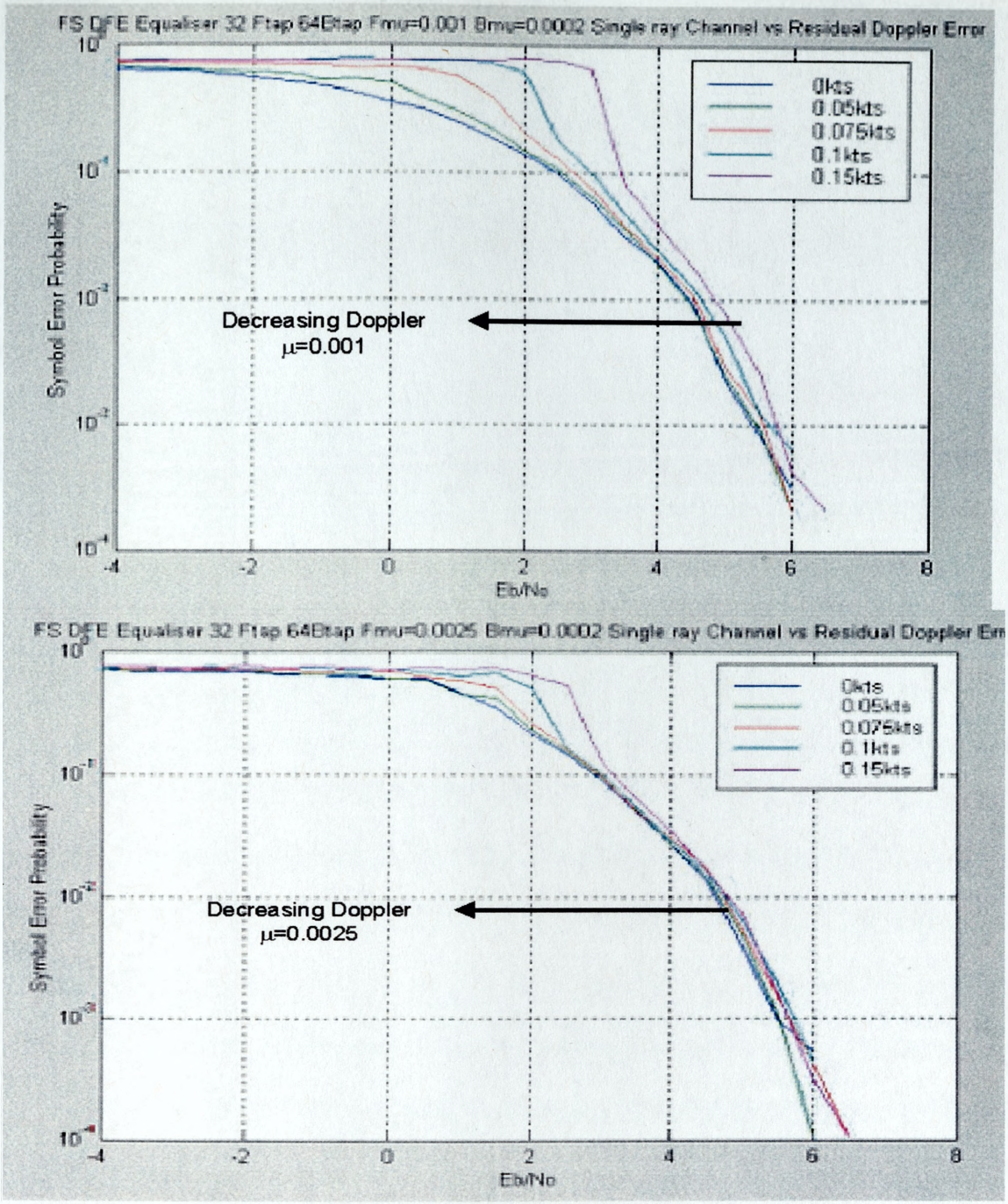

Note

- Doppler has greatest impact during convergence. Higher Doppler requires higher SNR for convergence. During steady state, equaliser Doppler performance within 1dB of zero Doppler case irrespective of PLL gain.

- Doppler tracking ability improves for increased adaption constant

Figure 44; STAP-DFE decoder performance for Residual Doppler error=0 to 0.15kts

9.11 Closed Loop PLL Performance vs Doppler

9.11.1 The previous open loop symbol error graphs have demonstrated that residual Doppler errors require higher signal-to-noise ratio for the structure to converge and once converged the adaptive receiver requires a large tracking constant in order to minimise the effect of Doppler error on bit error performance. The addition of a phase lock loop to relax the tracking burden of the adaptive receiver is an established technique in RF terrestrial communications and it is also possible to drive the phase lock loop adaptively in joint equalisation synchronisation schemes discussed earlier. Figure 45 shows symbol error performance when the structure is aided by a phase lock loop with tracking gains of 0.001, 0.0025, 0.005, 0.0075 and 0.01 for a residual Doppler error of 0.15kts. Also shown is the unaided symbol error graph.

9.11.2 The results demonstrate that the addition of the phase lock loop has a significant impact on the algorithm convergence and only a modest impact on steady state performance. Specifically it can be seen from the figure that when operating in the normal decision directed mode the addition of the PLL affords less than 1dB performance improvement. However, during initial training, higher bandwidth phase lock loops result in faster convergence. This is perhaps intuitively obvious. At low SNR the constellation points are diffuse and phase rotation results in a larger number of symbol errors. The feedback of these errors results in rapid breakdown. The addition of a high bandwidth, phase lock loop offloads phase tracking effort (and lag) from the adaptive filter such that convergence can be achieved at lower signal-to-noise ratios.

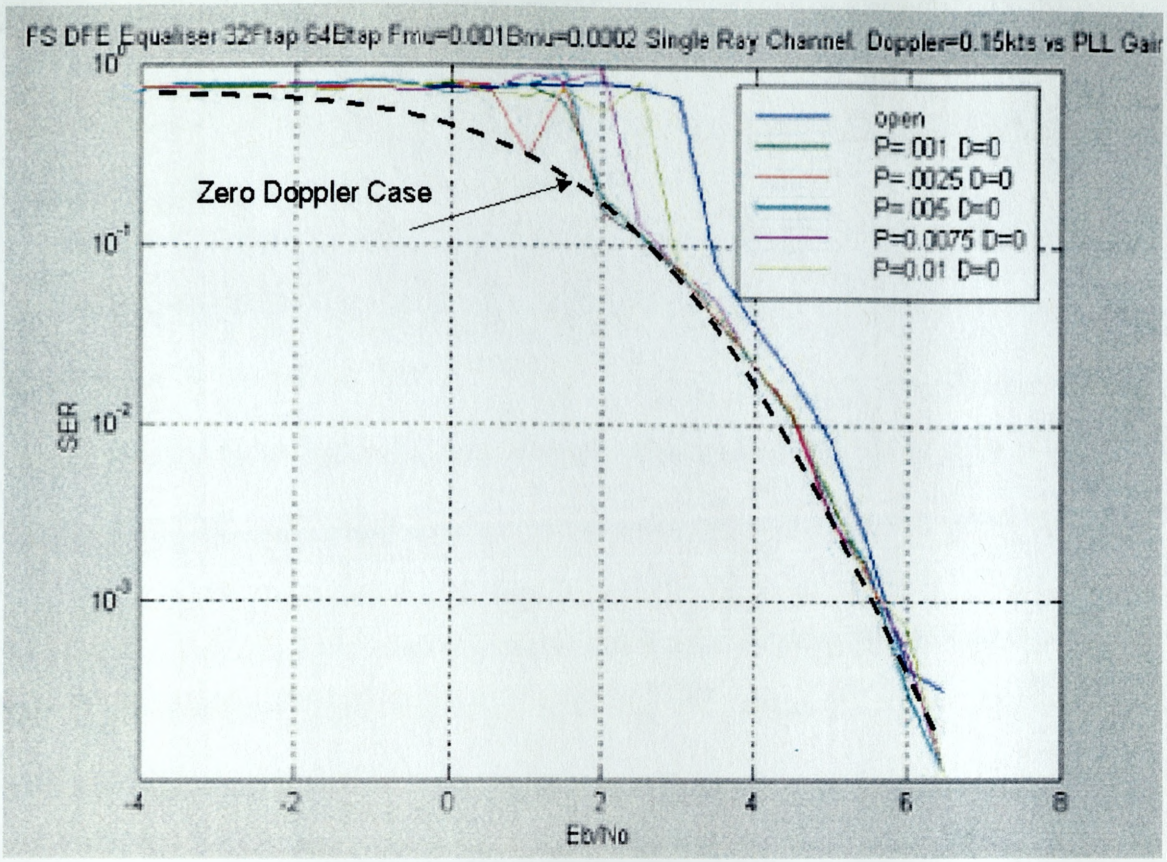

Note

- Increasing PLL gain/bandwidth, provides dramatic improvement in convergence at low SNR.
- At high SNR and during steady state PLL affords only modest improvement for Doppler=0.15kts.

Figure 45; STAP-DFE decoder performance for residual Doppler error=0.15kts and varying PLL gains 0.001 to 0.01

9.12 Closed Loop PLL+DLL Performance vs Doppler

9.12.1 The performance of the PLL aided receiver for higher residual Doppler errors (0.5kts) is shown in Figure 46.

9.12.2 Here the unaided receiver requires a signal-to-noise ratiosin excess of 6dB before convergence is achieved. The addition of a phase lock loop affords a significant improvement in system performance. However the performance improvement appears to 'saturate' for PLL gains 0.002-0.004.

9.12.3 In this case the addition of a delay lock loop affords further improvement in performance both in terms of convergence and steady state tracking. The adoption of a phase and delay lock loop provides the system the same bit error performance as the zero Doppler case at signal-to-noise ratios above 2dB. The results indicate that there is a transition signal-to-noise ratios below which the system cannot converge. The result also shows that both phase and delay timing loops have a key role to play in the overall performance of STAP receiver architectures.

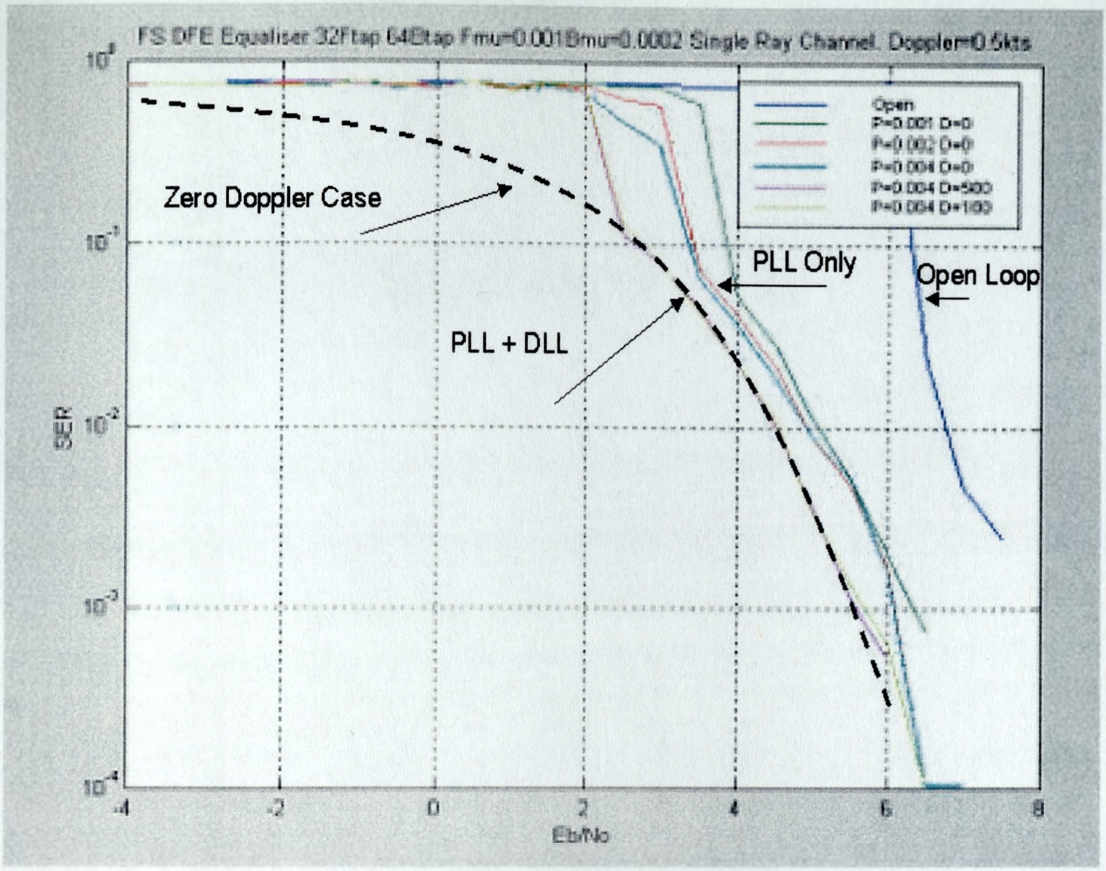

Note

- Doppler=0.5kts
- Increasing PLL gain/bandwidth provides improved performance.
- PLL performance improvement saturates 1dB from zero Doppler case
- Ideal performance only achieved using PLL+DLL.
- Result demonstrates the need for PLL+DLL for Doppler errors 0.5kts+.

Figure 46; STAP-DFE decoder performance for 0.5kts residual Doppler error and PLL+DLL support

9.13 Performance Vs Angular Rate

9.13.1 Large angular rates on path arrivals have an interesting effect on the STAP-DFE performance. Figure 47 shows the simulation results for a single ray channel at high signal-to-noise ratios for an angular rate of 20deg/s.

9.14 It is clear that the structure is able to accommodate high angular rate with little discernible impact on the received IQ constellation. It achieves this by reducing the taps weights at the extreme ends of the array. This is perhaps intuitively obvious since angular rate imposes the greatest tracking requirement on the extreme taps. So the structure adapts to reduce the weights of these taps in order to achieve the MMSE criteria. An alternative interpretation is that by de-emphasising the array end elements the effective beam width broadens, so accomodating large angular rates in received signal arrival angle.

9.15 Under more complex conditions where multipath and or noise exist, it is likely that the solution will adopt a different form, since the MMSE operating requirement must balance the need to accommodate high angular rates with the need to provide path discrimination and noise suppression. Clearly, in such instances, a single broad beam is unlikely to achieve an optimal solution.

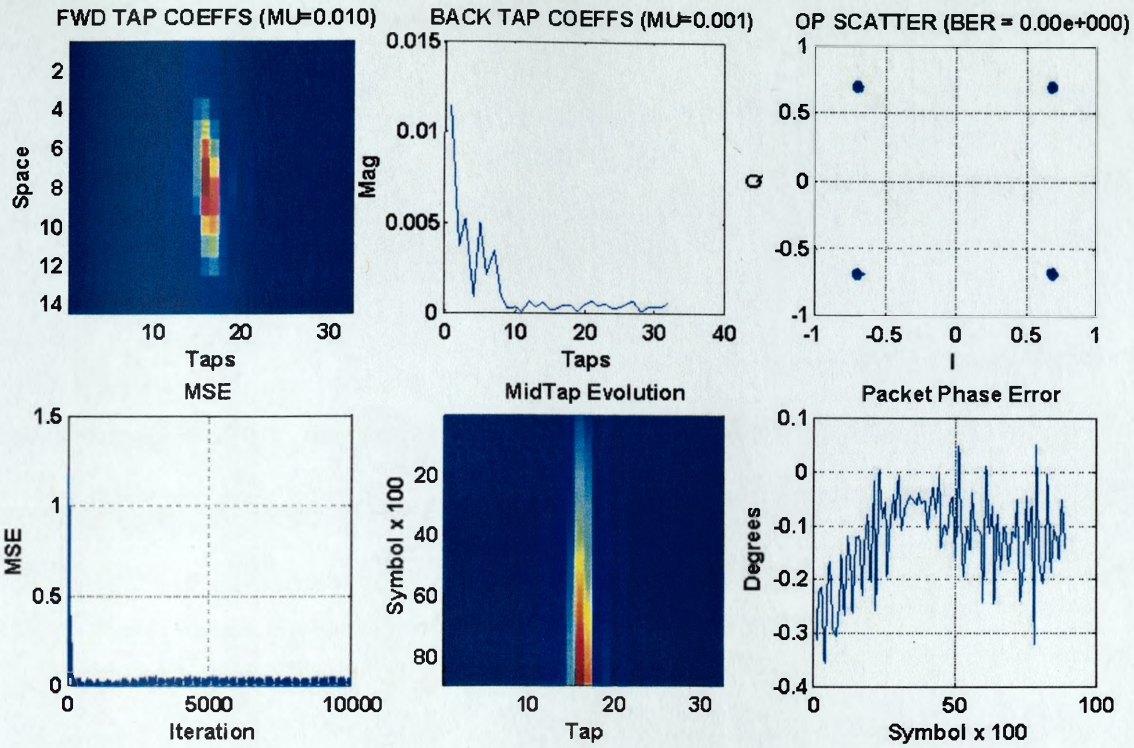

Single Ray Angular Rate = 20deg/s

Note

- High angular rates can be tracked
- This is achieved by the structure de-emphasising taps at array end

Figure 47; STAP-DFE decoder vs. angular rate

9.16 Performance Vs Sensor Separation

9.16.1 Sensor separation has an important role in the performance of STAP receiver architectures since it ultimately determines how the structure exploits the spatial characteristics of the incident field.

9.16.2 Since the spatial scales of acoustic data symbols are typically to centimetric order, a receiver array of comparable spatial scale can exploit the phase and, more importantly the temporal relationships between individual channels. This contrasts quite markedly from a typical RF receive array which merely exploits the phase relationship between channels. Put another way, in a RF array each channel effectively 'sees' the same data symbol and the phase relationship between channels is altered to effect coherent addition between channels (i.e beamforming). In an acoustic array, each channel 'sees' potentially different data symbols or the same data symbol at different delay and phase, depending on how far apart the elements are separated. In order to effect coherent addition of the data symbols appropriate phase and delays must be added to each channel to time align to a common symbol and sampling epoch. As the bandwidth of the data symbols is increased, or equivalently, their duration is reduced, so the spatial scale reduces further and the structure has a greater resolving power to discriminate between path arrivals in a temporal and angular sense.

9.16.3 Since the elements of a spatial temporal receiver 'see' data symbols at different delays rather than just different phases, the beamforming process is an inherently wideband process. Beam responses are no longer based on the addition of sinewaves of different phase (as in the RF case), but the addition of data symbols of both different phase and delay. It is therefore not surprising that the beampatterns of an acoustic STAP receiver bear little resemblance to the conventional sinc() patterns of narrowband beamformers.

9.16.4 In order to investigate this issue, a number of simulations were conducted to determine the beampattern response of the forward section of the STAP receiver for different sensor separations and numbers. At the completion of data decoding, beampatterns were determined by spatially convolving the forward filter complex coefficients with random complex baseband data and computing the resulting output power. The results, shown in Figure 48 depict four simulations.

- 14 element $\lambda/2$ spaced array.
- 7 element $\lambda/2$ spaced array.
- 7 element λ spaced array.
- 7 element $3\lambda/2$ spaced array.

9.16.5 The results demonstrate several important issues regarding the beampattern of a wideband spatial – temporal receiver architecture

- Sidelobe levels lower than a conventional uniformly weighted linear narrowband array
- Narrower beam patterns are obtained for larger sensor separations (as expected)
- At separations greater than $\lambda/2$ diffraction secondary effects are typically 10-15dB less than a conventional narrowband beamformer. This arises due to the aperiodic nature of the data symbol stream.

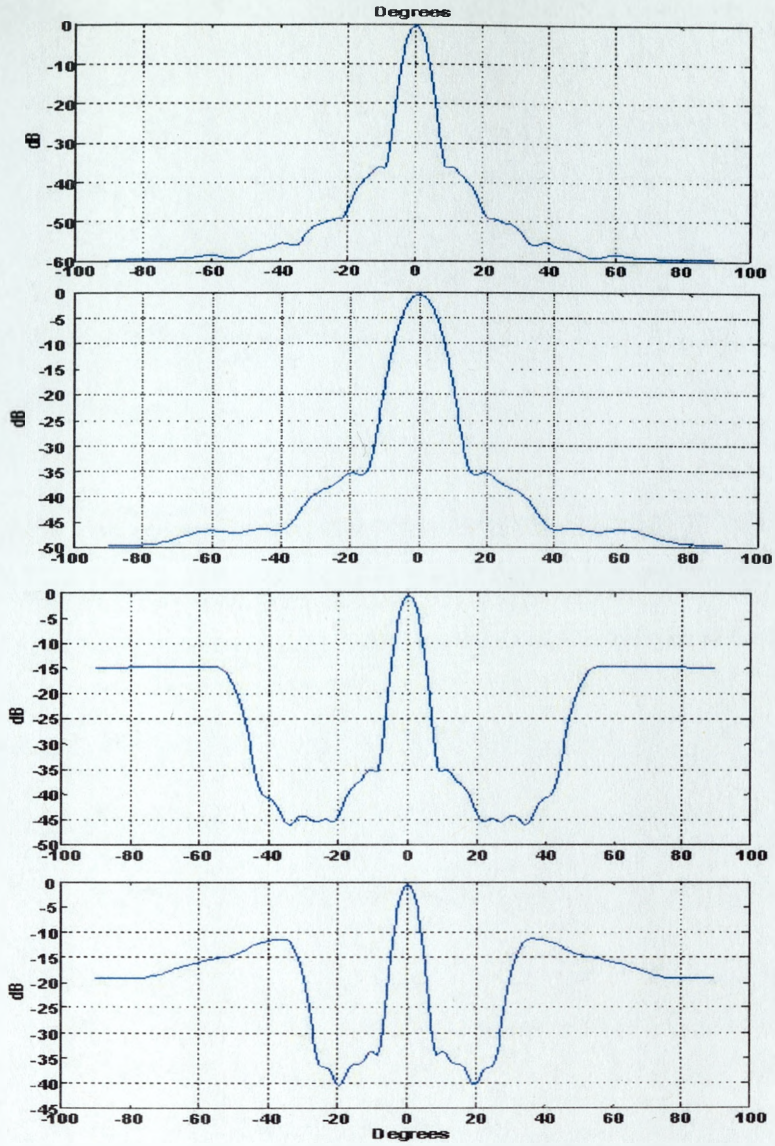

Note

- λ = wavelength of the centre carrier frequency of the SCM transmission.
- Low sidelobe levels for λ/2 case compared to conventional NB beamformer.
- Diffraction secondaries 10-15dB down compared to conventional NB beamformer
- Diffraction sidelobes for spacings of λ or greater extend typically 40deg either side of broadside. At medium-longer ranges little energy arrives outside +/-20deg
- Longer ranges require wider sensor separations: More like diversity combiner.

Figure 48; STAP-DFE BEAM RESPONSE

9.17 Performance vs. Differential Doppler and Angular Diversity

9.17.1 An important observation from earlier sections regarding the nature of the acoustic channel was the potential for multipath arrivals to exhibit rates of delay change with time i.e. differential Doppler. It was shown that differential Doppler arose due to the varying rates at which range changes for each path arrival and this was related to several mechanisms and exists at several scales.

9.17.2 An interesting issue with the decision feedback structure is the impact of differential Doppler between paths. It was shown in previous simulations that when Doppler scaling is the same for all paths, fractional forward filters compensate provided the Doppler error is not too great. In the case of differential Doppler, whilst delay distortion can be compensated for in the forward filter for the synchronised arrival, this cannot be achieved for postcursor arrivals in the feedback section due to the non fractional T spacing.

9.17.3 In order to investigate the capability of the structure to cope with this aspect of acoustic channel behaviour three simulations were conducted. For each simulation a minimum phase channel model of the form $H(z)=1+0.5z^{-10}$ was adopted. This model placed the second weaker path within the feedback filter span of the DFE.

9.17.4 Simulations were conducted as follows:-

- Simulation A: System performance was simulated for the case both paths arrive at broadside with zero differential Doppler.

- Simulation B: System performance was simulated for the case both paths arrive at broadside but with a differential Doppler between them of 0.2m/s.

- Simulation C: System performance was simulated for the case both paths arrive with a differential Doppler between them of 0.2m/s however in this case the paths arrive with an

angular separation of 2.5 degrees. The results of the simulations are depicted in Figure 49,50,51.

9.17.5 Figure 49 depicts the receiver performance for simulation A. From the figure it is evident that the structure manages to converge and decode the packet with zero errors. This is achieved primarily by the action of the DFE section cancelling the postcursor component of the channel impulse response as shown by the decision feedback graph.

9.17.6 Figure 50 depicts the receiver performance for simulation B. From the figure it is evident that the structure has much greater difficulty decoding this packet and errors occur.

9.17.7 Figure 51 depicts the receiver performance for simulation C. From the figure it can be seen that the small difference in arrival angles is exploited by the forward filter section by forming a null in the direction of the second arrival at 2.5degrees. By so doing the structure achieves decoding performance comparable to the zero Doppler case.

9.17.8 These results clearly demonstrate the ability of the spatial temporal processing to exploit both the temporal and spatial characteristics of the incident field to achieve the MMSE operating criteria. Specifically, small angular differences between paths with different Doppler can be exploited by the STAP receiver. This is achieved by spatially nulling the offending paths. The results underline the complex temporal and spatial responses of the STAP structure to typical acoustic channel behaviour.

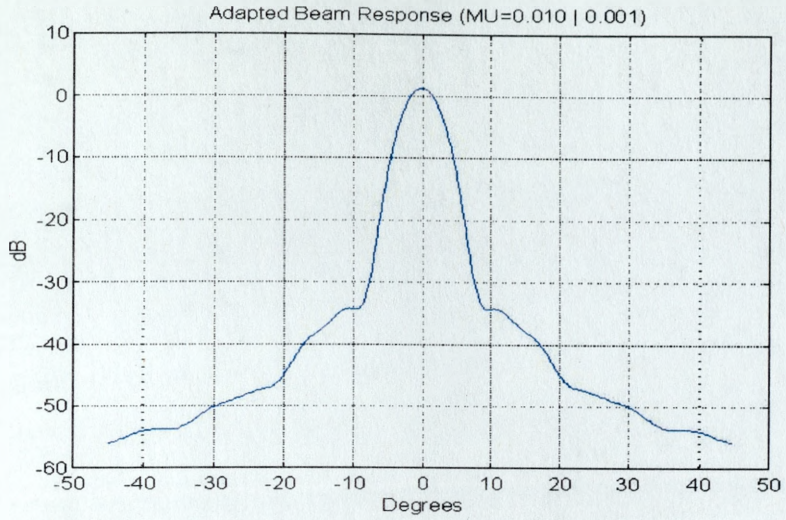

Two Rays ΔT=1ms W_1=1,W_2=0.5 Zero Diffferential Doppler

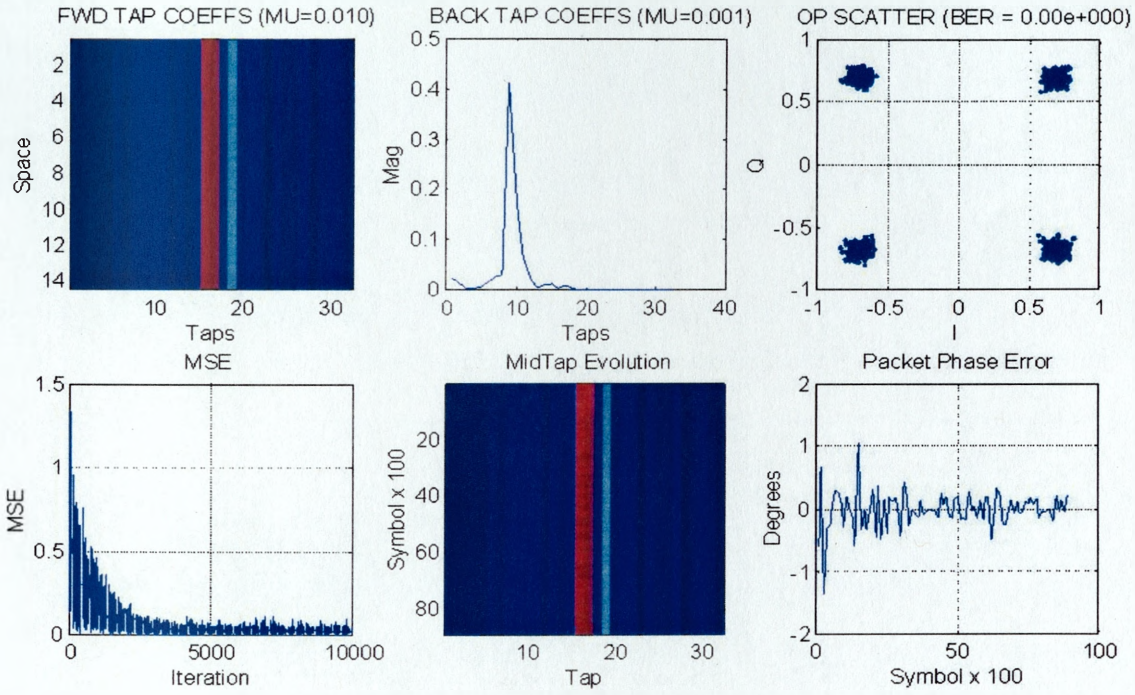

Note

- Zero differential Doppler
- Postcursor arrival cancelled in decision feedback section
- Relatively slow convergence
- Excellent decoding performance

Figure 49; Simulation A: Zero Differential Doppler

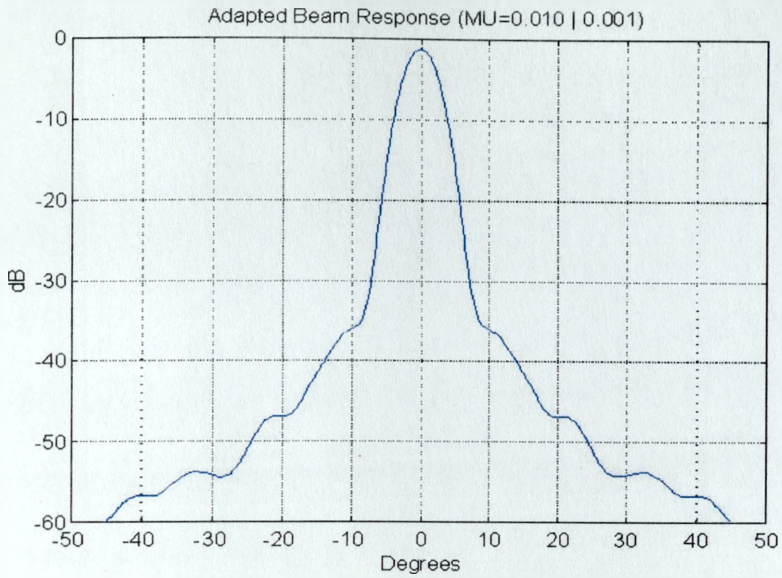

Two Rays ΔT=1ms W_1=1,W_2=0.5 Differential Doppler =0.2m/s

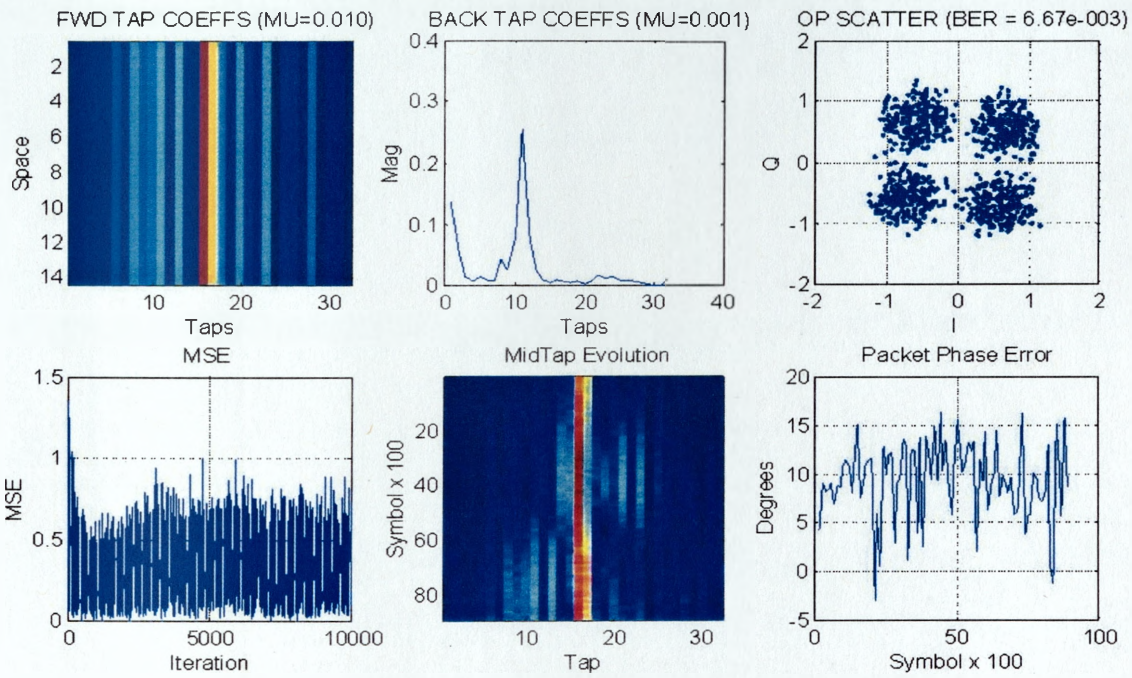

Note

- 0.2m/s differential Doppler
- Paths arrive at same angle
- Less postcursor cancellation in decision feedback section
- Unacceptable decoding performance

Figure 50; Simulation B: 0.2m/s Differential Doppler no angular separation between paths

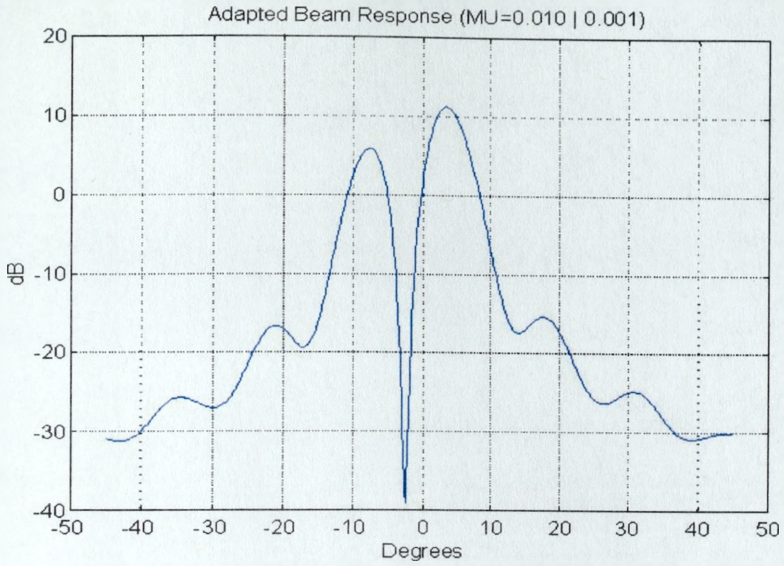

Two Rays DT=1ms W_1=1,W_2=0.5 Differential Doppler =0.2m/s q_1 =0, q_2=-2.5 deg

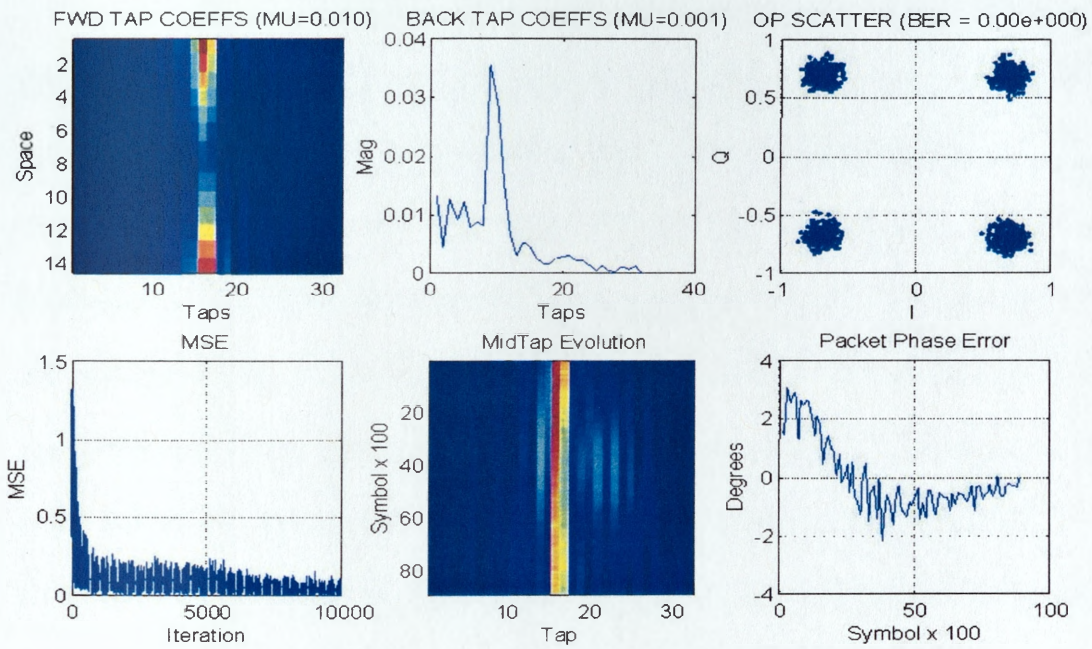

Note

- 0.2m/s differential Doppler
- Paths arrival angle separation = 2.5deg
- Negligible postcursor cancellation in decision feedback section
- Deep null in direction of second arrival
- Acceptable decoding performance

Figure 51; Simulation C: 0.2m/s Differential Doppler 2.5 degree separation between paths

9.18 Performance vs. Non Minimum Phase Channels

9.18.1 Of the acoustic channel conditions considered thus far, the potential for the channel to be non-minimum phase either at the start of decoding or, during the decoding process is a significant factor influencing receiver performance. This is particularly the case where paths have little or no angular separation. A simple example of a non-minimum phase channel which is difficult to cope with using the structures discussed thus far is of the form $H(z) = 0.5 + z^{-5}$. The reason why such a channel is difficult to cope is that it is non-minimum phase i.e. the channel does not have a stable inverse since some or all of its zeros lie outside the unit circle.

9.18.2 Figure 52 contrasts the zero positions for a channel of the form $H(z) = 1+ 0.5z^{-5}$ (top) and $H(z) = 0.5+z^{-5}$ (bottom). A potential solution to this problem is to time reverse the channel. In this case z^{-M} becomes z^{+M} and so the channel model becomes $H(z)=(0.5+z^{+5})=z^{+5}(1+0.5z^{-5})$. Since it is straightforward to make the system causal with the appropriate delay then the resulting inverse channel is both causal and stable. To apply this technique in practice requires that training sequences be applied at the start and at the end of the data packet. The training sequence applied at the end must also be time reversed to enable consistent training between forward and reverse directions as shown in Figure 53. The result of applying the time reversal method to this channel is shown in Figure 54. From the figure it can be seen that the data is decoded without error and, as expected the MMSE operating criteria achieved via feedback cancellation. Without time reversal the conventional DFE structure would be unable to reliably decode this transmission.

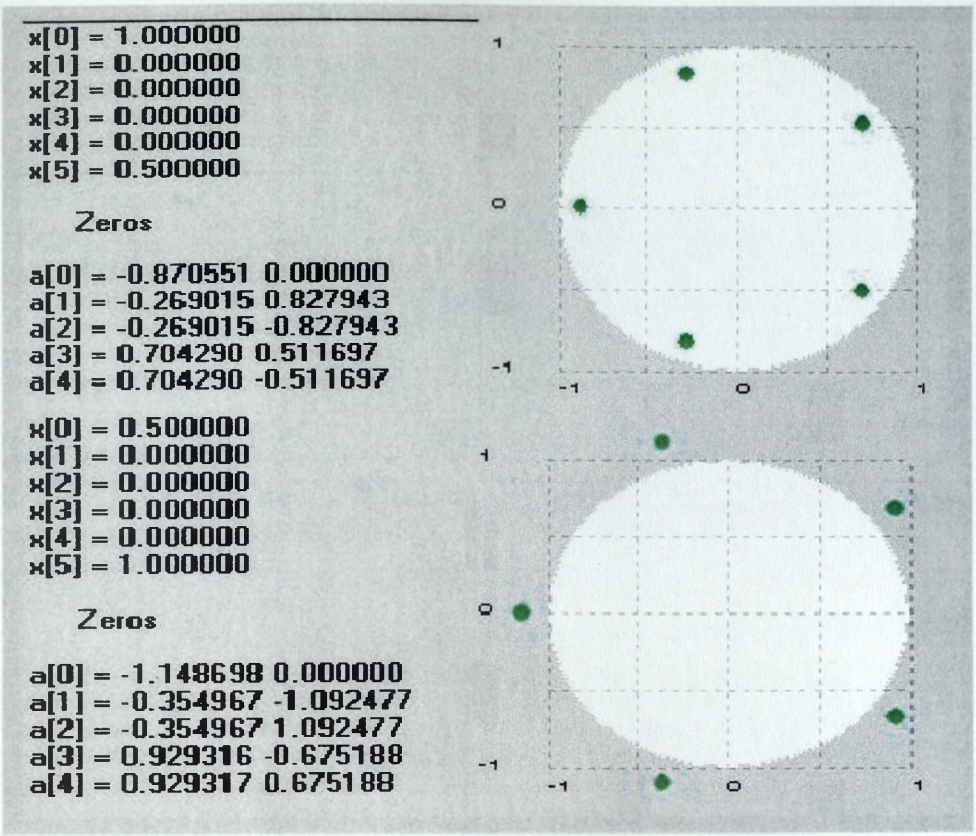

Note

- Minimum Phase Channel $H(z^{-1}) = 1 + 0.5z^{-5}$ (Top)
- Non minimum phase channel $H(z^{-1}) = 0.5+z^{-5}$ (Bottom)
- Zeros outside unit circle indicate unstable pole positions for inverse filter

Figure 52; Example non minimum phase system

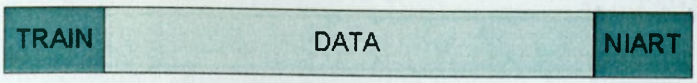

Note

- Minimum Phase Channel decoding occurs left to right
- Non minimum phase channel decoding occurs right to left
- Decoding direction based on MSE at end of training iterations

Figure 53; Forward and Reverse Training Sequences to cope with minimum phase and non minimum phase channels

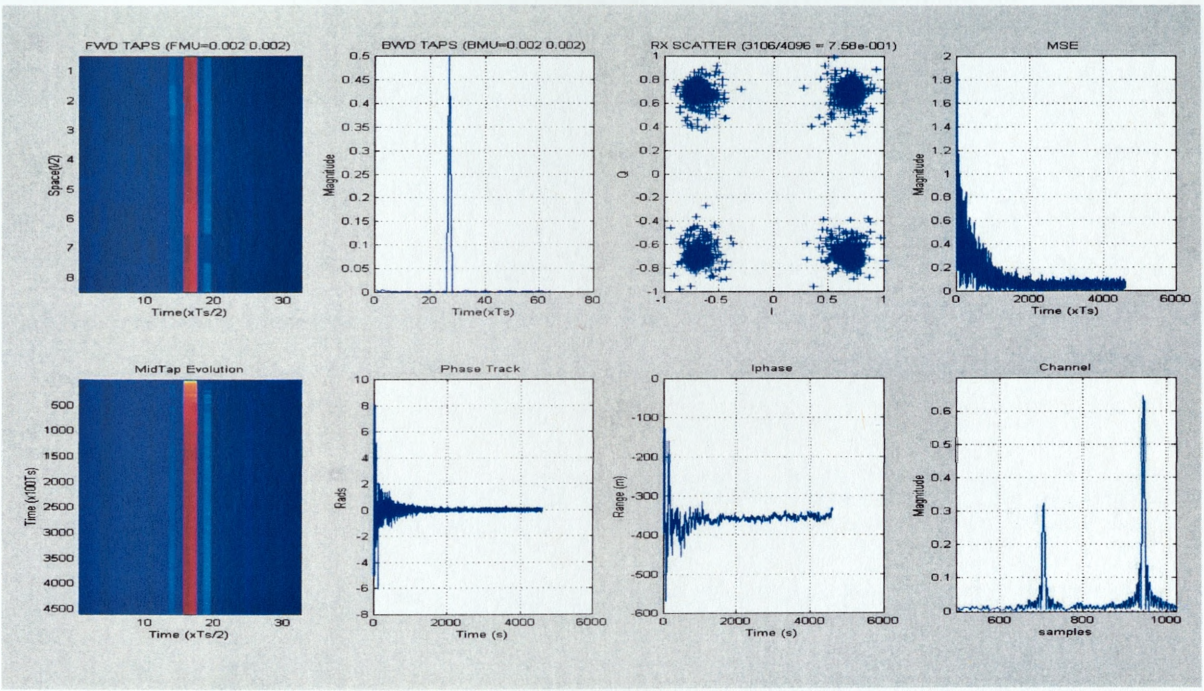

Note

- Non minimum phase channel cannot be equalised in forward direction
- Decoding occurs in time reverse, synchronised to second, larger, arrivals
- DLL gain term must be sign reversed
- Forward equalisation cannot decode this packet irrespective of synchronisation path

Figure 54; Time reverse decoding of non-minimum phase channel

9.18.3 The preceding investigation has determined the key issues which impact upon the performance of the STAP architecture under simulated acoustic channel conditions. It has been shown that the performance benefits obtained for more than eight channels are likely to be outweighed by the additional cost and complexity of additional channels.

9.18.4 It has been shown that equaliser convergence can be particularly slow for stochastic gradient algorithms in difficult channels however this can be offset by recycling training data.

9.18.5 It has been shown that acoustic Doppler influences both training and steady state performance. To counteract high residual Doppler errors a phase lock loop is necessary particularly during training. In steady state improved performance is obtained using both phase lock loop and delay lock loop closed loop tracking.

9.18.6 It has been shown that under non-minimum phase channel conditions where there is little angular or spatial diversity in the incident acoustic field, the structure is unlikely to operate effectively. Under such conditions decoding the packet transmission in time reverse can be an effective means to overcome the non-minimum phase channel problem.

9.18.7 Whilst the simulation studies presented here have provided valuable insight to the behaviour of the STAP under simulated channel conditions, the transition from synthetic to real operational environments introduces much greater levels of complexity and a more representative test for the algorithms. In the following section the performance of the STAP receiver is reported for a variety of trials environments.

"Nothing is too wonderful to be true,

if it be consistent with the laws of nature ,

and in such things as these,

experiment is the best test of consistency'

Michael Faraday, Diary 19 March 1849

10 IMPLEMENTATION, FIELD TRIALS AND EXPERIMENTAL RESULTS

10.1 Acknowledgements

10.1.1 In order to validate the performance of the STAP processing algorithms, a wide range of field trials have been conducted to verify algorithm performance and to better understand the behaviour of the STAP algorithms under real ocean (and platform) behaviour. The results collected are drawn from diverse geographical locations featuring a wide range of water depths, bathymetry, biological and man made noise.

10.1.2 The algorithms have been applied across a wide variety of operational frequencies and bandwidths reflecting the need to reduce frequencies in order to achieve improved range performance. Table 4 summarises the operational, geographical and environmental characteristics of the field trials data. Despite their cost, field trials remain the ultimate demonstration of any technology and the author is indebted to the efforts of the many people, organisations and funding bodies responsible for funding, organising and executing the field trials results reported here.

10.1.3 The support and funding from military sponsors, DEC(UWB) and DSc(SEA) is also greatfully acknowledged both for research programmes into high data rate acoustic

communications and ongoing research into acoustic modem technology for rapidly deployable sensors and systems. The author would like to acknowledge the efforts of the QinetiQ Winfrith Deployables and Acomms team for organising and executing trials under the Rapidly Deployable Sensor programe and for the development of the outboard systems and inboard MMI interfaces necessary for real time demonstrations. The author would also like to acknowledge the efforts of the Winfrith Active sonar team in transmitting and recording waveforms using low frequency projectors for several long-range acoustic communications performance experiments.

10.1.4 Over the course of this study much experimental data has been collected and analysed with a view to evaluating and improving algorithm performance. Practical realisation of the algorithms and techniques discussed thus far, represents in itself, a significant challenge. Real time implementation issues are therefore not discussed in depth here but are deferred to appendix V. Here the issues relevant to realising a practical telemetry link including algorithm implementation protocols and physical realisation are discussed.

10.1.5 Rather than provide an exhaustive review of the many field trials results reported in table 4, a single experimental scenario is considered which draws together theoretical and practical challenges in the development and implementation of acoustic communications for underwater vehicles. A more comprehensive discussion of the field trials results indicated in table 4 is presented in appendix U. The experiment reported here is a practical demonstration of autonomous underwater systems exchanging data in a demanding shallow water environment. The experiment pulls together many of the issues raised in previous discussions relating to the realisation of robust underwater acoustic communications at both low and high rate and provides a quantitative framework to assess the performance of these algorithms operating in autonomous systems

Figure	Location	Range	Bottom Type	Water depth	Static/Dynamic	Modulation	Data Rate	TX Config	RX Config	Frequency	Notes
		(meters)		(meters)	(kts)		(bps)			(kHz)	
55	Weymouth Harbour,1998	400	Sand/Silt	30-50	0.5	QPSK	21000	12in. Ball	14ch VLA	10.0-20.0	short range static configuration
56	Weymouth Harbour,1998	1200	Sand/Silt	30-50	0.5	QPSK	21000	12in. Ball	14ch VLA	10.0-20.0	medium range ststic configuration
57	Weymouth Harbour,1998	1200	Sand/Silt	30-50	0.5	QPSK	21000	12in. Ball	14ch VLA	10.0-20.0	Comparison 14ch vs. 7ch
58	Weymouth Harbour,1998	400	Sand/Silt	30-50	3.5	QPSK	21000	12in. Ball	14ch VLA	10.0-20.0	short range dynamic configuration
59	Weymouth Harbour,1998	400	Sand/Silt	30-50	0.5	QPSK	21000	12in. Ball	14ch VLA	10.0-20.0	Beam pattern comparison
60	Weymouth Harbour,1998	400	Sand/Silt	30-50	0.5	QPSK	21000	12in. Ball	14ch VLA	10.0-20.0	Doppler + BER evolution
61	Timor Sea, N.Australia,1999	1500	Clay	300	0.8	QAM16	41000	12in. Ball	14ch VLA	10.0-20.0	QAM16
62	Timor Sea, N.Australia,1999	2500	Clay	300	0.4	QPSK	21000	12in. Ball	14ch VLA	10.0-20.0	QPSK
63	Adriatic, E.Italy,2000	1000	Clay/Sand	200	1.3	QPSK	21000	4in. Flood Ring	8ch VLA	9.0-15.0	QAM
64	Portland Harbour,2000	1000	Clay/Sand	10	Static	QPSK	21000	4in. Flood Ring	8ch VLA	9.0-15.0	FWD-REV Decoding
65	Sound of Hura, NW Scotland,2001	20000	Sand/Silt	150	Static	QPSK	300	LF VLA	32ch VLA	<2kHz	Long range LF static
66	Narragansett Bay, Rhode Island	<1000	Clay	30	4.0-5.0	QPSK	12000	4in. Barrel Stave	2X8ch VLA	9.0-15.0	AUV telemetry link
67	Nova Scotian Shelf, NE Canada,2002	20000	Gravel/Rock	60	1	QPSK/DSSS	12000/60	4in. Flood Ring	8ch digital VLA	9.0-15.0	Subsea sensor data uplink TEXT
68	Nova Scotian Shelf, NE Canada,2002	1000	Gravel/Rock	60	0.5-1.0	QPSK/DSSS	12000/60	4in. Flood Ring	8ch digital VLA	9.0-15.0	Subsea sensor data uplink IMAGE
69	SW Approaches, SW UK, 2002	12000	Gravel/Rock	100	2.5-3.0	QPSK	1600	VLF VDS	8ch OBS	<2kHz	Medium Range LF dynamic

Table 4; Field trials and experimental results

10.2 Autonomous underwater vehicle acoustic communications

10.2.1 Mobile underwater vehicles present unique opportunities to explore the many issues relevant to mobile underwater communications. The author would like to acknowledge the underwater vehicle team at the Naval Underwater Warfare Center (NUWC), Newport Rhode Island for providing the opportunity to test modems developed by the Deployable and Acoustic Communications team on the Manta test vehicle (MTV). This section focuses on the results of a particular experimental demonstration designed to not only exercise the algorithms in demanding operational role and environment but to underpin the wider utility of acoustics in underwater sensor communications. Figure 55 depicts the run geometry for an experiment conducted in August 2002 at the Gould Island Acoustic tracking range (GIATR) facility at Newport, Rhode Island. This experiment involved MTV autonomously communicating with several underwater systems at both low and high data rate, initiating low data rate bidirectional links, and uplifting data via unidirectional high data rate link.

10.2.2 The experimental configuration was designed to demonstrate several features of the acoustic modem design namely:-

- Real time operation
- Bidirectionaldirect sequence spread spectrum communications;
- Unidirectional high data rate phase coherent communications;
- Automated Doppler measurement;
- Selective node addressing;
- Selective power control;

- Automated modulation detection;
- Spread spectrum mode @ 75bps;
- Phase Coherent mode @ 12000bps;

10.2.3 Commands issued by the MTV to nodes used a low data rate spread spectrum modulation scheme based on the waveform designs presented in section 7 and modulation techniques discussed in section 8. This mode provided bi-directional low data rate connectivity between MTV and rapidly deployable systems (RDS) nodes and also RDS to RDS. During the trial the low data rate mode was used primarily for RDS status interrogation by MTV and to initiate high data rate uplift from RDS nodes.

10.2.4 All acoustic commands and data transmission a link definition waveform (LDW) comprising a coded 12bit multi-field header designed to support acoustic network operations discussed in more detail in appendix V. The link definition header is used to provide Doppler measurement, definition of modulation type, power level control and selective addressing. This information provides the protocol a simple networking capability enabling MTV to connect to several RDS systems. For the demonstration run involving high data rate up lift of detection and targeting data, the RDS node modems provided a phase coherent uplink mode supporting data transfer at 12000bps. Command and control data exchanges occurred at 75bps.

10.3 RDS Data Seeding

10.3.1 For the demonstration trial, both RDS units were seeded with a fixed sonar data image. This provided a means to assess link bit error rates throughout the run. The data set shown in figure 56 comprised a 1kbyte image file.

10.3.2 The transmission of a common data set by all nodes enabled an accurate measurement of system's bit error rate performance to be made throughout the run. It should be stressed that whilst a single data set was transmitted by both RDS systems, the acoustic modem technology and protocol supported the transmission of any type of digital data including text, image, sound etc and selective transmission of arbitrary file data. So, for example, the uplifted data set could potentially have been changed on a transmission by transmission basis under the direction of MTV throughout the run.

10.4 Acoustic Conditions

10.4.1 Propagation conditions over the trial duration were noted to be extremely variable during engineering tests involving transmissions between GIATR nodes separated by approximately 1.5km. This was due to significant surface layer warming and layer mixing effects arising from strong tidal and current activity in the Narragansett Bay area. This led to dramatic variability in the sound velocity profiles for the area over the trial period as shown in figure 57. The profiles are seen to change from a mildly downwardly refracting profile on July 29th to strongly downwardly refracting profiles from July 31st onwards. In terms of acoustic modem performance these conditions served to limit direct path range to less than 500m often with one or more acoustically shadowed range regimes as shown in figure 58 which depicts a ray trace simulation for the SV profile of July 31st. These conditions represent a particularly demanding test for the acoustic modems and since the Summer seasonal profiles are usually the most challenging, the results presented here are most likely worst case for this environment.

10.5 Results

10.5.1 During the demonstration run all acoustic communication events including element level MTV array data, channel data, Doppler and of course decoded telemetry data were logged

and stored to disk within the vehicle. This data was subsequently fused off line with MTV mission log data in order to consolidate vehicle track and acoustic communication event data.

10.5.2 Figure 59 shows the MTV mission control position log showing the vehicle track during the demonstration run. Overlaid are the acoustic communication events, event time and approximate node positions.

10.5.3 The acoustic communication events 1-19 indicate the approximate position of the MTV at the time of each communication event. A communication event involved

- Acoustic modem transmits a 96bit acoustic command to selected node
- Node modem receives command and passes to node controller
- Node controller decodes command and protocol and passes requested data block to Node modem
- Node modem transmits 1024byte data block to MTV
- MTV receives data block and stores data plus diagnostics to disk.

10.5.4 All acoustic commands issued by MTV requested data uplift of the test data set of figure 56. MTV data uplift commands were issued approximately once every 25 seconds. The transmission of the same data set by both nodes provided a consistent basis to assess and compare modem performance over the run duration.

10.5.5 Events 1-19 depict three communication regimes as follows

- 1-7 MTV communicates with Node1 during over-flight;
- 8-14 MTV communicates with Node2 during circular manoeuvre;

- 15-19 MTV communicates with Node1during return over-flight.

10.5.6 In all cases, the vehicle was submerged to a depth of approximately 6-8m and moving at a velocity of between 4.5-5kts. The dynamic geometry involved forward and aft aspect communications with Node1 and multi-aspect communications with Node2.

10.5.7 Figure 60 depicts relative Doppler measurements logged by the QinetiQ acoustic modem on the MTV for events 1-19. The figure shows closing and receding speeds of up to 5kts consistent with the geometry of figure 55. Specifically

- Events 1-4 : MTV approaching Node 1 (Forward Aspect)
- Event 5 : MTV at Node 1 CPA (Close range broadside Aspect)
- Event 6-7 : MTV recedes from Node 1 (Stern Aspect)
- Event 8-4 ; MTV executes offset circular manoeuvre around Node2 (Multi-aspect)
- Event 15-17; MTV approaching Node 1 (Forward Aspect)
- Event 18-19; MTV recedes from Node 1 (Stern Aspect)

10.5.8 Figure 61 depicts the received bit error rate for events 1-19 and table 5 summarises bit error performance during each communication period with node 1 and node2. Figures 62-64 present actual logged data and decoded data files recovered from the MTV at the end of the run.

10.5.9 The bit error graph of figure 61 and the corresponding decoded image data in figures 62-64, identify several outlying results inconsistent with the overall data trend. In particular, events 5,7,10 and 11 indicate error rates at least one order of magnitude higher than the general trend.

10.5.10 Referring to figure 61 and 62, event 5 occurred during CPA with node 1. The measured Doppler at the packet start was almost zero indicating the vehicle to be extremely close to the node. Due to the close proximity, the Doppler rate is extremely high and it is likely that over the packet duration the system was unable to track the high Doppler variation. Referring to figure 62, this view is supported by the fact that the decoded image errors occurred toward the end of the transmission indicative of algorithm breakdown due to the high Doppler rate.

10.5.11 A similar effect is noted in event 10 where the vehicle goes through CPA with node 2. In this case the CPA occurs at slightly greater range and a reduced Doppler rate with the result that the breakdown in algorithm decoding occurs later in the packet and is less pronounced (refer figure 63).

10.5.12 In event 7 the consistent degradation in error rate is typical of degraded signal to noise. In this case errors are randomly distributed over the packet duration. This is likely due to a combination of the increased range coupled with stern aspect and downwardly refracting propagation conditions. Similar performance degradation occurs in event 11. In this event MTV self-noise is likely to be a more significant factor. Indeed system performance during the manoeuvre around node 2 was noticeably degraded. During the manoeuvre the vehicle self-noise levels were observed to increase significantly on the GIATR acoustic monitoring stations.

10.5.13 Table 5 summarises decoder bit error performance highlighting the performance degradation due to high MTV self noise levels arising from manoeuvres during events 8-14. With outliers removed the system demonstrated a mean raw bit error rate of 5.7e-3. It should be stressed that this error rate is a raw rate without any forward error correction coding. A forward error correction coding strategy would reduce this error rate by

typically 1-2 orders of magnitude. For an operational system this would mean that the majority of data packets, excluding outliers, would likely be decoded without error. Coding would however reduce the effective data rate by up to half.

10.6 Discussion

10.6.1 Of a total of 21 MTV requests for high data rate up lift, a total of 19 were successfully completed. This represents a packet request and delivery success rate of over 90%. This figure is particularly impressive given that each successful packet uplift was dependant not only on successful decoding of the uplink packet but also successful decoding of the downlink command word by the RDS node. The accuracy and fidelity of the acoustic modem Doppler estimation algorithm discussed in greater detail in section 6 was particularly impressive. In particular, with knowledge of own speed, the measured relative Doppler between MTV and deployed RDS nodes provides a means for the vehicle to estimate a relative bearing correction to 'home in' on RDS nodes.

10.6.2 Despite unfavourable aspect changes and increased noise levels during the manoeuvre around Node2 successful communications were maintained throughout the run. Full 360 degree aspect communications were achieved despite the potential for acoustic shadowing from MTV and DV structures particularly during stern aspect data transmissions. During this period all transmissions were successfully received and decoded albeit at degraded bit error performance. Optimum performance was achieved for forward aspect communications. Given the high noise levels both from MTV and other traffic in the vicinity of the test range the achieved raw bit error rates are good. An interleaved forward error correcting strategy would provide significant improvement in bit error performance particularly under bursty error conditions typified by the majority of transmissions decoded during the run.

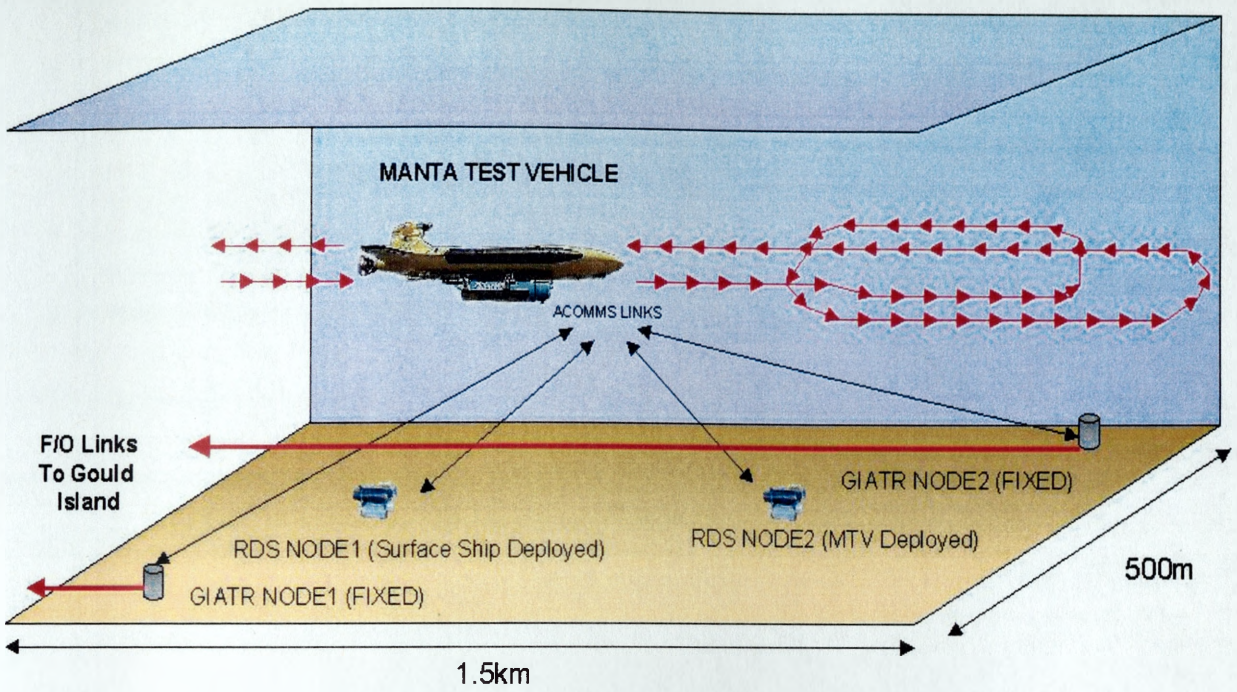

Figure 55; Subsea Sensor to AUV data telemetry uplink test scenario

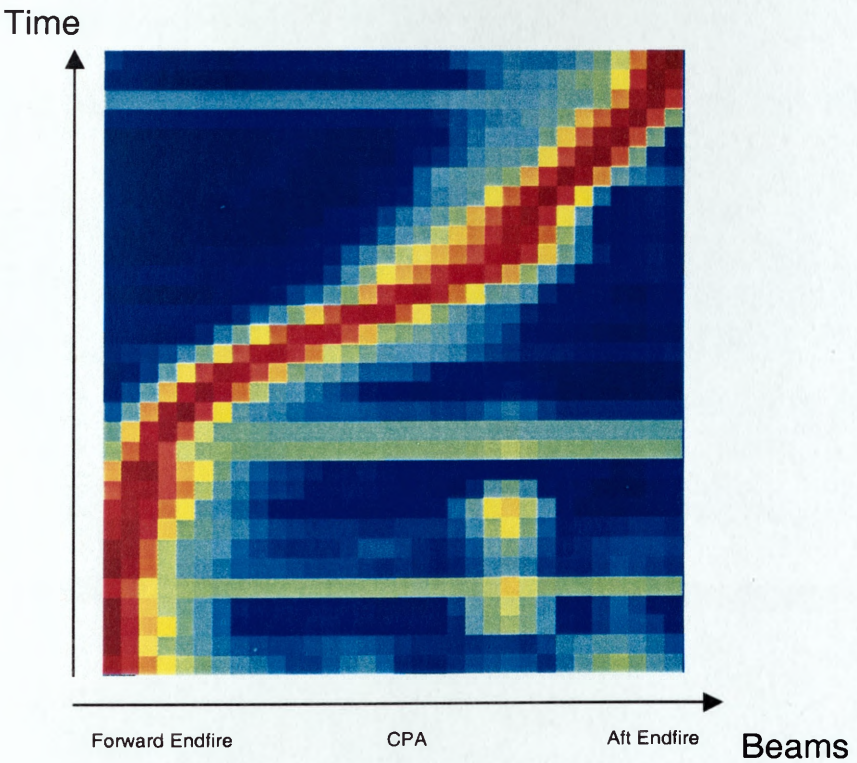

Figure 56; Sensor simulated test data set comprising 1kbyte image file

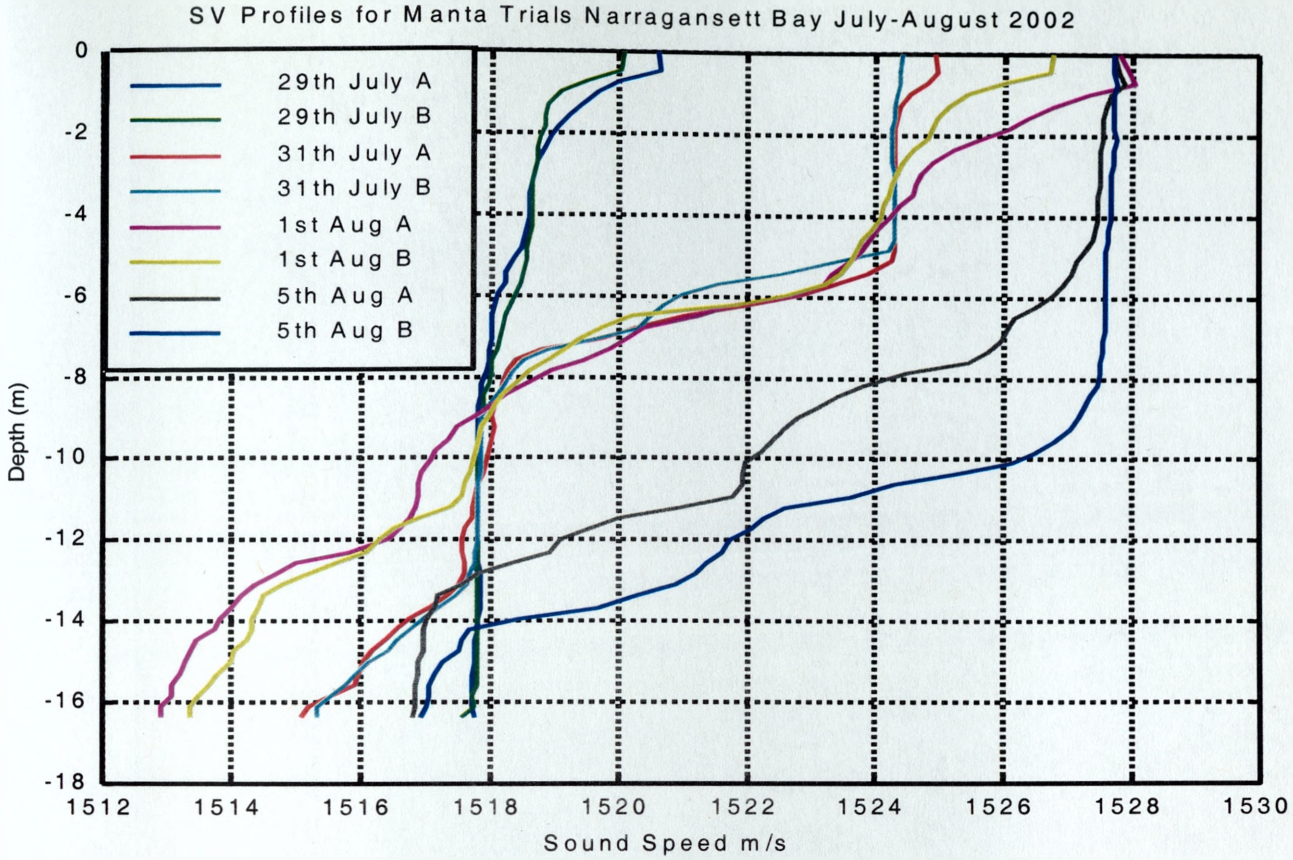

Figure 57; Sound velocity measurements over experimental duration demonstrating high variability

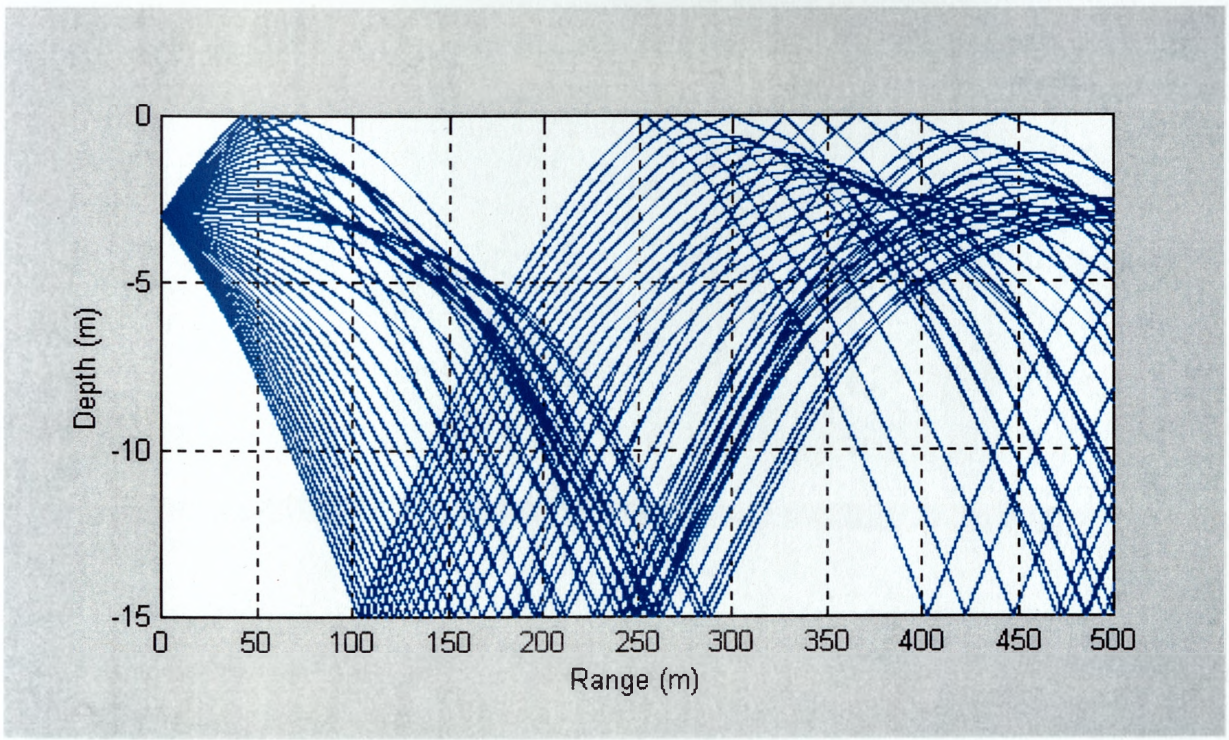

Figure 58; Ray trace simulation for experiment

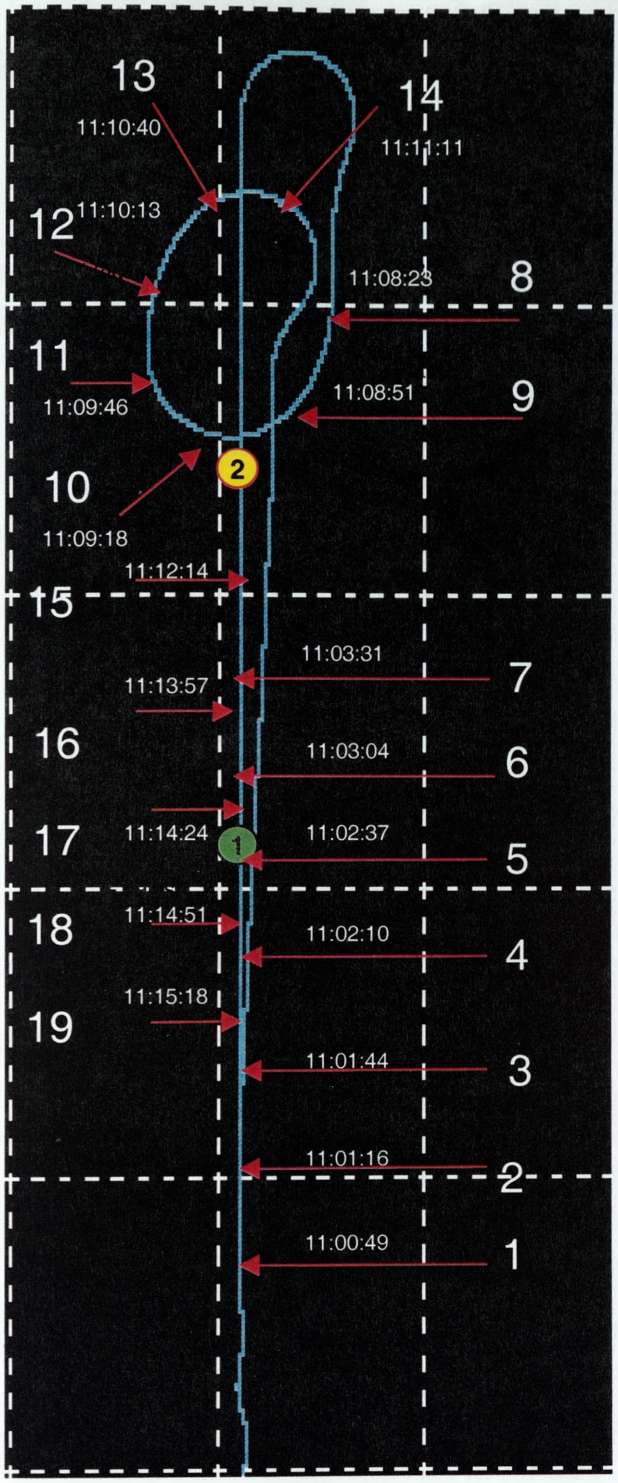

Figure 59; Fusion of vehicle INS data with acoustic communication event data

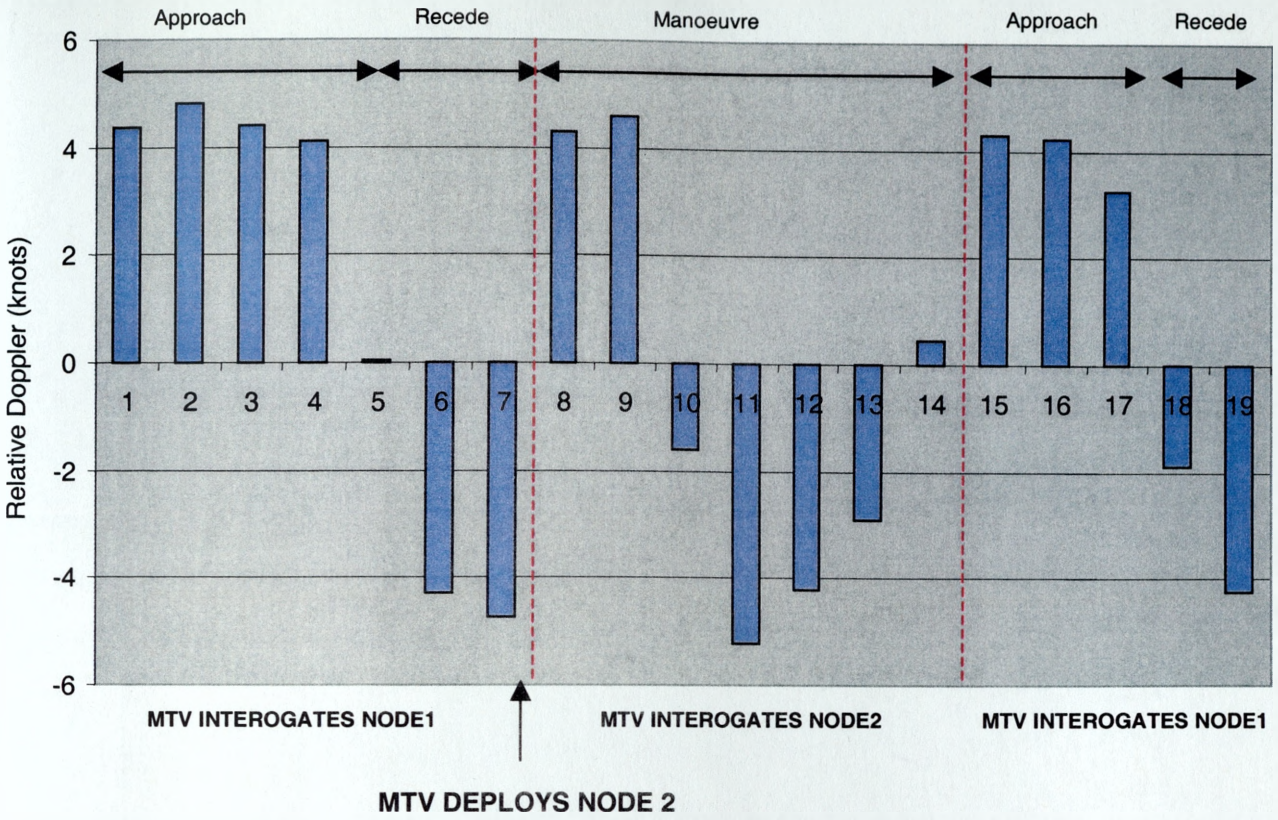

Figure 60; Communication event relative Doppler measurements abstracted from vehicle pos mission log

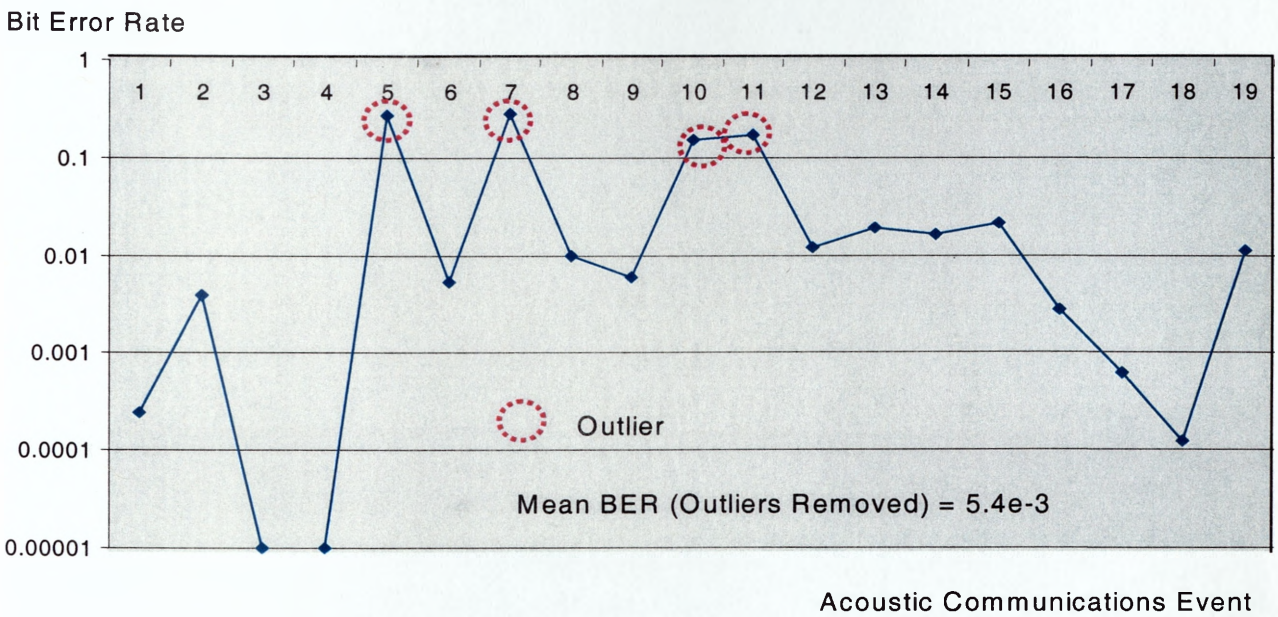

Figure 61; Data packet error rates measured during run

Events 1-7	Events 8-14	Events 15-19
1.3e-3	12.4e-3	3.6e-3
Mean BER (Outliers removed) = 5.7e-3		

Table 5; Raw error rates for modem high data rate packet transfers

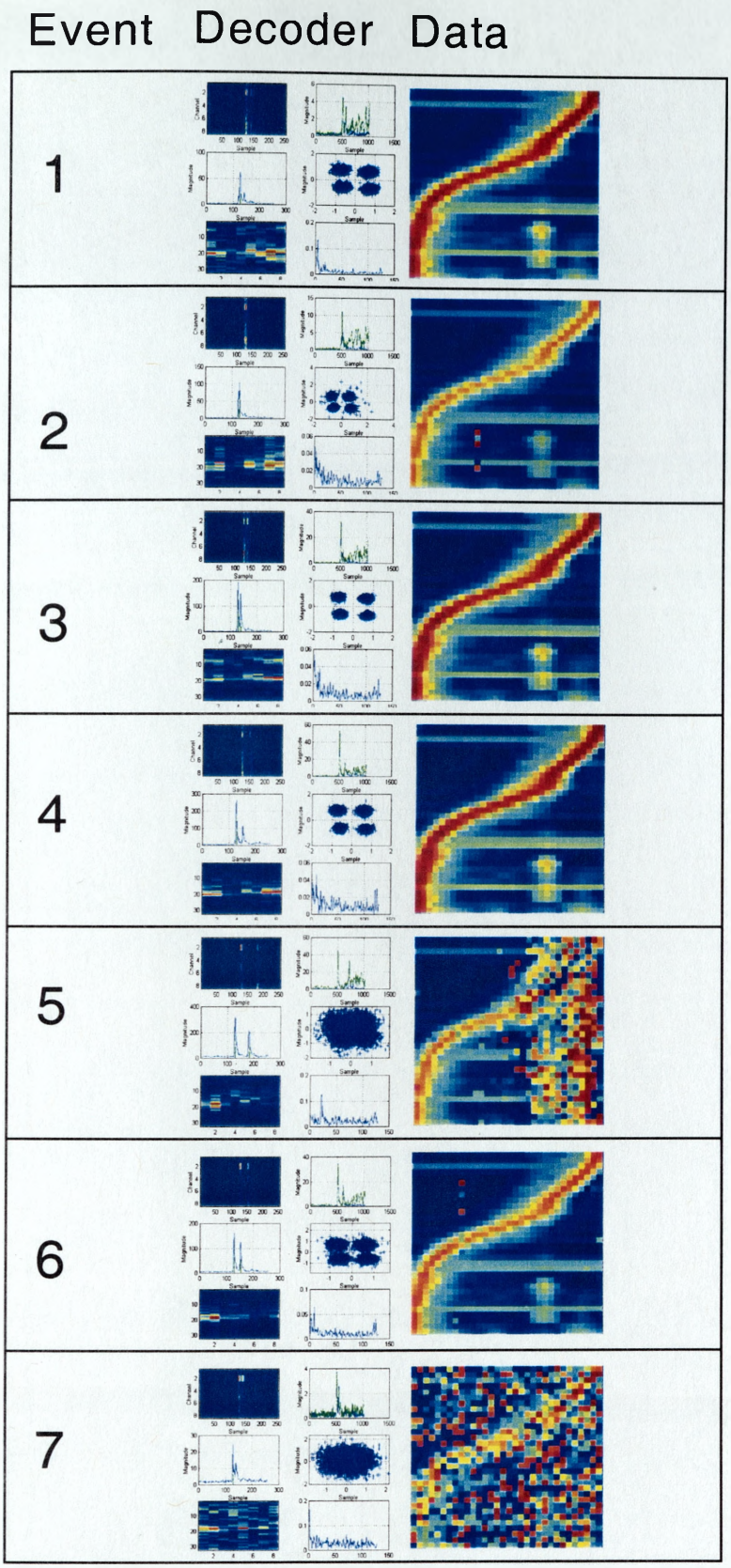

Figure 62; Decoder diagnostics and raw decoded data for events 1-7

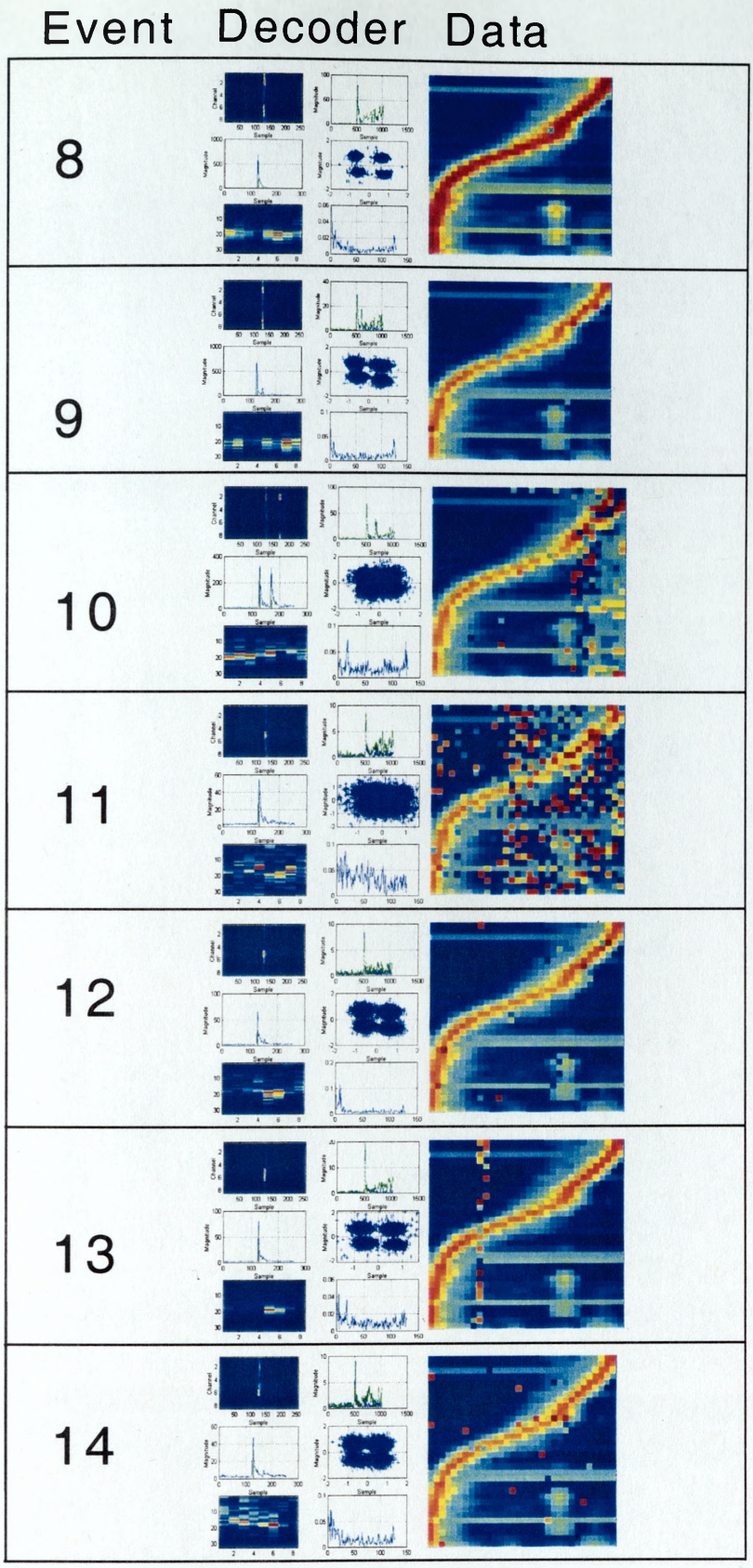

Figure 63; Decoder diagnostics and raw decoded data for events 8-14

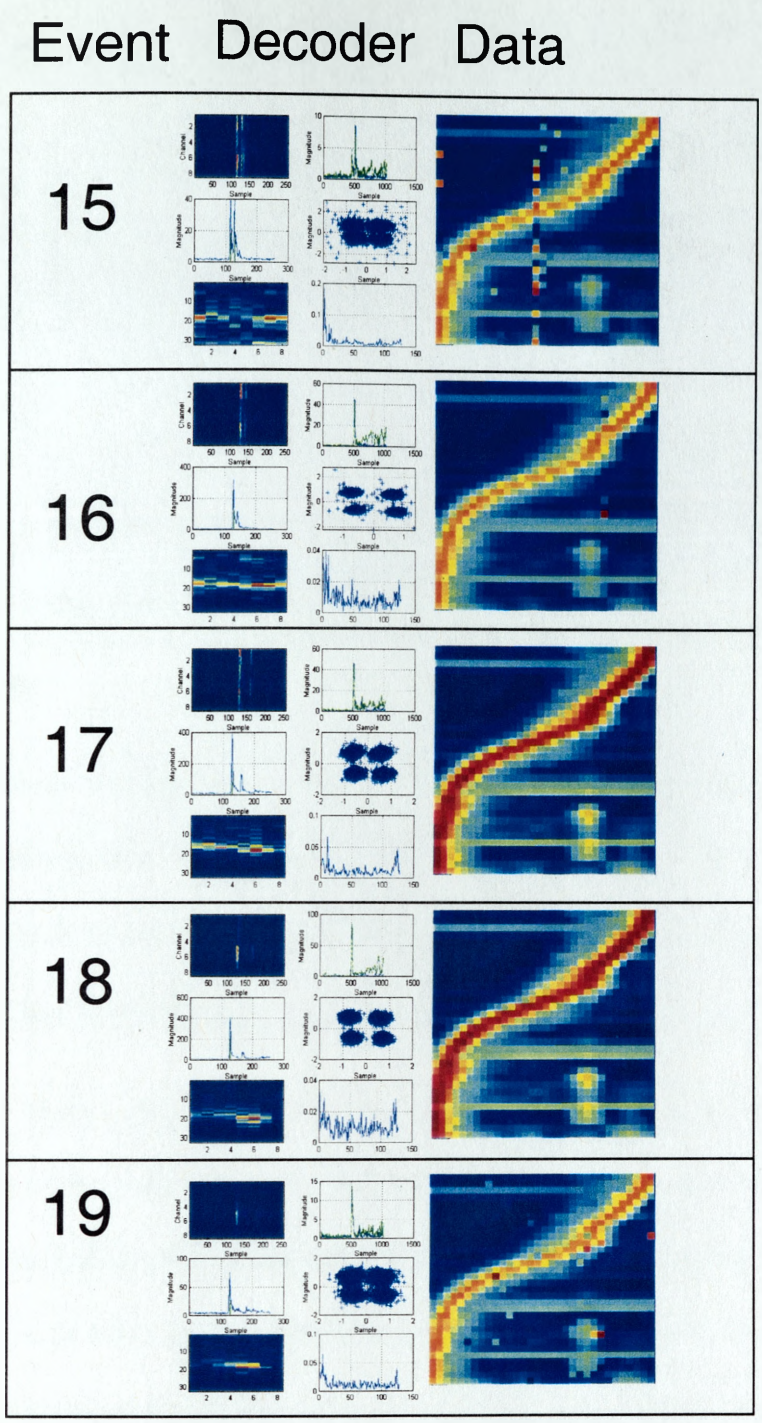

Figure 64; Decoder diagnostics and raw decoded data for events 15-19

Science means simply the aggregate of

all the recipes that are successful.

The rest is literature',

Paul Valery,1871-1945,Moralites(1932)

11 CONCLUSIONS AND FURTHER WORK

11.1 Conclusions

11.1.1 This work has investigated the problem of high data rate communications using acoustics. A key foundation has been the study of the physical ocean mechanisms that influence signal coherence and the relationship between the physical channel, signal coherence and the signal design problem.

11.1.2 It has been shown that the intrinsic coherence properties of the underwater acoustic environment differ markedly from terrestrial EM channels primarily due to the different spatial and temporal scales of the respective waveforms. This is in turn a consequence of the difference in propagation speeds of the two signal types. For underwater acoustic signals, the spatial and temporal scales of the waveforms are of comparable order to the inhomegineities and irregularities arising within the underwater medium. Such irregularities may be non-stationary surface waves, irregular bottom types or even temporal and/or spatial variability of the water propagation speed.

11.1.3 Experimental evidence has demonstrated that the underwater acoustic channel is doubly dispersive, exhibiting both temporal and Doppler spread. Simulation studies and field

experimental result have demonstrated the advantages of using wideband waveforms for measuring and tracking environmental variability These results have demonstrated that the complexity of the acoustic channel can often be greater at short to medium range than at longer ranges in the medium frequency band. This arises due to the more pronounced influence of path temporal scaling at shorter ranges arising from surface platform dynamics, and the potential for greater temporal smear.

11.1.4 The problem of optimised waveform design for doubly dispersive channels has been investigated. It has been shown that both temporal smear and Doppler scaling have a pronounced influence on the orthogonaliy properties of potential signalling waveforms. The well-defined correlation properties of classic code families such as maximal length sequences, Gold, Kasami and Walsh codes are all degraded under multipath conditions. Cyclic extension of such codes provides some protection against multipath. Temporal scaling due to Doppler rapidly erodes the correlation performance of such code designs, particularly for large BT product signals. Under such conditions explicit compensation is necessary. For high data rate communications, the potential advantages of spread spectrum techniques are often outweighed by the need to maximise data throughput.

11.1.5 The relative performance benefits of single carrier and multicarrier modulation have been investigated for the high data rate underwater acoustic communications application. It has been shown that the performance benefits of both approaches are constrained by the doubly spread nature of the acoustic channel. Single carrier modulation provides rapid sampling of the channel and so can track time varying fluctuations. However, extended multipath results in frequency selective fading requiring complex equalisation schemes. Multicarrier modulation, provides less rapid tracking of the environment. However, the equalisation problem is relaxed since one has greater control over subchannel bandwidths relative to the channel coherence bandwidth. For high platform velocity applications,

where the channel becomes more time selective, rapid sampling of the channel is essential. At short to medium range, differential path Doppler results in highly dynamic fluctuations in the magnitude and phase of the channel transfer function in the vicinity of channel nulls. Tracking such fluctuations in a frequency domain modulation technique such as COFDM requires rapid channel sampling and this offsets the inherent benefits of the technique to mitigate frequency selective fading since sub-band bandwidths may extend beyond the channel coherence bandwidth.

11.1.6 Single carrier modulation provides rapid sampling of the channel, however frequency selective fading will occur within the transmission bandwidth. For the modulation technique to be effective in high throughput underwater communications, techniques must be adopted to reduce the complexity of the equalisation task. Conventional equalisation schemes based either on zero forcing or MMSE optimisation criteria are suited to relatively benign acoustic channel conditions involving modest multipath spread. DFE structures provide some improvement, their ultimate performance is limited by the complexity and diversity of potential acoustic channel conditions.

11.1.7 Exploiting the spatial coherence properties of the acoustic field provides a means to relax the equalisation complexity. It has been shown for example that spatial temporal adaptive processing provides a means to effectively equalise non-minimum phase channels provided some angular diversity exists between path arrivals. In such cases the optimisation criteria is achieved by the structure adapting in a temporal and spatial sense. The exact solution so attained is strongly influenced by the spatial coherence properties of the incident field and the array geometry. For sensor separations up to lambda, the structure behaves much like a spatially coherent processor, capable of steering nulls in the direction of multipath arrivals to attain the MMSE operating criteria. For sensor separations exceeding lambda the structure behaves more like a spatial diversity combiner

which, with appropriate synchronisation at element level, can exploit path diversity in a wideband sense.

11.1.8 The results presented in this work have demonstrated the STAP-DFE structure with open and closed loop Doppler tracking, to be an effective means to combat a wide range of channel conditions. The adoption of relatively simple adaptive algorithms have enabled the techniques to be demonstrated in a real time system and the reliability of the techniques in terms of convergence and sensitivity to non minimum phase behaviour, have been improved using training data recycling and iterative forward and reverse decoding. Using these techniques data rates of up to 41kbps have been achieved and ranges of up to 3km in the MF band and 20km in the LF band using simple omindirectional projectors.

11.1.9 Achieving absolute repeatability and reliability in all potential acoustic environments remains a significant technical challenge. The complexity and diversity of acoustic channel behaviour are such that there is no single solution to the high data rate acoustic communications problem and the definition of high data rate ultimately rests with the complexity of the channel.

11.1.10 Field experience with the real time system has underlined the need for greater flexibility and automation in modulation mode and parameters. In the current system low data rate and high data rate modes are provided with a view to balancing the need for reliability with the need for high data rate communications. Whilst this technical solution has proved effective to demonstrate proof of concept, there are several areas in which the technology could be developed to improve reliability, flexibility and repeatability.

- Spread spectrum coding has been shown to be an effective means to combat the multipath problem. The adoption of a spread spectrum outer modulation layer

provides a means to improve noise performance, provide improved multi-user capability and increase the robustness of the system. The obvious price paid for these benefits is a reduction in the throughput of the system. This however is offset by the potential to provide a scalable data rate, wherein the data rate is tailored to the operating environment. Automating such a technique relies upon the effective assessment of the channel and optimisation of modulation parameters based on the coherence properties of the channel. The use of waveform coding with STAP processing potentially provides greater flexibility in the choice of operating data rate and system robustness.

- The results of this work have demonstrated that the STAP receiver can cope with a wide variety of channel behaviour by exploiting the temporal and spatial coherence characteristics of the received field. An obvious next step would be to investigate whether it is possible to reuse the adapted solution on transmit to exploit reciprocity in the channel. It has been shown that where angular diversity exists between paths the structure adapts to steer a null in the direction of the offending path arrival. On transmit using the time reversed, phase conjugated filter coefficients one essentially then beamsteers the transmission along the most favourable path or combination of paths. Such a technique has significant potential for increasing the reliability of the link under poor channel conditions and also providing spatial discrimination in multiuser environments.

- Ultra wideband, short-range acoustic links operating at several hundreds of kHz potentially afford much higher data throughputs due to the greater bandwidths achievable at higher frequencies. The key technical issues relating to such a link rest in a more thorough understanding of the signal coherence properties at such

frequencies. Such a link would be suited to data intensive applications including high fidelity video and imagery transfer between an AUV and host ship.

- Whilst this work has focussed primarily upon point to point data transfer applications, the issue of acoustically networking several users introduces genuinely new and technically challenging problems. In crowded acoustic environments, providing a reliable means for users to access and share the channel bandwidth whilst maximising data throughput and minimising latency represents a significant technical challenge. Conventional channel access schemes such as time and/or frequency multiplexing are subject to the extremely long latencies inherent in acoustic propagation. Code division multiplexing schemes are subject to the degradation in code orthogonality arising from the doubly spread nature of the acoustic environment. Spatial techniques are therefore likely to provide a key role in augmenting the performance of traditional multiplexing schemes. Optimising the physical layer modem technology and higher network layer technology for efficient, high throughput acoustic communications is an exciting and technically challenging avenue for future work.

11.1.11 In conclusion, this work has demonstrated several new techniques to provide high throughput point-to-point acoustic communications at data rates up to 41kbps and ranges of several tens of kilometres. The ultimate utility of any communication system however lies not in the rate at which data can be sent from point to point but the flexibility and reliability with which the data can be sent. This has been clearly demonstrated by the paradigm shift in terrestrial networking technology, where fixed infrastructures are giving way to more complex ad hoc networking infrastructures enabling users to enter and leave the network.

11.1.12 Translating such capabilities to the underwater acoustic environment represents a significant technological step. Acoustic networking infrastructures are currently in their infancy and there is, as yet, no technology capable of supporting multiple users at useful data rates and ranges. Achieving this vision will require continued research into understanding the acoustic environment, acoustic communications and networking technology.

12 REFERENCES

Acoustic Telemetry Reviews

1. Moore B.C.J., An introduction to the Psychology of Hearing, New York Academic Press, 1997
2. Evans B. G., Baughan K., Visions of 4G, IEE Electronics and Communications Engineering journal, Vol 12 Number 6, Dec 2000
3. Lau W.W., The Sonar of Dolphins, Springer-Verlag, New York, 1993
4. Space and Naval Warfare Systems Command, November 1992, Annex B, Submarine Communications shore infrastructure, http://www.fas.org/ma/dod-101/navy/docs/scmp/part06.htm
5. Urick R.J., Principles of Underwater Sound, McGraw-Hill, 3rd Ed, 1983,
6. Pierce A.D, Acoustics : An introduction to its Physical Principles and Applications, American Intitute of Physics , New York 1989
7. Jensen, F.B., Kuperman W. A., Porter M.B., Schmidt H., Computational Ocean Acoustics, AIP Series in Modern Acoustics and Signal Processing, 1994
8. Berktay H., Gazey B., Communications Aspects of Underwater Telemetry, Radio and Electronic Engineer, 33, 1967, pp295, May 1967
9. Quazi A., Knorad W., Underwater Acoustic Communications, IEEE Communications Magazine, 1982, Vol2, Part2, pp24-30
10. Baggeroer A.,Acoustic Telemetry - An overview, IEEE J.Oceanic Eng. Vol OE-09, No.4,1984
11. Catapovic J., Performance limitations in Underwater Acoustic Telemetry, IEEE J.Ocean Eng, Vol15, No. 3, July 1990.
12. Stojanovic M., Recent advances in High-Speed underwater acoustic communications, IEEE J.Ocean.Eng., Vol 21, No2, Apr 1996
13. McDonald J,., Performance Measurements of a diverse collection of Undersea Acoustic Communications Signals', Proc.Oceans 1999
14. Kilfoyle D.,'Research Directions in Underwater Acoustic Telemetry', Sea Technolgy, May 1999
15. Davies J.J, Pointer S.A., Wideband underwater communications techniques,

Proc IOA, Underwater communications and position fixing, University of Birmingham, December 1993.

16. Davies J.J., Pointer S.A, Dunn S.M., Wideband acoustic communications – Dispelling narrowband myths', Proc. IEEE/MTS Oceans2000, Rhode Island, USA, Sept 2000
17. **Nystuen**, 'Underwater ambient noise from rainfall', J.Acoust.Soc.Am, Vol.79, No.4,April 1986
18. **V.E.Otashev,'** Propagation of sound in a turbulent medium. I. Plane Waves',J,Acoust,Soc.Am 102(5),Pt 1, Nov.1997
19. Spindel R, Signal Processing in ocean tomography, Adaptive methods in underwater acoustics, 687-710,Urban H.G, 1985
20. Spiesberger J., Worcester P., Fluctuations of resolved multipaths at long range in the ocean, , J.Acoust Soc.Am, 70(2), Aug. 1981
21. Williams R., Battestin H., Coherent recombination of acoustic multipath signals propagated in the deep ocean, J. Acoust. Soc. Am,,Vol.60, No.1 , July 1976
22. Spiesberger J, Bushong P, Metzger K, Birdsall T.,Ocean Acoustic Tomography: Estimating the Acoustic Travel Time with Phase, J., IEEE Journal of Oceanic Eng. Vol. 14, No 1, Jan 1989
23. Jobst W., Dominijanni L., Measurements of the Temporal, Spatial and Frequency Stability of an underwater acoustic Channel, , J.Acoust Soc.Amer, 65(1) 1979
24. Veenkant R. , Investigation of the Propagation of a doubly Spread Underwater Acoustic Channel , Acoustics, Speech and signal processing, Vol ASSP25,No2, April 1977
25. Ewart T., Acoustic Fluctuations in the open ocean - A measurement using a fixed refracted path, J.Acoust. Soc. Am, Vol 60 No1, July 1976.
26. Birdsal T., Acoustic Telemetry For Ocean Acoustic Tomography, IEEE J.Ocean.Eng, Vol OE-9, No4, October 1984.
27. Coffey D., Paquette D, Accuracy of acoustic multipath timing and ranging predictions over extended ranges, Proc. Offshore Technology Conference, Houston TX, May19, 1985
28. Heard G., Schaumacher I., Time compression of M-sequence transmissions in a very long waveguide with a moving source and receiver, J.Acoust.Soc.Am, 99 (6), June 1996
29. Gerstoft P., Gingras D., Parameter estimation using multifrequency range-dependent acoustic data in shallow water, J. Acoust. Soc Am. 99(5), May 1996
30. Rouseff D., Porter R., Fox W., Acoustical characterisation of a shallow water environment from sparse data, Proc. Oceans'93, Vol. 1 pp71-75.
31. Franklin J., Barry P.,Underwater Acoustic Communication Channel Characterisation At Low Frequencies in Shallow Water, J., Proc. IOA Vol 15 Part 9,(1993)
32. Virovlyanski A., Saichev A, Slavinskii M, Spectrum of a signal received by a moving receiver in an underwater channel, Sov.Phys Acoust, 31(1), Jan-Feb 1985
33. Ali H., Oceanographic variability in shallow water acoustics and the dual role of the sea bottom, IEEE J. Ocean.Eng. Vol.18, No.1 Jan 1993
34. Ogilvy J.A., Wave scattering from rough surfaces, Rep. Prog. Phys. 50, 1553-

1608 (1987).

35. Robinson R., Chester J, Quazi A, Sensitivity of the Reverberation Spectrum to System and Environmental Parameters, NUSC Technical Document 7315, 1985

36. Rice J, Acoustic Signal Dispersion and Distortion by Shallow Undersea Transmission Channels, Proc. High Freq.Acoust in Shallow Water Conference, June1997

37. Owen R., An experimental study of rough surface scattering and its effects on communications coherence, IEEE Proc. Oceans 1994

38. Spindel R., Schultheiss P, Acoustic Surface Reflection Channel Characterisation through impulse response measurements, J.Acoust Soc.Am, Vol 51, Number 6, (Part 1), 1972.

39. Olson J., Nichols R., Correlation Measurements of Surface-reflected underwater acoustic signals at several sea states, J. Acoust Soc.Amer 71(6), June 1982

40. Boheme H.,Measurements of acoustic backscattering from very rough water surfaces, J.Acoust Soc.Am, 65(2), Feb 1979

41. Gulin E., Malyshev K, Amplitude and phase fluctuations of a sound wave reflected from a sinusoidal surface, Sov Phys. Acoust. Vol.8,No.3,July 1963

42. Gulin E., Malyshev K., Statistical Characteristics of sound signals reflected from the undulating sea surface, Sov. Phys.Acoustics, 1963, Vol 8, part 3, pp 228-234.

43. Gulin E., Amplitude and phase fluctuations of a sound wave reflected from a sinusoidal surface, Sov Phys Acoust, Vol8 No3, Jan 1963.

44. Gulin E., Malyshev K.,Experiments in the spatial correlation of the amplitude and phase fluctuations of acoustic signals reflected from a rough ocean surface, Sov Phys.Acoust, Vol 10, No.4, June 1965

45. Gulin E., Malyshev K., Some Results of an Investigation of the frequency correlation of the amplitude fluctuations in sound signals, Sov.Phys.Acoust, 1966, Vol12, Part1

46. Wilson M, Farwell R,Stanic S., Statistics of Shallow Water, High Frequency Acoustic Scattering and Propagation, Proc.IEEE Oceans'95, Victoria 1993, Vol2

47. Zheng M, Experimental study on Statistical characteristics of pulse transmissions in the shallow water, Proc. IOA, Dec 1993, Birmingham.

48. Hamilton, 'Geoacoustic modeling of the sea floor', J.Acoust Soc.Am, 68,1313-1340 , 1980

49. Jensen F,'Computational Ocean Acoustics', AIP Press, ISBN 1-56396-206-8, pp 42-54.

50. Ziomek L., Generalised Kirchoff Approach to the ocean surface scatter communication channel. Part 1: Transfer Function of the ocean surface., J.Acoust Soc.Am, 71(1), Jan 1982

51. Ziomek L., Generalised Kirchoff Approach to the ocean surface scatter communication channel. Part 2:Second Order Functions, J.Acoust Soc.Am, 71(6), June 1982.

52. Ventsanopolous A., Stochastic filter modelling for the sea surface scattering

channel, J.Acoust.Soc. Am., Vol.49,No.4 (pt1), 1971

53. McDonald J, Tuteur F., Moment characterisation of a doubly spread surface scattering channel, Proc. IEEE, Nov 1974

54. Mc Donald J., Tuteur F., Moment characterisation of a Doubly Spread Surface Scatter Channel at High Rayleigh Parameters, Proc IEEE, Nov 1974.

55. Venetsanopolous A., Modelling of the sea surface scattering channel and undersea communications, Comm. Sys. And Random Process Theory, ISBN 9028605681, pp 511-531, 1978

56. Acoustics, Propagation and Transducers, Post Experience course in underwater acoustics and sonar systems, School of Electronic and Electrical Eng., Volume 1, 1993

57. Kailath T., Measurements on time Variant Communication Channels, IRE Trans Infor.Theory,1962

58. Kailath T., Measurements on time Variant Communication Channels, IRE Trans Infor.Theory,1963

59. Kailath T., Measurements on time Variant Communication Channels, IRE Trans Infor.Theory,1962

60. Root W., On the measurement and use of time varying communication channels, ,Information and Control,1965

61. Bello P., Some techniques for the Instantaneous Real-Time measurement of Multipath and Doppler Spread, IEEE Trans on Commun vol(13) No3, Sept 1965

62. Spiliker J., On the characterisation and measurement of randomly varying filters, IEEE Trans.Circuit Theory, March 1965

63. Bello P., Time-Frequency Duality , IEEE Trans.Inform.Theory, Jan 1964

64. Middleton D. The underwater Medium as a generalised Communication Channel, Underwater Acoustics and Signal Processing, ISBN 9027712557, pp589-612

65. Gavin R., Coates R., Analysis of the performance of an underwater acoustic communications system and comparison with a stochastic model, IEEE Proc Oceans 1994

66. McCalla J., Baldwin K., James D., Blidberg D., Sivaprasad K., A ray tracing program for studying acoustic telemetry with AUV's, Proc. IEEE Oceans. 1992

67. Howse D., Zielenski A., Multipath Modelling For Acoustic Communication, Proc. Oceans 1982.

68. EsseBar A.,Underwater acoustic channel simulations for communications, IEEE Proc. Oceans 1994

69. Zielinski A, High Rate Shallow Water Acoustic Communication, IEEE Oceans'93, Victoria B.C,

70. Gerlach A., Acoustic Transfer Function of the Ocean For a Motional Source, IEEE trans. Acoust, Speech Sig Proc, Vol ASSP-26, No 6, December 1978

71. Estes L.,, Fain G.,, Carvalho D., A Shallow water Channel Characterisation for underwater acoustic Telemetry, Proc IEEE Oceans 93, Victoria , Vol1 pp 76-81

72. Adams S., Doubek J., Dispersive Properties of the Underwater Acoustic Channel, IEEE Int. Conf. Acoustics, Speech, Signal Proc., Philadelphia 1976, pp 664-667.

73. Morgera S., Digital filteriing and prediction for communications system time synchronisation ,IEE J.Oceanic Eng., Vol. OE-7, No.3, July 1982

74. Ludecke F., De-Dopplerisation of underwater acoustic data', J.Acoustic. Soc.Am, 92(5),Dec 1995

75. Solimon S., Synchronisation issues in ocean telemetry, IEEE J. Ocean Eng., Vol.16,No.1,Jan 1991

76. Sharif B., Neasham G., Hinton O., Adams A., Doppler compensation for underwater acoustic communications, Proc.Oceans 98

77. Iltis R., Joint estimation of PBN code delay and multipath using the extended Kalman filter, IEEE Trans. Comm,Vol. 38, No.10, Oct 1990

78. H.Van Trees ,Detection, Estimation and Modulation Theory, Part III, New York,Wiley,1971

79. Dooley S., Nandi A., Fast frequency estimation and tracking using Lagrange Interpolation, Electronic Letters, Oct 1998 Vol.34, No.20

80. Laasko T., Valimaki V., Karjalainen M., Laine U., Splitting the unit delay, IEEE Signal processing magazine Jan 1996

81. Hermanowicz E., Explicit formulae for weighing coefficients of maximally flat tuneable FIR delayers, Electronic Letters, Vol.28, No. 20, Sept 1992

82. Cain G., Evaluation of several variable FIR fractional sample delay filters, ICASSP'94, pp621-624

83. Glisson T., Sage S., On sonar signal analysis, IEEE. Trans. Aero.Elec.Sys., Vol.AES-6, No.1, Jan1970

84. S.Kramer,Statistical analysis of wideband pseudorandom matched filter sonars, IEEE. Trans.Aero.Sys., Vol.AES-5,No.2, Mar 1969

85. Mitchell R Rihaczek A,,*Matched filter response of the linear FM waveform*, IEEE Trans. Aero.Elec. Sys., Vol.AES-4, No.3, Jan 1968

86. Gaardner T., Signal design for fast fading Gaussian channels', IEEE Trans. Inf. Theory, Vol.IT-17,No.3, May 1971

87. S. Kramer, Doppler and acceleration tolerances of high gain , wideband linear FM correlation sonars, Proc. IEEE, Vol.55, No.5, 1967

88. Kobayashi H.,Simulataneous adaptive estimation and decision algorithm for carrier modulated transmission systems, IEEE Trans. Comm. Tech., Col.COM-19, No.13, June 1991

89. Ohkawa M., Orthogonal Multicarrier Frequency Hopping-Code Division Multiple Access Scheme for Frequency Selective Fading, Electronics and Communications in Japan, Part 1, Vol.78, No.8, 1995.

90. Le Floch B., Coded orthogonal frequency division multiplex, Proc.IEEE, Vol 83, No.6, June 1995

91. Zou W., Wu Y., COFDM: An overview, IEEE Trans. Broadcasting, Vol.41, No.1, March 1995

92. Wu Y.,Zou W., Orthogonal Frequency Division Multiplexing: A multicarrier modulation scheme, IEEE Trans. Consumer Electronics, Vol 41, No3,Aug 1995.

93. Coatelan S., Galvieux M, Design and Test of a coding OFDM system on the shallow water acoustic channel,, Proc Oceans 95, San Diego, October 1995

94. Bessios A., Fast Underwater Acoustic Data link design via multicarrier modulation and higher order statistics equalisation, , IEEE Journal Oceanic Eng,

95. Bessios A., Compound Compensation Strategies for Wireless Data Communications Over the Multimodal Acoustic Ocean Waveguide, , IEEE Journal Oceanic Eng, Vol 21, No2,1996
96. Proakis J.,' Adaptive equalisation techniques for acoustic telemetry channels', IEEEE J.Oceanic Eng., Vol.16, No.1, Jan 1991
97. Proakis J. G., Digital Communications, Third Edition, McGraw and Hill, ISBN 0-07-113814-5
98. Eleftheriou E., Falconer D., Tracking properties and steady state performance of RLS adaptive filter algorithms, IEEE Trans. ASSSP, Vol. ASSP-34, No.5 October 1986
99. Ariyavisitakul S., Decision Feedback Equaliser With Time Reversal Structure, IEEE J. Selected Areas In Communications Vol 10 No3 April 1992
100. Monsen P., MMSE equalisation of interference on fading diversity channels, IEEE Trans. Commun, Vol.Com-32,No1,Jan 1984.
101. Prasad S., Panthak S., On jointly adaptive decision feedback equalisation and carrier recovery, AEU, Vol.43,1989
102. Gitlin R., Weinstein B., Fractionally spaced equalisation : An improved digital transversal filter', The Bel System Technical Journal, Feb. 1981
103. Ungerboeck G. Fractional Tap-spacing equaliser and consequences for clock recovery in data modems, IEEE Trans. Comm., Vol. COM-24, No.8, Aug 1976
104. Brossier J., Jourdain G., Adaptive Equalisation and phase recovering application to underwater communications, IEEE Proc. Oceans 1993
105. Riter S., 'Design considerations for a pulse position modulation underwater Acoustic communications system', IEEE. Conf. Engineering in the Ocean Environment, Panama City Florida,1970.
106. Price R., Green R., A communication techiques for multipath channels', Proc. IRE,1958
107. Bitzer D., A rake system for tropospheric Scatter, EEE Trans. Ommun. Tech, Vol.COM-14, No.4, August 1966
108. Dillard R., Detectabilty of spread spectrum signals, IEEE Trans. Aero and Elect. Sys, Col.AES-15, No.4, Kuly 1979
109. Chandler E., Cooper G., Low probability of intercept performance for spread spectrum systems, IEEE J.Selected Areas in Communications, Vol.SAC-3,No.5,Sept 1985
110. Ayela G, Le Reste S., New innovative Multimodulation Acoustic Communication System, Proc Oceans 1994, Brest, France..
111. Ayela G., Le Reste S., A New Self Contained Multipath Protected Acoustic Transmission System for the offshore Environment, , Advances in Underwater Technology, Ocean Science and Offshore Engineering, Volume 16: Oceanology 1988
112. LeBlanc L., Beaujean M., Boubli C., Strutt.T., Chirp FSK modem for high reliability communication in Shallow water, Proc .Oceans 1998
113. Sozer e., Proakis J., Stojanovic M., Rice J., Benson A., Direct sequence spread spectrum based modem for underwater acoustic communciations and channel measurement,
114. Z.Zvonar,D.Brady,'Adaptive Multichannel Receiver for Fading CDMA Channels with Severe ISI', Proc IOA, 1993
115. M.Stojanovic,Z.Zvonar, 'Multichannel Processing of Broadband Multiuser Communication Signals in Shallow Water Acoustic Channels', IEEE J.Oceanic Eng.Vol.21, No.2, April 1996.

116. Kwon H., Birdsall T., Digital waveform codings for ocean acoustic telemetry, IEEE J.Oceanic Eng., Vol.16 Proc ICC,1991

117. Galvin R., Coates R.,'Analysis of the Performance of an Underwater Acoustic communications System and comparision with a stochastic Model', IEEE.Proc Oceans 1994

118. Catapovic J., Design and Performance Analysis of a Digital Acoustic Telemtry System for the Short Range Underwater Channel, IEEE J.Ocean.Eng., Vol OE-9,No 4,1984.

119. Freitag L., Catapovic J., A signal processing System for Underwater Acoustic ROV communication, Proc. 6th Int'l, Symp, Unmanned Untethered submersible tech, Baltimore,M.D, 1989

120. Eck C., Prota D., High Speed Digital Acoustic Telemtry System, Proc 4th Symp Unmanned, Untethered Submersible Tech (Durham) June 1987.

121. Chappel S., Acoustic Communication between two autonomous underwater vehicles, Proc 1994 Symph. AUV Technology, Cambridge MA,July 1994

122. Stojanovic M., Proakis J., Catapovic J., Analysis of the impact of Channel Estimation Errors on the performance of a Decision Feedback Equaliser in Fading Multipath Channels, IEEE Trans. Commun. Vol 43, No2, Feb 1995

123. D.Abrosimov, 'Vertical distribution of the sound intensity in an underwater sound channel', Sov.Phys.Acoust. 29(3), May 1983

124. Stojanovic M., Phase Coherent Digital Communications for Underwater Acoustic Channels, IEEE J. Ocean.Eng, Vol19,No1 Jan 1994

125. Jarvis S., Pendergrass N., Implementation of a Multichannel Decision Feedback Equaliser for shallow water acoustic telemtry using the stabilised fast transversal Filters Algorithm, IEEE. Proc Oceans 1993.

126. Stojanovic M., Performance of a highrate adaptive equalisation on a shallow water acoustic channel, J.Acoust Soc.Am, 100 (4) Pt1, Oct 1996

127. Stojanovic M., Proakis J., Catapovic J., Coherent communications over long range underwater acoustic telemetry channels, Acoustic Signal Processing for Ocean Exploration, Kluwer Academic Publishers,1993

128. Stojanovic M., Catapovic J, Proakis J., An algorithm for multichannel Coherent Digital communications over long range underwater acoustic telemetry channels, IEEE Proc Oceans 1992.

129. Henderson G., Investigation of adaptive Beamformer Performance and Experimental Verification of Applications in High Data Rate Digital Underwater Communications, Proc Oceans IEEE 94

130. Tarbit P., Development of a real time adaptive equaliser for a high rate underwater acoustic data communication link, et al, IEEE Proc Oceans1994

131. Kocic M., Brady D., Stojanovic M., Sparse Equalisation for Real Time Digital Underwater Acoustic Communications, Proc Oceans 95, San Diego,Oct1995

132. Feder M., Catapovic J., Algorithms for joint channel estimation and data recovery – Application to equalisation in underwater communications, IEEE J. Oceanic Eng., Vol.16,No.1,Jan 1991

133. Thompson D., Performance of coherent PSK receivers using adaptive combining, beamforming and equalisation in 50km underwater channels, IEEE Proc Oceans 1995

134. Howse G., Tarbit P., Hinton O., Sharif B., Adams A., Subsea acoustic remote

communications utilising an adaptive receiving beamformer and multipath suppresion, Proc Oceans 1994

135. Henderson G., Tweedy A., Howe G., Hinton O., Adams A., Investigation of adaptive beamformer performance and experimental verification of applications in high data rate digital underwater communications, IEEE proc. Oceans 1994

136. Stojanovic M., An algorithm for multichannel coherence digital communications over long range underwater acoustic telemetry channels, IEEE Proc. Ocenas 1990

137. Bragard P., Jourdain G., A fast self optimised LMS algorithm for non stationary identification. Application to underwater equalisation', IEEE Proc. Oceans 1990

138. Sandsmark G., Counteraction of multipath interference by a combination of Beamsteering and adaptive equalisation, Proc IOA, Vol.9, Pt.4, 1987

139. Davidson H., A reliable underwater acoustic data link employing an adaptive receiving array, Proc. IOA, Vol.9,Pt.4,1987

140. Hinto O., Performance of a stochastic gradient adaptive beamformer for subsea acoustic communications, Proc.Eusipco-94, Edinburgh, Sept 1994.

141. Stojanovic M., Freitag L., Johnson M, Channel estimation-based adaptive equalisation of underwater acoustic signals, Proc. Oceans 98

142. Performance of coherent PSK receivers using adaptive combining and beamforming for long range acoustic telemetry, 3rd European Conf. Underwater Acoustics, Heraklion, Crete June 1996.

143. Bragard P., A fast self optimised LMS algorithm for non-stationary identification. Application to underwater equalisation, IEEE Proc Oceans 1990.

144. Goalic A., Toward a Digital Acoustic Underwater Phone, IEEE Proc. Oceans 1994.

145. Barroso V., Belo C., A Model Based Equalisation Structure for Underwater Communications, Acoustic Sig.Proc for Ocean Exploration, 1993, pp601-606

146. Caimi F., Hassan G., Results of an alternative approach to channel equalisation using a pattern classification strategy, Proc. Oceans 98

147. Kennedy, 'Fading Dispersive Communication Channels', Chapter 2.

148. Paula, R.F., S.O. Rice and J.H Roberts,'Distribution of the phase angle between Two vectors Perturbed by Random noise',IEEE Transactions on communications vol COM-20, no.8, August 1982, pp1828-41..

149. Kema V., Laub A., The singular value decomposition, its computation and some applications. IEEE Trans. Automatic Control Vol. AC-25 ,No.2 April 1980

150. Slock D., Kailath T., Numerically stable fast transversal filters for recursive least squares adaptive filtering, IEEE Trans. Signal Proc., Vol.39, No.1, Jan 1991

151. Slock D, Chisci L.,Lev-Ari H., Kailath T., Modular and numerically stable fast transversal filters for multichannel and multiexperiment RLS, IEEE. Trans. Sig.Proc., Vol.40, No.4, April 1992

152. Cain J., 'Evaluation of several Variable FIR Fractional –sample delay filters, ICASSP'94,October 1994,pp 621-624

153. Haykin S., Digital Communication Techniques Signal Design and Detecton', Chapter 9

154. Kwon H., Birdsall T.,Channel Capacity in Bits Per Joule, IEEE J. Oceanic Eng., Vol. OE-11, No. 1 Jan 1986

155. Green M., Error correction coding for communication in adverse underwater

channels, IEE Proc. Ocenas 1997
156. Haykin S., Adaptive Filter Theory, ISBN 0-13-397985-7,Chapter 13
157. Collins, T., Atkins, P., Davies, J., Dunn,S., Robust video coding for underwater transmission, IS&T/SPIE Conf. Electronic Imaging, San Jose, CA, 20-26th Jan., 2001,4310,pp893-899
158. Davies J., Dunn S., High Data Rate Acoustic Communications Progress Report Year 1, DERA/S&P/UWS/CR980075/1.0, October 1998

13 Abbreviations

ACN	Acoustic Communications Node
AUV	Autonomous Underwater Vehicle
BER	Bit error rate
CATS	Continuous added training sequence
CLDL	Close loop Doppler compensation
DFE	Decision Feedback Equaliser
DLL	Delay Locked Loop
FEC	Forward Error Correction Coding
FFT	Fast Fourier Transform
HiDRAM	High Data Rate Acoustic Modem
ISI	Inter Symbol Interference
Kbps	Thousand bits per second
Ksps	Thousand samples per second
KHz	Signal Frequency in thousand cycles per second
LFM	Linear Frequency Modulation
MCM	Multicarrier Modulation
MSE	Magnitude squared error
OLDC	Open loop Doppler compensation
PLL	Phase Locked Loop
QPSK	Quadrature Phase Shift Keying
RDS	Rapidly Deployable Systems
ROV	Remote Operated Vehicle
SCM	Single Carrier Modulation
STAP	Spatial – Temporal adaptive processing
TD	Technical Demonstrator

A Channel Characterisation

A.1 Understanding Channel Behaviour

13.1.1 Channel characterisation provides a means to provide a quantitative basis for the assessment of the complexity of a channel as a communications medium. The time varying characteristics of many physical channels invariably raises a number of questions; 'how complex is the channel?', ' is channel A more complex channel than complex B ?','how can one optimise a signal design for a particular channel?'. Such considerations are particularly pressing in the underwater acoustic channel due to the degree and extent of the temporal and spatial variability, which is unlike any terrestrial channel. The measurement of channel characteristics, the interpretation of such characteristics and the development of a quantitative basis for signal design and modulation methodology are therefore important issues relevant to the underwater acoustic communications problem. These issues are now discussed.

A.2 Historical Perspective

A.2.1 Fundamental research into channel identification and characterisation was largely addressed in the 1950's and 1960's, albeit for RF channels, by researchers such as Kennedy, Bello, Spiliker, Root ,Price, Woodward, Turin and Kailath who conducted the pioneering research into time varying communications channels, techniques for measuring such channels and signal design techniques to mitigate their effects

A.2.2 One of the earlier investigators into randomly time varying multipath channels was Kailath [57] who sought a statistical analysis for such channels. The analysis focused on statistical models for the random scatter channel in the presence of additive noise for both phase coherent and incoherent systems. The analysis led to the well known Rayleigh distribution for path magnitude and uniform distribution for path phase. In practice the

usefulness of the Rayleigh model in fitting real observed data is limited as it is defined purely in terms of a single parameter. In many cases additional flexibility in defining the influence of real physical channels is desirable and so many other statistical models for signal fading statistics have been developed such as the Nakagami-m, Rician and log-normal based statistical models. Such models are now prevalent in RF channel modelling [97].

A.2.3 For engineers interested in the physical world, statistical modelling of a communications channel, whilst fine for simulation, relays little information as to the underlying physical mechanisms influencing channel behaviour. So whilst fading statistics of (narrowband) communications waveform envelope and its phase are of interest for system performance studies, often one is more interested in the statistics of the physical mechanisms within the medium itself which serve to distort the signal. This obviously raises the question of how one measures and quantifies these distortions. This question was largely tackled in the 1960's where the problems of actual measurement of time varying channels [57-63], characterising channels [63] and signal design for reliable communications over such channels [147] were addressed albeit for the narrowband RF terrestrial channel.

A.2.4 Kailath [59] presents an excellent paper on the measurement of time-variant communication channels and the problems of unambiguous resolution of the spreading characteristi0cs of the channel when the channel is overspread. The approach assumes linear systems identification theory and the analysis centres on first and second order statistical properties of the channel filter which models the temporal dispersion of the channel as a tapped delay line; a recurrent structure in time varying channel modelling.

A.2.5 Kailaith considers the auto and cross correlation between taps in the channel filter. Autocorrelation of the tap A_λ (t) at a delay t

$$R(\lambda,t,t+v) = \overline{A_\lambda(t)A_\lambda(t+v)} \qquad \textit{Eqn 22}$$

A.2.6 Cross correlation between taps at delays λ and λ'

$$R(\lambda,\lambda',t+v) = A_\lambda(t)A_{\lambda'}(t+v) \qquad \textit{Eqn 23}$$

A.2.7 The author assumes widesense stationarity (WSS) in the tap statistics, which are both individually and jointly stationary. The problem of identifying the filter parameters is considered. Kailath correctly notes that the correlation of the input signal with the output signal requires time averaging and yet the filter is itself time varying. This highlights the requirement for the channel Doppler spreading – time spreading product to be less than unity for unambiguous channel measurement.

A.2.8 An interesting technique credited to Green and Price [106] for the measurement of underspread channels considers the use of signals who's ambiguity function is localised within the Doppler and temporal spread of the channel.

A.2.9 The output power of a matched filter detector as a function of delay and Doppler frequency translation can be shown to involve the two dimensional convolution of the channel scattering function with the transmitted waveforms ambiguity function:-

$$P(\lambda',f') = \int_{\infty}\int \psi^2{}_x(\lambda'-\lambda,f'-f)S(\lambda,f)d\lambda df$$

where

$S(\lambda,f)$ = *channel Scattering function*

$\psi^2{}_x(\lambda,f)$ = *ambiguity function* $x(t)$ *the sounding waveform* *Eqn 24*

$$\psi^2{}_x(\lambda,f) = \left|\int_{-\infty}^{\infty} x(t)x^*(t+\lambda)\exp(j2\pi ft)dt\right|^2$$

A.2.10 Thus if the signal waveform is designed to be sharply peaked with its energy contained within the Doppler spread and time spread of the channel, $P(\lambda',f')$ will approximate $S(\lambda',f')$. This technique is of particular interest to the underwater acoustic communications problem since waveform ambiguity analysis is conducted as a function of temporal scaling rather than frequency translation for wideband signal designs. This means that channel scattering characteristics may be approximated by ambiguity analysis of the received signal provided the transmitted signal ambiguity function is suitably localised in time-Doppler. The requirement for unity spreading product remains. The design of channel characterisation signals and the role of waveform ambiguity and channel scattering functions in acoustic communications system design will be developed later.

A.2.11 Spiliker [62] considered the characterisation and measurement of randomly varying filters for the discrete case. This enables the channel transfer function to be modelled in terms of a random transfer matrix comprising a mean transfer matrix and a covariance transfer matrix. The advantage of this form is that both filters can be measured regardless of channel spreading product. Root [60] presents a comprehensive review of the time varying channel problem with emphasis on mathematical formulation rather than engineering application.

A.2.12 Fading dispersive communications channels is the subject of a classic text by Kennedy [147]. It is instructive to consider this text in the context of the acoustic communications channel as the approach serves to underline the significant differences in the channel and its characterisation.

A.2.13 Kennedy initially considers a point scatterer description of the channel whereby propagation occurs via single scattering from a large number of independent scatterers. For this model the contribution of a single i'th scatterer is given by:-

$$y_i(t) = A\rho \,\mathrm{Re}[u(t-\tau_i-\dot{\tau}_1 t)\exp j\omega_0(t-\tau_i-\dot{\tau}_1 t)] \qquad \textit{Eqn 25}$$

A.2.14 Kennedy argues that the variation of $\dot{\tau}_i$ over the time interval of interest can be ignored since it is supposed that the variation in $\dot{\tau}_i t$ is much less than the reciproacl of the bandwidth of *u(t)*. This is a reasonable assumption for terrestrial RF systems since the spatial scales of the transmitted waveform *u(t)* will typically be measured in kilometres and the influence of delay fluctuations due to either platform dynamics and or propagation speed fluctuations limited to typically metric scales.

A.2.15 Kennedy argues that for typical narrowband applications typical of RF systems the variation delay presented by $\dot{\tau}_i t$ whilst not significantly influencing u(t-$\dot{\tau}_i$) does significantly influence the exponent $\exp jw_0(t-\tau_i-\dot{\tau}_i t)$. This assumption forms the basis of most of the text and most of the work on channel characterisation research in the 1960's. Such assumptions are, however not always valid for the underwater acoustic channel since such systems are normally broadband with transmission bandwidths often comparable to carrier frequency.

A.2.16 The narrowband assumption is also used for the delay line model often used for channel modelling. Specifically the channel is modelled as

$$y(t) = \mathrm{Re}[\sum_{i}^{k} m_i(t)u(t-\Delta_i)\exp j\omega_0(t-\Delta_i)] \qquad \textit{Eqn 26}$$

A.2.17 where $m_i(t)$ are complex tap gain functions often assumed stationary and Gaussian in nature. The applicability of this model to simulate acoustic channel behaviour is limited

by the wideband nature of acoustic communications systems and the temporal scaling influence of acoustic Doppler.

A.3 Channel Characterisation Functions

A.3.1 The gross characterisation of linear, time varying, space varying communication channels is frequently considered in four domains [97] the base of which is the time variant, space variant random impulse response of the channel.

A.3.2 Time-frequency channel characterisation, or more specifically time-Doppler channel characterisation is particularly useful for underwater acoustic channels since platform velocities are typically only two to three orders of magnitude less than the sound propagation speed. This leads to significant temporal scaling of received waveforms for modest platform velocities. In terms of the channel time varying impulse response this results in not only tap phase rotation typical of the RF case but also tap 'slippage'.

A.3.3 Such considerations invariably impact upon much of the underlying theory of channel characterisation which was originally developed for radio frequency (RF) communications channels and interpreting these results for acoustic channel behaviour must be tempered with caution. Specifically, channel time coherence, which is derived from the channel spreading function, is based primarily on narrowband phase fluctuations of multipath components for RF systems. In the acoustic wideband case, it is more appropriate to consider delay fluctuations since it is usual for the ratio of carrier frequency to bandwidth to be less than 2-5 for a high rate medium range acoustic communications system.

A.3.4 Ziomek [159] derives the time varying, space varying channel impulse response denoted $h(\tau_d,\mathbf{Z}_o;t,\mathbf{Z}_r)$ can be considered as the channel impulse response h(t) due to a unit impulse

at time $t-\tau_d$ transmitted at space vector $\mathbf{Z_o}(x,y,z)$ and observed at space vector $\mathbf{Z_r}$ τ_d seconds later.

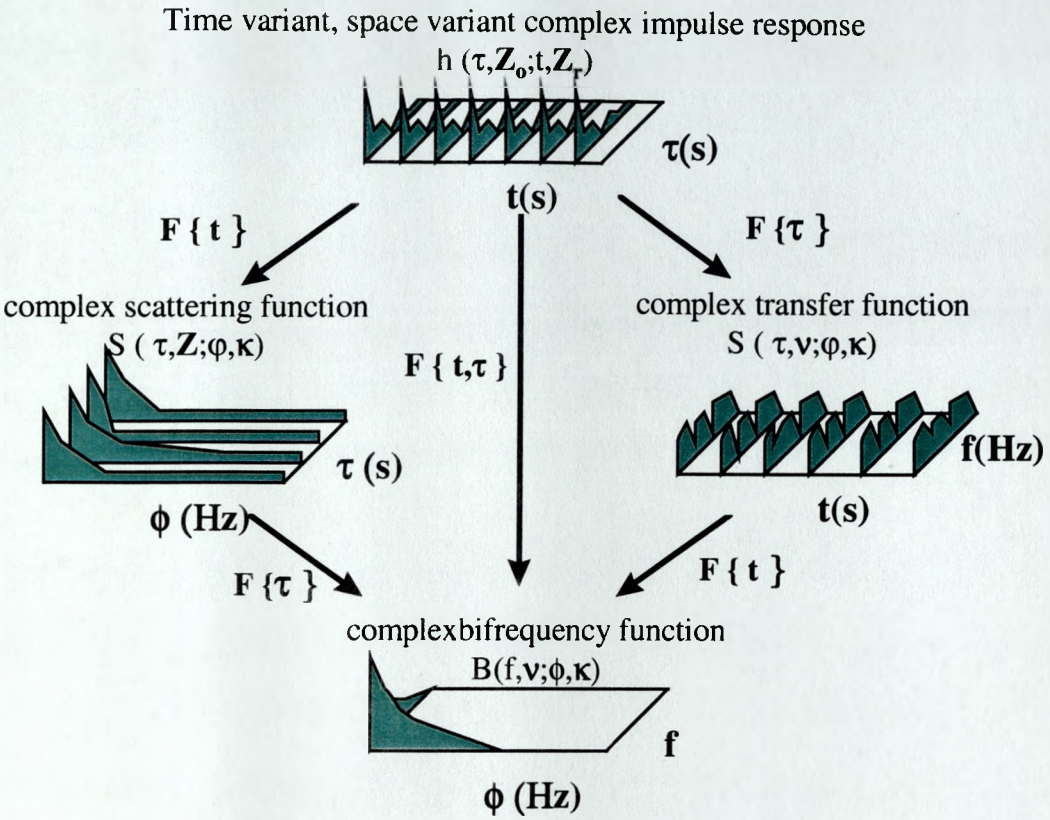

Figure 65; Channel Characterisation Functions and interrelationships

A.3.5 The Fourier transform of $h(\tau_d,\mathbf{Z_o};t,\mathbf{Z_r})$ with respect to τ_d gives the time varying, space varying channel transfer function $H(f, \boldsymbol{\nu};t,\mathbf{Z})$ where $\boldsymbol{\nu}$ denotes a spatial frequency vector. The Fourier transform $h(\tau_d,\mathbf{Z_o};t,\mathbf{Z_r})$ with respect to t gives the spreading function $S(\tau_d,\mathbf{Z}; \varphi, \boldsymbol{\kappa})$, where φ is Doppler shift in Hertz and $\boldsymbol{\kappa}$ is a spatial frequency vector. The relationship between each of the channel characterisation functions is shown in Figure 65.

A.3.6 The observed Doppler will be spatially dependent and this is reflected by the $\boldsymbol{\kappa}$ spatial frequency vector. Channel path length fluctuations arising through platform motion, boundary temporal (surface waves) and spatial variability and microscale variation of the ocean sound velocity profile, serves to 'blur' the channel tap phasor rotation and

amplitude such that the Fourier transform results in Doppler spreading in the φ axis. The spreading arises due to the combined effects of the amplitude and phase modulation processes. As stressed earlier, the effect is compounded by temporal scaling effects arising from acoustic Doppler. This means that the acoustic channel impulse 'taps' not only rotate but also time translate.

A.3.7 For a narrowband transmission, sinusoidal phase modulation transfers signal energy to sideband components which are Bessel distributed. The amplitude modulation gives rise to upper and lower sideband components the bandwidth of which are determined by the low pass nature of the random amplitude process.

A.3.8 Since all the foregoing channel characterisation functions are stochastic, it is more appropriate to consider each statistically as second order (power/energy) functions; specifically autocorrelation functions. Considering the time variant channel transfer function H(f,t) (ignoring spatial dependence for the time being), the two frequency mutual coherence function can be defined:

$$R_H(f_1,f_2,t_1,t_2) \equiv E\{H(f_1,t_1).H^*(f_2,t_2)\} \qquad \textit{Eqn 27}$$

A.3.9 E{} denotes expectation, and * complex conjugation. The two frequency mutual coherence function is therefore the two dimensional autocorrelation of the channel transfer function. This function is extremely useful for communications system signal design since it can be used to define the channel coherence bandwidth and coherence time: parameters fundamental to the choice of modulation scheme and symbol rate. One must however exercise care in the use of lumped channel characterisation parameters such as time coherence and frequency coherence since they convey little in terms of the fundamental channel physics. For discretely spread channels typified by macropath structure of shallow water acoustic channels it is appropriate to weight the coherence

measurements in accordance with ray energies. Further, due to the nature of acoustic Doppler one could argue that channel time coherence measurements should relate to specific ray arrivals rather than ensemble channel statistics. This point was raised in number of the tomographic papers discussed earlier where the distinction was made between the frequency coherence characteristics of forward scattered micropaths and the frequency coherence characteristics of macropaths.

B Models For Fading Dispersive Channels

B.1 Acoustic Channel Modelling vs RF channel modelling

B.1.1 RF channel modelling has underpinned the explosion in personal mobile communications and has provided a quantitative basis for the performance assessment of many communication systems. Perhaps the most fundamental factor which undermines the suitability of established RF models to the acoustic modelling problem, is the vastly different propagation speeds of the two wave types which result spatial scales differing by some five orders of magnitude . The impact of this on established fading dispersive channel models is discussed.

B.2 Point Scatterer Model Vs Delay Line Model

B.2.1 An established model for fading dispersive channels is based on the point scatterer model described by Kennedy [147]. In this approach a statistical model is assumed for the distribution of the phase and the statistical properties of the scatterer cross section. Specifically it is assumed that the scatterers are uncorrelated and independent such that the received process is Gaussian and as such completely characterised by the mean and correlation of the received waveform *y(t)*.

B.2.2 Alternative models are based on the delay line model of the form

$$y(t) = \sum_{i}^{k} m_i(t) u(t - \Delta_i) \exp j\omega_0 (t - \Delta_i) \qquad \textit{Eqn 28}$$

where $m_i(t)$ are complex tap gain functions and Δ_i are the delays corresponding to each tap. Such models are more general than the point scatterer approach, however it can be shown [147] that under certain assumptions the scatter model is actually equivalent to the delay line model. Specifically it is often assumed that the tap gain functions are uncorrelated Gaussian random possessing the same correlation function. In the point

scatterer model the received waveform is assumed the summation of multiple scatterers and the contribution of the I'th scatterer is a delayed and attenuated replica of the transmitted waveform defined as

$$s(t) = \mathrm{Re}[u(t)\exp(j\omega_0 t] \qquad \textit{Eqn 29}$$

where $u(t)$ is the complex envelope of $s(t)$ *and* ω_0 is the carrier frequency. In the point scatterer model each scatterer is characterised by its reflection energy cross section ρ_i^2 and by its propagation time delay $T_I(t)$. It is also assumed that the scatterer delays are linear functions of time i.e.

$$T_i(t) = \tau_i + \dot{\tau}_i t \qquad \textit{Eqn 30}$$

and that the variation of the delay over the observation interval is insignificant. This is equivalent to assuming that the symbolling rate is sufficiently rapid that delay change over each symbol snapshot is negligible. For the high data rate telemetry application this assumption is reasonable since the time scales of ocean delay fluctuations are rarely greater than a few fractions of a second (ref. Section 2-3).

B.2.3 A further assumption which is perhaps less applicable to the acoustic communications case is that the transmission bandwidth is very much less than the carrier frequency. This assumption implies that fluctuations of the scatterer delay term have no significant influence on the value $u(t-\tau_i)$ however they do significantly influence the received signal by virtue of the phase component $expj\omega_d(t-\tau_i)$. In an RF communication system this assumption effectively assumes that each symbol has a large number of carrier cycles. So small delays (a fraction of the symbol duration) between scatters result in constructive or destructive interference over the symbol duration.

B.2.4 The I'th scatter contribution in the received waveform is then

$$y_i(t) = A\rho_i \,\mathrm{Re}[u(t-\tau_i-\tau_i t)\exp(j\omega_0(t-\tau_i-\tau_i t) \qquad \textit{Eqn 31}$$

where A is an energy scaling constant introduced to ensure that the complex envelope energy scales to unit norm i.e.

$$\int |u(t)|^2 \, dt = 1 \qquad \textit{Eqn 32}$$

B.2.5 Assuming negligible variation of the delay over the symbol period and the narrowband approximation where the delay is assumed to comprise a bulk delay term plus delay perturbations expressed in terms of carrier phase i.e.

$$\tau_i = r_i + \frac{\theta_i}{\omega_0} \qquad \textit{Eqn 33}$$

B.2.6 The I'th scatter contribution in the received waveform can be expressed as

$$y_i(t) = A\mathrm{Re}[\textstyle\sum_i \rho_i u(t-r_i)\exp(j(\omega_0-\omega_i)t-\omega_0 r_i-\theta_i)]$$

where *Eqn 34*

$$\omega_i = \dot{\tau}_i\omega_0$$

B.2.7 The received signal comprises the sum all scatterer contributions

$$y(t) = A\,\mathrm{Re}\{\sum_i \rho_i u(t-r_i)\exp j([(\omega_0-\omega_i)t-\omega_0 r_i-\theta_i]\} \qquad \textit{Eqn 35}$$

B.2.8 Under the assumption that each scatterer delay and cross section are uncorrelated the received process is assumed zero mean Gaussian and characterised by the two dimensional correlation function of *y(t)*

$$R_y(t,\tau) = E[y(t)y(\tau)] = \mathrm{Re}[\sum_i \frac{A^2}{2}\overline{\rho_i^2}u(t-r_i)u^*(\tau-r_i)\exp j(\omega_0-\omega_i)(t-\tau)] \qquad \textit{Eqn 36}$$

B.2.9 Also, assuming the summation is performed over all scatterers at range $r_l=r$ and $\omega_l=2\pi f$, then the scatter weighting term $\sum_i \overline{\rho_i^2}$ can be replaced by the more useful average scatter cross section $\tilde{\sigma}(r,f)$ which introduces channel scattering as a function of range and frequency.

B.2.10 In practice however $\tilde{\sigma}(r,f)$ does not behave like a point function. Moreover channel scattering behaves more like a continuum and so it is more appropriate to replace the summation of equation 36 by an integration weighted by $\tilde{\sigma}(r,f)$ which behaves as a density function. i.e

$$R_y(t,\tau) = \mathrm{Re}[\frac{A^2}{2}\iint \tilde{\sigma}(r,f)u(t-r)u^*(\tau-r)\exp(j(\omega_0-\omega)(t-\tau)drdf] \quad \textit{Eqn 37}$$

B.2.11 The formal definition of $\tilde{\sigma}(r,f)$ as a channel scattering function requires that it be normalised

$$\sigma(r,f) = \frac{\tilde{\sigma}(r,f)}{\iint \tilde{\sigma}(r,f)drdf} \quad \textit{Eqn 38}$$

B.2.12 Assuming *u(t)* is normalised to unit norm through the scaling constant A, the received energy can be formulated directly in terms of the channel scattering function thus

$$E_r = \int \overline{y(t)}^2 dt = \frac{A^2}{2}\iint \sigma(r,f)drdf \quad \textit{Eqn 39}$$

B.2.13 This also enables the correlation function of the received signal to be formulated in terms of its complex envelope $y(t) = \sqrt{2E_r}\,\mathrm{Re}[z(t)\exp(j\omega_0 t]$ thus:-

$$R_y(t,\tau) = \mathrm{Re}[E_r R(t,\tau)\exp j\omega_0(t-\tau)]$$

where

$$R(t,\tau) = \iint \sigma(r,f)u(t-r)u^*(\tau-r)\exp j\omega(\tau-t)drdf = \overline{z(t)z^*(\tau)} \qquad \textit{Eqn 40}$$

B.2.14 $R_y(t,\tau)$ therefore completely characterises the zero mean Gaussian channel scatter process under the assumptions made above. In practice one is concerned with the influence of the channel scattering function on receiver performance as a function of waveform design since it is intuitively obvious that the time-frequency (and spatial) characteristics of the waveform intimately relate to the channel scattering function.

B.2.15 An alternative interpretation, which underlines the clear demarcation between RF and acoustic systems with respect to the point scatter model, is to consider spatial scales of the RF and acoustic waveforms and how these relate to spatial and temporal scales of scatter motion. Consider comparable temporal scales of the signalling waveform in each case, say a 10ksym/s phase modulated carrier and comparable temporal and spatial scales of scatterer motion, say 15cm movement over 1s.

B.2.16 In the acoustic case each symbol has a spatial scale of 1500/1e4=15cm and in the RF case each symbol has a spatial scale of 3e8/1e4 = 30km. Therefore over a 1 second interval (10,000symbols) the movement of the scatterer results in a complete symbol slip in the acoustic case and 0.000005 of a symbol in the RF case. In terms of carrier phase, the spatial scales of the acoustic carrier between 10-50kHz are comparable to the spatial scales of RF carrier at GHz. Thus whilst carrier phase is effectively decoupled from symbol timing for RF systems this is not so for the acoustic case and it is perfectly valid, for example to exploit phase information to effect symbol timing adjustments for example

C Acoustic Channel Modelling

C.1 Ray Models : Literature Overview

C.1.1 There are many papers in the open literature which consider modelling the underwater acoustic channel using ray trace techniques. In this section, several of these models are reviewed and compared. Adams and Doubek [72] consider a model where each path delay is assumed to comprise a bulk delay term T_0 and an additive random component e_n drawn from a uniformly distributed path length. The path delay model assumes a very simple structure where each ray is separated from its nearest neighbour by T_s/N where T_s denotes the channel time spread and N denotes the number of rays. Based on the assumption e_n are a set of statistically independent, identically distributed random variables, the authors derive generalised expressions for the mean, variance and cross covariance of the complex channel transfer function in terms of the probability density function of e_n. The derivation assumes the previous very simple path delay model. For a uniformly distributed path delay :-

$$\begin{aligned} p(e_n) &= \frac{1}{2e}, && |e_n| < e, \\ &= 0 && otherwise \end{aligned} \qquad Eqn\ 41$$

C.1.2 The author derives the following expressions for the channel transfer function:-

$$E\{H_N(\omega)\} = \sqrt{N}\exp(-j\omega T_0)\,sinc(\omega e)\frac{\sin(\frac{\omega T_s}{2})}{N\sin(\frac{\omega T_s}{2N})}, \qquad (mean) \qquad Eqn\ 42$$

$$V_N(\omega) = E\{H_N(\omega)H_N^*(\omega)\} - E\{H_N(\omega)\}.E\{H_N^*(\omega)\} = 1 - sinc^2(\omega e) \qquad (variance) \qquad Eqn\ 43$$

$$V_N(\omega_1,\omega_2) = \frac{E\{H_N(\omega_1)H_N^*(\omega_2)\} - E\{H_N(\omega_1)\}.E\{H_N^*(\omega_2)\}}{\sqrt{V_N(\omega_1)}\sqrt{V_N(\omega_2)}}$$

$$= exp(-j(\omega_1-\omega_2)T_0)\left[\frac{\sin(\omega_1-\omega_2)\frac{T_s}{2}}{N\sin\frac{(\omega_1-\omega_2)\frac{T_s}{2}}{2N}}\right]\left[\frac{\sin c((\omega_1-\omega_2)e)-\sin c(\omega_2 e)}{\sqrt{(1-\sin c^2(\omega_1 e))}\sqrt{(1-\sin c^2(\omega_2 e))}}\right]$$

(*Normalised Cross Co* var*iance*)
Eqn 44

C.1.3 Interpretation of this result is facilitated by considering the influence of the *sinc*(ω*e*)term which acts as a weighting term with nulls every 100π on the ωT_s axis. This term encompasses the influence of the random delay variation e on the mean transfer function. As the path length deviation increases relative to the channel delay spread, then the first null position will occur at lower frequency. As e tends to zero then the *sinc*(ω*e*) term tends to unity. The remaining terms result in interference fringes akin to due to the simple equ-ispaced path model adopted by the authors. As the number of paths is increased then the mean channel transfer function will be maximum for those frequencies of periods equal to an integer multiple of the path separation.

C.1.4 The uniform path separation model adopted by the authors results in well defined ridges in the mean transfer function. As the number of paths increases, the relative spacing reduces resulting in an increases between the frequency spacing of the peak transfer responses. The authors note that the cross coherence function when evaluated for a two path channel and small delay fluctuations results in significant coherence beyond the first null. They argue therefore that the coherence bandwidth does not always provide an accurate characterisation of the channel. This is an important result since it emphasises the role of channel time selectivity in determining channel frequency selective behaviour

and underlines the highly coupled time-frequency duality inherent in underwater acoustics.

C.1.5 Geralch [70] considers modelling ocean transfer function for a motional source based on discrete multipath structure predicted from ray tracing. The author argues that each ray can be modelled the cascade of a minimum phase system with an all pass system. The latter representing the bulk time delay and the former representing amplitude and delay variability. The simple model adopted assumes an iso-speed channel with ideal boundaries. Based on this simple model the ray path is given by:-

$$L_n(R,z) = \sqrt{\{[nD \pm (K_n - z)]^2 + R^2\}} = R / \cos\varphi_n$$

and

$$|\varphi_n| = \tan^{-1}\left(\frac{nD \pm (K_n - z)}{R}\right)$$

where

$L_n(R,z)$	$= Ray\ PathLength$		
R	$= Transmitter - receiver\ horizontal\ range$		
z	$= Transmitter\ depth$		
n	$= total\ number\ of\ boundary\ \text{int}eractions$		
D	$= water\ depth$		
d	$= receiver\ depth$		
φ_n	$= ray\ launch\ angle\ from horizontal$		
K_n	$= d$	$(n\ even)$	
	$= D - d$	$(n\ odd)$	*Eqn 45*

C.1.6 For a motional source the rate of change in path delay τ is given by:

$$\frac{d\tau}{dt} = \dot{\tau} = \frac{1}{c(R,z;t)}(\dot{R}\cos\varphi_n + \dot{z}\sin\varphi_n) \qquad \textit{Eqn 46}$$

C.1.7 Considering Gaussian random perturbations on the speed (v) and heading (Ψ) of the source relative to the receiver:-

$$v = v_0 + \sigma_v \xi_1$$
$$\Psi = \Psi_0 + \sigma_\psi \xi_2$$

where

Eqn 47

$\xi_{1,2}$ = *random Gaussian variables of unity variance*
v_0 = *mean speed*
ψ_0 = *mean heading*

C.1.8 The author derives the following approximate expressions for the rate of change of delay:-

$$\frac{d\tau}{dt} = k_0^{-1} - 1 - \varepsilon\xi$$

where

$$k_0 = \left(1 - \frac{v_o}{c}\cos\psi_0 \cos\varphi\right)^{-1} \qquad \textit{Eqn 48}$$
$$\varepsilon = \frac{\tilde{\sigma}_v}{c}\cos\varphi$$
$$\tilde{\sigma}_v = \sqrt{(\sigma_v \cos\psi_0)^2 + (v_0\sigma_\psi \sin\psi_0)^2}$$
$$\xi = \frac{1}{\tilde{\sigma}_v}\left[(\sigma_v \cos\psi_0)\xi_1 - (v_0\sigma_\psi \sin\psi_0)\xi_2\right]$$

C.1.9 The lumped parameter ξ represents all systematic error sources. k_0 represents the temporal scaling due to the resolved Doppler velocity. ε is a constant representing the standard deviation of the delay rate fluctuations.

C.1.10 Ray propagation time τ is obtained from the integral of $\frac{d\tau}{dt}$:-

$$\tau(x) = \tau_0 + (k_0^{-1} - 1)x - \varepsilon \int_0^x \xi dt$$

$$\tau(x) = \tau_0 + (k^{-1} - 1)x$$

where

$$k^{-1}(x) = k_0^{-1} - \frac{\varepsilon}{x} \int_0^x \xi dt$$

Eqn 49

C.1.11 The path delay time therefore consists of a bulk delay term τ_0 and a stochastic term k^{-1} which comprises a mean temporal scaling factor k_0 attributable to platform movement and the time delay fluctuation term fluctuation term ξ.

C.1.12 In terms of communications system design, the unknown time delay time τ_0 must be estimated (initial open loop synchronisation/acquisition) and the temporal fluctuations must be compensated for (closed loop tracking). For communications performance under time selective channel conditions, statistically characterising such fluctuations is obviously of interest.

C.1.13 Gerlach derives expressions for the mean and variance of the temporal excursions $\Delta\tau$ of the received signal. The author correctly notes that although the ensemble average is zero, over a finite observation interval T, the integration of the velocity fluctuation term ξ may be biased. The variance of the temporal excursions is given by:-

$$\sigma_{\Delta\tau} = \frac{\varepsilon T}{2\pi} \sqrt{\frac{\sum_1^\infty \frac{1}{n^2} P_\xi(\frac{n}{T})}{\sum_1^\infty P_\xi(\frac{n}{T})}} \leq \frac{\varepsilon T}{2\pi}$$

Eqn 50

where

$P_\xi(f)$ = *power spectral density of* ε

C.1.14 The author notes that the standard deviation is maximum and equal to $\frac{\varepsilon T}{2\pi}$ when the total power of the fluctuation term ξ is concentrated over a frequency equal to 1/T. Intuitively this is not difficult to see. If the velocity fluctuations are noiselike, then the spectral energy is smeared over a wider frequency range and so the path length variance, obtained from integrating the velocity fluctuations will be less than that obtained from sinusoidal velocity fluctuations. In the latter case, maximum path delay variance occurs when the velocity sinusoidal period is equal to the observation period. This clearly demonstrates the importance of ocean fluctuations time scales relative to observation period, or in the case of communications system design, symbol period.

C.1.15 The discrete path model is also adopted by Howse and Zielinski [67]. The authors focus on the losses incurred by each path and the role of spatial processing in containing the multipath problem. Losses associated with bottom interactions are modelled in terms of the respective acoustic impedance's of the media either side of the bottom interface.

$$\Gamma_b = -20\log\left|\frac{z_2 - z_1}{z_2 + z_1}\right|$$

where

Γ_b = *reflection loss at interface in dB* *Eqn 51*

z_2 = *acoustic impedance of water*

z_1 = *acousic impedance of bottom*

C.1.16 The authors assume specular reflection and comparable impedance's either side of the interface. For surface scattering losses the authors use the empirical model of Lord and Plemons [67].

$$\Gamma_s = \begin{cases} -10\log(1-0.57g) & for\ g < 1.4 \\ 7 & for\ g > 1.4 \end{cases}$$

$$g = \frac{8\pi\sigma f \sin(\theta)}{3} \qquad \textit{Eqn 52}$$

and

σ = *rms surface wave height in m*

θ = *grazing angle in* deg.

C.1.17 The surface reflection loss Γ_s is in dB and g is the surface roughness parameter. The intensity of the n'th eigen ray in dB is given by

$$I_n = T_\theta - L_s - L_a - L_a - s\Gamma_s - b\Gamma_b + R_\theta$$

where

I_n = int *ensity of the n'th eigenray in dB*,

s = *number of surface reflections*, *Eqn 53*

b = *number of bottom reflections.*,

T_θ = *TX transducer directivity term*,

R_θ = *RX transducer directivity term*,

C.1.18 Based on omnidirectional transmit and receive beam responses the authors derive the direct to multipath intensity ratio (DMR) versus horizontal distance as a function of frequency and ocean depth for a bottom mounted transmitter and surface receiver. A smooth surface and 5Mrayl bottom impedance is assumed. The results indicate highest DMR at short range. As the range increases the DMR reduces. At higher frequencies and greater ocean depths the DMR increases. The authors do not indicate the number of interface interactions as a function of range however they do note that at higher frequencies the absorption losses are significant at increased range. This latter point is an important one. The adopted bottom loss model does not account for scattering which will become significant at higher frequencies. Also at shorter range there is evidence that the DMR is substantially poorer than for increased range due to the role of bottom-surface energy scattering mechanisms.

C.1.19 McCalla et al [66] consider ray based modelling for the assessment of AUV acoustic telemetry links. A feature of the model is the use of very short range (<500m) ultra shallow channels (down to 10m). The approach mirrors that of many other authors whereby empirical models are adopted for bottom and surface scatter loss. The bottom loss model is that proposed by Brekhovskikh.

$$Bottom\,loss\,dB = 20\log(V)$$

where

$$V = \frac{m\cos(\vartheta) - \sqrt{n^2 - \sin^2(\vartheta)}}{m\cos(\vartheta) + \sqrt{n^2 - \sin^2(\vartheta)}}$$

and *Eqn 54*

$m = bottom\,density\,/\,water\,density$

$n = water\,acoustic\,velocity\,/\,bottom\,acoustic\,velocity$

$\vartheta = surface\,grazing\,angle.$

C.1.20 The surface loss model is that proposed by Schulkin, validated at frequencies up to 25kHz, and given by the empirical relation:-

$$Surface\,Loss\,(dB) = 1.64\sqrt{f.h}$$

where *Eqn 55*

$f = signal\,frequency\,(Hz)$

$h = wave\,height\,(m)$

C.1.21 Despite the proposed application to AUV telemetry assessment the model is essentially a simple ray trace program with no explicit support for range dependent, time dependent and spatial dependent platform motion and environmental variability. Since time variability is the most complex aspect of the shallow water acoustic communication problem, simple time-range independent ray based approach is unlikely to provide valid for any but the most simple environments.

C.1.22 Zielinski et al [69] consider the shallow water high data rate communications problem for differentially phase coherent modulation.. The impact of surface reflections are considered in terms of the associated Rayleigh roughness parameter

$$R = \frac{2\pi f}{c} W \sin \vartheta$$

where

f = *system operating frequency,* *Eqn 56*

W = *rms surface waveheight (crest to trough)*

ϑ = *surface grazing angle.*

C.1.23 Where for R>>1 the surface interface acts as a scatterer and for R<<1 as a specular reflector. The authors seek to characterise the channel in terms of the delay and loss attributed to four ray families each defined in terms of first and last boundary interaction. For each ray family the authors define terms for arrival angle, delay and pressure loss as follows:-

Arrival Angle

$$\vartheta = \tan^{-1}(\frac{A}{L})$$

where

$A = b - a;$	$k = -1$	*for direct path(D)*
$A = 2nh - a - b;$	$k = 1$	*for Surface – Surface(SS)*
$A = 2nh - a + b$	$k = -1$	*for Surface Bottom(SB)*
$A = 2nh + a - b$	$k = 1$	*for Bottom Surface(BS)*
$A = 2(n-1)h + a + b;$	$k = -1$	*for Bottom Bottom(BB)*

$n = 1,2..N$ *ray order*

$h =$ *water depth*

$a =$ *transmitter depth*

$b =$ *receiver depth*

$L =$ *receiver transmitter horizontal range*

Delay relative to direct path

$$\tau_{SS_n} \approx \rho[n^2h^2 - nh(a+b) + ab]$$

$$\tau_{SB_n} \approx \rho[n^2h^2 + nh(b-a)]$$

$$\tau_{BS_n} \approx \rho[(n-1)^2h^2 + (n-1)h(a+b) + ab]$$

where

$$\rho = \frac{2L}{c}$$

$c =$ *sound velocity*

Interaction Loss

$$RSS_n = (-1)^n r_s{}^n r_b{}^{n-1}$$

$$RSB_n = (-1) r_s{}^n r_b{}^n$$

$$RBS_n = (-1)^n r_s{}^n r_b{}^n$$

$$RBB_n = (-1)^{n-1} r_s{}^{n-1} r_b{}^n \qquad \textit{Eqn 57}$$

where

$r_s =$ *surface reflection coefficient*

$r_b =$ *bottom reflection coefficient*

C.1.24 The authors adopt a number of simplifying assumptions for r_s and r_b. It is assumed that for medium frequency operation (<50kHz) and shallow grazing angles the bottom reflection coefficient approaches unity. For the surface reflection coefficient the authors

adopt a low grazing angle form of the Bechman-Spechichino model where the coefficient becomes independent of grazing angle.

$$r_s = \sqrt{(1+(\frac{1}{f_1})^2 / (1+(\frac{1}{f_2})^2}$$

where

$f_2 = 378w^{-2}$ *Eqn 58*

$f_2 = \sqrt{10} f_2$

f = *frequency in kHz*

w = *wind speed in knots*

C.1.25 Based on this model the authors seek to determine a signal to multipath measure based on self and cross multipath components. The former are attributable to micropath scattering on a temporal scale shorter than one symbol, the latter attributable to micropath contributions on a temporal scale exceeding one symbol interval. Simulations are presented based on a 4-DPSK modulation scheme operating at 10kHz and bandwidth 1kHz. The simulations suggest an increase in signal to multipath ratio as wind speed increases due to the greater scattering loss from multipath boundary interactions

C.1.26 Estes et al [71], consider a composite ray model whereby the stochastic delay parameter is drawn from a first order Gaussian Markov model :-

$$\tau_{i,k+1} = \tau_{i,k}\rho_{12} + \sigma_\pi \sqrt{1-\rho^2{}_{12}}\, x(k)$$

wehre

$\tau_{i,k}$ = *delay of the i'th path at ins*tan*t k* *Eqn 59*

ρ_{12} = *normalised correlation coefficient*

σ_π = *s*tan*dard deviation of* τ_i

$x(k)$ = *zero mean unit* var*iance Gaussian random* var*iables*

C.1.27 The authors assume the channel impulse response is much shorter than the transmission bandwidth resulting in frequency nonselective fading. Under this assumption the received phase reduces to

$$\arg(S(t)) = -\omega_0 \tau(t) + \arg(H)$$
where
$S(t)$ = *narrowband CW transmission*
H = *channel complex phase at the transmission center frequency*

Eqn 60

C.1.28 The authors assume the delay autocorrelation coefficient to be of exponential form

$$\rho_{12} = \exp u|t_{k+1} - t_k| \qquad \textit{Eqn 61}$$

C.1.29 Based on experimental measurements model parameters $u, \sigma_{\omega_0 \tau}$ are derived for a number of environments and bit error rates simulated for a variety of modulation schemes. The limited set of results presented are however inconclusive in validating the model.

C.1.30 Essebar. Loubet and Vial [68] consider the underwater acoustic channel simulation problem for mobile platforms. The discrete channel model is again adopted

$$h(t) = \sum_{i=1}^{n} a_i e^{j\phi_i \delta(t-\tau_i)}$$
where
a_i = *is the magnitude of the i'th path*
ϕ_i = *path phase*
τ_i = *path delay*

Eqn 62

C.1.31 Here, again, the assumption is paths undergoing phase rather than delay variability. The authors comment on the intrinsic stability of the ray phase and note that platform dynamics contribute the most significant variability. Also the authors note that the most significant variation occurs primarily on path magnitude. The authors finally note that the short range channel, or more accurately channels exhibiting small range:depth ratios are

particularly difficult to deal with and longer range channels serve to average the random temporal variations introduced by the medium.

C.1.32 The channel model is ray based accepting geometry, environment and a limited number of system parameters. The bottom loss model is based on the Rayleigh formula:-

$$R = \frac{r_c \sin(\theta_i) - r_p \sin(\theta_t)}{r_c \sin(\theta_i) + r_p \sin(\theta_t)}$$

where

$\theta = incident\ angle_i$

$\theta_t = transmission\ angle$ *Eqn 63*

$$r_p = \frac{\rho_b}{\rho_w}$$

$$r_c = \frac{c_w}{c_b}$$

C.1.33 Interesting features of the model are the introduction of random perturbations in the ray launch angles to simulate platform motion and the introduction of a sinusoidal swell parameter to simulate platform heave motion. The simulation results presented, emphasise the importance of platform dynamics on both the complexity and stability of the received path structure.

D Ocean Surface Scatter Channel Transfer Function

D.1.1 Characterising the ocean medium transfer function as a time-space variant stochastic filter has been considered by a number of researchers [50-55]. In the context of acoustic channel simulation the scattering characteristics of the sea surface introduce signal distortions in a temporal and spatial sense. The following discussion briefly overviews the issues relevant to ocean surface scatter models for acoustic communications performance assessment.

D.1.2 Whilst it is not intended here to pursue the approach here, an overview of the relevant theory is presented to highlight the complexity of the surface scatter problem. Such models typically rely on a number of assumptions

- The ocean surface is locally plane i.e. surface curvature << acoustic wavelength.
- Shadowing, multiple scattering and diffraction ignored.
- Surface assumed to be in far field.
- Second order terms retained in the binomial expansion of the integrand position vector with respect to reference vector. (Fresnel assumption).

D.1.3 The theoretical approach is based on developing the time-space dependent channel transfer function H(f,t,r) for small amplitude acoustic signals from the scalar wave equation, using the geometrical optics approximation.

D.1.4 Ziomek [50,51] derives the time-space variant surface scatter channel transfer function for a bistatic communications channel as follows:-

$$H(f,t) = \frac{\exp(-jk_{att}(R_1 + R_2))}{R_1 R_2} \cdot$$

$$\int_x \int_y Z(k,x,y)\exp\{-jk_{att}[lx + my + \eta\xi(x,y,t')]\}\exp\{-jk_{att}(\frac{l_f}{2}x^2 + \frac{m_f}{2}y^2)\}dxdy$$

where

$$Z(k,x,y) \equiv D_T(k,x,y)K(x,y)D_R(k,x,y)$$
$$l = \sin\theta_1 - \sin\theta_2$$
$$m = -\sin\theta_2 \sin\psi_2$$
$$n = -(\cos\theta_1 + \cos\theta_2)$$
$$l_f = \frac{\cos^2\theta_1}{R_1} + \frac{[(1-\sin^2\theta_2\cos^2\psi_2)]}{R_2}$$
$$m_f = \frac{1}{R_1} + \frac{[(1-\sin^2\theta_2\sin^2\psi_2)]}{R_2}$$
$$k_{att} = k - j[\alpha(f) + \rho_v E\{\sigma_t\}]$$

Eqn 64

D.1.5 Z(k,x,y) encompasses the transmitter and receiver directivity terms D_T,D_R where frequency dependence is implied by $k=2\pi/\lambda$. The term K(x,y) basically introduces the necessary co-ordinate transformations between transmitter aperture attitude, receiver aperture attitude wave facet attitude and the reference co-ordinate system over which the integration is performed. k_{att} is a complex term the real part denoting wavenumber and the imaginary part an attenuation factor, comprising a frequency dependent absorption term α, and a volume scattering term ρ_v.

D.1.6 $\xi(x,y,t')$ introduces the time-variant, stochastic vertical displacement of the ocean surface observed at the retarded time t' to account for the propagation delay. It is evident that this single term underpins the complete model.

D.1.7 θ_1 and θ_2 are the angles between the transmitter and receiver position vectors and the reference Z axis respectively. φ_2 is the angle between the transmitter and reference X

axis. The l_f and m_f terms arise from the Fresnel approximation for the binomial expansion of the integrand position vector in terms of the transmit position vector.

D.1.8 The above definition for $H(f,t)$ forms the start point for the derivation of the second order channel characterising functions described earlier and have been derived [51]. The scattering function which can be derived from H(f,t) as shown earlier is developed by Ziomek and formulated in terms of the surface wave autocorrelation function $R_\xi(\Delta x, \Delta y, \Delta t)$.

D.1.9 Closed solutions for the ocean surface scatter transfer function are obviously dependent on knowledge of the surface wave second order functions. These have been addressed by numerous researchers [53,54]. In practice additional stochastic terms are introduced by time-space varying absorption terms, volume scatter from surface aeration, platform attitude variation and sound velocity speed-time variation.

E Wideband Channel Simulation Model

E.1 A Time-Space Convolver For Acoustic System Evaluation

E.1.1 The utility of any acoustic propagation model is ultimately determined by the fidelity and resolution of the data used to describe the environment which should be commensurate to the temporal and spatial scales of the communicating waveforms. For high data rate acoustic communications this is not a straightforward task..

E.1.2 An alternative approach to acoustic communications system performance modelling is to adopt a deterministic approach whereby the channel varied in an appropriate manner to exercise receiver equalisation/synchronisation and spatial processing.

E.1.3 A model for acoustic communications channel simulation may therefore comprises a sum of multipath components each with a time dependent delay, Doppler, magnitude and arrival angle term thus:-

$$h(t,\tau) = \sum_{n=0}^{N_p-1} R_n(\dot{\tau}_k(t), \alpha_k(t), A_k(t))$$

where

N_p = *number of discrete paths or macropaths,*

R_k = *k'th Ray arrival,* *Eqn 65*

$\dot{\tau}_k(t)$ = *k'th ray Doppler at time t*

$\alpha_k(t)$ = *k'th ray arrival angle at time t*

$A_k(t)$ = *k'th ray magnitude at time t*

E.1.4 Each ray arrival is characterised by time varying delay profile $\tau(t)$, a time varying Doppler profile $d\tau/dt$, a time varying magnitude profile A(t) and a time varying angular arrival profile $\alpha(\tau)$.

E.1.5 Each fluctuation term is assumed Gaussian in nature defined as follows

$$\tau_k(t) = T_k + \{D(t) + \Delta(t)\}.t + \{\xi(t) + \Psi_k(t)\} \qquad \textit{Eqn 66}$$

where

$\tau_k(t)$ = time delay for k'th multipath arrival at time t

T_k = Bulk delay term for k'th multipath arrival;

D(t) = Correlated Doppler fluctuation term;

$\Delta_k(t)$ = Uncorrelated Low Pass Doppler fluctuation term;

$\xi(t)$ = Correlated delay fluctuation term;

$\Psi_k(t)$ = Uncorrelated Low Pass delay fluctuation term.

E.1.6 Each ray arrival angle is considered in terms of a correlated and uncorrelated deterministic component and an additive noise term derived from a low pass Gaussian process. The bandwidth of this process is chosen to be commensurate with the time scales of delay and magnitude variability presented later.

$$\alpha_k(t) = \Phi_k + \vartheta(t) + \gamma(t) \qquad \textit{Eqn 67}$$

Φ_k = bulk angular term for k'th multipath arrival

$\vartheta(t)$ =Correlated angle fluctuation term

$\gamma_k(t)$ = Uncorrelated Low Pass angular fluctuation term

E.1.7 Similarly each ray will be subject to a magnitude term comprising correlated and uncorrelated terms

$$A_k(t) = M_k + \beta(t) + \rho(t) \qquad \textit{Eqn 68}$$

M_k = bulk magnitude term for k'th ray

$\rho_k(t)$ = Uncorrelated Low Pass magntiude for k'th ray

$\beta(t)$ = Correlated magnitude fluctuation term

E.1.8 By modelling each ray as above it is possible to exercise both deterministic and stochastic variability in the channel transfer function. The model also enables effects such as differential Doppler to be simulated. The low pass Gaussian process enables control over the timescales of each physical mechanism enabling tailoring of channel time, frequency and angular selectivity to intrinsic ocean time scales and spatial scales.

E.1.9 Since the model accepts ray magnitude, angle and delay parameters it is well suited to simulations based on the geometric or ray trace models presented earlier. The appropriate time scales for the respective fluctuation terms and nominal values are derived from field measurements presented in the main text.

F Channel Invertibility and Non-Minimum Phase Systems

F.1.1 The invertibility of the channel impulse response is an important consideration when attempting to equalise a particular channel [156]. Spatial processing somewhat confuses the equalisation problem since the invertibility of the channel becomes a function of the spatial coherence of the incident fled. This fact should be borne in mind for the subsequent discussion. Since digital systems operating at complex baseband are discretely sampled it is customary to model the channel transfer function as a discretely sampled ($1/T_s$) digital system.

F.1.2 Minimum phase systems are linear time-invariant systems that exhibit a stable and causal inverse system. For such a system the zeros as well as the poles must lie inside the unit circle. Further, the minimum phase transfer function $H_{min}(z)$ is uniquely determined and could be directly inferred from the systems magnitude-frequency response;-

$$\begin{aligned} |H(e^{j\omega})|^2 &= H(e^{j\omega})H^*(e^{j\omega}) \\ &= H(z)H^*(1/z^*)|_{z=e^{j\omega}} \end{aligned} \qquad \textit{Eqn 69}$$

F.1.3 Thus for a minimum phase system, the systems magnitude and phase response is unique. For a non-minimum phase system there is no unique phase response. In general however a non-minimum phase system can be considered the cascade of a minimum phase system $H_{min}(z)$ and an all pass system $H_{ap}(z)$.

$$H(z) = H_{\min}(z)H_{ap}(z) \qquad \textit{Eqn 70}$$

F.1.4 Here $H_{min}(z)$ contains the poles and zeros of $H(z)$ which lie inside the unit circle plus zeros that are the conjugate reciprocals of the zeros of $H(z)$ that lie outside the unit circle. $H_{ap}(z)$ comprises the zeros of $H(z)$ lying outside the unit circle together with poles to cancel the reflected conjugate reciprocal zeros in $H_{min}(z)$. Thus to make a minimum phase

system from a non-minimum phase system one reflects the zeros outside the unit circle to their conjugate reciprocal locations inside.

F.1.5 The practical implication is that if the channel is non minimum phase then by constructing $H_{min}(z)$ and $H_{ap}(z)$ it is possible to construct an inverse compensating filter $H_c(z)=1/H_{min}(z)$ such that the overall transfer function reduces to the all pass transfer function $H_{ap}(z)$ which ensures unity magnitude response however the overall phase response is modified to $\angle H_{ap}(e^{j\omega})$.

F.1.6 It is instructive to consider a specific example. A non minimum phase system with a real impulse response is given by

$$H(z) = (1-0.9e^{j0.6\pi}z^{-1})(1-0.9e^{-j0.6\pi}z^{-1})(1-1.25e^{j0.8\pi}z^{-1})(1-1..25e^{-j0.6\pi}z^{-1}) \qquad Eqn\ 71$$

F.1.7 The pole-zero and impulse response of this system is shown in figure 66 top. Since H(z) has only negative powers of z the system is causal and since H(z) has only zeros the system is stable. However two of the systems four zeros (top) lie outside the unit circle and so the system is nonminimum phase. By reflecting the two offending zeros to their conjugate reciprocal positions inside the unit circle (middle) the resulting system becomes minimum phase $H_{min}(z)$. By cascading this system with an allpass system $H_{ap}(z)$ characterised by poles located inside the unit circle to cancel the reflected poles of the minimum phase system and the zeros of H(z) (bottom) the original transfer function is obtained. If $1/H_{min}(z)$ is used as a compensating filter the resulting transfer function would be that of $H_{ap}(z)$.

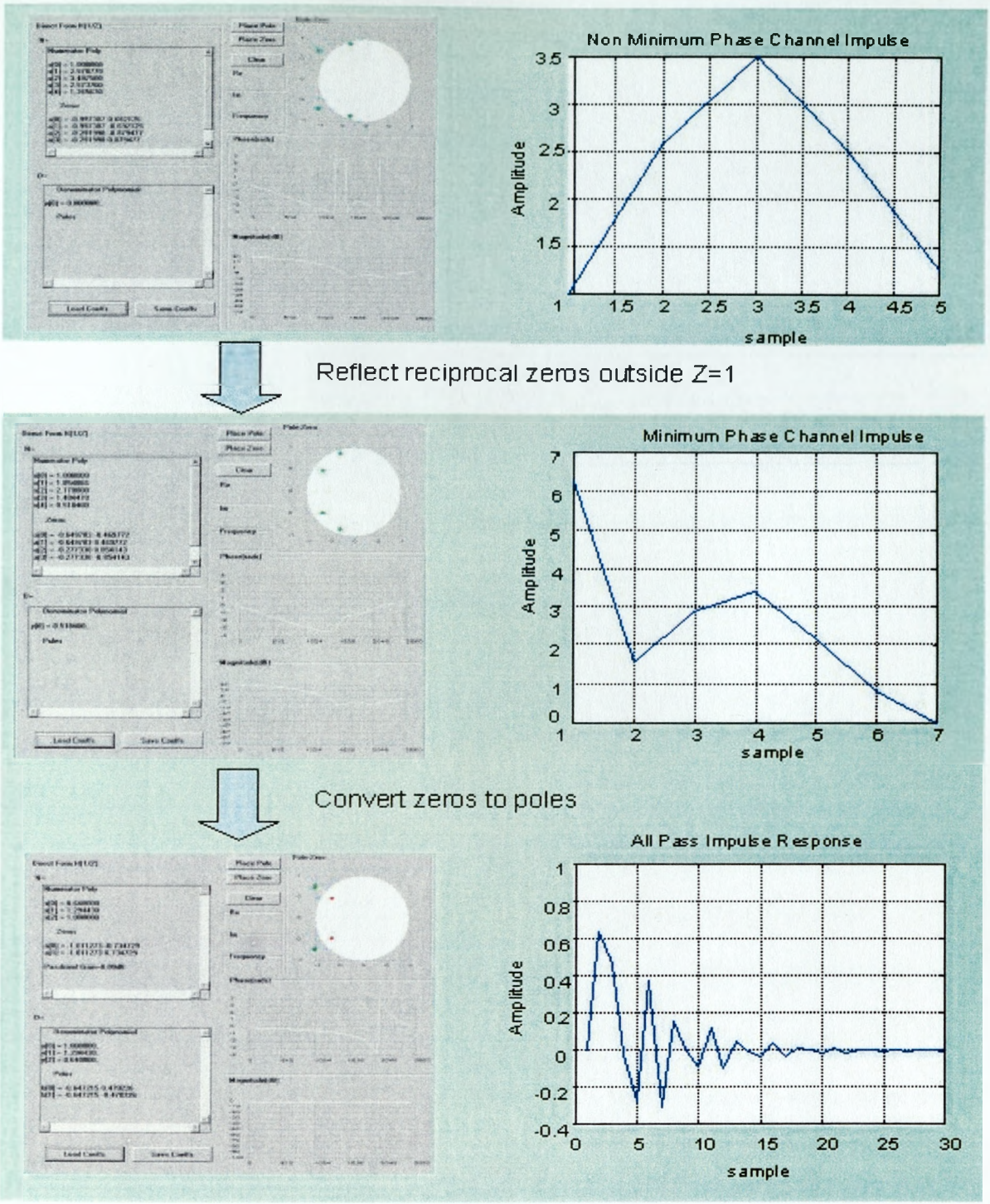

Figure 66; Non-Minimum phase transformation to equivalent cascaded minimum phase and all pass systems

G Phase Lock Loop Theory

G.1 Generic Model

G.1.1 The role of phase and delay in the analysis of an acoustic synchronisation system differs markedly from that of RF systems by virtue of the low ratio of transmission bandwidth to carrier frequency for acoustic systems.

G.1.2 Coherent modulation schemes rely on knowledge of carrier phase for demodulation. With the advent of phase coherent methods in underwater acoustics phase tracking loops have become well established in the field. Inevitably the main performance limitation is the influence of multipath and multipath variability on tracking loop behaviour. It is for this reason that it is difficult to split the synchronisation and equalisation problem and why adaptive structures operating at complex baseband are particularly powerful. These structures can compensate for modest phase rotation due to Doppler and, implemented in fractional form, can provide symbol timing compensation.

13.1.2 Phase lock loops [96] provide a means to offload the phase tracking effort from the equaliser and delay lock loops provide the means to offload symbol tracking effort. This appendix develops the fundamental theory of phase lock loop operation and also delay lock loop operation based on the material contained in [96]. The results form the basis for closed loop tracking loops reported in the main text.

G.1.3 Figure 67 depicts a typical model to analyse the performance of the phase lock loop. The input to the loop is assumed a narrowband process of the form

$$s(t,\Phi) = \sqrt{2}A(t)\sin\Phi(t) \qquad \textit{Eqn 72}$$

where

A(t) an amplitude modulation term introduced by either the transmitter or channel fading.

$\Phi(t) = \omega_0 t + \theta(t)$ is the instantaneous phase.

ω_0 is the carrier frequency term.

$\theta(t)$ is time varying phase term due to either the transmitter oscillator drift and/or channel fading.

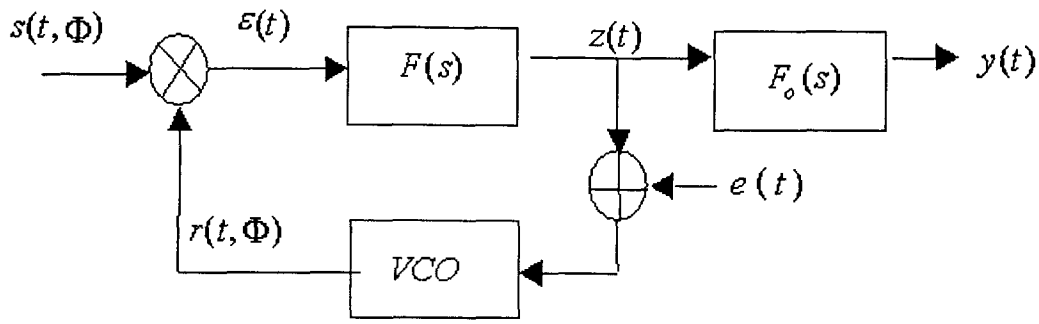

Figure 67; Generic PLL model

G.1.4 The input signal is multiplied by a voltage controlled oscillator (VCO) output

$$r(t,\hat{\Phi}) = \sqrt{2}K_1 \cos\hat{\Phi}(t) \qquad \textit{Eqn 73}$$

In the absence of noise, the instantaneous phase estimate $\hat{\Phi}(t)$ is given by

$$\hat{\Phi}(t) = \omega_0 t + \hat{\theta}(t) \qquad \textit{Eqn 74}$$

where

$\hat{\theta}(t)$ is the loop estimate of the received phase.

K_1 is the rms amplitude of the VCO output.

G.1.5 The phase discriminator in practice comprises a multiplier and low pass filter to remove double frequency terms arising from the multiplication process. The resulting filtered output is

$$\varepsilon(t) = AK_1K_m \sin\varphi(t) \qquad \textit{Eqn 75}$$

where

$$\varphi(t) = \Phi - \hat{\Phi} = \theta - \hat{\theta}$$

$\varepsilon(t)$ is the dynamic phase error which drives the closed loop.

G.1.6 Initial loop acquisition may be aided through $\varepsilon(t)$ which serves to tune the VCO toward pull in. The output phase estimate is then given by the integration of the VCO control signal considered in the S domain

$$\hat{\theta} = \frac{AK_1K_mK_vF(s)}{s}\sin\varphi + \frac{K_ve}{s} \qquad \textit{Eqn 76}$$

G.1.7 Letting the system open loop gain K=$K_1K_vK_m$ and since $\hat{\theta} = \theta - \varphi$ equation [76] becomes

$$\varphi = \theta - \frac{AKF(s)}{s}\sin\varphi - \frac{K_ve}{s} \qquad \textit{Eqn 77}$$

Or in the time domain

$$\frac{d\varphi(t)}{d(t)} = \frac{d\theta(t)}{d(t)} - K\int_0^t f(t-\lambda)(A(\lambda)\sin\varphi(\lambda))d\lambda - K_ve \qquad \textit{Eqn 78}$$

where

$f(t-\lambda)$ is the impulse response of the loop filter.

G.1.8 Equation [78] is the mathematical model for the loop behaviour and demonstrates the non-linear behaviour of the loop when the loop filter F(s) is not unity.

G.2 PLL Noise Model

G.2.1 Additive white noise and Instabilities in the VCO phase output and channel induced phase fluctuations on the received signal serve to cause fluctuations in the total phase error $\varphi(t)$.

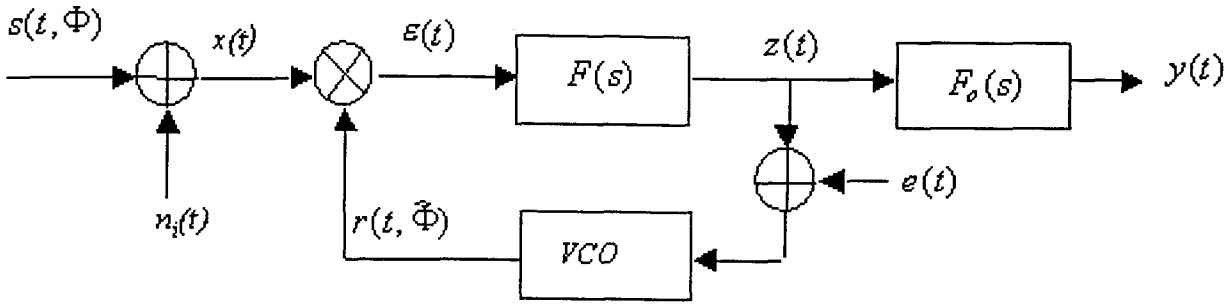

Figure 68: PLL with additive white noise model

G.2.2 The additive noise $n_I(t)$ is a narrowband Gaussian random process with symmetrical power spectral density.

$$n_i(t) = \sqrt{2}(n_c \cos\omega_0 t - n_s \sin\omega_0 t) = \sqrt{2}N_i(t)\cos\Theta_i = \sqrt{2}N_i(t)\cos(\omega_0 t + \theta_i(t)) \quad \textit{Eqn 79}$$

where

$N_I(t)$ is the envelope of the noise

$\theta_I(t)$ characterises the random phase.

G.2.3 The sum of the received signal and narrowband noise process is given by

$$x(t) = \sqrt{2}[(A(t) - N_s(t))\sin\Phi + N_c(t)\cos\Phi \quad \textit{Eqn 80}$$

where

$$N_c = N_i\cos(\theta_i - \theta) \quad N_s = N_i\sin(\theta_i - \theta)$$

G.2.4 The low pass product of the noise corrupted received signal and VCO output is

$$\varepsilon(t) = K_1 K_m[(A(t) - N_s(t))\sin\varphi + N_c(t)\cos\varphi \qquad \textit{Eqn 81}$$

where

$$\varphi = \Phi - \hat{\Phi} = \theta - \Theta$$

G.2.5 The instantaneous frequency of the VCO $\dot{\Theta}$ is given by the input phase derivative and comprises the sum of three terms :-

- The loop filter output $K_v F(s)\varepsilon(t)$;
- The VCO tuning voltage $K_v e(t)$;
- VCO phase instabilities $\dot{\psi}_2$.

G.2.6 Combining [80] and [81] gives the VCO output phase

$$\Theta = K\frac{F(s)}{s}[A\sin\varphi + N(t,\varphi)] + K_v\frac{e}{s} + \psi_2 \qquad \textit{Eqn 82}$$

where

$$N(t,\varphi) = N_c\cos\varphi - N_s\sin\varphi$$

$$K = K_1 K_m K_v$$

G.2.7 And substituting for $\varphi = \theta - \Theta$ gives

$$\varphi = \theta - K\frac{F(s)}{s}[A\sin\varphi + N(t,\varphi)] - \frac{K_v e}{s} - \psi_2 \qquad \textit{Eqn 83}$$

G.2.8 The signal phase modulation term θ also comprises the sum of three terms:-

- frequency translation Doppler *d(t)*;
- phase modulation term *M(t)*;
- transmitter oscillator/channel fluctuation phase term $\psi_1(t)$;

G.2.9 The resulting mathematical model for the performance of the PLL in white additive Gaussian noise with phase instabilities in received waveform and local VCO is

$$\frac{d\varphi}{dt} = \frac{dd(t)}{dt} + \frac{dM(t)}{dt} - \int_0^t Kf(t-\lambda)[A(\lambda)\sin\varphi(\lambda) + N(\lambda,\varphi)]d\lambda - K_v e + \frac{d\psi_1(t)}{dt} - \frac{d\psi_2(t)}{dt} \qquad \textit{Eqn 84}$$

G.2.10 The equivalent loop model of the system defined in [84] is shown in figure 69.

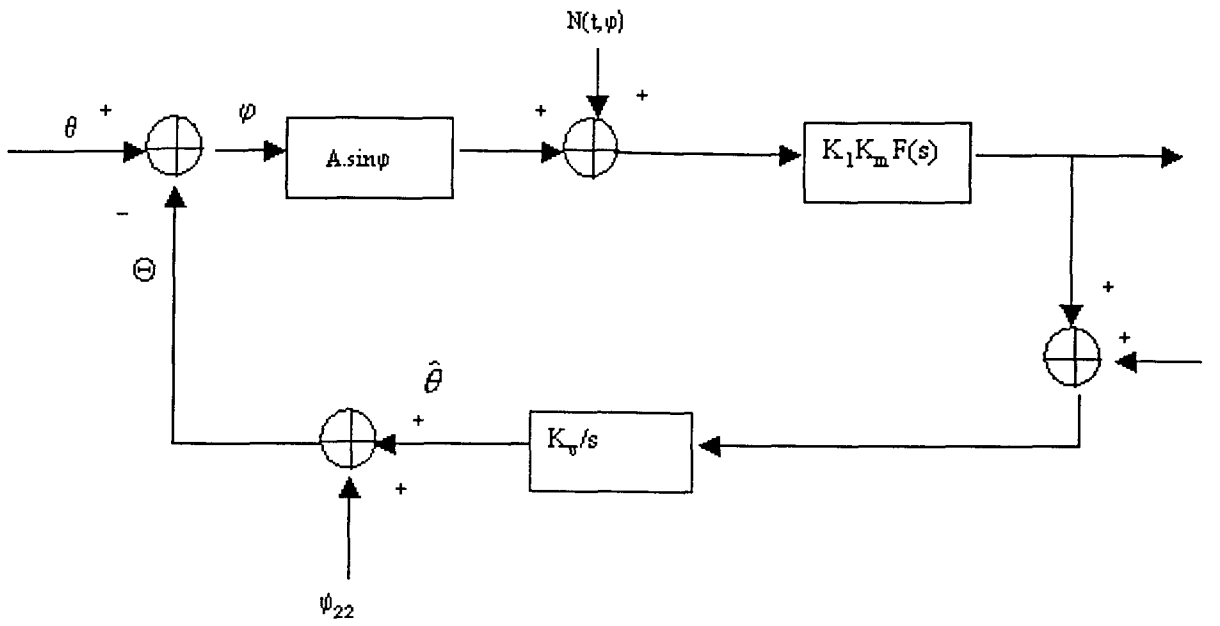

Figure 69: Equivalent PLL + noise model

G.3 PLL in coherent Communications

G.3.1 The phase error $\varphi(t)$ represents the total loop error and encompasses modulation *M(t)* , Doppler *d(t)*, transmitter/channel phase instabilities $\psi_1(t)$, local phase oscillator instabilities $\psi_2(t)$. In practice one wishes to track the phase instabilities introduced by unknowns in the system in order to recover the information bearing part of the signal, namely *M(t).*

G.3.2 These instabilities manifest as a carrier phase error term $\varphi_c(t)$ where

$$\varphi_c(t) = d(t) + \psi_1(t) - \hat{\theta}(t) \qquad \textit{Eqn 85}$$

such that

$$\varphi(t) = \varphi_c(t) + M(t) - \psi_2(t) \qquad \textit{Eqn 86}$$

G.3.3 This model defines the loop behaviour when the receiver tracks d(t)+ $\psi_1(t)$.

G.4 Linear PLL Model

G.4.1 The utility of the PLL in tracking phase relies on the total loop error $\varphi(t)$ being small. This enables the Taylor series approximation $\sin\varphi \approx \varphi$ to be used. i.e.

$$\varphi = \theta - K\frac{F(s)}{s}[A\varphi + N_c] - \frac{K_v e}{s} - \psi_2 \qquad \textit{Eqn 87}$$

G.4.2 Therefore, provided the initial phase error is small, phase pull in is readily achieved. However a significant limitation of the linear PLL approach is the 2π ambiguity in the phase track arising from the possibility of cycle slipping. Aspects of initial synchronisation of acoustic communications systems will be dealt with elsewhere, however it is useful to note that acoustic systems typically employ carrier frequencies much smaller than those of RF systems such that the ratio of transmission frequency to transmission bandwidth is often less than ten. This means that signal acquisition timing based on wideband correlation methods can often be immediately related to carrier phase.

G.4.3 The closed loop transfer function for the linearised loop model shown in figure 69 is defined by

$$H_\varphi(s) = \frac{L\{\Theta\}}{L\{\theta\}} = \frac{AKF(s)}{s + AKF(s)} \qquad \textit{Eqn 88}$$

where L{ } is the Laplacian operator.

G.4.4 It can be shown that the phase variance due to additive noise is inversely proportional to the signal-to-noise ratio of the loop $\rho = \frac{A^2}{N_0 B_l}$ where B_l is the single sided loop bandwidth. However reducing loop bandwidth impairs the tracking capability of the loop.

G.5 Tracking Performance

G.5.1 For a PLL system to track an Nth degree polynomial phase function with zero steady state error it can be shown that *F(s)* must have l>N-1 poles at the origin. This means that for the loop to track out any change in input phase $F(s) \neq 0$.

G.5.2 For the loop to track Doppler frequency shift i.e. $d(t) = \theta_0 + \Omega_0 t$, the tracking filter *F(s)* must exhibit two poles and to track Doppler rate i.e. acceleration $d(t) = \theta_0 + \Omega_0 t + \Omega_1 t^2$ the filter must exhibit three poles.

G.5.3 This can be seen by reorganising the closed loop transfer function to obtain an expression for the closed loop error $\varphi = \theta - \Theta$.

$$\begin{aligned} \varphi(s) &= \theta(s) - \Theta(s) \\ &= [1 - H_\varphi s)]\theta(s) \\ &= \frac{s\theta(s)}{s + AKF(s)} \end{aligned} \qquad \textit{Eqn 89}$$

G.5.4 Using the final value theorem

$$\lim_{t\to\infty} \varphi(t) = \lim_{s\to 0} s\varphi(s) \qquad \textit{Eqn 90}$$

then

$$\lim_{t\to\infty} \varphi(t) = \lim_{s\to 0} \frac{s^2\theta(s)}{s + AKF(s)} \qquad \textit{Eqn 91}$$

G.5.5 Substituting $\theta(s) = \frac{\Delta\theta}{s}$ into the final value theorem and applying limits for *F(s)*=1 indicates that the first order PLL can track the phase step with zero steady state error. In

the case of a phase ramp or frequency step $\theta(s) = \frac{\Delta\omega}{s^2}$ and the steady state error is given by:-

$$\lim_{t\to\infty} \varphi(t) = \lim_{s\to 0} \frac{s^2\Delta\omega}{s + AKF(s)} = \frac{\Delta\omega}{AKF(0)} \qquad \textit{Eqn 92}$$

G.5.6 For $F(s)=1$, $F(s)=w_1/(s+w_1)$ and $F(s)=(w_1 / w_2)(s+ w_1)/(s+w_2)$ the loop will track the ramp with a constant phase error $\frac{\Delta\omega}{AK}$. Zero error tracking of Doppler requires a perfect integrator in the feed back filter i.e.

$$F(s) = \frac{1}{s}.\frac{N(s)}{D(s)} \qquad \textit{Eqn 93}$$

G.5.7 For Doppler Rate it can be shown that the loop can track the input with a constant phase error only if it has an integrator in the feedback filter. For zero phase error tracking two integrators must exist in the filter transfer function.

G.6 Delay Lock Loops (DLL)

G.6.1 The delay lock loop can be considered to be a broadband analogue of the phase lock loop and much of the underlying theory of its operation is drawn from the foregoing PLL models. The main difference between the performance of the PLL and DLL lies in the calculation and nature of the phase discriminator characteristic.

G.6.2 In the case of a PLL the phase discriminator characteristic is formed from the multiplication of the reference carrier with the incoming signal and filtering the result to remove double frequency terms. This leads to a discriminator characteristic which, is itself, sinusoidal in nature and subject to cycle slipping.

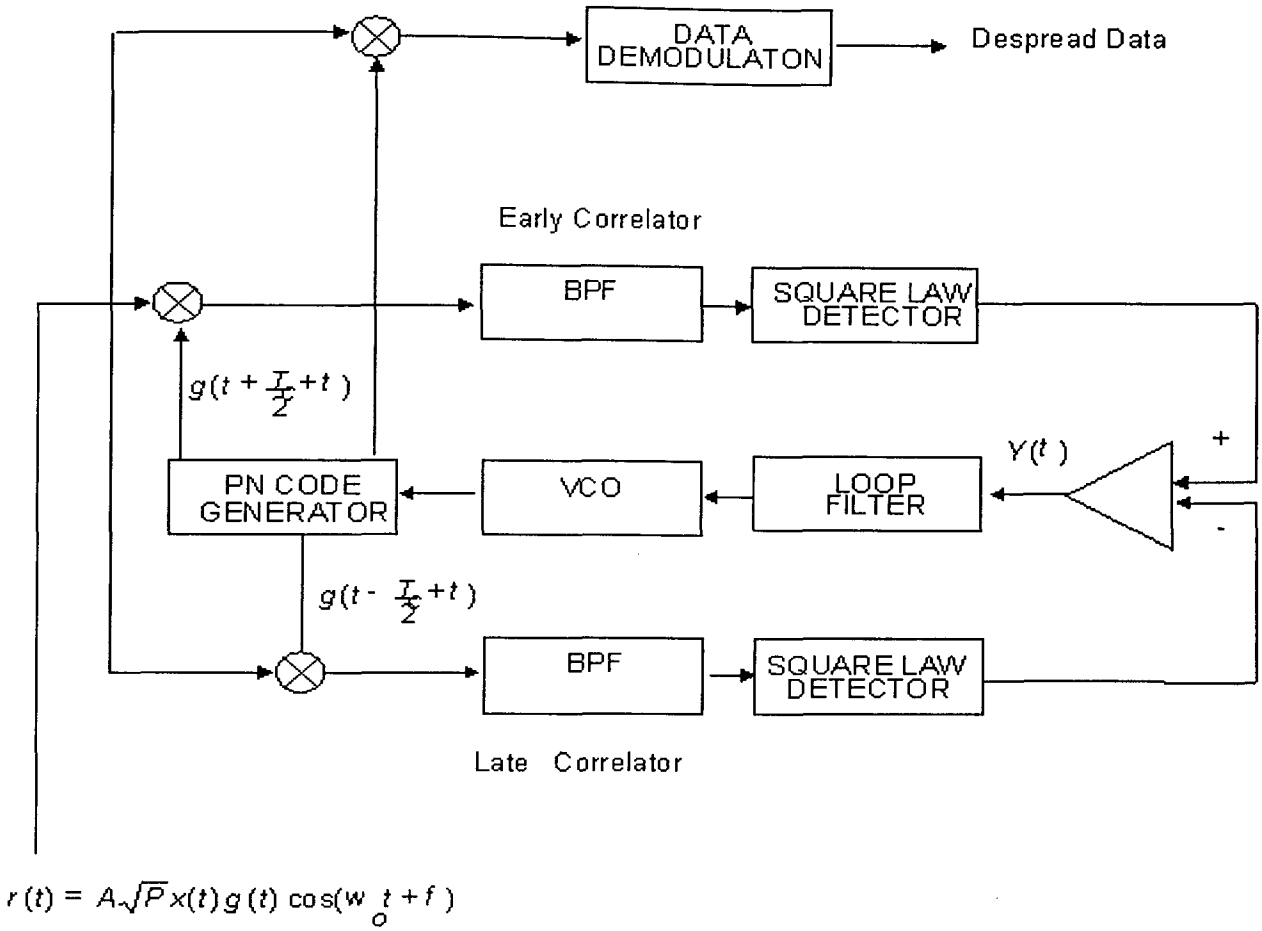

Figure 70: Early-Late Delay Lock Loop

G.6.3 In contrast, a DLL phase discriminator is formed from the multiplication and low pass filtering of two wideband signals and the performance of the loop draws heavily on the autocorrelation characteristics of these signals (see appendix N). Figure 70 depicts a typical noncoherent delay lock loop structure showing early and late correlator arms, comparator, loop filter VCO and wideband signal generator; in this case a pseudorandom sequence.

G.6.4 The tracking performance of the structure is essentially analysed as a conventional phase lock loop, however the difference lies in the implementation of the phase discriminator. In order for many wideband systems to operate at very low SNR, the phase discriminator is

normally based upon incoherent energy detection using multiple dwell versions of the received spreading waveform to establish timing phase. The simplest system, as shown uses a single early and late version of the system spreading waveform, separated by a single chip interval as shown in the figure.

G.6.5 In each arm of the structure, the respective early and late waveforms are multiplied with the received signal and the result integrated through the action of the bandpass filters whose bandwidth is determined by the system data rate. The square law detector removes the influence of data modulation, which is assumed in this case to be biphase.

G.6.6 For an ideal channel, the process of multiplication followed by integration simply forms the autocorrelation of the spreading waveform g(t), evaluated for lags +/- Tc/2

$$E[g(t)g(t \pm \tfrac{T_c}{2} + \tau)] = | R_g(\tau \pm \tfrac{T_c}{2}) | \qquad \textit{Eqn 94}$$

G.6.7 Under perfect synchronisation the symmetry of the autocorrelation $R_g(\tau)$ maintains the loop tracking error $Y(\tau)$ at zero. When the received timing epoch begins to slip, the loop tracking error will increase either advancing or retarding the phase of the PN code generator and so re-establishing zero error. By introducing a loop filter the transient response and tracking response of the structure can be tailored as discussed earlier.

G.6.8 Analysis of the performance of the delay lock loop is limited to the linear operating regime whereby the timing phase is limited to a single chip. Over this regime the transfer characteristic is linear and the system can be analysed in exactly the same manner as a conventional phase lock loop.

G.6.9 Figure 71 depicts the simulated phase discriminator characteristic of a pseudonoise signal for three correlator arm spacings corresponding to half a chip, one chip and two chips as shown in Figure 72. In the upper plot, the X-axis denotes normalised delay and the Y-

axis, normalised error. From the figure it can be seen that for relative dwell Tc/2, since the correlator arms overlap, the peak error is reduced from 1.0 to 0.707 for a delay error of Tc/4. Over the region $-0.25 < \frac{T_d}{T_c} < 0.25$ the discriminator characteristic is linear. Outside this region the error falls to zero. For a relative dwell of one chip the error is linear over the region $-0.5 < \frac{T_d}{T_c} < 0.5$. For relative dwell of two chips, the error is noticeably non-linear over the region $-1 < \frac{T_d}{T_c} < 1$. In particular, in the vicinity of $\frac{T_d}{T_c} = 0$ the error gradient approaches zero.

G.6.10 In practice the discriminator characteristic shown in the figure is rarely achieved. This is due to numerous impairments introduced by the channel such as noise, multipath, bandlimiting and Doppler. In the case of multipath, path arrivals outside one chip manifest as noise terms. Components arriving inside one chip will serve to distort the idealised characteristic shown in the figure. Also, the received signal may be subject to bandlimiting which will serve to broaden its autocorrelation function and again distort the ideal characteristics depicted in the figure.

G.6.11 The influence of acoustic Doppler on the performance of the loop is largely determined by the bandwidth of the tracking loop. Specifically, if the correlator integration period is too large, this will have a de-correlative effect depending upon the ambiguity performance of the particular waveform the DLL is using. This means for example, if the bandwidth is made small, to provide more robust tracking performance at low SNR, loop operation is likely to be impaired under high Doppler conditions.

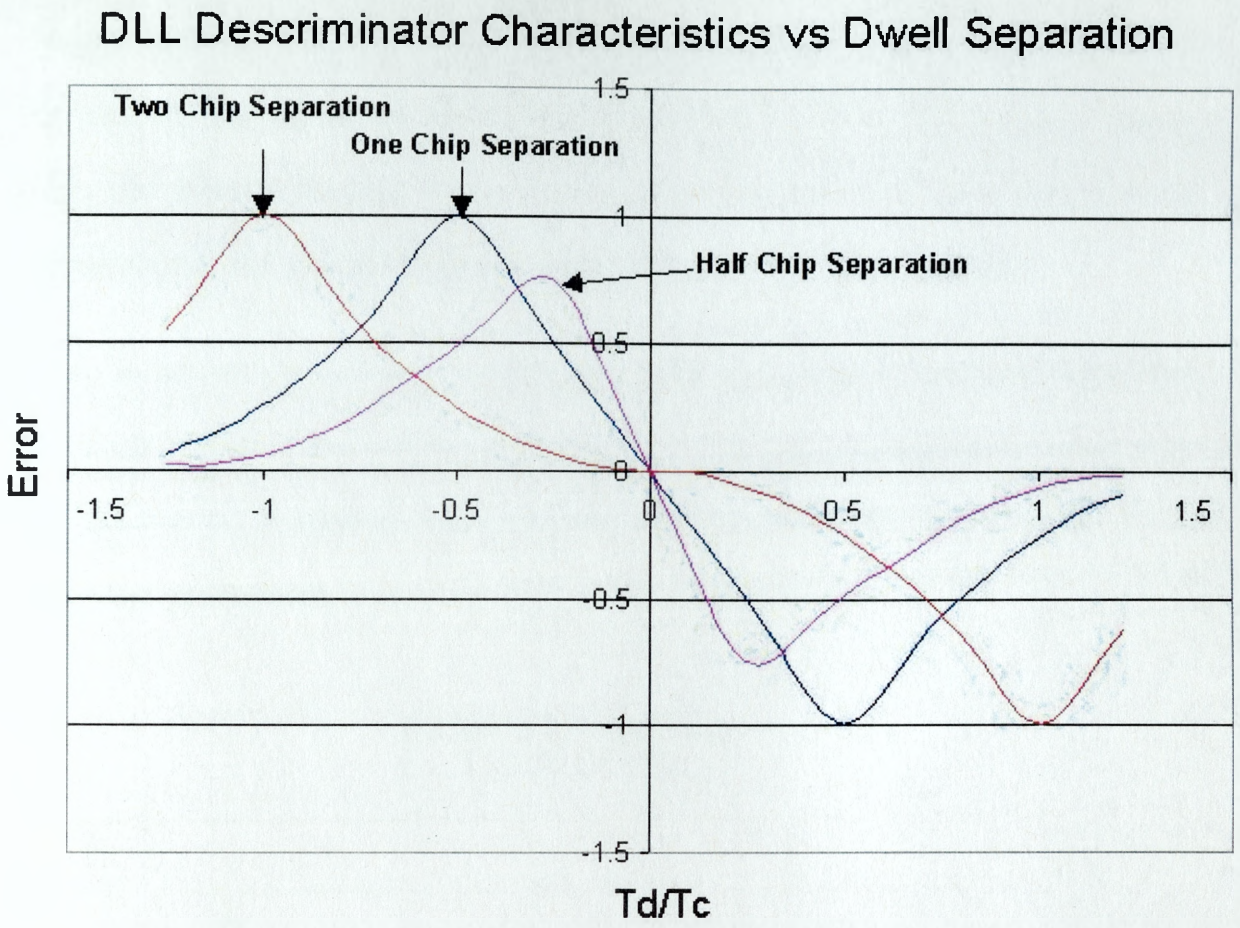

Figure 71: DLL Phase Discriminator Characteristic vs. Correlator Dwell Separation

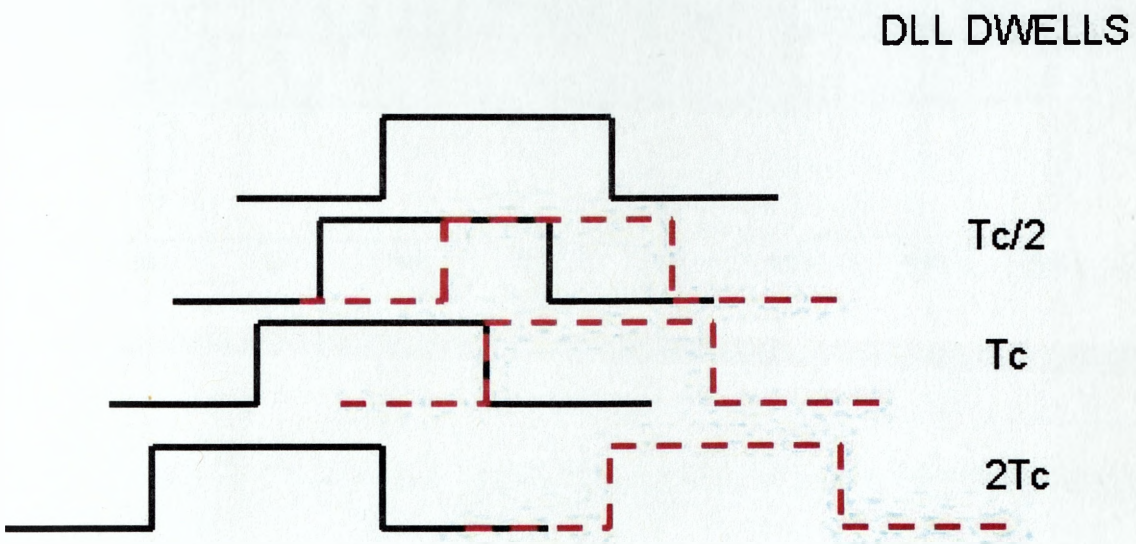

Figure 72; DLL dwells for discriminator characteristic above

G.6.12 Figure 73 depicts the simulated performance of an early-late delay lock with a two pole integrating filter to enable the loop to track out a step change in input signal Doppler. In the simulation a step change of 20 Doppler bins (1bin=0.1875m/s) is applied at sample 250. The transient response of the loop is shown for three loop gains demonstrating underdamped, and critically damped performance under noise free conditions.

G.6.13 In the acoustic channel, Doppler and Doppler variation can lead to significant degradation in correlator performance and this issue drives the choice of integration period used in the correlator arms. In practice on must balance loop bandwidth with tracking performance and noise performance.

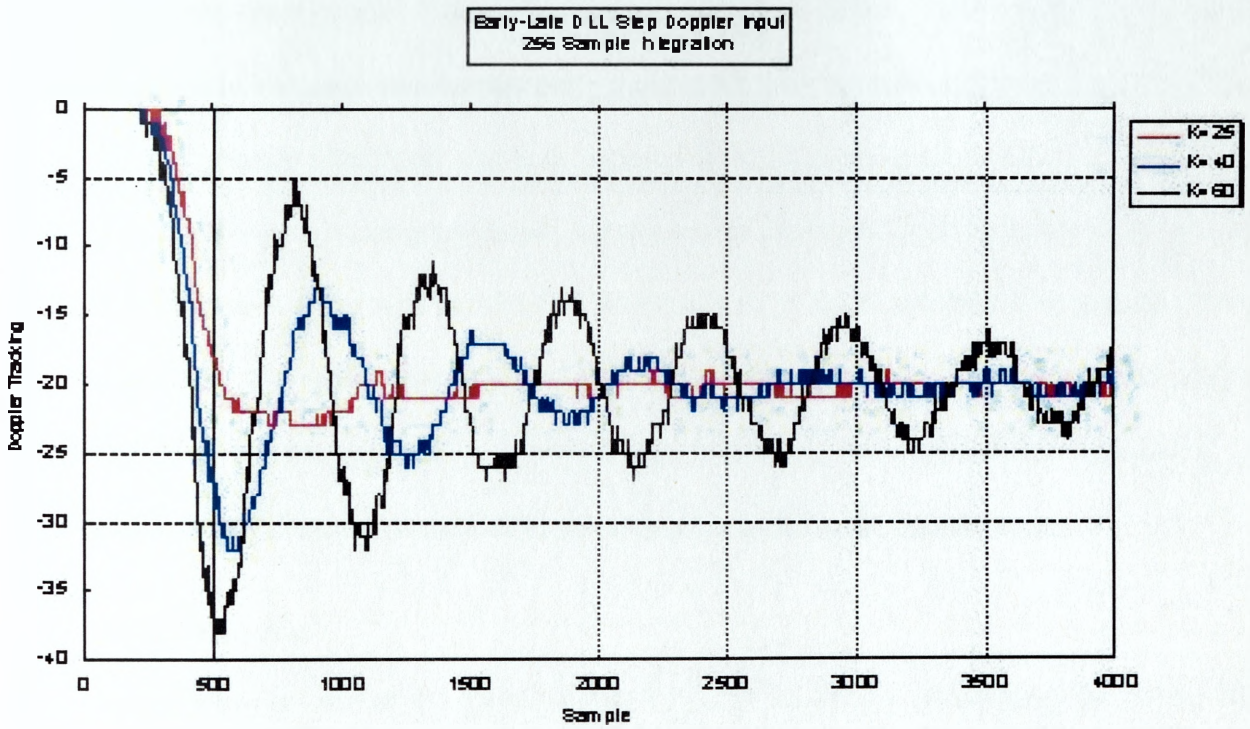

Figure 73; Early-Late digital DLL step Doppler response for three gain settings

H MSE and Peak Distortion Criteria for Equaliser Coefficient Optimisation

H.1.1 The transmission of digital signals through bandlimited channels and/or channels exhibiting multipath temporal dispersion, results in a smearing of information across data symbols often referred to as inter symbol interference (ISI). The process of compensating for ISI is one of equalisation. In many channels, the underwater acoustic channel included, the properties of the channel are unknown or are time varying. For acoustic channels, the equalisation task is particularly difficult due to both the time variability of the channel and the extremely long time spreads relative to RF channels.

H.1.2 Optimum equalisation of time dispersed channels involves brute force estimation of the most likely sequence transmitted using an estimate of the channel impulse response [153]. This maximum likelihood sequence estimation (MLSE) approach to channel equalisation whilst optimum, is computationally expensive for channels exhibiting long time spreads. Sub optimum techniques involve the minimisation of some performance measure of the equaliser. The most often used structure for equalisation is the linear transversal filter of the form shown previously in Figure 36. There are two criteria for optimising the coefficients of the transversal filter peak distortion and mean square error.

H.2 Peak distortion

H.2.1 Peak distortion where the performance index is based on minimising the worst case intersymbol interference at the output of the equaliser. Such a structure is the zero forcing equaliser whose transfer function is the reciprocal of the channel transfer function. The zero forcing criteria however suffers in the presence of additive white noise for channel exhibiting deep fades typical of multipath channels. In such conditions the inverse filter (if indeed it exists!) may have high gains at the fade frequencies. In the presence of noise

these high gains lead to noise enhancement such that whilst the peak distortion criteria is met, the filter output signal-to-noise ratio is degraded. It can be shown for example [96] that the output SNR of the infinite zero forcing equaliser is

$$SNR_{\infty} = \left[\frac{T^2 N_0}{2\pi} \int_{-\frac{\pi}{T}}^{+\frac{\pi}{T}} \frac{d\omega}{\sum_{n=-\infty}^{+\infty} |H(\omega + 2\pi n / T)|^2} \right]^{-2} \qquad \textit{Eqn 95}$$

Thus, if the folded transfer function H(ω) possesses any zeros, the integrand is infinite and the SNR is zero.

H.3 Mean Square Error

H.3.1 Mean square error (MSE) criterion where the tap weights are adjusted to minimise the mean square error terms computed from the difference between filter output and desired output. An obvious advantage of these criteria is the fact that the filter performance is driven equally by ISI and noise error terms. For an infinite length equaliser the minimum output noise is given by [96]

$$J_{\min} = \frac{T}{2\pi} \int_{n=-\infty}^{\infty} \left[\frac{N_0}{T^{-1} \sum_{n=-\infty}^{\infty} |H(\omega + 2\pi n / T)|^2 + N_0} \right] d\omega \qquad \textit{Eqn 96}$$

so in the absence of ISI (X(jwT)=1)

$$J_{\min} = \frac{N_0}{1 + N_0} \qquad \textit{Eqn 97}$$

and the output signal-to-noise is

$$SNR = \frac{1 - J_{\min}}{J_{\min}} \qquad \textit{Eqn 98}$$

I PDF of the Phase Angle Between Two Vectors Perturbed by AWGN

I.1 Overview

I.1.1 The probability distribution of the phase angle between two vectors perturbed by Gaussian noise is of interest in many communication systems including differential phase shift keyed modulation systems and systems which seek to exploit the phase difference between two complex vectors for the purpose of synchronisation and/or demodulation.

I.1.2 For synchronisation schemes using the change of phase between consecutive data vectors, the influence of noise on the delta phase estimate is clearly of interest. The probability distribution of the phase angle between two vector outputs pertubed by additive white noise has been derived by Paula, Rice and Roberts [148].

I.2 Geometry

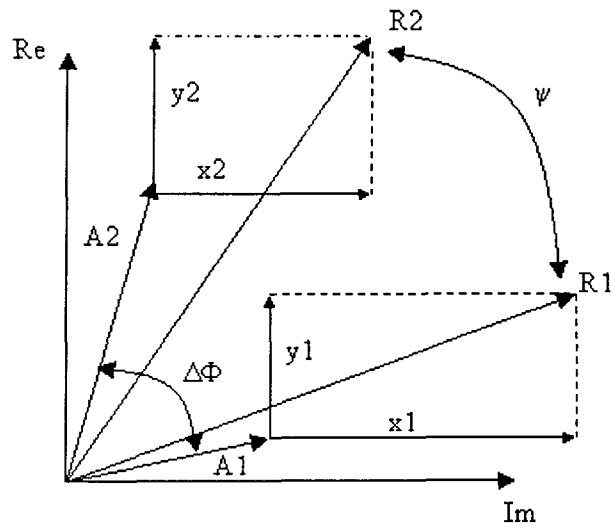

Figure 74; Phase angle between two vectors perturbed by AWGN

I.2.1 The problem is shown in Figure 74 which depicts two received signal vectors A1, A2 perturbed by random noise x1,y1 and x2,y2 resulting in received noisy vectors R1 and

R2. The problem at hand is to determine the probability distribution function of the modulo 2π difference Ψ. Defining the parameters

$$U=\frac{1}{2}\left[\frac{A_1^{\,2}}{2\sigma_1^{\,2}}+\frac{A_2^{\,2}}{2\sigma_2^{\,2}}\right],\qquad V=\frac{1}{2}\left[\frac{A_2^{\,2}}{2\sigma_2^{\,2}}+\frac{A_1^{\,2}}{2\sigma_1^{\,2}}\right],\qquad W=\sqrt{U^2-V^2} \qquad \textit{Eqn 99}$$

the probability distribution function $F(\Psi)$ can be defined for three different cases

Case 1 : Equal Signals and Uncorrelated Noise ($\Delta\Phi$=0, V=0)

$$F(\Psi)=\frac{-\sin\Psi}{4\pi}\int_{-\pi/2}^{\pi/2}\frac{\exp\{-U[1-\cos\Psi\cos t]\}}{1-\cos\Psi\cos t}dt \qquad \textit{Eqn 100}$$

Case 2 : Unequal Signals and Uncorrelated Noise

$$F(\Psi)=\frac{-W\sin(\Delta\Phi-\Psi)}{4\pi}\int_{-\pi/2}^{\pi/2}\frac{\exp\{-[U-V\sin t-W\cos(\Delta\Phi-\Psi)\cos t]\}}{U-V\sin t-W\cos(\Delta\Phi-\Psi)\cos t}dt \qquad \textit{Eqn 101}$$

Case 2 : Unequal Signals and Correlated Noise

$$F(\Psi)=\int_{-\pi/2}^{\pi/2}\frac{e^{-E}}{4\pi}\left[\frac{W\sin(\Delta\Phi-\Psi)}{U-V\sin t-W\cos(\Delta\Phi-\Psi)\cos t}+\frac{r\sin\Psi-p\cos\Psi}{1-(r\cos\Psi-p\sin\Psi)\cos t}\right]dt$$

Eqn 102

where

$$E=\frac{U-V\sin t-W\cos(\Delta\Phi-\Psi)\cos t}{1-(r\cos\Psi+p\sin\Psi)\cos t},\ r=\frac{\overline{x_1x_e}}{\sigma_1\sigma_2}=\frac{\overline{y_1y_e}}{\sigma_1\sigma_2},\ p=\frac{\overline{x_1y_e}}{\sigma_1\sigma_2}=\frac{\overline{y_1x_e}}{\sigma_1\sigma_2}$$

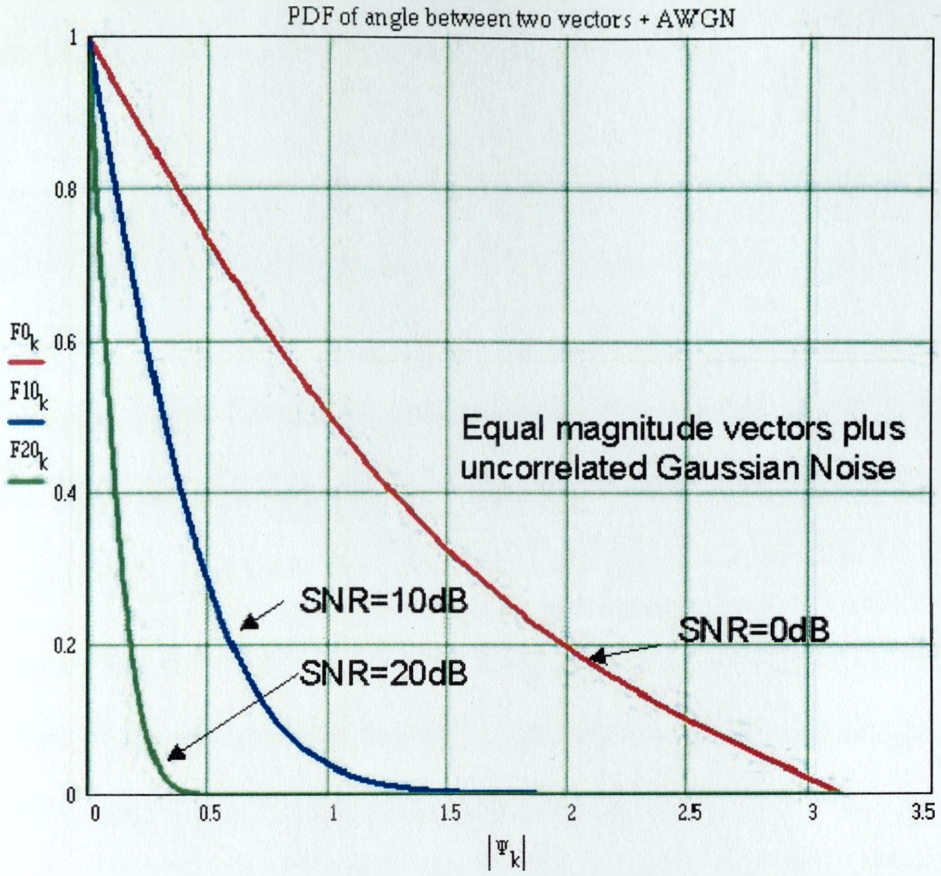

Figure 75; PDF of phase angle between two vectors perturbed by uncorrelated AWGN at SNR 0,10 and 20dB

I.2.2 Figure 75 depicts $F(\Psi)$ for the case of two equal vectors perturbed by uncorrelated AWGN and shows the PDF for SNR=0dB, 10dB, and 20dB. From the graph it can be seen that for fixed SNR, the probability of the phase difference between the two vectors assuming a particular phase difference ϕ_k , increases as ϕ_k reduces. As the received SNR increases so the probability of the phase difference assuming a lower value increases.

J Open Loop Synchroniser Detection Statistics Calculation

J.1 Overview

J.1.1 Initial synchronisation of an acoustic communications system forms a basic subset of detection theory. Open loop acquisition of a wideband signal requires that the signal be detected with a high probability whilst at the same time ensuring the system is not alerted to false alarms. The following discussion presents basic detection theory for the case of a single wideband pulse detector used for communication transmission acquisition..

J.2 Detection Statistics

J.2.1 Matched filter detection, i.e. coherent detection of a known signal in an additive white Gaussian noise environment realises a processing gain dependant upon the ratio of received signal energy E_s to noise spectral density N_0.

J.2.2 As a rough approximation it can be seen that the ratio of output signal-to-noise ratio (SNR) to input SNR is improved by a factor of BT i.e. the number of independent samples in the waveform.

$$\frac{E_s}{N_o} = \frac{\sigma_s^2 T}{\left[\frac{\sigma_s^2}{B}\right]} = BT\frac{\sigma_s^2}{\sigma_n^2} \qquad \textit{Eqn 103}$$

J.2.3 In practice the above relationship holds for AWGN channels only. In general realising any coherent processing advantage, whether by matched filter detection or spatial processing ultimately relies on the signal coherence characteristics which are greatly influenced by the acoustic environment, most notably by multipath propagation.

J.2.4 In the context of initial synchronisation, processing gain provides a system the means to synchronise at low signal-to-noise ratios. In addition to providing improvement in signal-

to-noise ratio, transmission bandwidth is extremely useful as a means to resolve multipath components. A receiver, who is able to resolve multipath components into several independent channels, may exploit the path diversity to improve overall receiver performance.

J.2.5 The problem of initial synchronisation is intimately linked to the signal detection problem. The classic detection problem considers the problem of detecting the presence or absence of a transmission in AWGN.

J.2.6 In sonar performance prediction detection performance is usually determined using Receiver Operating Curves (ROC) which indicates the signal-to-noise ratio required at the input to the thresholding algorithm to achieve stated probabilities of detection and false alarm. This parameter is usually termed the detection index (d). The detection threshold (DT) relates to the signal-to-noise ratio prior to the signal processing chain and before the thresholding algorithm. In the case of a coherent receiver using matched filter processing this processing chain will realise a 10log(BT) processing gain, in the case of an incoherent receiver using energy detection this processing chain will realise a 5log(BT) processing gain (assuming an exact match of time and bandwidth). For an incoherent energy detector the detection threshold is define thus

$$d = \frac{(\overline{Mean_{S+N}} - \overline{Mean_N})^2}{\overline{Var_N}}$$

$$d = \frac{(2BT\sigma_s^{\ 2})^2}{4BT\sigma_n^{\ 4}}$$

$$d = BT\left\{\frac{\sigma_s^{\ 2}}{\sigma_n^{\ 2}}\right\} \qquad \textit{Eqn 104}$$

$$d = BT\{DT\}^2$$

$$DT = 5\log d - 5\log BT(dB)$$

J.2.7 For a coherent receiver/synchroniser with exact knowledge of the received waveform

$$d = BT.DT$$
$$DT = 10\log(d) - 10\log(BT) \qquad \textit{Eqn 105}$$

J.2.7.1 Consider a windowed LFM chirp with the parameters shown in Table 6

SL	190dBre1 μPa @1m
B	8000Hz
N	35dBre1 μPa $Hz^{-1/2}$
DI	0dB
Tchirp	21.3ms
DF_w	4dB (Kaiser-Bessel Window)
POD	0.998
PFA	1e-2
d	36

Table 6; Simulation parameters for open loop synchroniser performance

J.2.8 It is assumed that for initial synchronisation the receiver has no spatial processing gain (DI=0dB). A single estimate, matched filter based synchroniser is required to detect the transmission with 99.8% certainty, and a probability of false alarm 1%. From standard Receiver Operating Curves (ROC) the input signal-to-noise ratio to the thresholding algorithm must be of the order d=100 (SNR=20dB) for a matched filter detector followed by envelope detector giving rise to exponential .

J.2.8.1 Hence the receiver detection threshold will be

$$\begin{aligned} DT &= 10\log(36) - 10\log(8000 * 21..3e-3) \\ &= 16 - 22 \\ &= -6dB \end{aligned} \qquad \textit{Eqn 106}$$

J.2.9 Assuming a signal excess of 0dB, it is possible to calculate the propagation loss which results in the system achieving the desired detection and false alarm probabilities for the system parameters specified in the table.

J.2.10 Assuming SE=0 then

$$PL = SL-(N+10\log B)+DI-10\log d+10\log BT_s-DF_w$$

SL	=	190dBrel μPa @1m
B	=	8000Hz
N	=	35dBrel μPa $Hz^{-1/2}$
DI	=	0dB
Tchirp	=	21.3ms
DF_w	=	4dB (Kaiser-Bessel Window)
POD	=	0.998
PFA	=	1e-2
d	=	36
PL_{psm}	=	122dB

J.2.11 So, for the given parameters, it can be seen that provided the total loses are less than 122dB, a single estimate matched filter based synchroniser will synchronise with a probability of 99.8% and a false alarm rate of 1%. In practice a much lower false alarm rate would be desirable. For example, in a practical implementation of such the

synchronisation system above, operating with sampling rate 48kHz, a false alarm would occur approximately once every fifty seconds. For a communication system false synchronisation is wasteful of resources and a practical open loop synchroniser would operate with a much lower false alarm probability such as the two chirp synchroniser discussed in the main text.

K Adaptive Algorithms

K.1 Overview

K.1.1 Adaptive filters are ideally suited to the problem of underwater acoustic channel equalisation by virtue of their ability to track the time varying nature of such channels. The following discussion develops the fundamental theory of several adaptive algorithms employed in the main text. The discussion is based on the material presented in [156] which provides a comprehensive treatment of many classes of adaptive algorithms.

K.2 Steepest Descent Algorithms

K.2.1 Steepest descent algorithms are recursive in nature and seek to locate a minimum point of an error performance surface without any a priori information of the surface. For a stationary process this solution is the optimal Weiner solution.

K.2.2 For a transversal filter implementation with weights $\mathbf{w(n)}= [w_0(n)\ w_1(n)\ ..\ w_{M-1}(n)]^T$ the estimation error *e(n)* is given by the difference between the desired output d(n) and the estimated output $\mathbf{w}^H(n)\mathbf{u}(n)$, where $\mathbf{u}(n)=[\ u(n)\ u(n-1)\ ..\ u(n-M+1)]^T$ is the input tap vector.

$$e(n) = d(n) - \sum_{k=0}^{M-1} w_k^* u(n-k) = d(n) - \mathbf{w}^H(n)\mathbf{u}(n) \qquad \textit{Eqn 107}$$

K.2.3 The first term is the variance of the desired response, the summation in the second and third terms is the cross correlation between the input tap vector and the desired response, the fourth term is the autocorrelation of the input tap vector for lag i-k. Denoting

$$\begin{aligned} p(-k) &= E[u(n-k)d^*(n)] \\ p^*(-k) &= E[u^*(n-k)d(n) \\ r(i-k) &= E[u(n-k)u^*(n-i)] \end{aligned} \qquad \textit{Eqn 108}$$

A suitable cost function J is provided by the mean square of this error.

$$J = \sigma_d{}^2 - \sum_{k=0}^{M-1} w_k{}^* p(-k) + \sum_{k=0}^{M-1} w_k{}^* p^*(-k) + \sum_{k=0}^{M-1}\sum_{i=0}^{M-1} w_k{}^* w_i r(i-k) \qquad \textit{Eqn 109}$$

K.2.4 The double summation indicates that the mean squared error cost function is a second order function of the tap weights of the filter. The dependence of J on the tap weights can be visualised as an (M+1) dimensional surface with M degrees of freedom. The global minimum point J_{min} has a gradient vector $\nabla \mathbf{J}$ equal to zero i.e.

$$\nabla_k J = 0 \qquad k = 0,1,...M \qquad \textit{Eqn 110}$$

K.2.5 Considering complex weights $w_k = a_k + jb_k$

$$\begin{aligned} \nabla_k J &= \frac{\partial J}{\partial a_k} + \frac{\partial J}{\partial b_k} \\ &= -2p(-k) + 2\sum_{i=0}^{M-1} w_i r(i-k) \end{aligned} \qquad \textit{Eqn 111}$$

or in matrix notation

$$\begin{aligned} \nabla \mathbf{J} &= \begin{bmatrix} \dfrac{\partial J(n)}{\partial a_0(n)} + j\dfrac{\partial J(n)}{\partial b_0(n)} \\ \dfrac{\partial J(n)}{\partial a_1(n)} + j\dfrac{\partial J(n)}{\partial b_1(n)} \\ \vdots \\ \vdots \\ \dfrac{\partial J(n)}{\partial a_{M-1}(n)} + j\dfrac{\partial J(n)}{\partial b_{M-1}(n)} \end{bmatrix} \\ &= -2\mathbf{p} + 2\mathbf{R}\mathbf{w}(n) \end{aligned} \qquad \textit{Eqn 112}$$

and applying the minimum condition for the optimal solution

$$\sum_{i=0}^{M-1} w_{opt_i} r(i-k) = p(-k) \quad k = 0,1,\ldots M-1 \qquad \textit{Eqn 113}$$

K.2.6 This is the Weiner-Hopf equation defining optimal filter solution for a stationary random process. An adaptive transversal filter seeks to attain this solution and the method of steepest descent seeks to achieve the solution by successive computation of the gradient vector and movement of the solution in a direction opposite to that of the gradient vector. i.e.

$$\begin{aligned} \mathbf{w}(n+1) &= \mathbf{w}(n) + \frac{1}{2}\mu[-\nabla \mathbf{J}(n)] \\ &= \mathbf{w}(n) + \mu[\mathbf{p} - \mathbf{R}\mathbf{w}(n)] \qquad n = 0,1,2,.. \end{aligned} \qquad \textit{Eqn 114}$$

K.2.7 This recursive formulation of the steepest descent approach therefore requires knowledge of the correlation matrix $\boldsymbol{R}$ of the input stochastic process and the cross correlation of the input process and desired response.

K.2.8 A simple solution is to use snapshot estimates for the correlation matrix $\boldsymbol{R}$ and crosscorrelation **p.** i.e.

$$\begin{aligned} \hat{\mathbf{R}}(n) &= \mathbf{u}(n)\mathbf{u}^H(n) \\ \hat{\mathbf{p}}(n) &= \mathbf{u}(n)d^*(n) \end{aligned} \qquad \textit{Eqn 115}$$

K.2.9 Whilst these estimate are subject to large variances, the recursive implementation of the tap update introduces the necessary averaging during the iterative convergence period.

K.2.10 The gradient estimate is then given by

$$\hat{\nabla}\mathbf{J}(n) = -2\mathbf{u}(n)d^*(n) + 2\mathbf{u}(n)\mathbf{u}^H(n)\hat{\mathbf{w}}(n) \qquad \textit{Eqn 116}$$

and substituting into equation [115] gives

$$\hat{\mathbf{w}}(n+1) = \hat{\mathbf{w}}(n) + \mu\mathbf{u}(n)[d^*(n) - \mathbf{u}^H(n)\hat{w}(n)] \qquad \textit{Eqn 117}$$

K.2.11 This recursive formulation is the complex form of the LMS algorithm. There are a number of variations of the algorithm aimed at improving implementation efficiency and convergence behaviour. Phase only implementations of the algorithm serve to quantise either the complex error and/or the input tap element prior to coefficient update. Averaging the gradient vector prior to coefficient update is a technique used to reduce noise and improve steady state performance.

K.3 Convergence Properties of LMS

K.3.1 The convergence properties of the LMS algorithms are directly related to the channel properties. It can be shown that convergence is ensured if the step size parameter satisfies the inequality

$$0 < \Delta < \frac{2}{\lambda_{max}} \qquad \textit{Eqn 118}$$

K.3.2 where λ_{max} is the largest eigenvalue of the received signal autocorrelation matrix Γ. It can be further shown that the convergence rate is determined by the ratio of the largest to smallest eigenevalue of Γ. Practically this means that if the channel has large spectral nulls and is close to non-minimum phase (poles close to unit circle), then the convergence rate of the algorithm will be slow.

K.4 Least Squares

K.4.1 The least squares approach to optimal filtering is a deterministic method which unlike Wiener filter theory, does not depend upon explicit assumptions regarding the input signal statistics, namely the signal auto and cross correlation functions.

K.4.2 A commonly adopted model for the least squares implementation is the transversal filter where the desired response d is modelled as

$$d(i) = \sum_{k=0}^{M-1} w_k^* u(i-k) + e(i) \qquad \textit{Eqn 119}$$

w_k are the unknown model parameters and e is the stochastic measurement error. Under the assumption that e has zero mean and variance σ^2, the ensemble average of the desired response output can be written

$$E[d(i)] = \sum_{k=0}^{M-1} w_k^* u(i-k) \qquad \textit{Eqn 120}$$

K.4.3 Considering the output error

$$e(i) = d(i) - \sum_{k=0}^{M-1} w_k^* u(i-k) \qquad \textit{Eqn 121}$$

the cost function adopted for least squares methods is based on the sum of error squares. The aim is then to define the optimum weights which minimise the error energy over a predefined observation interval over which the weights are fixed i.e

$$\varepsilon(w_0, w_1 \ldots w_{M-1}) = \sum_{i=i1}^{i2} |e(i)|^2 = \sum_{i=i1}^{i2} e(i)e^*(i) \qquad \textit{Eqn 122}$$

where *i1,i2* define the observation interval.

K.4.4 Assuming complex weights of the form

$$w_k = a_k + jb_k \qquad \textit{Eqn 123}$$

the output error can be written

$$e(i) = d(i) - \sum_{k=0}^{M-1} (a_k - jb_k) u(i-k) \qquad \textit{Eqn 124}$$

K.4.5 The gradient vector $\nabla\varepsilon$ is the derivative of the cost function with respect to the real and imaginary weights w

$$\nabla_k \varepsilon = \begin{bmatrix} \frac{\partial \varepsilon}{\partial a_0} + j\frac{\partial \varepsilon}{\partial b_0} \\ \frac{\partial \varepsilon}{\partial a_1} + j\frac{\partial \varepsilon}{\partial b_1} \\ . \\ . \\ . \\ \frac{\partial \varepsilon}{\partial a_{M-1}} + j\frac{\partial \varepsilon}{\partial b_{M-1}} \end{bmatrix} \qquad \textit{Eqn 125}$$

K.4.6 This gradient vector is normal to the error performance surface. Considering the cost function derivative for the k'th weight

$$\nabla_k \varepsilon = \frac{\partial \varepsilon}{\partial a_k} + \frac{\partial \varepsilon}{\partial b_k}$$

$$\nabla_k \varepsilon = -\sum_{i=M}^{N} e(i)\frac{\partial e^*(i)}{\partial a_k} + e^*(i)\frac{\partial e(i)}{\partial a_k} + je(i)\frac{\partial e^*(i)}{\partial b_k} + je(i)\frac{\partial e(i)}{\partial b_k} \qquad \textit{Eqn 126}$$

K.4.7 Now differentiating *e(I)* with respect to real and imaginary parts of w_k gives the following four partial derivatives

$$\begin{aligned} \frac{\partial e(i)}{\partial a_k} &= -u(i-k) \\ \frac{\partial e^*(i)}{\partial a_k} &= -u^*(i-k) \\ \frac{\partial e(i)}{\partial b_k} &= ju(i-k) \\ \frac{\partial e^*(i)}{\partial b_k} &= -ju^*(i-k) \end{aligned} \qquad \textit{Eqn 127}$$

K.4.8 When these are substituted back into the cost function expression and the minimisation applied i.e

$$\nabla_k \varepsilon = -2\sum_{i=M}^{N} u(i-k)e_{\min}{}^*(i) = 0 \qquad \textit{Eqn 128}$$

K.4.9 This relationship demonstrates that the least squares condition is achieved when the received input time series *u(i-k)* is orthogonal to the minimum error time series.

K.4.10 Under the assumption that the filter is operating in this condition then the minimum output error is

$$e_{\min}(i) = d(i) - \sum_{t=0}^{M-1} \hat{w}_t^* u(i-t) \qquad \textit{Eqn 129}$$

and substituting for e_{min} gives

$$\sum_{t=0}^{M-1} \hat{w}_t \sum_{i=M}^{N} u(i-k)u^*(i-t) = \sum_{i=M}^{N} u(i-k)d^*(i) \qquad k = 0..,M-1 \qquad \textit{Eqn 130}$$

which is a system of M simultaneous equations. The summations with respect to i represent time averages. The inner summation on the left hand side is the time averaged autocorrelation of the received signal *u(t) i.e*

$$\phi(t,k) = \sum_{i=M}^{i=N} u(i-k)u^*(i-t) \qquad 0 \le (t,k) \le M-1 \qquad \textit{Eqn 131}$$

K.4.11 The summation on the right hand side is the cross correlation between the tap inputs and desired response i.e

$$z(-k) = \sum_{i=M}^{N} u(i-k)d^*(i) \qquad 0 \le k \le M-1 \qquad \textit{Eqn 132}$$

or in matrix form

$$\Phi\hat{\mathbf{w}} = \mathbf{z}$$

where

$$\Phi = \begin{bmatrix} \phi(0,0) & \phi(1,0) & . & \phi(M-1,0) \\ \phi(0,1) & \phi(1,0) & . & . \\ . & . & . & . \\ . & . & . & . \\ \phi(0,M-1) & \phi(1,M-1) & . & \phi(M-1,M-1) \end{bmatrix} \qquad \textit{Eqn 133}$$

$$\hat{\mathbf{w}} = [w_0, w_1, w_2, \ldots w_{M-1}]^T$$

$$\mathbf{z} = [z(0), z(-1), z(0) \ldots z(-M+1)]^T$$

K.4.12 This is the matrix form of the linear least squares filtering problem and is the least squares counterpart of the Weiner-Hopf equation. The optimum filter coefficients are obtained from the solution of the Weiner-Hopf equation which relies on Φ being non singular.

K.4.13 An established technique for the solution of this problem is the singular value decomposition (SVD) method [149] that is applicable to real, complex overdetermined and underdetermined cases. In practical applications the introduction of noise in the measurement variables coupled with the need for real time implementation generally precludes the direct solution of [133] above.

K.4.14 In many cases, including real time filtering applications it is desirable to reformulate the least squares filtering problem such that the optimum tap weights are arrived at through recursive iteration. This is the basis for recursive least squares (RLS) adaptive filtering. The underlying theory is closely related to Kalman filtering and this relationship can be used to improve the characteristics of RLS implementations.

K.5 Recursive Least Squares

K.5.1 In deriving the normal equations, the optimisation criteria were based on the minimisation of the sum of the error squares over a period where the filter weights were fixed. If operating in a non-stationary environment it is desirable to track statistical variations. For this reason in RLS implementations it is customary to introduce an error weighting term $\beta(n,i)$ into the cost function i.e

$$\varepsilon(n) = \sum_{i=1}^{n} \beta(n,i) \mid e(i) \mid^2 \qquad \textit{Eqn 134}$$

K.5.2 Since the length of the data is variable the observation interval is also variable extending from index 1 to n. An established weighting function is the exponential which serves to weight recent errors more heavily than previous ones. This imparts the recursive algorithm the ability to track. The cost function becomes

$$\varepsilon(n) = \sum_{i=1}^{n} \lambda^{n-1} \mid e(i) \mid^2 \qquad \textit{Eqn 135}$$

and the exponential serves as a weighting term for the input tap vector i.e.

$$\Phi(n) = \sum_{i=1}^{n} \lambda^{n-i} \mathbf{u}(i)\mathbf{u}^H(i)$$
$$\mathbf{z}(n) = \sum_{i=1}^{n} \lambda^{n-i} \mathbf{u}(i)d^*(i) \qquad \textit{Eqn 136}$$

K.5.3 A recursive formulation for the correlation matrix can be obtained by isolating the term corresponding to i=n i.e

$$\Phi(n) = \sum_{i=1}^{n-1} \lambda^{n-1-i} \mathbf{u}(i)\mathbf{u}^H(i) + \mathbf{u}(i)\mathbf{u}^H(i)$$

so *Eqn 137*

$$\Phi(n) = \lambda\Phi(n-1) + \mathbf{u}(i)\mathbf{u}^H(i)$$

simillary one can obtain a recursive formulation for the cross correlation vector,

$$\mathbf{z}(n) = \lambda \mathbf{z}(n-1) + u(n)d^*(n) \qquad \textit{Eqn 138}$$

K.5.4 Since the solution of the normal equations requires the inverse to the correlation matrix it is necessary to reformulate the recursion for the correlation matrix to an equivalent recursion for the inverse correlation matrix.

K.5.5 This is realised by using the matrix inversion lemma. It can be shown that if ***A*** and ***B*** are two positive definite M by M matrices related by

$$\mathbf{A} = \mathbf{B}^{-1} + \mathbf{C}\mathbf{D}^{-1}\mathbf{C}^H \qquad \textit{Eqn 139}$$

where **C** is M by N positive definite and **D** is N by M positive definite then the inverse of **A** may be expressed

$$\mathbf{A}^{-1} = \mathbf{B} - \mathbf{B}\mathbf{C}(\mathbf{D} + \mathbf{C}^{\mathrm{H}}\mathbf{B}\mathbf{C})^{-1}\mathbf{C}\mathbf{B} \qquad \textit{Eqn 140}$$

K.5.6 Now letting

$$\begin{aligned} \mathbf{A} &= \Phi(n) \\ \mathbf{B}^{-1} &= \lambda\Phi(n-1) \\ \mathbf{C} &= \mathbf{u}(n) \\ \mathbf{D} &= 1 \end{aligned} \qquad \textit{Eqn 141}$$

and performing the substitution

$$\Phi^{-1}(n) = \lambda^{-1}\Phi^{-1}(n-1) - \frac{\lambda^{-2}\Phi^{-1}(n-1)\mathbf{u}(n)\mathbf{u}^H(n)\Phi^{-1}(n-1)}{1+\lambda^{-1}\mathbf{u}^H(n)\Phi^{-1}(n-1)\mathbf{u}(n)} \qquad \textit{Eqn 142}$$

letting

$$\mathbf{P}(n) = \Phi^{-1}(n)$$

and

$$\mathbf{k}(n) = \frac{\lambda^{-1}\mathbf{P}(n-1)\mathbf{u}(n)}{1+\lambda^{-1}\mathbf{u}^H(n)\Phi^{-1}(n-1)\mathbf{u}(n)} \qquad \textit{Eqn 143}$$

gives

$$\mathbf{P}(n) = \lambda^{-1}\mathbf{P}(n-1) - \lambda^{-1}\mathbf{k}(n)\mathbf{u}^H(n)\mathbf{P}(n-1)$$

K.5.7 The recursion in ***P(n)*** is the Ricatti equation for the RLS algorithm. **k*(n)*** is the gain vector in light of its correspondence with the Kalman gain term in Kalman filtering.

K.6 Square Root Adaptive Filters

K.6.1 The recursion in the Ricatti equation propagates the matrix correlation **P.** This formulation can lead to problems of numerical instability through quantisation and numerical round-off [150,151]. Square root adaptive filters overcome this problem by propagating a lower triangular form of the correlation matrix. One form of the square root adaptive filter is the QR decomposition based RLS algorithm or QR-RLS. This algorithm exploits the QR decomposition of the incoming data matrix rather than the time averaged correlation matrix as in the conventional RLS approach. In practice the QR decomposition may be realised through the repeated application of Givens rotations designed to zero selected elements in a pre-array as follows.

$$\begin{bmatrix} \lambda^{1/2}\Phi^{1/2}(n-1) & \mathbf{u}(n) \\ \lambda^{1/2}\mathbf{p}^H(n-1) & d(n) \\ \mathbf{0}^T & 1 \end{bmatrix} \Theta(n) = \begin{bmatrix} \Phi^{1/2}(n) & \mathbf{0} \\ \mathbf{p}^H(n) & \xi(n)\gamma^{1/2}(n) \\ \mathbf{u}^H(n)\Phi^{-H/2}(n) & \gamma^{1/2}(n) \end{bmatrix} \qquad \textit{Eqn 144}$$

$$\hat{\mathbf{w}}^H(n) = \mathbf{p}^H(n)\Phi^{-1/2}(n)$$

K.6.2 The algorithm proceeds by initialising the block matrix prearray with initial conditions

$\Phi^{1/2}(0) = \mathbf{0}$ and $\mathbf{p}(0)=\mathbf{0}$

K.6.3 The orthogonal matrix Θ implements a series of Givens rotations, otherwise known as Jacobi rotations which introduce the block zero column entry in the post array. The resulting post array matrix provides the updated $\mathbf{p}(n)$ and $\Phi(n)$ with which to repeat the recursions and to solve for the least squares weight vector. The application of Givens rotations is demonstrated below

Premultiplication Affects Rows Only
Rot(i,j) j>i

$$RowRot(0,1)\begin{bmatrix} c & s & 0 & 0 \\ -s & c & 0 & 0 \\ 0 & 0 & 1 & 0 \\ 0 & 0 & 0 & 1 \end{bmatrix}^T x \begin{bmatrix} a_{00} & a_{01} & a_{02} & a_{03} \\ a_{10} & a_{11} & a_{12} & a_{13} \\ a_{20} & a_{21} & a_{22} & a_{23} \\ a_{30} & a_{31} & a_{32} & a_{33} \end{bmatrix} = \begin{bmatrix} c.a_{00} - s.a_{10} & c.a_{01} - s.a_{11} & c.a_{02} - s.a_{12} & c.a_{03} - s.a_{13} \\ sa_{00} + ca_{10} & sa_{01} + ca_{11} & sa_{02} + ca_{12} & sa_{03} + ca_{13} \\ a_{20} & a_{21} & a_{22} & a_{23} \\ a_{30} & a_{31} & a_{32} & a_{33} \end{bmatrix}$$

$$RowRot(0,2)\begin{bmatrix} c & 0 & s & 0 \\ 0 & 1 & 0 & 0 \\ -s & 0 & c & 0 \\ 0 & 0 & 0 & 1 \end{bmatrix}^T x \begin{bmatrix} a_{00} & a_{01} & a_{02} & a_{03} \\ a_{10} & a_{11} & a_{12} & a_{13} \\ a_{20} & a_{21} & a_{22} & a_{23} \\ a_{30} & a_{31} & a_{32} & a_{33} \end{bmatrix} = \begin{bmatrix} c.a_{00} - s.a_{20} & c.a_{01} - s.a_{21} & c.a_{02} - s.a_{22} & c.a_{03} - s.a_{23} \\ a_{10} & a_{11} & a_{12} & a_{13} \\ sa_{00} + ca_{20} & sa_{01} + ca_{21} & sa_{02} + ca_{22} & sa_{03} + ca_{23} \\ a_{30} & a_{31} & a_{32} & a_{33} \end{bmatrix}$$

$$RowRot(0,3)\begin{bmatrix} c & 0 & 0 & s \\ 0 & 1 & 0 & 0 \\ 0 & 0 & 1 & 0 \\ -s & 0 & 0 & c \end{bmatrix}^T x \begin{bmatrix} a_{00} & a_{01} & a_{02} & a_{03} \\ a_{10} & a_{11} & a_{12} & a_{13} \\ a_{20} & a_{21} & a_{22} & a_{23} \\ a_{30} & a_{31} & a_{32} & a_{33} \end{bmatrix} = \begin{bmatrix} c.a_{00} - s.a_{30} & c.a_{01} - s.a_{31} & c.a_{02} - s.a_{32} & c.a_{03} - s.a_{33} \\ a_{10} & a_{11} & a_{12} & a_{13} \\ a_{20} & a_{21} & a_{22} & a_{23} \\ sa_{00} + ca_{30} & sa_{01} + ca_{31} & sa_{02} + ca_{32} & sa_{03} + ca_{33} \end{bmatrix}$$

$$RowRot(1,2)\begin{bmatrix} 1 & 0 & 0 & 0 \\ 0 & c & s & 0 \\ 0 & -s & c & 0 \\ 0 & 0 & 0 & 1 \end{bmatrix}^T x \begin{bmatrix} a_{00} & a_{01} & a_{02} & a_{03} \\ a_{10} & a_{11} & a_{12} & a_{13} \\ a_{20} & a_{21} & a_{22} & a_{23} \\ a_{30} & a_{31} & a_{32} & a_{33} \end{bmatrix} = \begin{bmatrix} a_{00} & a_{01} & a_{02} & .a_{03} \\ ca_{10} - sa_{20} & ca_{11} - sa_{21} & ca_{12} - sa_{22} & ca_{13} - sa_{23} \\ sa_{10} + ca_{20} & sa_{11} + ca_{21} & sa_{12} + ca_{22} & sa_{13} + ca_{23} \\ a_{30} & a_{31} & a_{32} & a_{33} \end{bmatrix}$$

$$RowRot(1,3)\begin{bmatrix} 1 & 0 & 0 & 0 \\ 0 & c & 0 & s \\ 0 & 0 & 1 & 0 \\ 0 & -s & 0 & c \end{bmatrix}^T x \begin{bmatrix} a_{00} & a_{01} & a_{02} & a_{03} \\ a_{10} & a_{11} & a_{12} & a_{13} \\ a_{20} & a_{21} & a_{22} & a_{23} \\ a_{30} & a_{31} & a_{32} & a_{33} \end{bmatrix} = \begin{bmatrix} a_{00} & a_{01} & a_{02} & .a_{03} \\ ca_{10} - sa_{30} & ca_{11} - sa_{31} & ca_{12} - sa_{32} & ca_{13} - sa_{33} \\ a_{20} & a_{21} & a_{22} & a_{23} \\ sa_{10} + ca_{30} & sa_{11} + ca_{31} & sa_{12} + ca_{32} & sa_{13} + ca_{33} \end{bmatrix}$$

$$RowRot(2,3)\begin{bmatrix} 1 & 0 & 0 & 0 \\ 0 & 1 & 0 & 0 \\ 0 & 0 & c & s \\ 0 & 0 & -s & c \end{bmatrix}^T x \begin{bmatrix} a_{00} & a_{01} & a_{02} & a_{03} \\ a_{10} & a_{11} & a_{12} & a_{13} \\ a_{20} & a_{21} & a_{22} & a_{23} \\ a_{30} & a_{31} & a_{32} & a_{33} \end{bmatrix} x \begin{bmatrix} a_{00} & a_{01} & a_{02} & .a_{03} \\ a_{10} & a_{11} & a_{12} & a_{13} \\ ca_{20} - sa_{30} & ca_{21} - sa_{31} & ca_{22} - sa_{32} & ca_{23} - sa_{33} \\ sa_{20} + ca_{30} & sa_{21} + ca_{31} & sa_{22} + ca_{32} & sa_{23} + ca_{33} \end{bmatrix}$$

Etc...

Postmultiplication Affects Columns Only

Rot(i,j) j>i

$$ColRot(0,1)\begin{bmatrix} a_{00} & a_{01} & a_{02} & a_{03} \\ a_{10} & a_{11} & a_{12} & a_{13} \\ a_{20} & a_{21} & a_{22} & a_{23} \\ a_{30} & a_{31} & a_{32} & a_{33} \end{bmatrix} x \begin{bmatrix} c & s & 0 & 0 \\ -s & c & 0 & 0 \\ 0 & 0 & 1 & 0 \\ 0 & 0 & 0 & 1 \end{bmatrix} = \begin{bmatrix} ca_{00} - sa_{01} & sa_{00} + ca_{01} & a_{02} & a_{03} \\ ca_{10} - sa_{11} & sa_{10} + ca_{11} & a_{12} & a_{13} \\ ca_{20} - sa_{21} & sa_{20} + ca_{21} & a_{22} & a_{23} \\ ca_{30} - sa_{31} & sa_{30} + ca_{31} & a_{32} & a_{33} \end{bmatrix}$$

$$ColRot(0,2)\begin{bmatrix} a_{00} & a_{01} & a_{02} & a_{03} \\ a_{10} & a_{11} & a_{12} & a_{13} \\ a_{20} & a_{21} & a_{22} & a_{23} \\ a_{30} & a_{31} & a_{32} & a_{33} \end{bmatrix} x \begin{bmatrix} c & 0 & s & 0 \\ 0 & 1 & 0 & 0 \\ -s & 0 & c & 0 \\ 0 & 0 & 0 & 1 \end{bmatrix} = \begin{bmatrix} ca_{00} - sa_{02} & a_{01} & sa_{00} + ca_{02} & a_{03} \\ ca_{10} - sa_{12} & a_{11} & sa_{10} + ca_{12} & a_{13} \\ ca_{20} - sa_{22} & a_{21} & sa_{20} + ca_{22} & a_{23} \\ ca_{30} - sa_{32} & a_{31} & sa_{30} + ca_{32} & a_{33} \end{bmatrix}$$

$$ColRot(0,3)\begin{bmatrix} a_{00} & a_{01} & a_{02} & a_{03} \\ a_{10} & a_{11} & a_{12} & a_{13} \\ a_{20} & a_{21} & a_{22} & a_{23} \\ a_{30} & a_{31} & a_{32} & a_{33} \end{bmatrix} x \begin{bmatrix} c & 0 & 0 & s \\ 0 & 1 & 0 & 0 \\ 0 & 0 & 1 & 0 \\ -s & 0 & 0 & c \end{bmatrix} = \begin{bmatrix} ca_{00} - sa_{03} & a_{01} & a_{02} & sa_{00} + ca_{03} \\ ca_{10} - sa_{13} & a_{11} & a_{12} & sa_{10} + ca_{13} \\ ca_{20} - sa_{23} & a_{21} & a_{22} & sa_{20} + ca_{23} \\ ca_{30} - sa_{33} & a_{31} & a_{32} & sa_{30} + ca_{33} \end{bmatrix}$$

$$ColRot(1,2)\begin{bmatrix} a_{00} & a_{01} & a_{02} & a_{03} \\ a_{10} & a_{11} & a_{12} & a_{13} \\ a_{20} & a_{21} & a_{22} & a_{23} \\ a_{30} & a_{31} & a_{32} & a_{33} \end{bmatrix} x \begin{bmatrix} 1 & 0 & 0 & 0 \\ 0 & c & s & 0 \\ 0 & -s & c & 0 \\ 0 & 0 & 0 & 1 \end{bmatrix} = \begin{bmatrix} a_{00} & ca_{01} - sa_{02} & sa_{01} + ca_{02} & a_{03} \\ a_{10} & ca_{11} - sa_{12} & sa_{11} + ca_{12} & a_{13} \\ a_{20} & ca_{21} - sa_{22} & sa_{21} + ca_{22} & a_{23} \\ a_{30} & ca_{31} - sa_{32} & sa_{31} + ca_{32} & a_{23} \end{bmatrix}$$

$$ColRot(1,3)\begin{bmatrix} a_{00} & a_{01} & a_{02} & a_{03} \\ a_{10} & a_{11} & a_{12} & a_{13} \\ a_{20} & a_{21} & a_{22} & a_{23} \\ a_{30} & a_{31} & a_{32} & a_{33} \end{bmatrix} x \begin{bmatrix} 1 & 0 & 0 & 0 \\ 0 & c & 0 & s \\ 0 & 0 & 1 & 0 \\ 0 & -s & 0 & c \end{bmatrix} = \begin{bmatrix} a_{00} & ca_{01} - sa_{03} & a_{02} & sa_{01} + ca_{03} \\ a_{10} & ca_{11} - sa_{13} & a_{12} & sa_{11} + ca_{13} \\ a_{20} & ca_{21} - sa_{23} & a_{22} & sa_{21} + ca_{23} \\ a_{30} & ca_{31} - sa_{33} & a_{32} & sa_{31} + ca_{33} \end{bmatrix}$$

$$ColRot(2,3)\begin{bmatrix} a_{00} & a_{01} & a_{02} & a_{03} \\ a_{10} & a_{11} & a_{12} & a_{13} \\ a_{20} & a_{21} & a_{22} & a_{23} \\ a_{30} & a_{31} & a_{32} & a_{33} \end{bmatrix} \begin{bmatrix} 1 & 0 & 0 & 0 \\ 0 & 1 & 0 & 0 \\ 0 & 0 & c & s \\ 0 & 0 & -s & c \end{bmatrix} \begin{bmatrix} a_{00} & a_{01} & ca_{02} - sa_{03} & sa_{02} + ca_{03} \\ a_{10} & a_{11} & ca_{12} - sa_{13} & sa_{12} + ca_{13} \\ a_{20} & a_{21} & ca_{22} - sa_{23} & sa_{22} + ca_{23} \\ a_{30} & a_{31} & ca_{32} - sa_{33} & sa_{32} + ca_{33} \end{bmatrix}$$

$$\begin{bmatrix} c & -s \\ s & c \end{bmatrix} \begin{bmatrix} a \\ b \end{bmatrix} = \begin{bmatrix} a\cos\theta - b\sin\theta \\ a\sin\theta + b\cos\theta \end{bmatrix} = \begin{bmatrix} r \\ 0 \end{bmatrix}$$

$$r = a\cos\theta - b\sin\theta$$
$$a\sin\theta = -b\cos\theta$$

$$\tau = \frac{b}{a} = \frac{\sin\theta}{\cos\theta} = \tan\theta$$
$$\frac{1}{\sqrt{1+\tau^2}} = \frac{1}{\sqrt{1+\tan^2\theta}} = \frac{1}{\sqrt{\sec^2\theta}} = \cos\theta$$

L Multirrate Systems and Fractional Delay Synthesis

L.1 Overview

L.1.1 In many signal processing problems there is often a need to implement delays which are a non integer multiple of the system sampling rate. This requirement is common in underwater acoustic signal processing and in communication synchronisation systems where optimum symbol timing epoch has to be maintained where, for example a fractional equaliser is not used. For signal processing chains involving multiple sampling rates, changing from one sampling rate to another requires the implementation of a fractional delay on a sample by sample basis. In this case implementation complexity as well as signal fidelity becomes a significant factor since the fractional delay filter design must be updated, often on a sample by sample basis, which could introduce significant processing overhead in real time applications.

L.1.2 Such multirate processing techniques are directly relevant to the acoustic Doppler processing problem since the variation in sampling frequency is analogous to the temporal scaling influence of Doppler. The problem of implementing non-integer delays is essentially one of interpolation.

L.1.3 There is fortunately an extensive source of literature on fractional delay filter synthesis for both FIR and IIR implementations. The following discussion is based on the excellent review paper by T.Laakso et al [80].

L.1.4 The Z transform of a delay D is implemented through z^{-D} i.e.

$$Z\{x(n-D)\} = z^{-D}X(z) \qquad \textit{Eqn 145}$$

L.1.5 For the case

$$D=INT(D)+d \qquad \text{Eqn 146}$$

one must approximate the fractional delay part d. Considering the problem in the frequency domain the ideal transfer function has unity magnitude response and linear phase i.e.

$$\begin{aligned} &H_{ideal}(\omega) = \exp - j\omega D \\ &|H_{ideal}(\omega)| = 1 \quad for all \omega \\ &\arg(H_{ideal}(\omega)) = \Theta_{ideal}(w) = -D\omega \end{aligned} \qquad \text{Eqn 147}$$

L.1.6 The group delay and the phase delay of the transfer function are defined

$$\tau_g(\omega) = -\frac{\partial\Theta(\omega)}{\partial\omega} \qquad \tau_p(\omega) = -\frac{\Theta(\omega)}{\omega} \qquad \text{Eqn 148}$$

L.1.7 The ideal filter implementation of the delay D is the impulse response obtained from the inverse Fourier transform of $H_{ideal}(\omega)$.

$$\begin{aligned} h_{ideal}(n) &= \frac{1}{2\pi}\int_{-\pi}^{+\pi} H_{ideal}(\omega)\exp(j\omega n)d\omega \qquad for\ all\ n \\ h_{ideal}(n) &= \frac{\sin(\pi(n-D))}{\pi(n-D)} = \sin c(n-D) \qquad for\ all\ n \end{aligned} \qquad \text{Eqn 149}$$

L.1.8 So, for integer delays the impulse response reduces to a single impulse at $n=D$ and for fractional delays the impulse response is an infinitely long shifted and sampled version of the sinc function. The significance of this result is that any fractional delay filter design must approximate this solution within the constraints imposed by practical implementation.

L.1.9 An obvious (and optimal in the Least Squared Error sense) solution to the FIR implementation is to truncate the ideal solution thus

$$h(n) = \begin{cases} \sin c(n-D) & for M \le n \le M+N \\ 0 & otherwise \end{cases} \qquad Eqn\ 150$$

where

M is the time index of the first nonzero value of the impulse response

N is the order of the FIR filter.

L.1.10 Unfortunately this solution suffers from ripples in the passband due to the Gibbs phenomenon which limits its practical application. However it is to be stressed that this solution is optimal in the sense of minimising the mean squared error between desired and achievable filter designs in either time or frequency domains.

L.1.11 Time domain weighting of the ideal sinc filter enables more flexible control over transition band and ripple characteristics. Practical implementation of such filter designs is fast and simple and readily suited to real time filter coefficient update as required for example in timing re-sampling loops such as Delay Lock Loops.

L.1.12 An alternative approach to minimising the least squared error function

$$E(e^{j\omega}) = H(e^{j\omega}) - H_{ideal}(e^{j\omega}) \qquad Eqn\ 151$$

over the complete band, is to ensure that the error function is maximally flat at a set frequency so that the approximation is best when close to this frequency. This means setting the derivatives of the frequency domain error function to zero at this point i.e

$$\left.\frac{d^n E(e^{j\omega})}{d\omega^n}\right|_{\omega=\omega_0} = 0 \qquad for\ n = 0,1,2...N \qquad Eqn\ 152$$

L.1.13 Differentiating and setting $\omega_0 = 0$ results in a set of $L=N+1$ linear equations which can be expressed in terms of the impulse response as

$$\sum_{k=0}^{N} k^n h(k) = D^n \quad for\, n = 0,1,2...N \qquad Eqn\ 153$$

or in matrix form

$$\mathbf{V.h} = \mathbf{v}$$

where

$$\mathbf{h} = [h(0)h(1)...h(N)]^T$$

$$\mathbf{v} = [1DD^2...D^N]^T$$

$$\mathbf{V} = \begin{bmatrix} 1 & 1 & 1 & .. & 1 \\ 0 & 1 & 2 & & N \\ 0 & 1 & 2^2 & & N \\ : & & & & : \\ 0 & 1 & 2^N & & N^N \end{bmatrix} \qquad Eqn\ 154$$

L.1.14 The solution to the above is equivalent to the Lagrangian interpolation formulae

$$h(n) = \prod_{k=0_{k\neq n}}^{N} \frac{D-k}{n-k} \quad for n = 0,1,2...N \qquad Eqn\ 155$$

L.1.15 A number of important issues arise from this form of interpolator:-

- the case N=1 corresponds to linear interpolation i.e h(0)=1-D,h(1)=D.;
- even length filters have the advantage of linear phase but suffer from rapid tail off in the magnitude response to zero at $\omega = \pi$;
- odd length filters have better magnitude response but the phase response is non-linear.
- whilst the performance of Lagrangian based FIR filter designs is good at low order, only modest improvement in fidelity is achieved as the filter order is increased.

L.1.16 The least squares and maximally flat techniques suffer from the lack of control one has over the peak error in a defined approximation band. Minimax design techniques strive to contain this error within a predefined tolerance scheme. The iterative nature of the solution to such an approach (such as the Remez algorithm) however, is not suited to real time coefficient update. In real time implementations of fractional delay filters, the time overhead of re-calculating filter coefficients often limits their use in practice. A technique for the efficient implementation of a continuously variable delay element has been proposed by Farrow [80]. The technique involves designing the filter coefficients off line and then implementing a P'th order polynomial in delay d as an approximation for each coefficient

$$h_d(n) = \sum_{m=0}^{P} c_m(n) d^m \qquad n = 0,1,2...N \qquad \textit{Eqn 156}$$

where

$c_m(n)$ are real valued approximating coefficients.

L.1.17 The transfer function of the filter is

$$H_d(z) = \sum_{n=0}^{N} h_d(n) z^{-n} = \sum_{n=0}^{N} \left[\sum_{m=0}^{P} c_m(n) d^m \right] z^{-n} = \sum_{m=0}^{P} \left[\sum_{n=0}^{N} c_m(n) z^{-n} \right] d^m = \sum_{m=0}^{P} C_m(z) d^m$$

where *Eqn 157*

$$C_m(z) = \sum_{n=0}^{N} c_m(n) z^{-n}$$

L.1.18 The form of the above equation implies the structure shown in Figure 76 below. characterised by fixed coefficients and a re-programmable delay d.

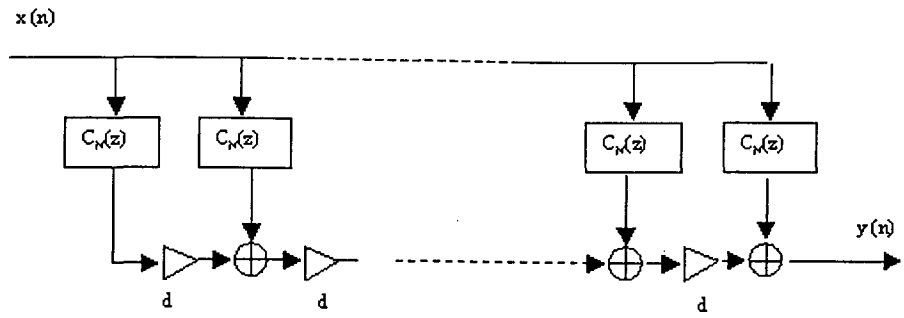

Figure 76: Farrow implementation of Fractional Delay Filter

L.1.19 A review of a number of fractional delay filters is presented by Cain. The review focuses on the performance trade offs inherent in each filter design as a function of measurement bandwidth and fractional delay. The author advocates the use of Polynomial based interpolators for full band applications where 15 or more taps are acceptable

L.1.20 Figure 77 shows the magnitude responses of Lagrangian interpolators or even and odd orders up to 10 for the fractional delay d=0.5 which represents the extreme limit on the filter performance. Also shown is the phase response for odd taps. The phase response for even taps is linear.

L.1.21 The top and middle graphs show the magnitude response of the filter for the cases n even and odd respectively. The results demonstrate that for filter lengths as low as 4-5 taps, the filter achieves flat, unity passband performance up to approximately Fs/5. However as the filter order is increased, there is only moderate increase in the passband performance, typically up to Fs/4 for 10-11 taps. Of note is the fact that the magnitude response falls to zero at Fs/2 for even implementations. However the advantage gained is the linear, zero phase response. For odd implementations, the phase response mirrors that of the magnitude response with non zero, non linear phase at frequencies typically above Fs/4.

L.1.22 Figure 78 shows the magnitude and phase response of a Kaiser windowed Sinc interpolator, based on a table lookup algorithm developed for real time DSP implementation.

L.1.23 The top graph depicts the magnitude response for the case d=0.5. Evident from the figure is passband ripple, reducing with filter order and a wider passband performance of 0.35.Fs for 11 taps. The filter phase response is also subject to passband ripple, which reduces with filter order. For filter orders of 9taps or more this ripple is typically less than 0.1 degrees.

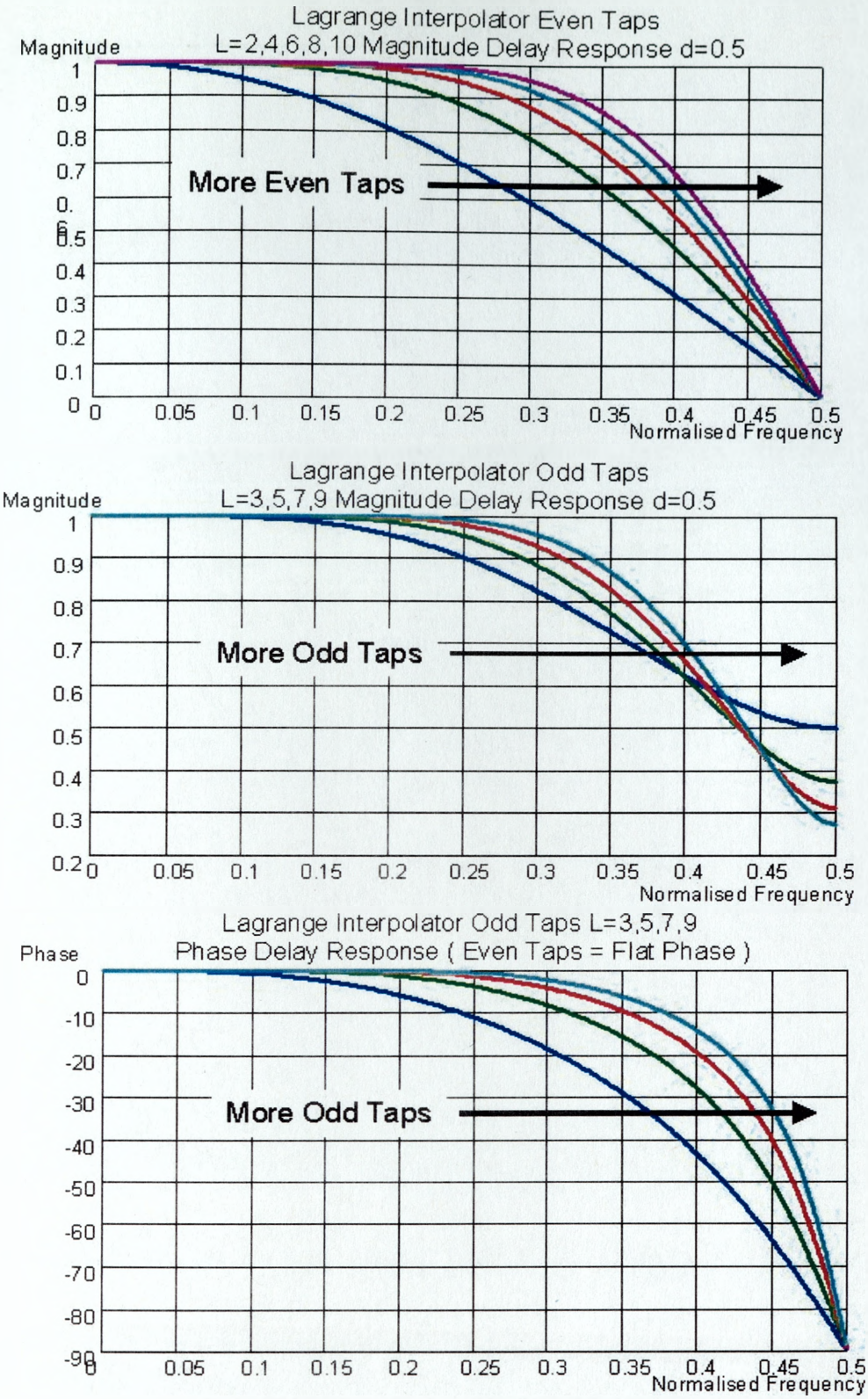

Figure 77; Magnitude and Phase response of Lagrange Fractional Delay Filter

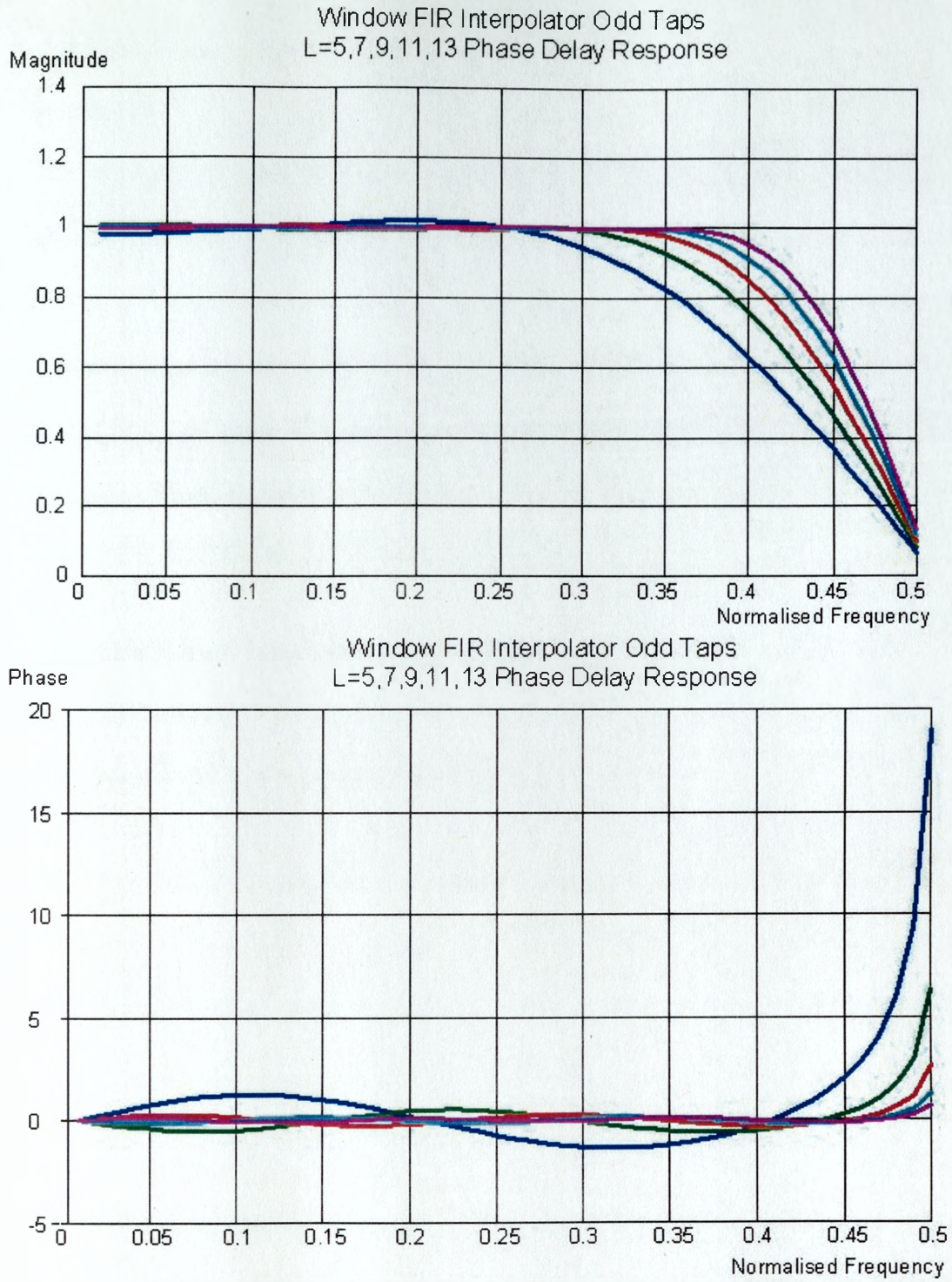

Figure 78: Magnitude and Phase response of windowed Sinc Fractional Delay Filter

M Optimum Binary Receiver In Doubly Spread Channels

M.1 Overview

M.1.1 The acoustic channel is dispersive in time and frequency and this has a profound influence on the performance of digital acoustic communication systems which are imprecisely synchronised. The following discussion considers the performance of an optimum binary receiver operating in a doubly dispersive channel for synchronised and unsynchronised cases. The analysis is formulated in terms of the transmission waveform ambiguity function and the channel scattering function and serves to highlight the need to best match the transmission characteristics to the channel in underwater acoustics.

M.2 Optimum Binary Receiver In Fading Dispersive Acoustic Channels

M.2.1 The optimum binary receiver is one which compares a likelihood ratio l with a threshold η to obtain two hypotheses H0,H1[78] thus:-

$$\begin{aligned} H0 &: \quad l < \eta \quad (noise\ only) \\ H1 &: \quad l > \eta \quad (signal + noise) \end{aligned}$$

where *Eqn 158*

$$l = \frac{1}{N_0{}^2} \int_{T1}^{T2} \int z^*(t) R(t,\tau) z(\tau) dt d\tau$$

M.2.2 Where $z(t)$ comprises the received waveform R() is the channel scattering function. Based on this condition Van Trees demonstrated that the probabilities of false alarm and detection are given by

$$P_F = Q(\frac{d}{2} + \frac{\eta}{d})$$

$$P_D = Q(\frac{\eta}{d} - \frac{d}{2})$$

where

$$d \equiv \sqrt{\frac{(E\{l|H_1\} - E\{l|\, H_0\})^2}{Var\{l \mid H_0\}}} \qquad \textit{Eqn 159}$$

and

$$Q(x) = \int_x^\infty \frac{1}{2\pi} \exp[\frac{-x^2}{2}]dx$$

M.2.3 In computing the signal-to-noise parameter *d,* it is necessary to consider the time averaged likelihood ratio for signal present and signal absent cases. By substituting the complex correlation envelope of the received process $R(t,\tau)$ into the likelihood ratio l, it is possible to compute *d* and hence determine the detection and false alarm probabilities.

M.2.4 Although presented in terms of signal-to-noise ratio, it is possible to consider the performance degradation of the optimum receiver under imprecise synchronisation conditions since the complex envelope of the received process can be expressed in terms of the transmitted waveform ambiguity function and channel scattering function.

M.2.5 In [75] Solimon presents a theoretical analysis of open and closed loop synchronisation techniques based on the optimum receiver approach. Solimon considers the case of a receiver operating under imprecise time and frequency synchronisation. In this case it is assumed that the true and estimated channel scattering functions are related by

$$\sigma_{est}(r,f) = \sigma_{true}(r - \Delta x_1, f - \Delta x_2) \qquad \textit{Eqn 160}$$

M.2.6 In this case the dimensionless decision parameter d is given by

$$d = \sqrt{\frac{\left[\iiint\int \sigma_{true}(r,f)\sigma_{true}(r',f')|\chi(r-r'+\Delta x_1, f-f'+\Delta x_2)|^2\, drdfdr'df'\right]^2}{\iiint\int \sigma_{true}(r,f)\sigma_{true}(r',f')|\chi(r-r',f-f')|^2\, drdfdr'df'}} \qquad \textit{Eqn 161}$$

which introduces the transmitted waveform ambiguity function

$$\chi(\tau,f) = \int_{-\infty}^{+\infty} u(t)u^*(t-\tau)\exp(j2\pi ft)dt \qquad \textit{Eqn 162}$$

M.2.7 The performance of an optimum detector is therefore a function of the channel scattering characteristics and transmission waveform ambiguity. Specifically d involves the two dimensional convolution of the transmission waveform ambiguity function with the channel scattering function. The result is multiply-integrated with the true channel scattering function which, when normalised for the perfect alignment case, results in the dimensionless 'signal-to-noise' parameter d with a value between 0 and 1. This is illustrated in Figure 79.

M.2.8 Evidently the performance of the receiver relies heavily on the ability of the receiver to synchronise in both time and frequency. The exact performance degradation under imprecise matching is heavily dependent on the nature of the channel scattering function and waveform ambiguity,

M.2.9 Based on knowledge of the transmitted waveform ambiguity function and the channel scattering statistics it is therefore possible to compute the probability of detection and false alarm for an optimum binary receiver.

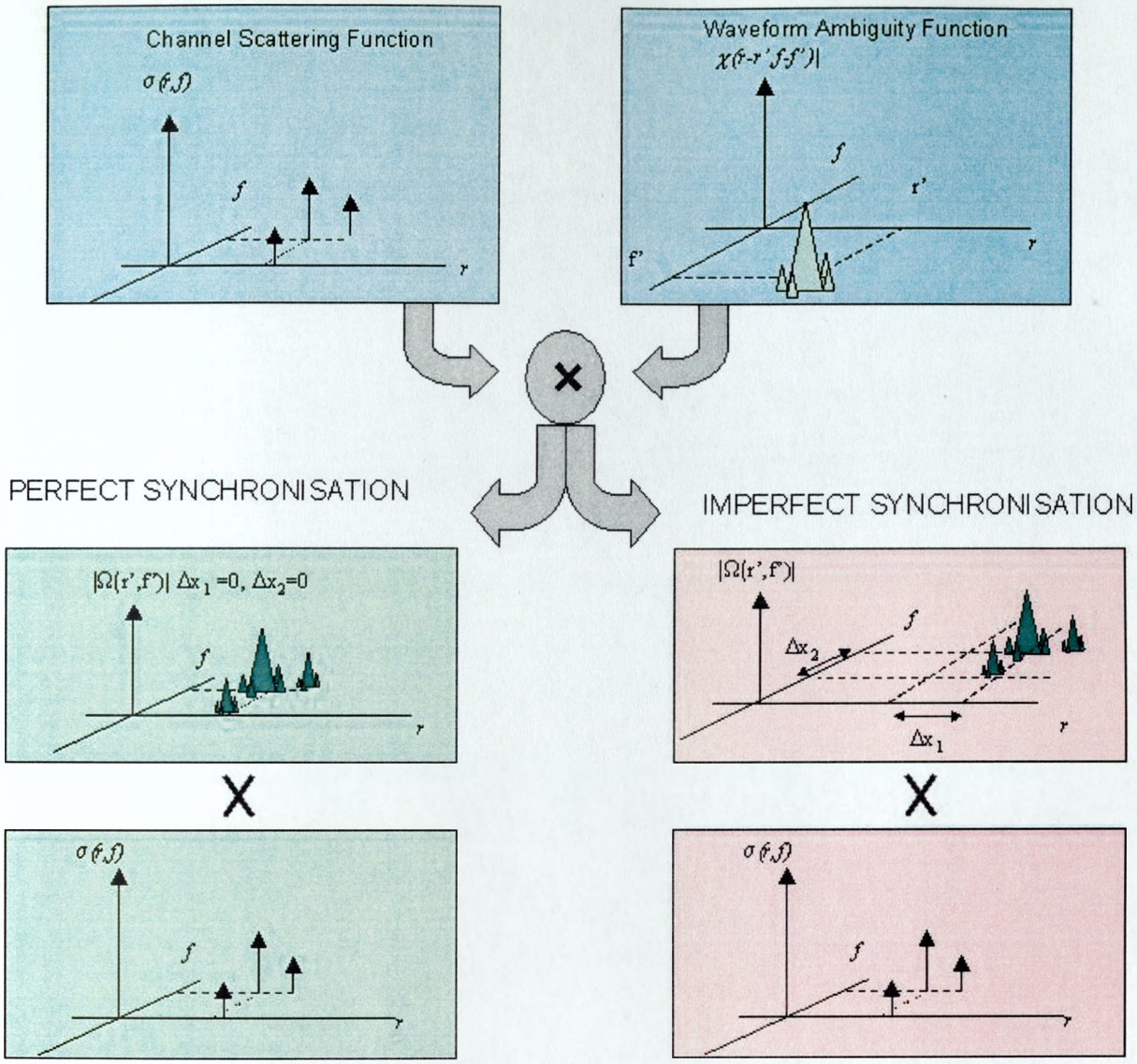

$$d^2 = \frac{\left[\iiint \sigma_{true}(r,f)\,\sigma_{true}(r',f')\,|\chi(r-r'+\Delta x_1, f-f'+\Delta x_2)|^2\, dr df dr' df'\right]^2}{\iiint \sigma_{true}(r,f)\,\sigma_{true}(r',f')\,|\chi(r-r', f-f')|^2\, dr df dr' df'}$$

Figure 79; Pictorial representation of the dimensionless decision parameter d

M.2.10 Based on a simple channel scattering function of the form

$$\sigma(r,f) = \frac{E_r}{2\pi BL}\exp(-r^2/2L^2 - f^2/2B^2)$$

where *Eqn 163*

E_r = *total received energy*
B = *channel Doppler Spread*
L = *channel multipath spread*

and a simple a simple waveform envelope as in an amplitude shift keyed telemetry system:-

$$u(t) = \begin{cases} \frac{1}{\sqrt{T}}, & 0 \le t \le T \\ 0 & \textit{elsewhere} \end{cases} \qquad \textit{Eqn 164}$$

it is possible to determine the probability of detecting such a waveform as a function of channel spread parameters B and L and time-frequency misalignment parameters *x1* and *x2*.

M.2.11 The ambiguity function of this simple waveform is given by

$$\phi(\tau,\omega) = \begin{cases} \frac{1}{T}\int_{-\frac{1}{2}(T-|\tau|)}^{\frac{1}{2}(T-|\tau|)} \exp j\omega t\,dt & \tau \le T \\ 0 & \textit{elsewhere} \end{cases}$$

so *Eqn 165*

$$|\chi(\tau,f)|^2 = \left(1-\frac{|\tau|}{T}\right)^2 \left(\frac{\sin\left[(\pi fT)\left(1-\frac{|\tau|}{T}\right)\right]}{(\pi fT)\left(1-\frac{|\tau|}{T}\right)}\right)^2$$

M.2.12 The empirical form of the ambiguity function for the rectangular symbol and the adopted scattering model lends to numerical evaluation of P_F and P_D. Table 7 depicts the simulated values computed for d.

Frequency Offset $\Delta x_2 T$	d	Time Offset $\Delta x_1 T$	d
0	1.0	0	1.0
0.1	0.839	0.1	0.937
0.2	0.5079	0.2	0.774
0.3	0.2476	0.3	0.565
0.4	0.1215	0.4	0.366

Table 7: Simulated values for d as a function of time and frequency synchronisation error

M.2.13 The results from the table indicate that for the simple complex envelope adopted for the simulation, system performance is subject to greater degradation in performance for frequency misalignment rather than time misalignment.

M.2.14 This is perhaps intuitively obvious from the nature of the waveforms ambiguity function since the range axis falls away as sinc(x) and the fall off in the time-range axis falls away linearly. The results differ slightly from those presented in [74] since the time frequency mismatch is expressed in terms of the rectangular pulse duration rather than the spread parameters of the channel.

M.2.15 Figure 80 depicts the ambiguity function of the rectangular pulse given in equation [165] (top right), the scattering function of the form given above for frequency spread

parameter B=1/(10T) and time spread parameter L=T/5. The bottom two graphs depict the two dimensional convolution of these functions for the case of perfect and imperfect synchronisation.

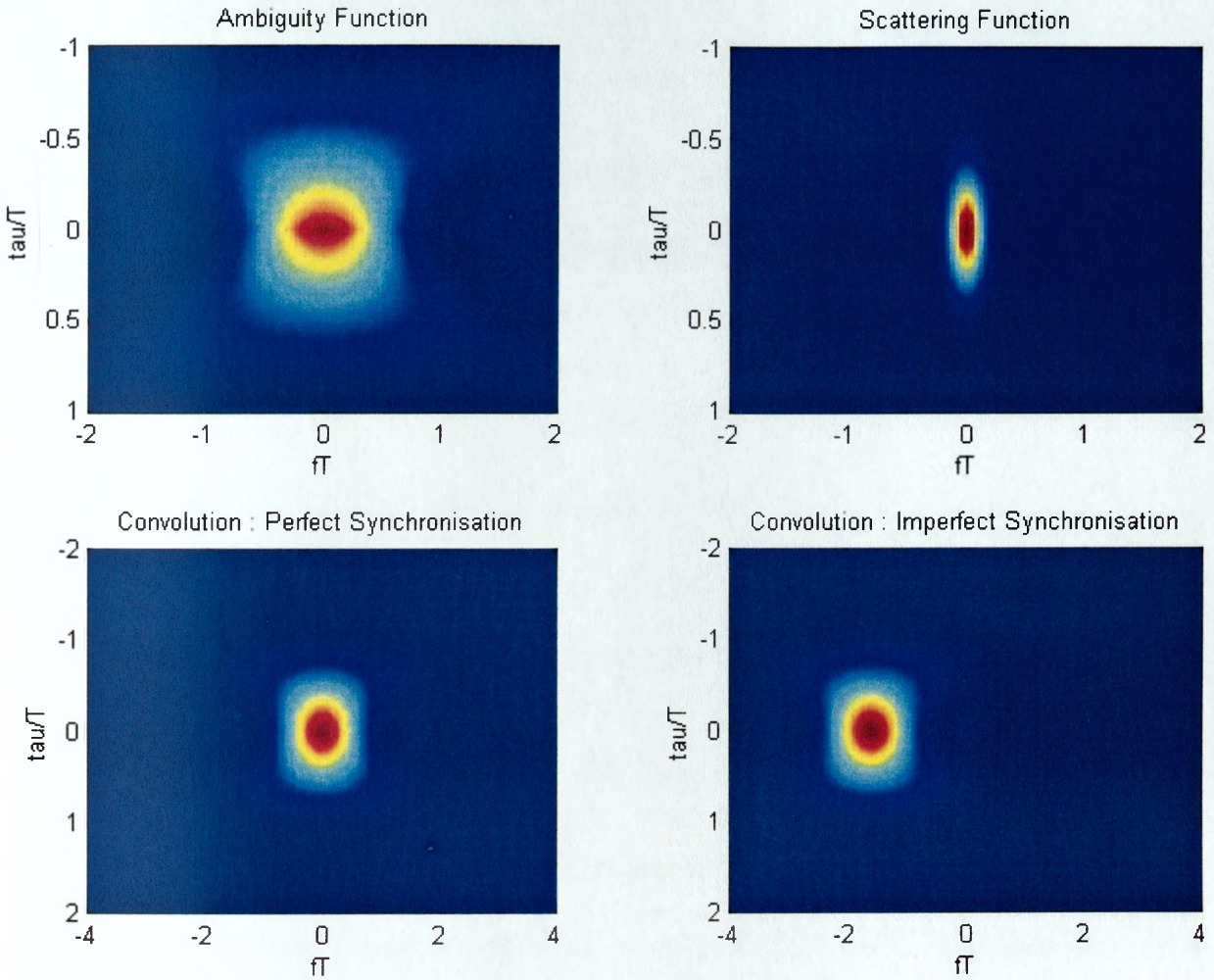

Figure 80; Simulated scattering simulation for CW pulse

N Ambiguity Functions

N.1 Acoustic Doppler

N.1.1 Assuming a waveform s(t) is transmitted the received signal r(t) is given by [83].

$$r(t) = \alpha(R)s(t - \tfrac{R}{c}) \qquad \textit{Eqn 166}$$

where $\alpha(r)$ is the range dependent attenuation, R is the radial range and c is the sound propagation. For dynamic platforms in a non-homogenous ocean the relative range R will be time dependent :

$$R(t) = R_0 + Vt \qquad \textit{Eqn 167}$$

N.1.2 Further, the relative platform Doppler V will be time dependent comprising a mean relative velocity and random perturbations induced both through platform velocity variations, aspect variations, and the influence of the ocean medium itself

$$V(t) = V_0 + \Psi(t)t \qquad \textit{Eqn 168}$$

where $\Psi(t)$ is a lowpass random stochastic process.

N.1.3 Under relative platform motion the received signal will be time translated, temporally scaled by virtue of the Doppler effect and attenuated.

$$r(t) = \alpha(R_0)s[(1-\sigma)t - \tau] \qquad \textit{Eqn 169}$$

where

$\tau = \dfrac{R_0}{c}$ denotes the bulk channel delay at range R_0

$\sigma = \dfrac{V}{c}$ denotes the Doppler temporal scaling parameter

c = sound velocity

α = attenuation

N.1.4 Burst synchronisation of the received signal waveform requires correlating the received waveform with a number of temporally scaled signal replicas which provide a systematic search of the delay-Doppler uncertainty. This process provides an estimate of the range and Doppler of the received signal, denoted $\hat{\tau},\hat{\sigma}$ respectively. The utility of waveform designs in providing unambiguous burst timing and Doppler estimation is demonstrated through their ambiguity functions which characterise the correlation performance of particular waveforms when subject to range and Doppler uncertainty.

N.1.5 The ability of a particular waveform design to instantaneously determine channel time and Doppler spreading is a function of the channel spreading factor given by the product of the channel delay spread and Doppler spread.

N.1.6 The correlation process is implemented as

$$\phi(\tau,\sigma) = \int_{-\infty}^{+\infty} r_\sigma{}^*(t)s(t+\tau)dt \qquad \textit{Eqn 170}$$

where

$r_\sigma(t) = s[(1-\sigma)t]$ is the scaled replica corresponding to Doppler parameter σ.

- * denotes complex conjugation

N.1.7 Under pure Doppler, this operation performs optimally in white Gaussian noise. In coloured noise conditions, pre-whitening filters are used to establish a uniform noise spectral density. The impulse response of the filter is given by the inverse Fourier transform of the noise spectral density N(f).

$$h(t) = \int_{-\infty}^{+\infty} \frac{e^{-j2\pi f(t-T)}}{N(f)} df \qquad \textit{Eqn 171}$$

N.2 The Ambiguity Function

N.2.1 Evaluating [170] under zero delay and Doppler conditions $\hat{\tau} = 0, \hat{\sigma} = 0$ gives the total signal energy

$$\phi(0,0) = \int_{-\infty}^{+\infty} s^*[(1-\sigma)t]s(t+\tau)dt = \int_{-\infty}^{+\infty} |s(t)|^2 \, dt = E_s \qquad \textit{Eqn 172}$$

N.2.2 This constitutes the maximum value of $|\phi(\tau,\sigma)|$ and using this as a normalisation term in 11 gives the uncertainty function $\psi(\tau,\sigma)$:-

$$\psi(\tau,\sigma) = \tfrac{1}{E_s} \int_{-\infty}^{+\infty} s^*[(1-\sigma)t]s(t+\tau)dt \qquad \textit{Eqn 173}$$

N.2.3 The ambiguity function is then given by the magnitude squared uncertainty function:-

$$X(\tau,\sigma) = |\psi(\tau,\sigma)|^2 \qquad \textit{Eqn 174}$$

N.3 The Narrowband Case

N.3.1 Temporal scaling in the time domain can be related to the frequency domain through the Fourier transform pair.

$$f(at) \leftrightarrow \frac{1}{|a|} F(\frac{\omega}{a}) \qquad \textit{Eqn 175}$$

N.3.2 By direct application of Parsevals theorem given by

$$\int_{-\infty}^{+\infty} |f(t)|^2 \, dt = \frac{1}{2\pi} \int_{-\infty}^{\infty} |F(\omega)|^2 \, dt \qquad \textit{Eqn 176}$$

the uncertainty function can be considered in the frequency domain.

$$\psi(\tau,\sigma) = \frac{1}{1-\sigma}\frac{1}{E_s}\int_{-\infty}^{+\infty} S^*[\tfrac{f}{1-\sigma}]S(f)e^{-j2\pi f\tau}df \qquad \textit{Eqn 177}$$

N.3.3 Since $\sigma << 1$ one can approximate $(1-\sigma)^{-1}$ using a series expansion and retain the first two terms:

$$(1-\sigma)^{-1} = 1+\sigma+\sigma^2+....\cong 1+\sigma \qquad \textit{Eqn 178}$$

giving

$$\psi(\tau,\sigma) = \frac{1}{E_s}\int_{-\infty}^{+\infty} S^*[f+\sigma f]S(f)e^{-j2\pi f\tau}df \qquad \textit{Eqn 179}$$

N.3.4 Assuming the signal is bandlimited to a bandwidth B and centred on a frequency f_o, in cases where $f_o >> B$ (the narrowband case) , the σf term will vary little over the integration limits and so can be replaced by the constant carrier term f_o. This gives the narrowband uncertainty function

$$\psi_{NB}(\tau,\sigma) = \frac{1}{E_s}\int_{+fo-B/2}^{+fo-B/2} S^*[f+\sigma f_0]S(f)e^{-j2\pi f\tau}df \qquad \textit{Eqn 180}$$

or equivalently

$$\psi_{NB}(\tau,\sigma) = \frac{1}{E_s}\int_{-\infty}^{\infty} s^*(t)s(t+\tau)e^{-j2\pi\sigma f_0 t}dt \qquad \textit{Eqn 181}$$

N.3.5 Letting $\beta = \sigma f_0$ the cross correlation is given by

$$\varphi_{NB}(\tau,\tfrac{\beta}{f_0}) = \int_{-T/2}^{T/2} s^*(t)x(t+\tau)e^{-j2\pi\beta t}dt \qquad \textit{Eqn 182}$$

N.3.6 This is simply the Fourier transform of the product of the received signal multiplied by the local replica and can be easily implemented using a heterodyne correlator. By using FFT based spectrum analysis the correlation output can simply be evaluated as a function of Doppler shift parameter β.

N.3.7 The applicability of the narrowband approximation is determined by both the transmission $Q=f_0/B$ and the characteristics of the signal. For communication synchronisation one requires that the synchronisation waveform design be capable of unambiguous range and Doppler estimation and that the estimation is sufficiently resolved in time and Doppler prior to the data demodulation process.

N.4 Swept Sine Waveforms

N.4.1 A common waveform used for channel sounding and synchronisation is the linear frequency modulated pulse.

$$s(t) = w(t)e^{j2\pi(f_o t+\frac{1}{2}mt^2)} \qquad \textit{Eqn 183}$$

where

$w(t)$ is an envelope window function defined over the interval -T/2 to +T/2.

$m = \frac{W}{T}$ is the sweep rate of the pulse

N.4.2 When subjected to Doppler the received signal is given by

$$s((1-\sigma)t) = w((1-\sigma)t)e^{j2\pi(f_o(1-\sigma)t+\frac{1}{2}m[(1-\sigma)t]^2)} \qquad \textit{Eqn 184}$$

which differs from the original signal by a frequency translation term $f_d = \sigma f_0$ and a slope mismatch term $\Delta m = (\sigma^2 - 2\sigma)m$. In the narrowband case the received signal is merely a frequency translated version of the transmitted signal. In the wideband case both frequency translation and slope mismatch serve to degrade correlator performance.

Considering the slope mismatch term, assuming the received and replica waveforms are aligned in centre frequency and delay, the maximum output of the normalised correlation function will be a function of Δm:

$$M(\Delta m) = \left| \frac{1}{T} \int_{-T/2}^{T/2} e^{-j\pi \Delta m t^2} dt \right| \qquad \textit{Eqn 185}$$

N.4.3 Through the approximation $\Delta m \approx 2\Delta m$ Glisson [83] formulates a wideband approximation for Doppler tolerance based on a 3dB correlation loss:-

$$V = \pm \frac{1300}{WT} ms^{-1} \qquad \textit{Eqn 186}$$

N.4.4 Whilst Doppler correlation loss is an important issue for acoustic communication system synchronisation, especially high platform Doppler, phase ambiguity or more accurately delay ambiguity is a more serious problem. In the case of LFM chirps the use of high sweep rates serves to increase the range ambiguity of the received signal. To contain the range ambiguity of the waveform it is desirable to :-

- reduce the carrier frequency f_o;
- increase the bandwidth W;
- reduce the pulse duration T.

N.4.5 The most immediate impact of reducing the pulse duration is to minimise its energy which degrades overall processing gain. This is obviously undesirable in a high noise applications.

N.5 Digital Phase Coded Waveforms

N.5.1 In order to achieve a more accurate instantaneous estimate of delay-Doppler, it is desirable for the ambiguity function of the channel sounding waveform to be localised at

$f = 0, \tau = 0$; the so called 'thumbtack' response. In practice such a response can be approximated by noiselike signals characterised by random magnitude and phase frequency components within the transmission bandwidth. Of course the sidelobe performance of such signals ultimately depends upon their dimensionality and/or specific orthogonality properties.

N.5.2 For a waveform exhibiting completely random phase and magnitude characteristics, orthogonality cannot be achieved in the mean sense under pure time translation $e^{j2\pi\omega\tau}$ and temporal scaling $f(\sigma t) \xleftrightarrow{F} \frac{1}{|\sigma|} F(\frac{\omega}{\sigma})$. Therefore such signals are subject to a noiselike self clutter in both time and Doppler axes. The level of self clutter is dependent on the dimensionality of the signal as measured by its bandwidth-time (BT) product. Since correlation is essentially an averaging process the use of large BT signals provides greater averaging against the random phase and magnitude 'mismatches' over the integration interval. So, for such signals to be beneficial for the purposes of communications signal synchronisation they must exhibit a suitably large BT to provide sufficient signal to self clutter (+noise) ratio in order to be detected and to minimise sidelobe contamination.

N.5.3 This self clutter limits the applicability of small BT noise signals as channel sounding signals. However as the BT product is increased, the self clutter level will reduce in inverse proportion resulting in a waveform ambiguity function localised at $\varphi(0,0)$ with self clutter levels 1/BT down to the main thumbtack peak response.

N.5.4 It is worth noting that the use of frequency in the range-Doppler ambiguity function is not appropriate for such signals in the wideband case. Since such signals are stochastic in nature the concept of instantaneous frequency has little meaning. Instead the signal spectra must be computed in a statistical sense by exploiting the Weiner-Khintchine relationship between signal autocorrelation and power spectra.

$$F\{\phi_{xx}(\tau) = |F_x(\omega)|^2 = \int_{-\infty}^{+\infty} \phi_{xx}(\tau) e^{-j\omega\tau} d\tau| \qquad \textit{Eqn 187}$$

N.5.5 For such signals the time-frequency analysis tools used for sinusoidal based waveforms such as the LFM chirp are no longer useful. Further, the ambiguity analysis of such signals can only be performed in a statistical sense. Such an analysis is presented by Kramer [29]. Assuming stationarity, the ensemble average of the cross correlation between replica and Doppler scaled replica is given by

$$\begin{aligned} E\{\varphi_0(\tau,\sigma)\} &= \frac{1}{T}\int_{-T/2}^{T/2} E\{s(t+\tau)s^*([1-\sigma]t)\}dt \\ &= \frac{1}{T}\int_{-T/2}^{T/2} \varphi_{xx}(\sigma t+\tau)dt \end{aligned} \qquad \textit{Eqn 188}$$

N.5.6 A reasonable approximation of the autocorrelation function of a pseudorandom noise (PRN) or other noiselike signal is to assume that the signals power spectral density is that of bandlimited white noise.

$$|S(f)|^2 = \begin{cases} \frac{1}{W} & , f_0 - \frac{W}{2} \le f \le f_0 + \frac{W}{2}; \quad 0 \quad otherwise \end{cases} \qquad \textit{Eqn 189}$$

N.5.7 The autocorrelation function is then given through the Fourier transform of the spectral density thus:-

$$\phi_{xx}(\tau) = \frac{\sin(\pi W\sigma\tau)}{\pi W\sigma\tau} e^{j2\pi f_0\tau} dt \qquad \textit{Eqn 190}$$

N.5.8 For the zero delay case $\tau = 0$, the ensemble correlation can be written

$$E\{\varphi_0(\sigma,0)\} = \frac{1}{T}\int_{-T/2}^{T/2} \frac{\sin(\pi W\sigma t)}{\pi W\sigma t} e^{j2\pi f_o\sigma t} dt \qquad \textit{Eqn 191}$$

N.5.9 Whilst this is difficult to evaluate analytically, the Doppler tolerance of noiselike signals can be easily calculated numerically and indicates that the signal Doppler tolerance is dictated primarily by the carrier frequency to signal duration ratio. For typical parameters, representative of a medium range communication system, the results demonstrate that Doppler compensation is a mandatory requirement for such systems to operate effectively.

O COFDM Modulation

O.1 Principle

O.1.1 The broad aim of OFDM and COFDM is to minimise the effect of the dispersive broadband channel by sub-dividing the available bandwidth into a number of very narrowband sub-channels, such that the performance of each sub-channel is almost ideal (i.e. they suffer from flat-band fading) [88-91].

O.1.2 By making the bandwidth of each sub-channel sufficiently narrow, the effects of inter-symbol interference (ISI) on that sub-channel are reduced and the equalisation requirement is effectively transformed to the frequency domain as a single complex phasor per carrier channel. In a typical, simplified, OFDM system, the original data stream is mapped into complex valued symbols by the modulation process, which can be any liner modulation method. The rate of these symbols is reduced by a factor N by multiplexing them into N parallel paths that are then modulated onto N carriers, as shown in Figure 81.

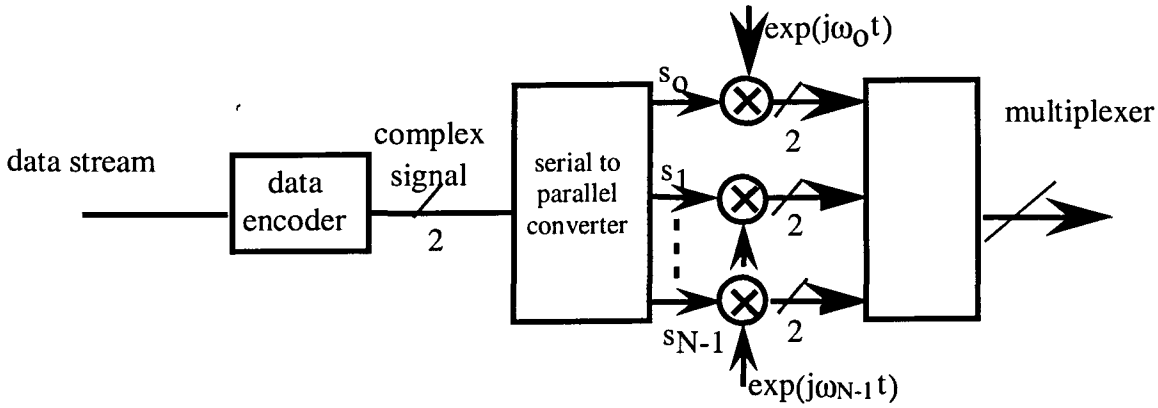

Figure 81 Schematic of generic OFDM transmitter

O.1.3 The key to the spectral efficiency of OFDM lies in the way in which the symbols are modulated onto the N carriers. Normally, it would be necessary to separate the frequency spacing of each carrier with a frequency guard-band to prevent the upper and lower sidebands of adjacent carriers from overlapping and producing aliasing. In OFDM, the carriers are all chosen to be *orthogonal* so that with an appropriate modulation scheme such as QPSK or QAM it is possible for upper and lower 'sidebands' of adjacent sub-carriers to fully overlap, yet still be correctly demodulated. Of course maintaining this orthogonality, particularly in the difficult underwater acoustic channel, is the most complex issue relating to OFDM schemes.

O.1.4 The discrete complex multi-carrier OFDM signal can be represented as [92]:

$$s(nT) = \frac{1}{N} \sum_{k=0}^{N-1} A_k e^{j(2\pi f_k nT + \phi_k} \qquad \textit{Eqn 192}$$

O.1.5 The sampling frequency is $1/T$ and the period of one data symbol is $2NT$ with interpolated inter-modulation frequencies between the sub-carriers.. A_n and ϕ_n are the amplitude and phase of the n^{th} sub-carrier respectively, and:

$$f_k = f_o + k(\Delta f) \qquad \textit{Eqn 193}$$

where f_o is the lowest frequency of the OFDM spectrum and $\Delta f = 1/NT$ is the frequency separation between carriers. In practice, the inverse Fast Fourier transform (IFFT) algorithm can be used to implement the parallel OFDM modulation structure and the FFT can be used for the corresponding matched-filter demodulation process in the receiver.

O.1.6 A typical transmitter using this principal is shown in Figure 82

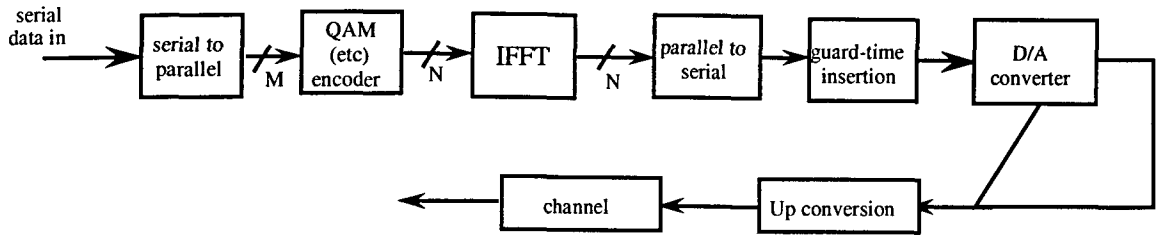

Figure 82; COFDM Transmitter block diagram

O.2 Effects caused by the channel on the transmitted signal

O.2.1 The orthogonality properties between the sub-carriers cannot be maintained in the presence of inter-symbol interference (ISI) caused by dispersion mechanisms due to the transmission channel and the main-lobe filtering in the transmitter and receiver. Also ,and more importantly, orthogonality cannot be maintained under acoustic Doppler conditions including frequency translation and frequency scaling..

O.2.2 The impact of ISI can be significantly reduced by increasing the period of each frame of data, i.e. increasing $N.T_s$, so that it is many times longer than the channel impulse response. Since the required data rate sets the value of T_s, this can only be achieved by increasing N and this increases the size of the DFT algorithm, and hence both the computation overhead, and the delay through the system is also increased. The extent to which N can be increased is limited by the temporal coherence of the channel and this is the most fundamental difficulty with OFDM techniques for underwater acoustic communications applications. Specifically, reducing symbolling rate increases synchronisation complexity.

O.2.3 To restore the orthogonality between the carriers under purely ISI conditions, a *time guard-band*, or, more accurately, a *cyclic prefix* that lasts for T_g seconds can be placed at the beginning of each symbol. Thus, in a system with cyclic prefix, the symbol period is increased to $T_s' = T_s + T_g$. The cyclic prefix ensures that signals which occur in a time

frame of $N.T'_S$ seconds are not carried over into the next time frame (due to the effect of the channel impulse), thus ensuring that the signals in each frame are kept independent. The cyclical nature of the prefix ensures that the received signal does not suffer from windowing, as would be the case if the signal had been set to zero amplitude for the duration of the guard-band.

O.2.4 If the channel impulse response is longer than the guard interval, then the orthogonality conditions no longer hold. The interfering term then comprises of inter-symbol interference from the preceding block and the loss of orthogonality in the remaining part of the integration interval. This combination of effects is termed inter-channel interference (ICI) and refers to the frequency domain contamination between sub-band carriers.

O.3 Coding and interleaving

O.3.1 Although the insertion of a cyclic prefix has meant that the effects of the channel impulse response on maintaining signal orthogonality are significantly reduced (i.e. low ICI), the received signal is still corrupted by random noise and this causes errors in the receiver. In addition, multipath propagation, Doppler effects and shadow loss give rise to deep time and frequency dependent fades that cause bursts of consecutive errors. In the OFDM system, these effects are called co-channel interference (CCI). To minimise these effects, it is usual to code the data.

O.3.2 Convolutional codes are effective against randomly distributed errors, whilst linear block codes together with interleaving are effective against burst errors. These two properties appear to lead to contradictory code requirements. However, they can be resolved through the use of a Reed-Solomon code where these two properties can be exploited simultaneously by associating an interleaving system matched to the length of the

symbols and a system for deleting the affected symbols in the case of a deep fade. If a simple convolutional coding strategy is used in a fading environment, it is important to use this in conjunction with interleaving. The reason is that by interleaving the data bits prior to transmission and de-interleaving in the receiver, bursts of consecutive errors in the channel are randomised, so that the convolutional code is better able to handle them.

O.4 Equalisation strategies with OFDM systems

O.4.1 The insertion of a cyclic prefix does not remove the need for equalisation. It can often be implemented using a simple one-tap equaliser on each output arm from the DFT. The reason for this is that the bandwidth of data on each sub-channel is very narrow and effectively suffers from flatband fading. This simply requires the sub-carrier to be amplitude and phase corrected by multiplication with a complex phasor. Most OFDM implementations use this structure, but more complex multi-tap equaliser structures operating in the frequency domain are feasible and operate in a manner completely analogous to the role of a time domain equaliser in combating ISI. However since these structures operate in the frequency domain instead of combating temporal dispersion they are potentially effective in combating ICI and CCI effects arising, for example from acoustic Doppler dispersion. This technique is shown in Figure 83. The structure of the feedforward section of the equaliser is identical to a simple time-domain equaliser used in conventional single carrier systems, except that it is being applied here in the frequency domain. The feedback part of the equaliser uses outputs Z_1, Z_{-1} etc. from the other adjacent equalisers. The coefficients C_0 and B_0 etc. have to be computed so that the mean square error at the output of the equaliser is minimum and one of the simplest adaptation algorithms is the LMS (stochastic gradient) algorithm. Other structures are possible. If one concentrates on the feedforward RAKE section of the equaliser, it will be

immediately apparent that this structure provides a good measure of resilience to Doppler frequency spread.

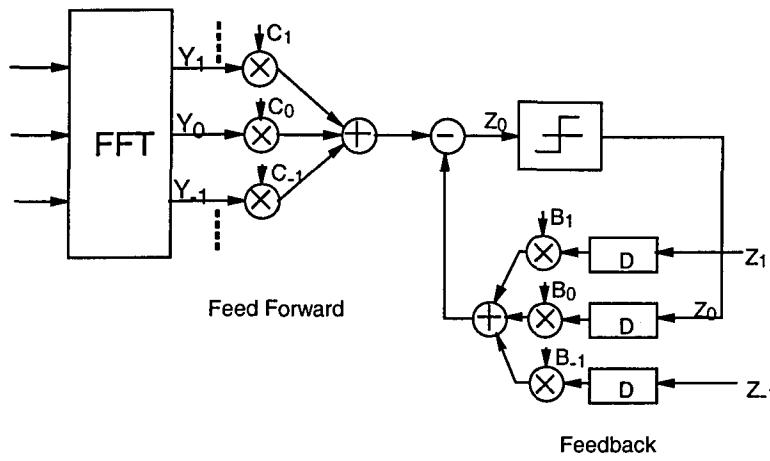

Figure 83; Frequency domain decision feedback equaliser

O.4.2 If there is an offset in frequency due to Doppler which corresponds to one or more of the adjacent frequency bins of the FFT algorithm, these will be raked in to the wanted tap by the multi-tap combiners. Of course acoustic Doppler involves not only a frequency translation of the COFDM spectrum, but also a frequency scaling. As in any adaptive process, the ability of the filter to track environmental uncertainty is intimately related to how rapidly one samples the environment. The dilemma faced with COFDM techniques is the balance to be struck between rapid sampling of the channel (wider bandwidth carriers) and equalisation complexity. This is a promising area for future research, particularly when combined with spatially adaptive structures.

P Fractional Spaced Equalisation

P.1 Fractionally Spaced Equalisation

P.1.1 An extremely important issue in the implementation of equalisers is the ability to compensate for delay distortion in the channel impulse response. A 1/T spaced equaliser is extremely sensitive to timing epoch and timing slip.

P.1.2 In the underwater acoustic channel path delay fluctuations invariably lead to timing slip by virtue of platform movement and environmental variability's. Consider, for example an equaliser operating at symbolling rate of 10ksym/s which equates to a symbol scale of 15cm. Platform heave motion, for example, would have a dramatic impact on equaliser performance since the equaliser would have to track delay fluctuations on a spatial scale of several symbols.

P.1.3 Such delay distortion would lead to significant performance degradation for a non-fractional forward filter. The performance benefits of fractional filters are discussed by Gitlen [102] and Ungerboeck [103]. Both papers consider the delay distortion issue for RF channels. Unfortunately the delay distortion problem is much greater in underwater acoustic channels

P.1.4 The inability of the 1/T spaced equaliser to cope with channel delay distortion can be considered in the frequency domain. Specifically the input to the equaliser can be expressed

$$Y_T(f) = \frac{1}{T}\sum_n X(f - \frac{n}{T}) e^{j2\pi(f - n/T)\tau_0} \qquad \textit{Eqn 194}$$

where

$Y_T(f)$ is the received, discrete frequency spectrum folded about 1/2T

X(f-n/T) are the aliased spectra of the received bandlimited symbol pulse

τ_0 is the delay uncertainty.

P.1.5 Evidently each aliased spectrum is subject to a linear phase term due to the delay uncertainty. For a T spaced equaliser the transfer function is given by

$$C_T = \sum_{-N/2}^{N/2} c_k e^{-j2\pi fkT} \qquad \textit{Eqn 195}$$

where the subscript T denotes T spacing.

P.1.6 Since

$$C_T(\omega) = C_T(\omega + \frac{2\pi}{T}) \qquad \textit{Eqn 196}$$

the synchronously spaced equaliser can only modify $Y_T(f)$ if and only if $\tau_0 = 0$.

P.1.7 If $\tau_0 \neq 0$ then the T synchronous equaliser cannot exercise independent control over both sides of the roll off region about $\omega = \frac{\pi}{T}$. If a fractional spaced equaliser is used however such control is possible prior to aliasing and this enables the equaliser to better cope with channel delay distortion.

P.1.8 The frequency response of the fractional spaced equaliser is given by

$$C_{T'} = \sum_{-N/2}^{N/2} c_k e^{-j2\pi fkT'} \qquad \textit{Eqn 197}$$

where

T'=MT/N and M and N are integers with N>M.

P.1.9 This enables equalisation of the received signal spectrum beyond the Nyquist frequency from 1/2T to N/MT. The importance of fractionally spaced equalisation in the underwater acoustic channel cannot be overstressed. It is shown in section 6 where synchronisation issues are developed, that open loop estimation of absolute time and Doppler is a difficult problem for channels exhibiting significant time and frequency spread.

P.1.10 Since the spatial scales of the symbolling waveforms in an acoustic communications system are comparable to the spatial scales of environmental variability and platform motion, initial 'burst' open loop synchronisation techniques are unlikely to achieve consistent, high fidelity, time and Doppler estimates in any but the most benign channels. Adaptive, fractionally spaced, equalisers provide a powerful means to 'pull in' delay error and, moderate residual Doppler error.

P.1.11 In order to demonstrate the importance of fractional spacing in the context of acoustic channel equalisation, a simulation was conducted based on a single channel T spaced adaptive equaliser and a single channel T/2 spaced equaliser.

P.1.12 In both cases the symbolling waveform comprised a root Nyquist filtered QPSK transmission and the standard form of the complex LMS algorithm for coefficient update with μ=0.02. In both cases a 10 tap equaliser was used. The signal was re-sampled to simulate Doppler of 0.5m/s in order to determine the relative behaviour of the fractional and non-fractional implementations.

P.1.13 Figure 84 shows the time evolution of the magnitude of each of the ten LMS coefficients for the fractional spaced equaliser and the corresponding magnitude squared error for the algorithm operating in training mode for the first 500 symbols.

P.1.14 Also shown, inset, in each MSE graph are the corresponding I-Q scatter diagrams of the received symbols. From the figure it can be seen that the relative slippage of the equaliser

taps corresponds to approximately 2 symbols over the 1600 symbols decoded. This equates to a slip of 4 taps in the T/2 equaliser and 2 taps for the T spaced equaliser.

P.1.15 For the fractional equaliser it is evident that the equaliser readily tracks the symbol timing drift introduced from the Doppler channel. This is demonstrated by the smooth transition in tap magnitudes throughout the simulation. The magnitude error is well behaved with convergence achieved in less than 100 samples and a steady state error of the order 0.05.

P.1.16 For the non-fractional spaced equaliser the behaviour is very different. The transition in tap magnitudes is disjointed, occurring in discrete steps, which are separated by a transient period in which the magnitude error increases significantly. The transition occurs when the timing slip corresponds to a half symbol period. This constitutes the worst case timing for the T spaced equaliser and results in significant increase in the magnitude error.

P.1.17 In addition the inability of the T spaced equalise to synthesise arbitrary delays severely degrades the equalisers convergence and steady state error performance, with convergence taking approximately four times as many symbols as in the fractional case. The steady state error is also significantly degraded relative to the fractional equaliser.

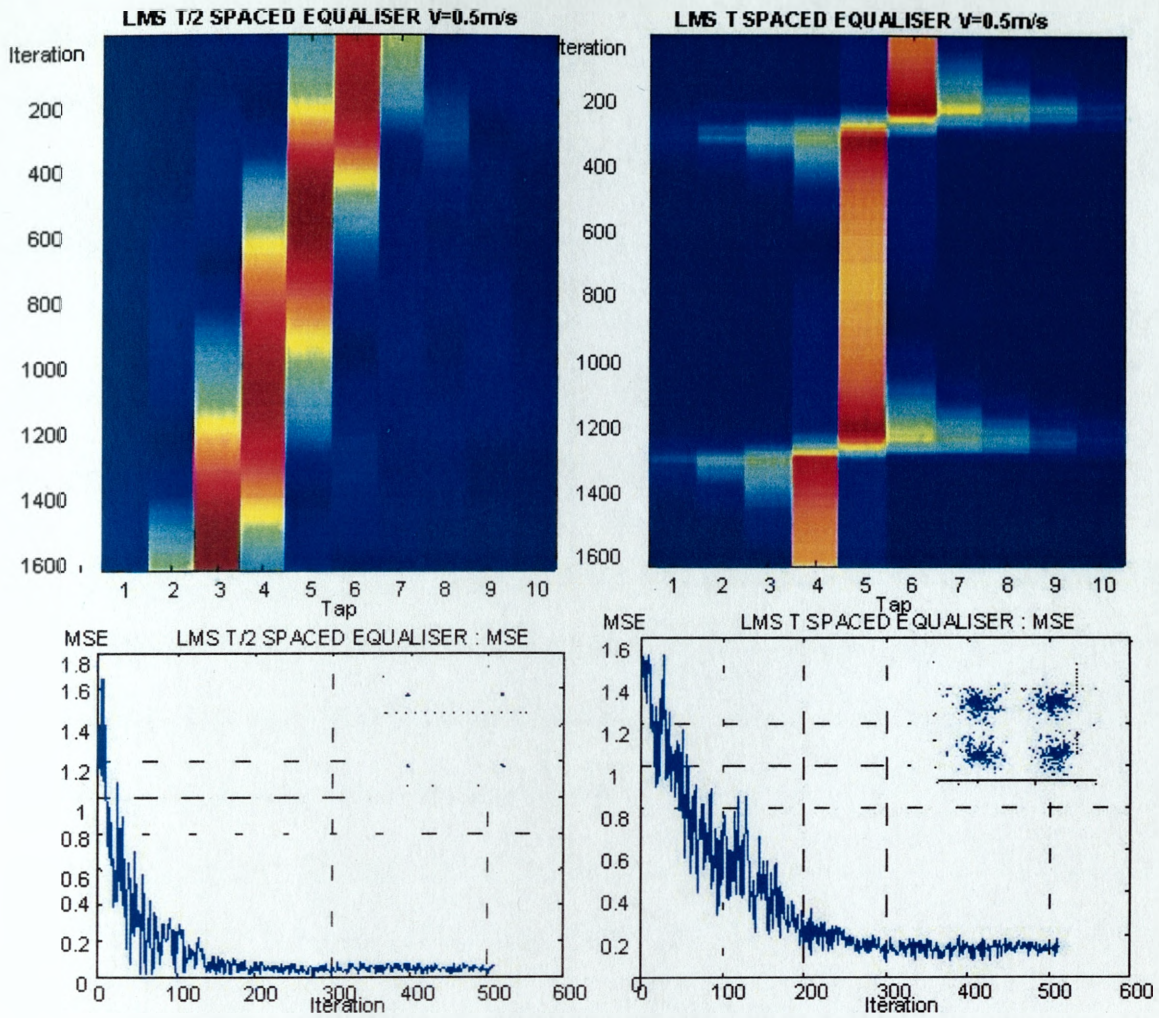

Figure 84: Fractional T/2 (Left) vs Non Fractional T spaced Equaliser for constant Doppler=1m/s

Q Orthogonal Coded Waveforms

Q.1 Optimum Designs

Q.1.1 In practice the utility of any wideband signal design is ultimately limited by its performance in time and frequency spread channels. In a multipath channel one seeks a waveform which exhibits good autocorrelation properties i.e. low correlation under time shift. Maintaining this performance in frequency selective and time selective channels is particularly challenging; especially so for the underwater acoustic channel.

Q.1.2 The matched filter output of a signal transmitted through a channel is given by the convolution of the channel scattering function with the waveform ambiguity function. If one considers the convolution the time axis only, the matched filter output comprises the convolution of the waveform ambiguity function with the channel multipath profile. If the waveform ambiguity function exhibits sidelobes then the convolution process results in each resolved path being subject to a self clutter noise term due to the sidelobe 'leakage' from all other paths. Clearly it is advantageous to reduce this noise term.

Q.1.3 An established technique to contain sidelobe spillage is to use either unilateral or bilateral weighting of the waveforms which serves to reduce the sidelobe level and/or redistribute sidelobes to minimise 'leakage'. An unfortunate consequence of such an approach is the reduction in system processing gain and range resolution. Processing gain is lost since the waveform energy is effectively reduced through the windowing process.

Q.1.4 Spread spectrum systems utilise phase coded waveforms based on codes exhibiting desirable autocorrelation properties or, in the case of multiuser communications, good cross correlation properties. Fortunately much work has been done toward identifying code families with these characteristics.

Q.1.5 The family of maximal length (ML) sequences is firmly established in direct sequence spread spectrum systems by virtue of their excellent autocorrelation properties. An important aspect of the ML code performance is the periodic autocorrelation function

$$\phi(j) = \sum_{i=1}^{n} (2b_i - 1)(2bi + j - 1), \quad 0 \le j \le n-1 \qquad \textit{Eqn 198}$$

where

n is the code period $\phi(j + rn) = \phi(j)$.

Q.1.6 Ideally the autocorrelation function of the code should be zero for $j \neq 0$. In the case of ML sequences the periodic autocorrelation function is

$$\phi(j) = \begin{cases} n & j = 0 \\ -1 & 1 \le j \le n-1 \end{cases} \qquad \textit{Eqn 199}$$

so for n large the codes approximate the ideal autocorrelation function.

Q.1.7 The cross correlation properties of the ML codes are however not so well behaved. For example for a m=9, n=511 sequence there exist 48 codes, the normalised cross correlation coefficient between any two codes can be as much as 0.22. For shorter codes the normalised cross correlation can be significantly higher. Gold codes improve on the cross correlation performance of ML sequence by exploiting selected pairs of ML sequences which exhibit a three valued correlation function.

Q.1.8 By exploiting this property by modulo two adding the two sequences new sequences are obtained by shifting the phase of one code relative to the other. In this way the peak cross correlation for $j \neq 0$ is significantly reduced

$$\phi_{\max\_mod\,d} = 2^{(m+1)/2} + 1, \phi_{\max\_meven} = 2^{(m+2)/2} + 1 \qquad \textit{Eqn 200}$$

Q.1.9 The achievable reduction is typically by a factor 5-10 depending on the code size, relative to ML sequences. Kasami codes are formed by decimating a ML code **a** of period 2^m–1 by $2^{m/2}$ to obtain a new code **b** which is periodic with period$2^{m/2}$-1. The Kasami code is formed by the modulo two addition of **b** with **a.** Since **b** has $2^{m/2}$-1 phases the total number of codes in the family is $2^{m/2}$ including **a.** Kasami codes achieve a maximum cross correlation of

$$\phi_{max} = 2^{m/2} + 1 \qquad \textit{Eqn 201}$$

Q.1.10 Figure 85 shows the auto and cross correlation properties of ML and Gold codes as follows

- Top : This shows the cross correlation properties of a degree 8 ML code with a number of other ML codes of the same degree. It is evident that the cross correlation is poorly behaved with peak values of around 90/255 = 0.35.

- Bottom: This graph shows the auto and cross correlation properties of a degree 9 Gold Code and its cross correlation with a Gold code from the same family. It is evident that in this case the code cross correlation properties are well behaved and bounded by $2^{\frac{(9+1)}{2}} = \pm 32$. The price paid is however, higher sidelobe levels on the autocorrelation, which are similarly bounded.

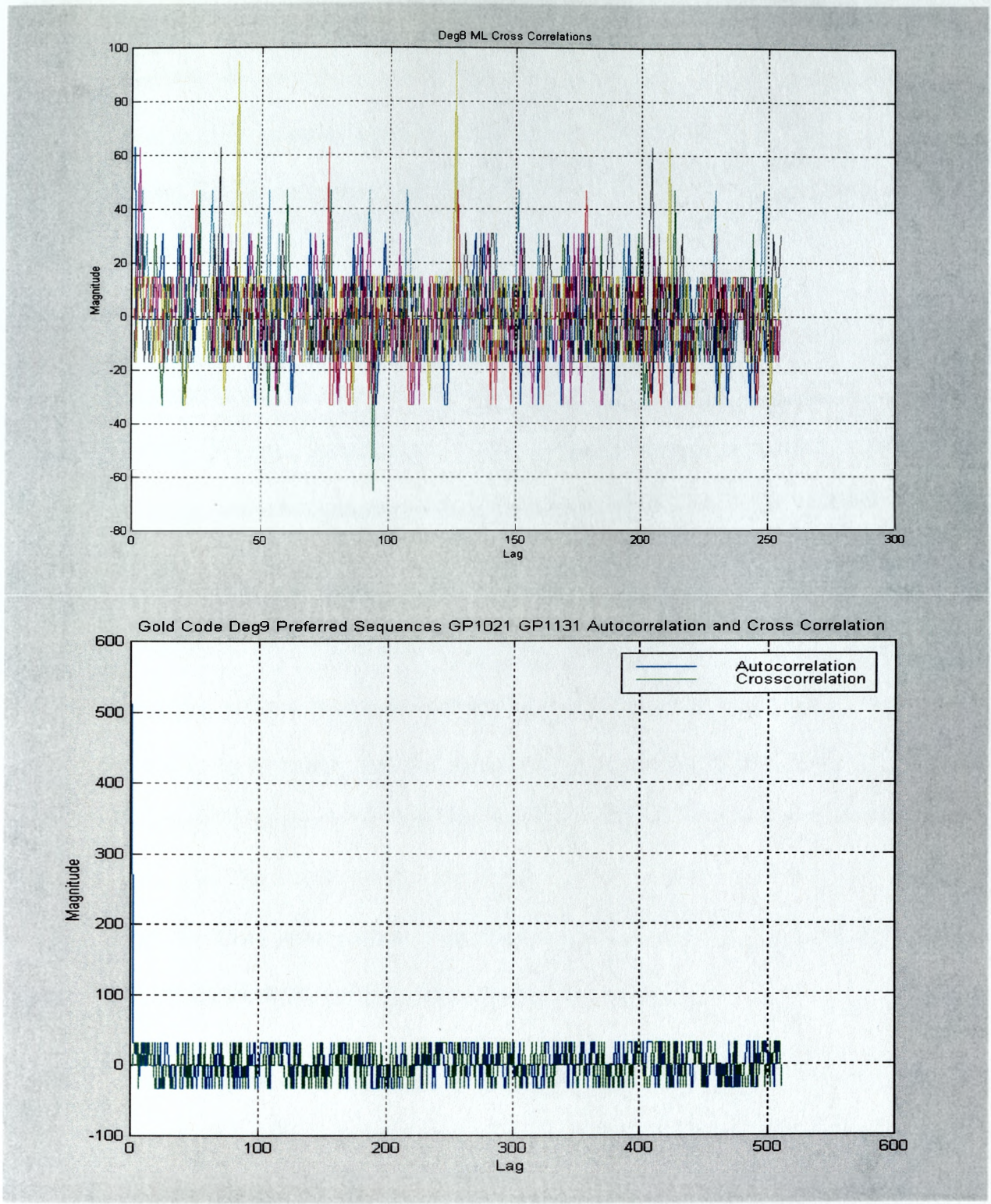

Figure 85: (Top) Crosscorrelation performance of ML Deg 8 Code (Middle) Auto and crosscorrelation performance of Deg 9 Gold

Q.1.11 The results demonstrate the trade off in code performance between achieving code designs with good autocorrelation properties which are essential for multipath channel

and codes with low cross correlation properties which are essential for multiuser applications, or Mary implementations which are based on maximum likelihood decoding. In practice, however, it is difficult to fully realise the potential of orthogonal signal designs since their orthogonality properties are often degraded under real channel conditions.

Q.1.12 For example multipath channels will degrade the performance of maximal length sequence codes if steps are not taken to ensure that the code correlation occurs as a circular process. Specifically a time guardband implementing a cyclic prefix of the maximal code is necessary to ensure all multipaths within a correlation window 'wrap round'.

Q.1.13 The addition of cyclic extensions to an orthogonal waveform is shown diagramatically in figure 86. Here an orthogonal waveform is extended to include a cyclic prefix and suffix. The aim is to ensure that the waveform's correlation properties are not degraded by multipath components provided the multipaths do not extend beyond the length of either extension. The addition of a cyclic prefix maintains the codes properties for paths arriving after the main synchronised path. The addition of a cyclic suffix maintains the codes properties for paths arriving before the synchronised path.

Q.1.14 The technique of course does not account for paths extending beyond the extension interval nor does it account for orthogonality degradation arising from Doppler and Doppler spread.

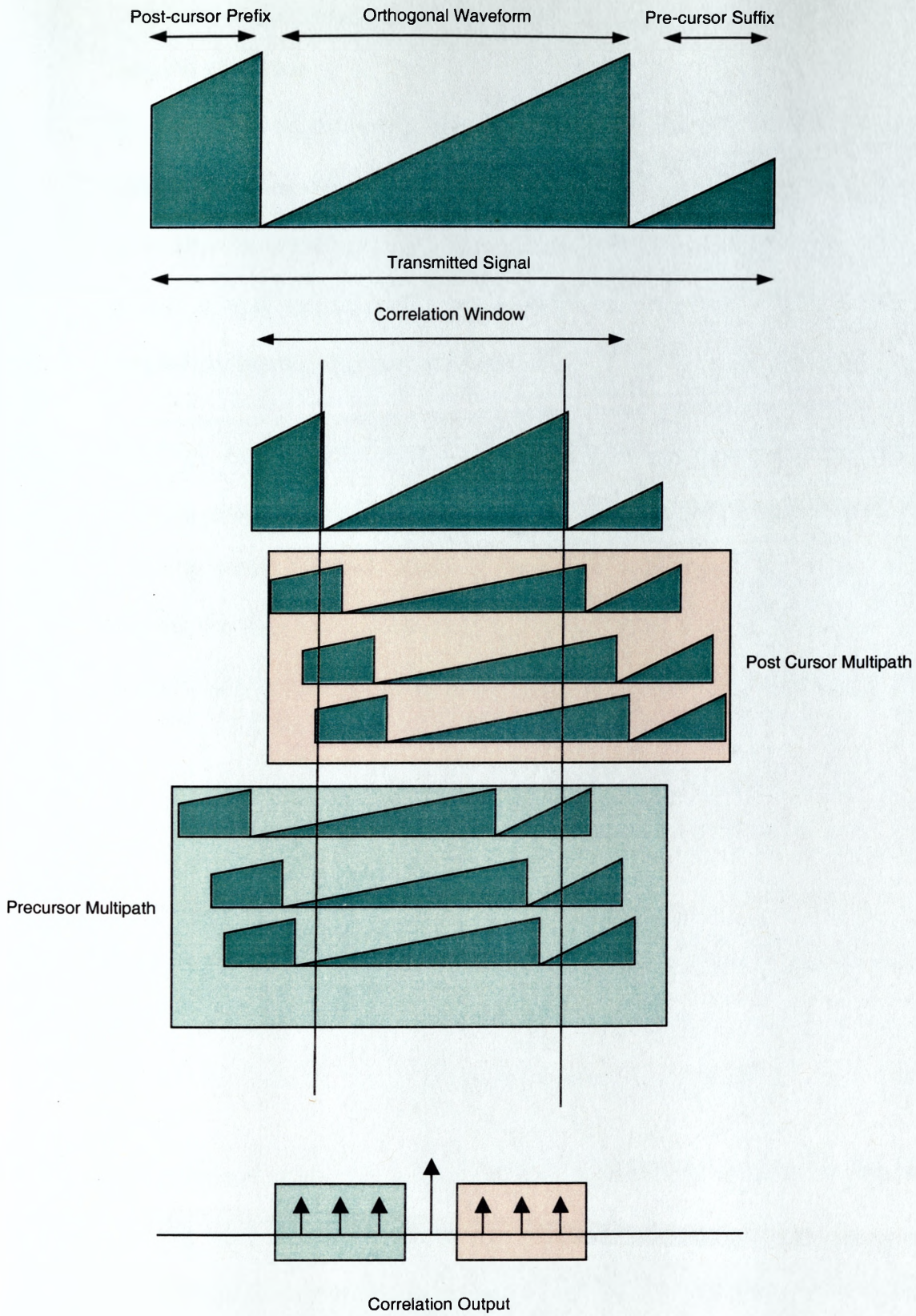

Figure 86; Application of cyclic prefixes to maintain waveform orthogonality

R Optimum Signal Design

R.1 Nyquist Criterion

R.1.1 Practical channels, the underwater channel included, have finite bandwidth which leads to symbol distortion commonly referred to as intersymbol interference (ISI). ISI manifests as a temporal smearing of data symbols such that they interfere with each other and so degrade overall system performance. Whilst this temporal smearing is not as severe as channel multipath, it can severely degrade system performance for nonadaptive receivers.

R.1.2 Optimum pulse shape design for such channels seeks to reduce the ISI problem by ensuring that the contamination between data symbols is reduced at the optimum sampling epoch for each symbol. The condition necessary to achieve zero ISI is the Nyquist criterion which seeks to ensure that for a discretely sampled data stream, pulses are finite only at their sampling epoch and are zero at all other sampling epochs

$$g_n = \int_{-\infty}^{+\infty} G(f) e^{j2\pi f n T_s} df = \begin{cases} 1; & n = 0 \\ 0; & n \neq 0 \end{cases} \qquad \textit{Eqn 202}$$

R.1.3 It can be shown [153] that this requirement is met if the overall frequency response when shifted and added to the original frequency response yields a uniform response

$$\sum_{k=-\infty}^{k=\infty} G(f + \tfrac{k}{T_s}) = T_s \qquad \textit{for all } f \qquad \textit{Eqn 203}$$

R.1.4 This criteria is satisfied by a brick wall frequency response for f=0 to f=1/(2T_s) which is desirable since it provides maximum throughput efficiency of 2sps/Hz. However, in the time domain the corresponding sinc() pulse design is impractical since it is defined over an infinite interval. Even if truncated, the use of a sinc() pulse design places impractical demands on the timing synchronisation circuitry since the pulse sidelobes extend for many symbols which lead to high levels of ISI for imprecise timing. The class of raised

cosine pulse designs enables the trade off between bandwidth and reduction in roll off rate. The impulse response is given by

$$g(t) = \left\{\frac{\sin \pi t / T_s}{\pi t / T_s}\right\}\left\{\frac{\cos \alpha \pi t / T_s}{1-(2\alpha t / T_s)^2}\right\} \qquad \textit{Eqn 204}$$

where the parameter α controls the bandwidth and roll off characteristics.

R.1.5 Figure 87 shows pulse designs, frequency characteristics and typical complex baseband symbol data for α=0,0.5,1.0. A Hamming weighting is also shown for comparison. The bottom figure shows simulated complex baseband symbol data for each of the pulse designs. The heavy line shows a single symbol sampling epoch for each pulse design. In each case the symbol {-0.707,-0.707} is correctly sampled. However for incorrect symbol timing, the influence of ISI is seen to substantially reduce for larger values of α. In applications where symbol timing is subject to uncertainty, as in the case of acoustic channels, higher values of α improve system robustness.

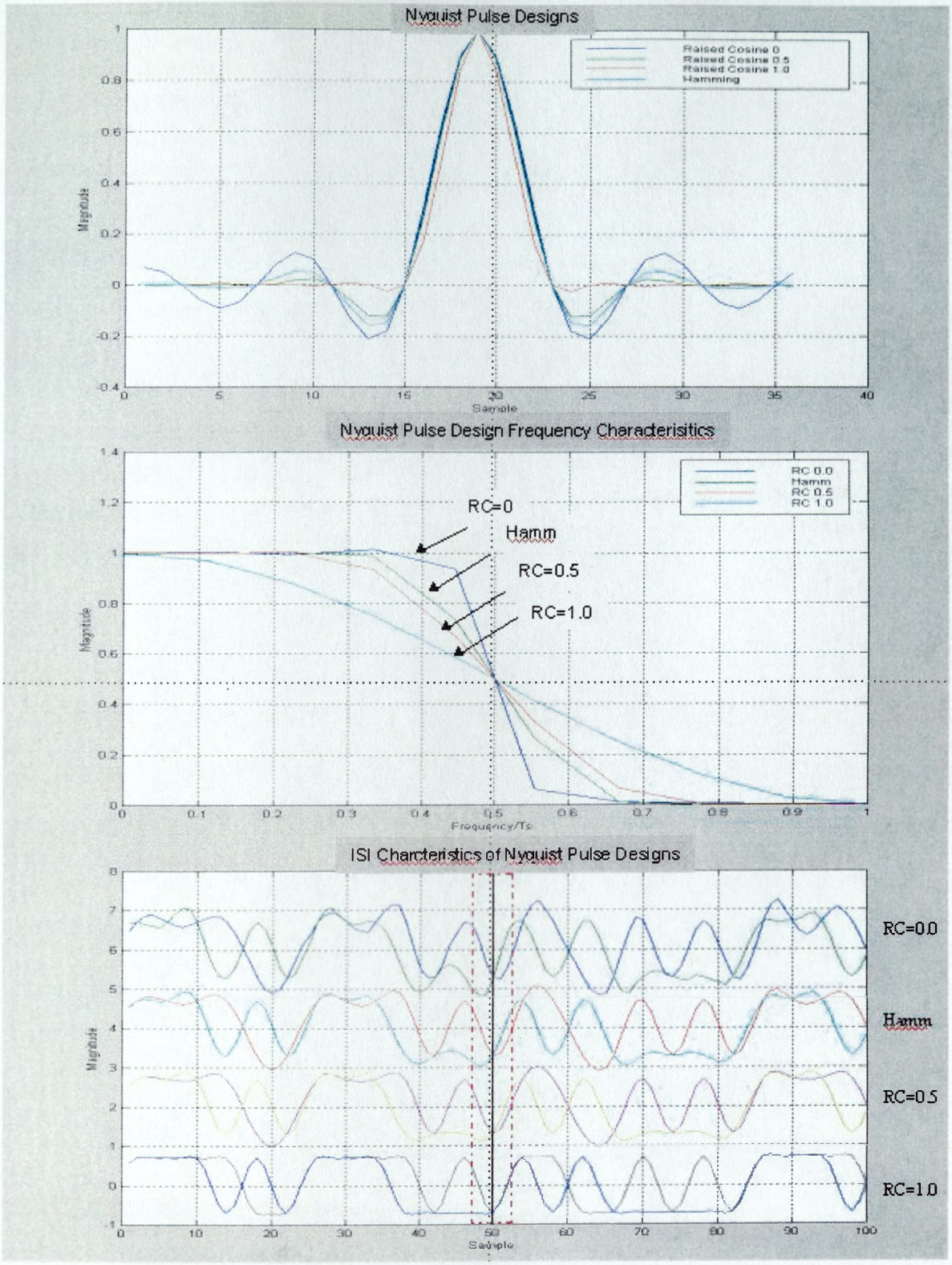

Figure 87: Nyquist pulse designs (top), Frequency Characteristics(middle), symbol timing sensitivity(bottom)

S Optimum Demodulation of ISI Corrupted Digital Signals

S.1 The Maximum Likelihood Sequence Estimator (MLSE)

S.1.1 Intersymbol interference occurs in acoustic channels by virtue of the bandlimited nature of the channel and, more importantly, by the acoustic multipath phenomenon. Transmitted digital complex data $\tilde{c}_n$ are time convolved with the channel impulse response $\tilde{h}(t)$, which smears data symbol energy between adjacent symbols. The received signal is then given by the convolution of the transmitted symbols and the channel impulse response plus noise

$$\tilde{r}(t) = \sum_{n=-\infty}^{n=+\infty} \tilde{c}_n \tilde{h}(t - nT_s) + \tilde{n}(t) \qquad \textit{Eqn 205}$$

S.1.2 It is therefore, perhaps intuitively obvious that an optimum detector for ISI corrupted digital signals is one which operates on sequences of data symbols rather than on a symbol by symbol basis since the convolutional process introduces memory. By this one means that the ISI per symbol is due to the combined contribution from many symbols. So, if one can measure or estimate the channel, one could use this information to systematically evaluate all possible combinations of symbol sequences for a given channel memory.

S.1.3 The optimum detector is one which maximises the a posteriori probability of detecting the transmitted sequence. Such a detector is the maximum likelihood sequence estimator.

S.1.4 The mathematical derivation of the decision rule is well documented in relevant texts [153] and is reproduced here

Choose the sequence $\hat{\tilde{\mathbf{c}}} = \{..., \tilde{c}_{-2}, \tilde{c}_{-1}, \tilde{c}_0, \tilde{c}_1, \tilde{c}_2, ...\}$ *which maximises*

$$F_0(\tilde{\mathbf{c}}) = 2\mathrm{Re}\{\sum_{n=-\infty}^{n=+\infty} \tilde{c}_n^{\,*}\tilde{y}_n\} - \sum_{n=-\infty}^{n=+\infty}\sum_{m=-\infty}^{m=+\infty} \tilde{c}_n^{\,*}\tilde{c}_m\tilde{g}_{m-n} \qquad \textit{Eqn 206}$$

S.1.5 The index n refers to the sequence length over which the decision is based and is determined ultimately by the spread characteristics of the channel. The index m refers to all the symbols transmitted.

S.1.6 The samples $\tilde{y}_n$ are obtained from the correlation of the channel impulse response and the received temporally smeared digital data stream $\tilde{r}(t)$, under the assumption of perfect sampling epoch.

$$\tilde{y}_n \cong \tilde{y}(nT_s) = \int_{-\infty}^{+\infty} \tilde{r}(t)h(t-nT_s)dt \qquad \textit{Eqn 207}$$

where

$$\tilde{y}(t) = \int_{-\infty}^{+\infty} \tilde{r}(\tau)\tilde{h}(\tau-t)d\tau \qquad \textit{Eqn 208}$$

S.1.7 The samples g_{m-n} constitute the ISI contribution from each transmitted to each symbol involved in the sequence estimation

$$\tilde{g}((m-n)T_s) \cong \tilde{g}_{m-n} = \int_{-\infty}^{+\infty} \tilde{h}^*(t-nT_s)\tilde{h}(t-mT_s) \qquad \textit{Eqn 209}$$

where

$$\tilde{g}(t) = \int_{-\infty}^{+\infty} \tilde{h}(\tau)^*\tilde{h}(\tau+t)d\tau \qquad \textit{Eqn 210}$$

S.1.8 Figure 88 illustrates the underlying principle of MLSE detection. The transmitted, complex baseband symbol vector $\hat{\tilde{\mathbf{c}}} = \{\tilde{c}_1, \tilde{c}_2, \tilde{c}_3, \tilde{c}_4\}$ comprises a total of four symbols. For the purpose of illustration, the channel impulse response is assumed of the form

$$h(t) = \begin{cases} 1 & t = 0 \\ 0.5 & -T_s < t < T_s \\ 0 & otherwise \end{cases} \qquad Eqn\ 211$$

S.1.9 The convolution of the transmitted data sequence with the channel $\tilde{c}_n$ with the channel impulse response *h(t)* and the addition of noise gives the received signal $\tilde{r}(t)$ where the noise term $\tilde{n}(t)$ is assumed zero.

S.1.9.1 The autocorrelation of the channel impulse response *g(t)* extends $2T_s$ either side of *t=0.*

S.1.10 The correlation of the channel impulse response *h(t)* with $\tilde{r}(t)$ results in the function $\tilde{y}(t)$.The discrete samples taken at $\tilde{y}(nT_s)$ now comprise the required symbol component and ISI contributions from adjacent samples as shown.

$$F_0(\tilde{\mathbf{c}}) = 2\mathrm{Re}\{\sum_{n=-\infty}^{n=+\infty} \tilde{c}_n^{\,*} \tilde{y}_n\} - \sum_{n=-\infty}^{n=+\infty} \sum_{m=-\infty}^{m=+\infty} \tilde{c}_n^{\,*} \tilde{c}_m \tilde{g}_{m-n} \qquad Eqn\ 212$$

S.1.10.1 The MLSE decision rule therefore involves two terms

- The summation over the sequence length (three in the figure) of the product of each $\tilde{y}(nT_s)$ with the corresponding symbol estimate $\tilde{c}_n^{\,*}$ which is conjugated to ensure a real result.

- The inner summation (over m) of the ISI contribution from adjacent symbols to the outer summation symbol n and the subsequent outer summation over the sequence length of the total ISI contribution over the sequence

13.1.3 The subtraction of the two terms to give $F_0(\tilde{\mathbf{c}})$ provides a quantitative basis for determining the most likely sequence $\hat{\tilde{\mathbf{c}}} = \{\tilde{c}_1, \tilde{c}_2, \tilde{c}_3, \tilde{c}_4\}$ for all possible combinations which in this case would be 16 for a binary system and 256 for a QPSK system.

13.1.4 Recursive formulation of [212] lends to computationally efficient implementation using the Viterbi algorithm

$$F_n(\tilde{\mathbf{c}}_n) = F_{n-1}(\tilde{\mathbf{c}}_{n-1}) + \mathrm{Re}[\tilde{c}^*_n(2\tilde{y}_n - \tilde{g}_0\tilde{c}_n - 2\sum_{m=1}^{L}\tilde{g}_m\tilde{c}_{n-m})] \qquad \textit{Eqn 213}$$

S.2 Practical Considerations

S.2.1 It is evident that the complexity of the MLSE detector scales exponentially with the length of the sequence over which the detection is made. Since this is itself dependant on the time spread of the channel, one would presume that the utility of MLSE based detection is limited for typical underwater channels.

S.2.2 Assuming a time spread of 10ms for a typical shallow water channels and a 10ksym/s QPSK transmission, the time spread of the channel equates to 100symbols. So the direct implementation of an MLSE detector would have to evaluate $4^{100} = 1.61\text{x}10^{60}$ sequence combinations! Whilst there are efficient techniques to implement the MLSE, most notably the Viterbi algorithm, the problem, in its current form, is sufficiently complex to preclude real time implementation.

S.2.3 In many practical acoustic channels however, the channel spread is discrete due to the multipath phenomenon. This suggests that significant savings in computational complexity could be made by considering the ISI contribution only from significant paths.

S.2.4 Such an approach could greatly reduce the complexity of an MLSE decoding algorithm. In this case the discrete nature of path arrivals is exploited to reduce the number of

potential combinations. For example it is possible that an acoustic channel comprises 4 significant paths over the 10ms time spread. Assuming a 0.2ms (2 symbol) temporal smear is associated with each path then $8^4 = 4096$ sequence combinations would have to be searched. Such complexity is well within the capability of current signal processing devices.

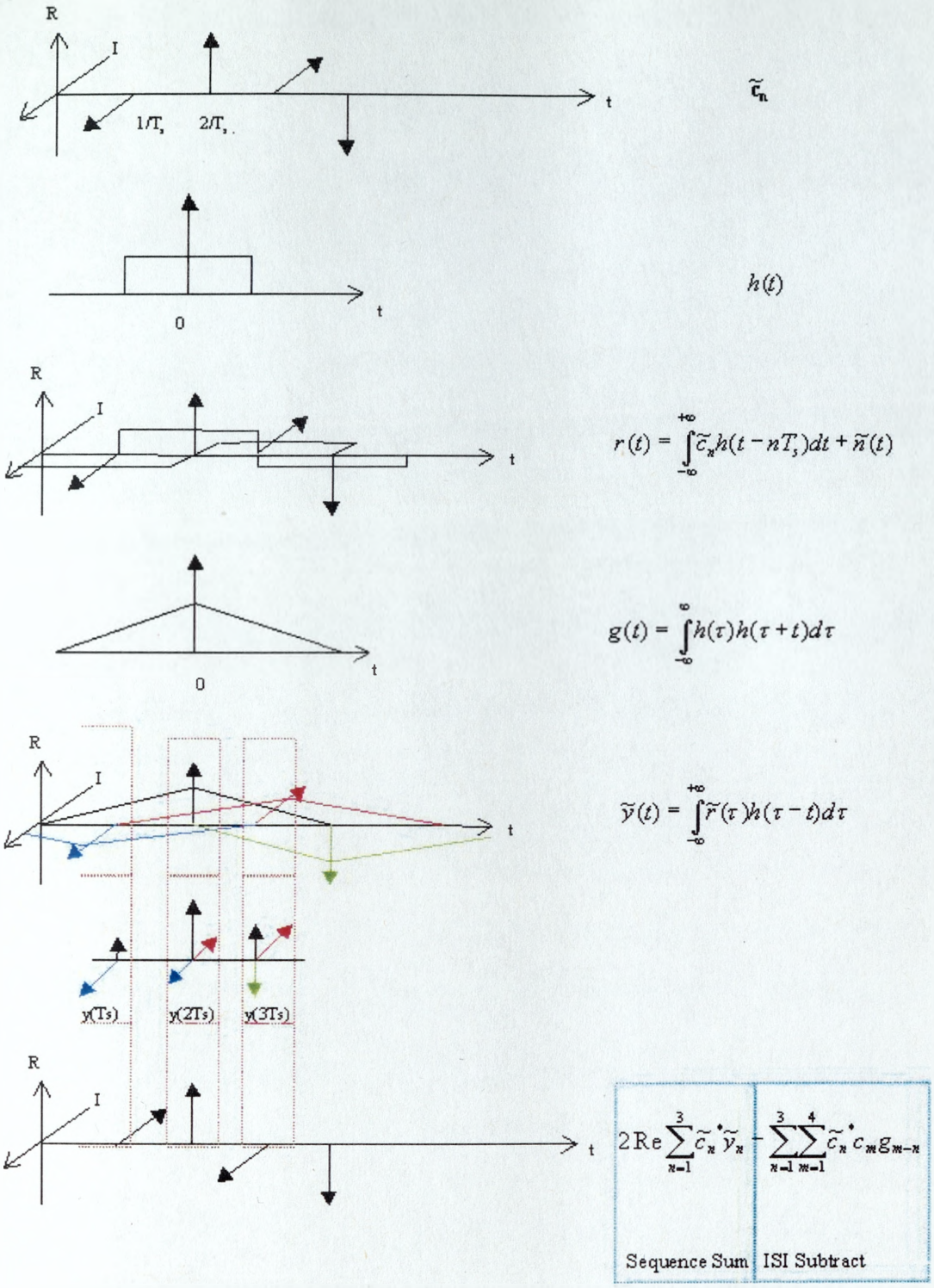

Figure 88:Pictorial Representation of the operation of a MLSE detector

T Swimmer Speed Measurement Device

T.1 Problem

T.1.1 During training the ability to measure a swimmers speed time profile provides a valuable aid to coaches and trainers seeking to improve technique and efficiency. The use of acoustics to measure swimmer speed is greatly complicated by the acoustic multipath problem, which is both extremely long due to the smooth hard faces of the pool enclosure and extremely variable due to the confined geometry. Narrowband transmissions are subject to fading and rapid phase variability by virtue of the multipath extent and temporal variability. In order to achieve greater speed measurement fidelity a wideband system was developed using direct sequence spread spectrum modulation techniques.

T.1.2 The ability to use consecutive channel estimates to determine Doppler were reported in section 6. The overarching aim is to first resolve path multipath structure and then to use successive channel estimates to determine acoustic Doppler.

T.1.3 In the swimmer device, acoustic Doppler is first estimated using the two-chirp open loop Doppler estimation technique (see section 6). This estimate is then used to provide a coarse Doppler correction during the data-decoding phase. Data modulation is implemented as a direct sequence spread spectrum code modulation using two M sequence codes to encode a fixed data transmission. The first Msequence transmission is cyclically prefixed to improve its correlation properties as discussed in section 7. This provides the reference for subsequent data decoding and path combining.

T.1.4 During data decoding phase an M=2 maximum likelihood decoder determine the most likely transmitted code sequence. This comprises two parallel correlators which form the cross correlation result of the received signal transmission with the two potential codes. The correlation is weighted by the previous channel estimate, i.e. raked.. In order to

ensure the channel remains reasonably stable over two observation intervals the system operates at an effective symbol rate of 50Hz which provides an acceptable trade off between maximising system processing gain and channel tracking performance.

T.1.5 The channel estimate from the detection decision is then cross correlated with the previous channel estimate to determine phase advance or retard arising from relative motion between transmitter and receiver. This cross correlation result is computed for early, on time and late lags and the resulting phase correction used to provide the velocity estimate

T.2 Results

T.2.1 Figure 89 shows swimmer speed profiles for male and female swimmers performing the breast stroke. The breast stroke was found to provide the best results due to the consistent body posture during the stroke. The results clearly demonstrate deceleration, acceleration and glide phases of the stroke. The channel evolutions for each stroke demonstrate significantly different path structures. The top graph data was taken for an Olympic size pool and the bottom a 25m x 8m pool. The path structures demonstrate significant variability in structure, and path extent between pools. Not indicated, but equally important is the swimmer position within the pool

T.2.2 Figure 90 shows swimmer speed profiles for a slow front crawl stroke with initial push off (top) and butterfly stroke. More evident in these strokes is the dramatic loss of signal which occurs within the stroke. This is most evident in the butterfly stroke and corresponds to the power phase where the swimmer surfaces and draws both arms forward. In this case complete loss of signal occurs due to water aeration in front of the transducer. The effect was also noticeable during front crawl stroke however it was unclear if signal loss was due to water aeration or acoustic shadowing whereby the line of

sight propagation path is lost as the swimmer's body twists. Refinement of the system and ongoing development will seek to address the signal loss problem.

T.2.3 Potential solutions include a more thorough study of the siting and design of the swimmer transducer mounting arrangement and the use of more than one transducer to provide some spatial diversity. The potential benefits of both approaches require underwater video of the swimmer stroke viewed along the acoustic path. This is the subject of ongoing investigation. The ultimate aim will be to time synchronise video footage with the swimmer speed profile to highlight and correct technique deficiencies.

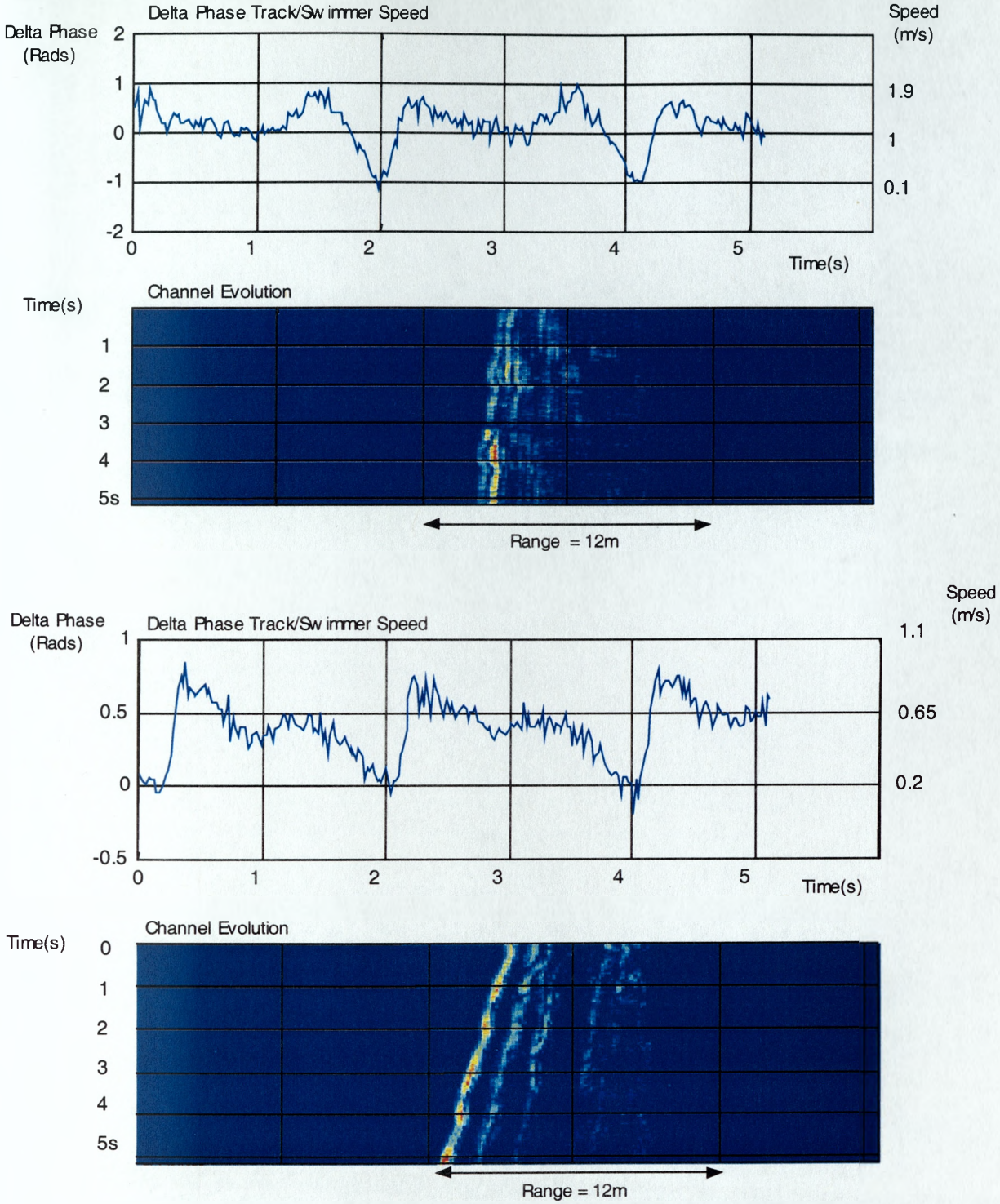

Figure 89; Comparison of Male (top) and Female (bottom) breast stroke profiles

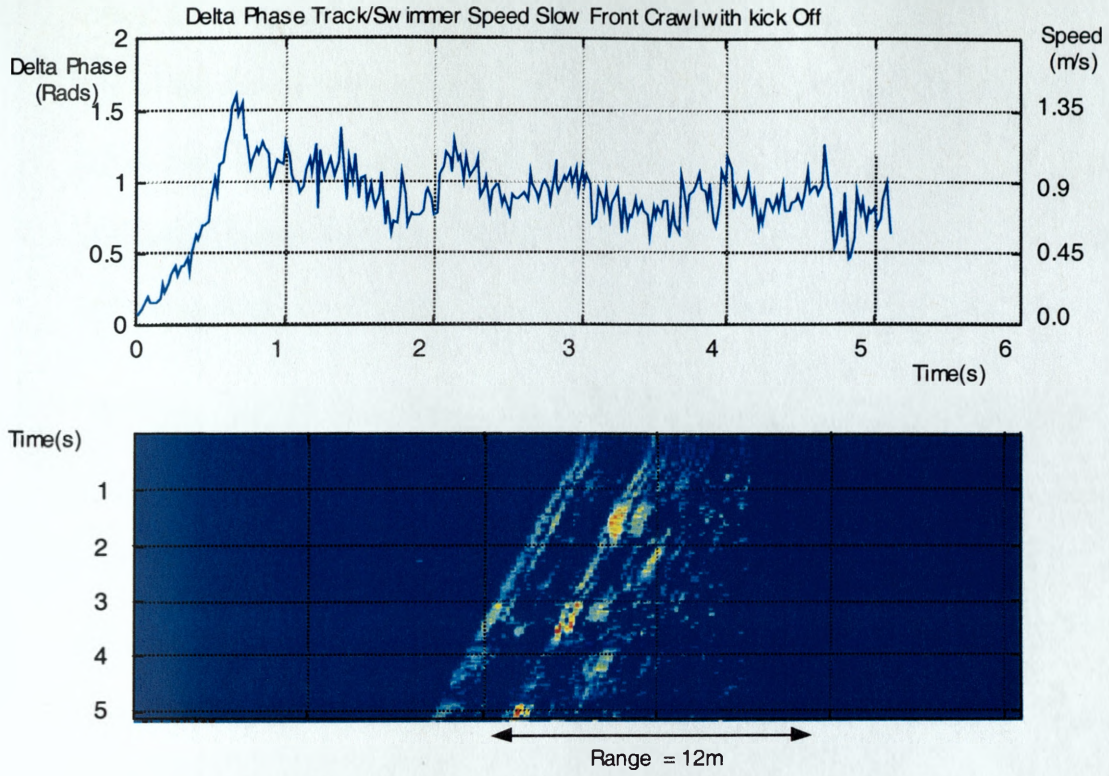

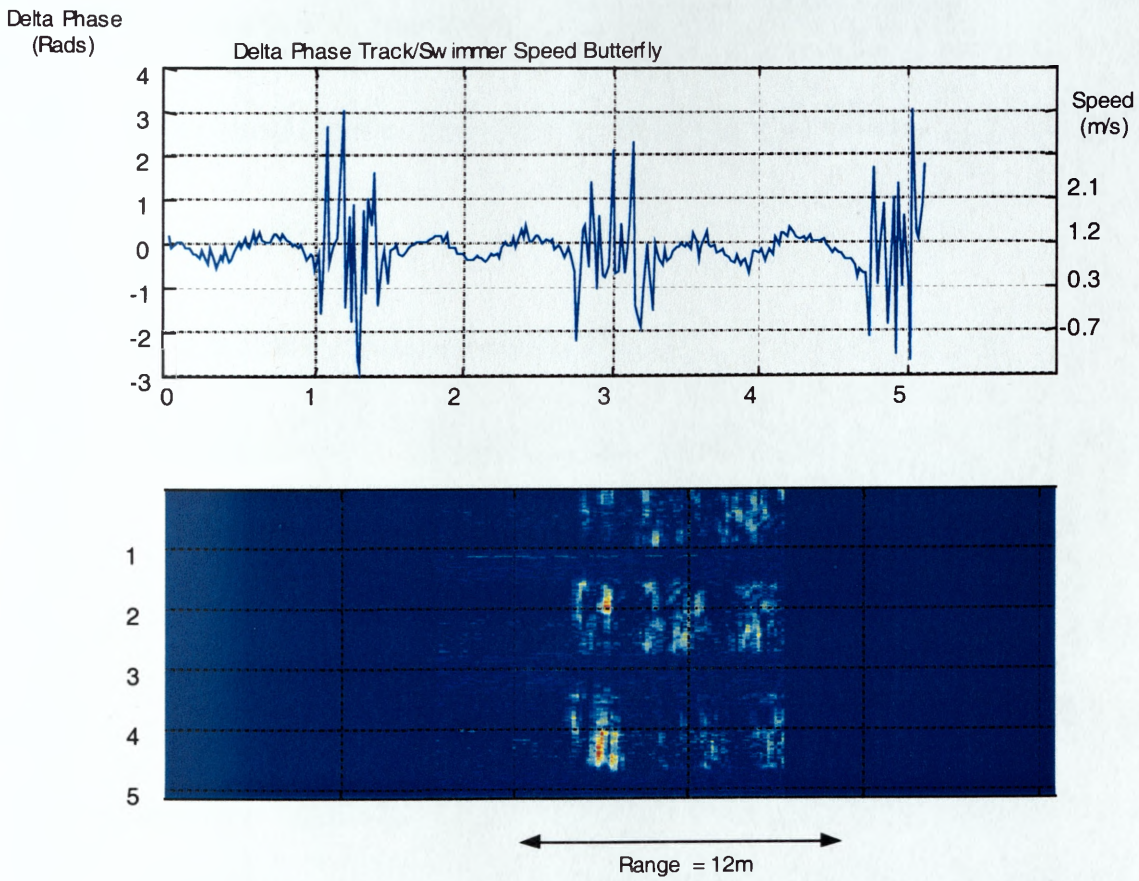

Figure 90; Male Slow Front Crawl with push off (top) and butterfly (bottom)

U Field Trials Results and Analysis

U.1.1 Initial sea trials investigating the performance of a vertical line array (VLA) receiver were conducted during August 1998 in Weymouth Bay using a 14-element analogue VLA reciever. Signals from the receiver were digitised and stored on a Racal Storeplex data recording system and archieved to CD-ROM for subsequent offline analysis.

U.1.2 The array configuration comprised 14 ball hydrophone receive elements spaced at 5cm spacing. The data transmission comprised a 10000symbol pseudorandom data transmission at 10.5ksym/s between 10-20kHz using phase coherent QPSK modulation equating to 2bps/Hz. This configuration provided a net throughput rate of 21kbps. Water depth was typically between 15-20m with the receiver deployed midwater and the transmitter deployed to a depth of 5m. A more comprehensive discussion of the field trials results and experimental configuration is provided in [158].

U.1.3 Experimental results from four trials geoemetries were recorded as follows

- Static400 – Static transmitter and receiver separated by 400m
- Static1200 – Static transmitter and receiver separated by 1200m
- Dynamic400_1 – Transmitter moving toward static receiver at 3.5kts,range 100m-400m
- Dynamic400_2 – Transmitter moving away from static receiver at 3.5kts,range 100m

U.1.4 Figure 91 depicts offline analysis results for the static400 scenario. The figure depicts algorithm diagnostic displays top and bottom for two arbitrary packet transmissions selected from the total of 60 packets transmitted. The middle figure depicts the evolved channel impulse response computed from individual packet headers and demonstrates the temporal variability of the channel and the nature and extent of channel multipath. The

figure indicates typically 5-6 path arrivals with highly variable relative magnitudes. The time evolution of the channel demonstrates temporal perturbations in the arrival time of the respective paths believed attibutable to the transmitter – receiver platform heave dynamics.

U.1.5 For this configuration all packets were successfully decoded with error rates of better than 1e-3. Considering the algorithm diagnostic displays it is evident that both packets were correctly decoded as indicated by the I-Q constellation diagram shown upper right and this is reflected in the MSE plot shown bottom left. Of particular interest is the time variability of the decoder phase error, which indicates a consistent error of approximately 10degrees for the first packet, and between –5 to +5 degrees phase error for the second packet. It should be noted that the mean Doppler drift component was preprocessed out prior to decoding for each packet. The phase error therefore reflects temporal variabilty in the path length arising from platform dynamics over the transmission duration. The error itself represents the phase tracking lag as the fractionally spaced forward filters in the recevier decoder attempt to compensate for the temporal fluctuation in the received signal.

U.1.6 The impact of this tracking effort on overall receiver performance is demonstrated in figure 92, which represents results for the static1200 geometry. Here the evolved channel impulse response has notably less time spread and the relative path magnitudes appeart more stable than the static400 geometry. There remains however temporal perturabations in the path arrival times. For this configuration again, all packets were successfully decoded with error rates less than 1e-3 and this is reflected in the two algorithm diagnostic figures shown top and bottom. Of particular note in this data set, is the time variability in the receiver phase error, which exhibits sinusoidal variations on time scales of 1-2s. Further, it is evident from the upper diagnostic figure, that high phase tracking

errors equate to increased magnitude squared error. This underlines the need to offload the phase tracking effort from the adaptive filters in order to achieve robust performance in time selective environments. This is in broad agreement with the results presented in section 9.12 which identified the requirement for close loop phase tracking and its role in improving algorithm performance under time selective conditions.

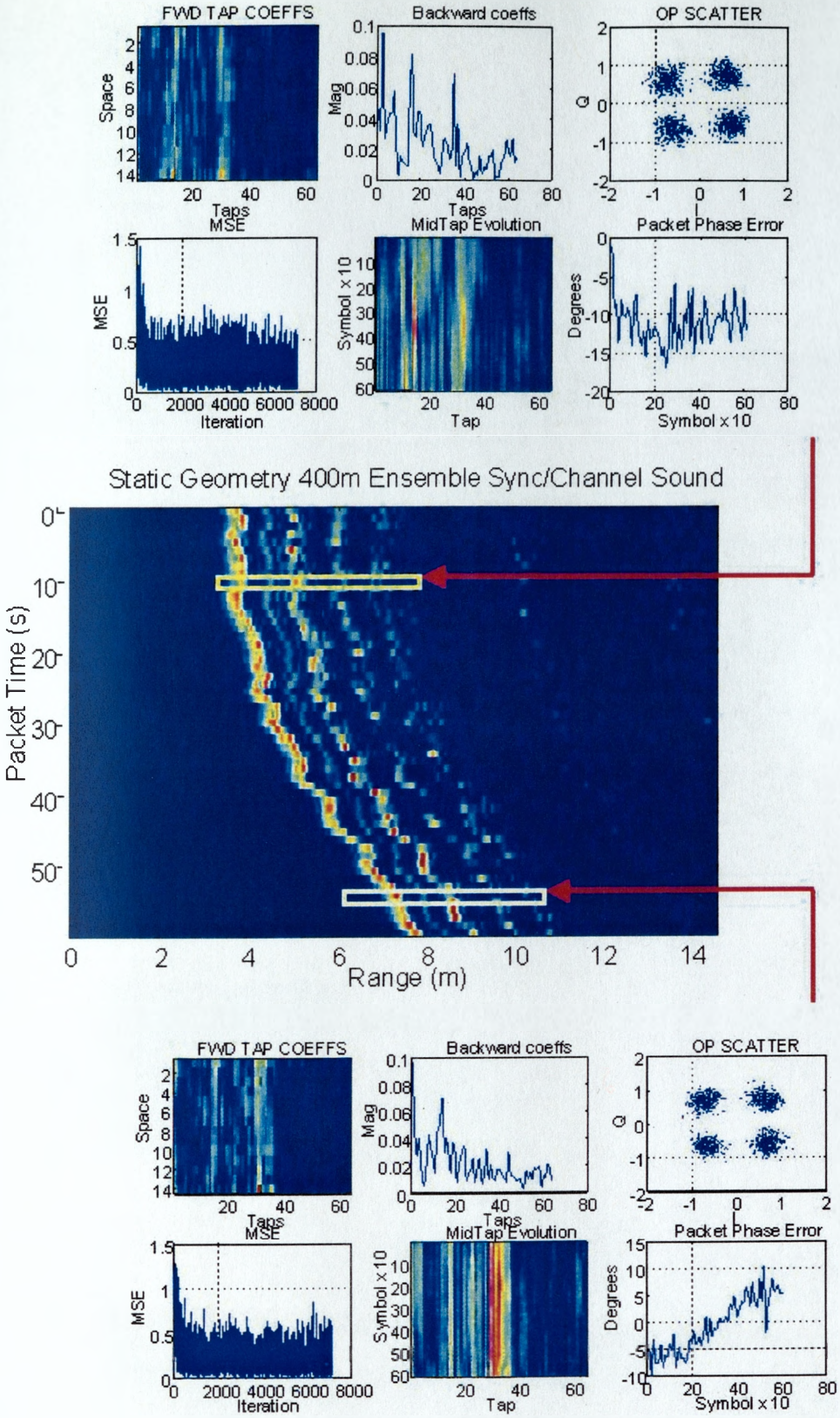

Figure 91; Weymouth Bay Range 400m

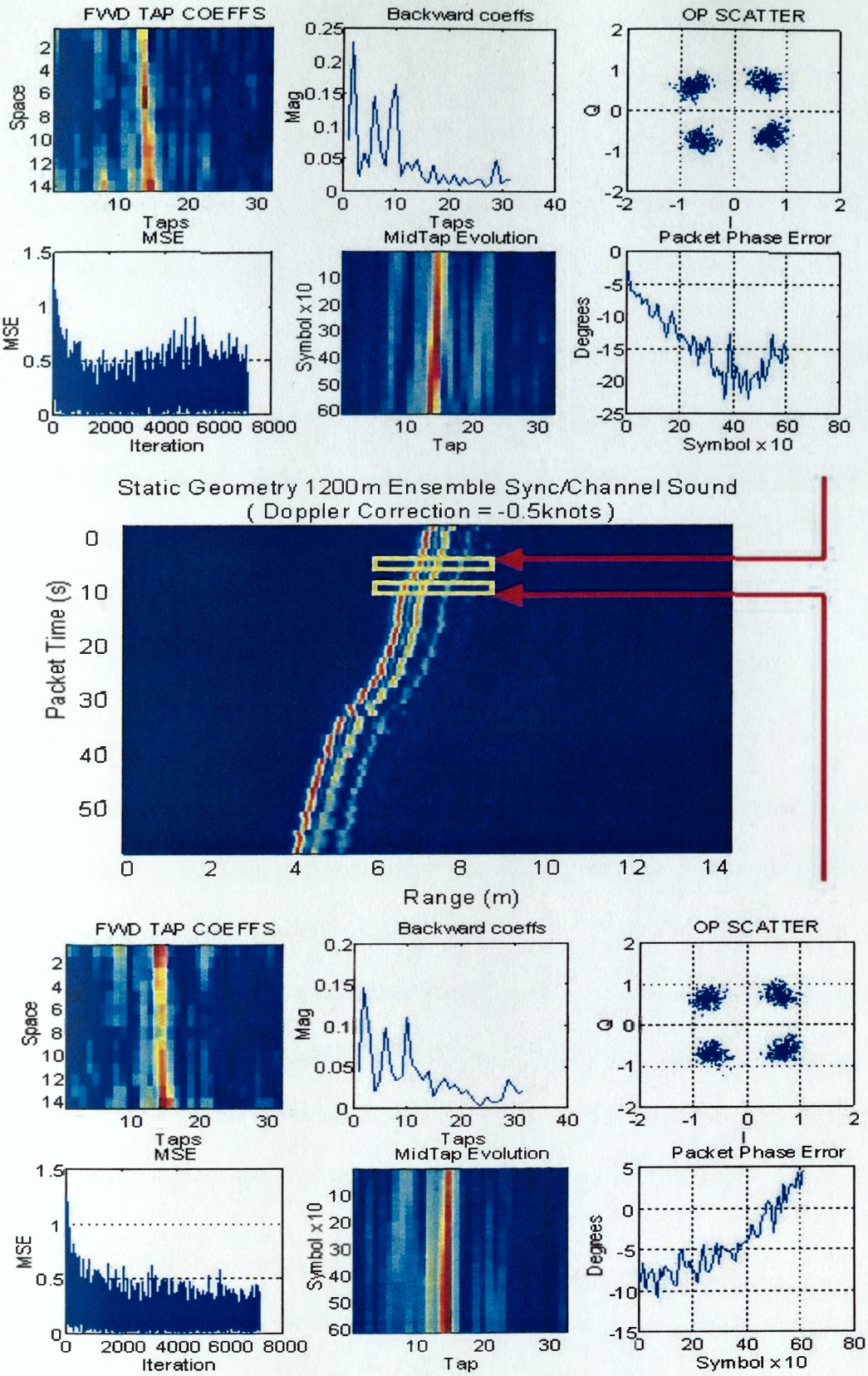

Figure 92; Weymouth Bay Range 1200m

U.1.7 In figure 93, decoder performance is compared for data packet transmitted for the static 1200 configuration where the array geometry is altered. Specifically, the upper diagnostic display depicts decoder performance for the full array aperture based on 14 elements at 5cm spacing. The lower figure depicts decoder performance based on the same array aperture, but in this case the aperture comprises 7 elements at 10cm spacing.

U.1.8 The result indicates that there is only a marginal performance improvement in sampling the acoustic field at lambda/2 spacing relative to lambda spacing for fixed acoustic aperture. This is indicated by the MSE curves for each case which exhibit broadly similar behaviour with the full aperture array at lambda/2 spacing having slightly reduced error during the acceleration occuring over the packet duration. This result supports the conclusions from the simulation studies conducted in section 9.16 relating to algorithm performance versus sensor separation.

U.1.9 Specifically, it was shown that comparable decoding performance can be achieved for fixed acoustic aperture for lambda and half lambda spacing in an isotropically noisefree environment. In the lambda spacing case, it was shown in section 9.16 that at the frequencies of interest, the diffraction secondaries fell 50-60degrees eitherside of broadside and they were typically 15dB. The practical significance of this result is that provided there are no significant path components outside of this angular limit and that there are no significant noise sources outside the limit then high diffraction secondaries will not necessarily limit overall performance.

U.1.10 This assumption is likely to be satisfied at moderately long range to depth ranges. At shorter range to depth ratios, path angular arrivals may occur at angles equal to or greater than 50-60degrees. Such arrivals may potentially lead to degraded performance.

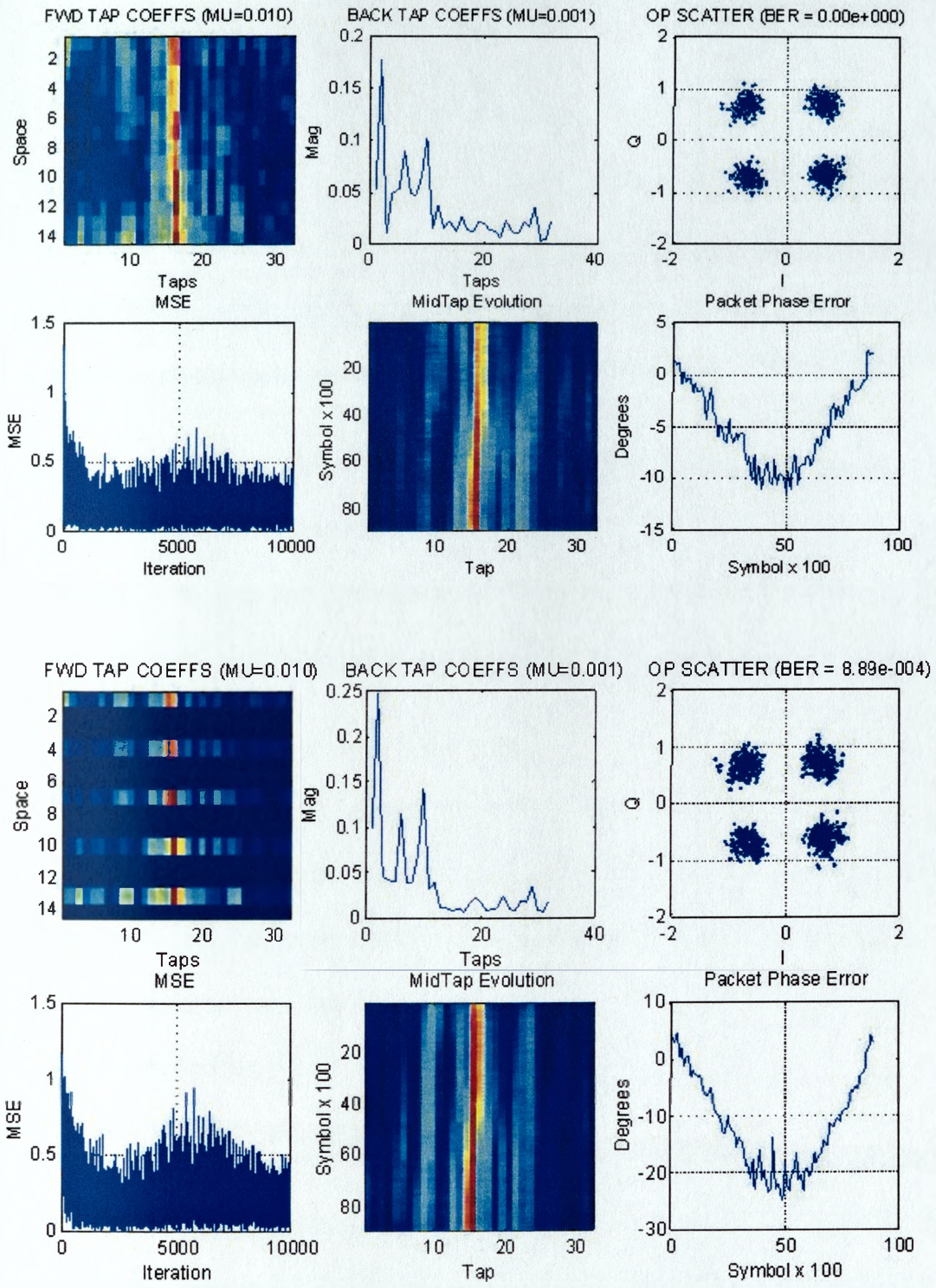

Figure 93; Weymouth Bay Range 1200m, comparison of full array and subarray performance

U.1.11 Figure 94 depicts algorithm diagnostic displays for the dynamic400_1 geometry. Here the transmitter approached the static receiver at a relative velocity of 3.5kts. The figure shows analysis results where this mean Doppler component has been removed prior to algorithm application.

U.1.12 The evolved channel impulse response demonstrates three significant arrivals that are subject to appreciable residual Doppler variation despite the removal of the mean Doppler bias prior to decoding. This underlines a key point, namely that any channel or Doppler estimation algorithm represents merely a snap shot of the complex temporal variability of the acoustic channel

U.1.13 This is further emphasised by the variability in the phase tracking error commensurate with platform heave dynamics. Despite this variabilty, and with appropriate open loop Doppler correction, the algorithm is able to track the temporal fluctuation of the multipath and successful decoding was achieved for the majority of packets.

U.1.14 The figure also depicts array beam pattern responses at the end of the decoding phase. The two beam pattern results demonstrate that the multipath arrival angles were approximately broadside. The rich structure of the two beampatterns and the disparity between these structures further underlines the complex spatial-temporal coherence characteristics of shallow water channels and how STAP receiver processing copes with these complexities.

U.1.15 This issue is developed further in figure 95. Here the STAP decoder is synchronised to each of the arrivals shown in the channel impulse response of figure 95. The channel snapshot is shown in the upper figure and the resulting beam pattern response at the end of synchronising to each of the path arrivals is shown in the lower figure. The result demonstrates the ability of the STAP decoder to not only adaptively beamsteer to the

synchronised path arrival and adjust the beam beam response in accordance with the path magnitude, but also the ability to selectively spatially cancel other paths that manifest as uncorrelated noise in the receiver. This is most clearly demonstrated by the nulls in the beam pattern at 5degrees corresponding to the direct path arrival when the receiver is synchronised to the second and third arrivals.

U.1.16 Doppler and perhaps more importantly Doppler variability within a data packet is a key factor influencing overall algorithm performance. In figure 96 Doppler estimates based on synchronisation to one of two different rays are shown for a series of 20 data packet transmissions. The upper figure depicts range and Doppler estimates for each ray based on twenty consecutive packet transmissions. This figure demonstrates a closest point of approach between transmitter and receiver in the vicinty of packet 16. The range profile demonstrates that between packets 15-19 the platform Doppler was changing relatively rapidly. It is interesting to compare the performance of the decoding algorithms during constant Doppler and accelleration conditions. In particular it can be seen that the algorithms perform effectively with an error rate of between 1e-2 to 1e-5 for packets 1-15 and performance is noticeably degraded during the accelleration period where the error rate increases and the system is unable to synchronise to several packets during this period. This was believed attributable to acoustic screening effects from wake of the transmitter boat during the transition from forward aspect to stern aspect.

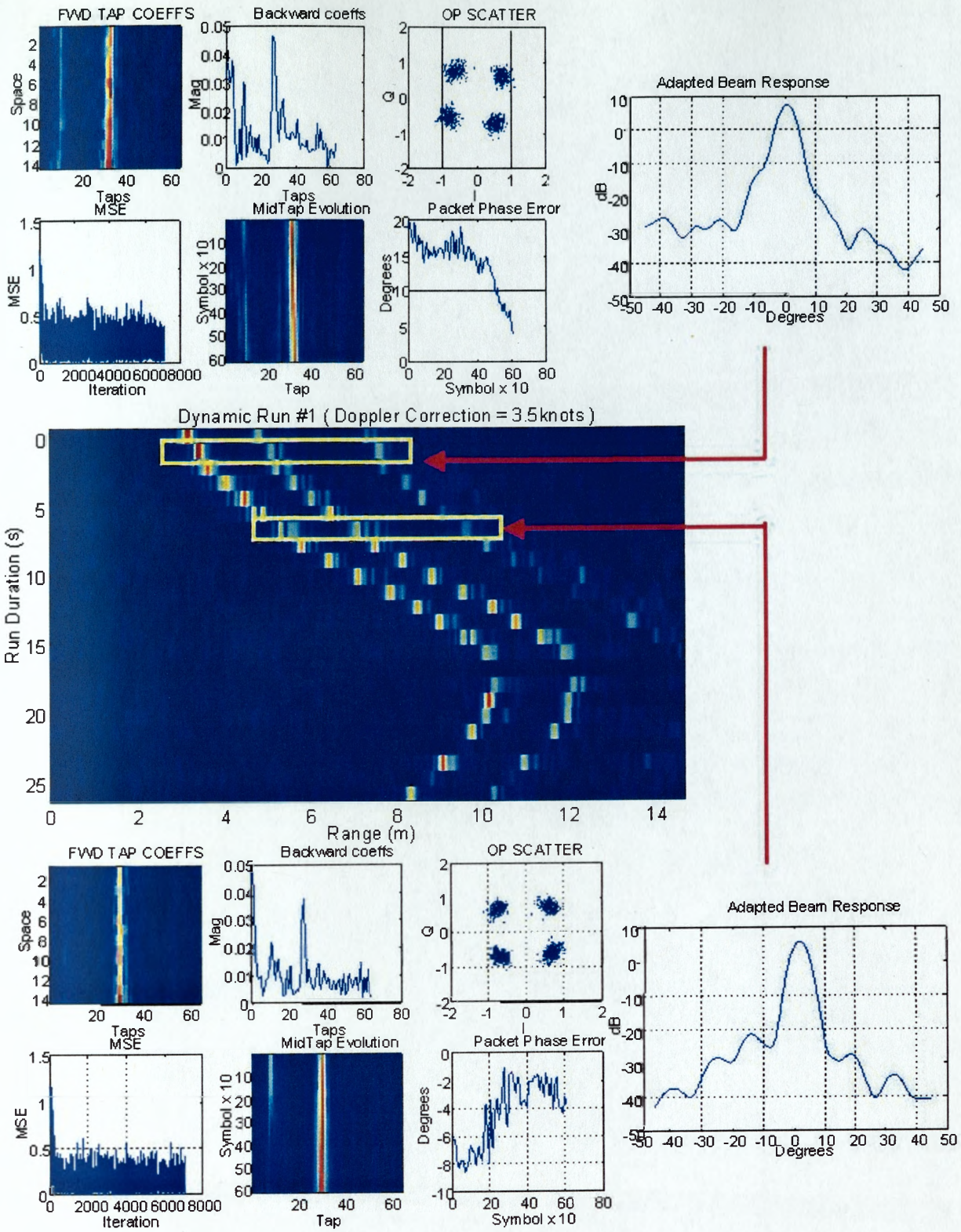

Figure 94; Weymouth Bay Range=400m Doppler=3.5kts

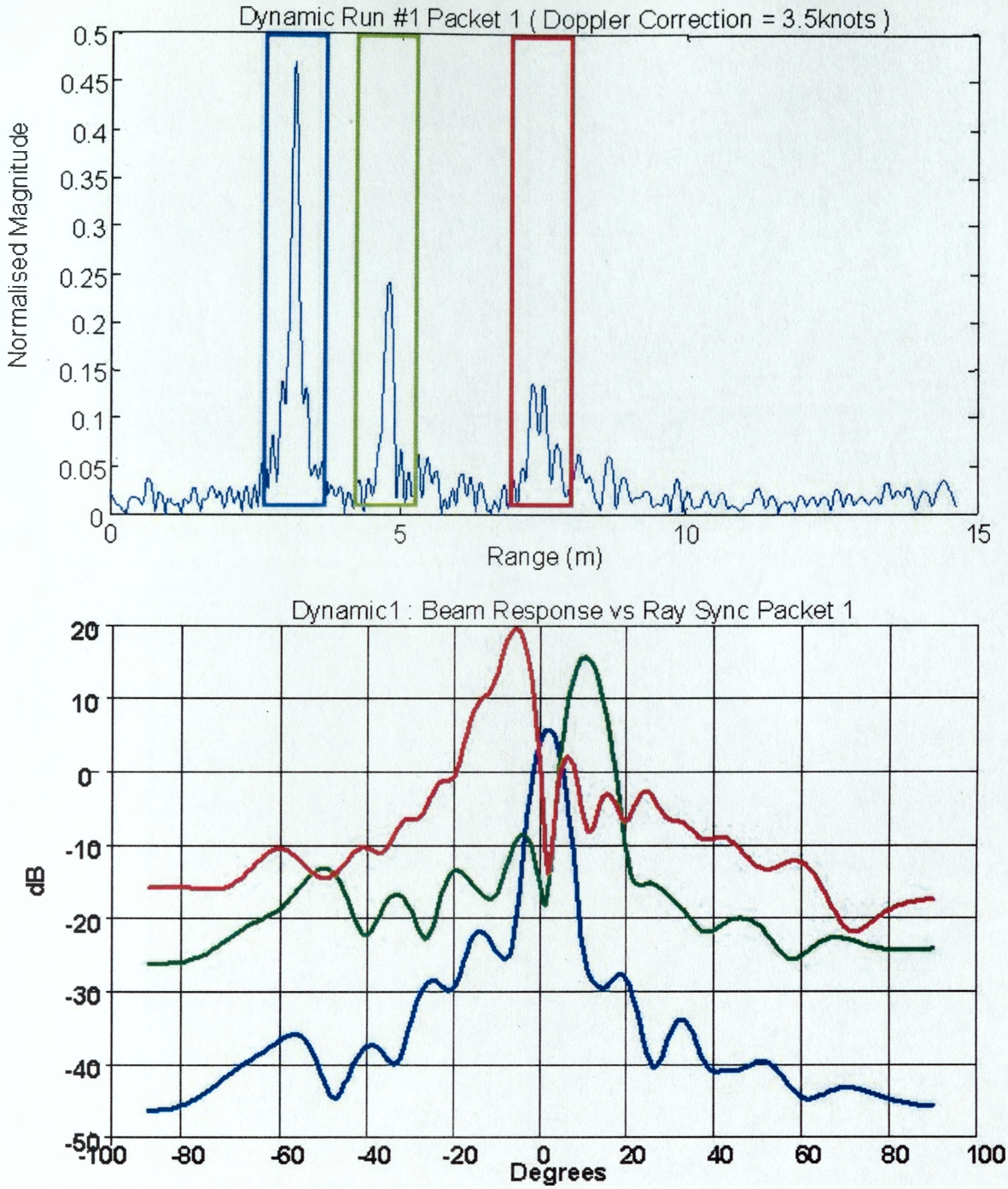

Figure 95; Weymouth Bay Range=400m, Comparison of beam responses when synchronised to different path arrivals

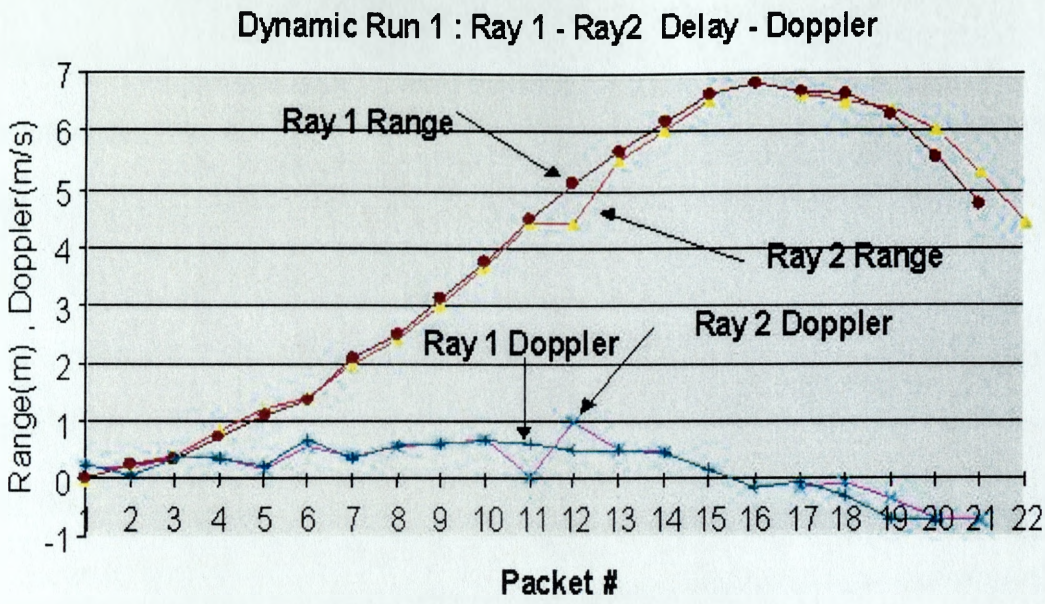

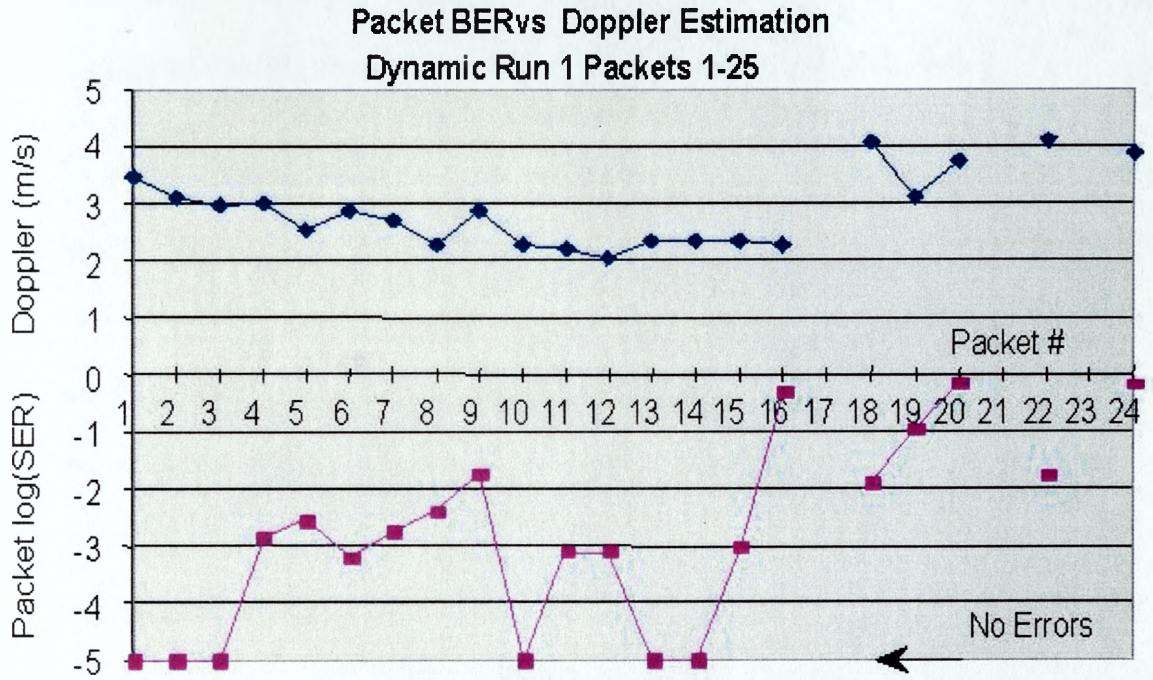

Figure 96; Doppler variability for first and second path arrivals (top), system symbol error performance plotted versus Doppler

U.1.17 Under favourable channel conditions very high data throughputs are possible. This is demonstrated in figure 97 which illustrates decoder performance for a 41kbps transmission in the band 10-20kHz using the same 14 element receive configuration described previously. This data, collected during a collaborative trial in the Timor sea, NW Darwin, Australia, demonstrates the potential for very high data throughputs under favourable channel conditions. The middle figure depicts the channel magnitude impulse response evolved over 16 packet transmissions and indicates two path arrivals, separated by 0.6m. Despite the fact the transmissions were made in a shallow horizontal channel, at a range of 1500m and water depth 300m, the prevalent propagation conditions resulted in a relatively benign channel capable of supporting very bandwidth efficient modulation schemes. Such an efficient scheme is the QAM16 phase coherent modulation depicted in the figure affording 4bps/Hz and an overall data throughput in excess of 40kbps.

U.1.18 Of course, channel conditions are often less benign and highly variable in both time and space. Figure 98 for example depicts the same system operating in the same environment two days later. Here the channel can no longer reliably support 41kbps and the figure shows system operation at the reduced rate of 20kbps. Of particular note in this figure is the existence of large transients in the MSE graphs for both packets. These were due to biological activity in the vicinity of the receive array which introduced bursty errors indicated by outliers in the IQ constellation plot.

U.1.19 Figure 99 depicts decoder performance for a more complex environment. This data, collected from field trials conducted in the NE Adriatic, demonstrates a more severe channel character exhibiting greater time spread extending some 20-25ms with a more complex structure. The difficult nature of this environment is reflected in the more diffuse IQ constellation and the more complex distribution of energy in the forward space time matrix. A further point of note was that this data set represented a reduced data

throughput of 12kbps in the 9-16kHz band compared to 20-40kbps from previous results. This was a result of the transition from data gathering experiments to real time embedded modem operation. In the latter case the transducer technology was based on cheaper flooded ring designs which represented a cost – performance trade off biased toward cost.

U.1.20 Figure 100 depicts STAP decoder performance for a 12kbps transmission decoded in forward and time reversed directions. The upper group of eight graphs depict algorithm performance in the forward direction and the lower group of eight graphs depict algorithm performance in the backwward or time reversed direction. The key point to note from this analysis is that the channel itself is moderately complex exhibiting time spread in excess of 20ms with a strong first arrival followed by numerous weaker paths.

U.1.21 This channel is a classic candidate for the conventional forward implementation of the STAP decoding algorithm, and as can be seen from the figure the algorithm successfully decodes this particular channel. However it is also clear that the algorithm is also successful when implemeted in time reverse as discussed in section 8. Here one notes the trajectory of the integrated phase error is the inverse of the forward case and the forward space time tap magnitudes are also time reversed.

U.1.22 Although not indicated in the figure the successof the time reversed decoding stems from the angualr diversity of the incident multipath arrivals. Without this spatial information it is unlikely that the algorithm could reliably converge for this minimum phase channel.

U.1.23 Figures 101 and 102 depict algorithm performance operating at lower frrquencies and longer ranges. Figure 101 shows results from field trials data collected by the Active sonar group at QinetiQ Winfrith, involving the transmission of phase coherent waveforms over a range of 21km in a reverberant littoral environment. Figure 102 shows results from

field trials involving transmission of phase coherent waveforms over a range of 12km at a rate of 1.6kbps using a low frequency towed projector.

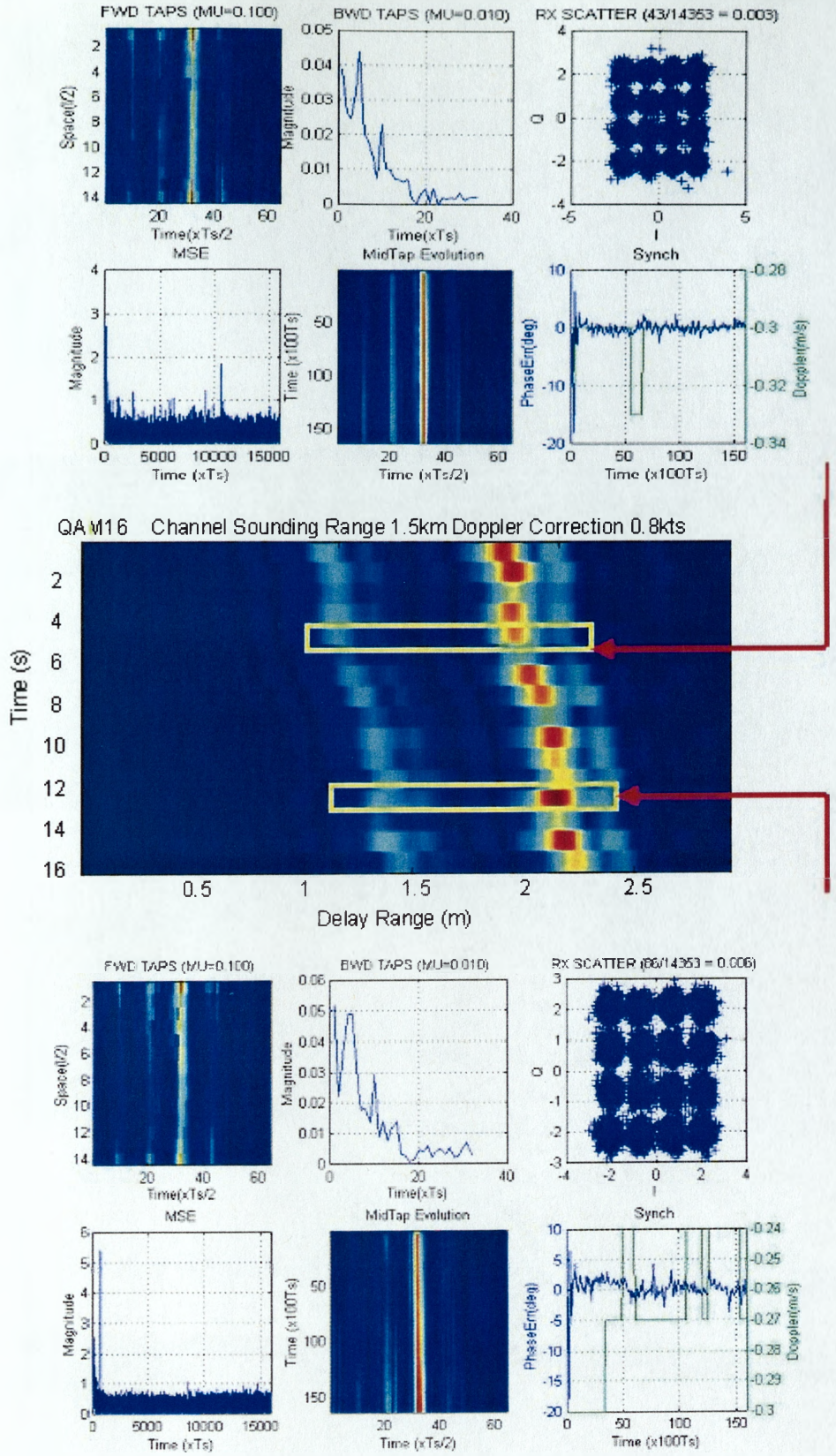

Figure 97; QAM16 Transmission at 1.5km, 41kbps Timor Sea, North Australia, October 1999

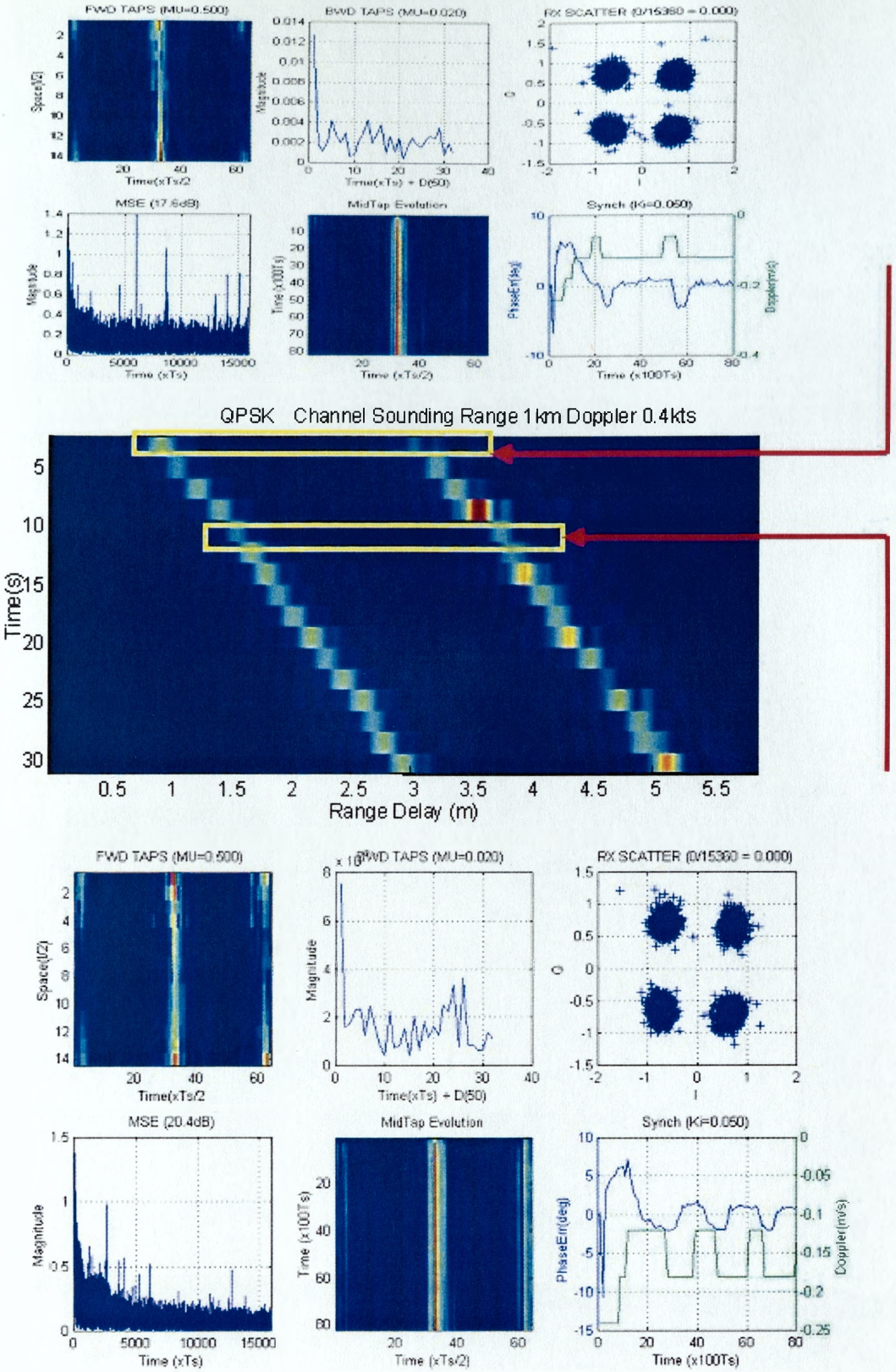

Figure 98; QPSK @ 20kbps Range 1.5km Timor Sea, North Australia

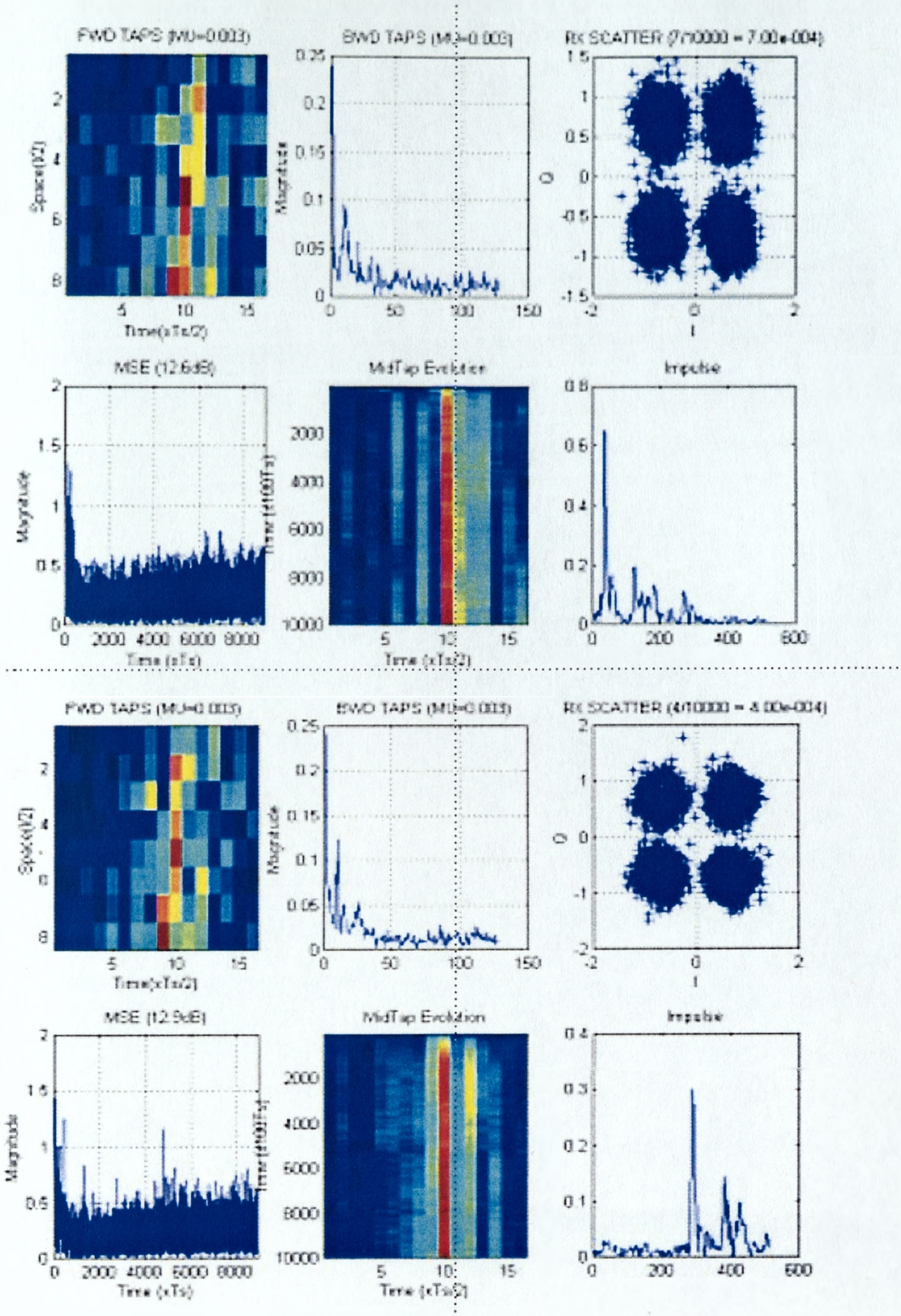

Figure 99; QPSK Data Uplink @ 12kbps Range 1.2km from Subsea Node North East Adriatic, 2000

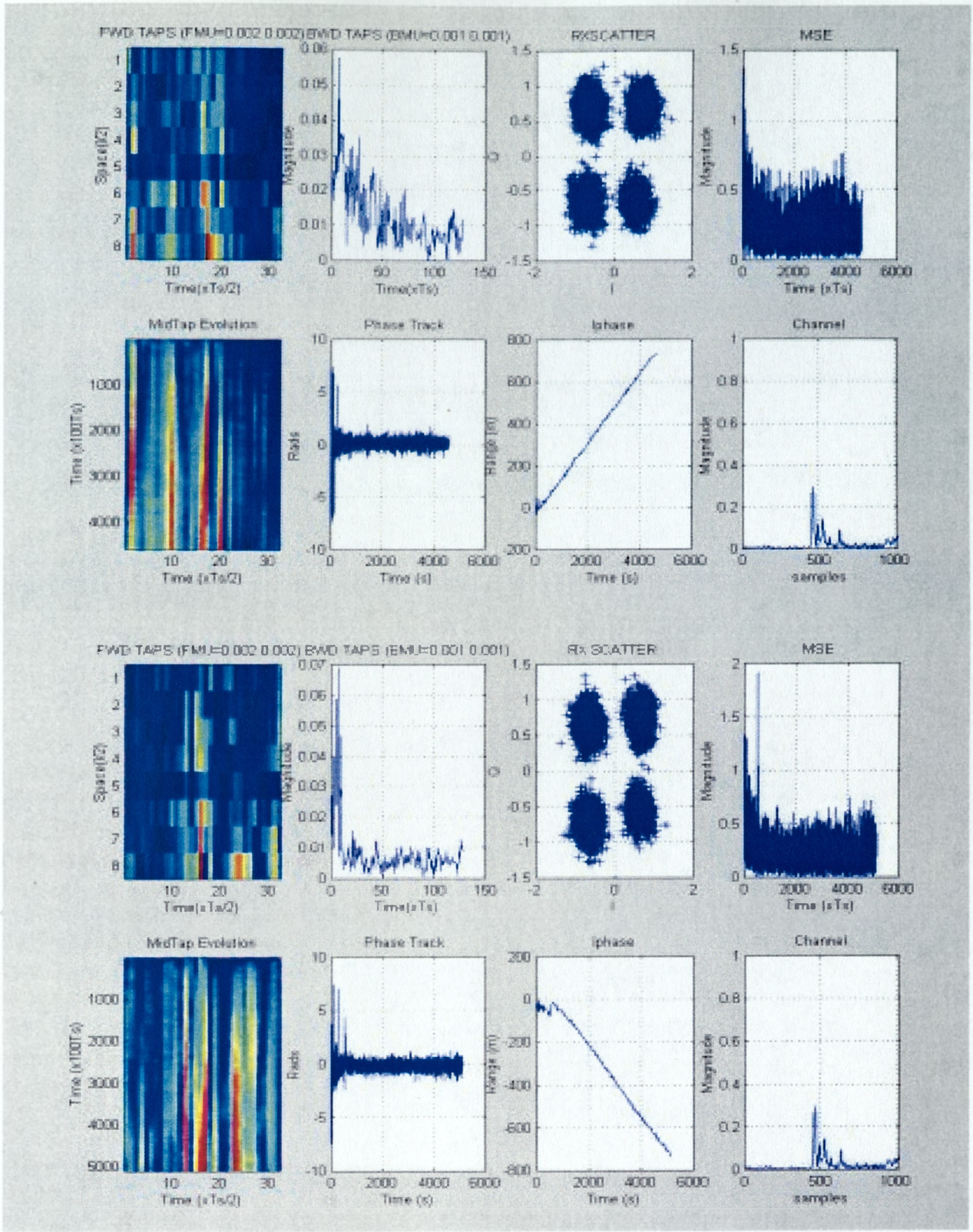

Figure 100 Forward (top) and Time Reversed (Bottom) STAP decoding 12kbps @ 1km, Portland Harbour ,2001

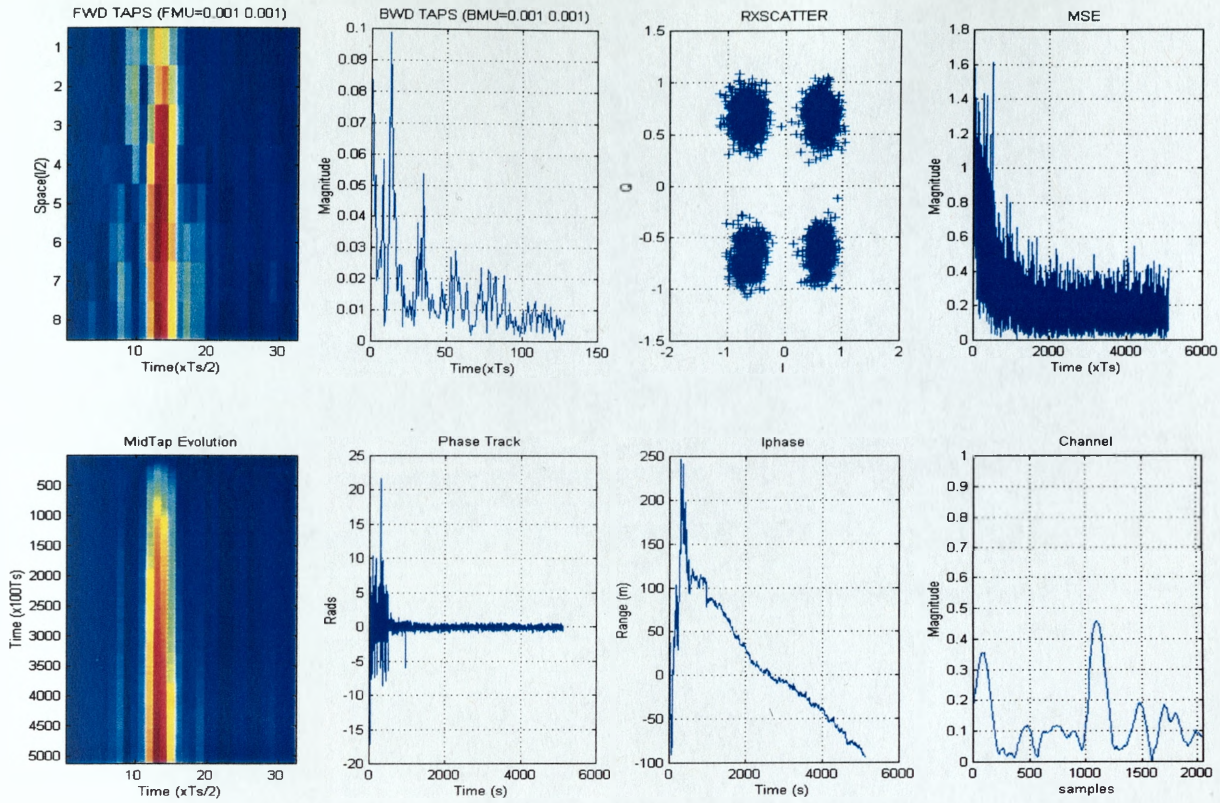

Over the last ten years there has been a paradigm shift in underwater acoustic communications technology and performance brought about by advances in signal processing technology and a greater understanding of the issues relating to acoustic communications performance particularly in shallow water environments This report explores the potential roles of acoustic communications technology in the modern underwater battlespace and identifies existing force command, control and communications shortfalls based on current and future submarine platforms and roles. The need to support future off platform technologies and the underwater C3 requirement of these technologies is discussed and developed in the context of future network centric warfare applications. It is concluded that acoustic communications is a key enabling technology to underpin future operational concepts, roles and technologies and should be supported within both pure and applied research programs.

Figure 101; Text Message Transmission from LF moving source to static receiver at 1.6kbps range 12km

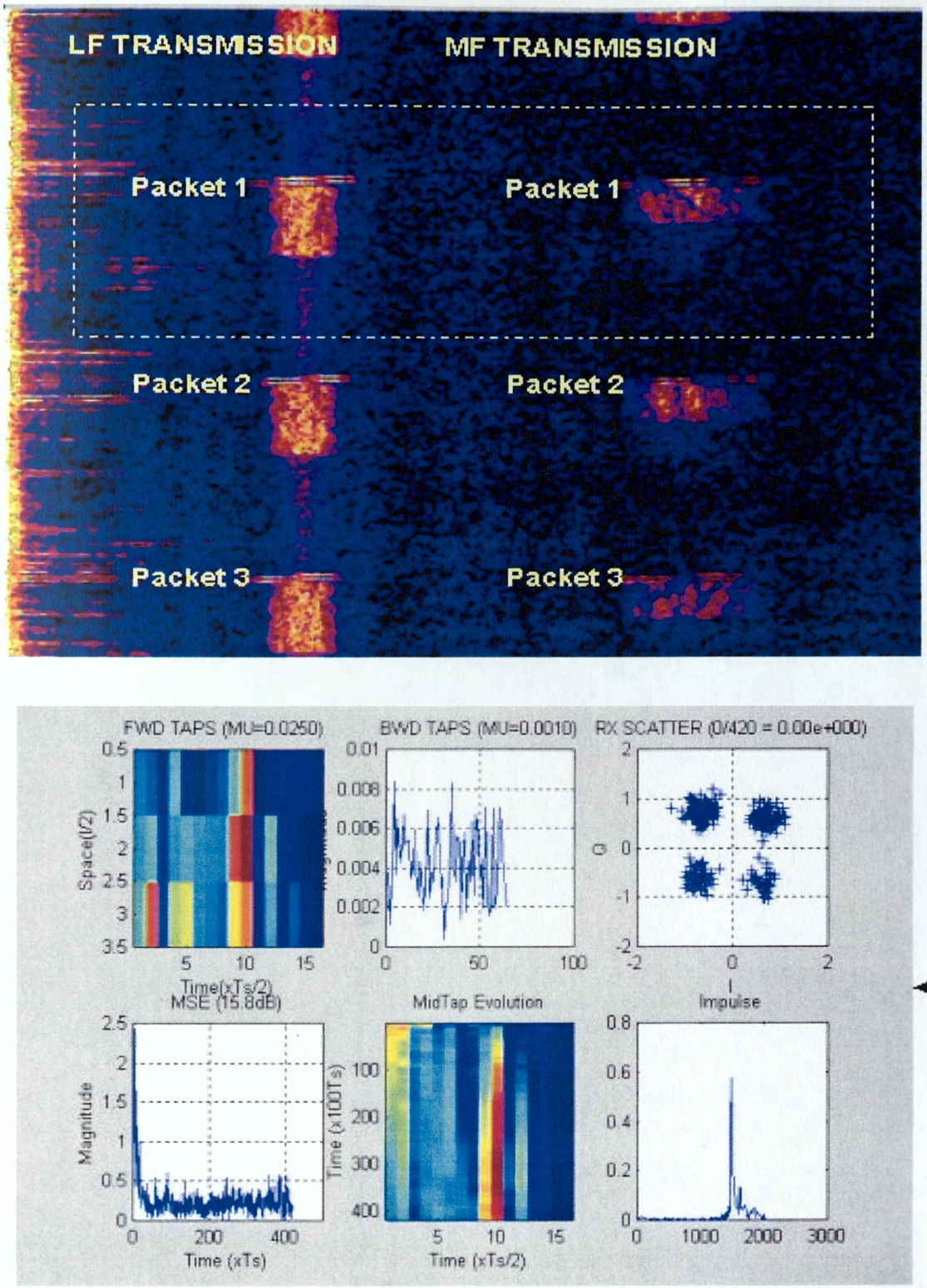

Figure 102; Operation at 20km using dual band low frequency (<2kHz) projectors at 300bps. Sound of Jura, NW Scotland.

V Real Time Implementation

V.1 Background

V.1.1 The preceding discussion has served to identify key technologies and processing algorithms for high data rate, acoustic communications. Of course a key feature of many communications systems is the need to support real time operation, enabling users to initiate and control data exchanges. In the majority of cases effective acoustic communications cannot be achieved using a single operating mode.

V.1.2 This is especially true in acoustic communications where the requirement is often to communicate with power sensitive, autonomous subsea sensor systems. Since acoustic transmission often places the greatest energy demands on the system, it is desirable to minimise acoustic transmission times by using high rate power efficient modulation techniques. In many applications the volume of data stored within the autonomous device will preclude a full data upload and so provision must be made to enable the user to interrogate the autonomous sensor and upload selected data subsets. The provision of a low rate, robust, bi-directional acoustic link naturally complements the high data rate uplink mode by providing a means to interrogate the autonomous system, select data subsets, and initiate high rate acoustic transmissions. In practice a third mode is also necessary, which enables the remote activation of the modem from sleep modes. This is essential for power sensitive systems. Also, in applications involving several undersea users, the initiation and control of high data rate exchanges must be arbitrated by robust point to point and point to multipoint acoustic links.

V.1.3 Over the course of this study there have been two real time demonstrations of the high data rate acoustic communications techniques

- Real time acoustic video telemetry;

- Real time subsea unit interrogation and data uplift.

V.2 Real Time acoustic video telemetry

V.2.1 The demonstration of real time acoustic video telemetry was the result of a collaborative effort between DERA and the University of Birmingham [157]. The aim of this work was to demonstrate the feasibility of using an acoustic communications link to uplift real time video images from a small remotely operated vehicle (ROV). This involved interfacing a video capture and compression subsystem developed by Birmingham to an embedded acoustic modem developed by DERA. Figure 103 shows the ROV and pressure vessel housing the video subsystem, modem electronics and power amplifier. The transducer, a free flooded ring design was mounted forward of the pressure vessel. The video processing subsystem comprised a frame grabber and a wavelet based, error tolerant image compression algorithm developed by Birmingham University specifically for the underwater acoustic telemetry application. The output of the image compression system was input to the acoustic modulator and power amp chain as shown in the figure. Figure 104 demonstrate images taken and decoded in real time for the vehicle operating in the QinetiQ tank facility at Winfrith, and Figure 105 shows a decoded image from the vehicle during field trials in Weymouth bay. The poor quality is attributable to imprecise adjustment of the camera focussing mechanism. Due to the latency in receiving the images, camera focusing could not easily be achieved manually.

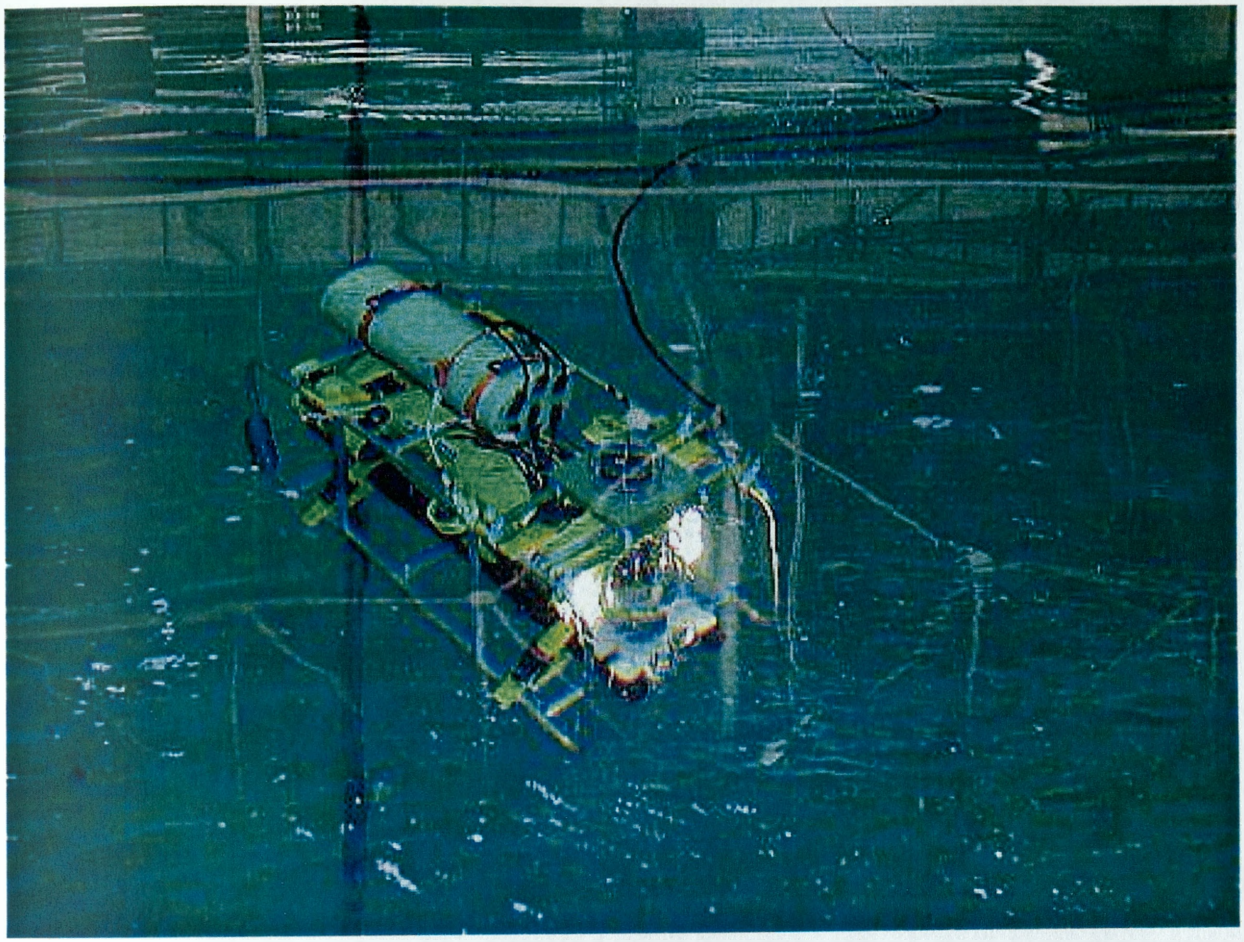

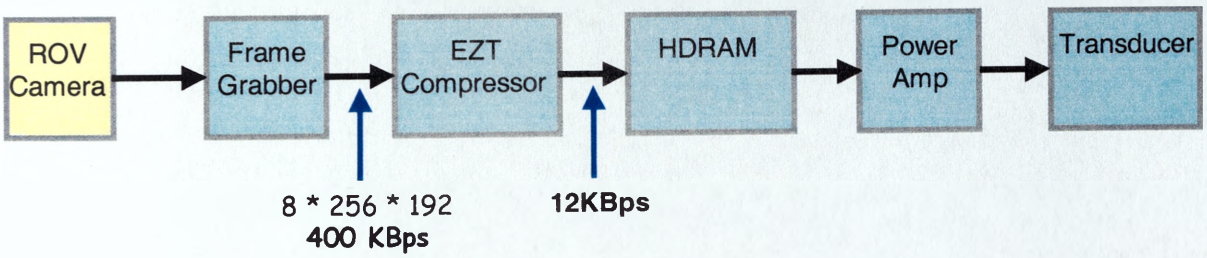

Figure 103; Real time video uplink demonstration

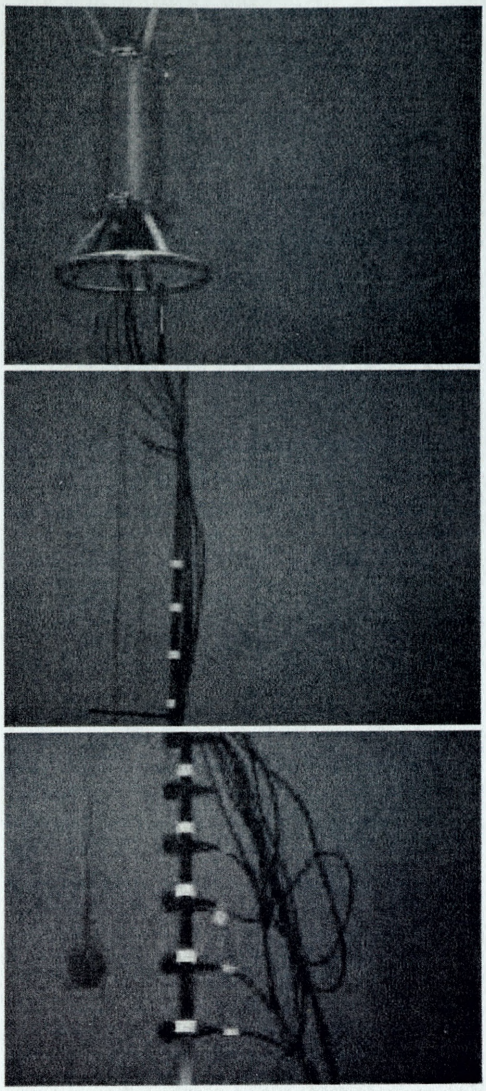

Figure 104; Images taken from ROV during initial tank tests at QinetiQ

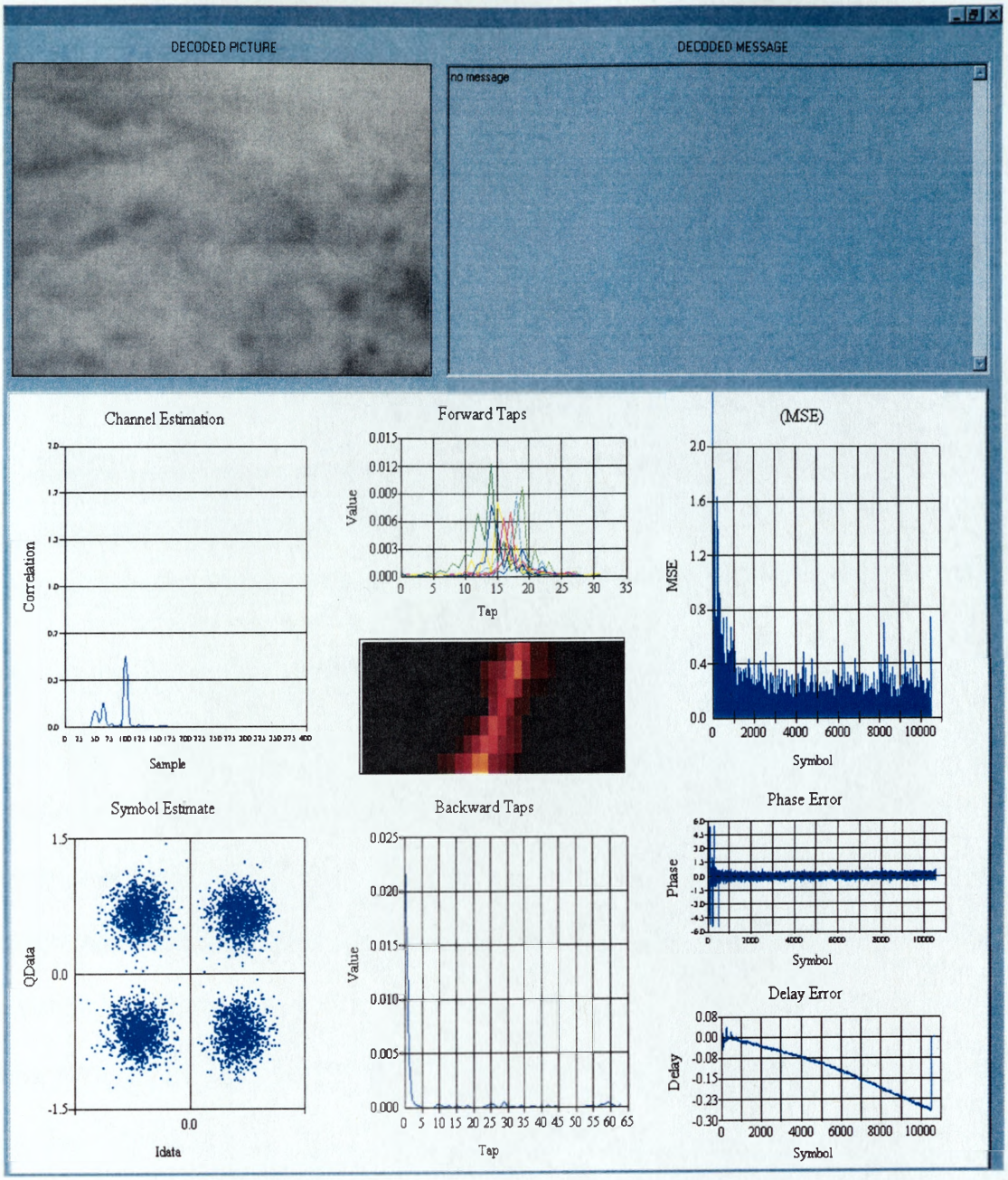

Figure 105; Decoded Sea Floor Image taken from ROV during field trials

V.3 Subsea Node Communications

V.3.1 Acoustic communications, both low and high data rate, is a key technology to enable connectivity with a variety of underwater sensor systems. The acoustic connectivity requirements to these systems exists at three levels

- Acoustic activation / deactivation
- Low data rate bi-directional acoustic communications
- High data rate uplink communications

V.3.2 Acoustic activation and deactivation essentially relates to simple commands to switch the subsea unit on or off. Due to limited energy resources, power management is an integral part of any subsea system and during the low power state, some means is necessary to wake up the system. Such systems must be simple and robust commensurate with the power constraints in sleep mode which are typically a few mW at most. Once the unit is awake, more powerful signal processing becomes available to receive and decode commands. Such techniques lend, for example, to asking the node simple questions regarding status and as a precursor to higher bandwidth data uplift, using the final high data rate mode. Figure 106 depicts an experimental subsea node designed to demonstrate the above three operational modes. Figure 107 depicts the system block diagram. The node comprised three processors

- Low Power Microcontroller
- 21061 digital signal processor
- Embedded PC

V.3.3 The low power micro controller was responsible for several system functions

- Real time clock and alarm modes
- Acoustic command detection

- Power control and sequencing

V.3.4 The DSP board was responsible for implementing acoustic modem functions. The embedded PC was used to provide data logging functions and to act as a data source for high data rate transmit requests.

V.3.5 Figure 108 depicts typical displays during node interrogation.

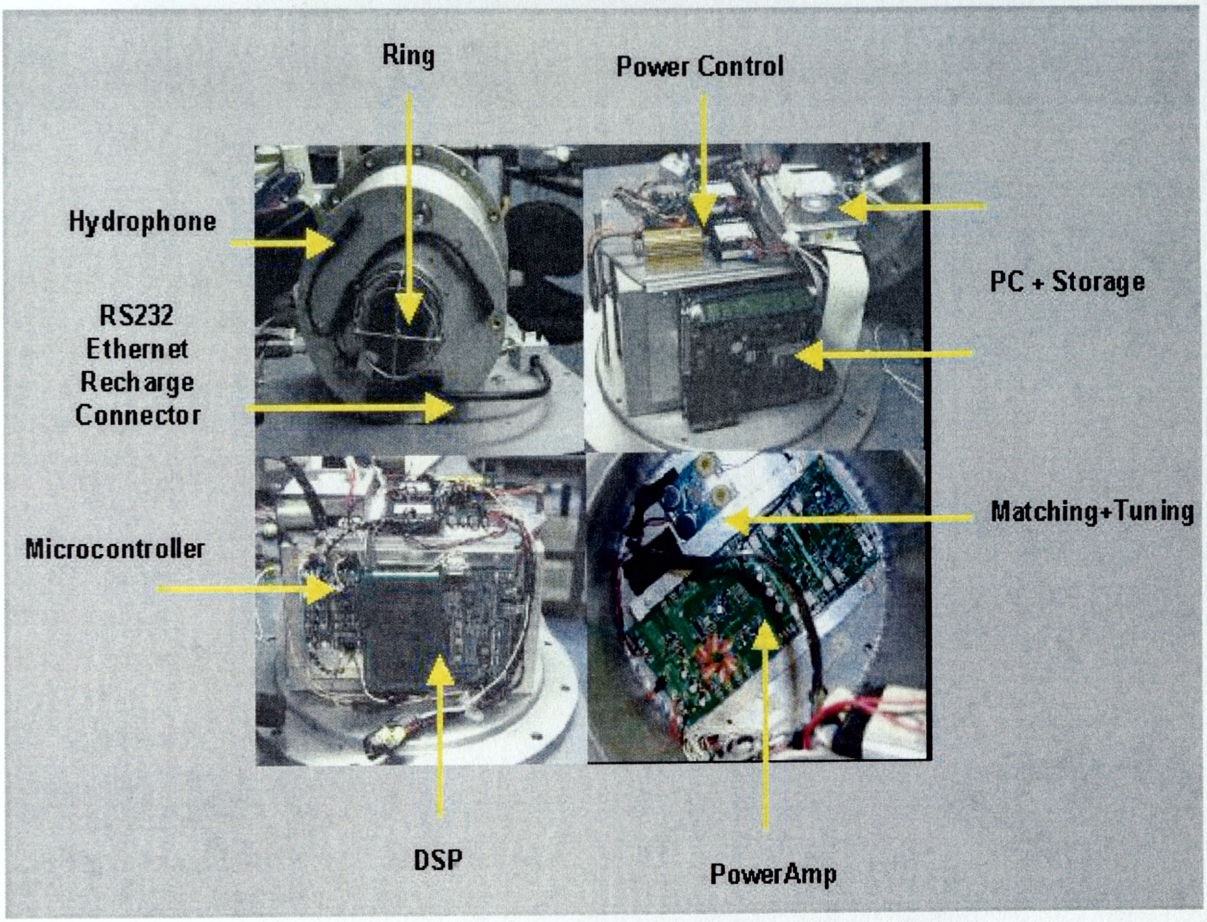

Figure 106; Subsea node and acoustic modem

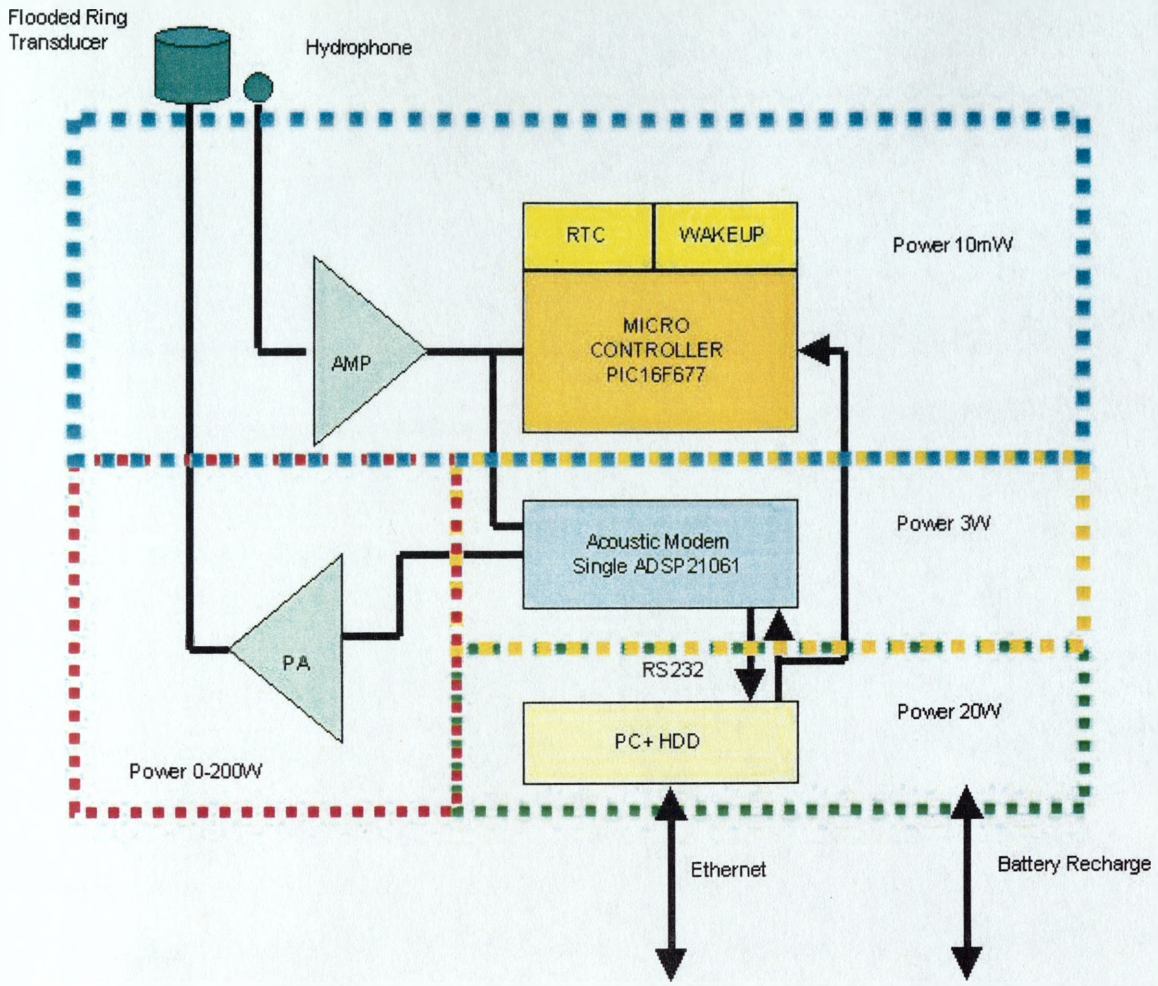

Figure 107; Subsea node and modem block diagram

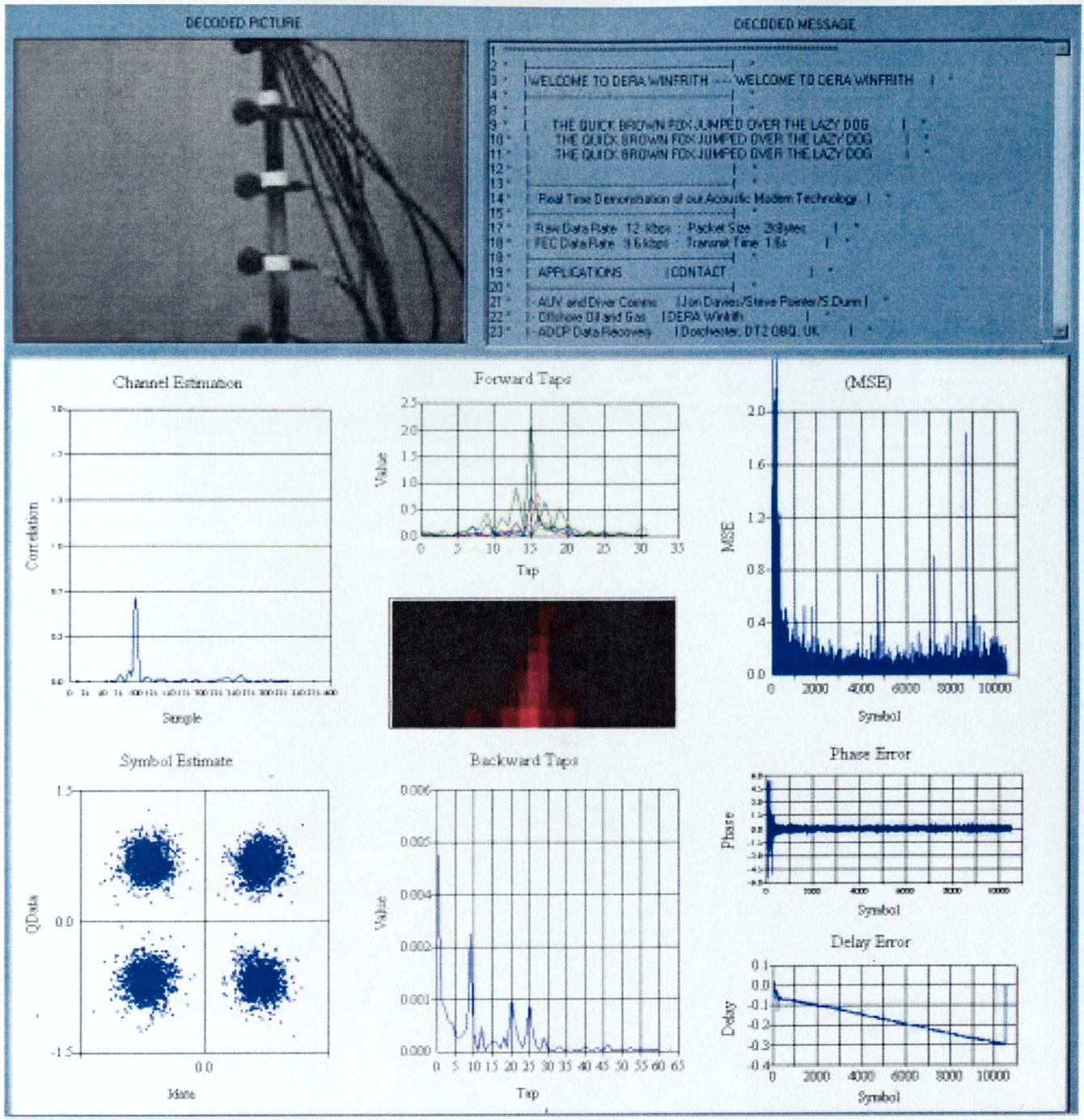

Figure 108; Image and text uplink data decoded in real time from subsea node

V.4 Handshake Protocol

V.4.1 There are several considerations relating to the design and implementation of packet design and data exchange protocol. As well as user data there are several systematic parameters which underpin the initiation and sustained reliability of an acoustic link

- Robust synchronisation
- Selective addressing and packet ID.
- Automated modulation detection
- Automated power control
- Automated preemphasis
- Automated transponding

V.4.2 Packet synchronisation is the most fundamental aspect of the communication problem ideally affording high probability of packet detection and low probability of packet false alarm, both of which are wasteful of processing resources. Selective addressing relates to the ability to individually address selected users and to provide a means for users to know the origin of the packet transmission and packet ID provides a number identifier to enable lost packets to be identified. Automating the detection and choice of modulation parameters provides a means for the receiver to identify how the user information part of the transmission is modulated. This is useful for example to provide the bandwidth efficiency of phase coherent techniques with the robustness and reliability of spread spectrum techniques.

V.4.3 Automated power control is essential for power efficiency. Establishing an acceptable power level between communicating parties relies on a co-operative power control mechanism. At longer ranges, the differential absorption losses across the transmission

bandwidth can total several tens of dB's or more. In such circumstance applying emphasis to the higher frequency components may partly redress the loss.

V.4.4 Automated transponding relates to the ability of the surface unit to interrogate the subsea unit and use its reply to determine range and possibly bearing based on the two way time of flight. All of the preceding information may be obtained during an initial communication phase or handshake protocol. The aim of this initial phase is to determine

- Time (range), Doppler (velocity) and bearing estimates
- Modulation mode
- Power level
- Prefiltering requirements

V.5 Packet Design

V.5.1 Figure 109 depicts the packet structure adopted for the acoustic telemetry link. The structure comprises two chirps (Table 8) at the start. This provides the means for the receiver to obtain time and Doppler (and bearing) synchronisation prior to data decoding. Following the two initial chirps are four protocol definition waveforms. These waveforms (Table 10) comprise maximum length sequences. The first sequence is cyclically extended by a time guard prefix to maintain the codes good time correlation properties in multipath channels for spread times up to the guard time interval. This waveform is fixed and used to provide channel estimation. The protocol definition comprises twelve bits of header information (Table 11). These bits are distributed over five fields and used to control transmission source level, pre-filtering modulation mode and automated retransmission request.

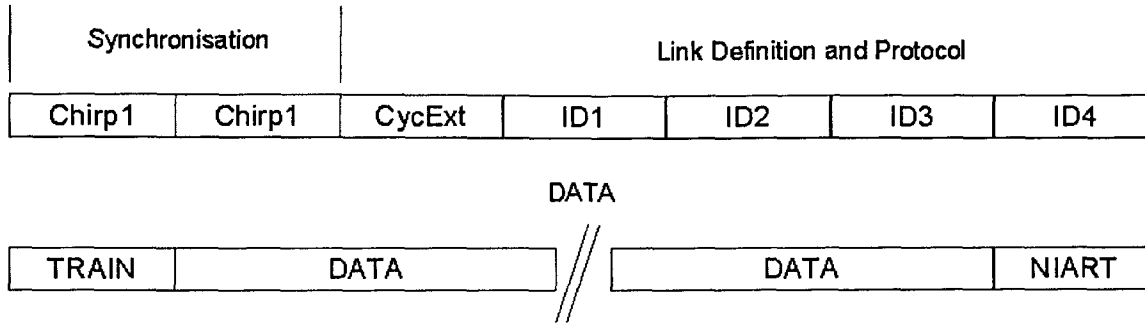

Figure 109; Packet Design

SYNCHRONISATION PARAMETERS	
Coding	LFM
Frequency	8 to 16kHz
Weighting	Kaiser Window Beta=0.8
Duration	21.33ms

Table 8; Synchronisation Chirp Header Parameters

Protocol Definition	
Frequency	8 to 16kHz
Time Guardband	Variable nominal 10.67ms
Duration	85.16ms (511x8/48000)
Modulation	2PSK DS Spread Spectrum
ID1-4 Waveform	511chip M=8, ML Sequence

Table 9; Protocol definition Waveform Parameters

Data Modulation						
Mode	bps/Hz	Chips	Rate (bps)	Syms (bytes) per packet	Sym Duration (ms)	Data Duration (s)
LoData	3	255	70.58	32(12)	42.5	1.36
HiData	2	N/A	12000	4096	0.17	0.683s

Table 10; Modem Operating Modes

V.6 Description

V.6.1 The need for open loop Doppler estimation and compensation has been emphasised throughout this thesis and the technique adopted is that described in section 6 based on two consecutive chirp soundings as shown in Table 8.

V.6.2 ID1 Bit 0 indicates the modulation modes as shown in Table 10. Low rate mode provides a spread spectrum link operating at 71bps. High rate mode provides a phase coherent link operating at 12000bps.

V.6.3 ID1 bit 1 indicates whether the transmission has been pre-emphasised. The problems of differential absorption across wideband transmissions was discussed in section 4. This field essentially implements a long range switch to improve system performance at longer ranges.

V.6.4 ID1 bit 2 indicates whether the destination should transpond. If set the destination, responds by transmitting a link definition response. The transpond transmission is offset a fixed delay from absolute synchronisation time and at a power level deduced from that encoded in the transpond request.

V.6.5 ID 2 bits 0-2 indicate the power level at which the transmission was initiated. This enables a remote receiver to adjust its power level based on the transmitter power level and received signal-to-noise ratio. During handshaking, the receiver may respond with a power indication higher or lower than the transmitted level depending upon the received signal-to-noise ratio. At the transmitter, the new source level is then used for subsequent transmissions.

V.6.6 A typical handshake/transpond exchange may proceed as follows. The interrogating unit initiates transpond request with sub sea node 3. On the downlink the transmitter sets ID1 bit2 = 1, encodes its source level using ID2 bits 0-2, indicates whether the transmission is preemphasised in ID1 bit 2 and sets the source node address in ID3 and destination address in ID4. The transmission comprising chirp header and protocol definition (total duration less than 250ms) is then transmitted to the subsea unit.

V.6.7 At node 3 the transmission is detected and decoded. Once the initial synchronisation is achieved the node uses a background timer to time offset the response to allow for host latency. At the transmitter the total transpond time is measured and a range estimate computed. The source level field of the uplink message is compared to the downlink and if modified, subsequent transmissions are adjusted. In this way the interrogating unit establishes an appropriate power level with the node. A typical data exchange may proceed as follows. The interrogating unit indicates a data packet transmission by encoding ID2 bit2 =0. Transmission source level is encoded in ID2 bits 1,0. Since the packet is now a data packet ID1 bits 0,1 are used to flag the modulation mode and the data rate. Individual node addressing if required, is defined within the packet data structure

ID4	ID3	ID2	ID1		
Bit0-2 Dest ID	Bit0-2 Source ID	Bit0-2 Source Level	Bit 2 Transpond	Bit 1 Pre-emphasis	Bit 0 Packet Type*
0-7	0-7	Ref + 0-36dB	0=No 1=Yes	0=No 1=Yes	0=LoData 1=HiData

Table 11; Protocol Definition Bit Fields (Data Mode)

V.7 Node Acoustic Modem Design

V.7.1 Figure 110 depicts the block diagram of the node acoustic modem operation. A single digitised hydrophone output is processed using the two chirp synchronisation algorithm. This algorithm determines the precise time of arrival of the transmission, the relative Doppler between the transmitter and receiver and the channel. Using this information the received signal is Doppler compensated using a multirate processing algorithm. The Doppler compensated data is then decoded using a low data rate decoding algorithm which computes the maximum likelihood transmitted symbol using a weighted correlator bank. This structure performs maximal ratio combining and maximum likelihood symbol estimation. The decoded data is passed via RS232 to the host platform. Response data from the host platform, which may be a low data rate reply or high data rate transmission is appropriately modulated and packetised for uplink transmission.

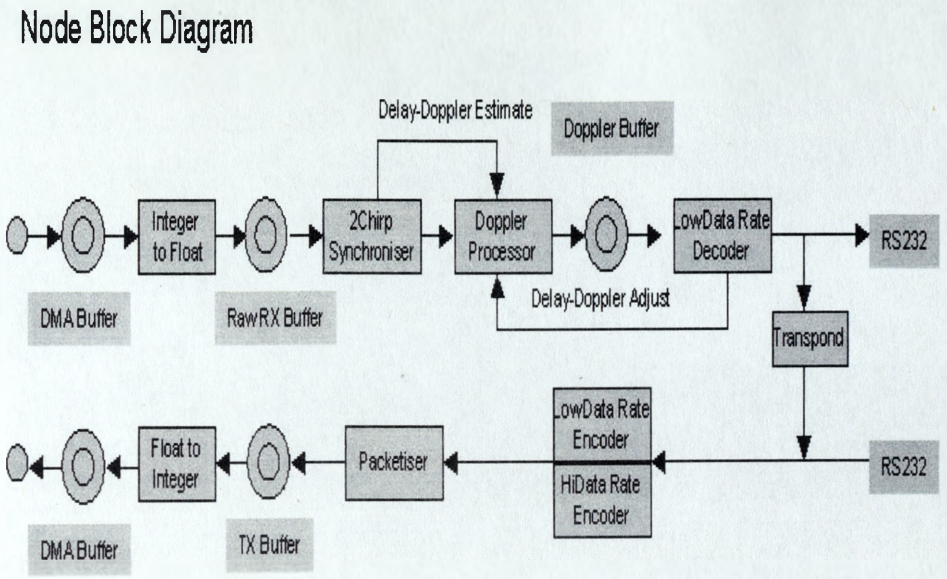

Figure 110; Subsea Node Block Diagram

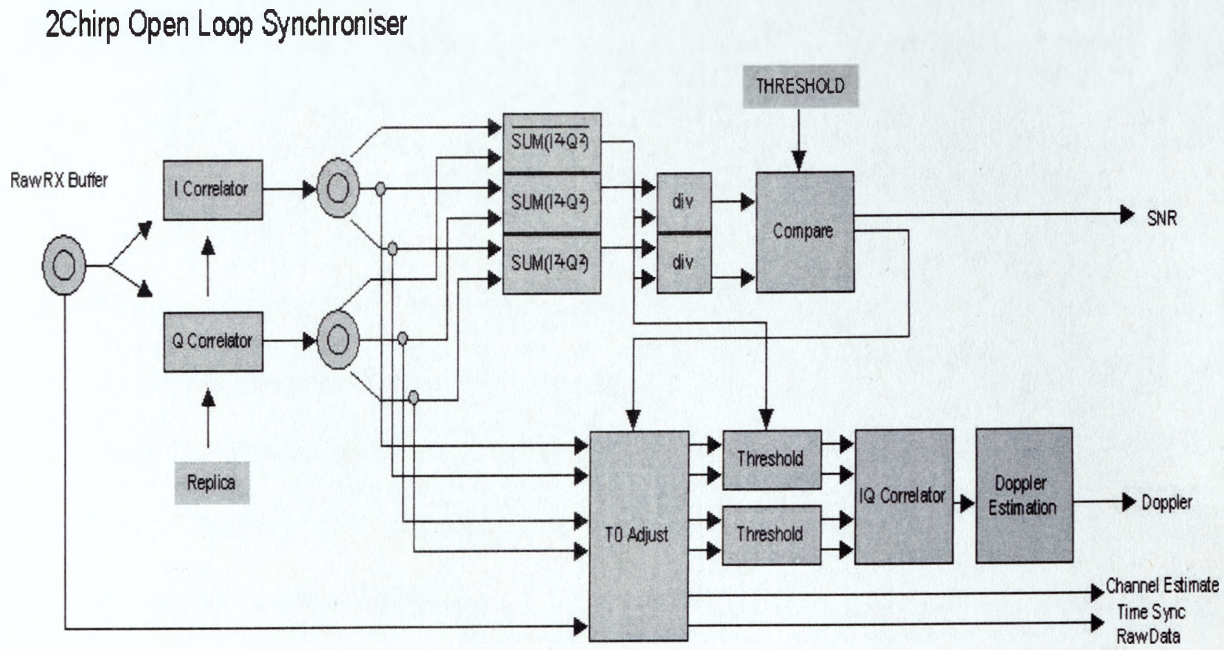

Figure 111; Two Chirp open Loop Synchroniser processing block diagram

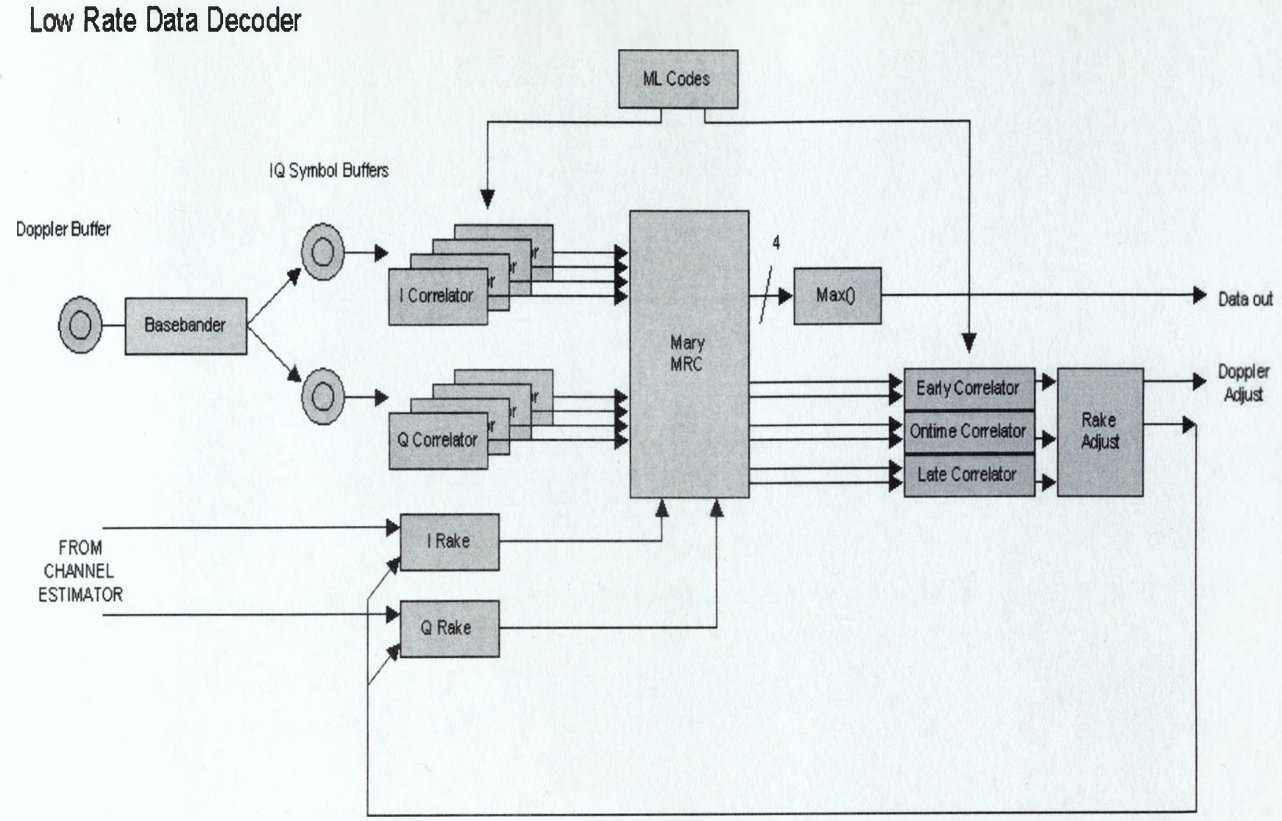

Figure 112; Low data rate spread spectrum decoding block diagram

V.7.2 The synchroniser algorithm, shown in Figure 111 implements the two chirp processing technique described in section 6. This processing block provides open loop time, Doppler and channel estimates. The low rate decoder algorithm shown in Figure 112 implements a Mary (M=8) orthogonal maximum likelihood detection algorithm using M sequence codes. Maximal ratio combining is used to rake path energies and rake taps are updated on a symbol-by-symbol basis.

V.8 Surface Unit Modem Design

V.8.1 The operation of the surface unit differs in principle from the subsea node. In particular, the surface unit must not only decode low rate replies from the node, but also decode the high data rate uplink transmissions. This dual functionality is shown in Figure 113. A further level of functionality is afforded by the use of two sub-arrays horizontally

separated. The use of these arrays allows highly accurate bearing information to be obtained.

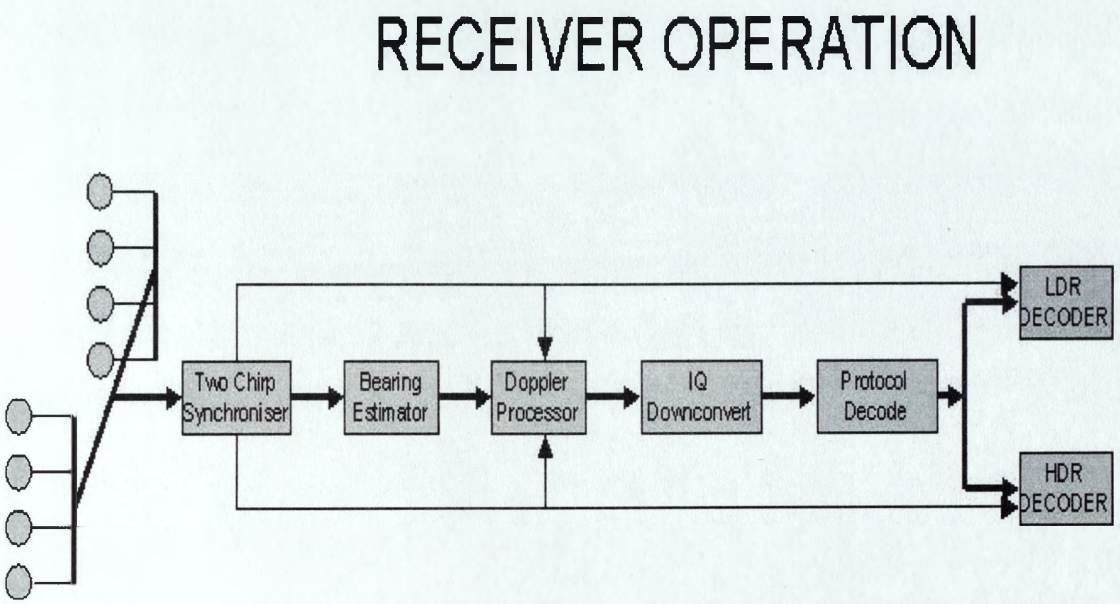

Figure 113; Surface unit receiver block diagram

V.8.2 The principle of operation for the surface unit involves determining the type of uplink message as defined in the link protocol header at the start of the transmission. This information enables the receiver to determine whether the transmission is a low rate transmission or high rate transmission and the appropriate decoding algorithm is applied. If low rate the decoding algorithm is that shown in Figure 114 and Figure 115. If high data rate, the receiver decoding proceeds in both forward and reverse directions

V.8.3 Figure 114 depicts the forward-reverse iterative training algorithm. Complex baseband packet data incorporating forward and reversed training sequences are applied to two concurrent STAP-DFE structures one operating on forward time data, one operating on reverse time data. Both structures are concurrently trained and the MSE output error monitored. At each training iteration the MSE output error is compared with a threshold.

If the error exceeds this threshold training is repeated Training iterations continue until either the error falls below the threshold or the total number of iterations exceeds a predefined limit.

V.8.4 If both forward and reverse training iterations converge below the threshold, then both are subsequently decoded in the decision directed mode and the MSE error computed. The MSE outputs from both forward and reverse directions are compared and the one affording the lowest error chosen. Potential benefits from exploiting both forward and reverse decoded symbol streams have not been studied. For example, where the channel response does not demonstrate marked maximum or nonminimum phase behaviour, and where the structure converges in both forward and reverse directions, there may be advantages in combing the two symbol streams to improve overall system performance.

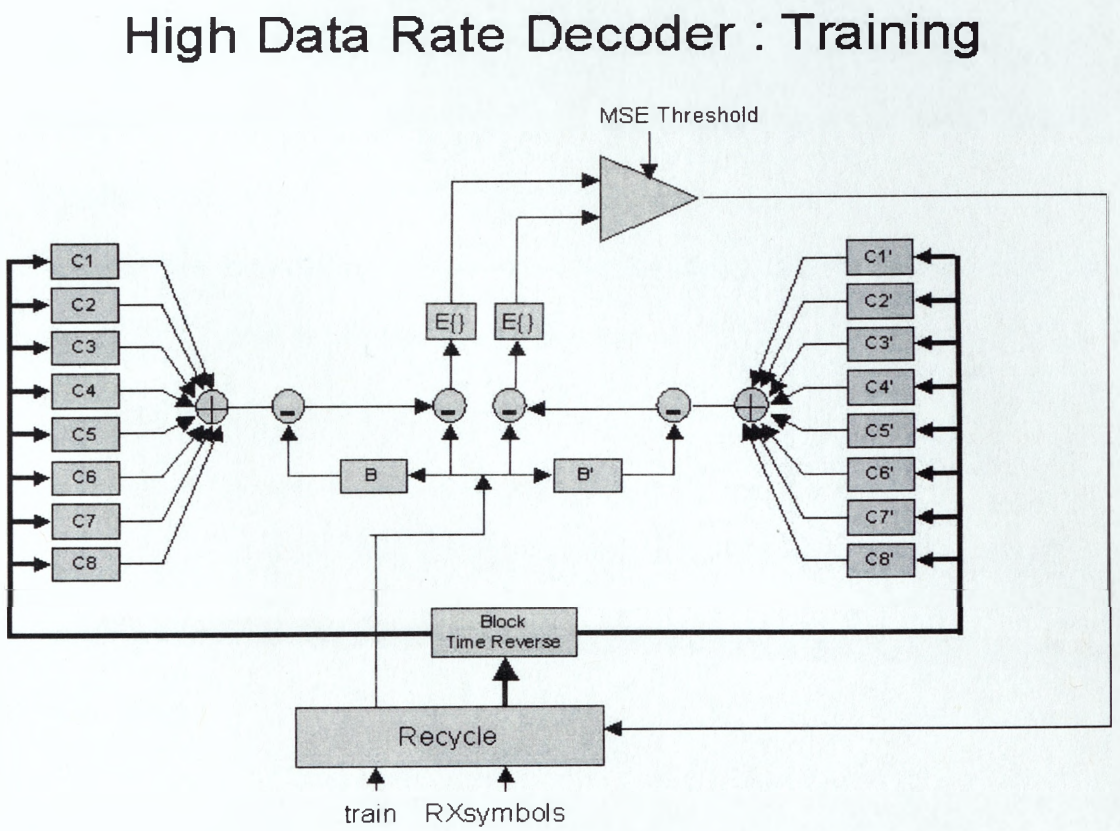

Figure 114; High data rate forward-reverse iterative training

High Data Rate Decoder : Decoding

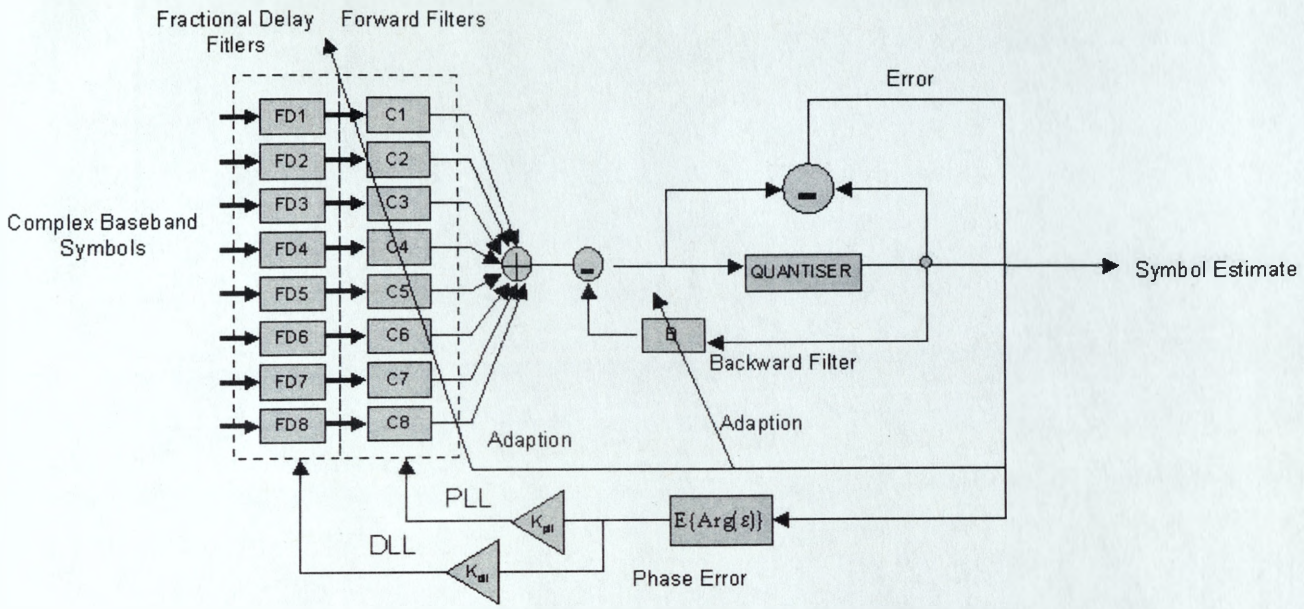

Figure 115; High data rate decision directed decoding with closed loop PLL+DLL support

V.8.5 Figure 115 depicts receiver performance during the closed loop data decoding phase. Here the receiver structure reverts to conventional form with the addition of two synchronisation loops. Both PLL and DLL tracking algorithms are driven by the phase of the complex tracking error. Symbol timing adjustments are implemented by a fractional delay filter section FD1-8, using the techniques discussed in appendix L. Phase tracking is implemented as a phase rotation of the fractionally delayed symbol data prior to the forward STAP filter block. This contrasts to the position adopted by several authors, whereby the phase correction is applied after the STAP filter block. In simulations it was found that the former position provided better performance over a wider range of channel conditions.